Molecular models for 267 binary mixtures validated by vapor-liquid equilibria: a systematic approach

Jadran Vrabec * [1], Yow-lin Huang[1], Hans Hasse[2]

[1] Lehrstuhl für Thermodynamik und Energietechnik, Universität Paderborn, 33098 Paderborn, Germany

[2] Laboratory for Engineering Thermodynamics, University of Kaiserslautern, 67663 Kaiserslautern, Germany

Keywords: molecular model; mixture; unlike interaction; vapor-liquid equilibrium

Abstract

By assessing a large number of binary systems, it is shown that molecular modeling is a reliable and robust route to vapor-liquid equilibria (VLE) of mixtures. A set of simple molecular models for 78 pure substances from prior work is taken to systematically describe all 267 binary mixtures of these components for which relevant experimental VLE data is available. The mixture models are based on the modified Lorentz-Berthelot combining rule. Per binary system, one state independent binary interaction parameter in the energy term is adjusted to a single experimental vapor pressure. The unlike energy parameter is altered usually by less than 5 % from the Berthelot rule. The mixture models are validated regarding the vapor pressure at other state points and also regarding the dew point composition, which is a fully predictive property in this work. In almost all cases, the molecular models give excellent predictions of the mixture properties.

* corresponding author, tel.: +49-5251/60-2422, fax: +49-5251/60-3522,
email: jadran.vrabec@upb.de

1 INTRODUCTION

In previous work of our group, a set of molecular models has been developed for 78 real pure fluids using the dipolar or quadrupolar two-center Lennard-Jones (2CLJD and 2CLJQ) potential [1,2]. This model type has been proposed more than three decades ago [3], however, it is far from being fully exploited. Polar 2CLJ models consider the basic molecular interactions repulsion and dispersive attraction and also feature anisotropy and polarity in a simple way. 78 small molecules consisting of up to nine atoms that belong to different classes of real fluids, including noble gases, alkanes, halogens and numerous refrigerants, were covered in [1,2]. For many of the 78 molecules, the polar 2CLJ model strongly simplyfies the intermolecular interactions. E.g., the asymmetry of the molecules is neglected and the polar interaction is always aligned along the main molecular axis. Also the polarizability, which is often assumed to be a crucial molecular property for thermodynamics, is only implicitly considered by Lennard-Jones interaction sites. Furthermore, the internal degrees of freedom are neglected as the polar 2CLJ models are rigid.

The aim of this work is to investigate whether these crude assumptions for pure substance models have an impact on mixture properties, in particular on binary vapor-liquid equilibria (VLE). It can be argued that oversimplified molecular models can be adjusted to a few experimental pure substance properties, but major deficiencies should be visible when applied to mixtures.

Molecular simulations on binary VLE containing some of the 78 components, but using other models or parameter sets, are available from different authors: Potoff and Siepmann [4] (N_2, CO_2 and alkanes), de Pablo et al. [5] (hydrocarbons), Gao et al. [6] (hydrofluorocarbon and hydrochlorofluorocarbon mixtures), Kronome et al. [7] (N_2 + C_2H_6), Nath et al. [8] (alkane mixtures), Cui et al. [9] (CO_2 + perfluoroalkanes), Potoff et al. [10] (mixtures of various polar and non-polar components), Delhommelle and Millié [11] (Ne, Ar and Kr), Liu and Beck [12] as well as Vrabec and Fischer [13,14] (CH_4, C_2H_6 and CO_2). However, each of these publications is restricted to a few mixtures only.

Some of the abovementioned 78 pure substance models [1,2] have successfully been used in simulation studies by others: Several authors used them as solute models for predictions of the

Henry's law constant: Boutard et al. [15] for O_2 in Ethanol, Krishnamurthy et al. [16] for N_2 and O_2 in Ethylene oxide and Shah and Maginn [17] for C_2H_6 and C_2H_4 in an ionic liquid. Grimm et al. [18] used the CH_2I_2 model to investigate local density effects on photoinduced isomerization kinetics of this substance in supercritical CO_2. Müller et al. [19,20] used several models (C_2H_6, C_2H_4, N_2 and C_2F_6) for simulations on adsorption regarding micro-porous carbon. Jia and Murad [21,22] took the N_2 and O_2 models to simulate zeolite membrane separations of gas mixtures. The same models were taken by Chialvo and Horita [23] for a study on vapor-liquid fractionation factors. Schumacher et al. [24] used the N_2, O_2 and CO_2 models for investigations on the optimization of organic/inorganic adsorbents. Carrero-Mantilla and Llano-Restrepo [25] used them to predict VLE of binary mixtures containing CH_4, C_2H_6, C_2H_4 and Propylene, they also regarded reactive systems [26]. Furthermore, Smith and Lísal [27,28] used the N_2 model for non-reacting and reacting systems regarding ammonia synthesis.

It should be noted that polar 2CLJ models are not suited for hydrogen bonding molecules as they cannot mimic their very strong short-range interaction. However, it was shown for 35 binaries [29,30] that they are, e.g. for CO_2 compatible with appropriate molecular models, e.g. for Methanol, for hydrogen bonding fluids.

Reasonable molecular modeling of mixtures requires the definition of the unlike interactions only. While unlike polar interactions are straightforwardly known on a sound physical basis, i.e. by using the laws of electrostatics, there is still no such framework for the unlike dispersive interactions [31]. Therefore, combining rules have been proposed that determine the parameters of that unlike interaction, where, among many others, the most well-known is the Lorentz-Berthelot rule. Regarding binary VLE of 44 systems we have recently shown in [32] that *(a)* the Lorentz rule is excellent, *(b)* the unlike dispersion energy parameter is crucial for accurate predictions of the pressure, *(c)* none of a set of eleven investigated combination rules yields really optimal values for it and *(d)* it should be adjusted to one experimental vapor pressure of the mixture.

Based on the 78 pure substance models [1,2], the unlike energy parameter was adjusted in

previous work [33–35] to the experimental binary vapor pressure for 44 systems in order to very accurately describe their VLE. The viability of this approach was also shown with VLE predictions of five ternary mixtures [33–35]. Galbraith and Hall [36] took some of those adjusted mixture models and calculated VLE of four binaries containing N_2, O_2, CO_2 and C_2H_6 by Gibbs-Duhem integration and obtained an excellent agreement with experimental data.

However, as in most fields of science, there is a danger that results are biased by a selection of the studied subjects. Moreover, successful approaches are generally more likely to be published than failures. To counter this, a combinatorial approach was used here. Theoretically, out of the $N = 78$ components $N(N-1)/2 = 3\ 003$ binary mixtures can be formed, but of course, not all of these systems have been studied experimentally. To our knowledge, the VLE was measured for a subset of 267 out of the 3 003 binaries. In the present work, *all* those 267 binary mixtures were studied. This is by far the largest set of binaries that was used to probe the application of molecular modeling and simulation to mixtures.

The presented simulation results are compared to experimental data and in most cases to the Peng-Robinson equation of state (EOS). For parameter adjustments of the molecular models and the Peng-Robinson EOS always the same experimental data were used to achieve a fair comparison.

2 EXPERIMENTAL DATABASE

In this work, experimental data were predominately retrieved using Dortmunder Datenbank (DDB) [37], which collects *all* publicly available mixture VLE data sets, covering more than a century of experimental work. For a subset of 286 of the potential 3 003 binary mixtures experimental VLE data is available. That data is contained in 203 publications [38]-[240]. These 286 binaries include 66 of the 78 pure components, i.e. for 12 substances no mixture data was found with any of the other 77 components. A list of these 66 components, including their CAS RN number for proper identification, is given in Table 1. Please note that the ASHRAE nomenclature is preferred in the following due to its brevity, despite its deficiencies [241].

Of those 286 binary mixtures, 44 have been modeled in previous work of our group [33–35] but the resulting VLE data were published only partly.

The term VLE data is used here for information on vapor-liquid coexistence at finite mole fractions, i.e. not for properties at infinite dilution like the Henry's law constant. For an additional 66 binary mixtures experimental Henry's law constant data were found, however, they are not regarded here but will be discussed in a forthcoming paper.

For 55 of the 286 systems experimental data is available only from a single source. Among them are 8 binaries, where exclusively data on the dew line were published. Such cases, cf. Table 1 of the supplementary material, are of little use for the present modeling and validation procedure so that these mixtures were excluded here. For 11 binaries VLE data are available only for very dilute state points, i.e. the bubble point mole fraction of the low boiling component is $x_1 < 0.02$ mol/mol, cf. Table 2 of the supplementary material. Such data rather present gas solubilities which are related to the Henry's law constant. For direct VLE simulations they are not well suited so that they were excluded as well. The total number of investigated systems is therefore 286-8-11=267 binaries.

3 PURE FLUID MODELS

Due to the binary VLE experimental data situation 66 polar 2CLJ based molecular models, taken from [1,2], were used here. These are five spherical non-polar (LJ) models for noble gases and CH_4, three spherical dipolar (Stockmayer) models for R30, R32 and R30B2, furthermore 32 elongated dipolar (2CLJD) models which include carbon monoxide and numerous refrigerants, and finally 26 elongated quadrupolar (2CLJQ) models which include halogens, alkanes, refrigerants and CO_2.

The polar two-center Lennard-Jones pair potential writes as

$$u_{\mathrm{2CLJP}}(\boldsymbol{r}_{ij}, \boldsymbol{\omega}_i, \boldsymbol{\omega}_j, L, P) = u_{\mathrm{2CLJ}}(\boldsymbol{r}_{ij}, \boldsymbol{\omega}_i, \boldsymbol{\omega}_j, L) + u_{\mathrm{P}}(\boldsymbol{r}_{ij}, \boldsymbol{\omega}_i, \boldsymbol{\omega}_j, P),$$

where u_{2CLJ} is the Lennard-Jones part

$$u_{\mathrm{2CLJ}}(\boldsymbol{r}_{ij},\boldsymbol{\omega}_i,\boldsymbol{\omega}_j,L)=\sum_{a=1}^{2}\sum_{b=1}^{2}4\epsilon\left[\left(\frac{\sigma}{r_{ab}}\right)^{12}-\left(\frac{\sigma}{r_{ab}}\right)^{6}\right].$$

Herein, is $\boldsymbol{r}_{ij}$ the center-center distance vector of two molecules i and j, r_{ab} is one of the four Lennard-Jones site-site distances; a counts the two sites of molecule i, b counts those of molecule j. The Lennard-Jones parameters σ and ϵ represent size and energy, respectively. The polar contribution, written in a general form u_{P} here, is also dependent on the vectors $\boldsymbol{\omega}_i$ and $\boldsymbol{\omega}_j$ representing the orientations of the two interacting molecules. P is a general notation for the polar momentum.

In the case of a dipolar model, the polar contribution is given by [242]

$$u_{\mathrm{D}}(\boldsymbol{r}_{ij},\boldsymbol{\omega}_i,\boldsymbol{\omega}_j,\mu)=\frac{1}{4\pi\epsilon_0}\cdot\frac{\mu^2}{|\boldsymbol{r}_{ij}|^3}\left(s_i s_j\cos\phi_{ij}-2c_i c_j\right), \tag{1}$$

with $c_k=\cos\theta_k$ and $s_k=\sin\theta_k$. θ_i is the angle between the axis of the molecule i and the center-center connection line and ϕ_{ij} is the azimuthal angle between the axis of molecules i and j. The number of parameters related to the dipole is one, namely the dipolar momentum μ, as its position in the center of the model and orientation along the molecular axis are fixed and it is reduced by the large distance approximation to a point dipole.

A point dipole may, e.g. when a simulation program does not support this interaction site type, be approximated by two point charges q separated by a distance l. Limited to small l, one is free to choose this distance as long as $\mu=ql$ holds. However, the computational effort increases through this separation for the interaction between two dipoles roughly by a factor of four.

The 2CLJQ model has a point quadrupole of momentum Q also placed in the geometric center of the molecule and oriented along the molecular axis. The quadrupolar contribution is [242]

$$u_{\mathrm{Q}}(\boldsymbol{r}_{ij},\boldsymbol{\omega}_i,\boldsymbol{\omega}_j,Q)\;=\;\frac{1}{4\pi\epsilon_0}\cdot\frac{3}{4}\frac{Q^2}{|\boldsymbol{r}_{ij}|^5}\left[1-5\left(c_i^2+c_j^2\right)-15c_i^2c_j^2+2\left(s_i s_j\cos\phi_{ij}-4c_i c_j\right)^2\right]. \tag{2}$$

As for the point dipole, also the point quadrupole may be approximated by three linearly aligned point charges in the sequence q, $-2q$, q, each separated by l. The small distance l can also be chosen arbitrarily as long as $Q=2ql^2$ holds. The computational effort for the interaction between two quadrupoles increases then roughly by a factor of nine.

Most polar 2CLJ models have four parameters: size σ, energy ϵ, elongation L and dipolar momentum μ or quadrupolar momentum Q; Stockmayer models have a vanishing elongation, while the non-polar spherical LJ models have only two parameters: σ and ϵ. Both their elongation and polarity are zero. Model parameters were adjusted in [1,2] to experimental pure fluid VLE data using global correlations of critical temperature, saturated liquid density and vapor pressure as functions of these molecular parameters [243,244]. These pure substance model parameters are not repeated here. It should be noted that a wide range of polar momenta are covered by the 66 pure substance models. Starting from a non-existent polar momentum in case of the noble gases and methane, it ranges to up to 4.7919 D for the dipolar R130a and up to 16.143 DÅ for the quadrupolar R1110.

The advantage of these molecular models is their simplicity, which reduces simulation time considerably, and their accuracy: typically, the relative deviations between simulation and experiment are below 1 % for the saturated liquid density, below 3 % for the vapor pressure, and below 3 % for the enthalpy of vaporization [1,2]. They also have shown to predict reliably Joule-Thomson inversion curves for pure fluids and mixtures [245,246] covering a wide range of state points but also transport properties [247–251].

4 MOLECULAR MIXTURE MODELS

On the basis of defined pairwise additive pure fluid models, molecular modeling of mixtures reduces to modeling the interactions between unlike molecules. Unlike interactions consist of two different types here. The electrostatic interactions, e.g. between dipole and dipole, dipole and quadrupole, as well as quadrupole and quadrupole, belong to one type. These interactions are treated here in a physically straightforward way, simply using the laws of electrostatics. Interactions between different dipoles and different quadrupoles are already defined by equations (1) and (2), when $\mu^2 = \mu_i\mu_j$ or $Q^2 = Q_iQ_j$ is specified, respectively. The dipole-quadrupole interaction, present here in 108 mixtures, is given by [242]

$$u_{\mathrm{DQ}}(\boldsymbol{r}_{ij}, \boldsymbol{\omega}_i, \boldsymbol{\omega}_j, \mu_i, Q_j) = \frac{1}{4\pi\epsilon_0} \cdot \frac{3}{2} \frac{\mu_i Q_j}{|\boldsymbol{r}_{ij}|^4} (c_i - c_j) \left[1 + 3c_ic_j - 2s_is_jc\right]. \tag{3}$$

Repulsion and dispersive attraction are other interaction types and are present between all molecules. If a mixture A + B is modeled on the basis of Lennard-Jones potentials, the knowledge of the unlike Lennard-Jones parameters σ_{AB} and ϵ_{AB} is required. For their determination, the broadly used Lorentz-Berthelot combining rule is a good starting point [32]

$$\sigma_{AB} = (\sigma_A + \sigma_B)/2, \tag{4}$$

and

$$\epsilon_{AB} = \sqrt{\epsilon_A \epsilon_B}. \tag{5}$$

Applying σ_{AB} and ϵ_{AB}, as given by equations (4) and (5), allows the prediction of mixture properties from pure fluid data alone [25,32–35]. But as shown in [25,32–35], a significant improvement can be achieved by introducing one state independent binary interaction parameter ξ to adjust the unlike energy parameter

$$\epsilon_{AB} = \xi \sqrt{\epsilon_A \epsilon_B}. \tag{6}$$

For VLE, it was shown in [32] that ξ should be adjusted to a single experimental binary vapor pressure. Specifying temperature and bubble point composition, ξ has hardly any influence on the bubble density and a minor influence on the dew point composition. The benefit of ξ lies in an excellent representation of the experimental two-phase envelope that is predominantly superior to adjusted cubic EOS. The binary interaction parameter was adjusted here following the same procedure as in [33–35]. It should be pointed out that the dew point composition was not included in the adjustment so that dew point simulation data is fully predictive and thus can well be used to assess the mixture models.

Table 2 gives the state point (i.e. temperature T and bubble point mole fraction of the lower boiling component x_1) and the experimental vapor pressure p^{exp} which was used for the adjustment as well as the resulting binary interaction parameter ξ. A first validating VLE simulation at this state point with the adjusted mixture model was performed. The resulting vapor pressure p^{sim} and dew point composition from simulation are also listed in Table 2 and can numerically

be compared to experimental data there. Note that for 80 binaries no experimental dew point composition is available.

5 PENG-ROBINSON EQUATION OF STATE

Cubic EOS offer a compromise between generality and simplicity that is suitable for many purposes. They are valuable tools for correlating experimental data and are therefore often used in technical applications. In the present work, the Peng-Robinson EOS was used for comparison and as a guide for the eye in the numerous phase diagrams presented subsequently.

The Peng-Robinson EOS [253] is given by

$$p = \frac{RT}{v-b} - \frac{a}{v(v+b)+b(v-b)}, \tag{7}$$

where the temperature dependent parameter a is defined by

$$a = \left(0,45724\ \frac{R^2{T_c}^2}{p_c}\right)\left[1+\left(0.37464+1.54226\ \omega-0.26992\ \omega^2\right)\left(1-\sqrt{\frac{T}{T_c}}\right)\right]^2, \tag{8}$$

and the constant parameter b is

$$b = 0.07780\ \frac{RT_c}{p_c}. \tag{9}$$

Therein, the critical temperature T_c, the critical pressure p_c, the acentric factor ω, and the ideal gas constant R of the pure substance are needed. These data were taken from Merseburger Datenbank [254].

To apply the Peng-Robinson EOS to mixtures, mixed parameters a_m and b_m have to be defined. For this purpose, a variety of mixing rules has been presented in the literature. The Van der Waals one-fluid mixing rule [253] was chosen here. It defines the temperature dependent parameter as

$$a_m = \sum_i \sum_j x_i x_j a_{ij}, \tag{10}$$

where i and j indicate the components with

$$a_{ij} = \sqrt{a_i a_j}(1-k_{ij}), \tag{11}$$

including k_{ij} as an adjustable binary parameter. The constant parameter is defined as

$$b_m = \sum_i x_i b_i. \tag{12}$$

In the present work, the binary parameter k_{ij} of the Peng-Robinson EOS was adjusted for each mixture to the experimental vapor pressure at the same state point as the molecular mixture model.

6 RESULTS AND DISCUSSION

The results are presented here in pressure vs. mole fraction phase diagrams, cf. Figures 1 to 20 and supplementary material. Full numerical VLE simulation data are given as supplementary material as well which also contains the saturated densities and the heat of vaporization from simulation. Due to the fact that such data is rarely available from experiment for comparison, they are not discussed in the present work.

By addressing the binaries, the lower boiling component is always mentioned first, i.e. in mixture A + B, A is lower boiling one. In all phase diagrams, also the pure substance vapor pressure of the molecular models is indicated. These were obtained via the vapor pressure correlations for polar 2CLJ fluids as given in [243,244].

To assess the quality of the mixture models, VLE calculations were made at other state points than those used for the adjustment of the binary interaction parameter ξ. Preferably, state points were chosen for which a direct comparison to experimental data is possible. The near-critical region was not covered to avoid difficulties in the simulations. The first criterion of the present assessment is the resulting slope of the bubble line which can directly be compared with experimental data in most cases. The second criterion is the resulting dew point composition as a function of pressure which is fully predictive here. These data may also directly be compared to experimental data in most cases. However, for 80 mixtures no experimental dew line data was published.

A similar assessment was made in the Third Industrial Fluid Property Simulation Challenge

2007 [255] for molecular simulation data regarding the binary system R227ea+Ethanol.

We have rated the mixture models according to the two criteria mentioned above: if the slope of the simulative bubble line was in agreement with the experiment roughly within the statistical uncertainty and the average deviation between simulation and experiment for the dew point mole fraction was below 0.05 mol/mol, it was assumed that the mixture model is *successful*. For a few pure fluids, e.g. R23 between around 260 to 300 K, the pure substance vapor pressure shows noticeable deviations when compared with experimental data, cf. Figure 1. Thus, the binary two-phase envelope must deviate in the region which is rich of this component. However, it was found that such deficiencies usually do not translate into the remaining composition range. If the mixing behavior was generally predicted correctly in that sense, the mixture model was also rated as successful.

The successful cases are discussed here at a glance due to the large number of systems, however, they are all shown in the supplementary material. The regarded vapor pressure range, depending on the availability of experimental data, was extensive. It covers more than three orders of magnitude from around 0.016 MPa (R140a + R10, cf. Figure 2) to above 30 MPa (Ne + CO_2, cf. Figure 3).

For zeotropic mixtures, it can be seen that very different shapes of the two-phase envelope were predicted correctly. At sub-critical temperatures, there are very narrow envelopes (e.g. R22 + R134a, cf. Figure 4), wider envelopes (e.g. Propylene + R114, cf. Figure 5) and very wide envelopes (e.g. R14 + R152a, cf. Figure 6), where the vapor phase contains little of the high boiling component. There are qualitatively different slopes of the bubble line: convex (e.g. Xe + R40, cf. Figure 7), straight (e.g. N_2 + Ar, cf. Figure 8), concave (e.g. R23 + R152a, cf. Figure 1) or S-shaped (e.g. R14 + Propylene, cf. Figure 9). Also qualitatively different slopes of the dew line were predicted correctly: convex (e.g. R22 + R12, cf. Figure 10), straight (e.g. R22 + R134a, cf. Figure 4), concave (e.g. CH_4 + C_2H_6, cf. Figure 11), or S-shaped (e.g. R22 + CS_2, cf. Figure 12).

Analyzing the VLE envelopes further, it was found that 36 binaries show an azeotropic behavior,

thereof one exhibits a pressure minimum (R134 + R152a, cf. Figure 13). It should be noted that the location of the azeotropic point is a fully predictive property in the present work.

To limit the computational effort, for most mixtures only one isotherm was simulated and, of course, it can be argued that the binary interaction parameter ξ and thus the mixture model might only be valid for the temperature where it was adjusted. This would significantly restrict the applicability of the present mixture models. To counter this, a subset of 53 binaries was regarded for two to up to four different temperatures. A good example is CO + CH_4, cf. Figure 14, which is experimentally well explored. It can be seen there for four isotherms that the present mixture model is successful in a temperature range of 55 K in the entire composition range. Also larger temperature intervals were regarded, e.g. 100 K for R22 + CS_2, cf. Figure 12.

For 22 mixtures only isobaric experimental data is available, mostly at ambient pressure. Then, usually only these state points were simulated (e.g. R116 + R115, cf. Figure 15) and thus the predictive quality with respect to temperature and composition was assessed.

In case of 12 binaries experimental data is only available for a fixed bubble point composition (e.g. SF_6 + R13B1, cf. Figure 16). There, the predictions regarding temperature and pressure were evaluated.

In summary, for a total of 267 binaries useful experimental VLE data were found. Based on the criteria mentioned above we have rated the present modeling approach in 259 cases as successful, i.e. only for eight binaries, listed in Table 3, larger deviations were found. The quota of successful mixture models is hence 97 %.

It is worthwhile to examine the unsatisfactory cases as well, which are listed in Table 3. Different deviation types can be distinguished: For five binaries, the agreement between simulation and experiment is good on the bubble line, however, the predicted dew point composition is off by more than 0.05 mol/mol on average. This is the case for Ne + Xe (Figure 17), Ne + R13, Ne + R14, N_2 + R14 and Propylene + R30. It should be noted that three of those mixtures contain Neon. In case of C_2H_2 + Propylene, cf. Figure 18, a modest temperature extrapolation over 21 K failed, where significant deviations in pressure were found. The simulated binary data for

C_2H_2 + Propyne, cf. Figure 19, also shows deviations from experimental dew line data, however, the slope of the bubble line seems qualitatively wrong as well. Finally, a significant mismatch between experiment and simulation was found for R13 + R114. The experimental data for that system, taken from DDB, is from an anonymous author [240] and is the only available source. By inspection of Figure 20 it can be concluded the binary data from [240] seems doubtful as it does not correspond with the pure substance vapor pressure of the two components in the pure substance limit.

On the basis of such a large data set it is useful to examine the distribution of the optimized unlike interaction parameter ξ, cf. Figure 21. It can be seen that the modus of this distribution lies at $\xi = 1$ and that on average ξ is below unity. For 71 % of the binaries it is within 5 % of the Berthelot rule ($\xi = 1$). Six systems (Ne + Kr, Ne + CO_2, SF_6 + R32, R32 + R134a, R116 + R32, and R116 + R41) require binary parameters that significantly differ from unity, i.e $\xi < 0.8$ or $\xi > 1.1$. Among them two again contain Ne, which indicates together with the three unsatisfactory cases that the Lennard-Jones potential does not well represent the intermolecular interactions of Ne. Three of the remaining four binaries contain R32, which was modeled by the Stockmayer potential. It might be argued that the large deviation from unity is caused by this oversimplification of the molecular structure of R32.

For 263 systems, the results of the Peng-Robinson EOS with adjusted binary parameter k_{ij} are also shown. Due to the fact that this model is a reliable correlation tool, making it a workhorse in process engineering, it performs well in most cases too. Beside the fact that it sometimes overshoots in the critical region, which is a well known fact, only for few mixtures significant deviations were found. Examples are Ar + Propylene, CO_2 + CS_2 and R23 + CS_2 (all presented in the supplementary material) as well as R14+R152a (Figure 6), Xe+R40 (Figure 7), C_2H_2+Propylene (Figure 18) and R13+R114 (Figure 20).

7 CONCLUSION

It was shown that molecular modeling, and simulation as the most versatile method at that level, is a reliable and robust approach to VLE of mixtures. To verify this issue, a large scale simulation effort was made to cover 267 binary mixtures in a combinatorial way. The employed molecular models in many cases oversimplify the molecular features of the substance that they represent. They were, however, adjusted to pure substance VLE data in a quantitatively sound way. Unexpectedly, it was found that the molecular models are almost always able to compensate such oversimplifications and nonetheless adequately cover the effects of mixing.

To optimally represent the phase behavior of all regarded binary mixtures, the unlike dispersive energy parameter was adjusted to a single experimental vapor pressure of each mixture. It was found that the Berthelot rule is a good choice. In 71 % of all binaries, unlike dispersion was modified by 5 % or less. On average, unlike dispersion should by slightly weaker than the Berthelot rule suggests.

Following that procedure, a large number of 259 molecular mixture models was presented that accurately cover the diverse fluid phase behavior of binary systems. Compared to the Peng-Robinson EOS, molecular modeling and simulation are superior, particularly in the critical region. Due to the comparably weak nature of three body interactions, reliable VLE predictions for ternary and polynary mixtures can be expected.

Due to their numerical efficiency and accuracy, the presented molecular mixture models are also well suited to be used in simulations on a larger scale to investigate processes like evaporation, adsorption, flow etc.

ACKNOWLEDGEMENTS

We gratefully acknowledge Deutsche Forschungsgemeinschaft for funding this project. The simulations were performed at the Höchstleistungsrechenzentrum Stuttgart and at the Steinbuch Centre for Computing Karlsruhe.

APPENDIX, SIMULATION DETAILS

The technical simulation details of the present work are similar to those published in [33]. A center-center cut-off radius of 17.5 Å was used for the explicit evaluation of the intermolecular interactions. The Lennard-Jones tail corrections for internal energy, pressure, and chemical potential were calculated employing angle averaging as proposed by Lustig [260]. Long-range corrections for the dipolar part of the potential model were calculated with the reaction field method [261,262]. The quadrupolar interaction needs no long range correction as it disappears by orientational averaging. The same holds for the mixed polar interaction between dipoles and quadrupoles, cf. Weingerl et al. [263].

Vapor-liquid equilibria were obtained with the Grand Equilibrium method [264]. Depending on thermodynamic conditions, three different levels of computational effort were employed:

(A) In simple cases (e.g. Ar + R22, Kr + Propylene and R116 + R134a) VLE can be obtained with small statistical uncertainties sampling $N = 500$ molecules for the liquid phase and about 200 molecules for the vapor phase. Liquid simulation runs were carried out using molecular dynamics with 100 000 time steps, vapor simulation runs were performed using the Monte Carlo technique with 100 000 cycles. Within one cycle, N attempts to translate or rotate, and two attempts to insert or delete molecules were performed. The chemical potentials were calculated by Widom's insertion technique [257] using 2000 test molecules each time step.

(B) In intermediate cases (e.g. R14 + R13, R116 + CO_2 and SF_6 + R13B1) where experimental data is present only for dense liquid phases, 864 molecules were used for liquid simulations and about 600 molecules for vapor simulations. Liquid runs were carried out using molecular dynamics with 300 000 time steps, vapor runs were performed by Monte Carlo with 200 000 cycles. The number of test molecules was 3456 every time step.

(C) In difficult cases (e.g. R14 + R10, R32 + R143a and R1120 + R1110) where experimental data is present only for highly dense strongly polar liquid phases where the vapor pressure is usually very low, the more elaborate gradual insertion scheme had to be employed to obtain the chemical potentials.

The gradual insertion method is an expanded ensemble method [265] based on the Monte Carlo technique. The version as proposed by Nezbeda and Kolafa [266], extended to the NpT ensemble [267], was used in case *(C)*. In comparison to Widom's insertion technique, where real molecules are inserted into the fluid, gradual insertion introduces one fluctuating molecule that undergoes changes in a predefined set of discrete states of coupling with all other real molecules of the fluid. Preferential sampling is done in the vicinity of the fluctuating molecule. This concept leads to considerably improved accuracy of the residual chemical potential. Gradual insertion simulations were performed with $N = 864$ molecules in the liquid phase. Starting from a face-centered cubic lattice arrangement, every simulation run was given 5000 Monte Carlo cycles to equilibrate. Data production was performed over 100 000 Monte Carlo cycles. One Monte Carlo cycle is defined here as N trial translations, $(2/3)\,N$ trial rotations, and one trial volume change. Further simulation parameters for runs with the gradual insertion method were taken from Vrabec et al. [267].

LIST OF SYMBOLS

Latin Letters

a	component index
a	parameter of Peng-Robinson equation of state
b	component index
b	parameter of Peng-Robinson equation of state
c	short-cut notation for cosinus
i	molecule index
j	molecule index
k_B	Boltzmann's constant, $k_B = 1.38066 \cdot 10^{23}$ J/K
k_{ij}	binary parameter of the Peng-Robinson equation of state
L	elongation
p	pressure
P	polarity representing a point dipole or a point quadrupole
Q	quadrupolar momentum
R	ideal gas constant
s	short-cut notation for sinus
r	distance
T	temperature
u	pair potential
v	volume
x	mole fraction in liquid phase
y	mole fraction in vapor phase

Greek Letters

γ	precession angle between the orientation vectors of two molecules
ϵ	Lennard-Jones energy parameter
μ	dipolar momentum
ξ	binary interaction parameter

θ	dihedral angle between the orientation vectors of two molecules
σ	Lennard-Jones size parameter
ϕ	azimuthal angle between the orientation vectors of two molecules
ω	acentric factor

Subscripts

a	count variable for molecule sites
a	constant
A	related to component A
b	count variable for molecule sites
b	constant
B	related to component B
c	critical value
D	dipole
i	related to component i
ij	related to components i and j
j	related to component j
m	mixture
Q	quadrupole

Superscripts

exp	experimental data
sim	simulation data

Abbreviations

1CLJ	one-center Lennard-Jones
1CLJD	one-center Lennard-Jones plus point dipole

2CLJ	two-center Lennard-Jones
2CLJD	two-center Lennard-Jones plus point dipole
2CLJQ	two-center Lennard-Jones plus point quadrupole
DDB	Dortmunder Datenbank
EOS	equation of state
VLE	vapor-liquid equilibria

Vector properties

$\boldsymbol{r}_{ij}$	center-center distance vector between two molecules i and j
$\boldsymbol{\mu}$	dipole vector
$\boldsymbol{\omega}$	orientation vector of a molecule

References

[1] J. Vrabec, J. Stoll, H. Hasse, J. Phys. Chem. B 105 (2001) 12126-12133.

[2] J. Stoll, J. Vrabec, H. Hasse, J. Chem. Phys. 119 (2003) 11396-11407.

[3] W.B. Streett, D.J. Tildesley, Proc. Roy. Soc. Lond. A 355 (1977) 239-266.

[4] J.J. Potoff, J.I. Siepmann, AIChE J. 47 (2001) 1676-1682.

[5] J.J. de Pablo, M. Bonnin, J.M. Prausnitz, Fluid Phase Equilib. 73 (1992) 187-210.

[6] G.T. Gao, W. Wang, X.C. Zeng, Fluid Phase Equilib. 158-160 (1999) 69-78.

[7] G. Kronome, I. Szalai, M. Wendland, J. Fischer, J. Mol. Liq. 85 (2000) 237-247.

[8] S.K. Nath, F.A. Escobedo, J.J. de Pablo, I. Patramai, Ind. Eng. Chem. Res. 37 (1998) 3195-3202.

[9] S.T. Cui, H.D. Cochran, P.T. Cummings, J. Phys. Chem. B 103 (1999) 4485-4491.

[10] J.J. Potoff, J.R. Errington, A.Z. Panagiotopoulos, Mol. Phys. 97 (1999) 1073-1083.

[11] J. Delhommelle, P. Millié, Mol. Phys. 99 (2001) 619-625.

[12] A. Liu, T.L. Beck, J. Phys. Chem. B 102 (1998) 7627-7631.

[13] J. Vrabec, J. Fischer, Int. J. Thermophys. 17 (1996) 889-908.

[14] J. Vrabec, J. Fischer, AIChE J. 43 (1997) 212-217.

[15] Y. Boutard, Ph. Ungerer, J.M. Teuler, M.G. Ahunbay, S.F. Sabater, J. Pérez-Pellitero, A.D. Mackie, E. Bourasseau, Fluid Phase Equilib. 236 (2005) 25-41.

[16] M. Krishnamurthy, S. Murad, J.D. Olson, Mol. Sim. 32 (2006) 11-16.

[17] J.K. Shah, E.J. Maginn, J. Phys. Chem. B 109 (2005) 10395-10405.

[18] C. Grimm, A. Kandratsenka, P. Wagener, J. Zerbs, J. Schroeder, J. Phys. Chem. A 110 (2006) 3320-3329.

[19] E.A. Müller, Environ. Sci. Technol. 39 (2005) 8736-8741.

[20] S. Curbelo, E.A. Müller, Adsorpt. Sci. Technol. 23 (2005) 855-865.

[21] W. Jia, S. Murad, J. Chem. Phys. 120 (2004) 4877-4885.

[22] W. Jia, S. Murad, J. Chem. Phys. 122 (2005) 234708:1-11.

[23] A.A. Chialvo, J. Horita, J. Chem. Phys. 125 (2006) 034510:1-11.

[24] C. Schumacher, J. Gonzalez, M. Pérez-Mendoza, P.A. Wright, N.A. Seaton, Ind. Eng. Chem. Res. 45 (2006) 5586-5597.

[25] J. Carrero-Mantilla, M. Llano-Restrepo, Mol. Sim. 29 (2003) 549-554.

[26] J. Carrero-Mantilla, M. Llano-Restrepo, Fluid Phase Equilib. 242 (2006) 189-203.

[27] M. Lísal, M. Bendová, W.R. Smith, Fluid Phase Equilib. 235 (2005) 50-57.

[28] W.R. Smith, M. Lísal, Phys. Rev. E 66 (2002) 011104-011106.

[29] T. Schnabel, J. Vrabec, H. Hasse, Fluid Phase Equilib. 233 (2005) 134-143 and 239 (2006) 125-126.

[30] T. Schnabel,A. Srivastava, J. Vrabec, H. Hasse, J. Phys. Chem. B111 (2007) 9871-9878.

[31] A.J. Haslam, A. Galindo, G. Jackson, Fluid Phase Equilib. 266 (2008) 105-128.

[32] T. Schnabel, J. Vrabec, H. Hasse, J. Mol. Liq. 135 (2007) 170-178.

[33] J. Stoll, J. Vrabec, H. Hasse, AIChE J. 49 (2003) 2187-2198.

[34] J. Vrabec, J. Stoll, H. Hasse, Mol. Sim. 31 (2005) 215-221.

[35] J. Stoll, Molecular Models for the Prediction of Thermalphysical Properties of Pure Fluids and Mixtures, Fortschritt-Berichte VDI, Reihe 3, Vol. 836, VDI-Verlag, Düsseldorf, 2005.

[36] A.L. Galbraith, C.K. Hall, Fluid Phase Equilib. 241 (2006) 175-185.

[37] Dortmunder Datenbank, Mixture Properties, Version 1.3.0.211 (2004).

[38] M.J. Hiza, A.G. Duncan, Adv. Cryog. Eng. 15 (1969) 42-45.

[39] H. Destaillats, R. Fernández Prini, J. Chem. Thermodyn. 29 (1997) 1209-1221.

[40] R.B. Fang, S.H. Zhang, W.H. Zhang, Chem. J. Chin. Univ. (Changchun) 18 (1997) 869-872.

[41] J.M. Prausnitz, P.R. Benson, AIChE J. 5 (1959) 161-164.

[42] N.V. Kuskova, V.F. Kukarin, V.G. Martynets, E.V. Matizen, J. Chem. Thermodyn. 23 (1991) 523-530.

[43] I.V. Volobuev, V.I. Los, L.V. Los, M.G. Khmelnyuk, Kholod. Tekh. Tekhnol. 39 (1984) 65-67.

[44] H. Hiraoka, J.H. Hildebrand,
J. Phys. Chem. 68 (1964) 213-218.

[45] Y. Kobatake, J.H. Hildebrand,
J. Phys. Chem. 65 (1961) 331-334.

[46] O.V. Efstigneev, M.B. Santimova, S.G. Dunaev, S.B. Levanova, Khim. Prom. 6 (1985) 342-343.

[47] L.A. Makarevich, E.S. Sokolova,
Termodin. Termokhim. Konstanty (1970) 120-124.

[48] H. Jaster, P.G. Kosky, J. Chem. Eng. Data 21 (1976) 66-71.

[49] E. Wilhelm, R. Battino, J. Chem. Thermodyn. 3 (1971) 379-392.

[50] W.B. Streett, J. Chem. Phys. 46 (1967) 3282-3286.

[51] N.J. Trappeniers, J.A. Schouten, Physica 73 (1974) 546-555.

[52] R.J. Burch, J. Chem. Eng. Data 9 (1964) 19-23.

[53] W.B. Streett, C.H. Jones, Adv. Cryog. Eng. 11 (1966) 356-366.

[54] V. Sasinovskii, Trudy Moskovskogo Energeticheskogo Instituta 364 (1979) 13-18.

[55] H. Schmidt, Z. Phys. Chem. Neue Folge 24 (1960) 265-274.

[56] L.V. Shatskaya, N.A. Zhirnova, Russ. J. Phys. Chem. 50 (1976) 515.

[57] A.M. Clark, F. Din, J. Robb, Proc. Roy. Soc. Lond. A 221 (1954) 517-534.

[58] G.I. Kaminishi, Y. Arai, S. Saito, S. Maeda, J. Chem. Eng. Jpn. 1 (1968) 109-116.

[59] I.M. Elshayal, B.C.Y. Lu, Cryogenics 11 (1971) 285-289.

[60] N.A. Orobinskii, Yu.P. Blagoi, E.L. Semyannikova, Ukr. Fiz. Zh. (Russ. Ed.) 13 (1968) 263-268.

[61] E.B. Graham, K.E. Weale, Prog. Int. Res. Therm. Trans. Prop. (1962) 153-158.

[62] V.A. Baginskii, N.D. Zakharov, N.I. Lapardin, Sb. Issled. Teplofiz. Svoistva Raboch. Veshch. Prots. Teploobm. Kholod. Tekh. 9 (1989) 9-15.

[63] J. Nohka, E. Sarashina, Y. Arai, S. Saito, J. Chem. Eng. Jpn. 6 (1973) 10-17.

[64] J.C.G. Calado, E. Chang, W.B. Streett, Physica A 117 (1983) 127-138.

[65] J.C.G. Calado, M. Nunes Da Ponte, V.A.M. Soares, L.A.K. Staveley, J. Chem. Thermodyn.10 (1978) 35-44.

[66] C.D. Holcomb, J.A. Zollweg, Fluid Phase Equilib. 75 (1992) 213-224.

[67] M. Nunes Da Ponte, D. Chokappa, J.C.G. Calado, P. Clancy, W.B. Streett, J. Phys. Chem. 89 (1985) 2746-2751.

[68] J.C.G. Calado, E.J.S. Gomes de Azevedo, V.A.M. Soares, K. Lucas, K.P. Shukla, Fluid Phase Equilib. 16 (1984) 171-183.

[69] I.M.A. Fonsecax, L.Q. Lobo, Fluid Phase Equilib. 113 (1995) 127-138.

[70] S.C. Aldersley, L.Q. Lobo, L.A.K. Staveley, J. Chem. Thermodyn. 11 (1979) 597-604.

[71] J.C.G. Calado, L.A.K. Staveley, Trans. Faraday Soc. 67 (1971) 1261-1269.

[72] J. Davalos, W.R. Anderson, R.E. Phelps, A.J. Kidnay, J. Chem. Eng. Data 21 (1976) 81-84.

[73] R.C. Miller, A.J. Kidnay, M.J. Hiza, J. Chem. Thermodyn. 9 (1977) 167-178.

[74] I. Wichterle, R. Kobayashi, J. Chem. Eng. Data 17 (1972) 9-12.

[75] F. Steckel, Swensk. Kem. Tidskr. 57 (1945) 209-216.

[76] M. Yorizane, S. Yoshimura, H. Masuoka, Y. Miyano, Y. Kakimoto , J. Chem. Eng. Data 30 (1985) 174-176.

[77] M. Simon, C.M. Knobler, J. Chem. Thermodyn. 3 (1971) 657-662.

[78] K.L. Lewis, L.A.K. Staveley, J. Chem. Thermodyn. 7 (1975) 855-864.

[79] S.G.J. Mastera, Dampf-Flüssig-Gleichgewichtsdaten der Systeme Ar-N2, Kr-Ar, Kr-N2 und Xe-Kr sowie Löslichkeitsgrenzen des festen Xenons und des festen Kryptons in flüssigen Luftkomponenten, Thesis, Technical University Aachen, 1976.

[80] A.J. Kidnay, R.C. Miller, W.R. Parrish, M.J. Hiza, Cryogenics 15 (1975) 531-540.

[81] B.F. Dodge, Chem. Metall. Eng. 10 (1927) 622.

[82] F.B. Sprow, J.M. Prausnitz, AIChE J. 12 (1966) 780-784.

[83] F.A. Somait, A.J. Kidnay, J. Chem. Eng. Data 23 (1978) 301-305.

[84] L. Grausø, A. Fredenslund, J. Mollerup, Fluid Phase Equilib. 1 (1977) 13-26.

[85] V.Ya. Maslennikova, N.P. Goryunova, D.S. Tsiklis, Russ. J. Phys. Chem. 41 (1967) 735-737.

[86] J.S. Lim, J.-D. Kim, J. Chem. Eng. Data 42 (1997) 112-115.

[87] A. Laitinen, M. Jäntti, J. Chem. Eng. Data 41 (1996) 1418-1420.

[88] J. Nohka, E. Sarashina, Y. Arai, S. Saito, J. Chem. Eng. Jpn. 6 (1973) 10-17.

[89] J. Kulka, G.M. Schneider, Fluid Phase Equilib. 63 (1991) 111-128.

[90] W.G. Fastowskij, Ju.W. Petrowskij, Russ. J. Phys. Chem. 30 (1956) 589-592.

[91] A. Fredenslund, G.A. Sather, J. Chem. Eng. Data 15 (1970) 17-22.

[92] E.G. Komarova, G.F. Sosoreva, T.V. Petrova, E.D. Finyakina, Sb. Issled. Appar. Tekhnol. Oforml. Avtomatiz. Khim. Protses. (Leningrad) (1983) 60-61.

[93] W.M. Spicer, J. Kruger, J. Am. Chem. Soc. 72 (1950) 1855-1856.

[94] W.M. Spicer, L.H. Meyer, J. Am. Chem. Soc. 73 (1951) 934-938.

[95] A.G.Duncan, L.A.K. Staveley, Trans. Faraday Soc. 62 (1966) 548-552.

[96] L.J. Christiansen, A. Fredenslund, J. Mollerup, Cryogenics 13 (1973) 405-413.

[97] L.J. Christiansen, A. Fredenslund, N. Gardner, Adv. Cryog. Eng. 19 (1974) 309-319.

[98] D.B. Trust, F. Kurata, AIChE J. 17 (1971) 415-419.

[99] A. Jónasson, O. Persson, P. Rasmussen, D.-U. Astrath, J. Chem. Eng. Data 45 (2000) 642-646.

[100] E. Kimura, S. Fukushima, J. Jpn. Inst. Metals 43 (1979) 223-229.

[101] W.-E Reiff, H. Roth, K. Lucas, Fluid Phase Equilib. 73 (1992) 323-338.

[102] J.P. Kuenen, Philos. Mag. 44 (1897) 174-199.

[103] A. Fredenslund, J. Mollerup, J. Chem. Soc. Faraday Trans. I 70 (1974) 1653-1660.

[104] K. Nagahama, H. Konishi, D. Hashino, M. Hirata, J. Chem. Eng. Jpn. 7 (1974) 323-328.

[105] G.K. Lavrenchenko, V.A. Nikolovsky, O.V. Baklai, Kholod. Tekh. 6 (1983) 41-45.

[106] A.M. Scurto, C.M. Lubbers, G. Xu, J.F. Brennecke, Fluid Phase Equilib. 190 (2001) 135-147.

[107] H. Roth, P. Peters-Gerth, K. Lucas, Fluid Phase Equilib. 73 (1992) 147-166.

[108] A.V. Gonzalez, R. Tufeu, P. Subra, J. Chem. Eng. Data 47 (2002) 492-495.

[109] A. Diefenbacher, M. Türk, J. Chem. Thermodyn. 34 (2002) 1361-1375.

[110] C.M.A. Hartman, Metingen omtrent de dwarsploi van het psi-vlak van van der Waals bij mengsels van chloormethyl en koolzuur, Thesis, 1899.

[111] C.D. Holcomb, J.W. Magee, J.L. Scott, S.L. Outcalt, W.M. Haynes, Proceedings of the 15th Symposium on Energy Engineering Sciences, National Technical Information Service Report (1997) A1-A87.

[112] G. Di Nicola, M. Pacetti, F. Polonara, R. Stryjek, J. Chem. Eng. Data 47 (2002) 1145-1153.

[113] G. Silva-Oliver, L.A. Galicia-Luna, Fluid Phase Equilib. 199 (2002) 213-222.

[114] S. Sengupta, S. Gupta, K.M. Dooley, F.C. Knopf, J. Supercrit. Fluids 7 (1994) 201-209.

[115] S.D. Fink, H.C. Hershey, Ind. Eng. Chem. Res. 29 (1990) 295-306.

[116] B. Bian, Measurement of Phase Equilibria in the Critical Region and Study of Equation of State, Thesis, 1992.

[117] K. Hlavaty, Collect. Czech. Chem. Commun. 35 (1970) 2878-2884.

[118] G.C. Schmidt, Z. Phys. Chem. (Leipzig) 121 (1926) 221-253.

[119] K. Prochazka, T. Boublik, Collect. Czech. Chem. Commun. 40 (1975) 497-506.

[120] G.A. Gaziev, Ya.D. Zelvenskii, V.A. Shalygin, Zh. Prikl. Khim. (Leningrad) 31 (1958) 1220.

[121] E.A. Moelwyn-Hughes, R.W. Missen, Trans. Faraday Soc. 53 (1957) 607-615.

[122] N.D. Litvinov, Zh. Fiz. Khim. 14 (1940) 782-788.

[123] S.M. Khodeeva, R.P. Kukina, Russ. J. Phys. Chem. 42 (1968) 2444-2449.

[124] J.S. Lim, Y.-W. Lee, J.-D. Kim, Y.Y. Lee, J. Chem. Eng. Data 41 (1996) 1168-1170.

[125] M. Nunes Da Ponte, D. Chokappa, J.C.G. Calado, J. Zollweg, W.B. Streett, J. Phys. Chem. 90 (1986) 1147-1152.

[126] J. Mollerup, J. Chem. Soc. Faraday. Trans. I 71 (1975) 2351-2360.

[127] R.J. Hogan, W.T. Nelson, G.H. Hanson, M.R. Cines, Ind. Eng. Chem. 47 (1955) 2210-2215.

[128] F.F. Karakhorin, Foreign Petr. Techn. 9 (1941) 411-422.

[129] G.G. Haselden, F.A. Holland, M.B. King, R.F. Strickland-Constable, Proc. Roy. Soc. Lond. A 240 (1957) 1-28.

[130] G.D. Efremova, G.G. Leonteva, Tr. Gosudarst. Nauch. Issled. I Proekt. Inst. Azot. Prom. 3 (1954) 5-12.

[131] J. Shim, J.P. Kohn, J. Chem. Eng. Data 9 (1964) 1-2.

[132] X. Yang, Beitrag zur experimentellen Untersuchung und Berechnung von Dampf-Flüssigkeits-Phasengleichgewichten, Thesis, 1991.

[133] E.S. Lebedeva, S.M. Khodeeva, Tr. Gosudarst. Nauch. Issled. I Proekt. Inst. Azot. Prom. 13 (1963) 79-90.

[134] E.S. Lebedeva, A.S. Kashirina, V.P. Grokholskaya, Tr. Gosudarst. Nauch. Issled. I Proekt. Inst. Azot. Prom. 12 (1971) 92-100.

[135] V.S. Zernov, V.B. Kogan, S.G. Lyubetski, V.M. Kobyakov, Viniti, Code no. 1479-78 dep. Leningrad (1978) 1-11.

[136] J.L. McCurdy, D.L. Katz, Ind. Eng. Chem. 36 (1944) 674-680.

[137] B.H. Sage, W.N. Lacey, Some Properties of the Lighter Hydrocarbons, Hydrogen Sulfide, and Carbon Dioxide, American Petroleum Institute, New York, 1955.

[138] R. Takahashi, K. Nagahama, Thesis, Tokyo Metropolitan Univ., 1989.

[139] T. Hakuta, K. Nagahama, M. Hirata, Bull. Jap. Petrol. Inst. 11 (1969) 10-15.

[140] K.-E. Doering, H. Preuss, FIZ Report 6191 (1967).

[141] B.I. Konobeev, V.V. Lyapin, Khim. Prom. 43 (1967) 114-116.

[142] M. Kleiber, Fluid Phase Equilib. 92 (1994) 149-194.

[143] K. Ohgaki, M. Kageyama, T. Katayama, J. Chem. Eng. Jpn. 23 (1990) 763-764.

[144] O.Y. Guzechak, V.N. Sarancha, I.M. Romanyuk, O.M. Yavorskaya, G.P. Churik, Russ. J. Appl. Chem. 57 (1985) 1662-1665.

[145] A. Kovac, J. Dykyj, Petrochemia 11 (1971) 91-93.

[146] A. Bayer, Untersuchungen zum Blasensieden von binären Stoffgemischen in einem grossen Druckbereich, Thesis, TH Karlsruhe, 1988.

[147] F.N. Kissell, F.S. Manning, J. Chem. Eng. Data 7 (1962) 205-206.

[148] P. Perez, J. Valero, M. Gracia, J. Chem. Eng. Data 39 (1994) 789-792.

[149] V. Fried, D.R. Franceschetti, A.S. Gallanter, J. Phys. Chem. 73 (1969) 1476-1479.

[150] R. Xie, Y. Liu, P. Yu, C. He, H. Qin, B. Dong, H. Shiyou, Petrochem. Tech. 17 (1988) 155-161.

[151] N.D. Loi, Luft- und Kältetech. 19 (1983) 37-40.

[152] G. Hackstein, Ein Beitrag zur experimentellen Bestimmung thermodynamischer Stoffwerte an halogenierten Kohlenwasserstoffen, deren Gemische sowie deren Gemische mit Kältemaschinenöl, Thesis, 1975.

[153] H. Kubota, T. Ikawa, Y. Tanaka, T. Makita, K. Miyoshi, J. Chem. Eng. Jpn. 23 (1990) 155-159.

[154] J. Lee, J. Lee, H. Kim, J. Chem. Eng. Data 41 (1996) 745-747.

[155] K. Wang, Y. Shi, H. Liu, J. Fu, Y. Hu, J. East China Inst. Chem. Techn. 19 (1993) 653-659.

[156] A.A. Fedorova, L.V. Kruglova, L.P. Danishevskii, Sb. Teor. Osn. Khim. Tekhnol. (Leningrad) (1980) 14-18.

[157] M. Kriebel, H.J. Löffler, Kältetechnik 18 (1966) 34-36.

[158] J. Mollerup, A. Fredenslund, J. Chem. Eng. Data 21 (1976) 299-301.

[159] M. Kleiber, Thesis, 1994.

[160] M. Meskel-Lesavre, D. Richon, H. Renon, J. Chem. Eng. Data 27 (1982) 160-165.

[161] Y. Takaishi, K. Oguchi, Int. J. Thermophys. 7 (1986) 721-730.

[162] M. Hongo, M. Kusunoki, H. Matsuyama, T. Takagi, K. Mishima, Y. Arai, J. Chem. Eng. Data 35 (1990) 414-417.

[163] K. Mishima, M. Hongo, T. Takagi, Y. Arai, J. Chem. Eng. Data 38 (1993) 49-52.

[164] L.V. Utrobina, E.G. Komarova, T.V. Petrova, Sb. Teor. Osn. Khim. Tekhnol. (Leningrad) (1980) 37-41.

[165] N.A. Orobinskii, Y.P. Blagoi, E.L. Semyannikova, L.N. Vyunnik, Fiz. Khim. Rastvorov (1972) 233-238.

[166] V.V. Altunin, E.V. Skopintsev, M.O. Zhekshenbaev, Tr. Mosk. Energ. Inst. 206 (1989) 59-64.

[167] J. Storm, Anwendung der UNIFAC-Methode zur Vorausberechnung der Verdampfungsgleichgewichte von Kaeltemittelgemischen, Thesis, TU Braunschweig, 1989.

[168] W.L. Kubic, F.P. Stein, Fluid Phase Equilib. 5 (1981) 289-304.

[169] A. Piacentini, F.P. Stein, Chem. Eng. Progr. Symp. Ser. 63 (1967) 28-36.

[170] I.M.A. Fonseca, G.G. Sardinha, L.Q. Lobo, J. Chem. Thermodyn. 30 (1998) 1271-1274.

[171] M.L. McGlashan, J.E. Prue, I.E.J. Sainsbury, Trans. Faraday Soc. 50 (1954) 1284-1292.

[172] P. Dakshinamurty, C.V. Rao, Vapor-Liquid Equilibria. Systems: Acetone - Tetrachloroethylene, Chloroform - Tetrachloroethylene, Metals Miner. Rev., 1955.

[173] Y.W. Kang, S.Y. Cho, I.W. Nah, J. Chem. Eng. Data 43 (1998) 611-613.

[174] N. Xu, J. Yao, Y. Wang, J. Shi, B.C.-Y. Lu, Fluid Phase Equilib. 69 (1991) 261-270.

[175] M. Meskel-Lesavre, D. Richon, H. Renon, Fluid Phase Equilib. 8 (1982) 37-53.

[176] H. Nishiumi, S. Kohmatsu, T. Yokoyama, A. Konda, Fluid Phase Equilib. 104 (1995) 131-143.

[177] Y. Feng, G. Wu, C. Li, J. Chen, J. Gu, Z. Wang, J. Chem. Ind. Eng. (China) 36 (1985) 93-99.

[178] A. Valtz, S. Laugier, D. Richon, Int. J. Refrig. 9 (1986) 282-289.

[179] J. Togo, K. Nagahama, Thesis, Tokyo Metropolitan Univ., 1972.

[180] G.V. Blinova, A.B. Kovaleva, L.P. Danyushevskii, Teor. Osn. Khim. Tekhnol. 6 (1980) 19-24.

[181] H. Nishiumi, M. Komatsu, T. Yokoyama, S. Kohmatsu, Fluid Phase Equilib. 83 (1993) 109-117.

[182] W. Cao, H. Yu, W. Wang, J. Chem. Ind. Eng. (China) 48 (1997) 136-142.

[183] E.I. Geller, V.F. Chaikovskii, A.V. Egorov, Kholod. Tekh. Tekhnol. 15 (1972) 70-75.

[184] F.P. Stein, P.C. Proust, J. Chem. Eng. Data 16 (1971) 389-393.

[185] A. Valtz, S. Laugier, D. Richon, J. Chem. Eng. Data 32 (1987) 397-400.

[186] S. Laugier, D. Richon, H. Renon, Fluid Phase Equilib. 93 (1994) 297-316.

[187] Y.V. Semenyuk, V.P. Zheleznyi, Y.M. Aftenev, Kholod. Tekh. Tekhnol. 51 (1990) 79-81.

[188] J.S. Lim, K.H. Park, B.G. Lee, J.-D. Kim, J. Chem. Eng. Data 46 (2001) 1580-1583.

[189] J.S. Lim, K.H. Park, B.G. Lee, J. Chem. Eng. Data 47 (2002) 582-586.

[190] G. Rulewicz, H. Schuberth, E. Leibnitz, J. Prakt. Chem. 37 (1968) 122-136.

[191] A. Apelblat, J. Wisniak, A. Tamir, J. Chem. Eng. Data 26 (1981) 144-147.

[192] R.L. Rowley, R.H. Powell, Dippr Data Series 2 (1994) 116-142.

[193] Yu.V. Golubkov, N.V. Kotenkova, T.G. Repneva, V.E. Markovich, V.P. Papsueva, Zh. Prikl. Khim. (Leningrad) 53 (1980) 1666-1667.

[194] M. Artal, J.M. Embid, S. Otin, I. Velasco, Fluid Phase Equilib. 154 (1999) 223-239.

[195] Y.W. Kang, Y.Y. Lee, J. Chem. Eng. Data 41 (1996) 303-305.

[196] J.S. Lim, Y.-W. Lee, Y.Y. Lee, J. Chem. Eng. Data 42 (1997) 566-569.

[197] W.H. Mears, J.V. Sinka, P.F. Malbrunot, P.A. Meunier, A.G. Dedit, G.M. Scatena, J. Chem. Eng. Data 13 (1968) 344-347.

[198] J. Lee, J. Lee, H. Kim, Fluid Phase Equilib. 150 (1998) 297-302.

[199] M.Y. Jung, C.N. Kim, Y.M. Park, J.S. Yoo, J. Chem. Eng. Data 46 (2001) 750-753.

[200] J.V. Widiatmo, T. Fujimine, H. Sato, K. Watanabe, J. Chem. Eng. Data 42 (1997) 270-277.

[201] C.N. Kim, Y.M. Park, J. Chem. Eng. Data 45 (2000) 34-37.

[202] B.G. Lee, J.Y. Park, J.S. Lim, S.Y. Cho, K.Y. Park, J. Chem. Eng. Data 44 (1999) 190-192.

[203] J.S. Lim, Y.-W. Lee, Y.Y. Lee, J. Chem. Eng. Data 42 (1997) 566-569.

[204] A.M.P. Serna, I.M.A. Fonseca, L.Q. Lobo, J. Chem. Thermodyn. 35 (2003) 1051-1057.

[205] L. Hnědkovský, V. Dohnal, I. Cibulka, J. Chem. Thermodyn. 19 (1987) 1145-1154.

[206] H. Hinrichsen, Kältetechnik Klimatisierung 21 (1969) 290-293.

[207] Y.Y. Lee, Y.W. Kang, W.H. Hong, H. Lee, J. Chem. Eng. Data 33 (1988) 155-157.

[208] N. Yada, M. Uematsu, K. Watanabe, Int. J. Thermophys. 10 (1989) 639-647.

[209] M.B. Shiflett, S.I. Sandler, Fluid Phase Equilib. 147 (1998) 145-162.

[210] A.D. Leu, C.J. Chen, D.B. Robinson, AIChE Symp. Ser. 85 (1989) 11-16.

[211] M.B. Shiflett, A. Yokozeki, B. Minor, Azeotropic Compositions of Perfluoroethane, and Trifluoromethane, or Oxide, or Nitrous Oxide, or Carbon Dioxide, or Fluoromethane, Patent WO/1994/001512. 1994.

[212] N.G. Zenkevich, E.G. Komarova, T.V. Petrova, Osnovy Khim. Tekhnol. L (1980) 3-6.

[213] B.A. Mahler, M.J. Nappa, M.A. Casey, R.N. Miller, Distillation Processes for Removing CFC-115 and Hydrofluoric Acid from HFC-125, Patent WO/1997/003936, 1997.

[214] M. Nagel, K. Bier, Int. J. Refrig. 18 (1995) 534-543.

[215] M. Nagel, K. Bier, Int. J. Refrig. 19 (1996) 264-271.

[216] H. Nishiumi, H. Akita, S. Akiyama, Korean J. Chem. Eng. 14 (1997) 359-364.

[217] P.L. Bartlett, D.B. Bivens, B.S. Lunger, A. Yokozeki, Azeotropic and Azeotrope-Like Compositions of 1,1,2,2-Tetrafluoroethane, US-Patent 5968406, 1992.

[218] H. Kubota, Q. Zheng, X.-Y. Zheng, T. Makita, J. Chem. Eng. Jpn. 24 (1991) 659-661.

[219] X.Y. Zheng, H. Kubota, Q. Zheng, T. Makita, J. Chem. Eng. Data 35 (1990) 441-444.

[220] Y. Shi, K. Wang, H. Liu, Y. Hu, J. East China Univ. Sci. Technol. 21 (1995) 613-618.

[221] A. Kovac, J.M. Svoboda, I. Ondrus, Chemical Papers 39 (1985) 737-742.

[222] P. Rathbone, "Vapour Liquid Equilibrium Data on Binary Chlorinated Hydrocarbon Systems", Conf. Int. Thermodyn. Chim. (1975) 64-74.

[223] E.L. Meijer, N. Brouwer, J.C. Van Miltenburg, J. Chem. Thermodyn. 8 (1976) 703-708.

[224] L.A. Weber, A.M. Silva, Int. J. Thermophys. 17 (1996) 873-888.

[225] J.S. Lim, J.-Y. Park, B.-G. Lee, Y.-W. Lee, Fluid Phase Equilib. 193 (2002) 29-39.

[226] S.I. Kaplan, Z.D. Monakhova, Zh. Obshch. Khim. 7 (1937) 2499-2512.

[227] F. Gölles, O. Wolfbauer, F. Still, Monatsh. Chem. 106 (1975) 1437-1447.

[228] A.P. Kuznetsov, I.V. Volobuev, M.G. Khmelnyuk, Kholod. Tekh. Tekhnol. 30 (1980) 54-56.

[229] N. Yada, M. Uematsu, K. Watanabe, Trans. JAR 5 (1988) 107-115.

[230] B.G. Bian, N.P. Xu, J.H. Dong, Y.R. Wang, J. Shi, J. Eng. Thermophys. 14 (1993) 238-240.

[231] G. Guglielmo, Acad. Naz. Lincei, Cl. Sci. Fis. Mat. Natur., Rend 1 (1892) 242-249.

[232] Anonymous, Vapor-Liquid Equilibria of the System Difluoromethane (F32) - Tetrafluoroethylene (TFE), Confident. Comp. Res. Rep., 1978, cf. [34]

[233] M. Sagnes, V. Sanchez, J. Chem. Eng. Data 16 (1971) 351-354.

[234] J.L. Owens, C.J. Brady, J.R. Freeman, W.V. Wilding, G.M. Wilson, AIChE Symp. Ser. 83 (1987) 18-41.

[235] I.Ya. Azbel, A.A. Panfilov, A.V. Vdovets, N.M. Gavrilchuk, Khim. Prom. 44 (1968) 269-273.

[236] A. Deerenberg, J.A. Schouten, N.J. Trappeniers, Physica A 101 (1980) 459-476.

[237] N.D. Zakharov, V.G. Semenov, E.V. Domnina, Zh. Fiz. Khim. 56 (1982) 2575.

[238] V.F. Chaikovskii, N.D. Zakharov, A.K. Grezin, Yu.I. Matyash, Kholod. Tekh. Tekhnol. 22 (1976) 51-55.

[239] R.J. Burch, M.W. Leeds, Ind. Eng. Chem., Chem. Eng. Data Series 2 (1957) 3-7.

[240] Anonymous, Flüssigkeits-Dampf-Gleichgewicht des Systems Frigen 13 - Frigen 114, Confident. Comp. Res. Rep., 1970, cf. [34].

[241] U.K. Deiters, Fluid Phase Equilib. 132 (1997) 265-270.

[242] C.G. Gray, K.E. Gubbins, Theory of molecular fluids, Vol. 1, Fundamentals, Clarendon Press, Oxford, 1984.

[243] J. Stoll, J. Vrabec, H. Hasse, J. Fischer, Fluid Phase Equilib. 179 (2001) 339-362.

[244] J. Stoll, J. Vrabec, H. Hasse, Fluid Phase Equilib. 209 (2003) 29-53.

[245] J. Vrabec, G.K. Kedia, H. Hasse, Cryogenics 45 (2005) 253-258.

[246] J. Vrabec, A. Kumar, H. Hasse, Fluid Phase Equilib. 258 (2007) 34-40.

[247] G.A. Fernández, J. Vrabec, H. Hasse, Int. J. Thermophys. 25 (2004) 175-186.

[248] G.A. Fernández, J. Vrabec, H. Hasse, Fluid Phase Equilib. 221 (2004) 157-163.

[249] G.A. Fernández, J. Vrabec, H. Hasse, Int. J. Thermophys. 26 (2005) 1389-1407.

[250] G.A. Fernández, J. Vrabec, H. Hasse, Mol. Sim. 31 (2005) 787-793.

[251] G.A. Fernández, J. Vrabec, H. Hasse, Cryogenics 46 (2006) 711-717.

[252] M.P. Allen, D.J. Tildesley, Computer simulations of liquids, Clarendon Press, Oxford, 1987.

[253] J.M. Smith, H.C. Van Ness, M.M. Abbott, Introduction to chemical engineering thermodynamics, 5th Edition, McGraw-Hill, New York, 1996.

[254] Merseburger Datenbank.

[255] F.H. Case, J. Brennan, A. Chaka, K.D. Dobbs, D.G. Friend, D. Frurip, P.A. Gordon, J. Moore, R.D. Mountain, J. Olson, R.B. Ross, M. Schiller, V.K. Shen, Fluid Phase Equilib. 260 (2007) 153-163.

[256] H.C. Andersen, J. Chem. Phys. 72 (1980) 2384-2393.

[257] B. Widom, J. Phys. Chem. 39 (1963) 2808-2812.

[258] D.M. Heyes, Mol. Sim. 8 (1992) 227-238.

[259] H. Flyvbjerg, H.G. Petersen, J. Chem. Phys. 91 (1989) 461-466.

[260] R. Lustig, Mol. Phys. 65 (1988) 175-179.

[261] J.A. Barker, R.O. Watts, Mol. Phys. 26 (1973) 789-792.

[262] B. Saager, J. Fischer, M. Neumann, Mol. Sim. 6 (1991) 27-49.

[263] U. Weingerl, J. Fischer, Fluid Phase Equilib. 202 (2002) 49-66.

[264] J. Vrabec, H. Hasse, Mol. Phys. 100 (2002) 3375-3383.

[265] S.V. Shevkunov, A.A. Martinovski, P.N. Vorontsov-Velyaminov, High Temp. Phys. (USSR) 26 (1988) 246-254.

[266] I. Nezbeda, J. Kolafa, Mol. Sim. 5 (1991) 391-403.

[267] J. Vrabec, M. Kettler, H. Hasse, Chem. Phys. Lett. 356 (2002) 431-436.

Table 1

List of the 66 components included in the present work. The model parameters were taken from [1,2].

Fluid	CAS RN	Fluid	CAS RN
Non-polar, 1CLJ		R141b (CH_3–$CFCl_2$)	1717-00-6
Ne	7440-37-1	R142b (CH_3–CF_2Cl)	75-68-3
Ar	13965-95-2	R143a (CH_3–CF_3)	420-46-2
Kr	7439-90-9	R150a ($CHCl_2$–CH_3)	75-34-3
Xe	7440-63-3	R152a (CH_3–CHF_2)	75-37-6
CH_4	74-82-8	R160B1 (CH_2Br–CH_3)	74-96-4
Dipolar, 1CLJD		R1122 (CHCl=CF_2)	359-10-4
R30 (CH_2Cl_2)	75-09-2	R1140 (CHCl=CH_2)	75-01-4
R30B2 (CH_2Br_2)	74-95-3	**Quadrupolar, 2CLJQ**	
R32 (CH_2F_2)	75-10-5	N_2	7727-37-9
Dipolar, 2CLJD		O_2	7782-44-7
CO	630-08-0	Cl_2	7782-50-5
CH_3I	74-88-4	Br_2	7726-95-6
R11 ($CFCl_3$)	75-69-4	I_2	7553-56-2
R12 (CF_2Cl_2)	75-71-8	CO_2	124-38-9
R12B1 ($CBrClF_2$)	353-59-3	CS_2	75-15-0
R12B2 (CBr_2F_2)	75-61-6	C_2H_2	74-86-2
R13 (CF_3Cl)	75-72-9	C_2H_4	74-85-1
R13B1 ($CBrF_3$)	75-63-8	C_2H_6	74-84-0
R20 ($CHCl_3$)	67-66-3	Propadiene (CH_2=C=CH_2)	463-49-0
R21 ($CHFCl_2$)	75-43-4	Propyne (CH_3–C≡CH)	74-99-7
R22 (CHF_2Cl)	75-45-6	Propylene (CH_3–CH=CH_2)	115-07-1
R23 (CHF_3)	75-46-7	SF_6	2551-62-4
R30B1 (CH_2BrCl)	74-97-5	R10 (CCl_4)	56-23-5
R40 (CH_3Cl)	74-87-3	R14 (CF_4)	75-73-0
R41 (CH_3F)	593-53-3	R113 ($CFCl_2$–CF_2Cl)	76-13-1
R112a (CCl_3–CF_2Cl)	76-11-9	R114 (CF_2Cl–CF_2Cl)	76-14-2
R123 ($CHCl_2$–CF_3)	306-83-2	R114B2 ($CBrF_2$–$CBrF_2$)	124-73-2
R123B1 (CHClBr–CF_3)	151-67-7	R115 (CF_3–CF_2Cl)	76-15-3
R124 (CHFCl–CF_3)	2837-89-0	R116 (C_2F_6)	76-16-4
R125 (CHF_2–CF_3)	354-33-6	R134 (CHF_2–CHF_2)	359-35-3
R130a (CH_2Cl–CCl_3)	630-20-6	R150B2 (CH_2Br–CH_2Br)	106-93-4
R134a (CH_2F–CF_3)	811-97-2	R1110 (C_2Cl_4)	127-18-4
R140 ($CHCl_2$–CH_2Cl)	79-00-5	R1114 (C_2F_4)	116-14-3
R140a (CCl_3–CH_3)	71-55-6	R1120 (CHCl=CCl_2)	79-01-6

Table 2

Binary interaction parameter ξ, experimental bubble point used for the adjustment with reference, simulation results with adjusted ξ, and binary parameter of the Peng-Robinson EOS k_{ij}.

Mixture (1+2)	ξ	T	x_1	p^{exp}	p^{sim}	y_1^{exp}	y_1^{sim}	k_{ij}	Ref.
		K	mol/mol	MPa	MPa	mol/mol	mol/mol		
Ne + Ar	0.826	110.78	0.024	2.734	2.78 (7)	0.670	0.69 (1)	0.203	[50]
Ne + Kr	0.733	178.15	0.072	10.12	9.8 (2)	0.638	0.666(7)	0.035	[51]
Ne + N_2	0.928	82.70	0.089	3.04	3.02 (2)	0.906	0.904(3)	0.111	[52]
Ne + O_2	0.921	110.39	0.252	20.94	20.5 (3)	0.808	0.844(4)	0.139	[53]
Ne + CO_2	1.124	273.15	0.038	8.84	8.84 (1)	0.445	0.466(1)	0.100	[54]
Ar + Kr	0.989	138.15	0.176	0.772	0.766(7)	0.583	0.590(3)	0.010	[55]
Ar + CH_4	0.964	123.05	0.541	0.912	0.915(8)	0.848	0.839(3)	0.037	[56]
Ar + O_2	0.988	104.51	0.148	0.386	0.389(5)	0.190	0.178(4)	0.015	[57]
Ar + CO_2	0.999	288.15	0.099	8.754	8.48 (8)	–	0.243(4)	0.170	[58]
Ar + C_2H_6	0.978	115.50	0.505	0.68	0.65 (4)	–	0.995(1)	0.050	[59]
Ar + Propylene	1.019	150.00	0.328	4.374	4.3 (2)	–	0.910(8)	–	[60]
Ar + R10	0.964	348.15	0.292	27.86	26.0 (1)	–	0.980(8)	0.130	[61]
Ar + R14	1.024	203.68	0.179	3.65	3.67 (5)	0.431	0.436(5)	0.010	[62]
Ar + R22	0.989	323.15	0.227	10.13	10.1 (2)	0.596	0.60 (1)	0.104	[63]
Kr + Xe	0.989	200.64	0.463	2.07	2.09 (2)	0.787	0.805(2)	0.010	[64]
Kr + C_2H_4	1.020	115.77	0.492	0.048	0.050(4)	0.990	0.998(1)	0.050	[65]
Kr + C_2H_6	1.023	278.98	0.225	4.751	4.82 (5)	0.424	0.398(1)	0.033	[66]
Kr + Propylene	1.001	200.00	0.333	1.648	1.65 (4)	–	0.980(5)	0.050	[60]
Xe + C_2H_6	0.984	292.00	0.528	4.737	4.80 (5)	0.561	0.579(2)	0.010	[67]
Xe + R40	0.973	182.32	0.478	0.18	0.18 (2)	0.993	0.990(6)	0.074	[68]
Xe + R41	0.928	182.33	0.472	0.235	0.23 (2)	0.831	0.91 (4)	0.120	[69]
Xe + R116	1.010	173.11	0.552	0.153	0.154(3)	0.857	0.877(6)	0.120	[70]
CH_4 + Kr	0.998	174.55	0.455	2.268	2.284(1)	0.516	0.516(3)	0.005	[71]
CH_4 + CO_2	0.962	230.00	0.318	5.57	5.61 (4)	0.764	0.766(3)	0.084	[72]
CH_4 + C_2H_4	1.022	223.15	0.398	4.053	4.09 (4)	0.734	0.696(5)	0.034	[73]
CH_4 + C_2H_6	0.997	172.04	0.504	1.24	1.21 (1)	0.966	0.969(3)	0.001	[74]
CH_4 + Propylene	1.032	190.00	0.667	2.815	2.80 (2)	0.992	0.997(1)	0.010	[75]
CH_4 + R12	1.052	298.20	0.431	7.4	7.28 (7)	0.829	0.827(4)	0.030	[76]
CH_4 + R14	1.030	98.00	0.688	0.026	0.023(2)	0.982	0.998(1)	0.115	[77]

Table 2: continued.

CH_4 + R22	1.021	263.20	0.540	9.80	9.2 (2)	0.844	0.884(5)	0.055	[76]
N_2 + Ar	1.010	122.89	0.390	2.006	1.999(9)	0.495	0.501(2)	-0.015	[78]
N_2 + Kr	0.989	125.00	0.247	1.044	1.02 (3)	0.852	0.855(6)	0.008	[79]
N_2 + CH_4	0.958	140.00	0.519	3.080	3.07 (2)	0.777	0.785(2)	0.026	[80]
N_2 + O_2	1.007	105.00	0.500	0.743	0.734(9)	0.702	0.709(4)	0.012	[81]
N_2 + CO	1.007	83.82	0.445	0.167	0.174(1)	0.56	0.544(1)	0.028	[82]
N_2 + CO_2	1.041	270.00	0.132	9.290	9.2 (4)	0.417	0.43 (2)	0.017	[83]
N_2 + C_2H_4	0.926	200.00	0.181	6.033	6.9 (2)	0.829	0.849(6)	0.065	[84]
N_2 + C_2H_6	0.974	200.00	0.026	1.043	1.07 (1)	0.753	0.766(1)	0.052	[84]
N_2 + Propylene	0.959	290.00	0.203	11.138	10.5 (1)	0.751	0.766(6)	0.088	[84]
N_2 + R12	1.000	295.15	0.370	15.199	14.8 (4)	0.830	0.850(5)	0.002	[85]
N_2 + R12B1	0.942	313.20	0.106	7.0	6.85 (8)	0.882	0.884(2)	0.054	[86]
N_2 + R13	1.045	253.15	0.285	7.0	6.92 (4)	0.680	0.677(5)	0.060	[87]
N_2 + R13B1	1.022	313.20	0.200	7.4	7.5 (2)	0.385	0.371(9)	0.076	[86]
N_2 + R22	1.000	348.15	0.145	8.26	8.3 (1)	0.380	0.36 (1)	0.000	[88]
N_2 + R23	1.042	179.80	0.450	15.8	15.8 (6)	–	0.852(9)	0.030	[89]
O_2 + Kr	1.050	100.00	0.536	0.162	0.163(6)	0.944	0.946(3)	0.030	[90]
O_2 + CO_2	0.979	253.15	0.092	6.079	6.68 (9)	0.537	0.556(7)	0.048	[91]
Cl_2 + R12	0.975	298.15	0.532	0.805	0.81 (3)	0.571	0.59 (2)	0.026	[92]
Cl_2 + R140	0.948	313.00	0.083	0.101	0.100(6)	–	0.91 (5)	0.010	[46]
Cl_2 + R140a	0.930	313.00	0.063	0.101	0.102(4)	–	0.72 (2)	0.020	[46]
Cl_2 + R150a	0.967	293.00	0.104	0.101	0.099(3)	–	0.78 (1)	0.030	[46]
Br_2 + R10	0.995	336.25	0.342	0.098	0.098(3)	0.536	0.55 (1)	0.020	[93]
Br_2 + R112a	0.967	344.15	0.238	0.101	0.101(2)	0.600	0.60 (1)	0.030	[94]
CO + Ar	0.992	83.00	0.534	0.108	0.108(5)	–	0.65 (2)	0.040	[95]
CO + CH_4	1.003	123.40	0.360	0.988	1.07 (1)	0.800	0.796(3)	0.026	[96]
CO + CO_2	1.080	263.15	0.210	10.32	11.2 (2)	0.496	0.392(9)	0.034	[97]
CO + C_2H_6	1.000	248.15	0.056	2.758	3.15 (3)	0.452	0.487(7)	0.020	[98]
CO + R30	0.816	333.15	0.014	2.45	2.37 (4)	0.885	0.91 (1)	0.050	[99]
CO_2 + Cl_2	0.936	243.15	0.140	0.507	0.57 (1)	0.800	0.778(8)	0.093	[100]
CO_2 + CS_2	0.918	360.00	0.354	11.5	11.6 (1)	0.875	0.914(3)	0.002	[101]
CO_2 + C_2H_2	1.000	297.90	0.500	5.5	5.50 (1)	–	0.520(5)	0.007	[102]
CO_2 + C_2H_6	0.954	263.15	0.425	2.9	2.98 (3)	0.514	0.524(3)	0.132	[103]
CO_2 + Propylene	0.915	273.15	0.231	1.51	1.52 (1)	0.630	0.631(5)	0.095	[104]
CO_2 + R12	0.927	273.00	0.714	2.65	2.67 (2)	–	0.932(4)	0.069	[105]

Table 2: continued.

CO_2 + R20	0.945	333.15	0.569	6.45	6.3 (1)	0.962	0.972(4)	0.032	[106]
CO_2 + R22	1.006	273.15	0.560	1.99	2.07 (2)	0.848	0.853(3)	0.007	[107]
CO_2 + R23	0.997	263.35	0.417	2.292	2.34 (2)	0.482	0.503(5)	0.011	[107]
CO_2 + R30	0.923	326.95	0.550	6.246	6.3 (1)	–	0.970(7)	0.063	[108]
CO_2 + R32	1.050	280.00	0.486	2.51	2.48 (2)	0.724	0.732(4)	0.033	[109]
CO_2 + R40	0.990	282.65	0.534	2.53	2.45 (7)	0.861	0.90 (1)	0.001	[110]
CO_2 + R41	1.024	290.00	0.662	4.53	4.42 (8)	0.720	0.720(8)	0.010	[111]
CO_2 + R125	1.021	304.60	0.450	3.34	3.31 (4)	0.630	0.640(7)	0.050	[112]
CO_2 + R134a	0.982	329.60	0.510	5.37	5.43 (9)	0.707	0.710(8)	0.010	[113]
CO_2 + R140	0.902	323.20	0.662	6.89	7.26 (7)	0.995	0.990(1)	0.092	[114]
CO_2 + R140a	0.889	323.17	0.462	4.88	4.85 (6)	0.983	0.983(5)	0.080	[115]
CO_2 + R142b	0.952	318.30	0.551	4.71	4.73 (5)	0.848	0.873(4)	0.200	[116]
CO_2 + R152a	1.004	347.70	0.392	5.53	5.58 (7)	0.580	0.610(7)	0.005	[116]
CS_2 + R10	1.029	318.15	0.468	0.069	0.069(2)	0.717	0.72 (1)	0.002	[117]
CS_2 + R20	1.007	353.15	0.500	0.247	0.23 (4)	–	0.7 (1)	0.020	[118]
CS_2 + R1110	1.025	318.15	0.298	0.04	0.041(2)	0.880	0.89 (1)	0.020	[119]
CH_3I + CS_2	1.000	317.15	0.122	0.101	0.102(4)	–	0.16 (1)	0.040	[120]
CH_3I + R10	0.971	298.15	0.558	0.04	0.038(1)	0.811	0.80 (1)	0.010	[121]
CH_3I + R20	0.994	308.15	0.492	0.06	0.059(2)	–	0.68 (2)	0.010	[122]
C_2H_2 + R10	0.890	393.15	0.480	9.11	9.1 (2)	–	0.895(8)	0.080	[123]
C_2H_2 + R152a	1.090	303.20	0.569	2.5	2.45 (8)	0.837	0.87 (2)	0.085	[124]
C_2H_4 + Xe	1.010	269.54	0.499	3.98	4.00 (3)	0.502	0.499(4)	0.020	[125]
C_2H_4 + CO_2	0.944	243.15	0.087	1.588	1.51 (2)	0.156	0.162(5)	0.055	[126]
C_2H_4 + C_2H_2	0.975	255.37	0.980	2.682	2.72 (2)	0.979	0.994(2)	0.064	[127]
C_2H_4 + C_2H_6	1.037	233.15	0.500	1.132	1.151(9)	0.622	0.622(4)	0.040	[128]
C_2H_4 + Propylene	0.996	263.07	0.625	2.067	2.08 (1)	0.884	0.882(2)	0.021	[129]
C_2H_4 + R10	1.003	323.15	0.473	4.37	4.33 (7)	0.981	0.985(3)	-0.010	[130]
C_2H_4 + R20	1.001	323.15	0.539	5.066	4.9 (1)	0.976	0.93 (2)	0.030	[131]
C_2H_4 + R22	1.026	213.15	0.030	0.062	0.063(2)	–	0.29 (1)	0.022	[132]
C_2H_4 + R30	1.070	423.15	0.250	6.03	6.20 (8)	0.60	0.647(8)	0.080	[133]
C_2H_4 + R30B1	0.946	373.15	0.210	6.08	6.02 (6)	0.905	0.915(5)	0.050	[134]
C_2H_4 + R1140	0.945	313.15	0.539	4.9	4.94 (4)	0.902	0.856(2)	0.100	[135]
C_2H_6 + C_2H_2	0.968	277.59	0.180	3.544	3.89 (2)	0.243	0.262(3)	0.156	[136]
C_2H_6 + Propylene	1.015	310.93	0.260	2.41	2.51 (2)	0.447	0.438(4)	0.007	[137]
C_2H_6 + R22	0.981	293.24	0.551	2.76	2.78 (3)	0.762	0.753(3)	0.090	[138]

Table 2: continued.

Propylene + Propadiene	0.991	293.15	0.464	0.852	0.88 (2)	0.545	0.56 (1)	0.020	[139]
Propylene + Propyne	1.003	313.15	0.566	1.442	1.46 (2)	–	0.639(6)	0.050	[140]
Propylene + R10	1.005	333.15	0.282	0.766	0.79 (4)	–	0.90 (2)	0.020	[141]
Propylene + R12	0.998	283.00	0.529	0.63	0.62 (1)	0.654	0.66 (1)	0.026	[142]
Propylene + R20	0.975	293.15	0.361	0.455	0.46 (3)	–	0.950(1)	0.010	[141]
Propylene + R22	0.982	283.00	0.147	0.73	0.71 (2)	0.187	0.171(6)	0.036	[142]
Propylene + R114	0.966	298.00	0.514	0.745	0.72 (2)	0.807	0.810(7)	0.050	[142]
Propylene + R115	0.948	298.00	0.549	1.244	1.24 (2)	0.607	0.59 (1)	0.080	[142]
Propylene + R134a	0.924	298.00	0.204	0.95	0.95 (2)	0.399	0.383(8)	0.105	[142]
Propylene + R142b	0.987	298.00	0.443	0.73	0.71 (1)	0.701	0.705(9)	0.035	[142]
Propylene + R152a	0.933	298.15	0.281	0.94	0.95 (1)	0.431	0.483(6)	0.100	[143]
Propylene + R1110	1.008	293.15	0.441	0.534	0.49 (6)	–	0.998(5)	0.010	[141]
Propylene + R1120	0.983	303.15	0.275	0.507	0.55 (4)	–	0.94 (3)	0.050	[144]
Propylene + R1140	1.029	293.15	0.542	0.687	0.69 (1)	0.781	0.775(5)	0.050	[145]
SF_6 + R12	0.984	319.78	0.330	2.1	2.10 (3)	0.534	0.540(5)	0.050	[146]
SF_6 + R13B1	0.999	296.70	0.339	1.93	1.94 (4)	0.407	0.410(7)	0.035	[146]
SF_6 + R22	0.915	318.58	0.154	2.406	2.42 (4)	0.307	0.300(8)	0.100	[146]
SF_6 + R32	0.790	310.00	0.480	4.041	4.07 (7)	0.523	0.517(8)	0.190	[109]
SF_6 + R114	1.050	270.80	0.011	0.087	0.088(4)	–	0.065(4)	0.070	[48]
R10 + R140	0.955	360.05	0.490	0.099	0.097(3)	0.750	0.74 (1)	0.120	[147]
R10 + R150B2	0.987	323.15	0.533	0.028	0.027(2)	–	0.88 (1)	0.000	[148]
R10 + R1110	0.967	343.15	0.488	0.05	0.05 (2)	0.808	0.81 (1)	0.005	[149]
R10 + R1120	0.998	354.64	0.506	0.101	0.097(3)	0.577	0.588(1)	0.010	[150]
R12 + R10	0.991	297.75	0.090	0.101	0.101(3)	–	0.877(5)	0.040	[49]
R12 + R11	1.001	343.00	0.439	1.025	0.99 (1)	0.739	0.721(5)	0.010	[151]
R12 + R113	1.014	293.15	0.513	0.27	0.28 (2)	0.936	0.94 (2)	0.030	[152]
R12 + R114	0.989	313.15	0.523	0.668	0.69 (2)	0.727	0.70 (2)	0.010	[153]
R12 + R142b	0.960	303.00	0.414	0.583	0.59 (4)	–	0.58 (3)	0.040	[154]
R12 + R152a	0.936	323.01	0.269	1.39	1.40 (3)	–	0.320(5)	0.060	[155]
R12B2 + R114B2	1.030	306.70	0.500	0.101	0.099(3)	0.670	0.70 (1)	0.010	[156]
R13 + Propylene	0.970	273.00	0.568	1.5	1.48 (2)	0.738	0.743(4)	0.059	[142]
R13 + R11	0.975	253.15	0.568	0.73	0.73 (2)	–	0.986(2)	0.030	[157]
R13 + R12	0.971	290.00	0.549	1.836	1.80 (3)	0.809	0.800(6)	0.030	[158]

Table 2: continued.

R13 + R13B1	0.992	273.00	0.566	1.46	1.42 (2)	0.712	0.699(6)	0.010	[159]
R13 + R113	0.980	348.15	0.499	3.55	3.54 (6)	–	0.890(6)	0.010	[160]
R13 + R134a	0.955	273.00	0.464	1.28	1.27 (1)	0.809	0.806(5)	0.090	[159]
R13B1 + Propylene	0.998	298.00	0.545	1.5	1.49 (1)	0.591	0.607(5)	0.032	[142]
R13B1 + R12	1.002	364.36	0.214	3.42	3.42 (3)	–	0.270(4)	0.003	[161]
R13B1 + R22	0.975	328.15	0.635	2.95	2.99 (4)	–	0.674(4)	0.031	[162]
R13B1 + R114	1.038	343.15	0.534	2.09	2.07 (3)	–	0.777(6)	0.030	[163]
R13B1 + R115	1.018	343.15	0.509	3.24	3.20 (3)	–	0.554(4)	0.015	[163]
R13B1 + R125	0.969	298.15	0.514	1.682	1.68 (1)	0.538	0.548(4)	0.063	[164]
R14 + Propylene	0.872	210.00	0.479	1.75	1.73 (4)	0.970	0.968(4)	0.050	[165]
R14 + SF_6	0.978	273.00	0.388	3.83	3.75 (5)	0.618	0.619(6)	0.010	[166]
R14 + R12	0.893	174.60	0.133	0.32	0.32 (4)	0.992	0.987(6)	0.130	[167]
R14 + R13	0.972	288.70	0.108	3.699	3.59 (6)	0.175	0.190(5)	0.050	[168]
R14 + R22	0.895	289.65	0.285	5.287	5.30 (8)	–	0.720(7)	0.105	[62]
R14 + R23	0.876	224.82	0.435	2.29	2.26 (4)	0.776	0.790(5)	0.115	[169]
R14 + R41	0.920	130.00	0.061	0.03	0.03 (1)	0.990	0.998(1)	–	[170]
R14 + R152a	0.982	174.91	0.550	0.459	0.45 (7)	0.998	0.998(1)	0.100	[167]
R20 + R10	0.958	328.15	0.499	0.068	0.068(2)	0.618	0.61 (1)	0.005	[171]
R20 + R1110	0.931	356.95	0.358	0.101	0.10 (1)	0.805	0.80 (5)	0.023	[172]
R22 + Cl_2	0.955	283.15	0.100	0.59	0.58 (1)	–	0.22 (1)	0.061	[173]
R22 + CS_2	0.950	323.15	0.509	1.448	1.47 (2)	0.923	0.928(2)	0.092	[107]
R22 + R10	0.929	383.00	0.524	3.097	3.08 (3)	0.907	0.916(3)	0.003	[174]
R22 + R11	0.956	348.15	0.543	1.98	2.00 (2)	–	0.827(4)	0.045	[175]
R22 + R12	0.974	343.81	0.498	2.61	2.61 (3)	0.574	0.570(5)	0.034	[176]
R22 + R21	0.982	293.33	0.536	0.585	0.59 (2)	0.891	0.87 (2)	0.010	[177]
R22 + R113	0.929	372.20	0.506	2.5	2.55 (4)	–	0.833(7)	0.040	[178]
R22 + R114	0.924	338.15	0.487	1.732	1.73 (3)	0.722	0.73 (1)	0.060	[153]
R22 + R115	0.931	336.75	0.518	2.781	2.75 (4)	0.546	0.549(7)	0.055	[179]
R22 + R123	0.976	383.15	0.374	2.52	2.50 (3)	0.642	0.645(7)	0.010	[176]
R22 + R124	0.999	283.15	0.500	0.444	0.428(4)	0.706	0.700(1)	-0.005	[180]
R22 + R134a	0.988	343.81	0.506	2.66	2.65 (2)	0.550	0.563(5)	0.010	[181]
R22 + R142b	0.985	328.15	0.560	1.52	1.50 (3)	0.732	0.730(8)	0.010	[182]
R22 + R152a	1.019	313.15	0.519	1.19	1.20 (3)	0.624	0.61 (3)	0.000	[182]
R23 + CS_2	0.852	398.15	0.191	14.07	13.6 (5)	0.774	0.790(8)	0.150	[107]

Table 2: continued.

R23 + Propylene	0.891	265.00	0.189	1.0	1.00 (2)	0.552	0.580(6)	0.115	[159]
R23 + SF_6	0.849	295.00	0.476	3.905	3.84 (4)	0.542	0.548(4)	0.120	[109]
R23 + R11	0.849	348.10	0.400	5.23	5.15 (7)	–	0.847(5)	0.130	[95]
R23 + R12	0.883	243.00	0.600	0.774	0.74 (3)	–	0.897(6)	0.100	[183]
R23 + R13	0.902	273.15	0.538	2.732	2.75 (3)	0.564	0.562(6)	0.101	[184]
R23 + R13B1	0.906	268.15	0.415	1.619	1.57 (3)	0.600	0.629(9)	0.100	[164]
R23 + R22	0.962	323.15	0.524	4.575	4.55 (3)	0.644	0.646(4)	0.025	[107]
R23 + R113	0.812	348.10	0.415	4.72	4.65 (5)	–	0.910(5)	0.100	[185]
R23 + R114	0.836	348.00	0.300	3.54	3.55 (3)	–	0.680(6)	0.120	[186]
R23 + R115	0.880	330.14	0.202	3.253	3.29 (4)	0.349	0.342(6)	0.120	[146]
R23 + R116	0.840	280.15	0.299	3.04	2.92 (3)	–	0.370(5)	0.120	[187]
R23 + R134a	0.956	293.15	0.401	1.75	1.79 (2)	0.750	0.715(7)	0.001	[188]
R23 + R142b	0.930	273.11	0.362	0.99	1.00 (2)	0.861	0.873(7)	0.050	[167]
R23 + R143a	0.956	293.15	0.550	2.52	2.54 (2)	0.727	0.719(3)	0.000	[189]
R23 + R152a	0.982	293.15	0.550	2.11	2.12 (3)	0.835	0.828(7)	0.000	[189]
R30 + CH_3I	1.040	298.15	0.498	0.058	0.058(1)	0.516	0.54 (1)	0.001	[121]
R30 + R10	0.979	318.15	0.450	0.082	0.081(2)	0.753	0.741(9)	0.001	[190]
R30 + R20	1.014	318.15	0.500	0.090	0.091(2)	0.676	0.709(9)	-0.010	[190]
R30 + R30B1	0.990	322.35	0.502	0.101	0.102(2)	0.717	0.745(7)	0.005	[191]
R30 + R30B2	1.000	331.25	0.436	0.101	0.101(2)	0.775	0.800(1)	0.010	[191]
R30 + R140a	0.994	432.40	0.500	1.36	1.36 (1)	–	0.660(4)	0.001	[192]
R30 + R1110	0.950	333.00	0.350	0.101	0.102(2)	0.907	0.908(6)	0.010	[193]
R30B1 + R10	0.921	313.15	0.242	0.034	0.035(2)	0.340	0.37 (2)	0.010	[194]
R30B1 + R30B2	0.972	355.08	0.372	0.101	0.102(2)	0.599	0.527(9)	0.010	[191]
R32 + Cl_2	0.965	283.15	0.352	1.111	1.12 (2)	–	0.595(8)	0.148	[173]
R32 + R12	0.941	283.15	0.180	0.783	0.782(9)	0.502	0.488(6)	0.013	[195]
R32 + R22	1.052	283.15	0.502	0.908	0.92 (1)	0.604	0.567(7)	0.130	[195]
R32 + R30	0.812	313.20	0.440	1.372	1.39 (2)	0.912	0.917(2)	0.055	[196]
R32 + R40	1.012	283.15	0.392	0.777	0.772(9)	0.663	0.649(6)	0.061	[195]
R32 + R115	0.827	298.15	0.736	1.92	1.93 (2)	–	0.724(5)	0.130	[197]
R32 + R123	0.982	313.95	0.478	1.29	1.303(1)	0.909	0.894(3)	0.045	[198]
R32 + R125	0.910	308.15	0.495	2.066	2.150(8)	0.53	0.54 (1)	0.015	[199]
R32 + R134a	1.109	289.99	0.566	1.005	0.994(2)	–	0.709(6)	0.001	[200]
R32 + R142b	0.955	314.95	0.435	1.45	1.50 (1)	0.725	0.730(4)	0.035	[189]
R32 + R143a	0.883	313.15	0.439	2.22	2.30 (4)	0.491	0.490(6)	0.015	[201]

Table 2: continued.

R32 + R152a	0.995	323.15	0.260	1.775	1.76 (2)	0.463	0.419(5)	0.041	[202]
R40 + R30	0.964	278.15	0.476	0.151	0.145(3)	–	0.900(6)	0.020	[203]
R41 + R40	0.982	182.33	0.584	0.032	0.031(2)	0.975	0.974(4)	0.020	[204]
R113 + Br_2	0.940	319.25	0.820	0.101	0.103(9)	0.370	0.33 (6)	0.001	[94]
R113 + R123B1	0.998	308.15	0.103	0.06	0.059(2)	–	0.130(8)	0.006	[205]
R114 + R21	0.950	338.37	0.404	0.695	0.71 (1)	0.479	0.440(7)	0.030	[206]
R114 + R113	1.019	294.15	0.442	0.101	0.101(3)	0.770	0.79 (1)	0.010	[207]
R115 + R114	1.000	369.50	0.269	1.98	1.99 (2)	–	0.428(4)	0.010	[208]
R116 + CO_2	0.867	227.60	0.583	0.88	0.964(1)	0.380	0.382(1)	0.028	[209]
R116 + Propylene	0.888	275.00	0.563	1.8	1.82 (3)	0.687	0.702(6)	0.150	[142]
R116 + R22	0.878	288.15	0.560	2.325	2.30 (5)	0.741	0.688(4)	0.100	[210]
R116 + R32	0.768	253.55	0.385	1.20	1.21 (2)	–	0.624(3)	0.180	[209]
R116 + R41	0.775	225.45	0.529	0.69	0.68 (1)	–	0.44 (2)	0.170	[211]
R116 + R115	1.000	285.10	0.500	1.52	1.48 (1)	0.682	0.716(3)	0.020	[212]
R116 + R134a	0.881	275.00	0.300	1.17	1.17 (3)	0.730	0.72 (1)	0.095	[142]
R123B1 + R10	1.002	318.15	0.431	0.06	0.057(2)	0.651	0.64 (1)	0.010	[205]
R123B1 + R20	0.978	318.15	0.452	0.074	0.074(2)	0.544	0.55 (1)	0.001	[205]
R123B1 + R140a	1.006	318.15	0.456	0.059	0.058(1)	0.646	0.63 (1)	-0.007	[205]
R124 + R142b	0.990	312.15	0.508	0.536	0.536(8)	0.536	0.530(7)	0.000	[154]
R125 + R115	0.927	298.15	0.821	1.369	1.33 (5)	0.836	0.815(7)	0.070	[213]
R125 + R134a	0.999	323.00	0.484	1.9	1.85 (2)	0.590	0.588(4)	0.009	[214]
R125 + R143a	0.987	264.01	0.503	0.466	0.504(5)	0.516	0.526(6)	–	[215]
R125 + R152a	0.989	333.02	0.551	2.35	2.35 (3)	0.674	0.641(6)	0.000	[216]
R134 + R142b	0.998	254.95	0.596	0.101	0.103(3)	–	0.72 (1)	0.010	[142]
R134 + R152a	1.075	253.45	0.278	0.101	0.101(3)	–	0.167(7)	0.070	[217]
R134a + R12	0.943	298.00	0.219	0.772	0.74 (2)	0.302	0.30 (1)	0.090	[142]
R134a + R114	0.899	298.00	0.534	0.538	0.54 (1)	0.746	0.76 (1)	0.080	[159]
R134a + R123	0.940	332.74	0.489	0.99	0.99 (2)	0.791	0.81 (1)	0.045	[218]
R134a + R124	0.971	307.25	0.486	0.707	0.72 (2)	0.605	0.59 (1)	0.030	[154]
R134a + R141b	0.935	333.15	0.520	1.07	1.08 (2)	0.822	0.840(6)	0.052	[219]
R134a + R142b	0.960	298.00	0.451	0.51	0.51 (3)	0.600	0.60 (3)	0.025	[142]
R134a + R152a	1.003	323.08	0.485	1.226	1.22 (3)	0.505	0.50 (1)	0.001	[220]
R140 + R130a	1.003	399.75	0.186	0.101	0.100(2)	0.260	0.262(8)	0.020	[221]
R140 + R1110	0.974	390.50	0.232	0.101	0.100(3)	0.308	0.289(1)	0.010	[222]
R140a + R10	1.010	298.15	0.506	0.017	0.016(1)	–	0.53 (2)	-0.001	[223]

Table 2: continued.

R141b + R140a	0.996	323.25	0.200	0.076	0.075(2)	0.502	0.50 (1)	0.010	[195]
R142b + R113	0.952	373.00	0.502	1.25	1.27 (4)	–	0.77 (2)	0.030	[186]
R142b + R140a	0.945	323.25	0.481	0.383	0.42 (4)	0.931	0.94 (2)	0.030	[195]
R142b + R141b	0.994	323.25	0.490	0.433	0.44 (2)	0.749	0.74 (2)	0.010	[195]
R143a + R12	0.936	313.00	0.600	1.71	1.65 (4)	–	0.675(8)	0.080	[183]
R143a + R22	1.023	275.00	0.500	0.589	0.58 (3)	0.546	0.54 (3)	0.000	[224]
R143a + R134a	0.994	293.15	0.442	0.798	0.816(7)	0.567	0.570(5)	0.013	[225]
R143a + R152a	0.977	313.15	0.447	1.34	1.40 (1)	0.571	0.570(4)	0.001	[225]
R143a + R1122	0.958	313.50	0.708	1.57	1.56 (2)	–	0.800(4)	0.030	[132]
R150a + R10	0.937	335.63	0.506	0.101	0.104(3)	0.661	0.65 (1)	0.030	[226]
R150a + R20	1.000	302.86	0.456	0.033	0.032(1)	0.494	0.51 (2)	–	[227]
R150a + R140	1.010	349.15	0.500	0.101	0.09 (2)	0.853	0.87 (5)	0.015	[221]
R152a + R12B1	0.921	293.15	0.385	0.44	0.44 (2)	–	0.63 (2)	0.085	[228]
R152a + R113	0.883	348.20	0.462	1.246	1.24 (3)	–	0.85 (1)	0.080	[185]
R152a + R114	0.897	345.50	0.392	1.53	1.471(2)	–	0.592(5)	0.110	[229]
R152a + R142b	0.963	347.60	0.461	1.72	1.74 (2)	0.544	0.550(5)	0.045	[230]
R152a + R150a	0.963	323.20	0.488	0.67	0.64 (7)	0.900	0.91 (2)	0.030	[124]
R152a + R1140	0.975	323.20	0.505	1.05	1.06 (1)	0.578	0.600(4)	0.030	[203]
R160B1 + CS_2	1.018	286.15	0.074	0.032	0.032(2)	0.145	0.10 (1)	0.040	[231]
R1114 + R32	0.932	253.15	0.391	0.885	0.88 (4)	0.607	0.64 (3)	0.130	[232]
R1120 + R1110	0.954	380.85	0.262	0.101	0.102(3)	0.512	0.50 (2)	0.010	[233]
R1140 + R140	0.980	346.15	0.517	0.703	0.72 (5)	–	0.95 (1)	0.010	[234]
R1140 + R1120	1.037	298.15	0.180	0.067	0.065(2)	–	0.886(9)	-0.030	[235]

Table 3

List of the eight binary mixtures for which the present molecular mixture models show larger deviations.

Ne + Xe [236]	Ne + R14 [237]	C_2H_2 + Propylene [239]	Propylene + R30 [99]
Ne + R13 [237]	N_2 + R14 [238]	C_2H_2 + Propyne [239]	R13 + R114 [240]

List of Figures

Fig. 1.

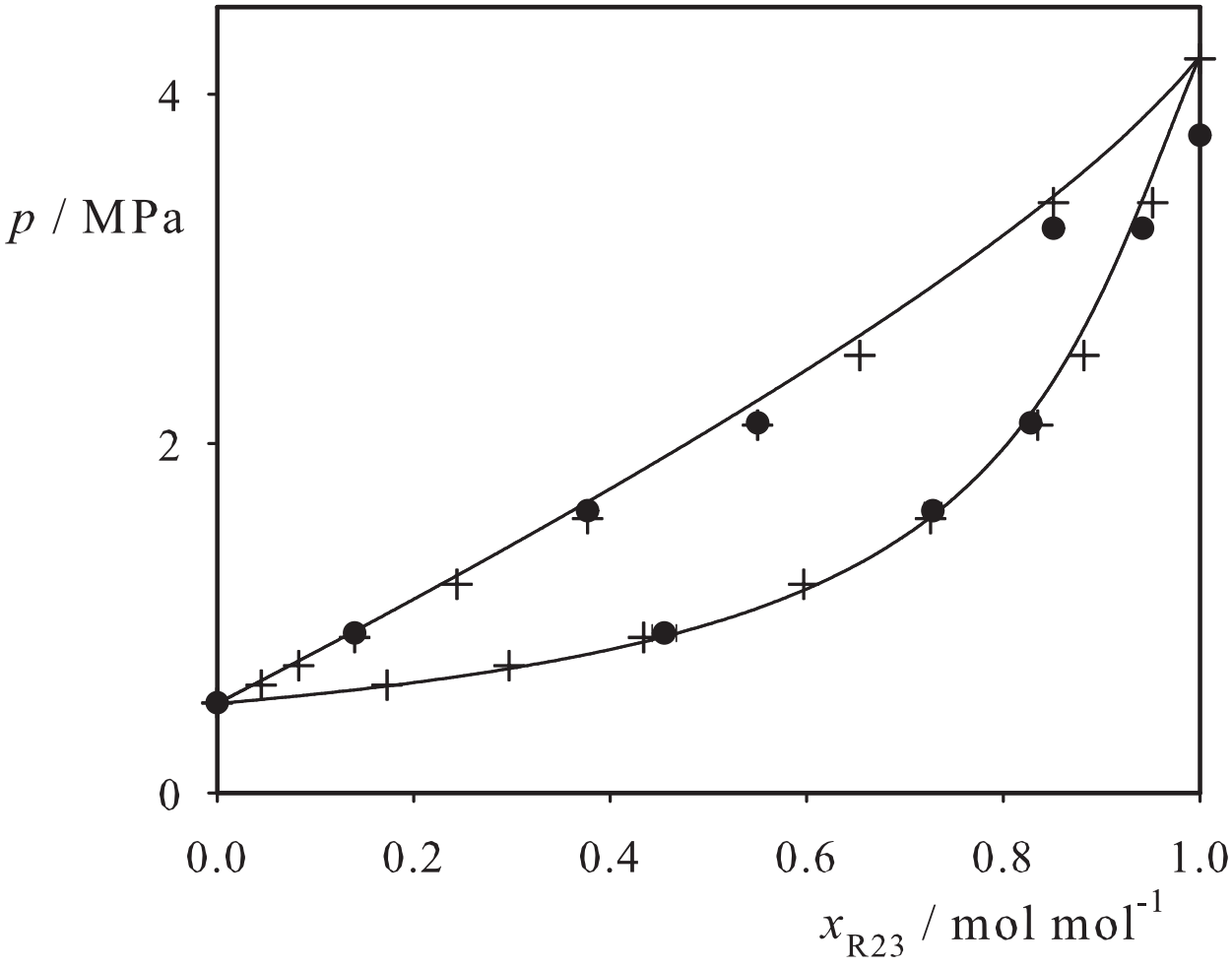

Fig. 2.

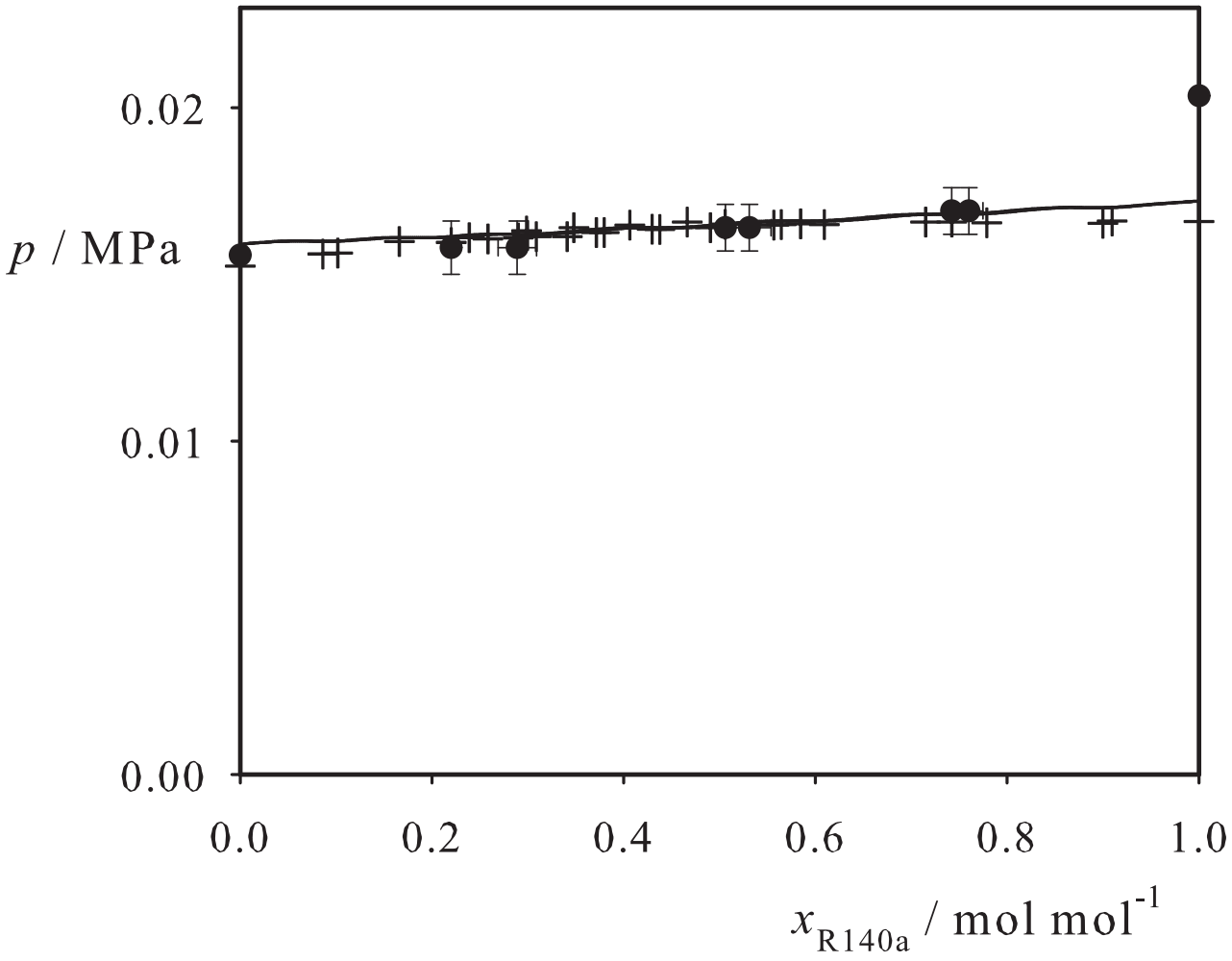

Fig. 3.

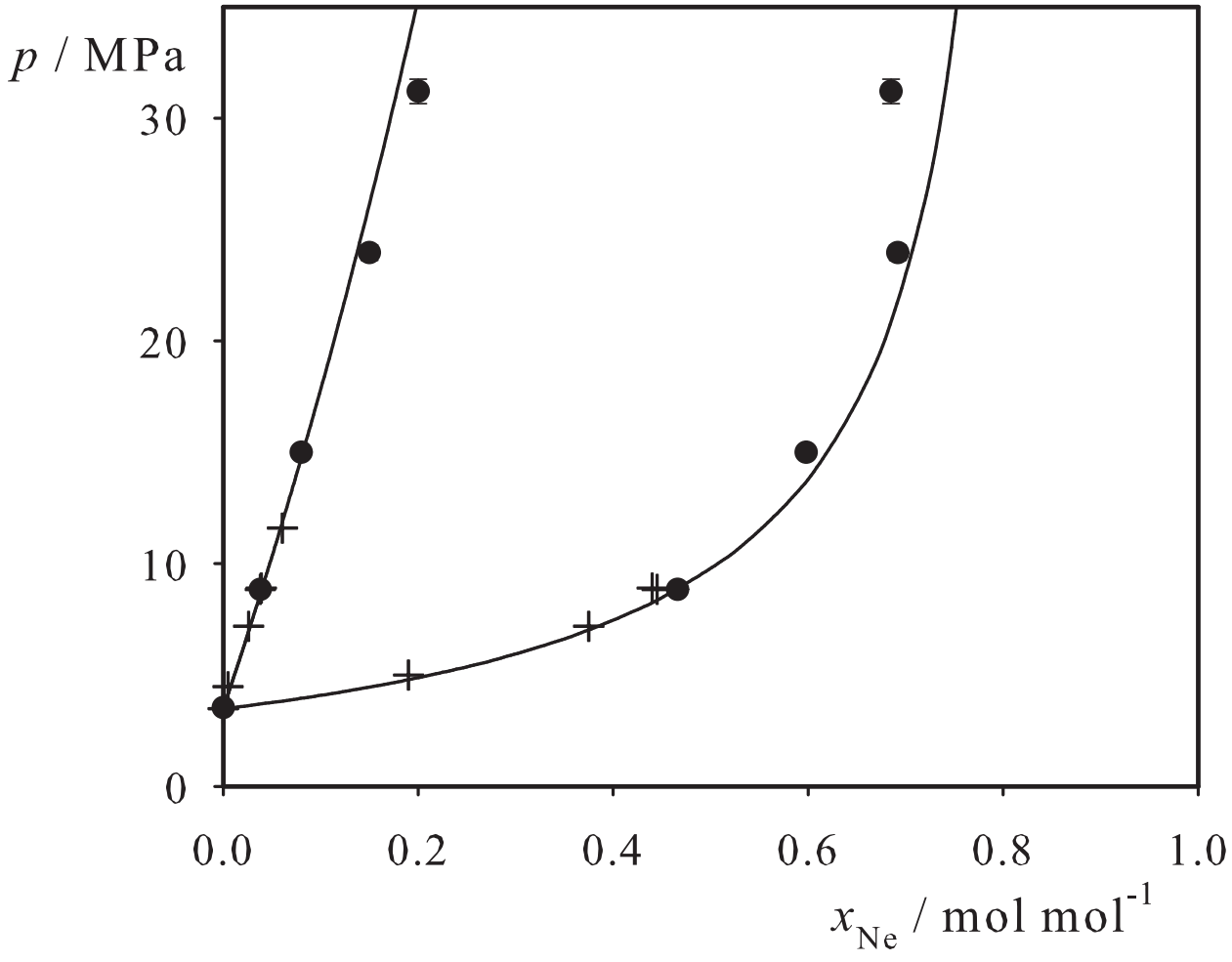

Fig. 4.

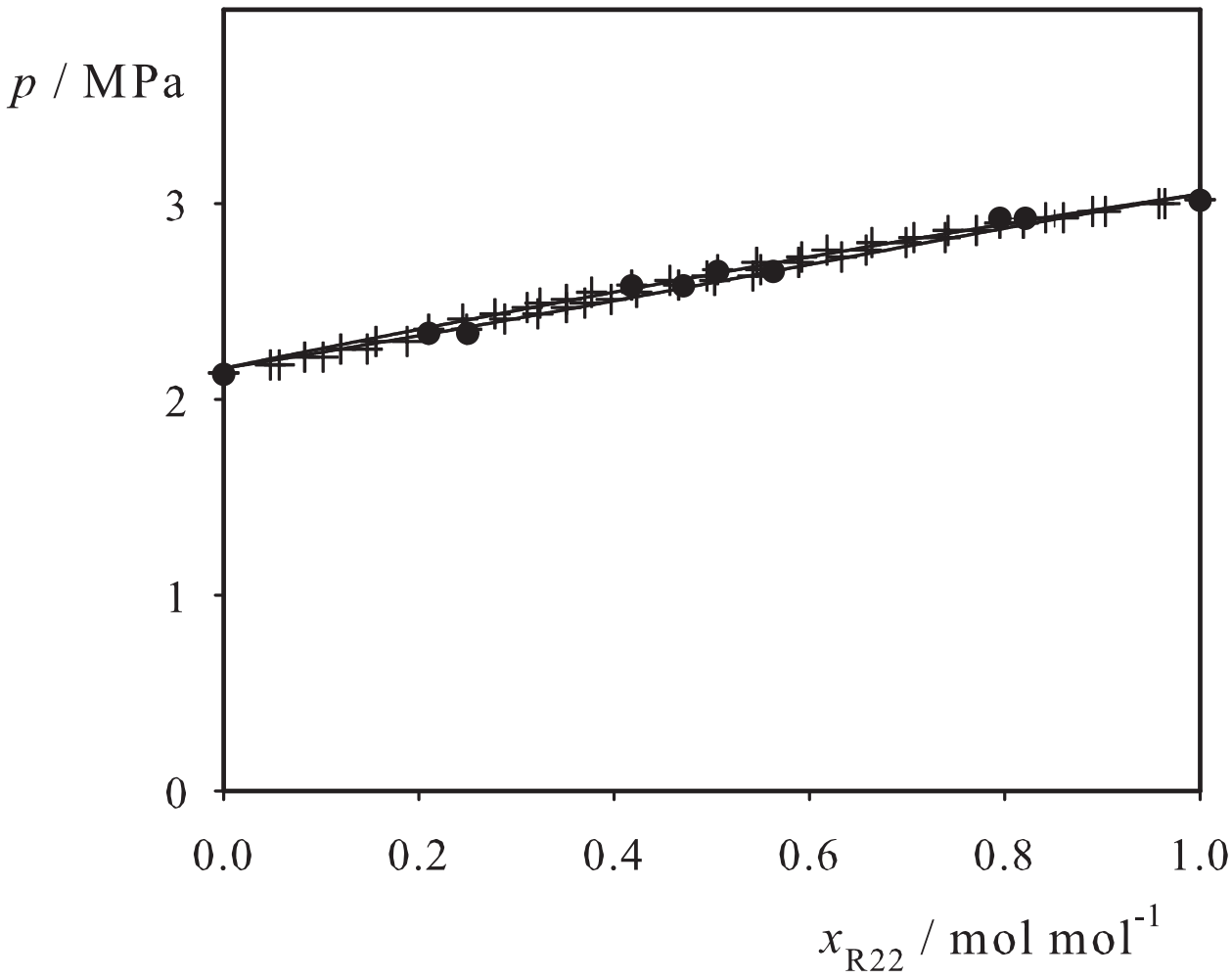

Fig. 5.

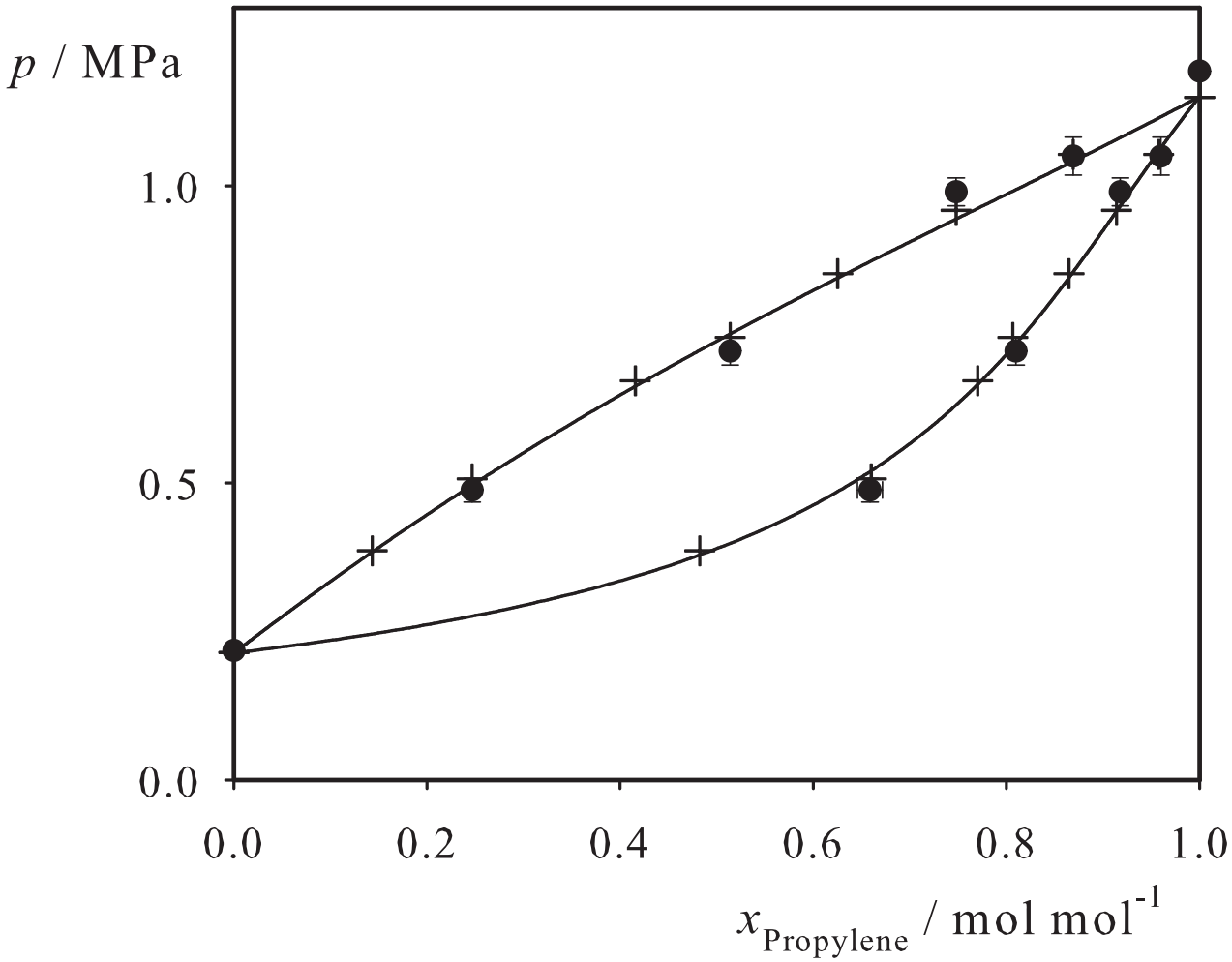

Fig. 6.

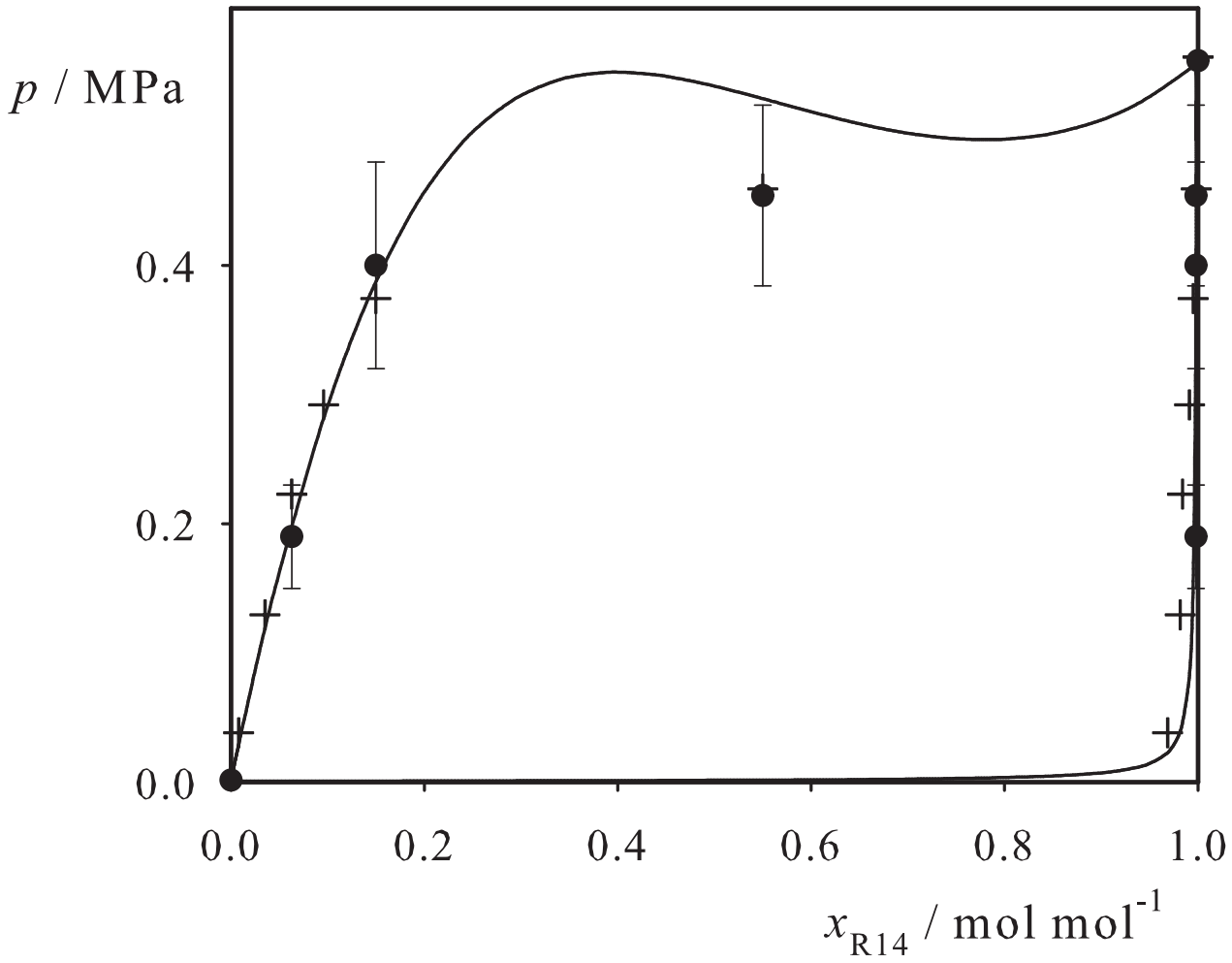

Fig. 7.

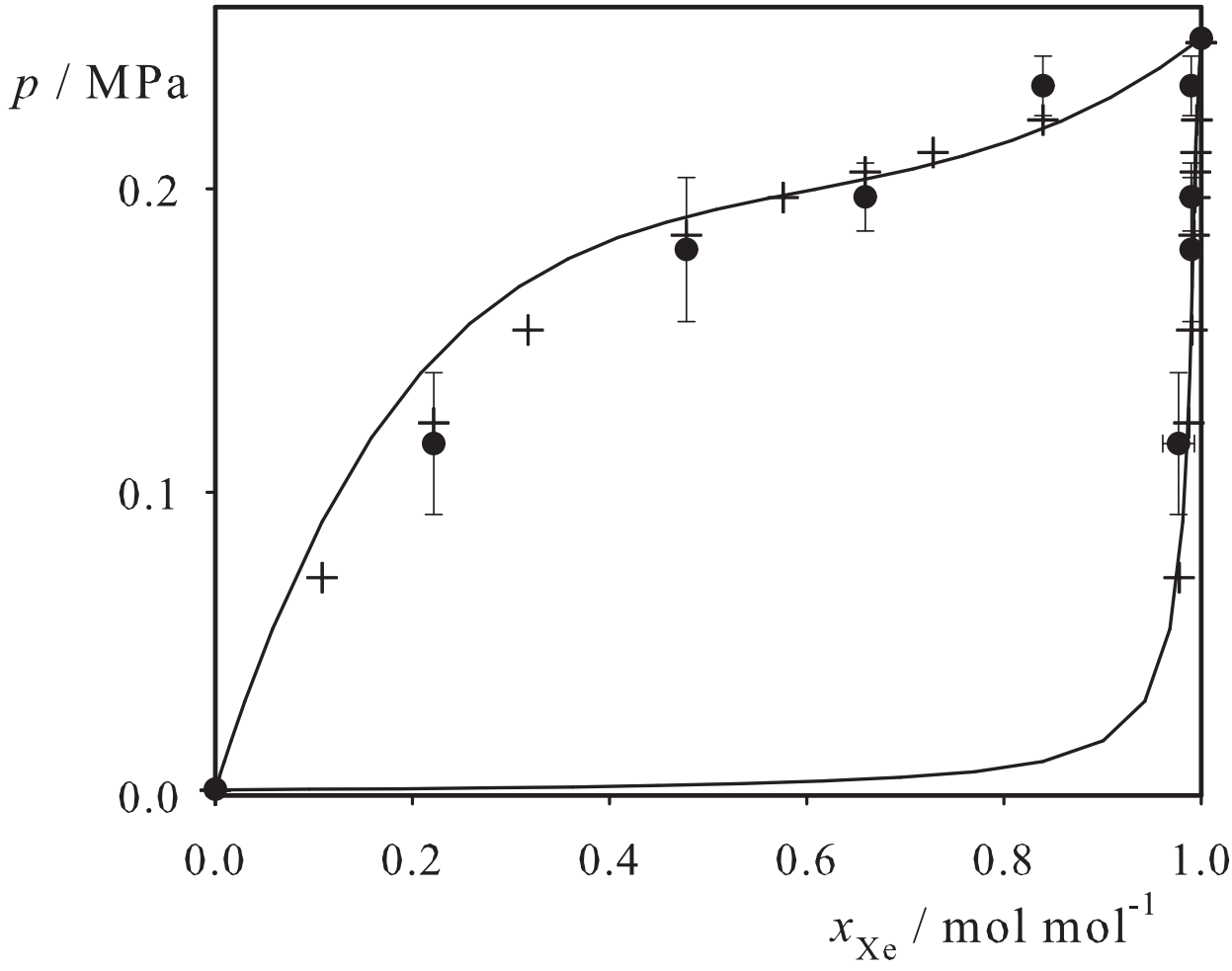

Fig. 8.

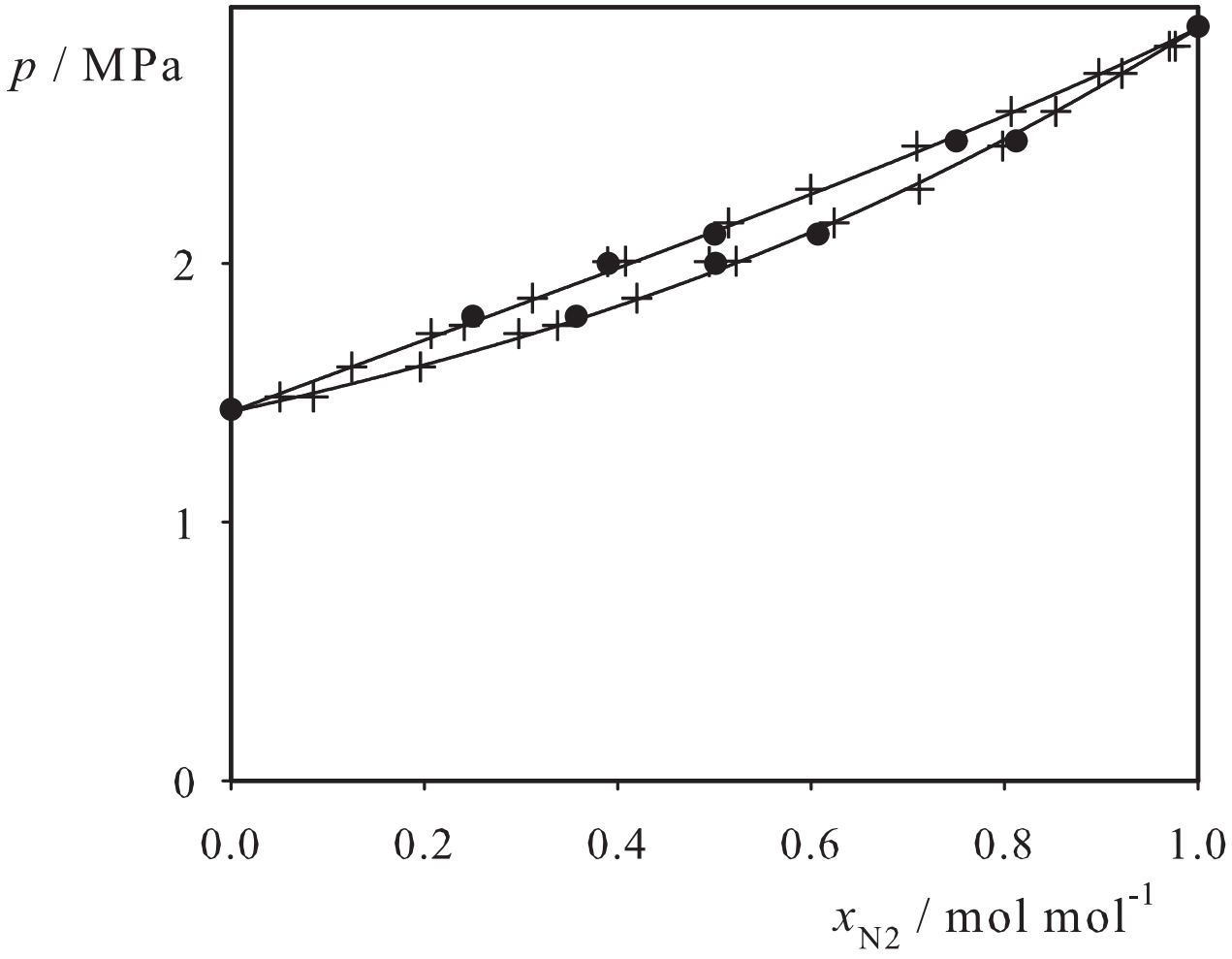

Fig. 9.

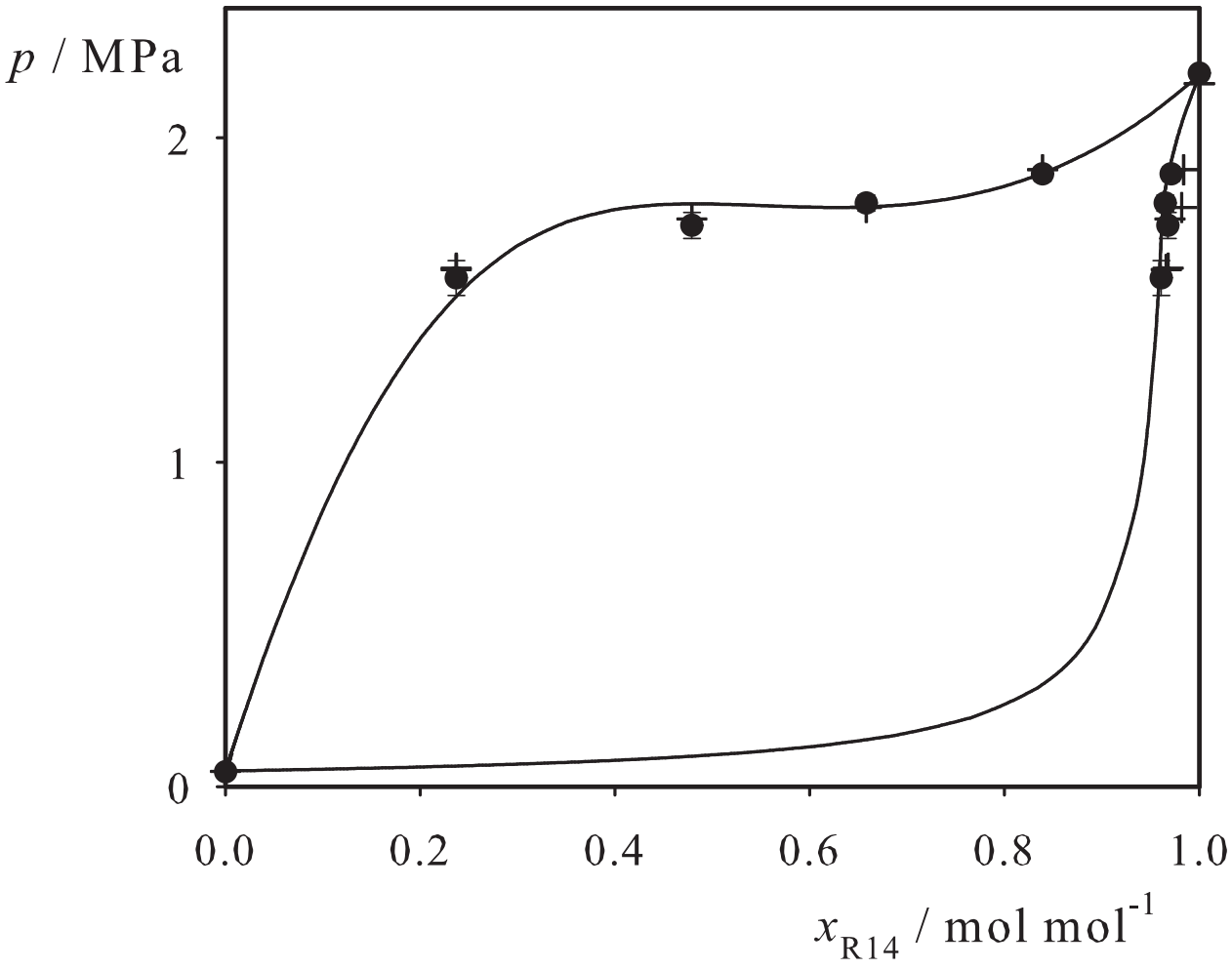

Fig. 10.

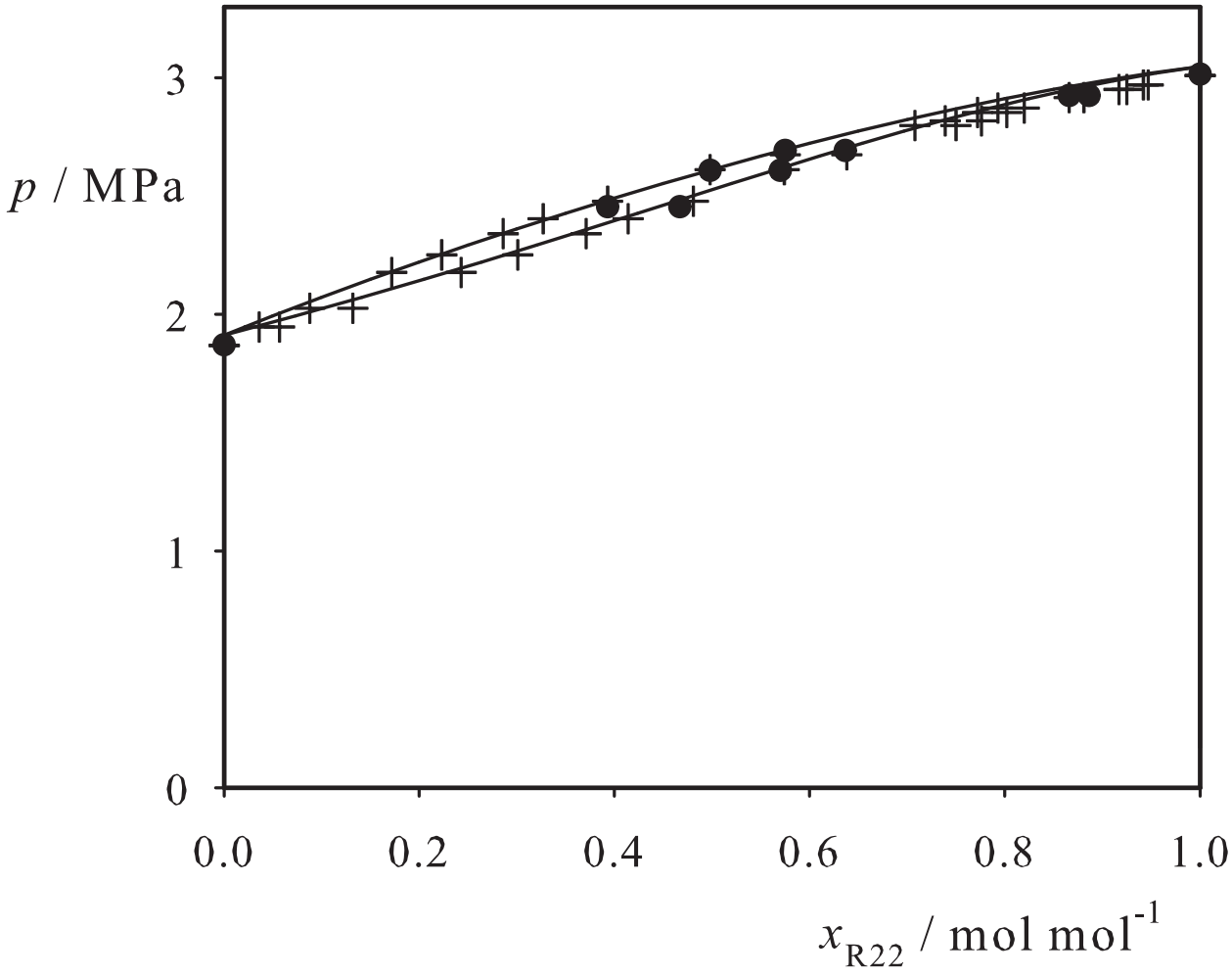

Fig. 11.

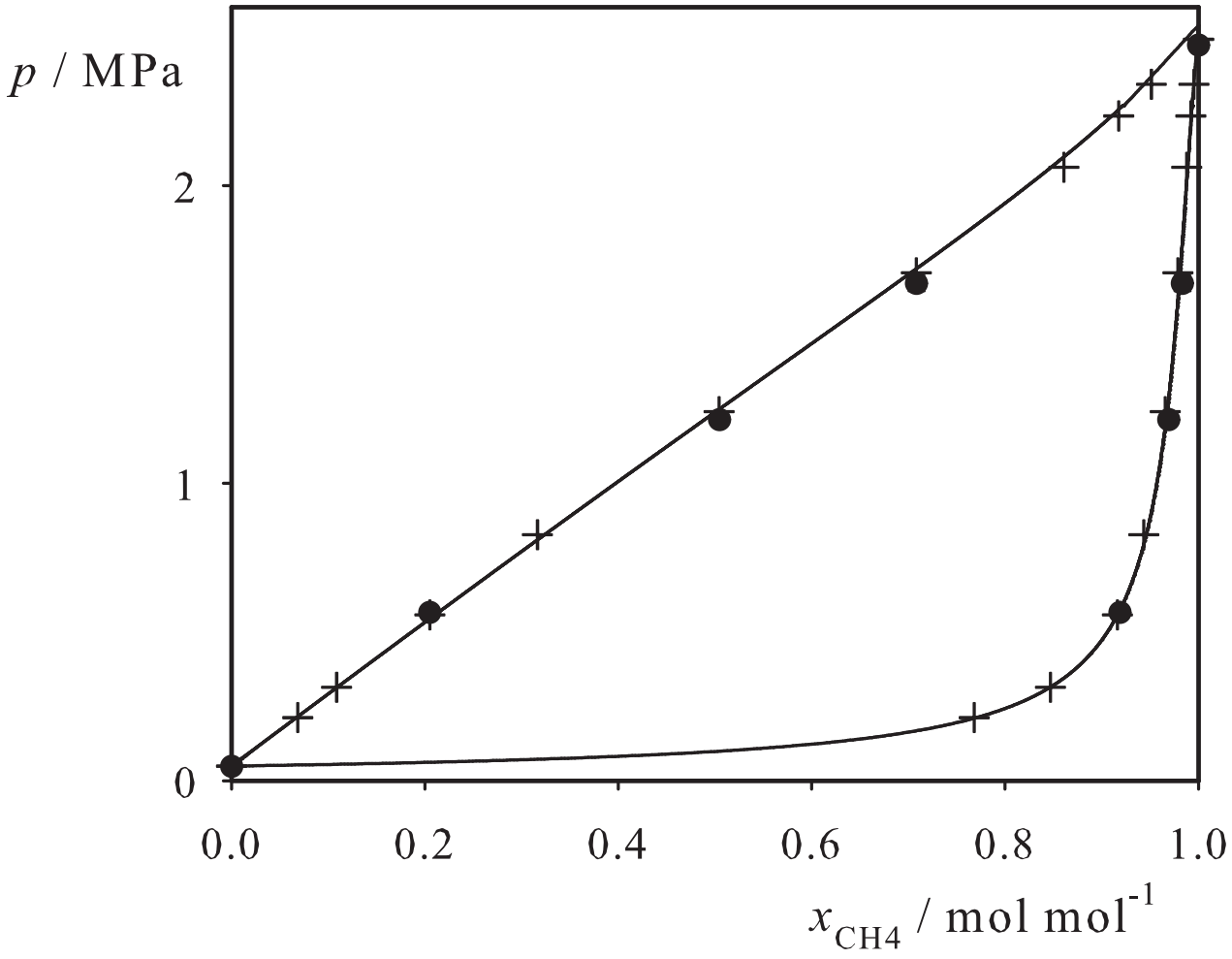

Fig. 12.

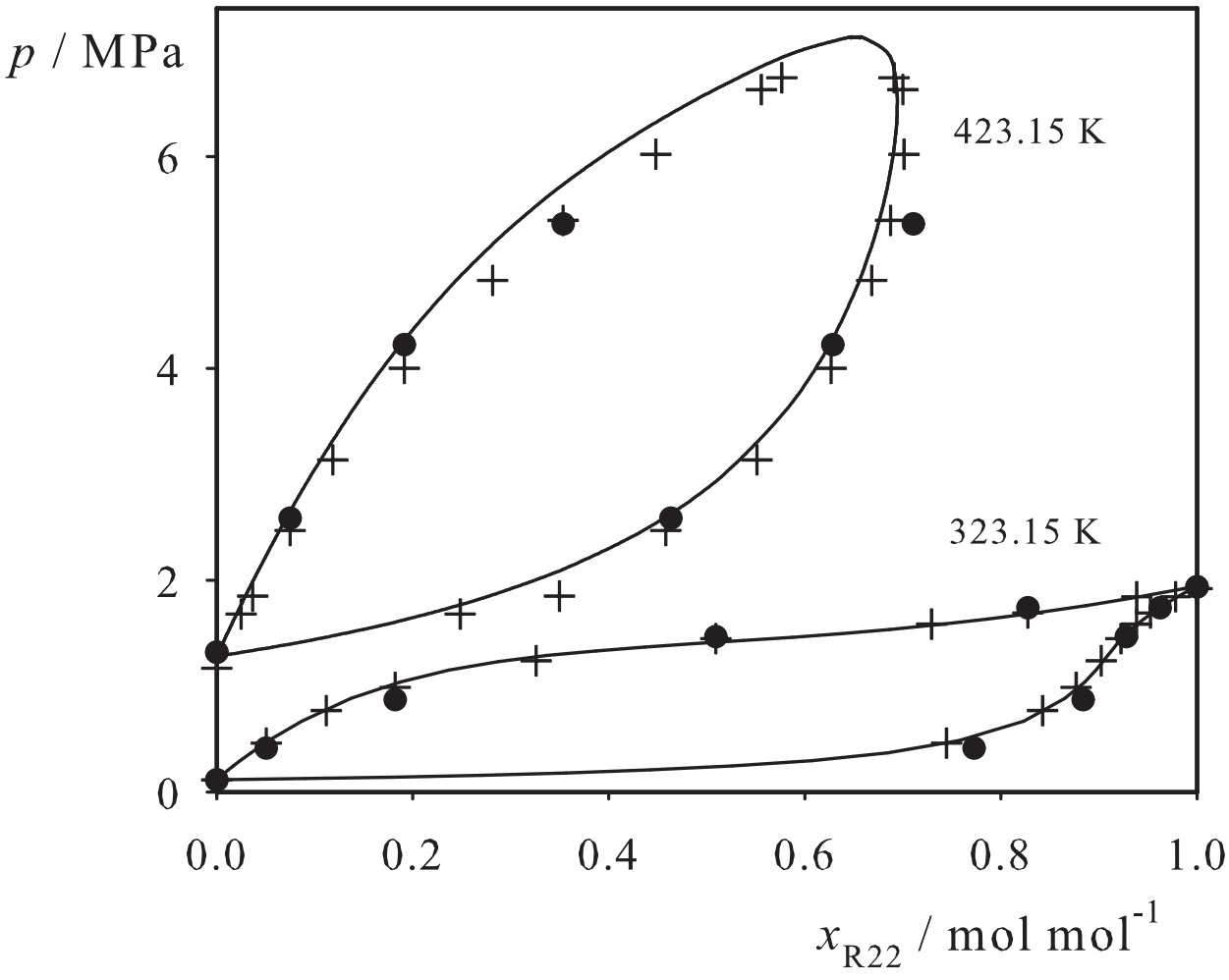

Fig. 13.

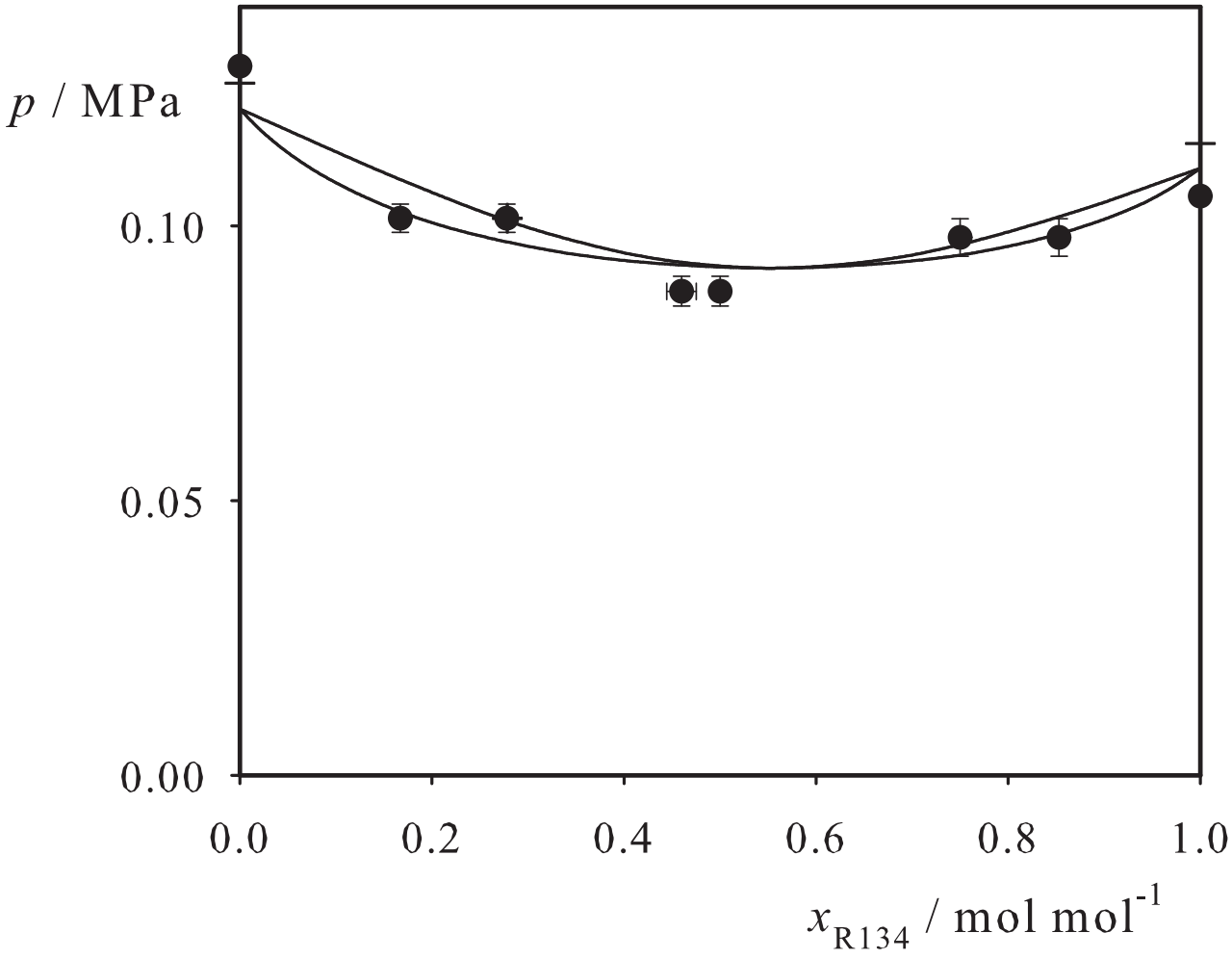

Fig. 14.

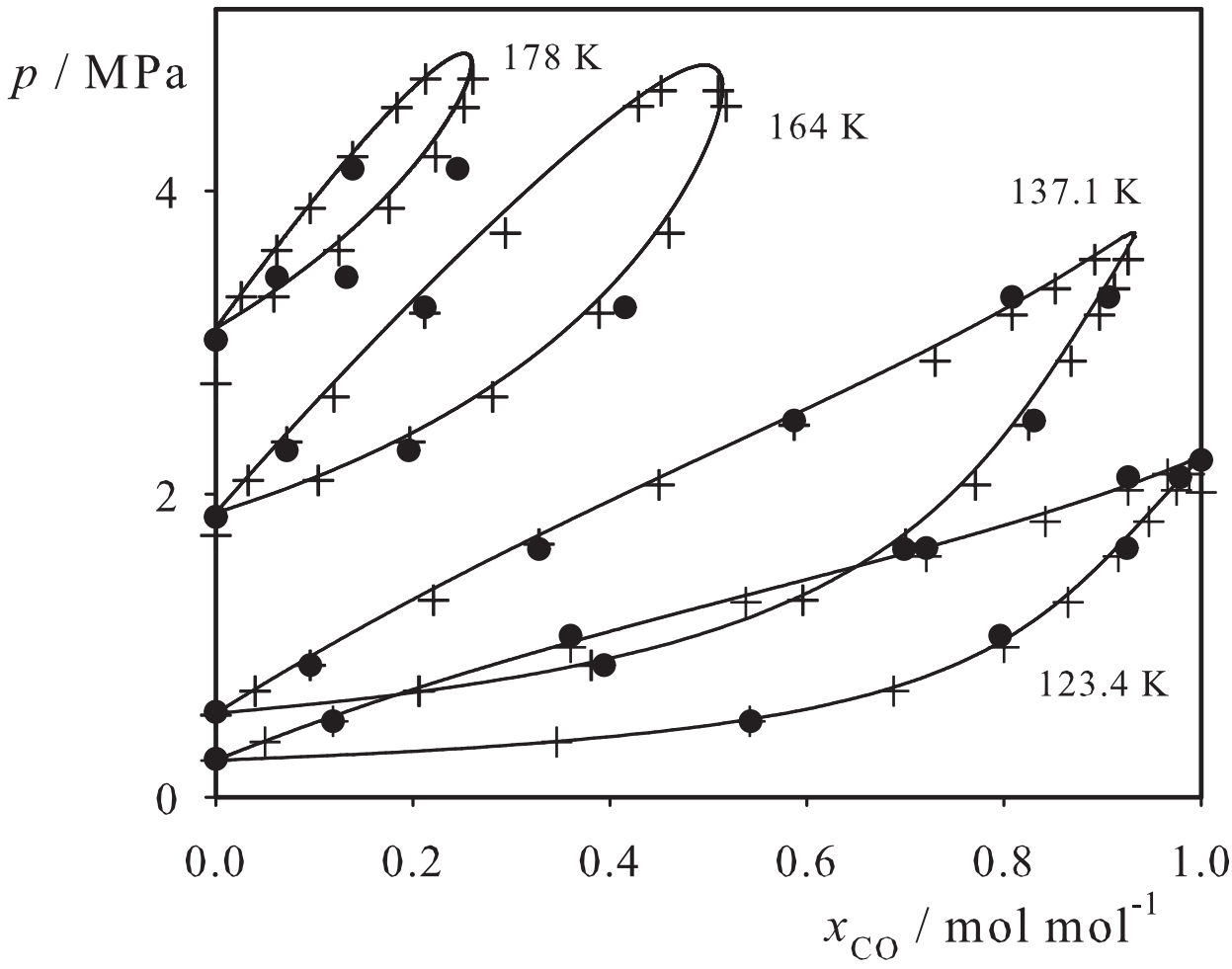

Fig. 15.

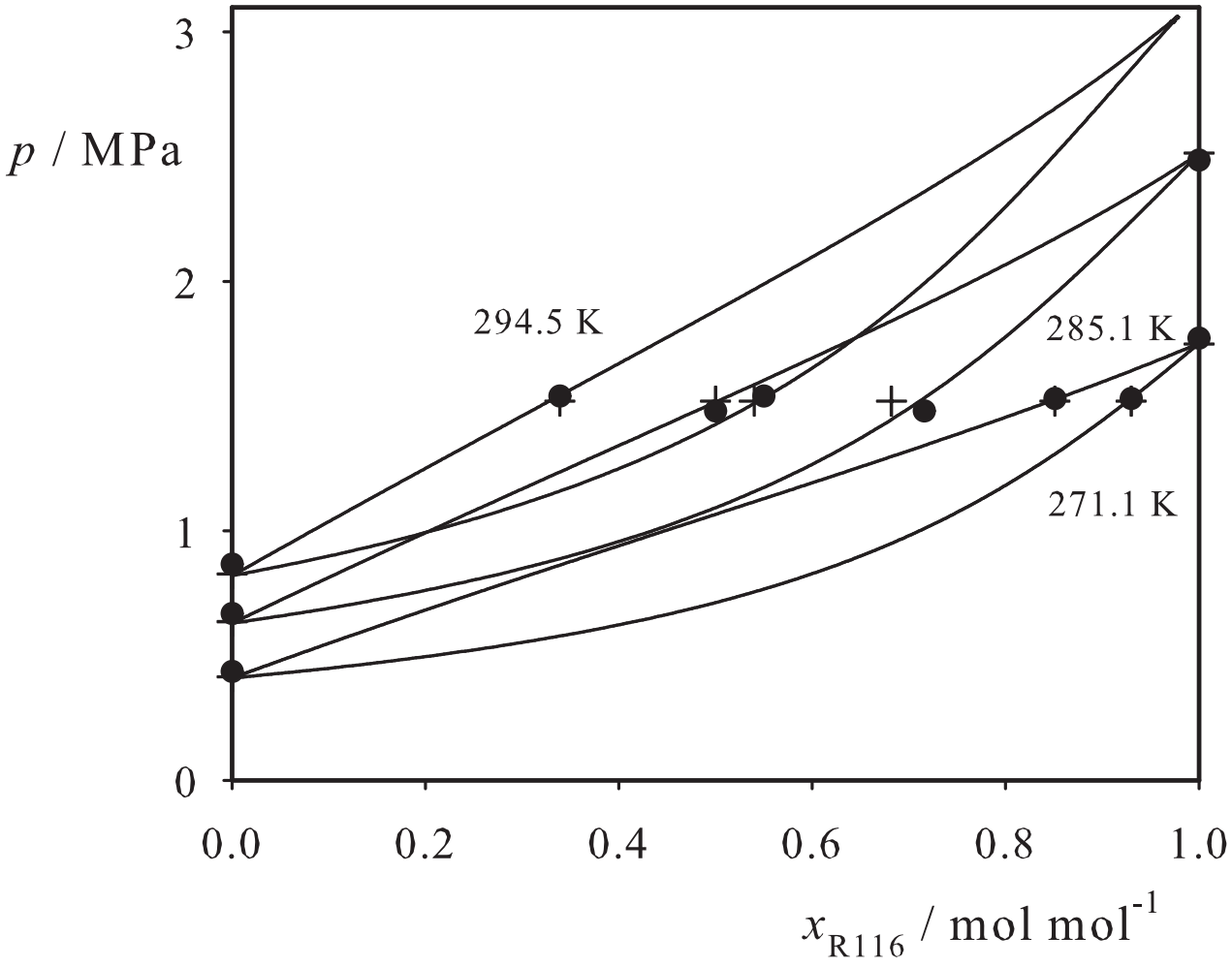

Fig. 16.

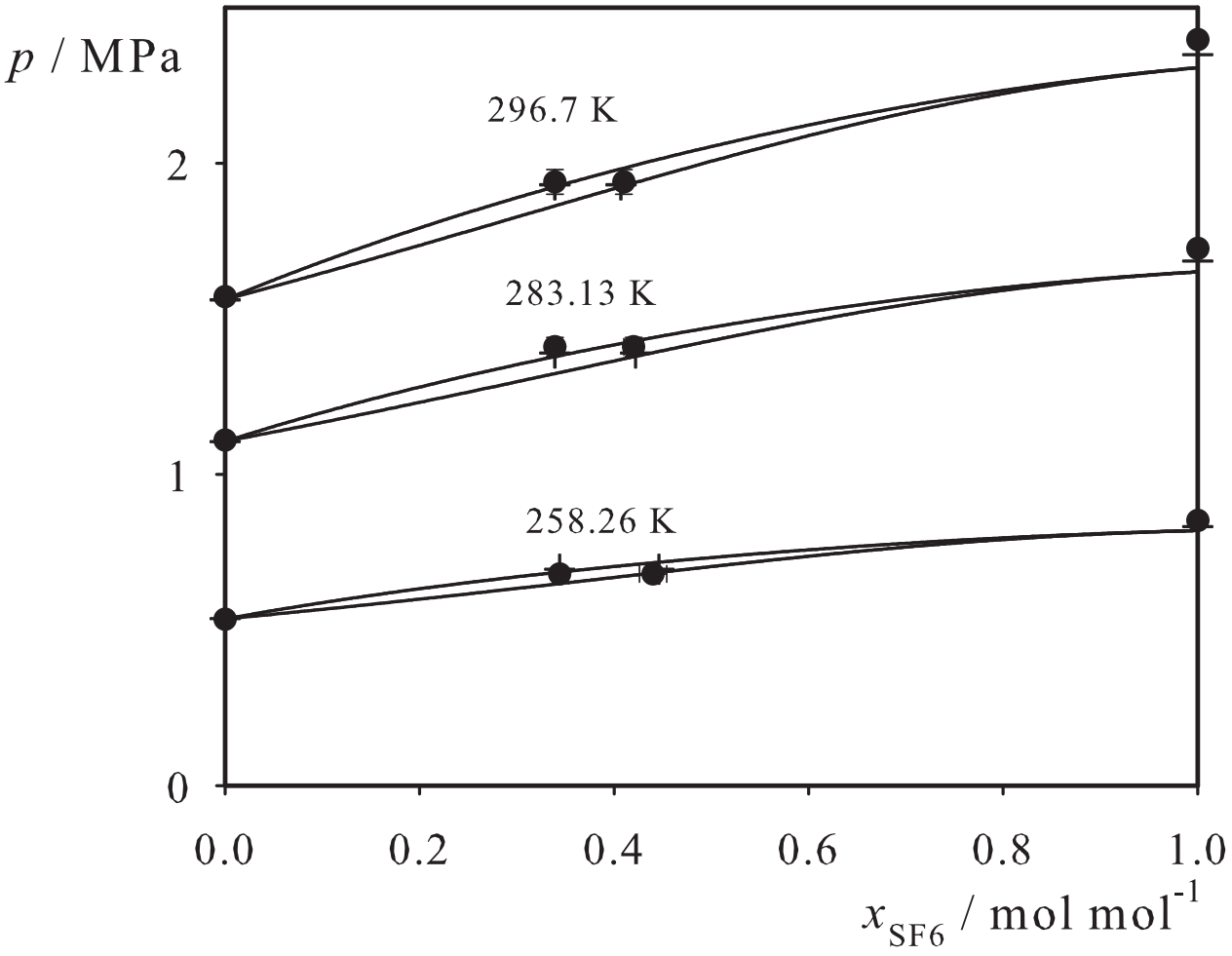

Fig. 17.

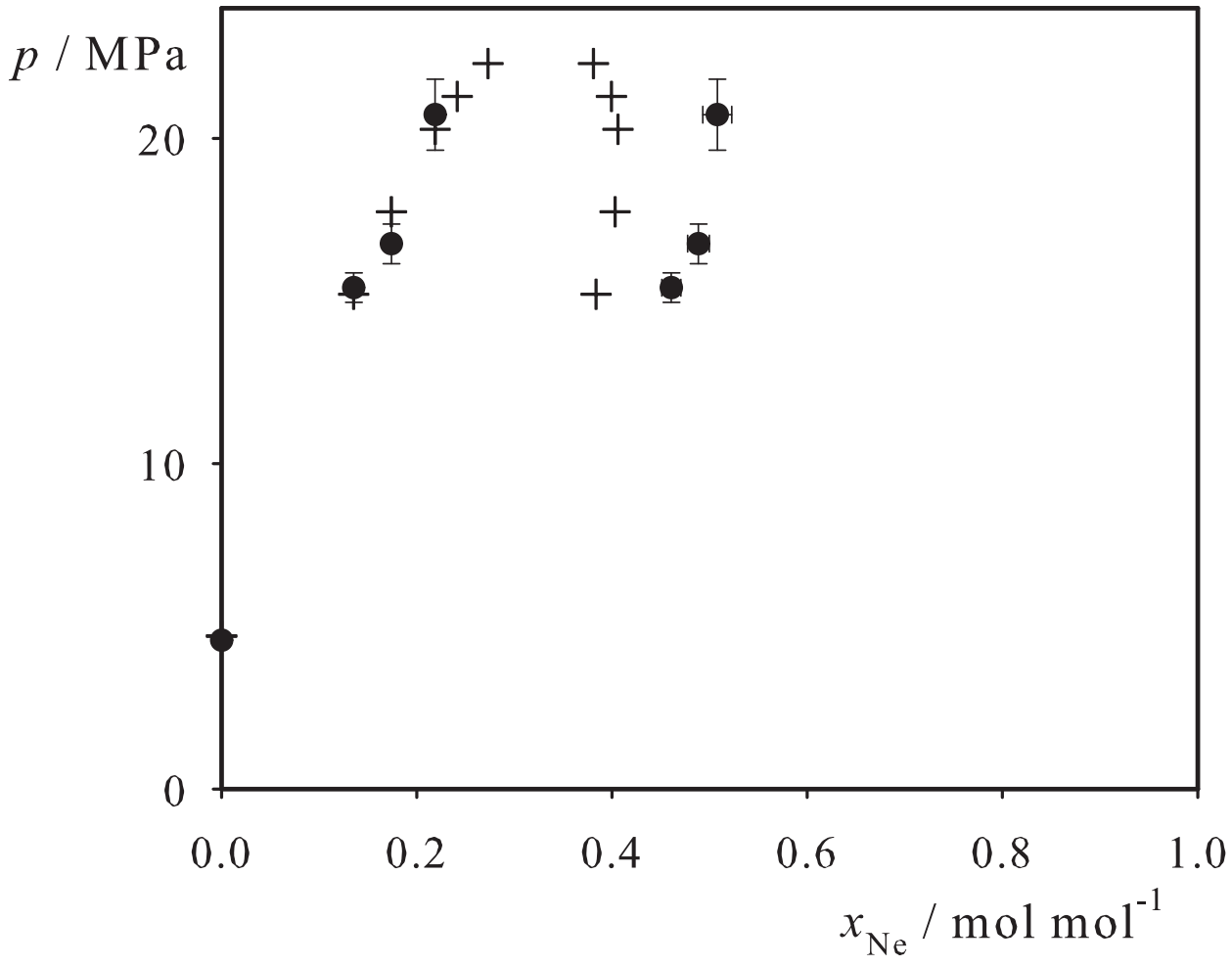

Fig. 18.

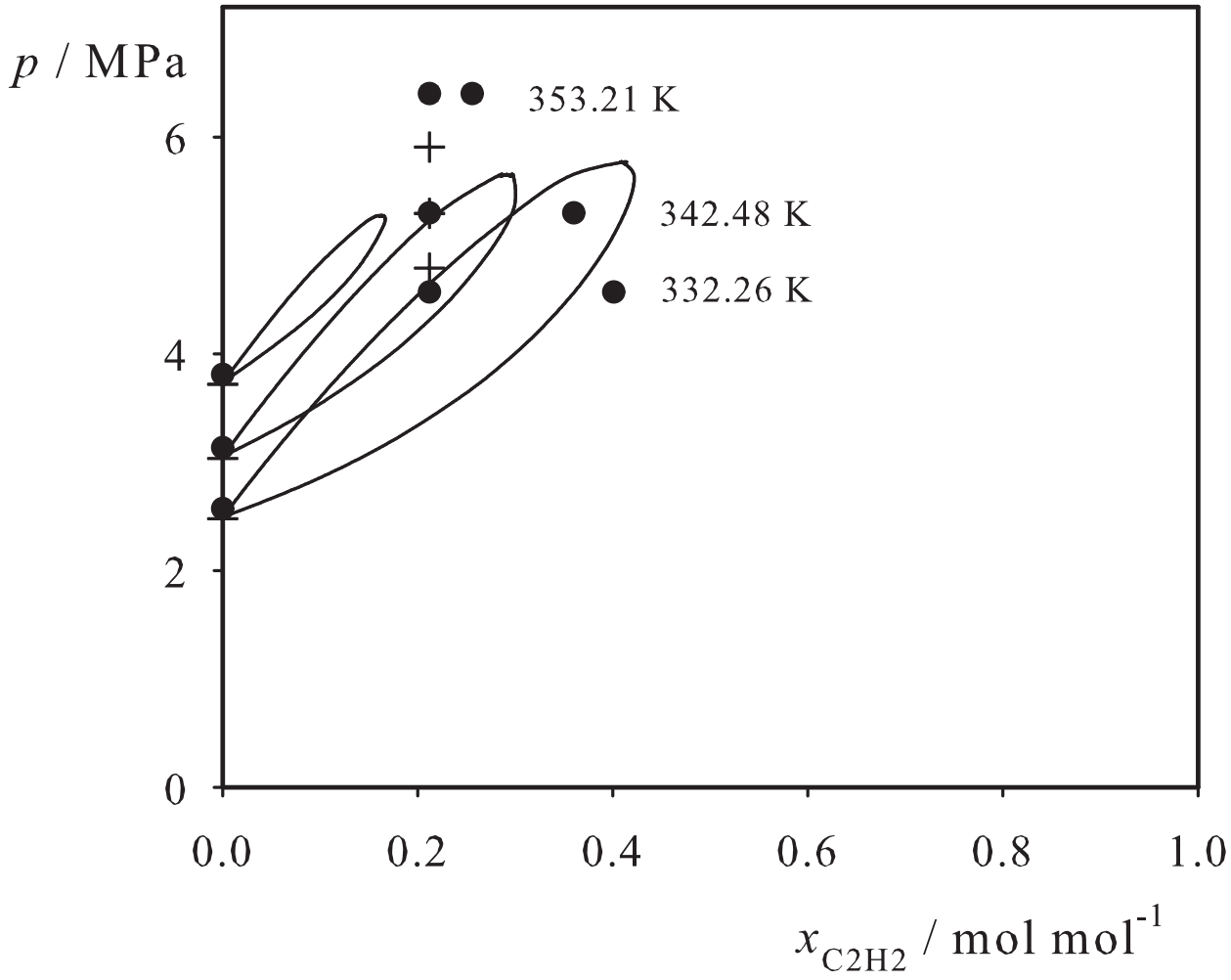
p / MPa
353.21 K
342.48 K
332.26 K
6
4
2
0
0.0
0.2
0.4
0.6
0.8
1.0
x C2H2 / mol mol-1

Fig. 19.

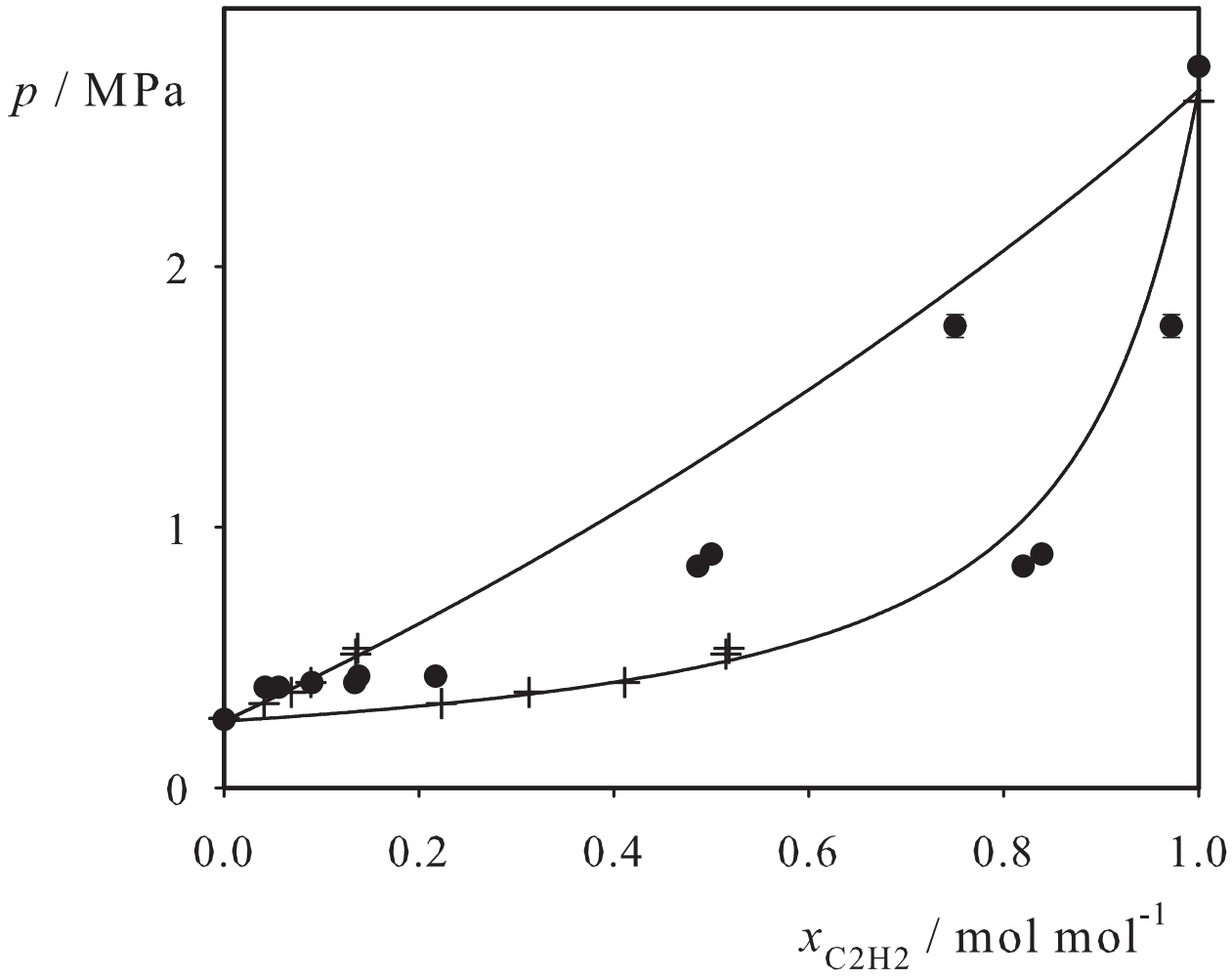

Fig. 20.

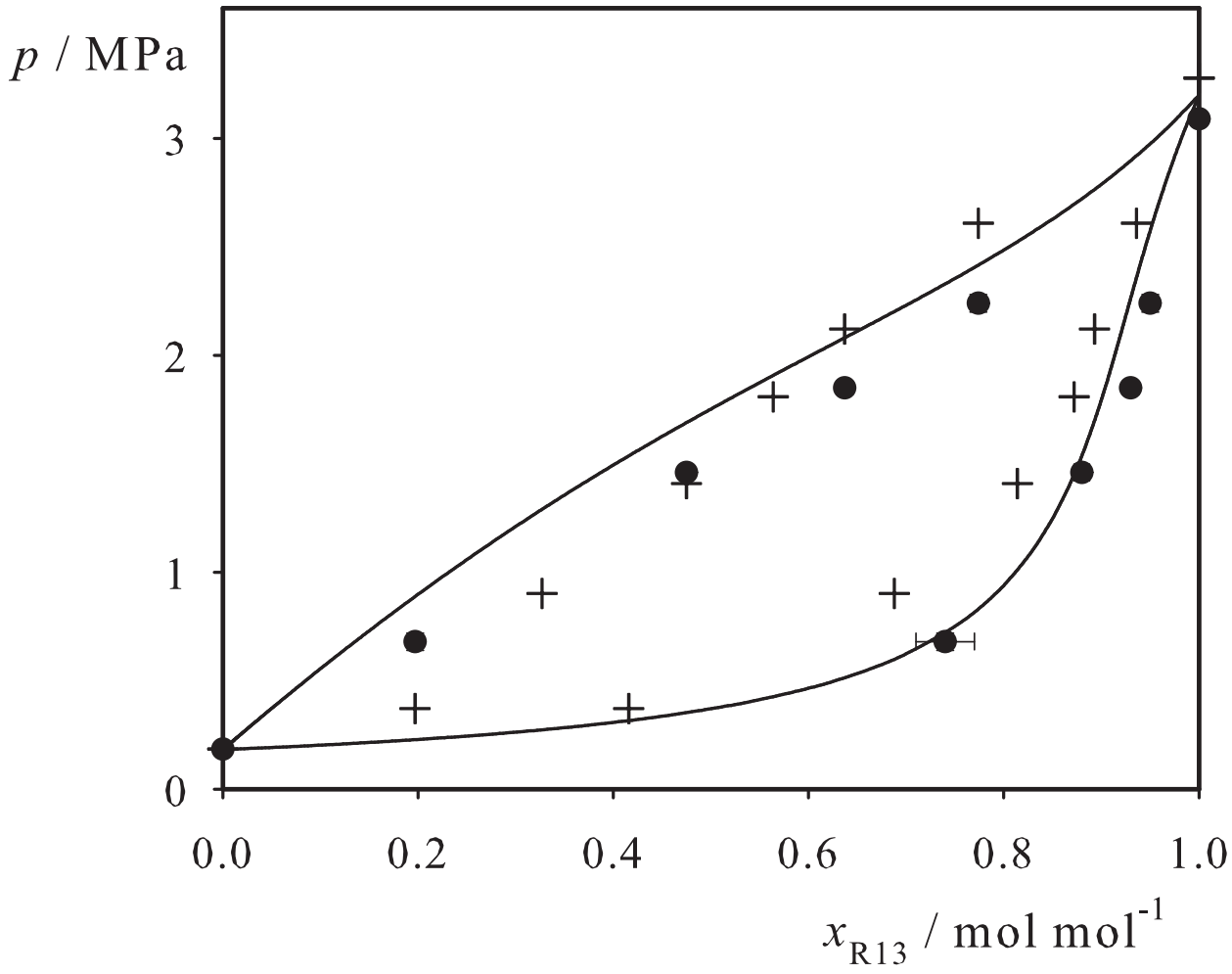

Fig. 21.

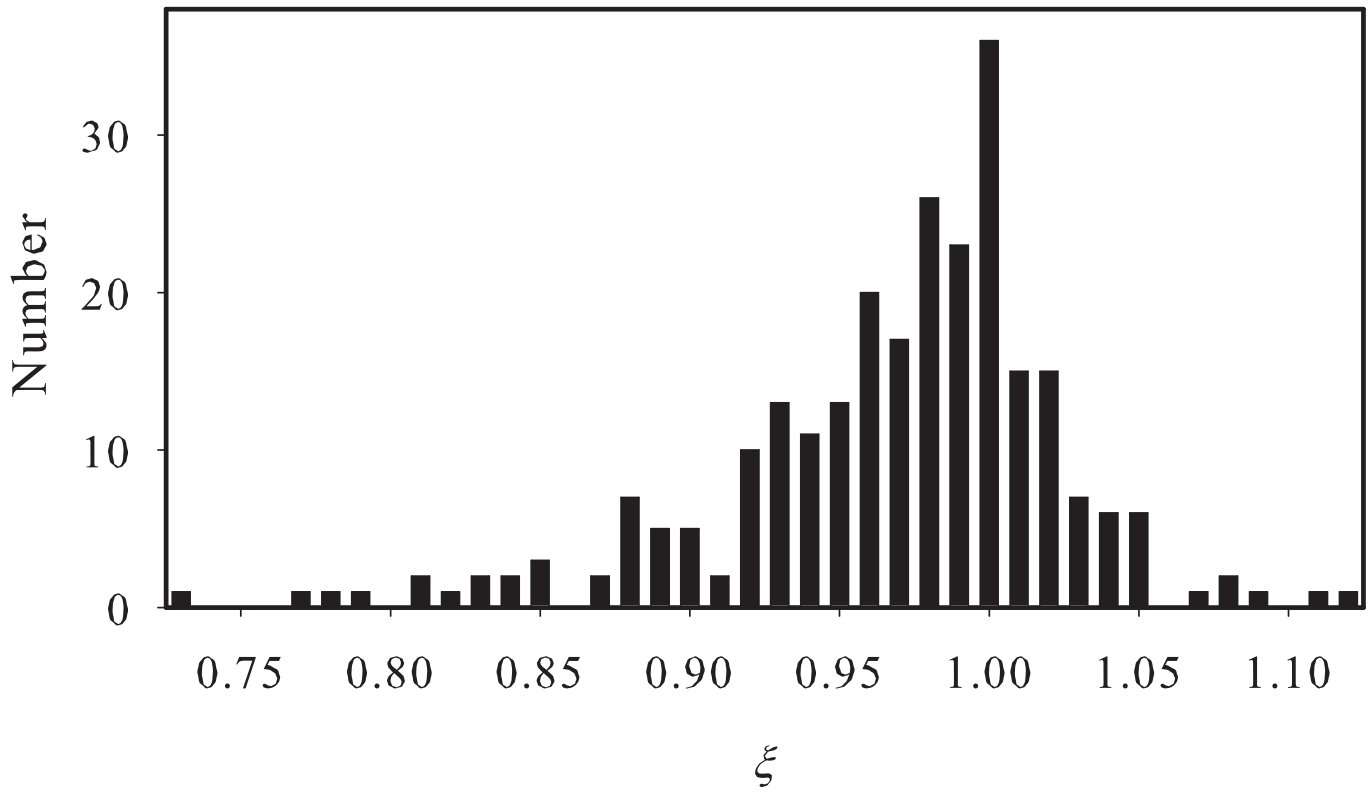

Supplementary Material to: Molecular models for 267 binary mixtures validated by vapor-liquid equilibria: a systematic approach

Jadran Vrabec * [1], Yow-lin Huang[1], Hans Hasse[2]

[1] Lehrstuhl für Thermodynamik und Energietechnik, Universität Paderborn, 33098 Paderborn, Germany

[2] Laboratory for Engineering Thermodynamics, University of Kaiserslautern, 67663 Kaiserslautern, Germany

* corresponding author, tel.: +49-5251/60-2422, fax: +49-5251/60-3522,
email: jadran.vrabec@upb.de

Table 1

List of the eight binary mixtures for which experimental VLE data is available on the dew line only.

Ne + C_2H_6 [1]	Xe + I_2 [2]	N_2 + R10 [4]	CO_2 + R10 [4]
Ne + C_2H_4 [1]	I_2 + CO_2 [3]	CO_2 + Kr [5]	R143a + R12B1 [6]

Table 2

List of the 11 binary mixtures for which experimental VLE data is available for dilute state points only.

Ar + R113 [7]	N_2 + CS_2 [8]	CO_2 + SF_6 [10]	SF_6 + R113 [11]
CH_4 + CS_2 [8]	N_2 + R113 [7]	CO_2 + R113 [7]	R13 + R10 [12]
CH_4 + R113 [7]	Cl_2 + R130a [9]	SF_6 + CS_2 [8]	

References

[1] M.J. Hiza, A.G. Duncan, Adv. Cryog. Eng. 15 (1969) 42-45.

[2] H. Destaillats, R. Fernández Prini, J. Chem. Thermodyn. 29 (1997) 1209-1221.

[3] R.B. Fang, S.H. Zhang, W.H. Zhang, Chem. J. Chin. Univ. (Changchun) 18 (1997) 869-872.

[4] J.M. Prausnitz, P.R. Benson, AIChE J. 5 (1959) 161-164.

[5] N.V. Kuskova, V.F. Kukarin, V.G. Martynets, E.V. Matizen, J. Chem. Thermodyn. 23 (1991) 523-530.

[6] I.V. Volobuev, V.I. Los, L.V. Los, M.G. Khmelnyuk, Kholod. Tekh. Tekhnol. 39 (1984) 65-67.

[7] H. Hiraoka, J.H. Hildebrand,
J. Phys. Chem. 68 (1964) 213-218.

[8] Y. Kobatake, J.H. Hildebrand,
J. Phys. Chem. 65 (1961) 331-334.

[9] O.V. Efstigneev, M.B. Santimova, S.G. Dunaev, S.B. Levanova, Khim. Prom. 6 (1985) 342-343.

[10] L.A. Makarevich, E.S. Sokolova,
Termodin. Termokhim. Konstanty (1970) 120-124.

[11] H. Jaster, P.G. Kosky, J. Chem. Eng. Data 21 (1976) 66-71.

[12] E. Wilhelm, R. Battino, J. Chem. Thermodyn. 3 (1971) 379-392.

Fig. 1. Binary vapor-liquid equilibrium phase diagram: simulation data ●, experimental data + (cf. Table 2 of the manuscript for the reference) and Peng-Robinson equation of state —.

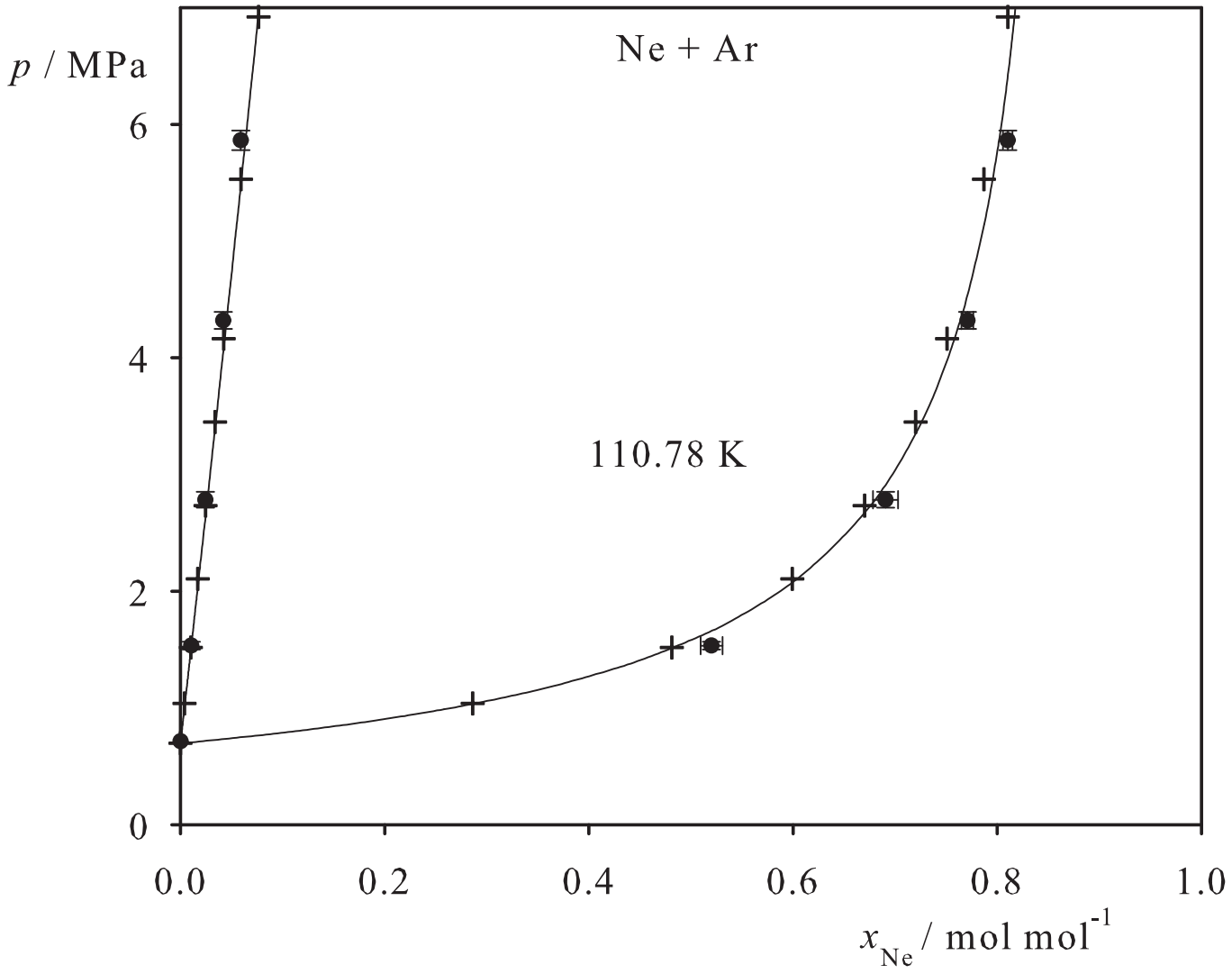

Fig. 2. Binary vapor-liquid equilibrium phase diagram: simulation data ●, experimental data + (cf. Table 2 of the manuscript for the reference) and Peng-Robinson equation of state —.

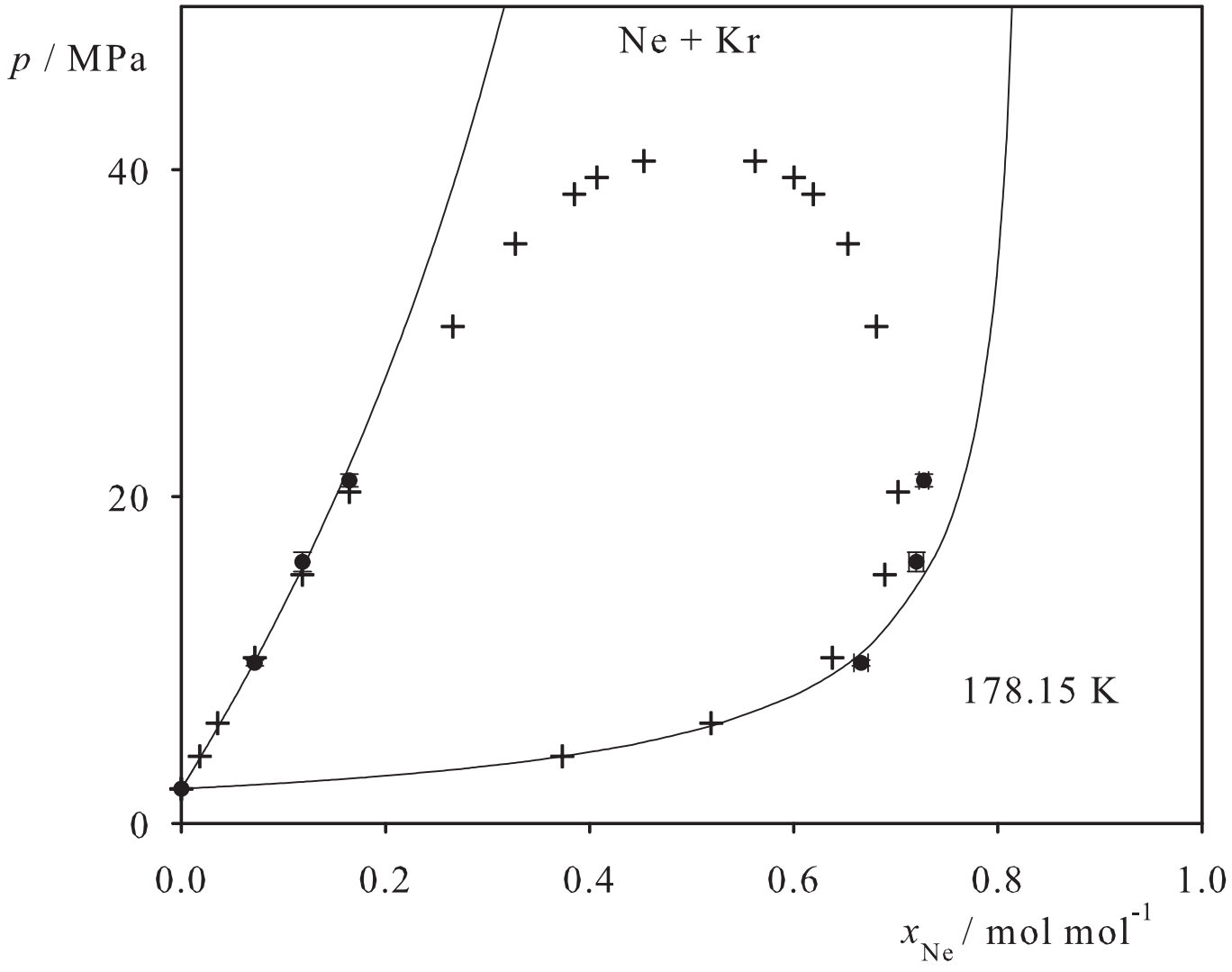

Fig. 3. Binary vapor-liquid equilibrium phase diagram: simulation data ●, experimental data + (cf. Table 2 of the manuscript for the reference) and Peng-Robinson equation of state —.

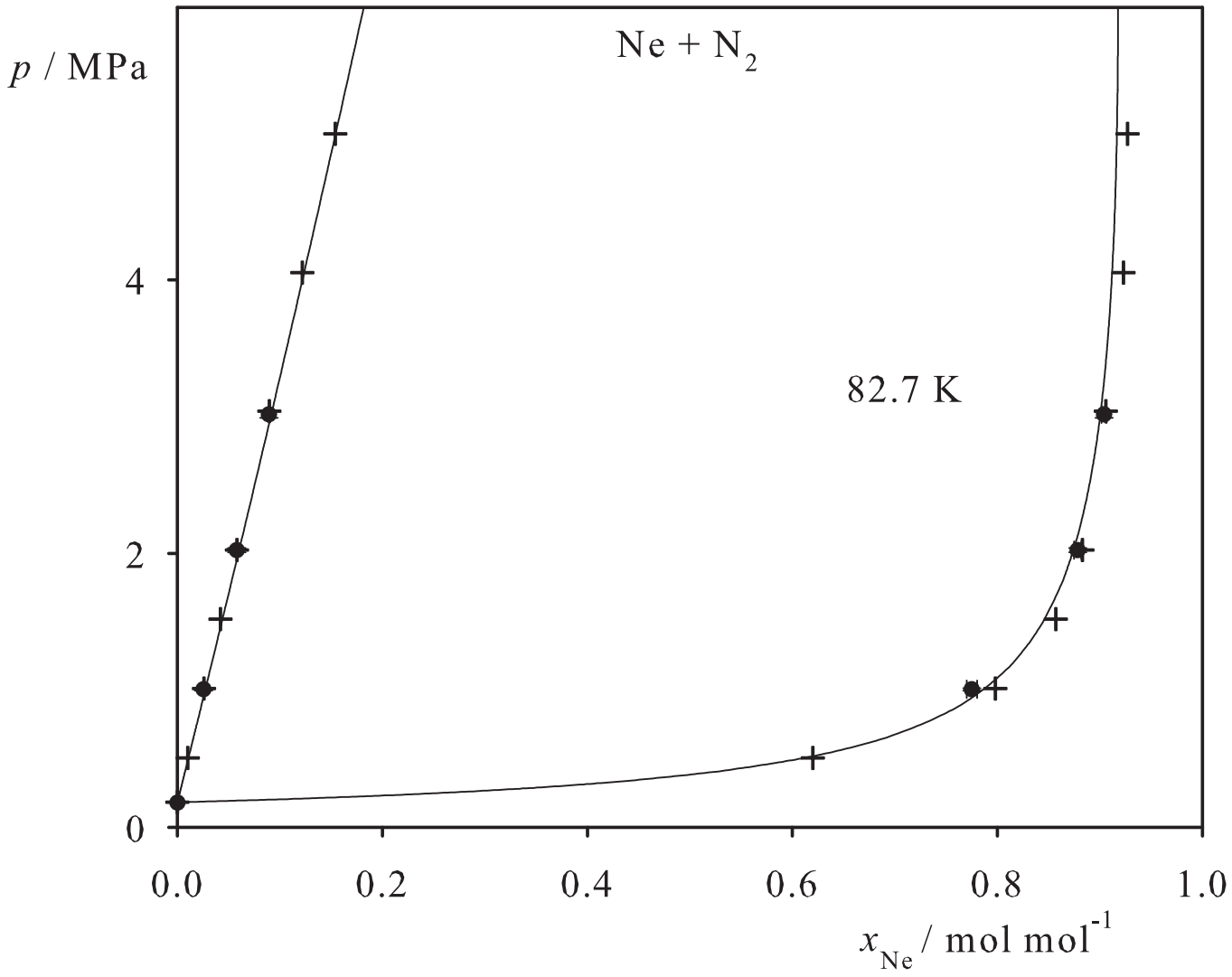

Fig. 4. Binary vapor-liquid equilibrium phase diagram: simulation data ●, experimental data + (cf. Table 2 of the manuscript for the reference) and Peng-Robinson equation of state —.

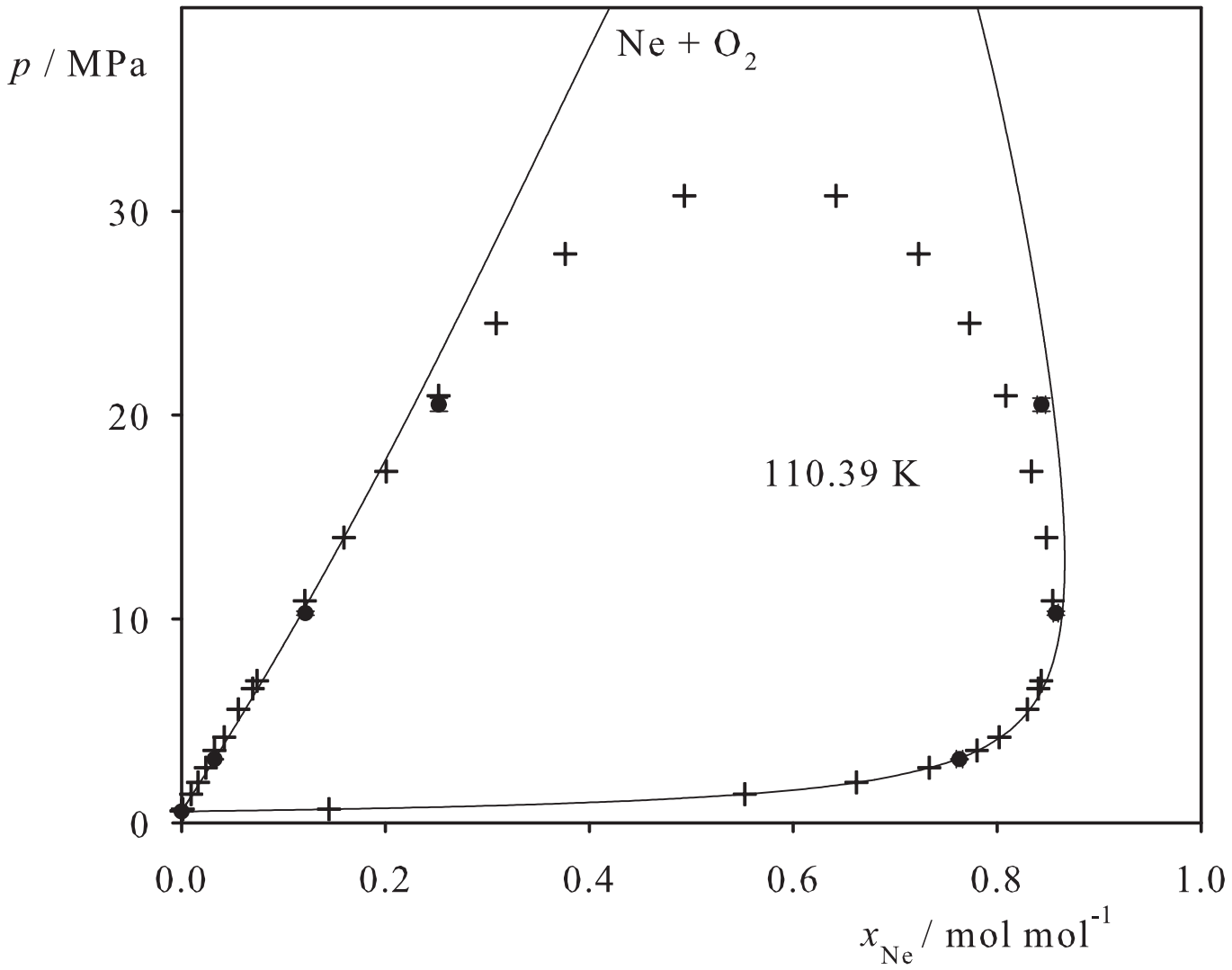

Fig. 5. Binary vapor-liquid equilibrium phase diagram: simulation data ●, experimental data + (cf. Table 2 of the manuscript for the reference) and Peng-Robinson equation of state —.

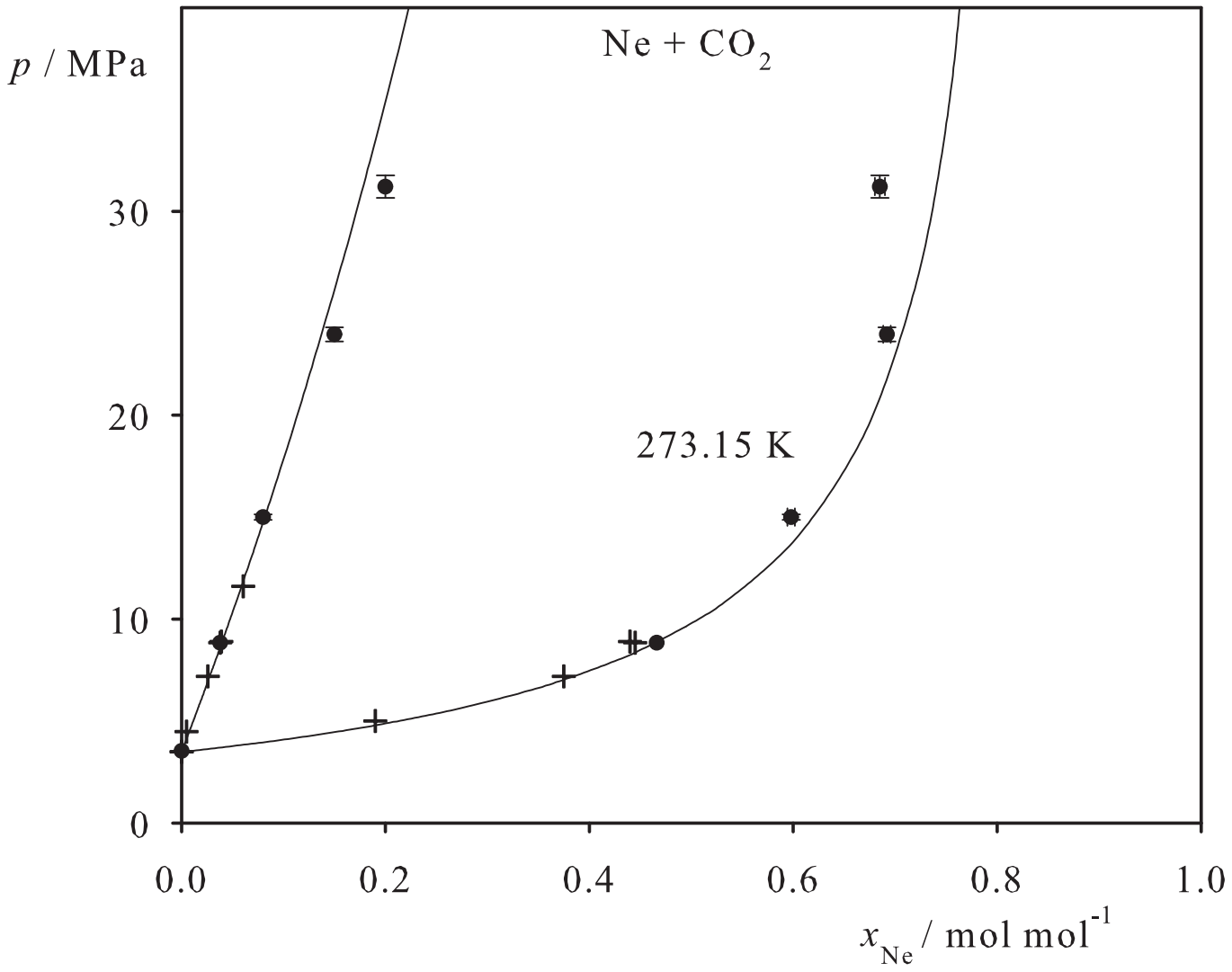

Fig. 6. Binary vapor-liquid equilibrium phase diagram: simulation data ●, experimental data + (cf. Table 2 of the manuscript for the reference) and Peng-Robinson equation of state —.

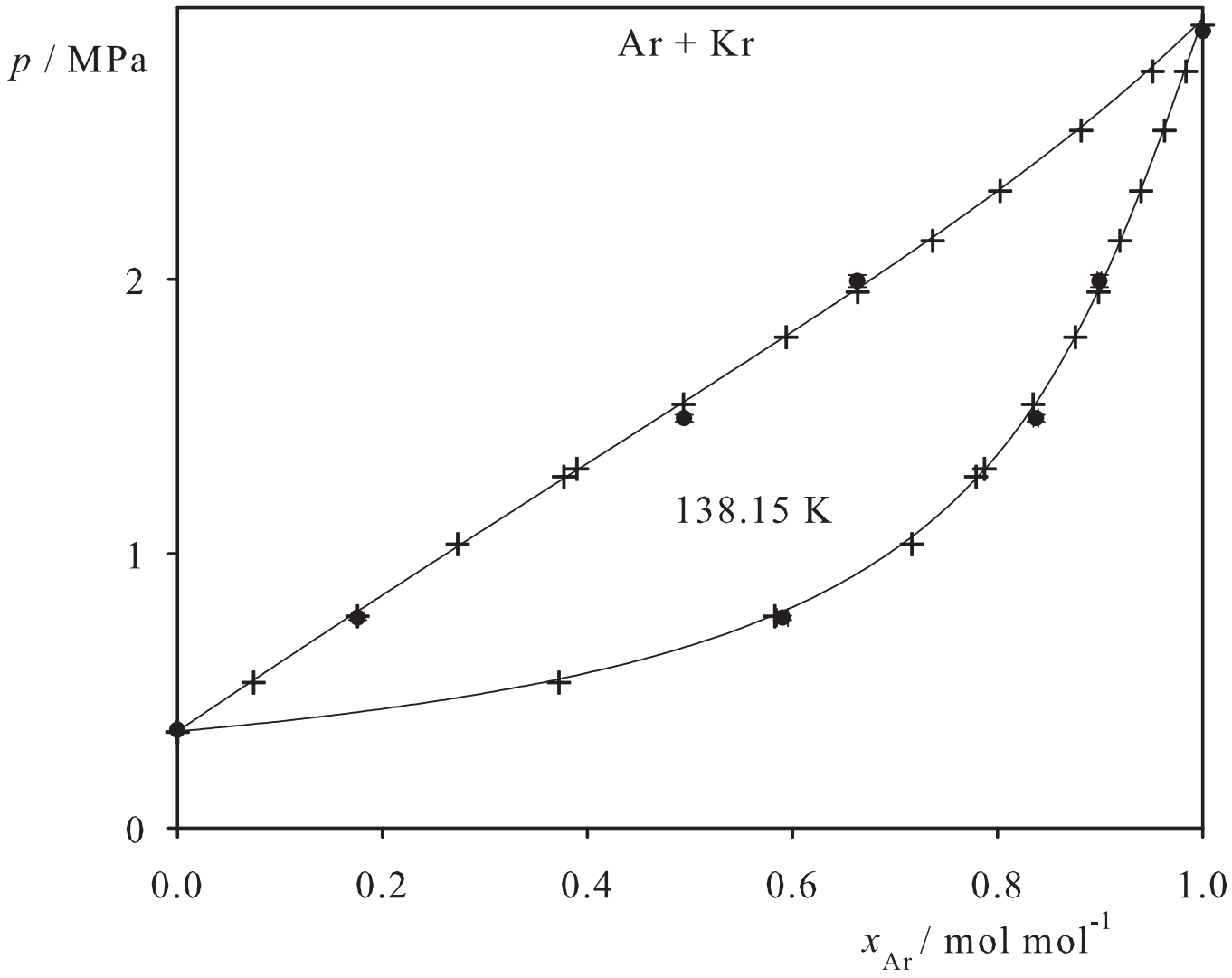

Fig. 7. Binary vapor-liquid equilibrium phase diagram: simulation data ●, experimental data + (cf. Table 2 of the manuscript for the reference) and Peng-Robinson equation of state —.

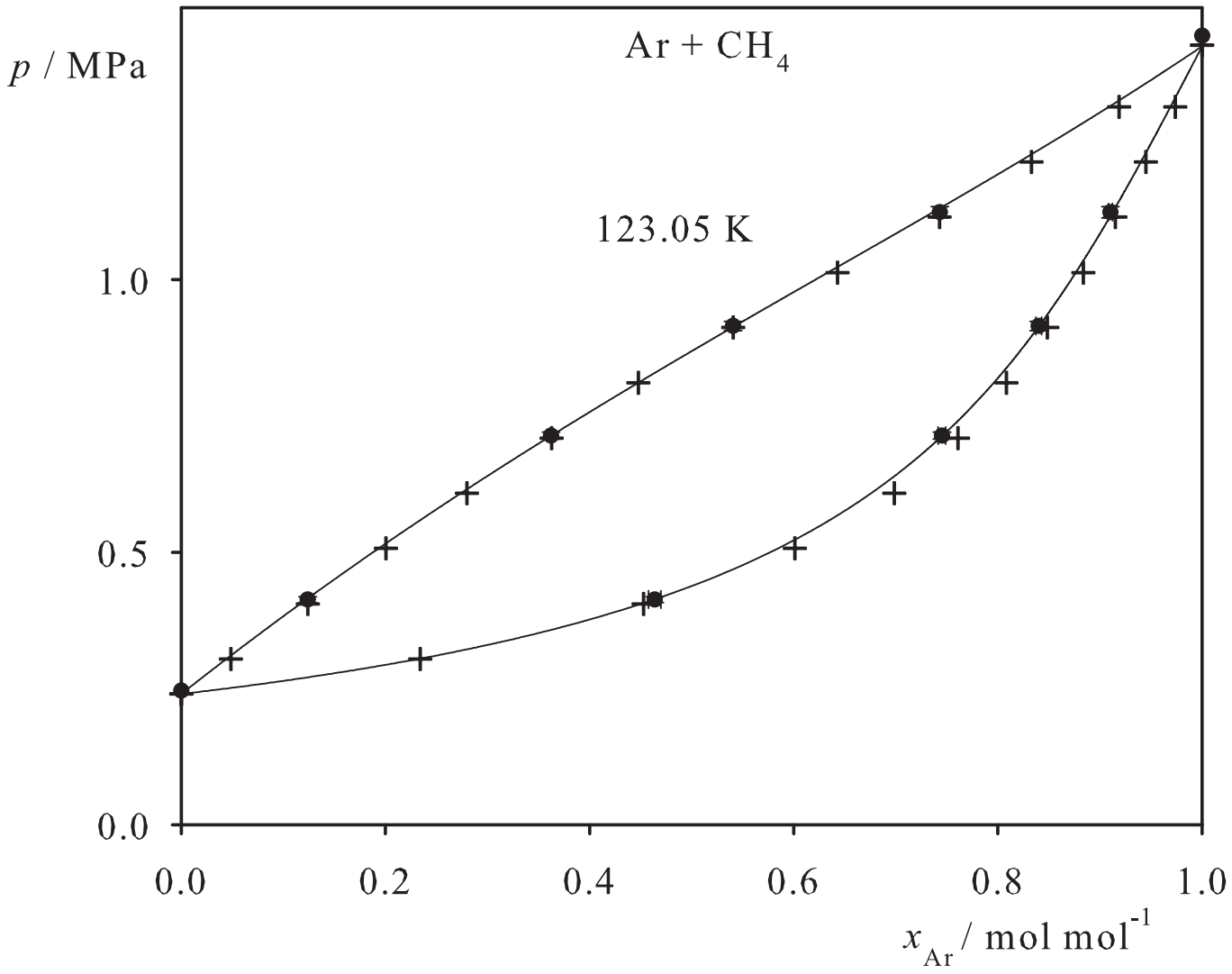

Fig. 8. Binary vapor-liquid equilibrium phase diagram: simulation data ●, experimental data + (cf. Table 2 of the manuscript for the reference) and Peng-Robinson equation of state —.

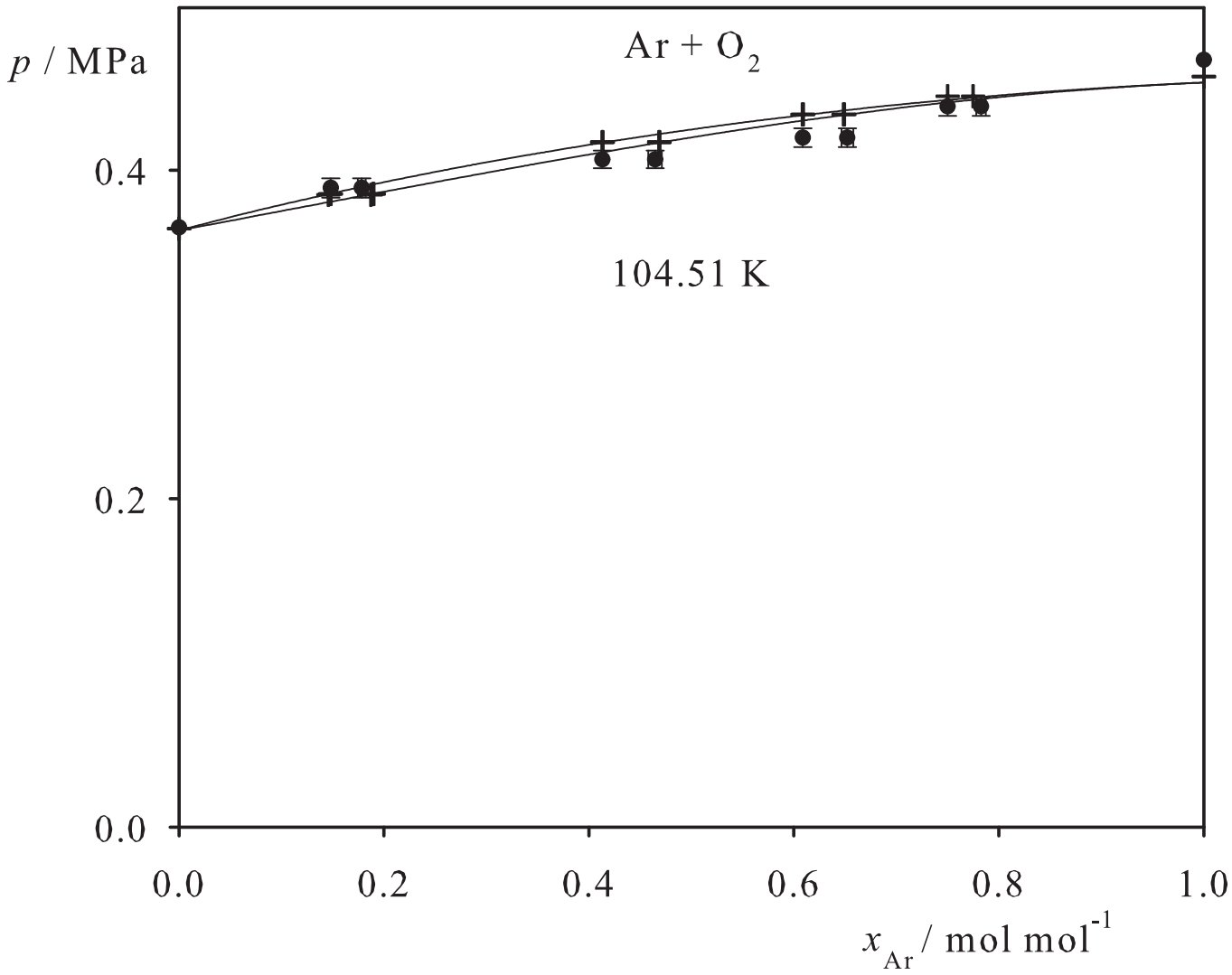

Fig. 9. Binary vapor-liquid equilibrium phase diagram: simulation data ●, experimental data + (cf. Table 2 of the manuscript for the reference) and Peng-Robinson equation of state —.

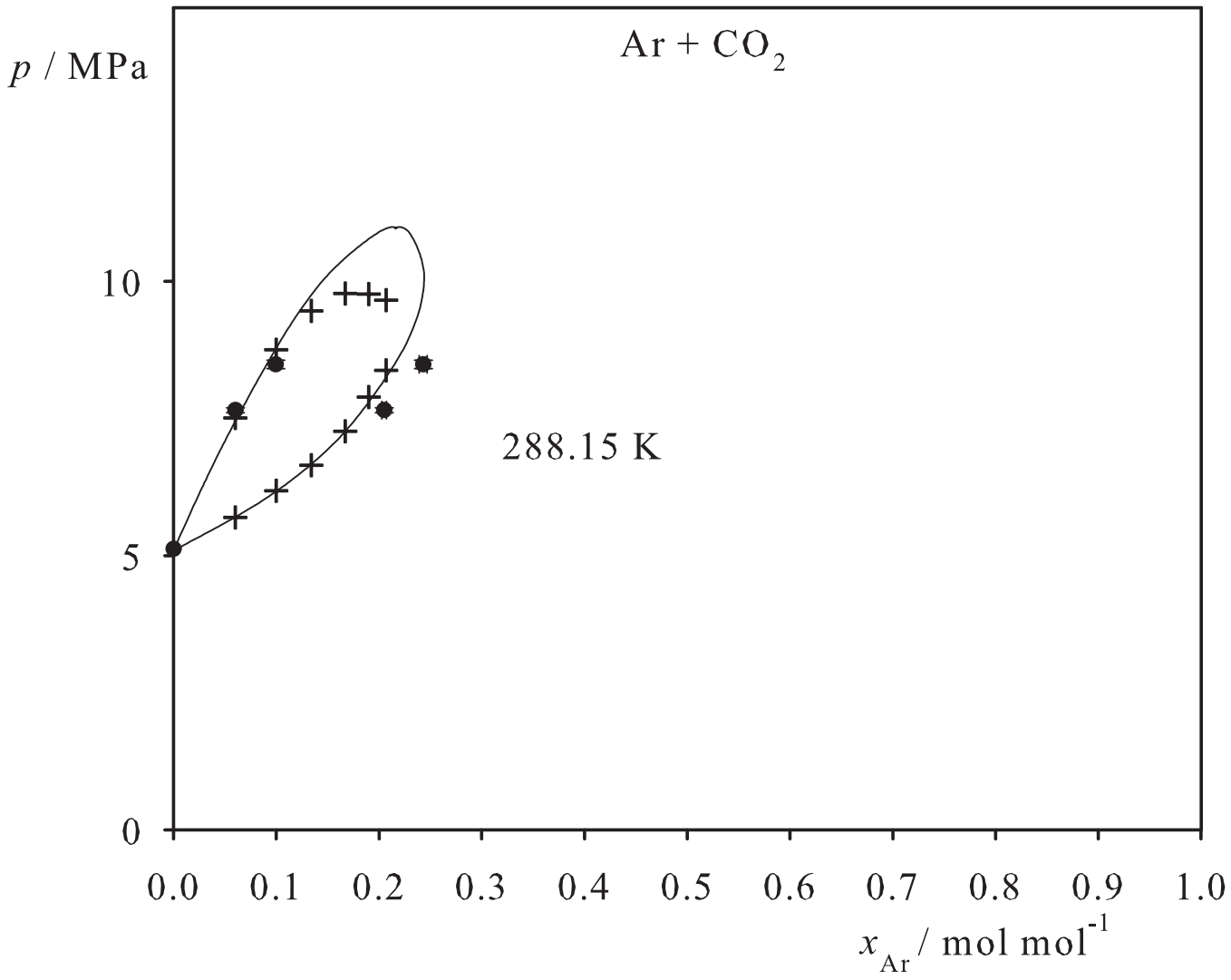

Fig. 10. Binary vapor-liquid equilibrium phase diagram: simulation data ●, experimental data + (cf. Table 2 of the manuscript for the reference) and Peng-Robinson equation of state —.

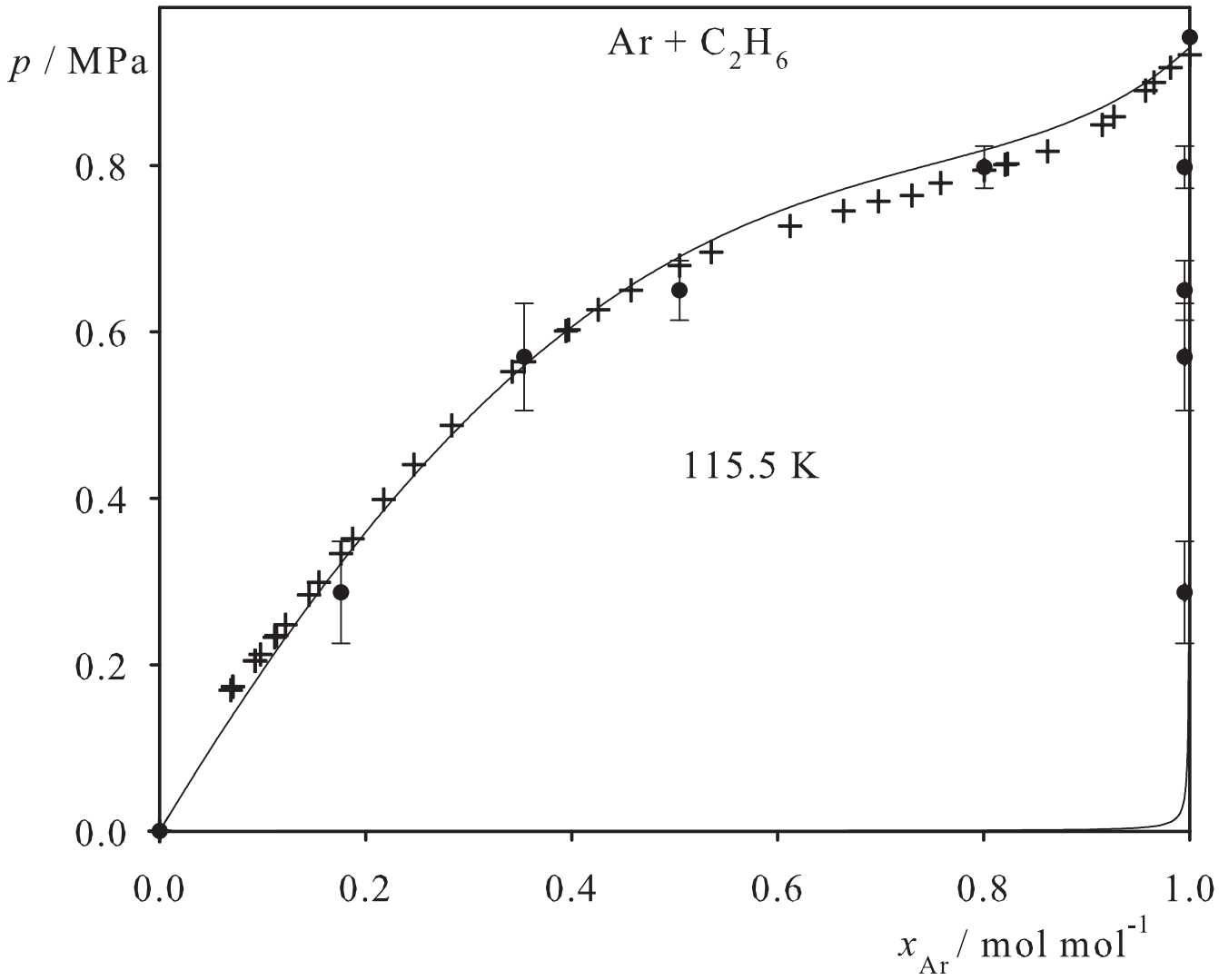

Fig. 11. Binary vapor-liquid equilibrium phase diagram: simulation data ●, experimental data + (cf. Table 2 of the manuscript for the reference) and Peng-Robinson equation of state —.

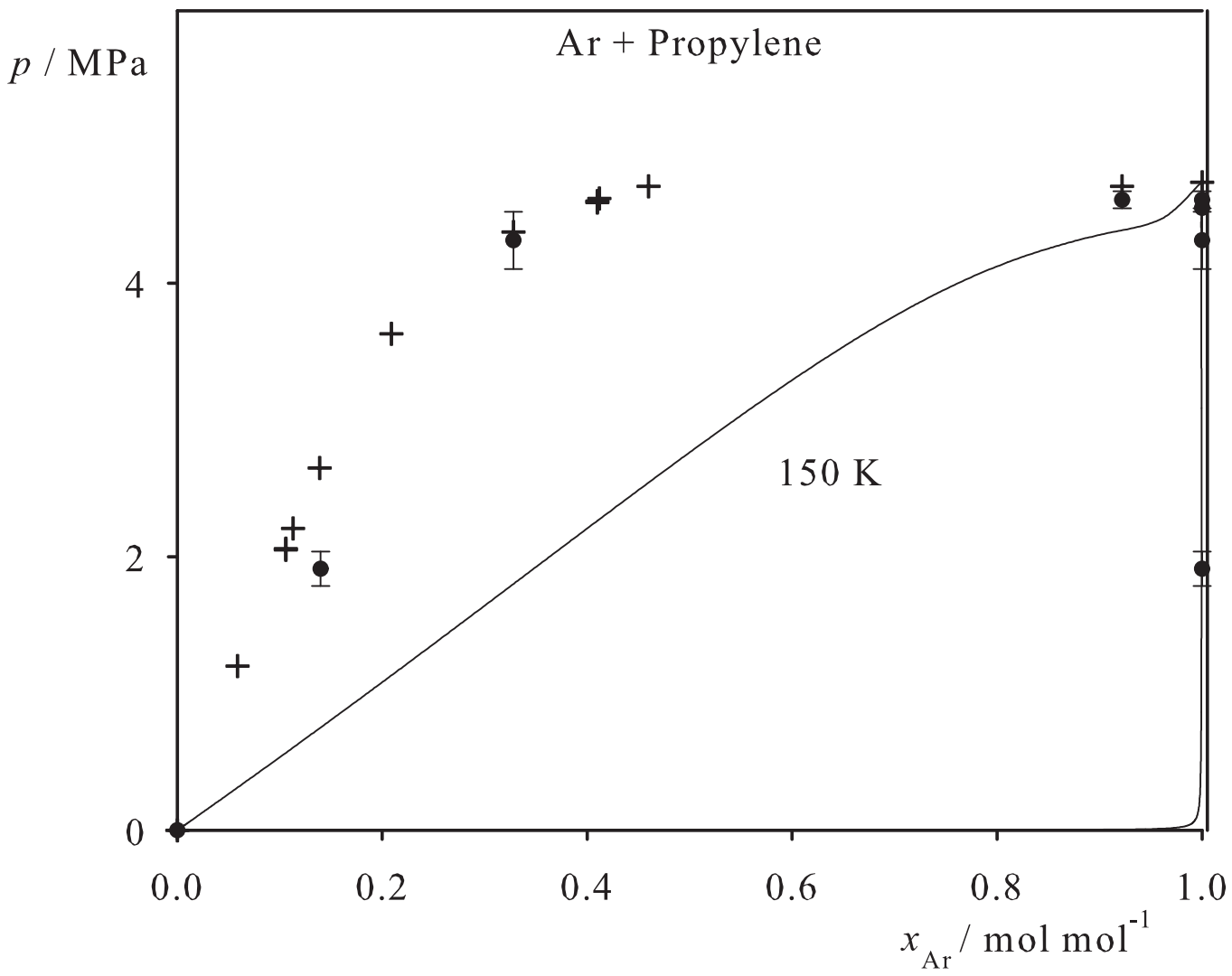

Fig. 12. Binary vapor-liquid equilibrium phase diagram: simulation data ●, experimental data + (cf. Table 2 of the manuscript for the reference) and Peng-Robinson equation of state —.

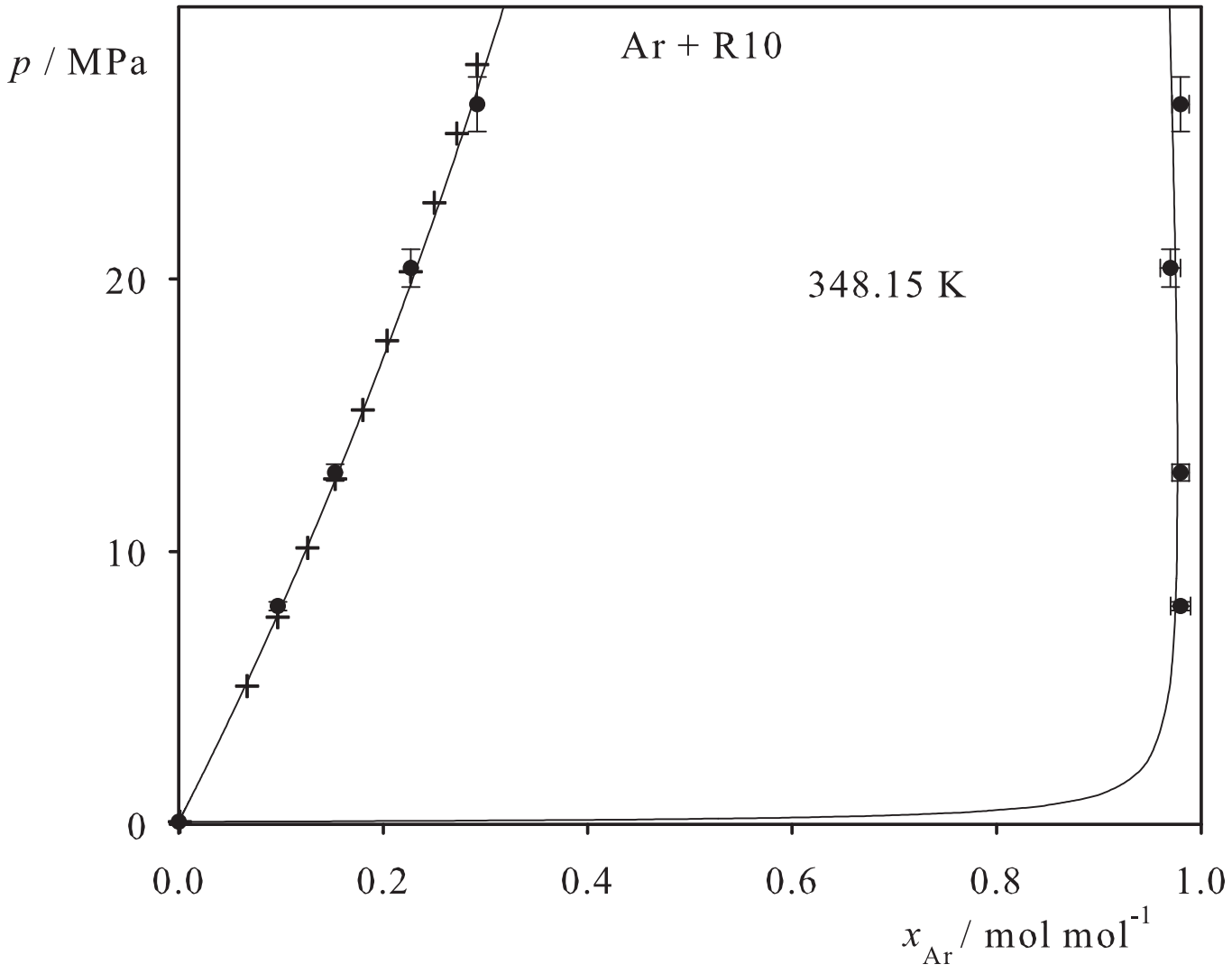

Fig. 13. Binary vapor-liquid equilibrium phase diagram: simulation data ●, experimental data + (cf. Table 2 of the manuscript for the reference) and Peng-Robinson equation of state —.

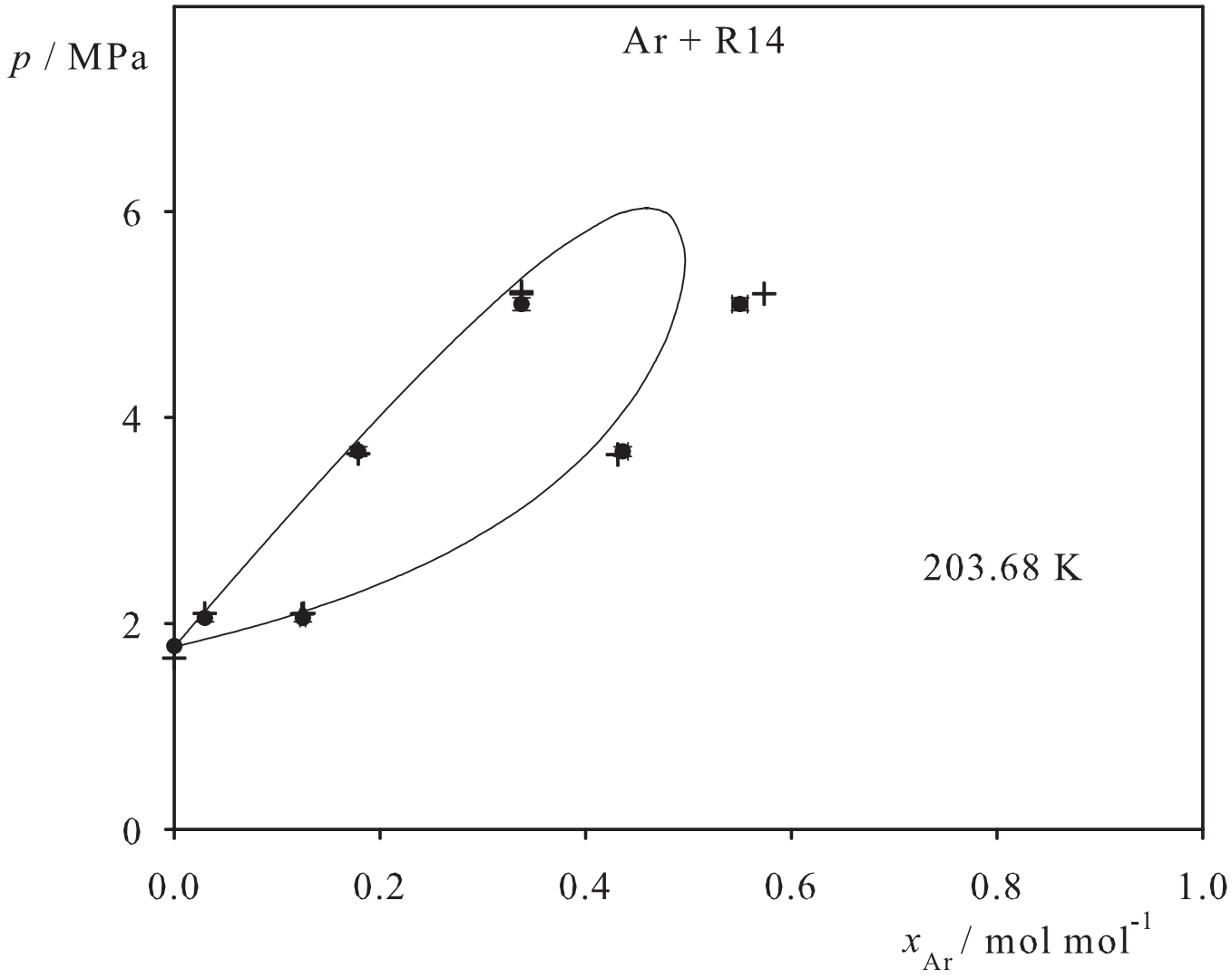

Fig. 14. Binary vapor-liquid equilibrium phase diagram: simulation data ●, experimental data + (cf. Table 2 of the manuscript for the reference) and Peng-Robinson equation of state —.

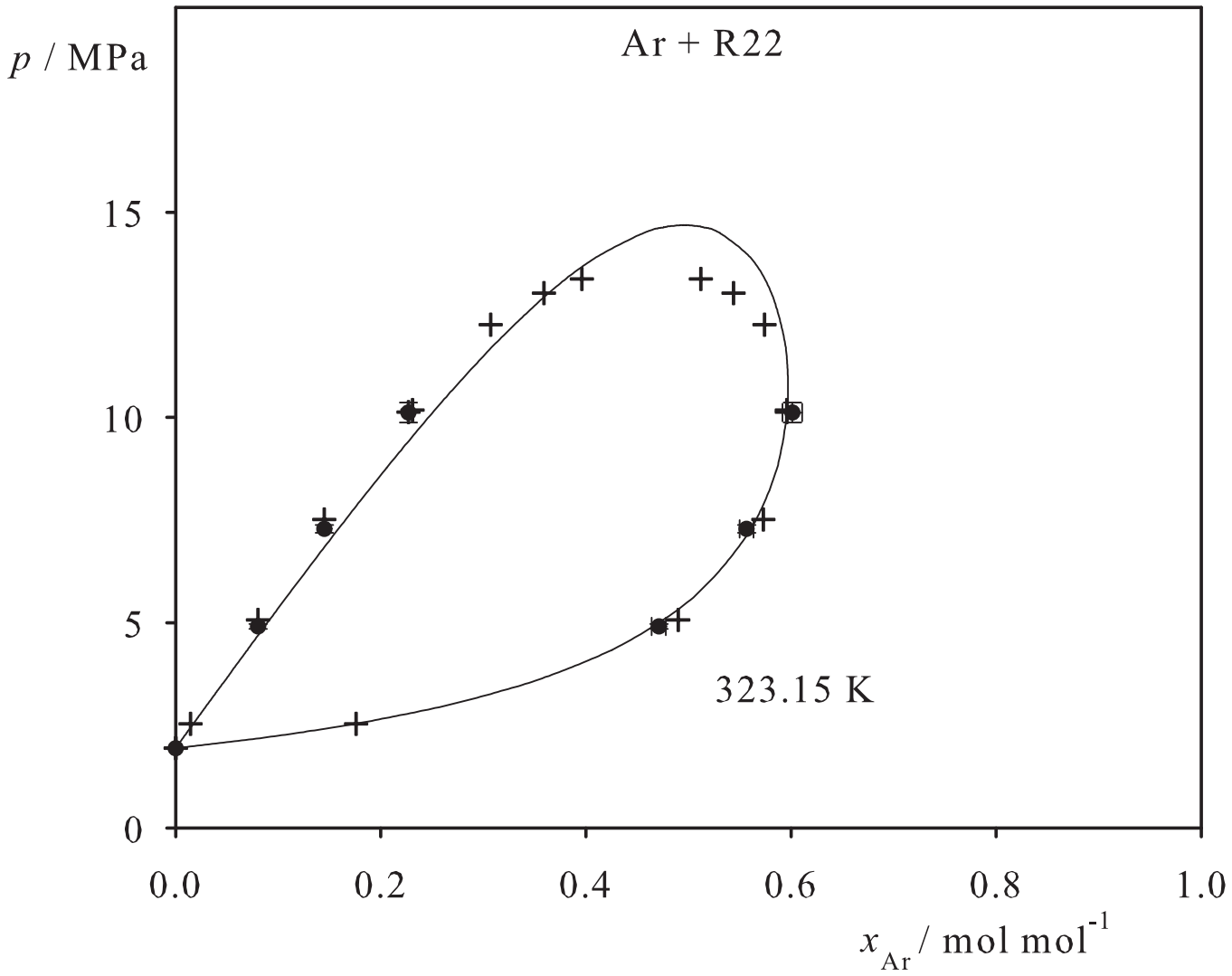

Fig. 15. Binary vapor-liquid equilibrium phase diagram: simulation data ●, experimental data + (cf. Table 2 of the manuscript for the reference) and Peng-Robinson equation of state —.

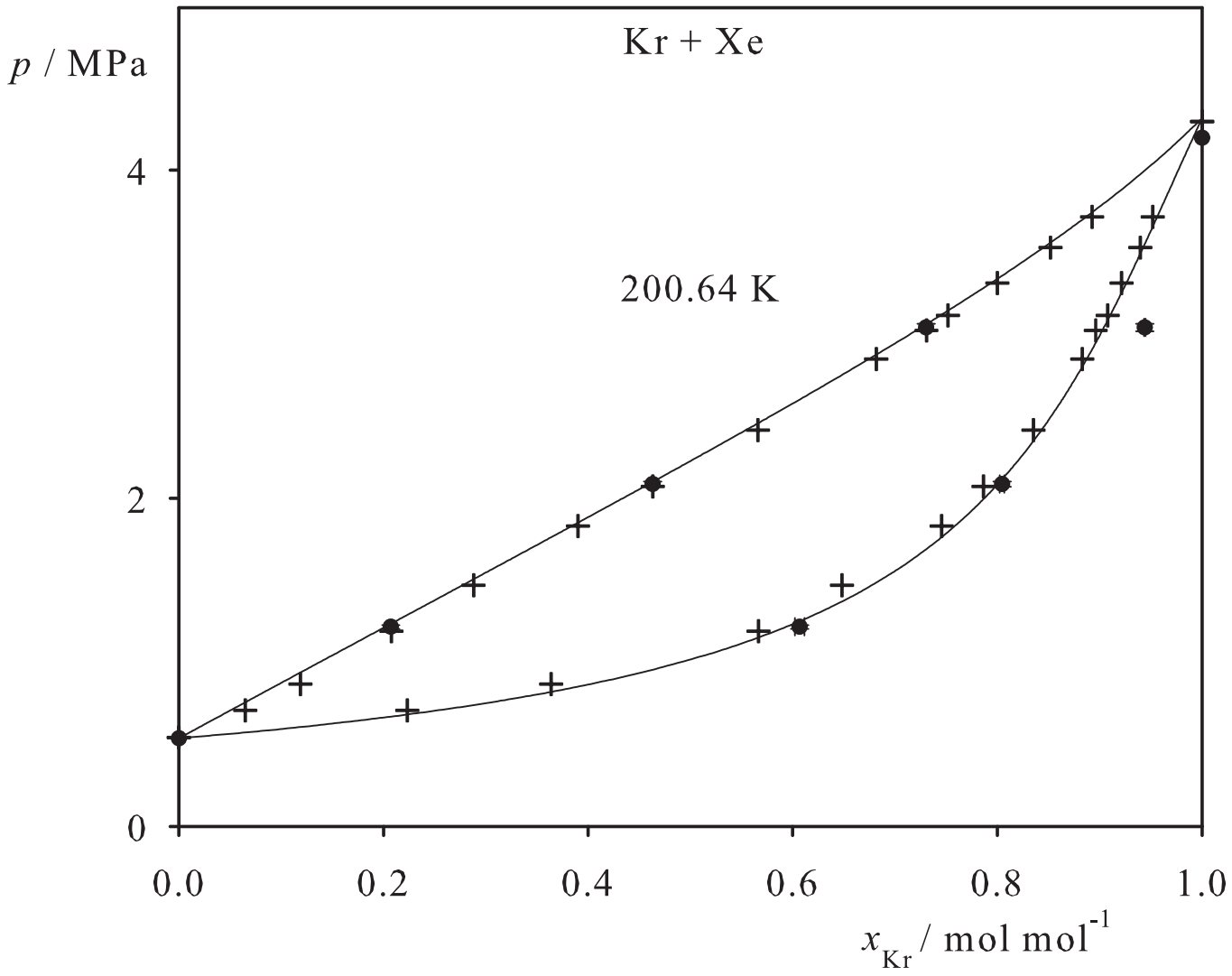

Fig. 16. Binary vapor-liquid equilibrium phase diagram: simulation data ●, experimental data + (cf. Table 2 of the manuscript for the reference) and Peng-Robinson equation of state —.

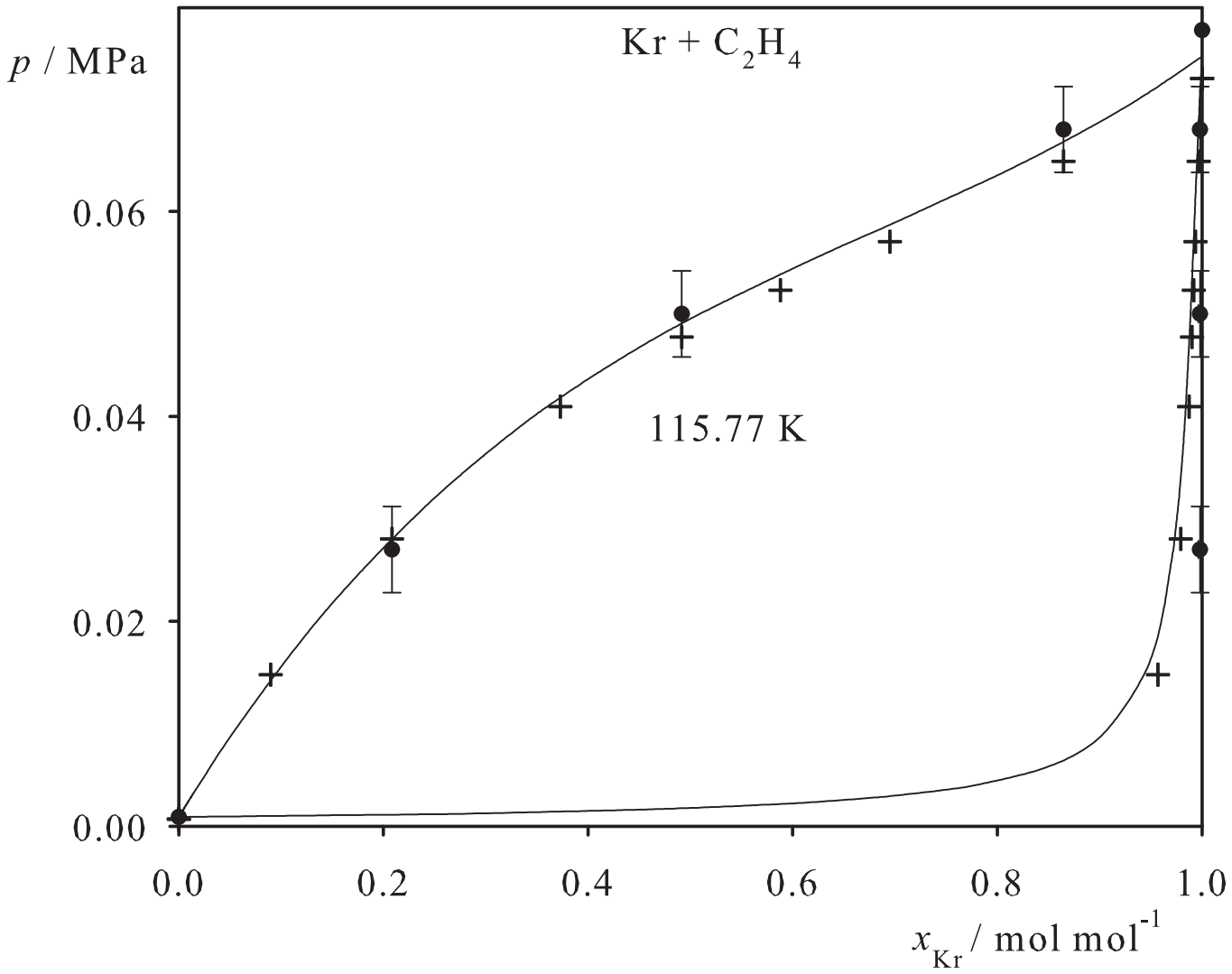

Fig. 17. Binary vapor-liquid equilibrium phase diagram: simulation data ●, experimental data + (cf. Table 2 of the manuscript for the reference) and Peng-Robinson equation of state —.

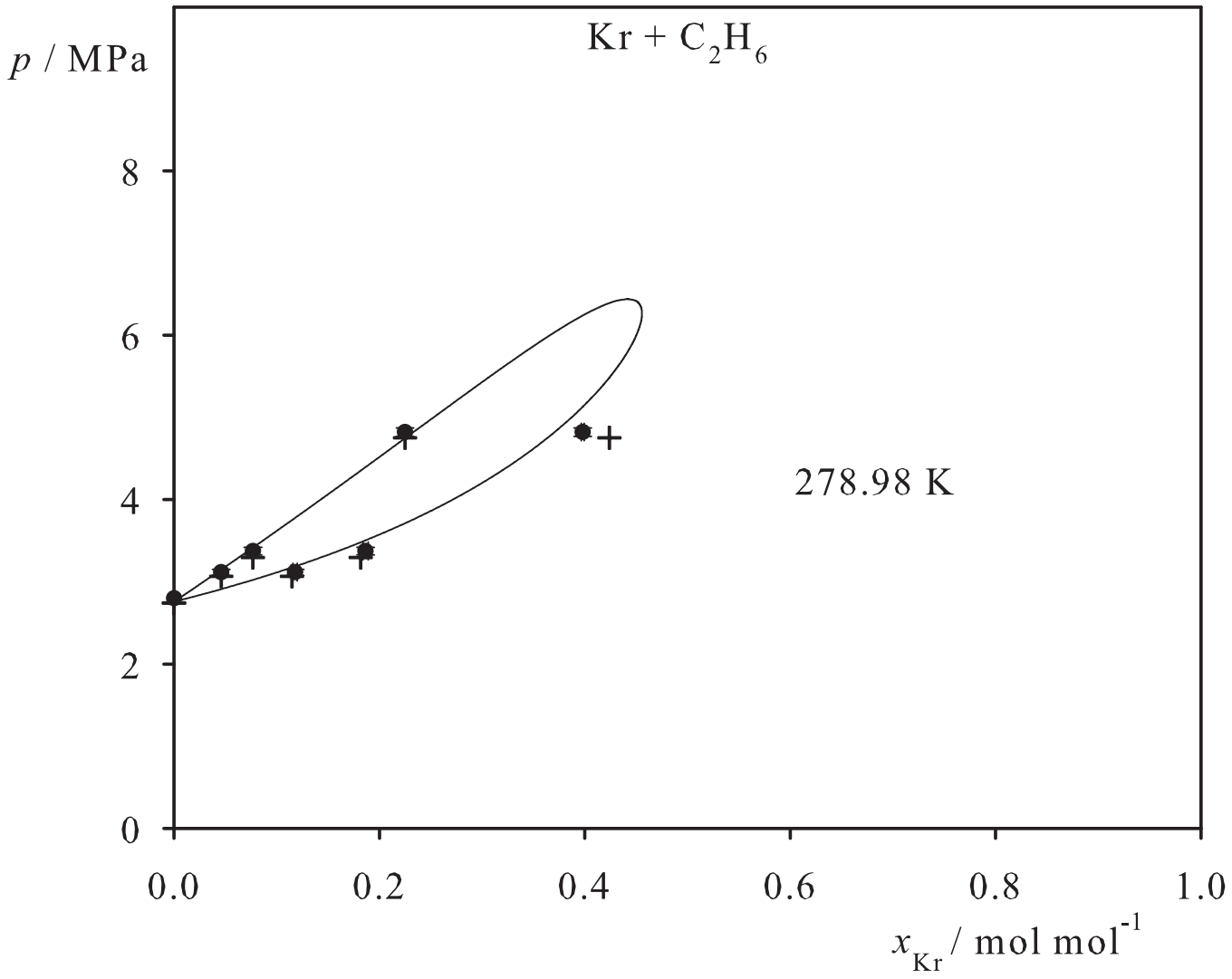

Fig. 18. Binary vapor-liquid equilibrium phase diagram: simulation data ●, experimental data + (cf. Table 2 of the manuscript for the reference) and Peng-Robinson equation of state —.

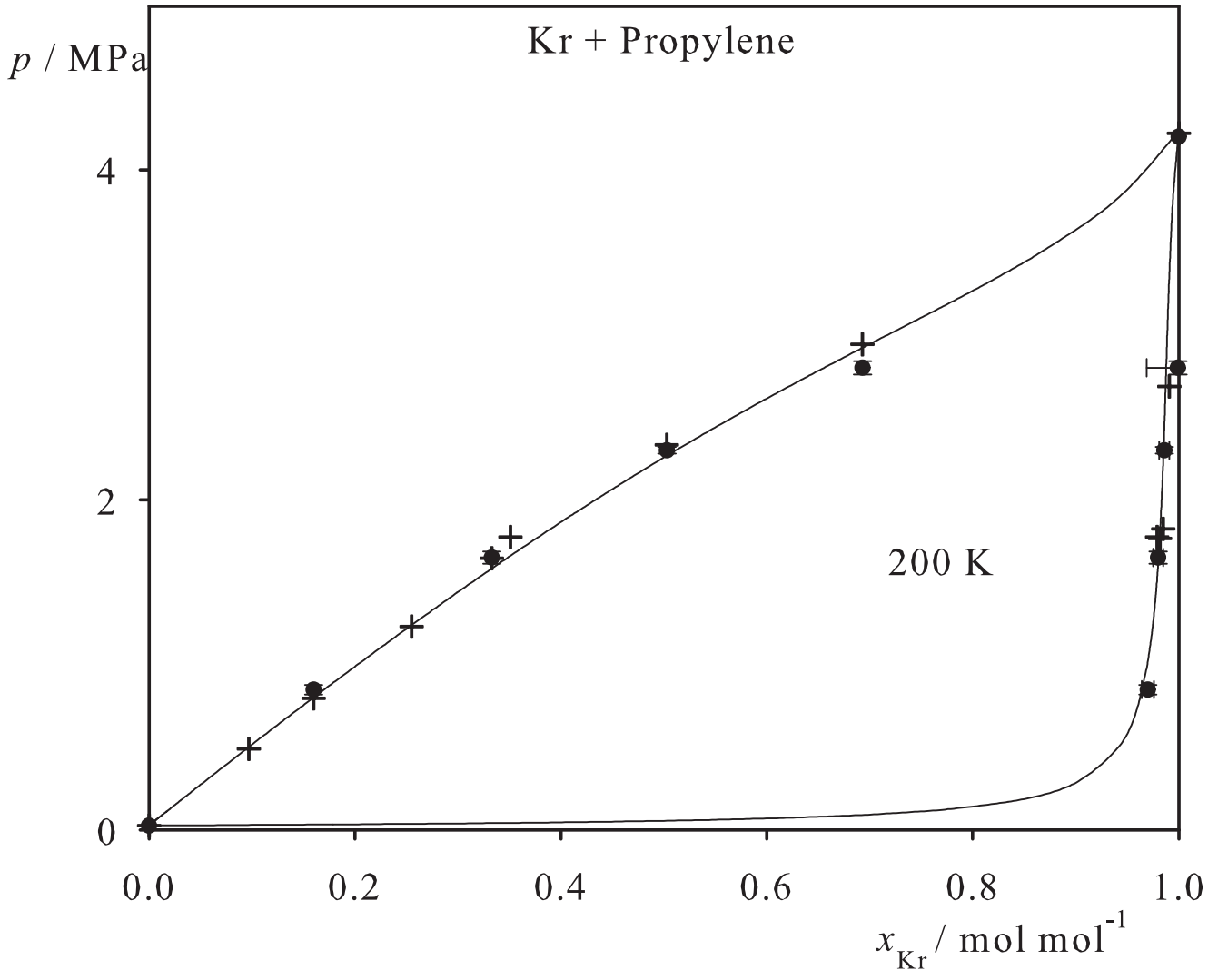

Fig. 19. Binary vapor-liquid equilibrium phase diagram: simulation data ●, experimental data + (cf. Table 2 of the manuscript for the reference) and Peng-Robinson equation of state —.

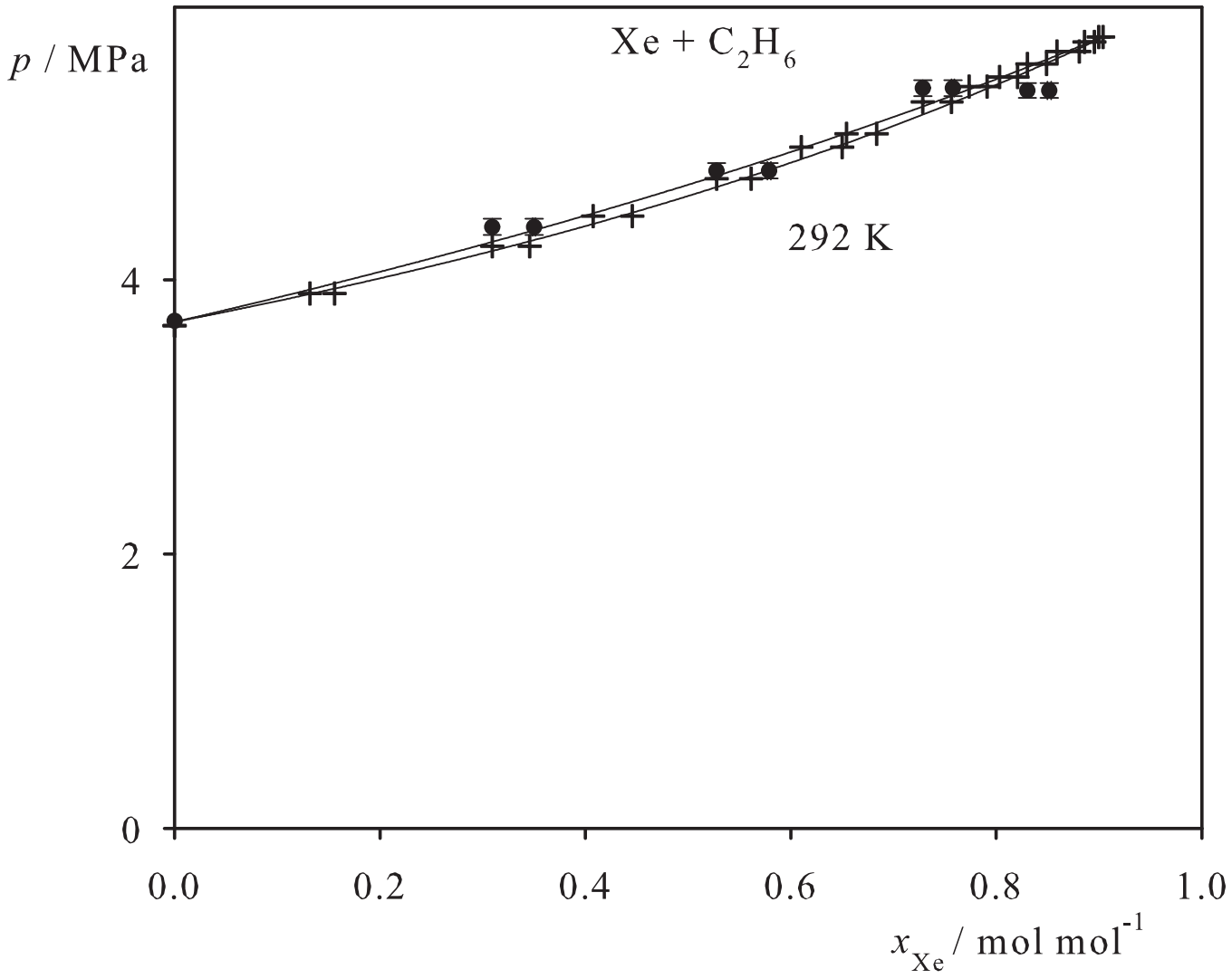

Fig. 20. Binary vapor-liquid equilibrium phase diagram: simulation data ●, experimental data + (cf. Table 2 of the manuscript for the reference) and Peng-Robinson equation of state —.

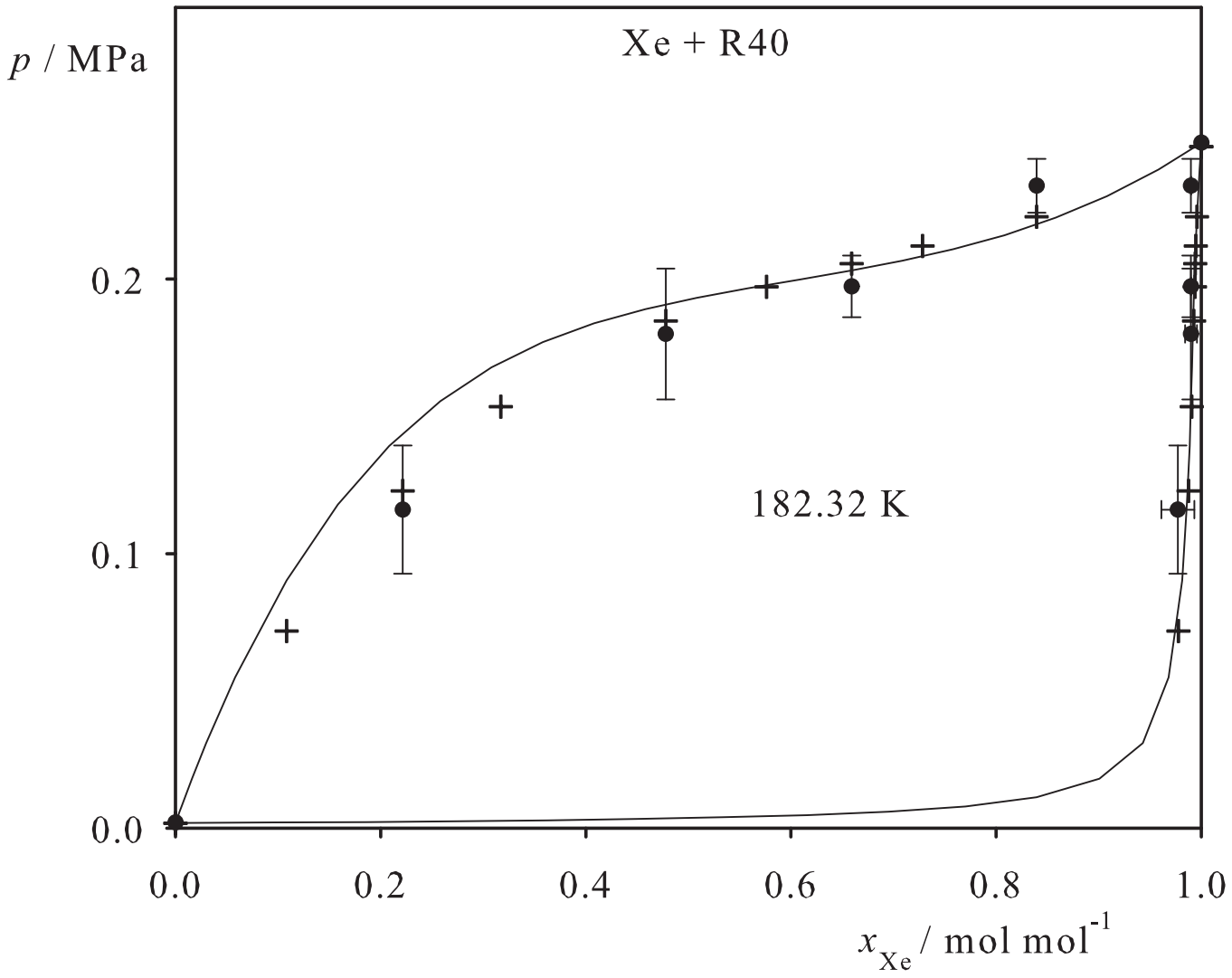

Fig. 21. Binary vapor-liquid equilibrium phase diagram: simulation data ●, experimental data + (cf. Table 2 of the manuscript for the reference) and Peng-Robinson equation of state —.

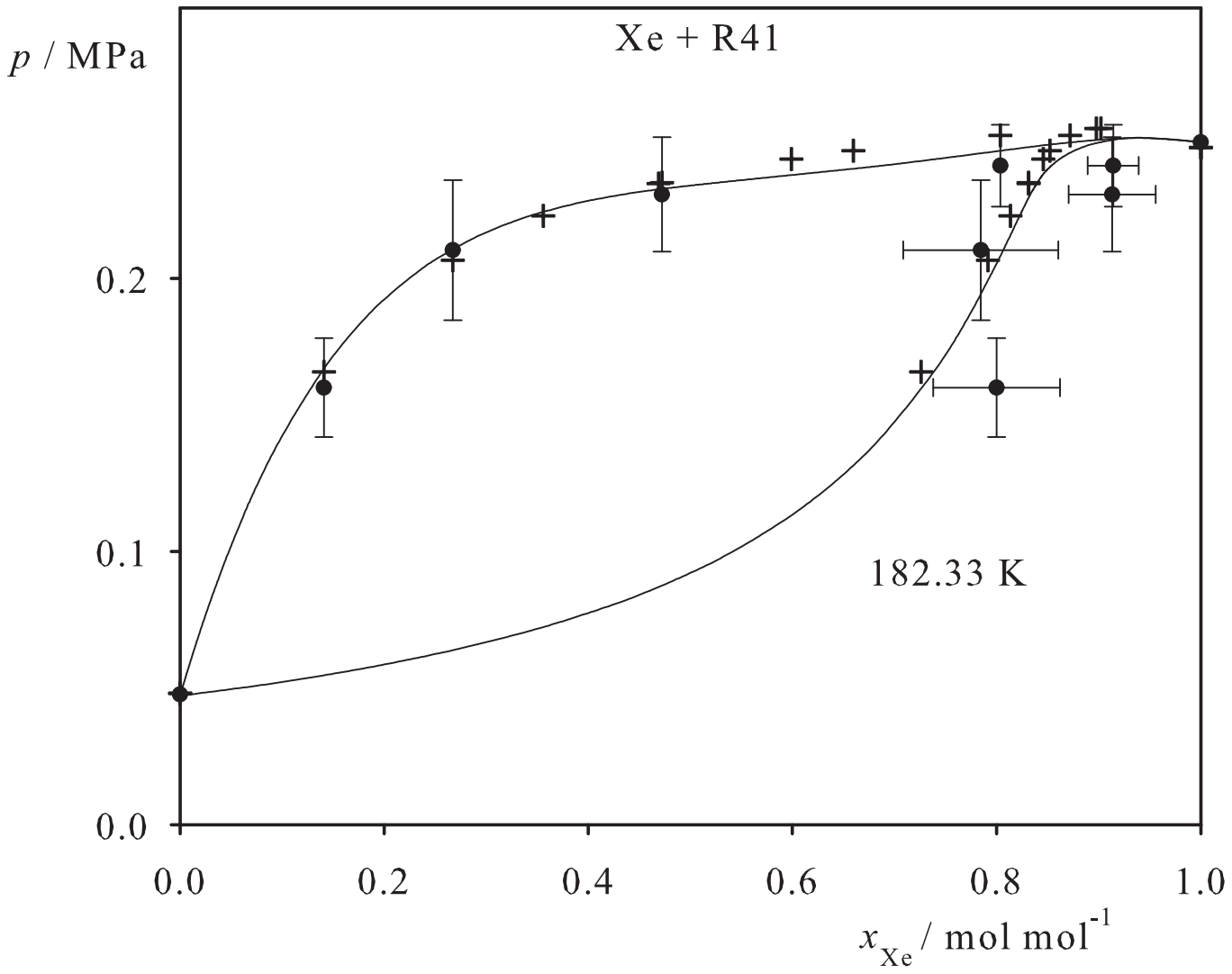

Fig. 22. Binary vapor-liquid equilibrium phase diagram: simulation data ●, experimental data + (cf. Table 2 of the manuscript for the reference) and Peng-Robinson equation of state —.

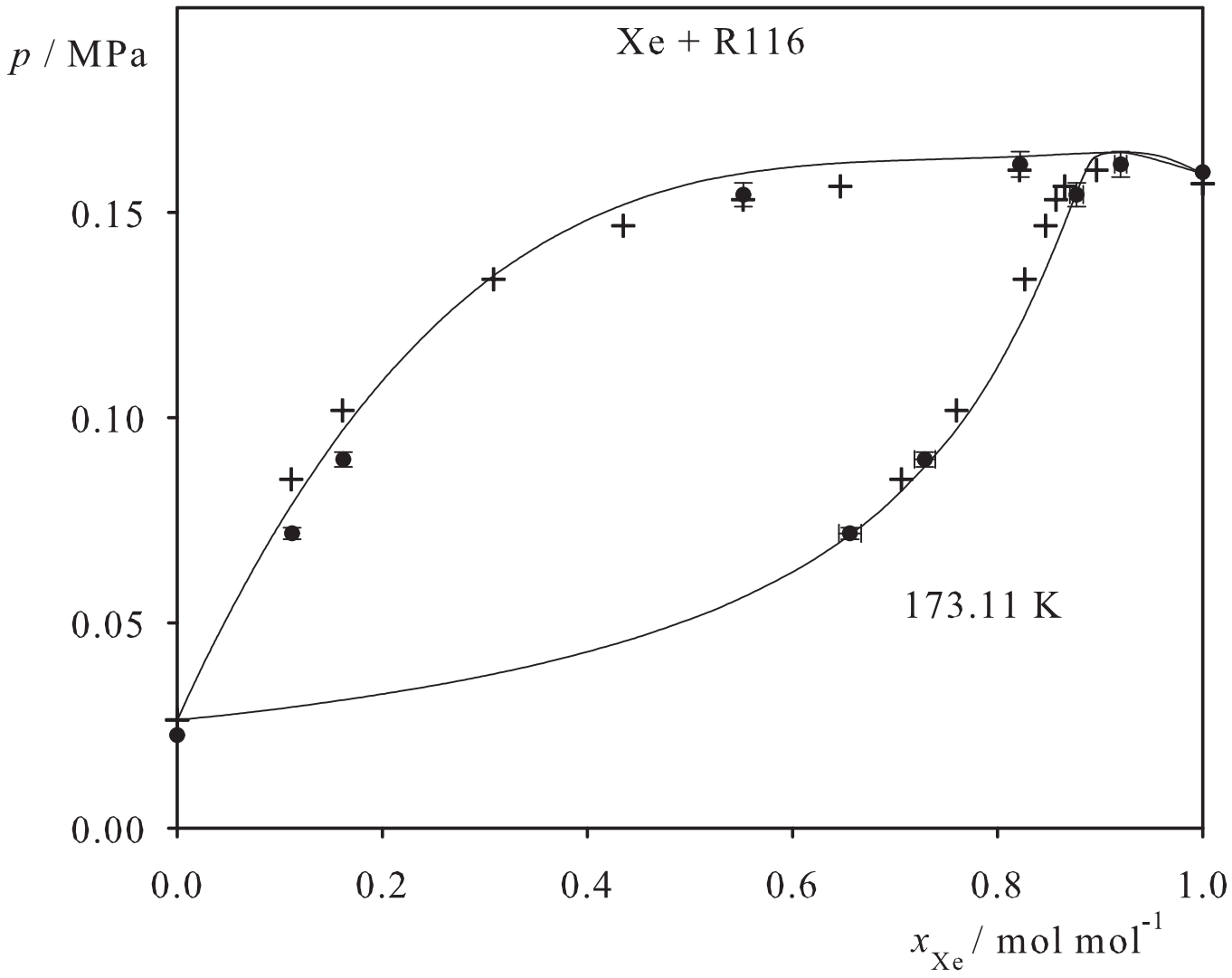

Fig. 23. Binary vapor-liquid equilibrium phase diagram: simulation data ●, experimental data + (cf. Table 2 of the manuscript for the reference) and Peng-Robinson equation of state —.

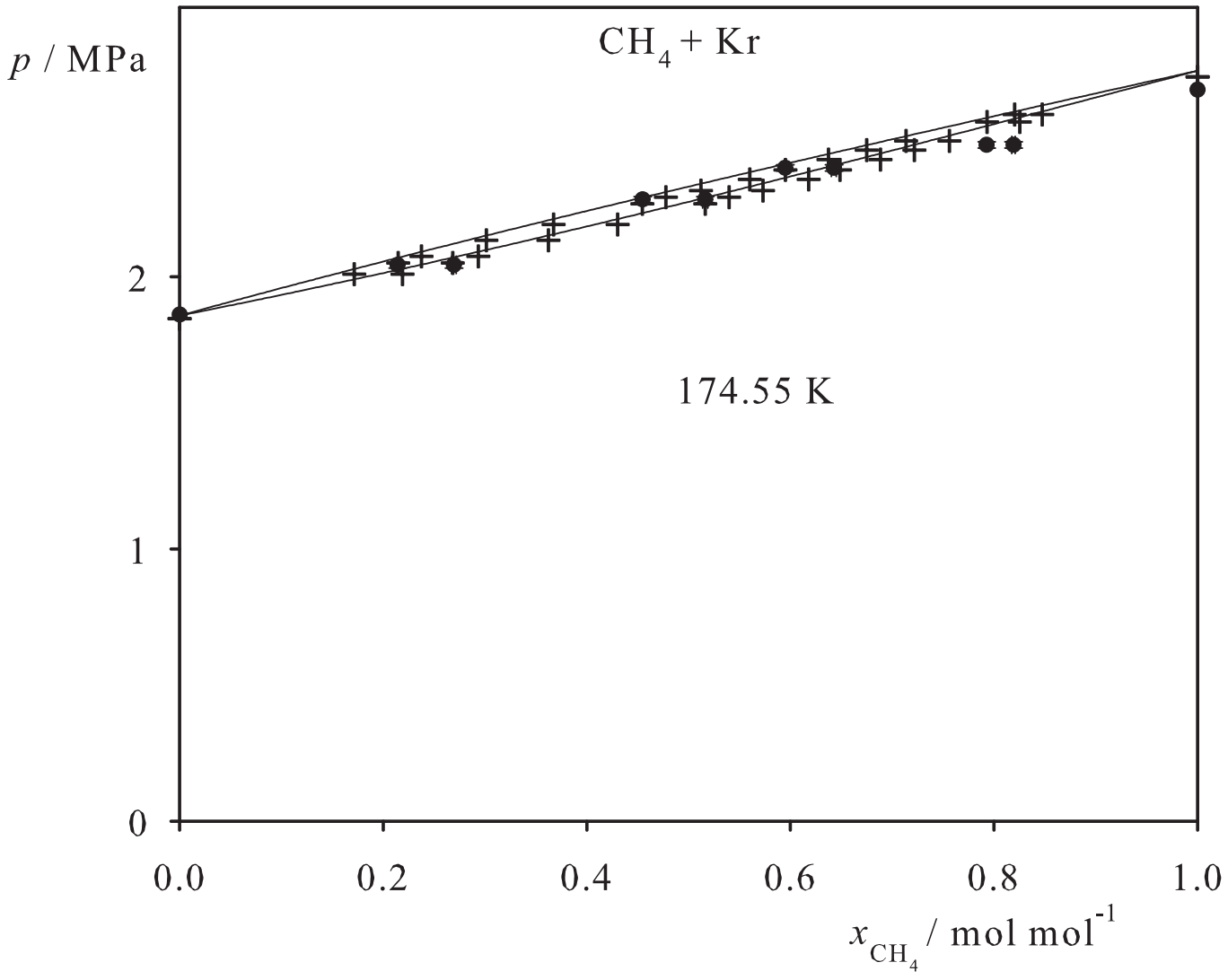

Fig. 24. Binary vapor-liquid equilibrium phase diagram: simulation data ●, experimental data + (cf. Table 2 of the manuscript for the reference) and Peng-Robinson equation of state —.

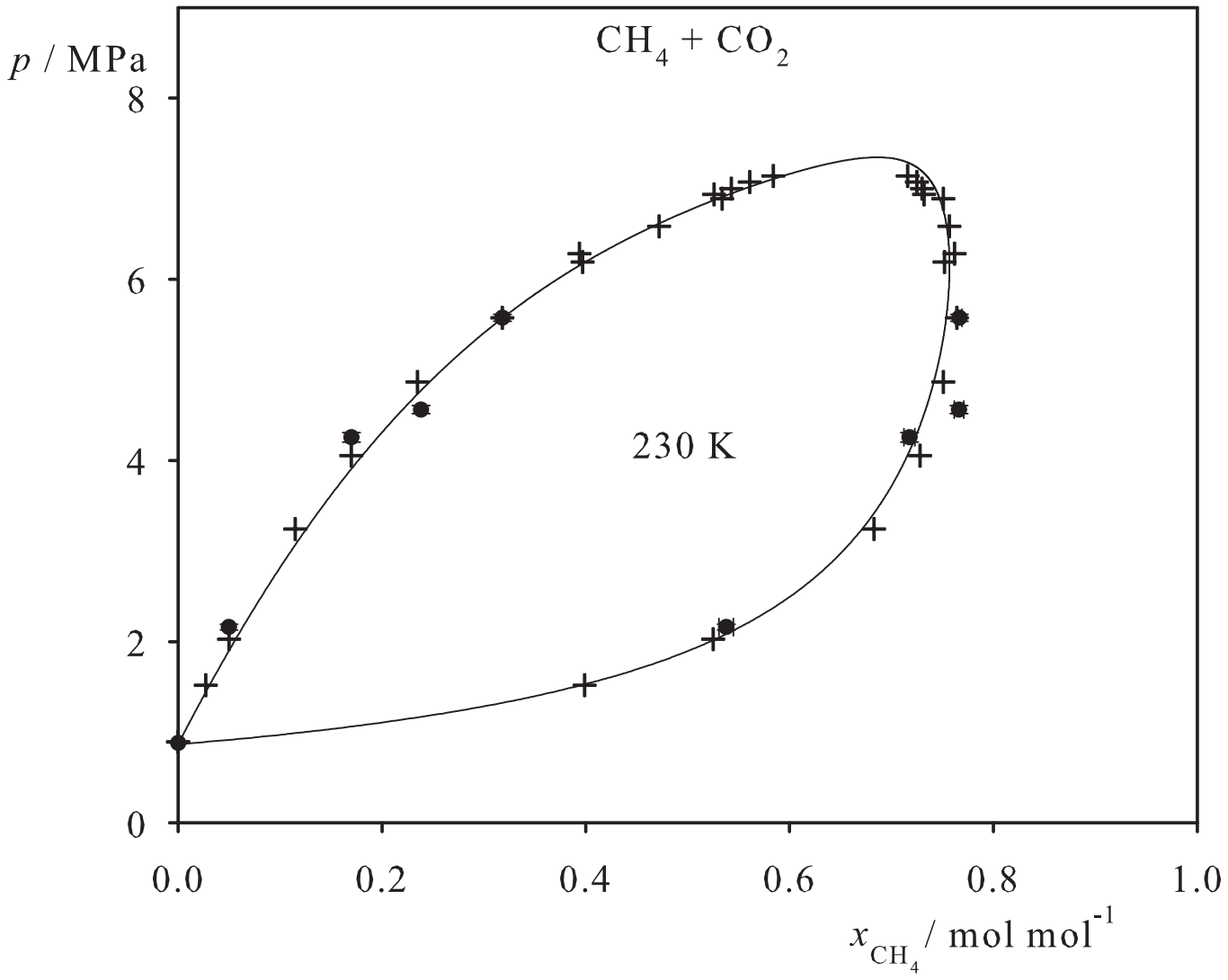

Fig. 25. Binary vapor-liquid equilibrium phase diagram: simulation data ●, experimental data + (cf. Table 2 of the manuscript for the reference) and Peng-Robinson equation of state —.

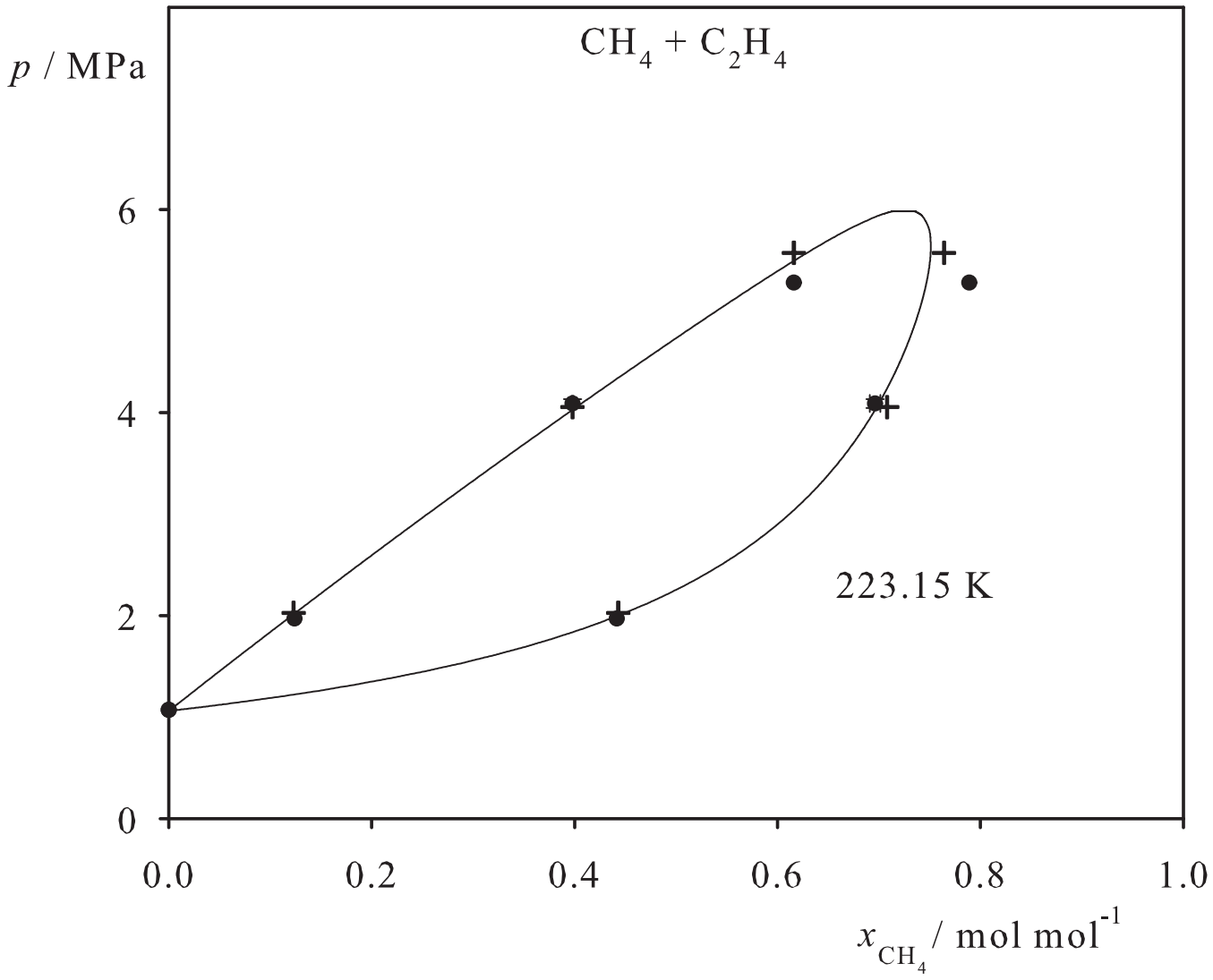

Fig. 26. Binary vapor-liquid equilibrium phase diagram: simulation data ●, experimental data + (cf. Table 2 of the manuscript for the reference) and Peng-Robinson equation of state —.

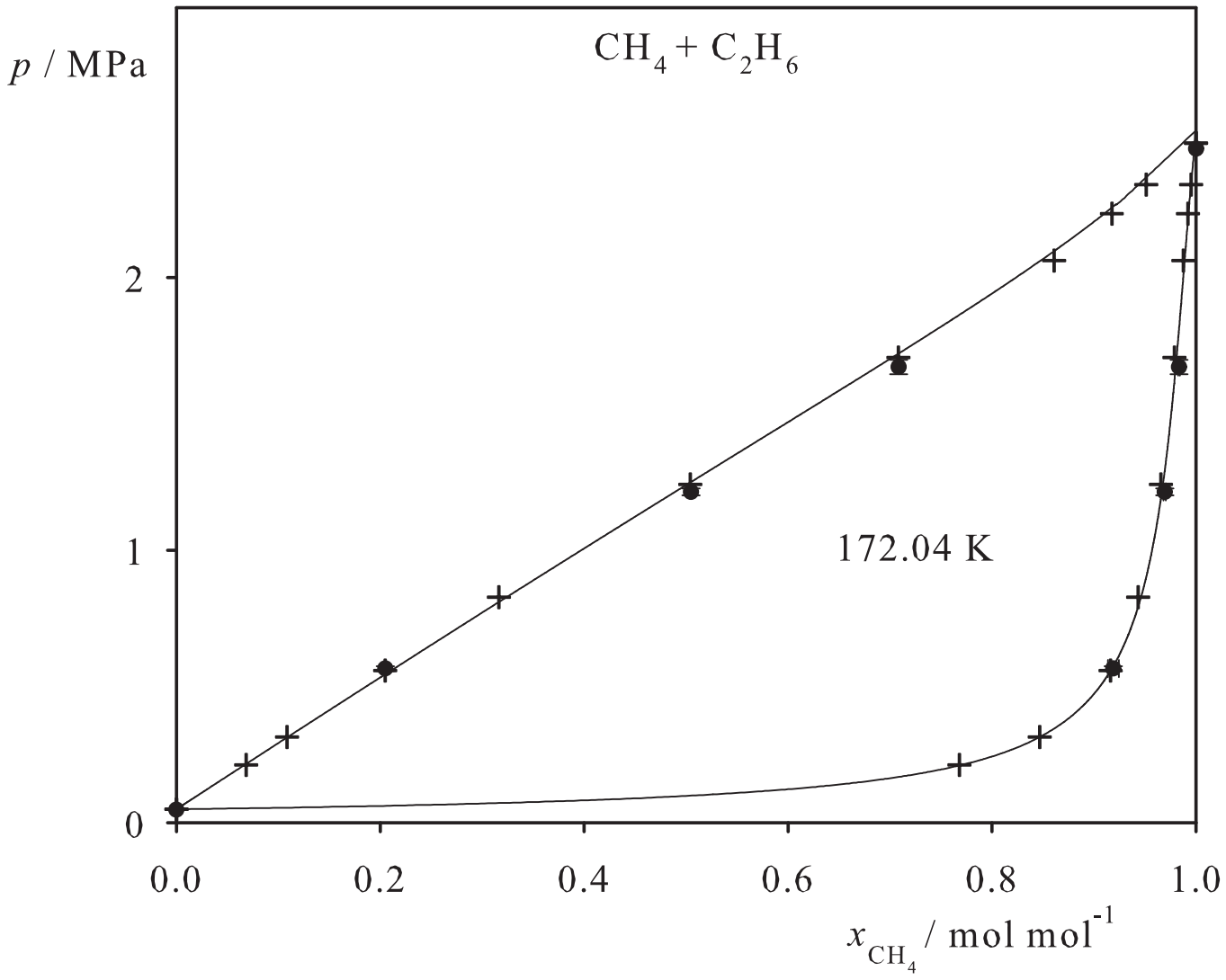

Fig. 27. Binary vapor-liquid equilibrium phase diagram: simulation data ●, experimental data + (cf. Table 2 of the manuscript for the reference) and Peng-Robinson equation of state —.

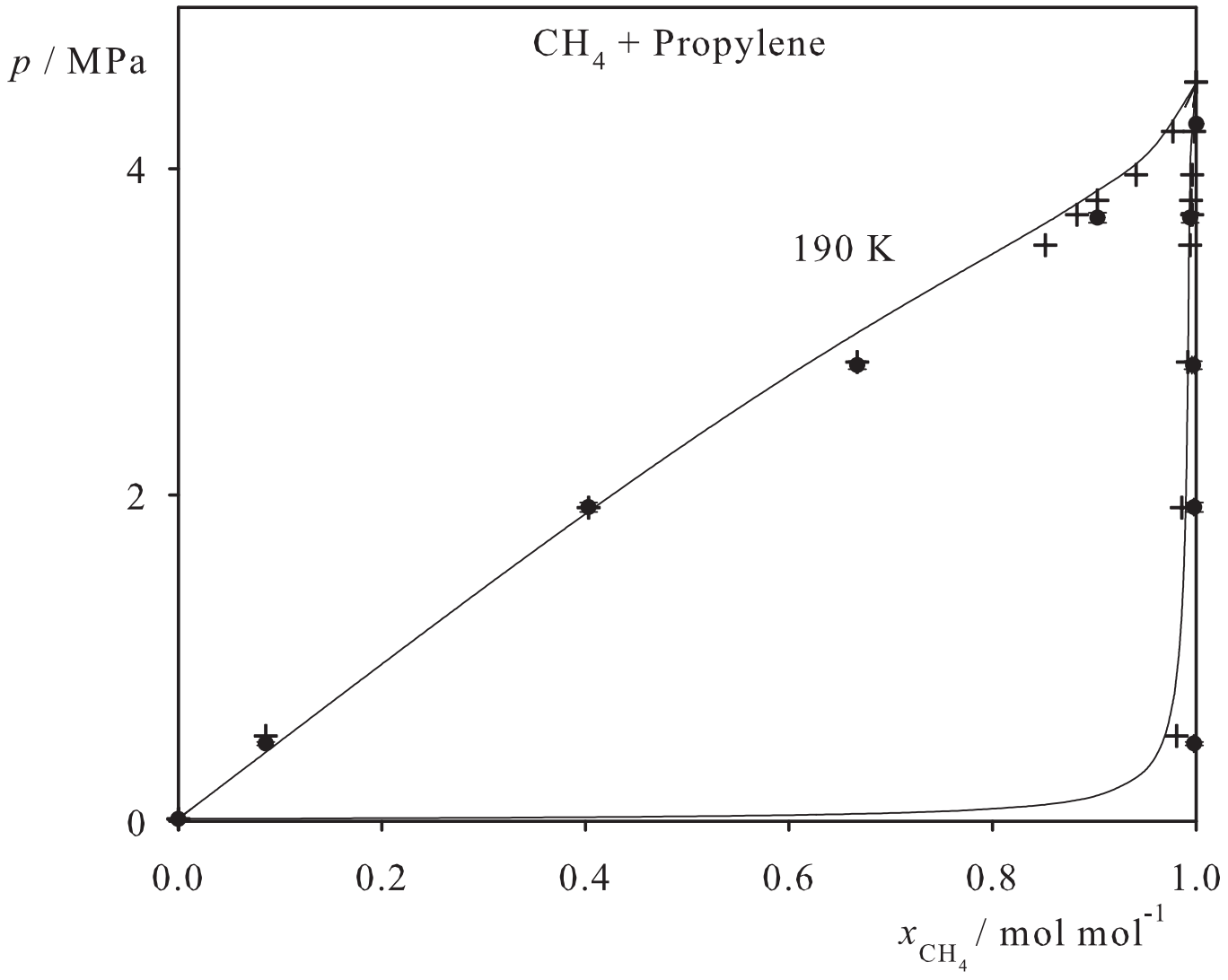

Fig. 28. Binary vapor-liquid equilibrium phase diagram: simulation data ●, experimental data + (cf. Table 2 of the manuscript for the reference) and Peng-Robinson equation of state —.

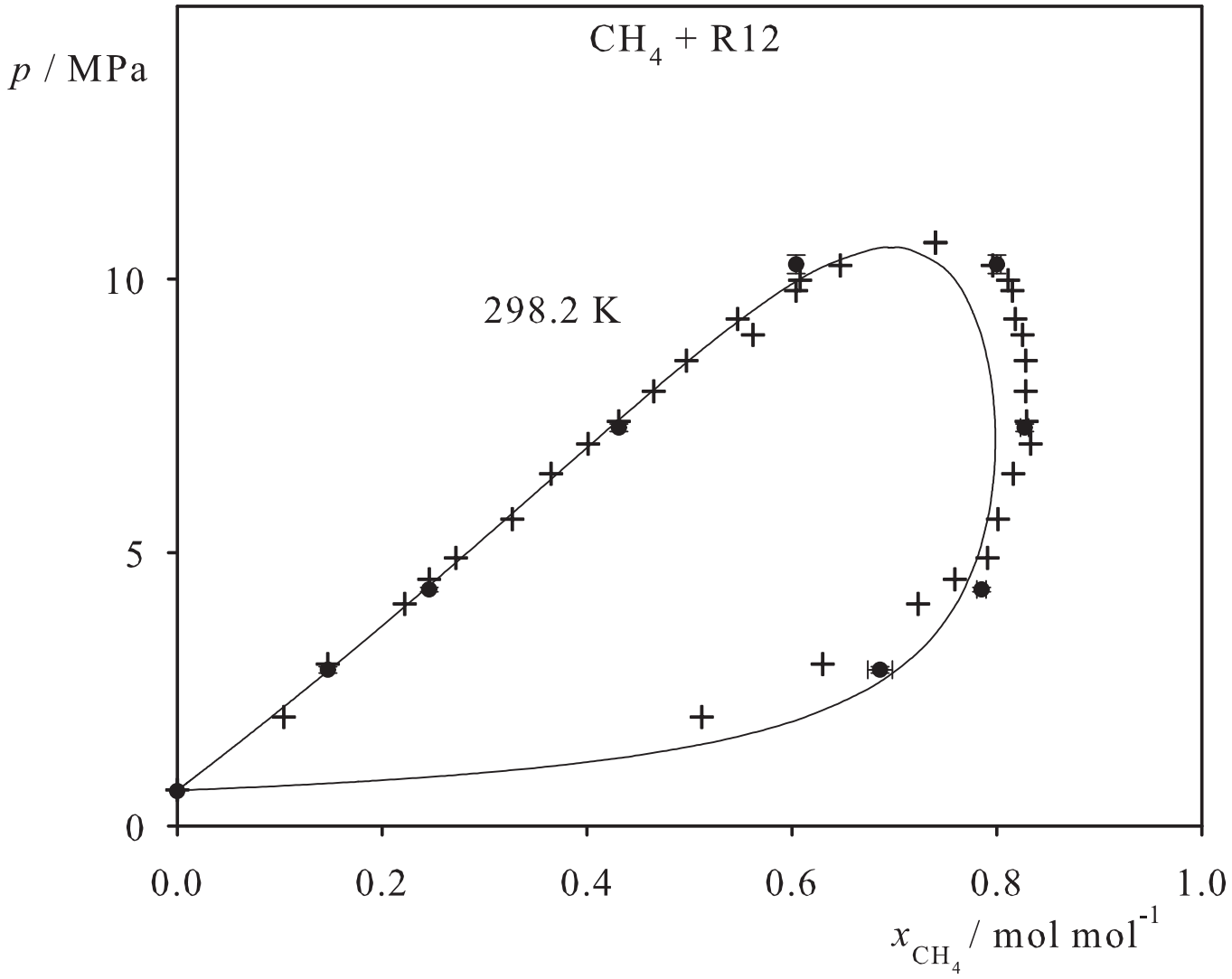

Fig. 29. Binary vapor-liquid equilibrium phase diagram: simulation data ●, experimental data + (cf. Table 2 of the manuscript for the reference) and Peng-Robinson equation of state —.

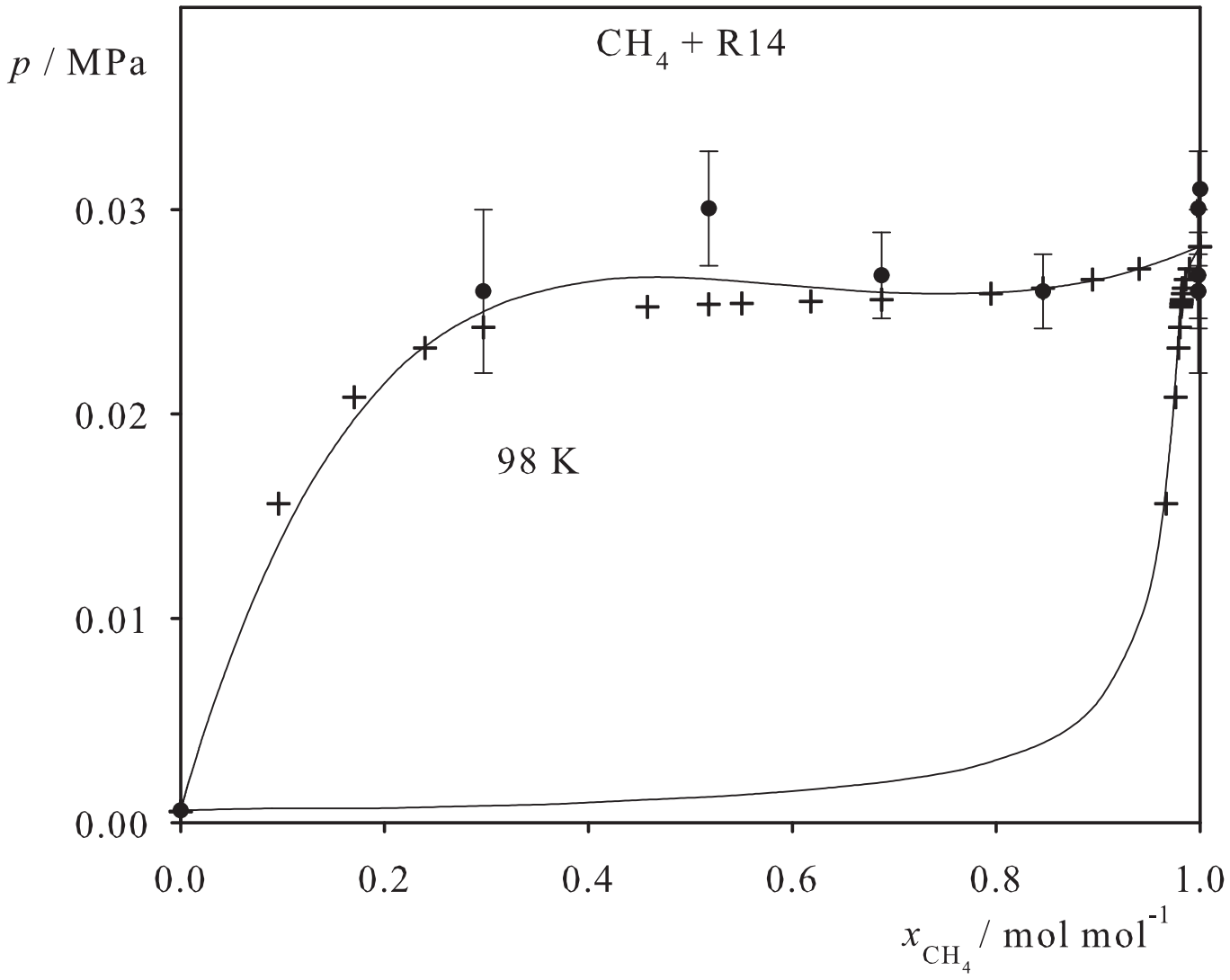

Fig. 30. Binary vapor-liquid equilibrium phase diagram: simulation data ●, experimental data + (cf. Table 2 of the manuscript for the reference) and Peng-Robinson equation of state —.

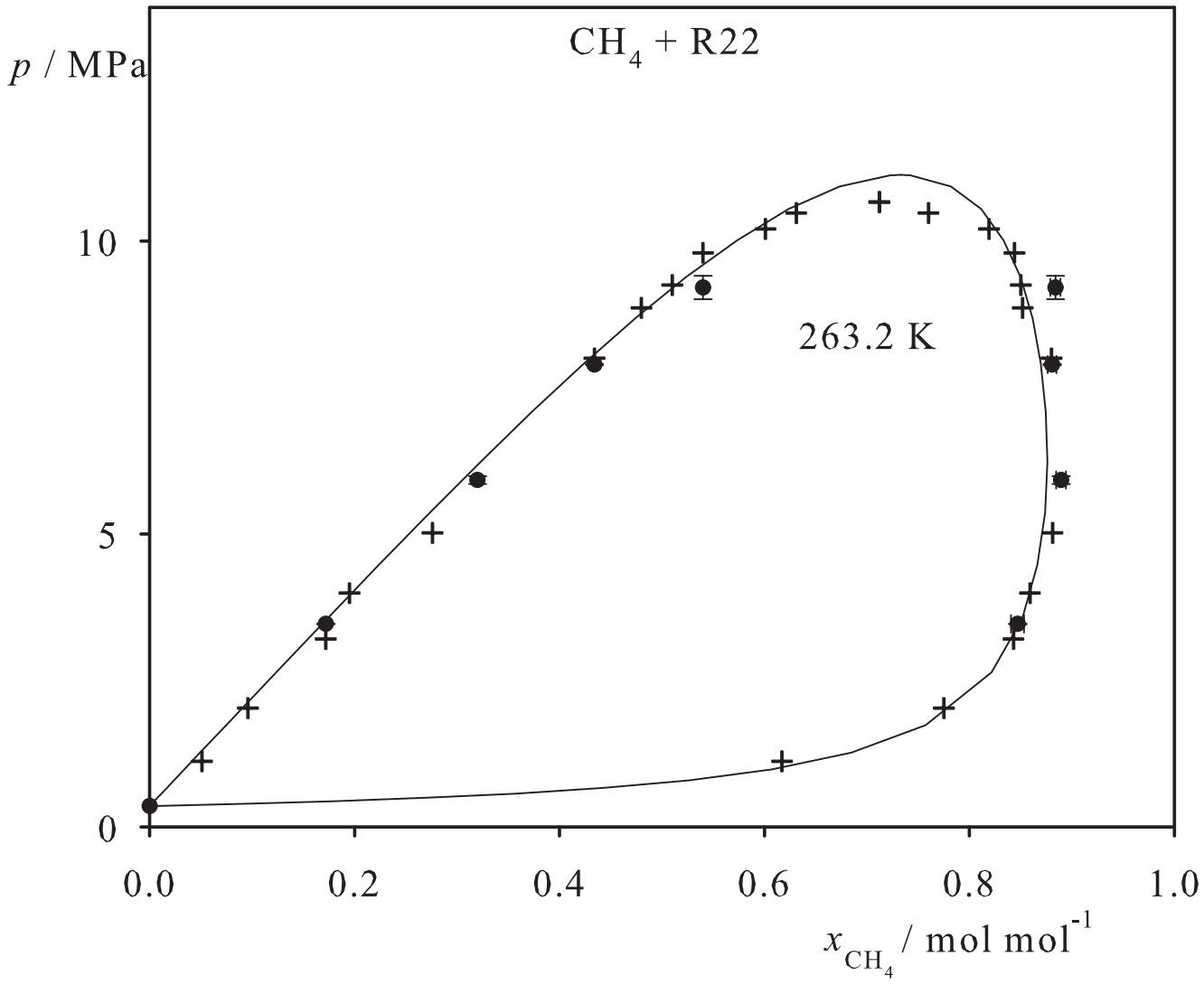

Fig. 31. Binary vapor-liquid equilibrium phase diagram: simulation data ●, experimental data + (cf. Table 2 of the manuscript for the reference) and Peng-Robinson equation of state —.

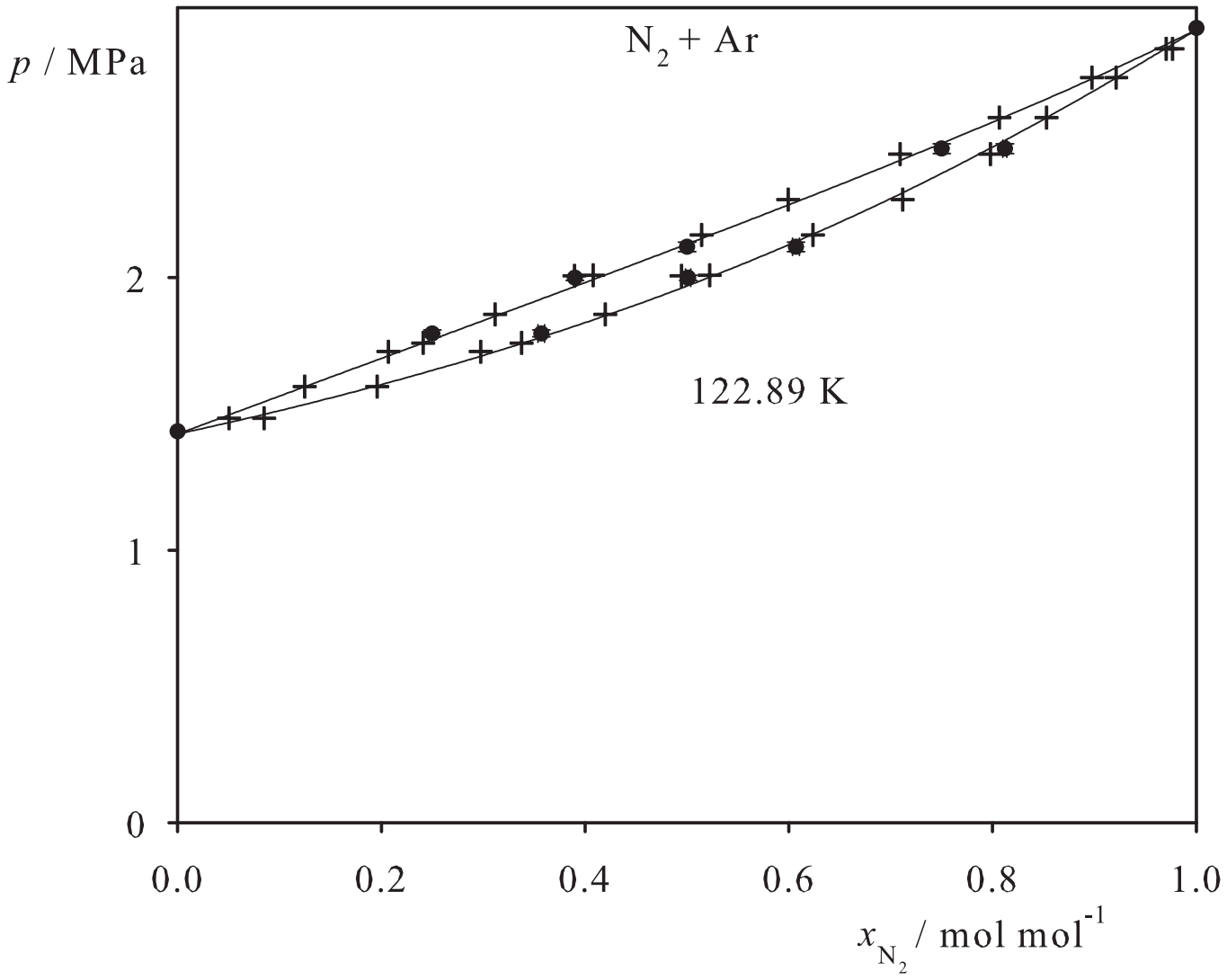

Fig. 32. Binary vapor-liquid equilibrium phase diagram: simulation data ●, experimental data + (cf. Table 2 of the manuscript for the reference) and Peng-Robinson equation of state —.

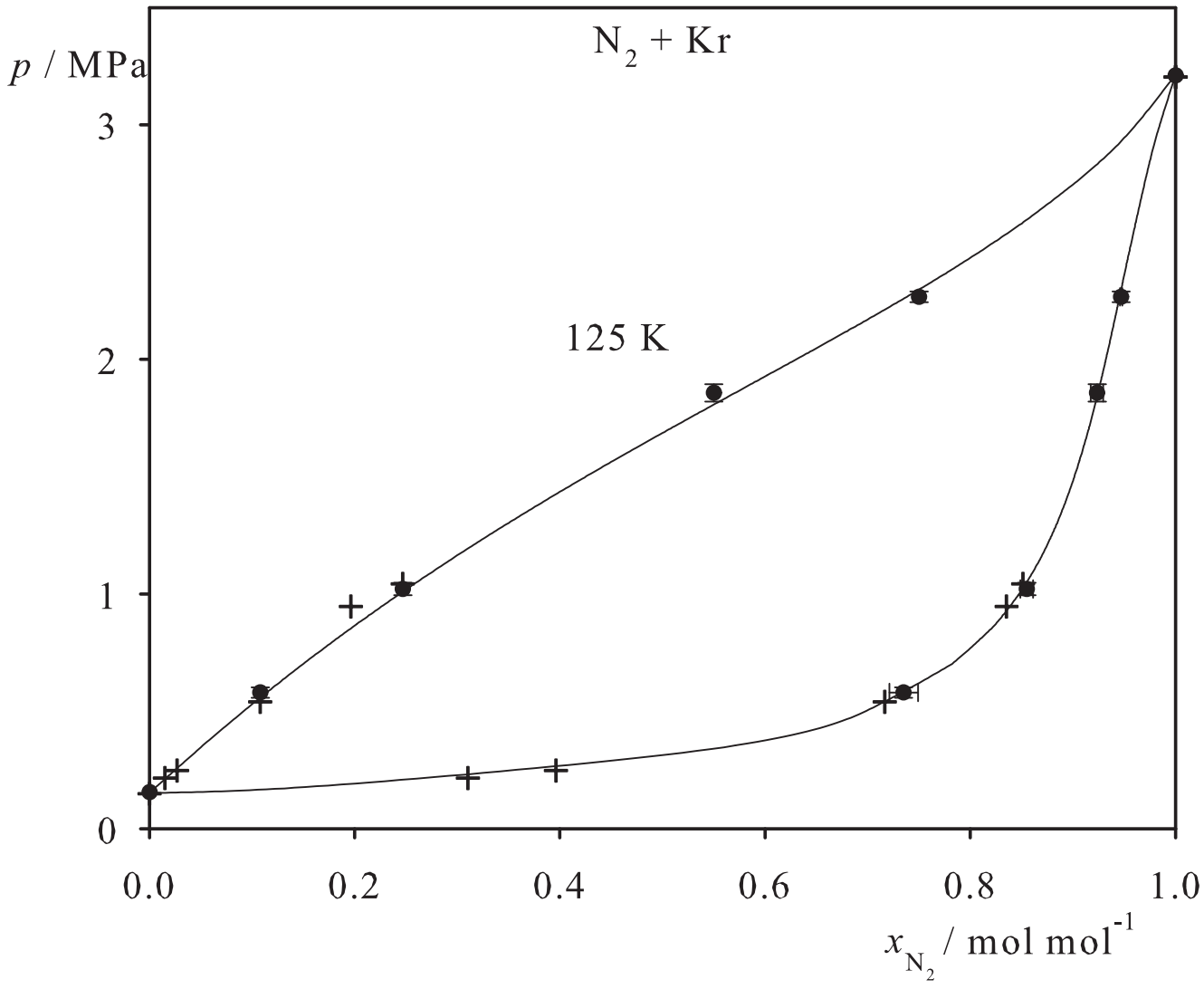

Fig. 33. Binary vapor-liquid equilibrium phase diagram: simulation data ●, experimental data + (cf. Table 2 of the manuscript for the reference) and Peng-Robinson equation of state —.

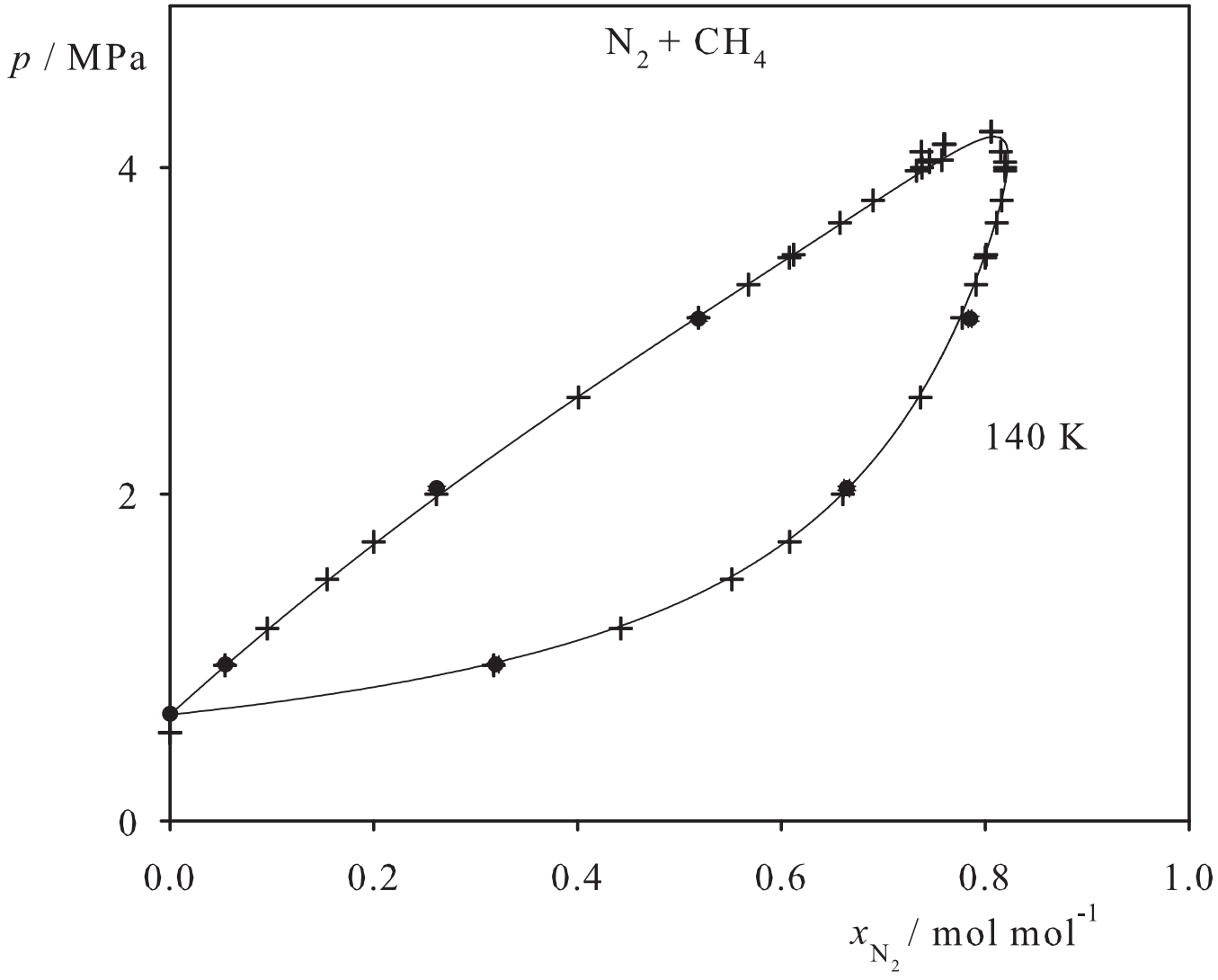

Fig. 34. Binary vapor-liquid equilibrium phase diagram: simulation data ●, experimental data + (cf. Table 2 of the manuscript for the reference) and Peng-Robinson equation of state —.

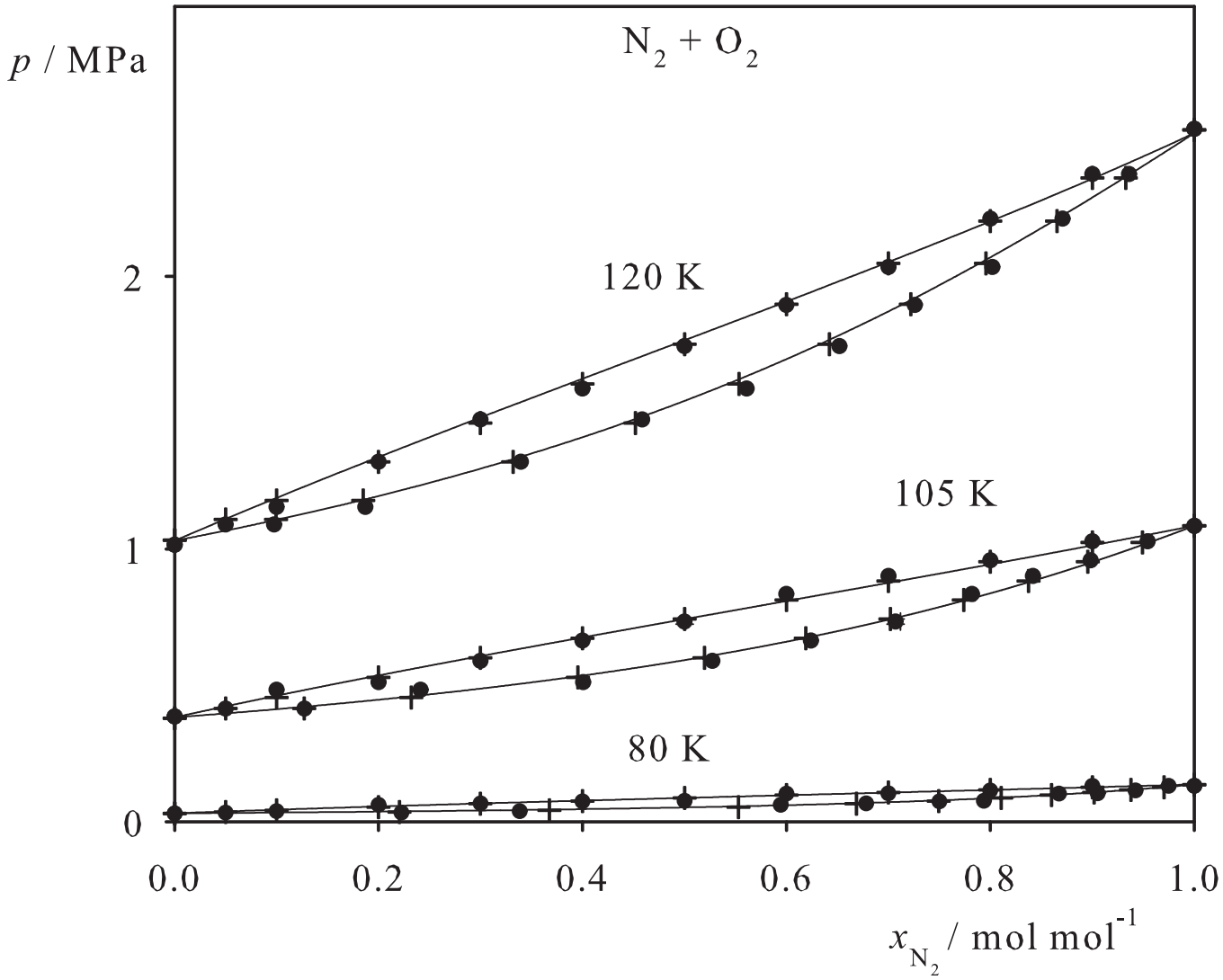

Fig. 35. Binary vapor-liquid equilibrium phase diagram: simulation data ●, experimental data + (cf. Table 2 of the manuscript for the reference) and Peng-Robinson equation of state —.

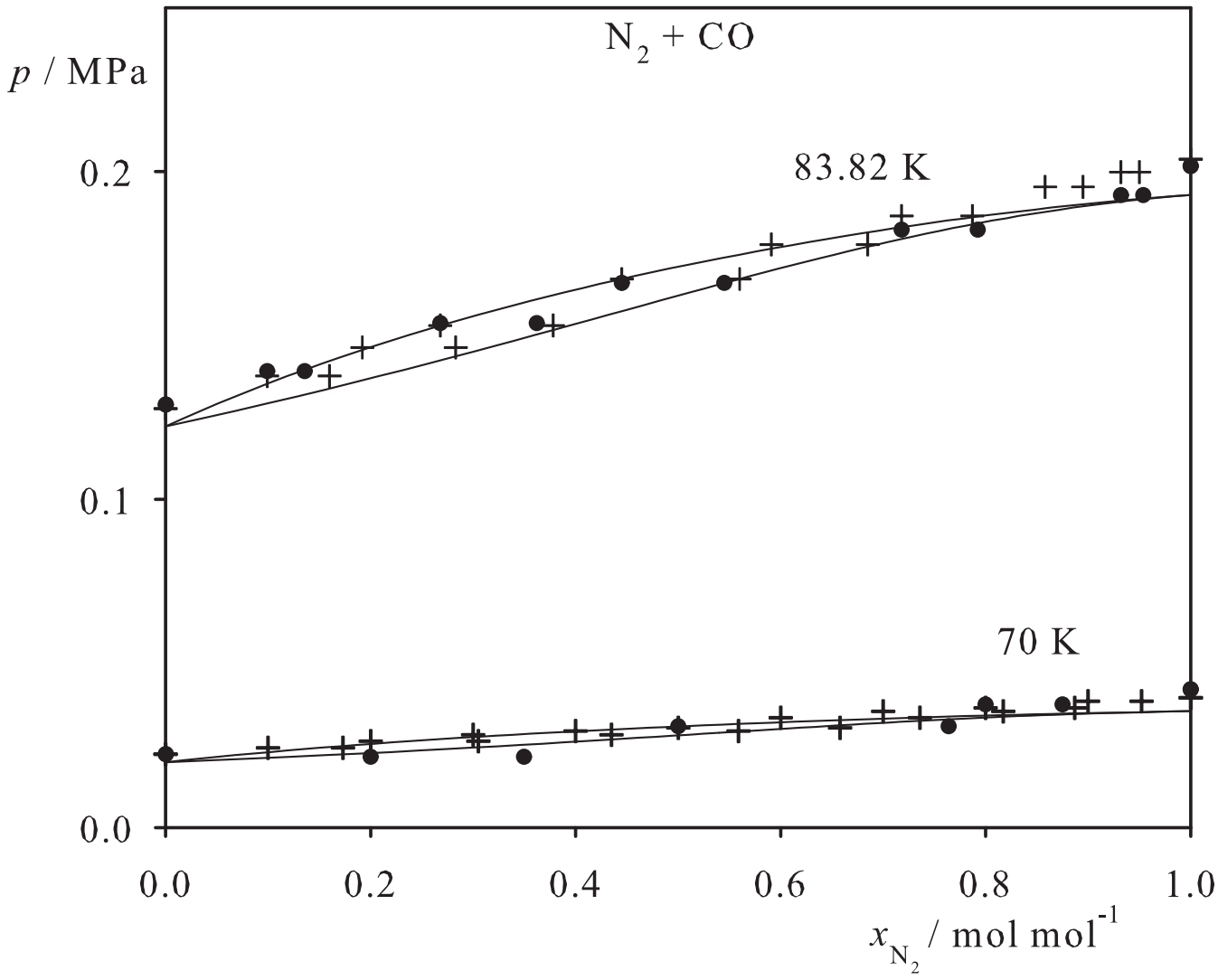

Fig. 36. Binary vapor-liquid equilibrium phase diagram: simulation data ●, experimental data + (cf. Table 2 of the manuscript for the reference) and Peng-Robinson equation of state —.

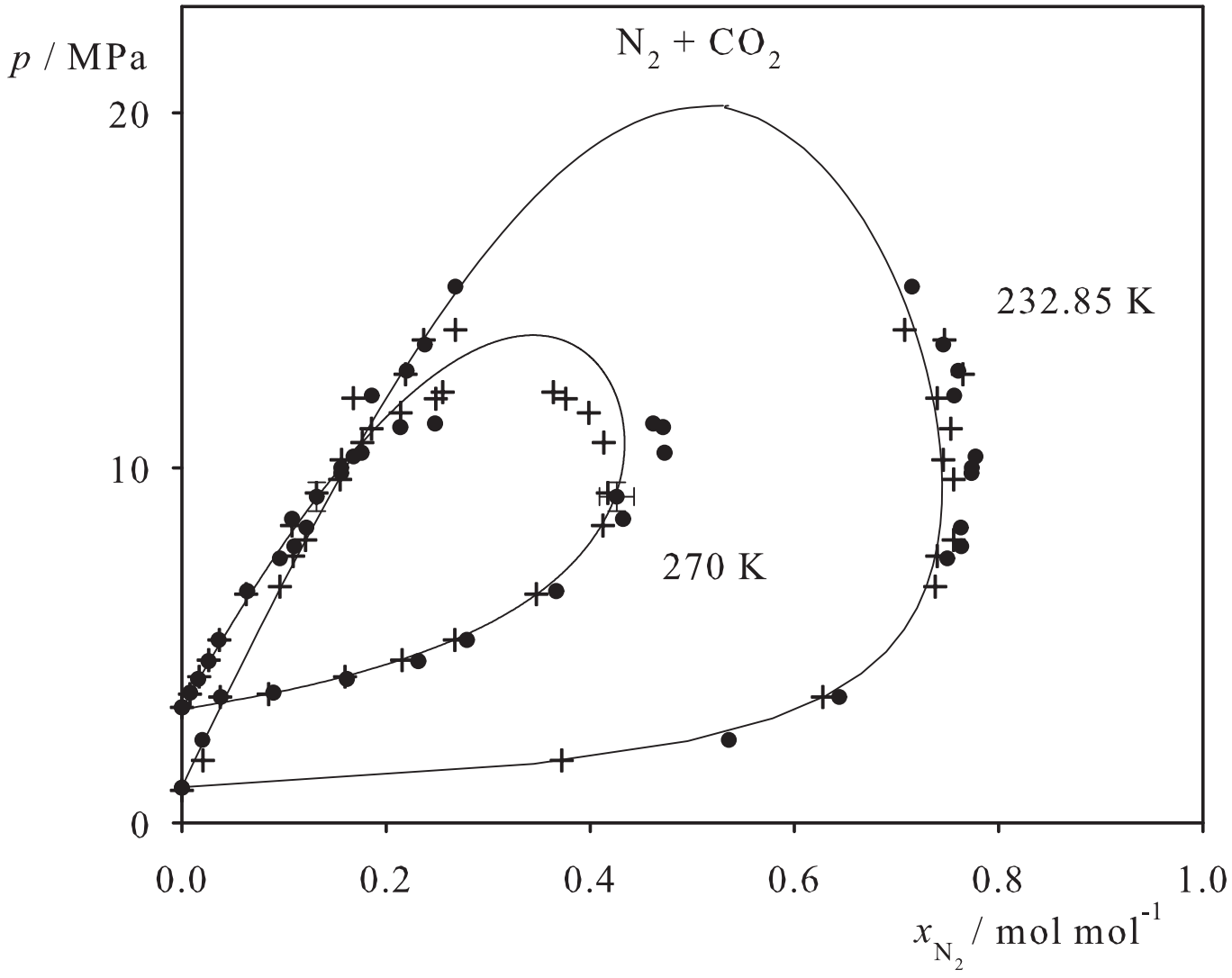

Fig. 37. Binary vapor-liquid equilibrium phase diagram: simulation data ●, experimental data + (cf. Table 2 of the manuscript for the reference) and Peng-Robinson equation of state —.

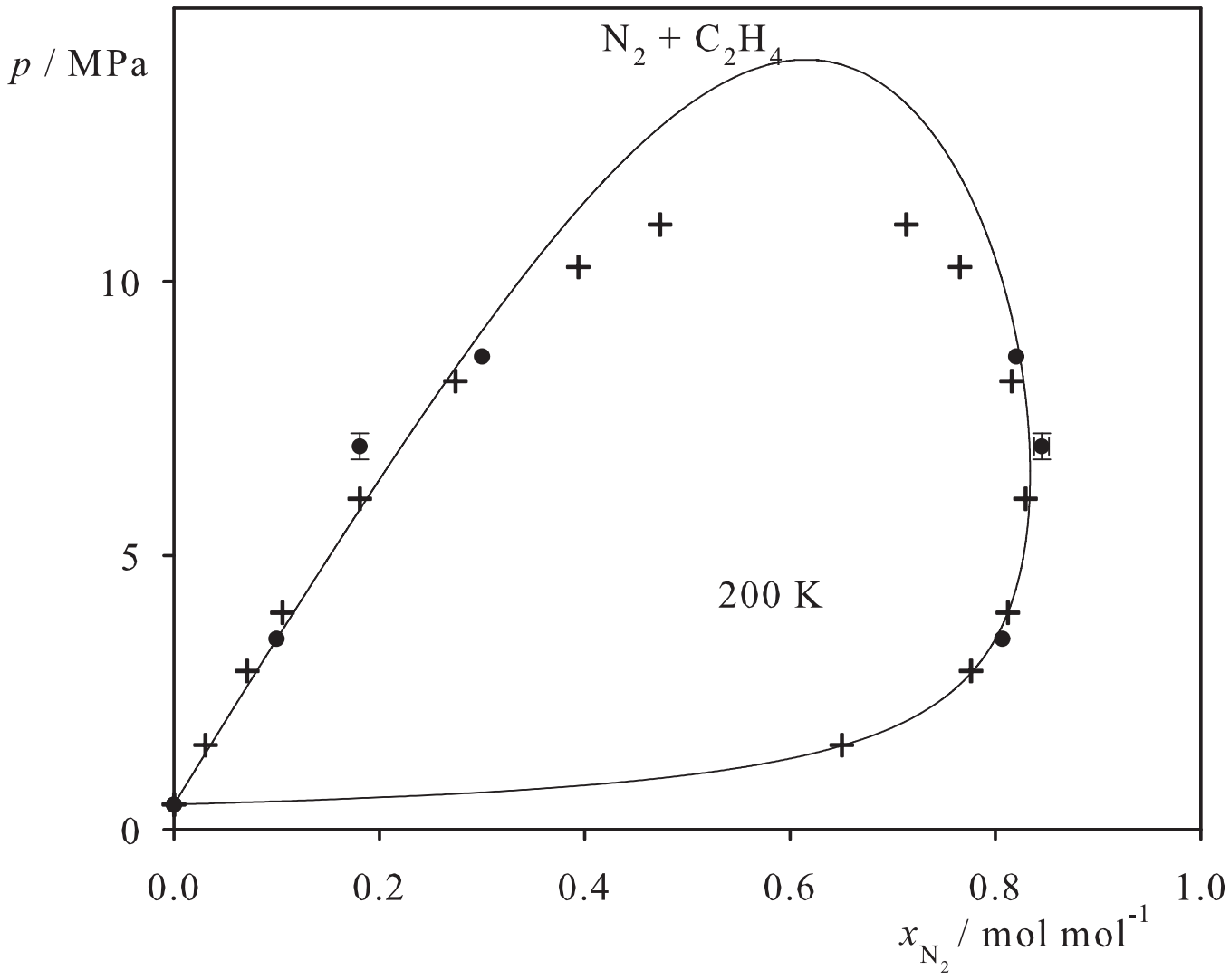

Fig. 38. Binary vapor-liquid equilibrium phase diagram: simulation data ●, experimental data + (cf. Table 2 of the manuscript for the reference) and Peng-Robinson equation of state —.

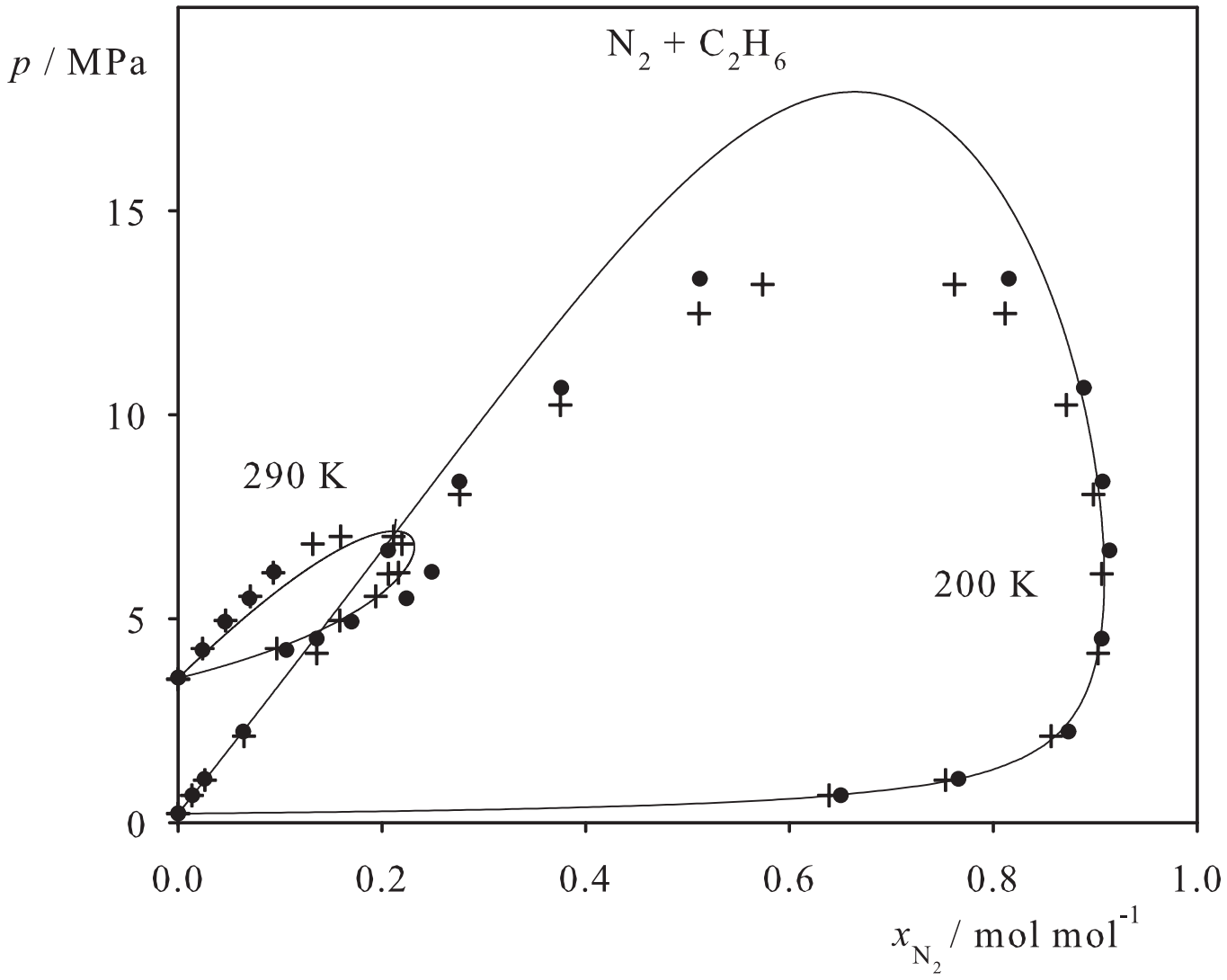

Fig. 39. Binary vapor-liquid equilibrium phase diagram: simulation data ●, experimental data + (cf. Table 2 of the manuscript for the reference) and Peng-Robinson equation of state —.

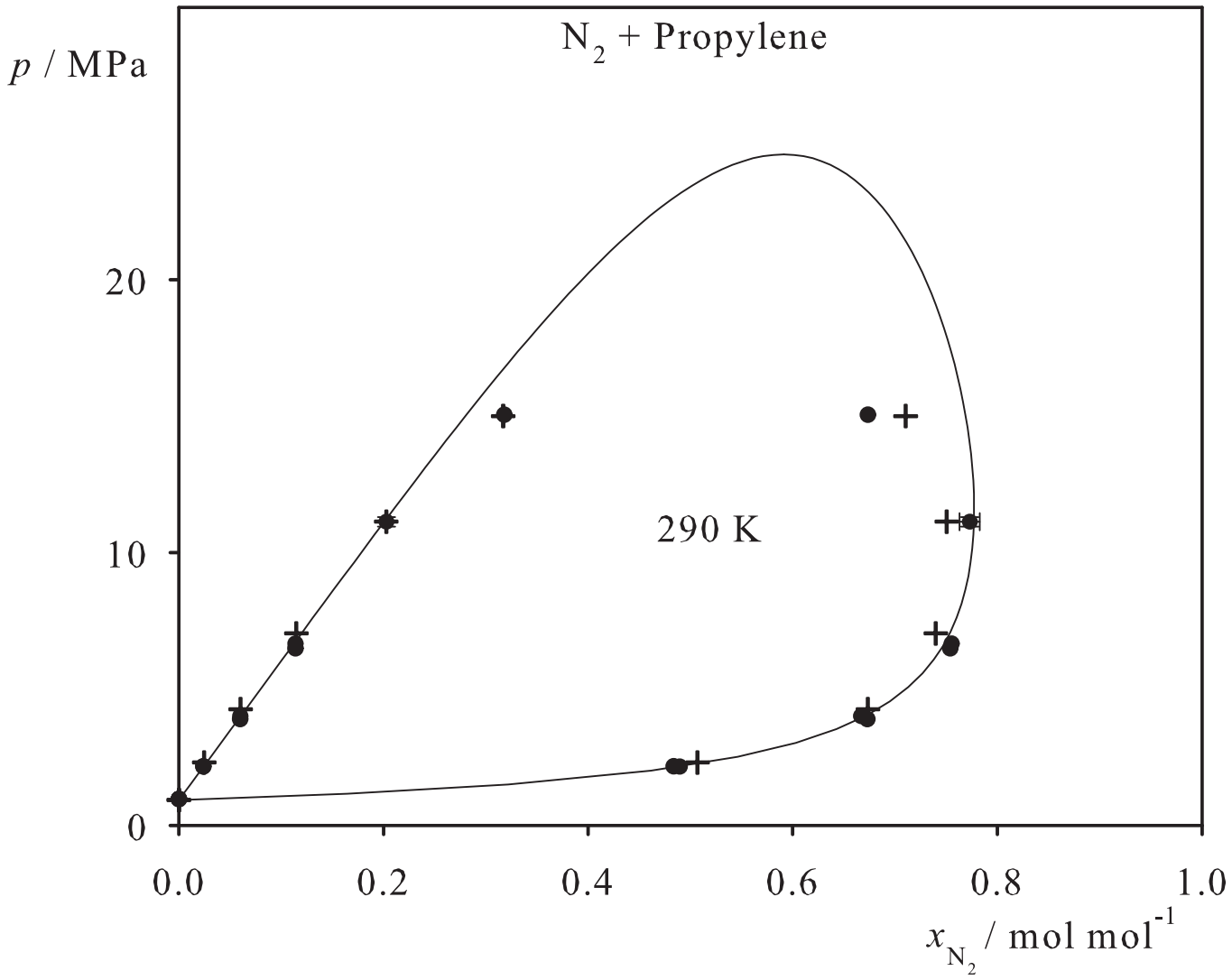

Fig. 40. Binary vapor-liquid equilibrium phase diagram: simulation data ●, experimental data + (cf. Table 2 of the manuscript for the reference) and Peng-Robinson equation of state —.

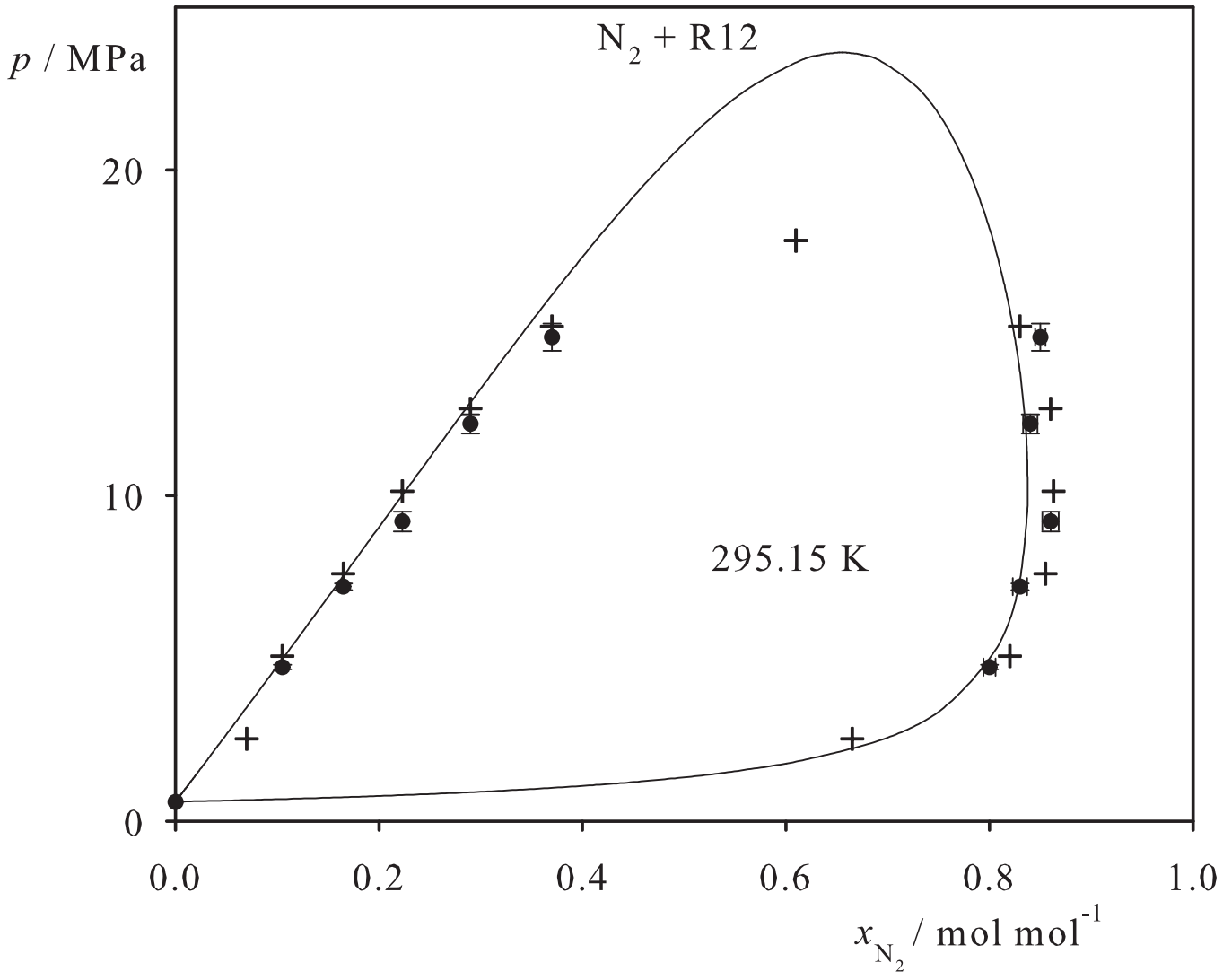

Fig. 41. Binary vapor-liquid equilibrium phase diagram: simulation data ●, experimental data + (cf. Table 2 of the manuscript for the reference) and Peng-Robinson equation of state —.

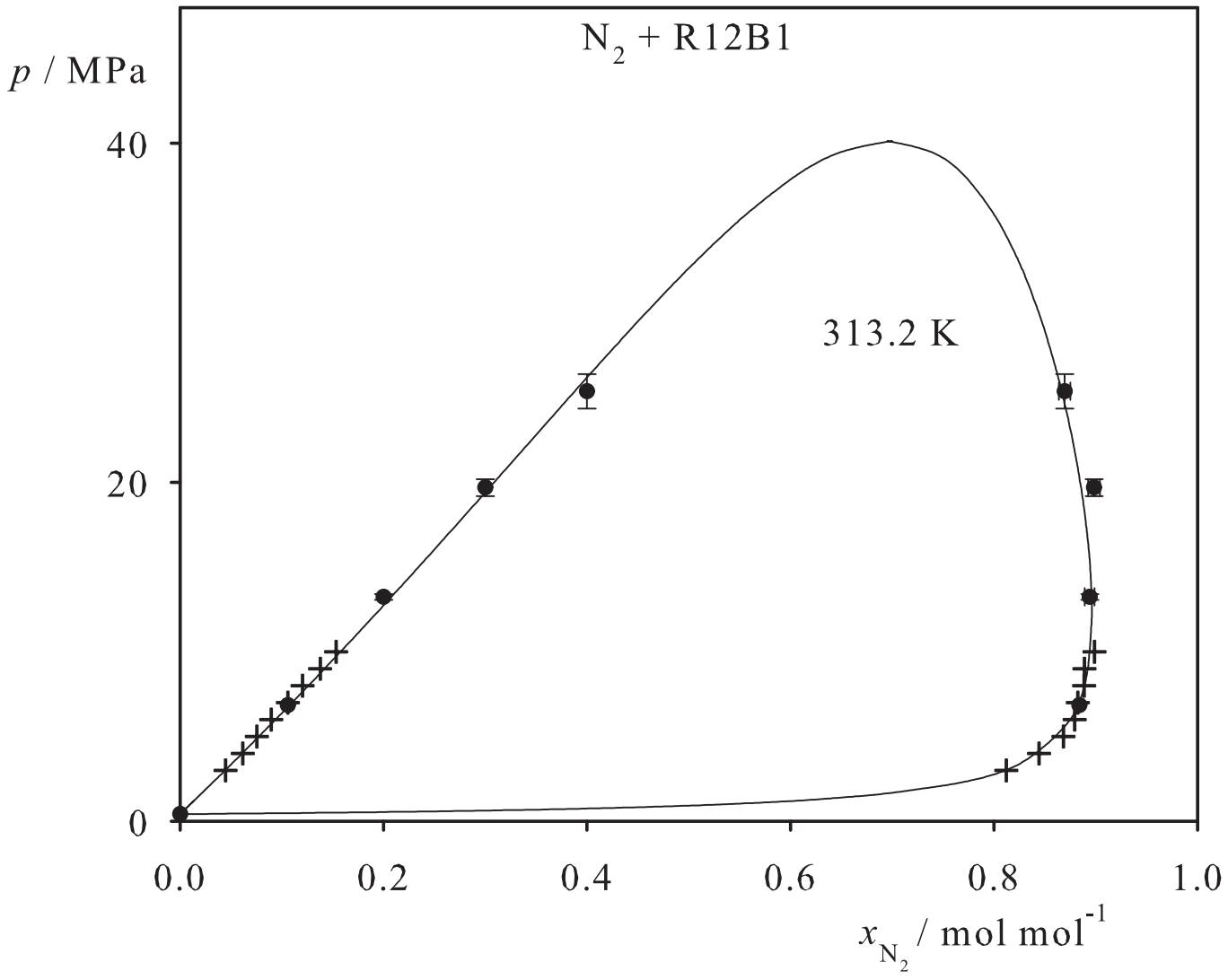

Fig. 42. Binary vapor-liquid equilibrium phase diagram: simulation data ●, experimental data + (cf. Table 2 of the manuscript for the reference) and Peng-Robinson equation of state —.

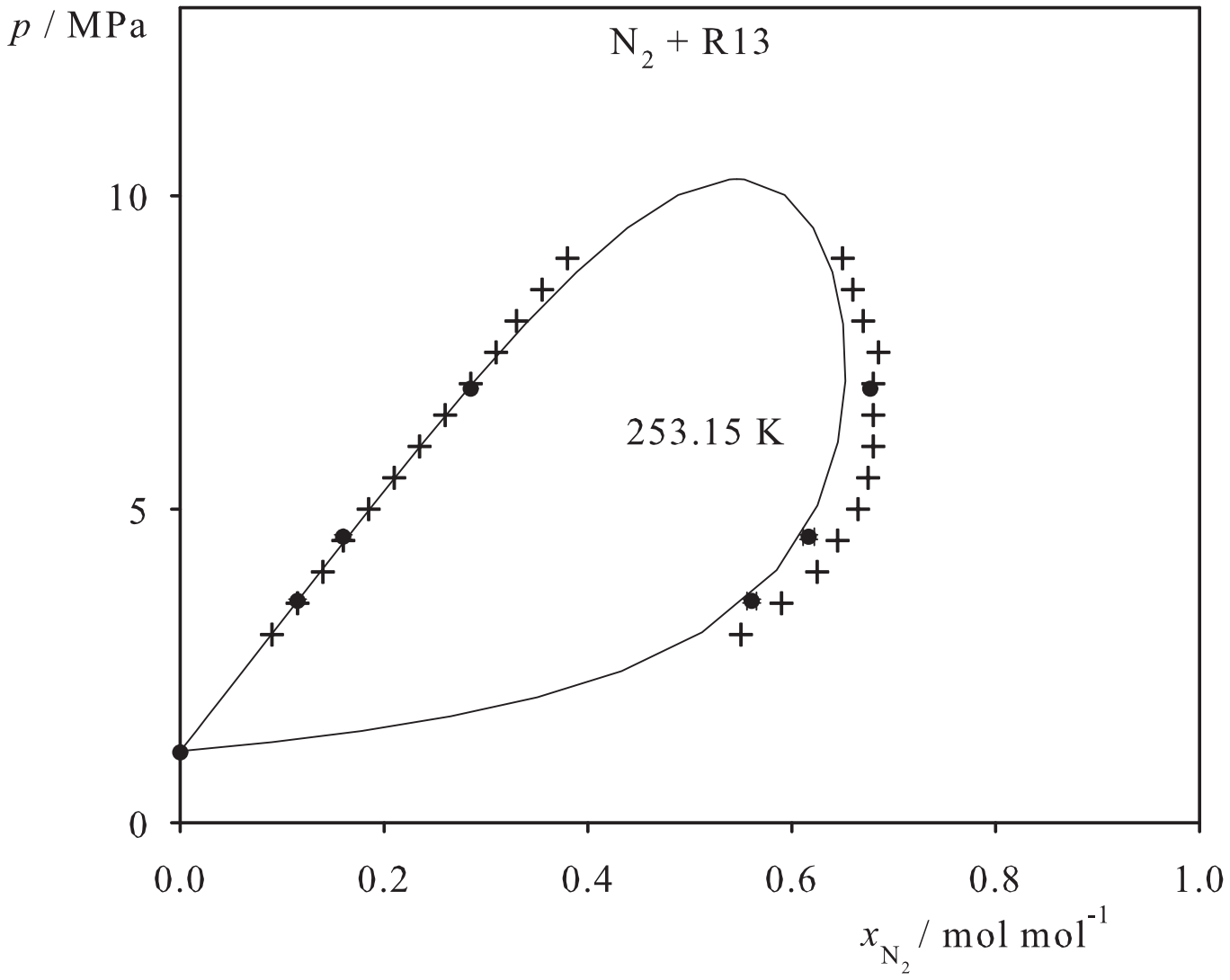

Fig. 43. Binary vapor-liquid equilibrium phase diagram: simulation data ●, experimental data + (cf. Table 2 of the manuscript for the reference) and Peng-Robinson equation of state —.

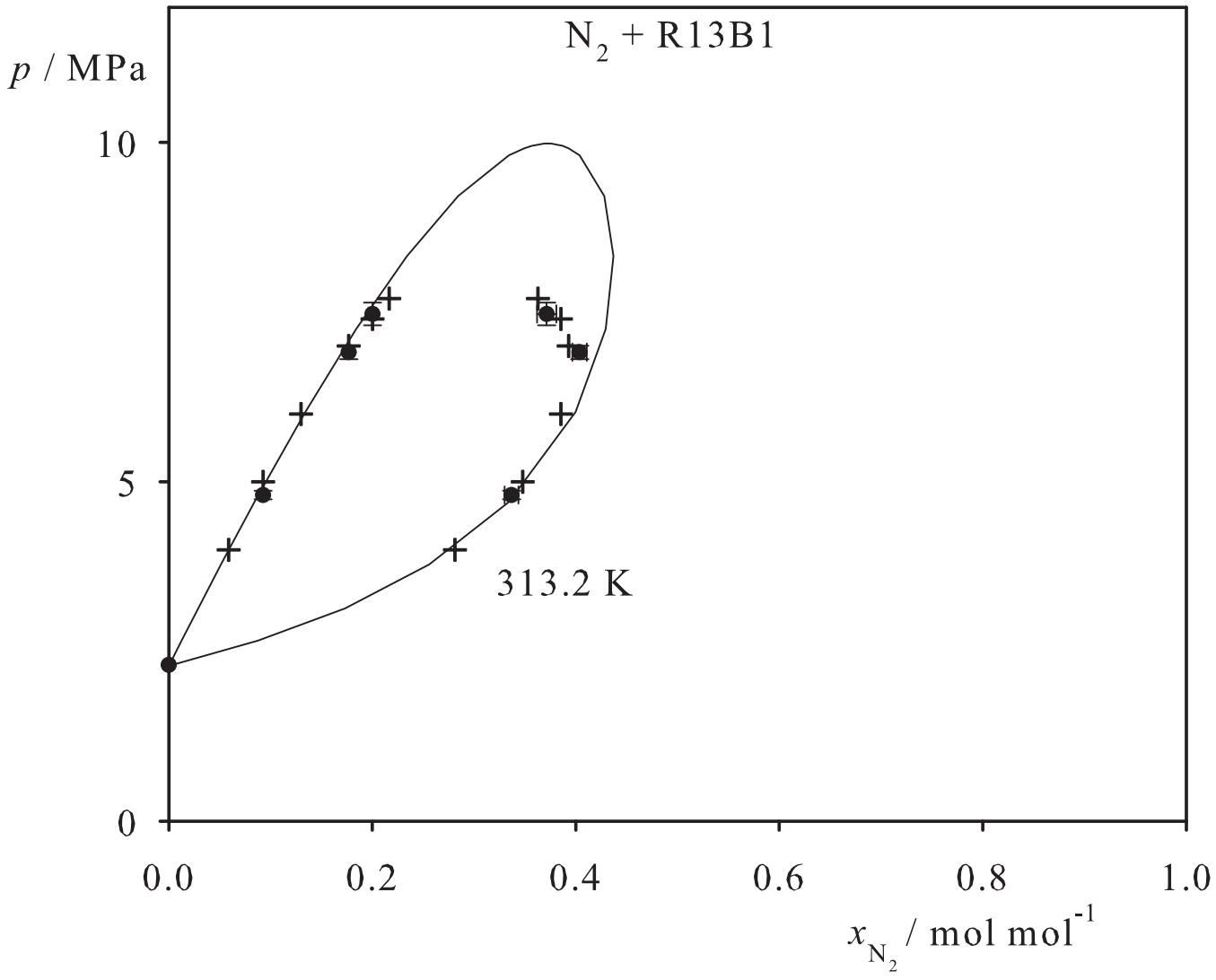

Fig. 44. Binary vapor-liquid equilibrium phase diagram: simulation data ●, experimental data + (cf. Table 2 of the manuscript for the reference) and Peng-Robinson equation of state —.

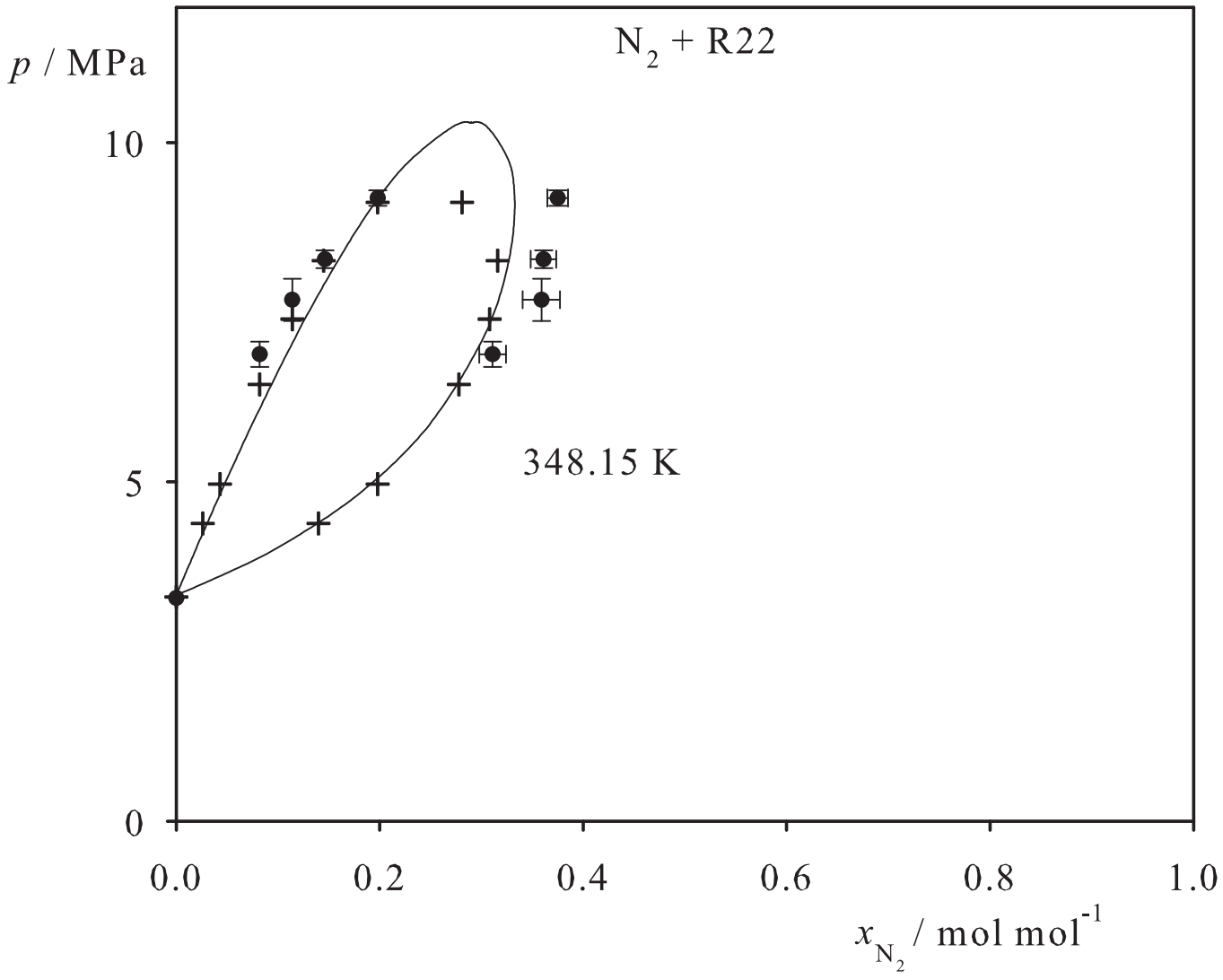

Fig. 45. Binary vapor-liquid equilibrium phase diagram: simulation data ●, experimental data + (cf. Table 2 of the manuscript for the reference) and Peng-Robinson equation of state —.

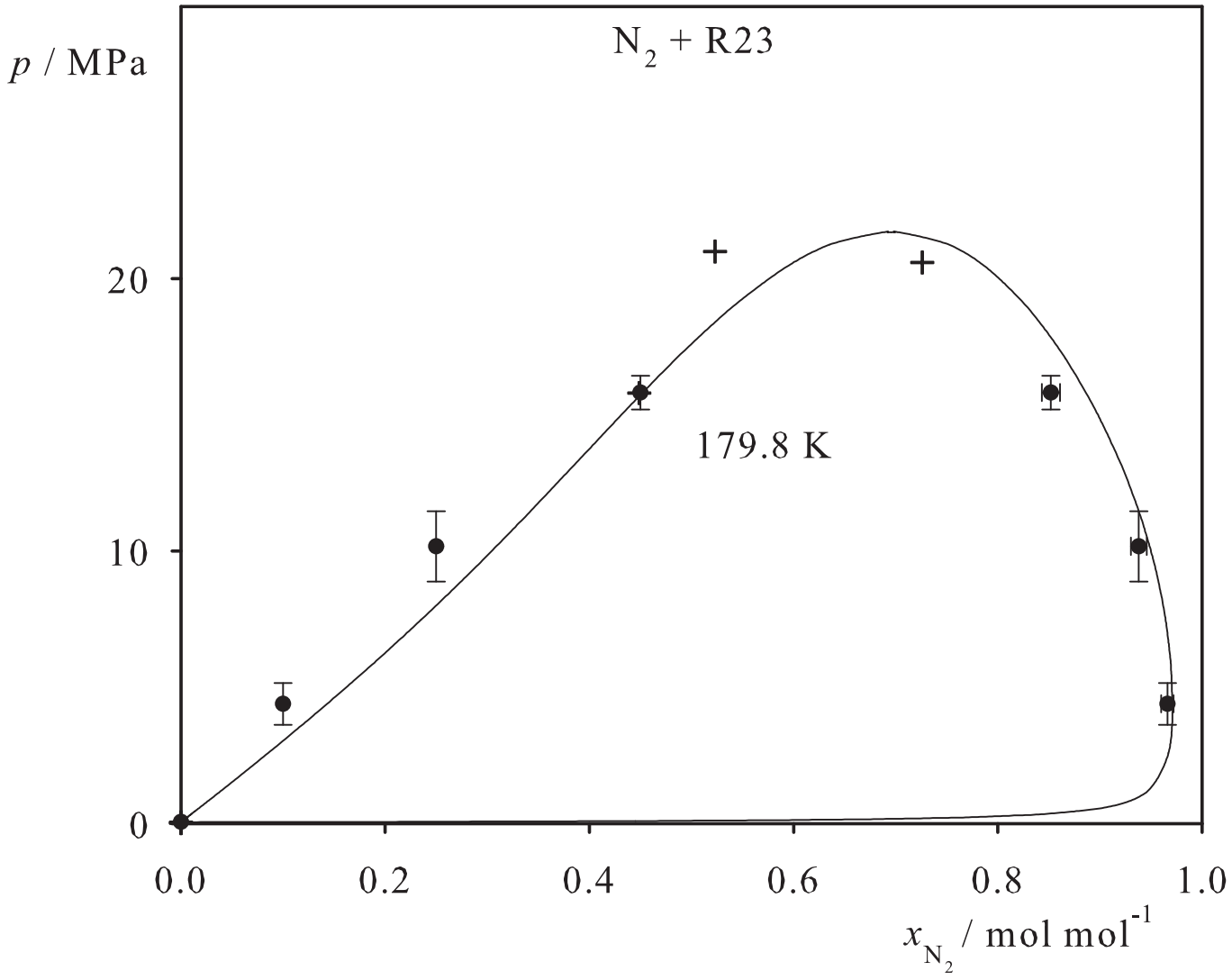

Fig. 46. Binary vapor-liquid equilibrium phase diagram: simulation data ●, experimental data + (cf. Table 2 of the manuscript for the reference) and Peng-Robinson equation of state —.

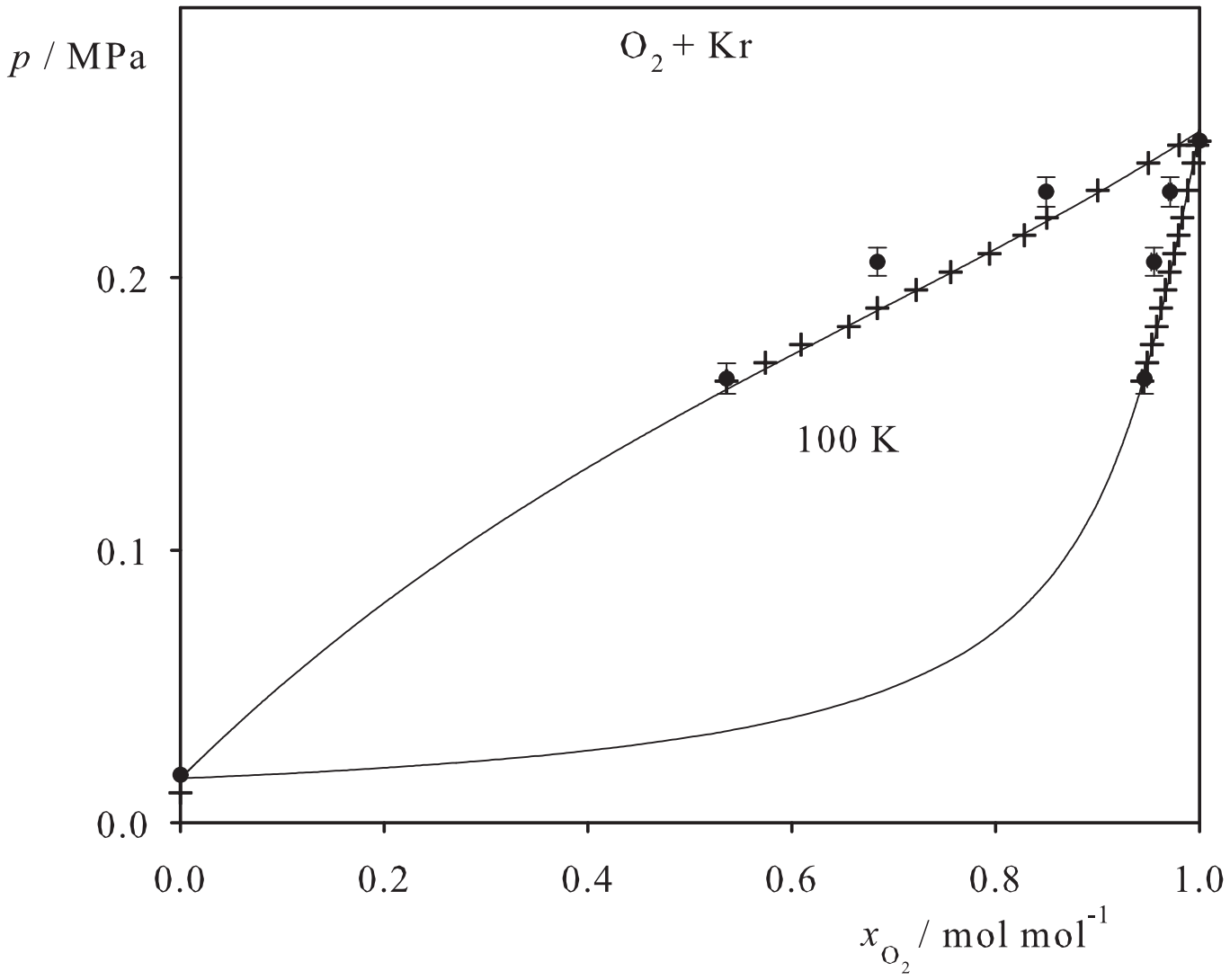

Fig. 47. Binary vapor-liquid equilibrium phase diagram: simulation data ●, experimental data + (cf. Table 2 of the manuscript for the reference) and Peng-Robinson equation of state —.

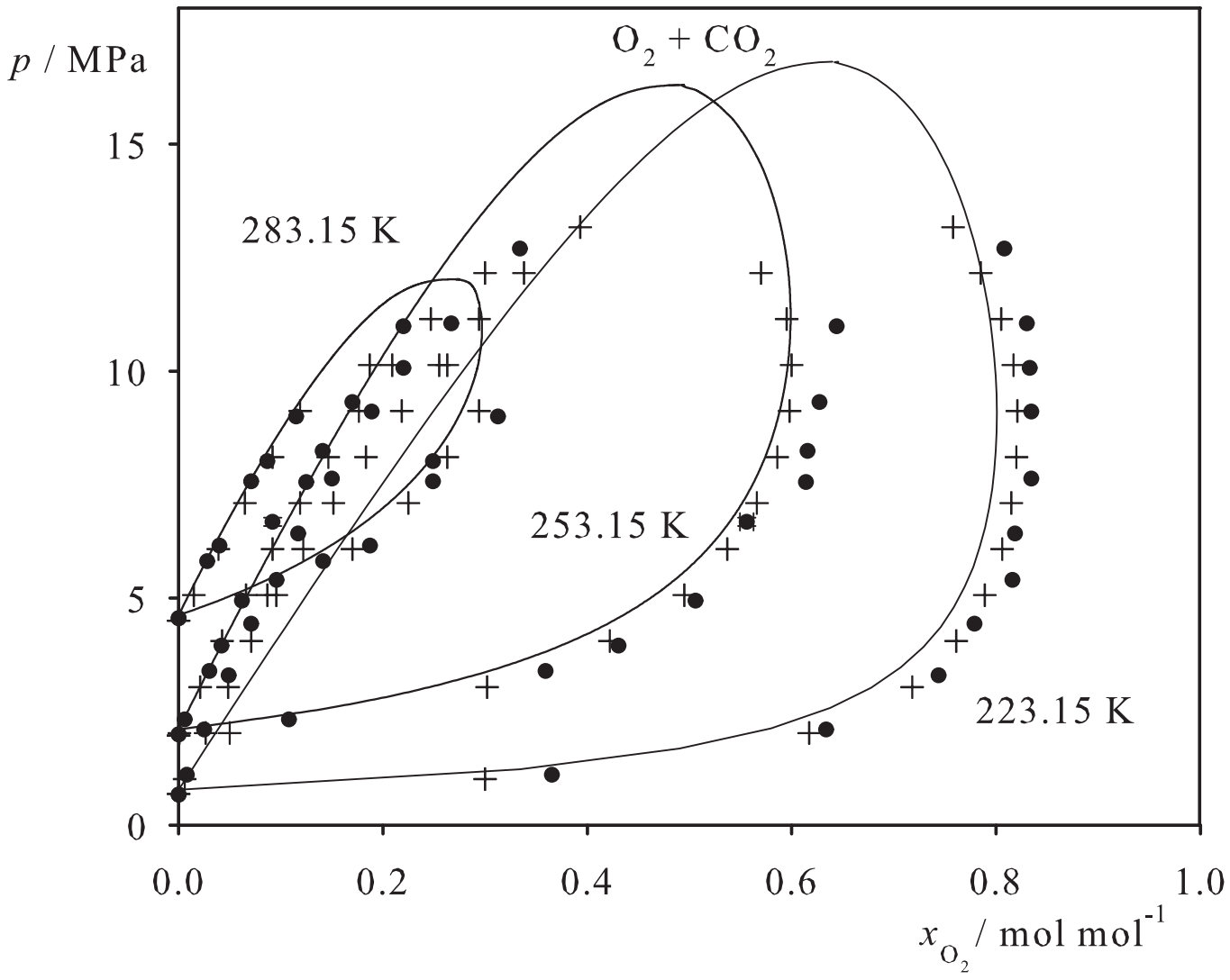

Fig. 48. Binary vapor-liquid equilibrium phase diagram: simulation data ●, experimental data + (cf. Table 2 of the manuscript for the reference) and Peng-Robinson equation of state —.

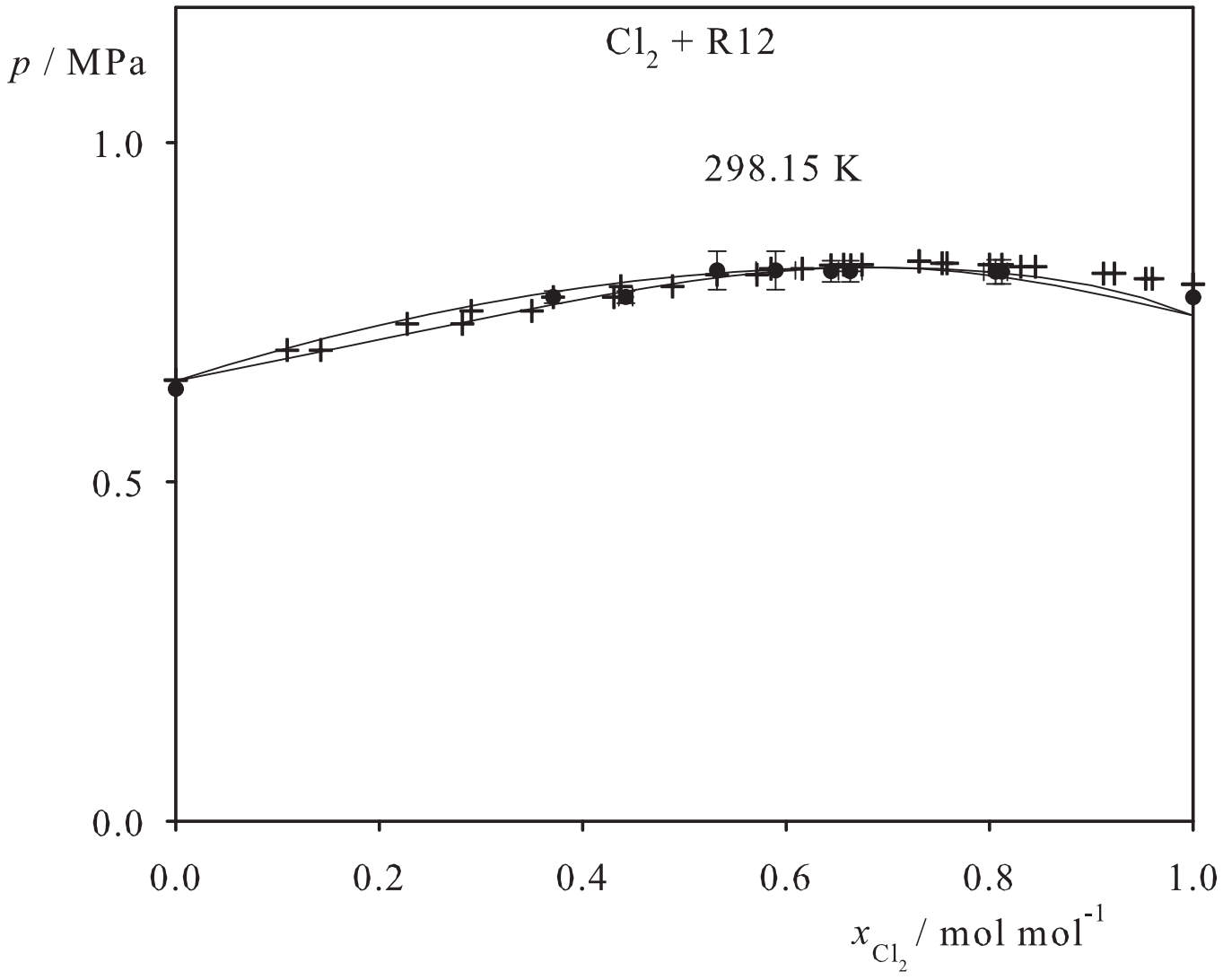

Fig. 49. Binary vapor-liquid equilibrium phase diagram: simulation data ●, experimental data + (cf. Table 2 of the manuscript for the reference) and Peng-Robinson equation of state —.

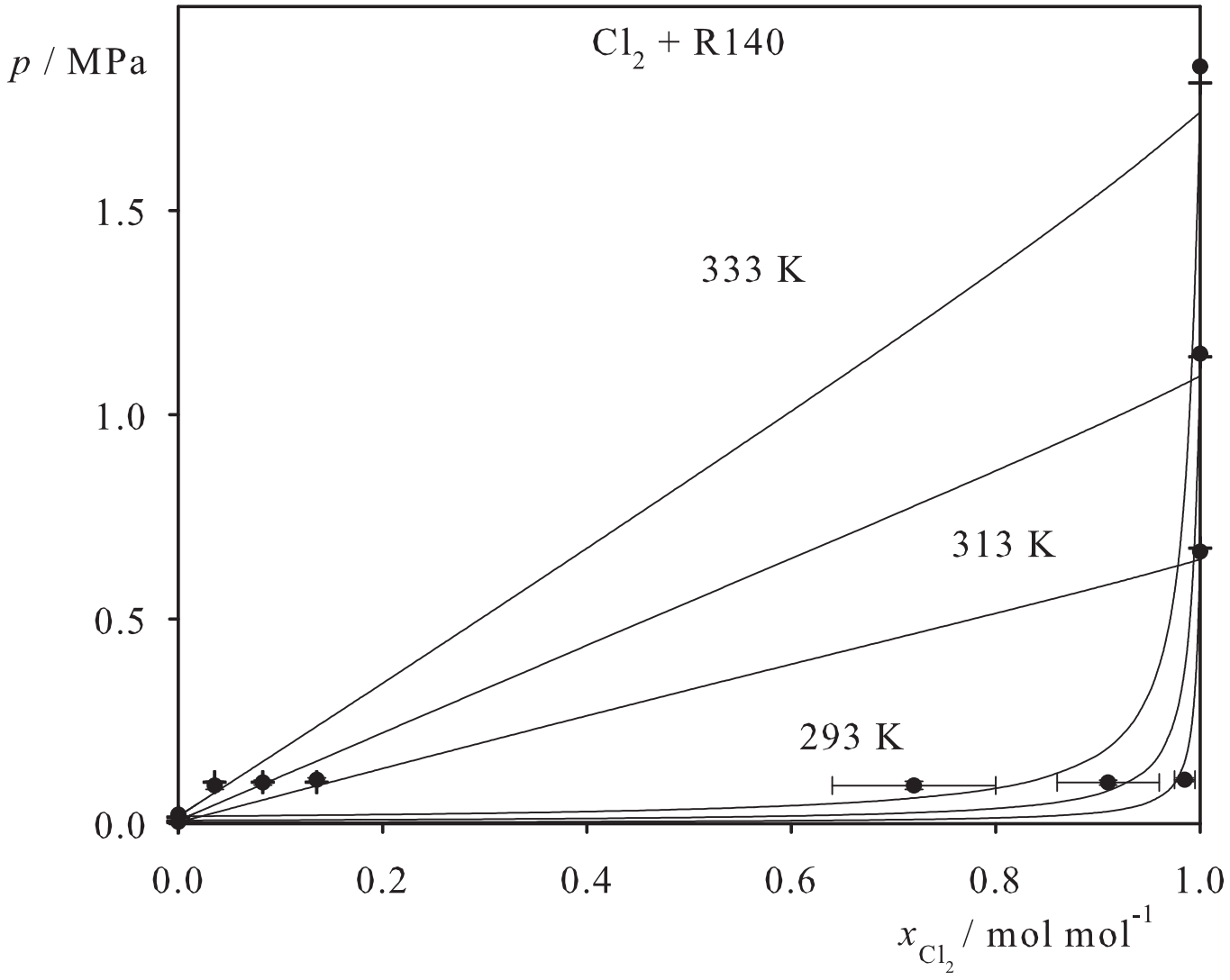

Fig. 50. Binary vapor-liquid equilibrium phase diagram: simulation data ●, experimental data + (cf. Table 2 of the manuscript for the reference) and Peng-Robinson equation of state —.

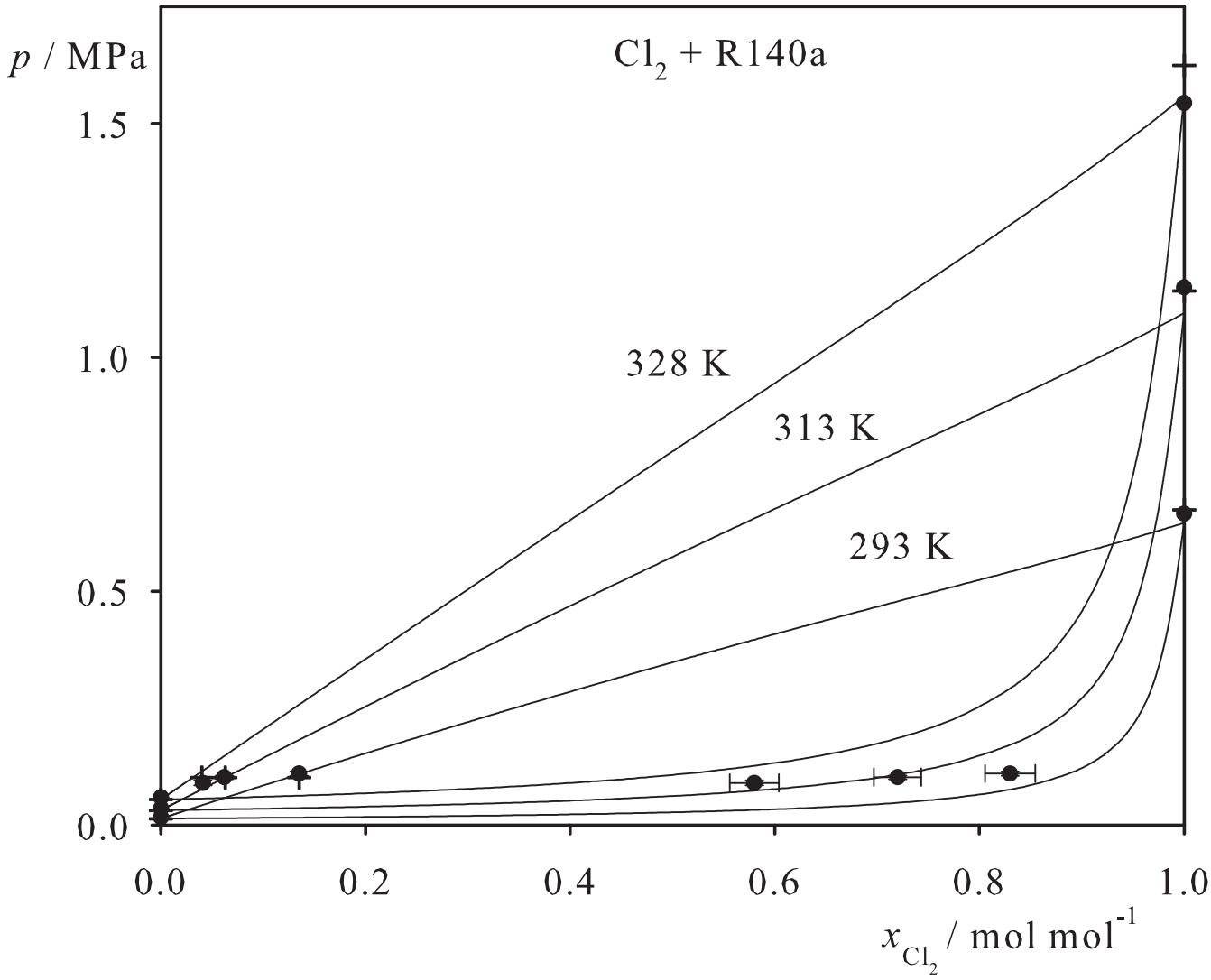

Fig. 51. Binary vapor-liquid equilibrium phase diagram: simulation data ●, experimental data + (cf. Table 2 of the manuscript for the reference) and Peng-Robinson equation of state —.

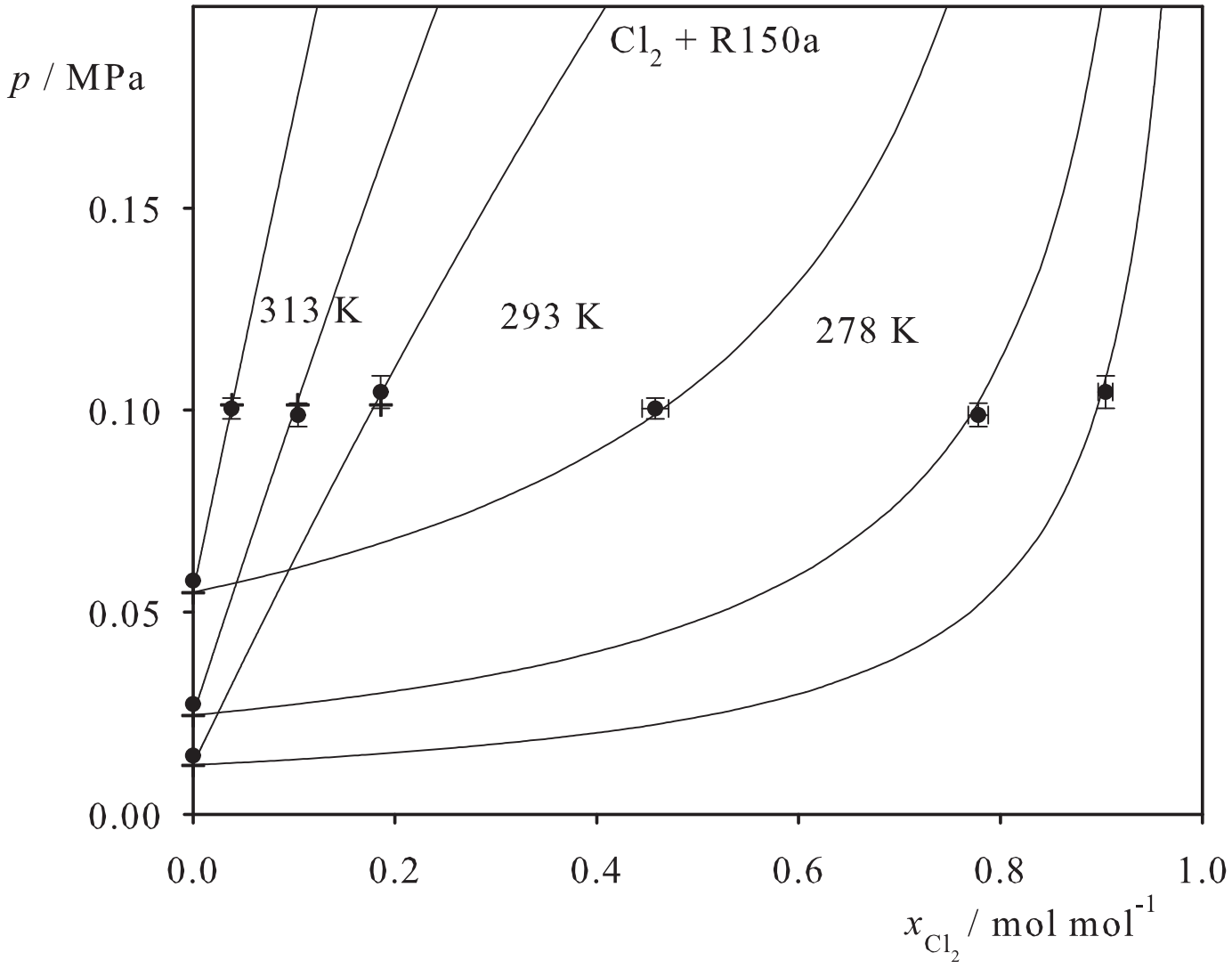

Fig. 52. Binary vapor-liquid equilibrium phase diagram: simulation data ●, experimental data + (cf. Table 2 of the manuscript for the reference) and Peng-Robinson equation of state —.

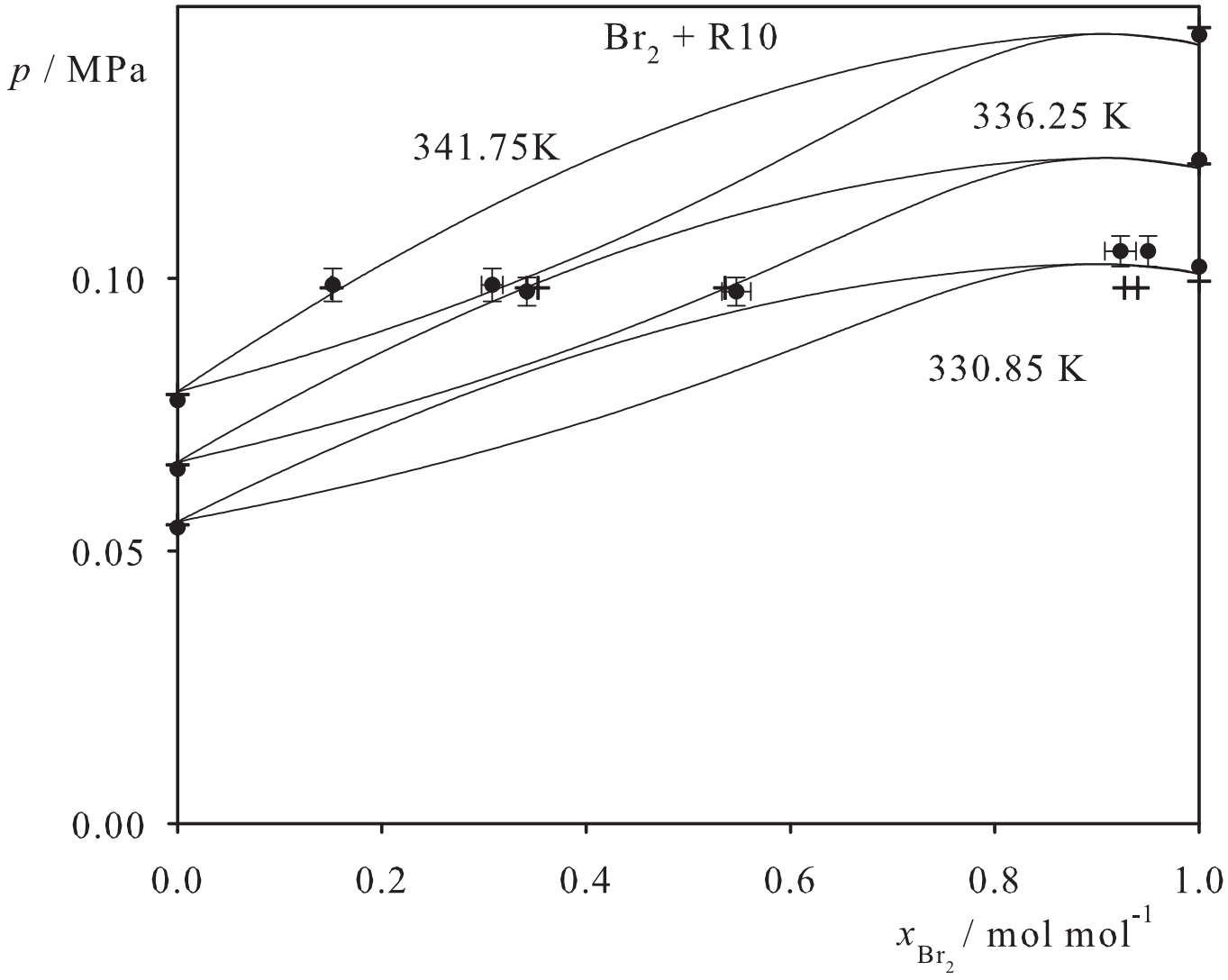

Fig. 53. Binary vapor-liquid equilibrium phase diagram: simulation data ●, experimental data + (cf. Table 2 of the manuscript for the reference) and Peng-Robinson equation of state —.

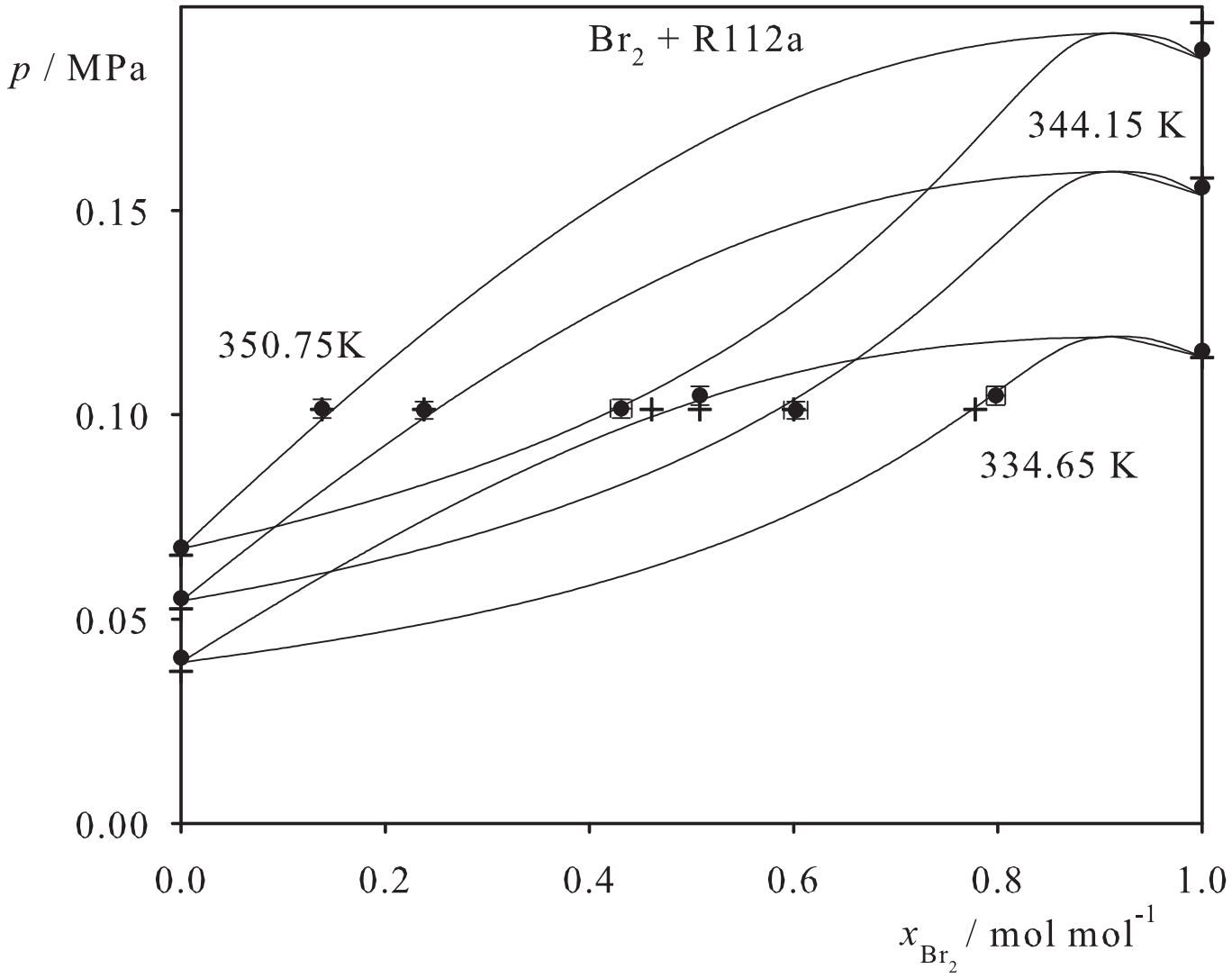

Fig. 54. Binary vapor-liquid equilibrium phase diagram: simulation data ●, experimental data + (cf. Table 2 of the manuscript for the reference) and Peng-Robinson equation of state —.

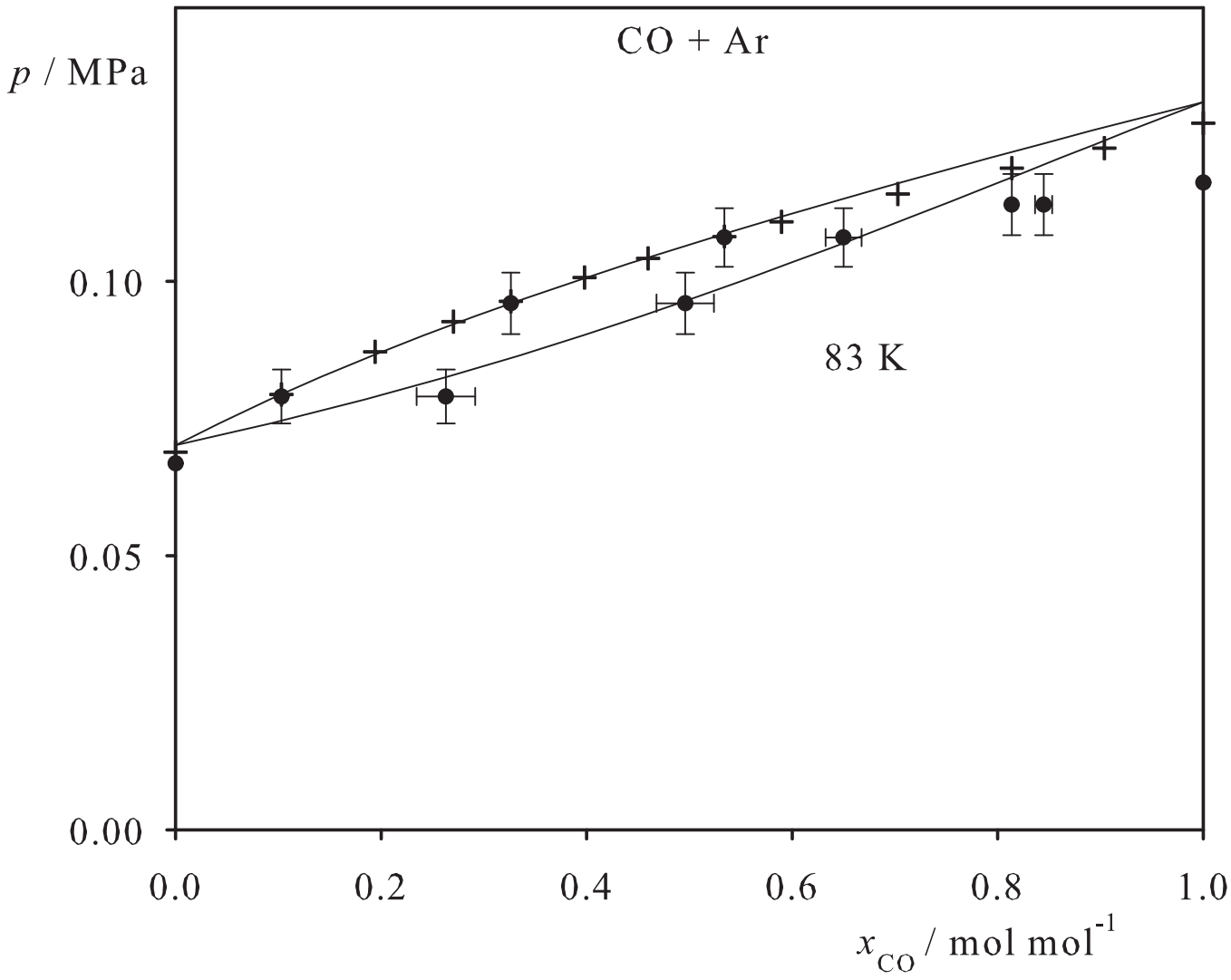

Fig. 55. Binary vapor-liquid equilibrium phase diagram: simulation data ●, experimental data + (cf. Table 2 of the manuscript for the reference) and Peng-Robinson equation of state —.

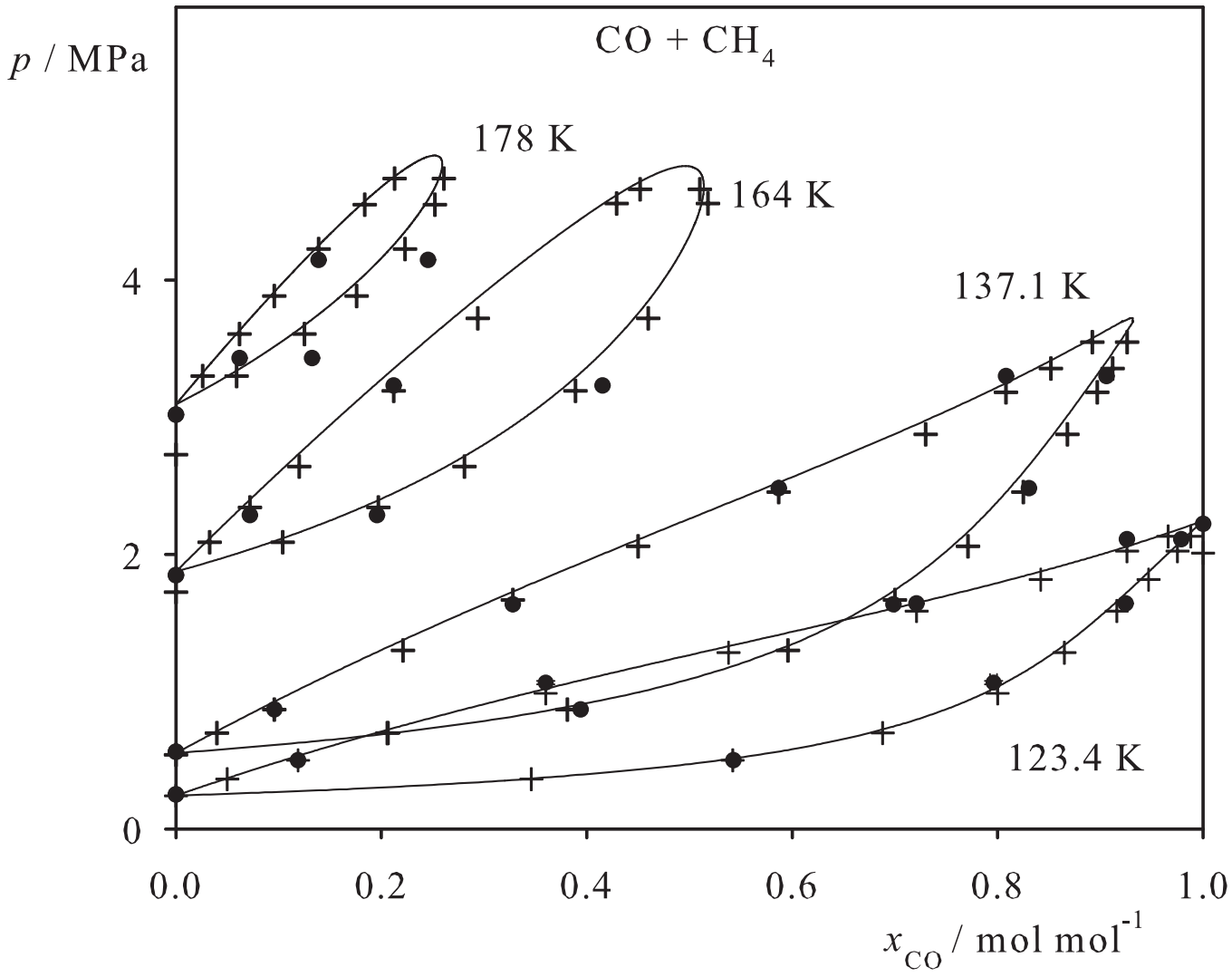

Fig. 56. Binary vapor-liquid equilibrium phase diagram: simulation data ●, experimental data + (cf. Table 2 of the manuscript for the reference) and Peng-Robinson equation of state —.

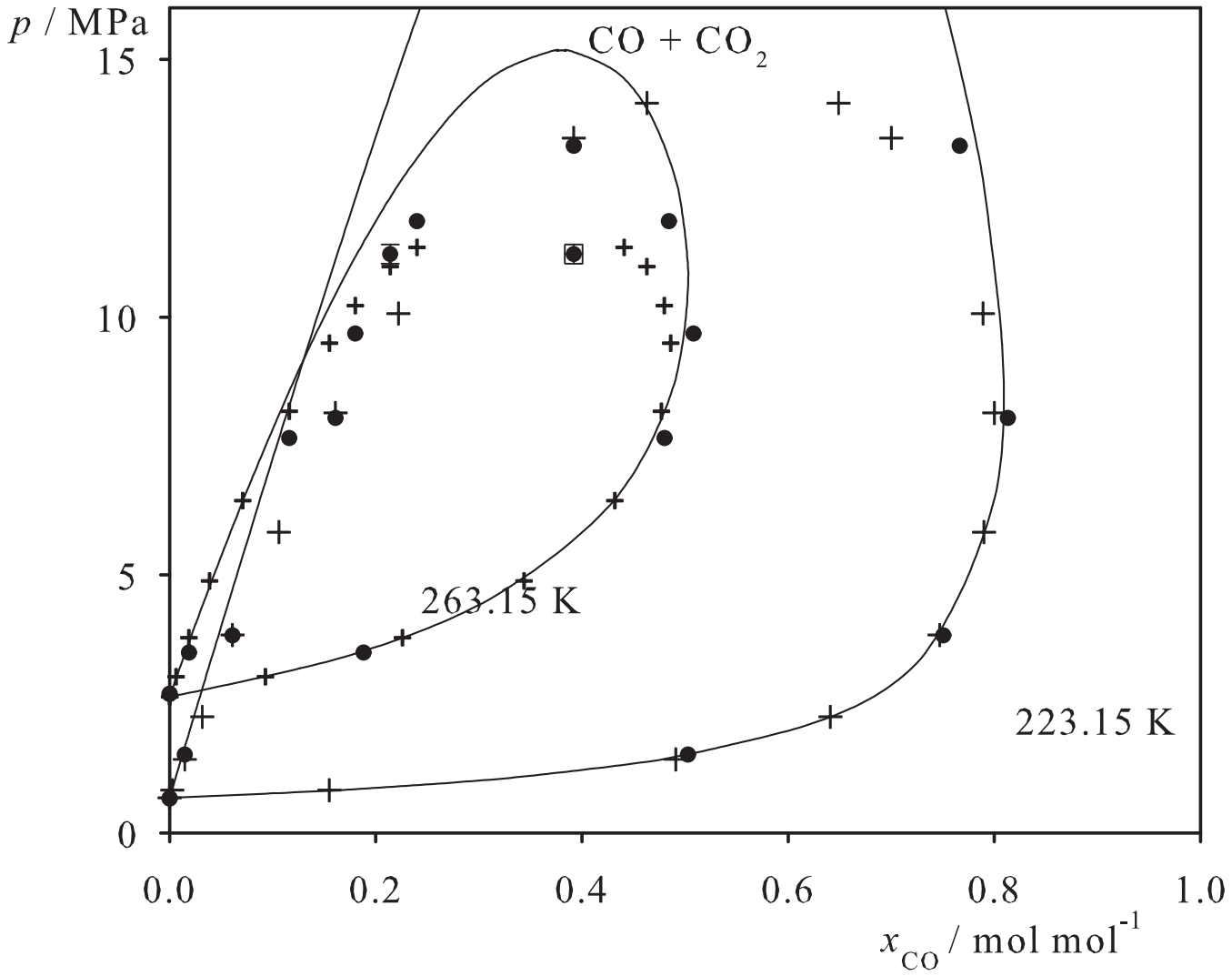

Fig. 57. Binary vapor-liquid equilibrium phase diagram: simulation data ●, experimental data + (cf. Table 2 of the manuscript for the reference) and Peng-Robinson equation of state —.

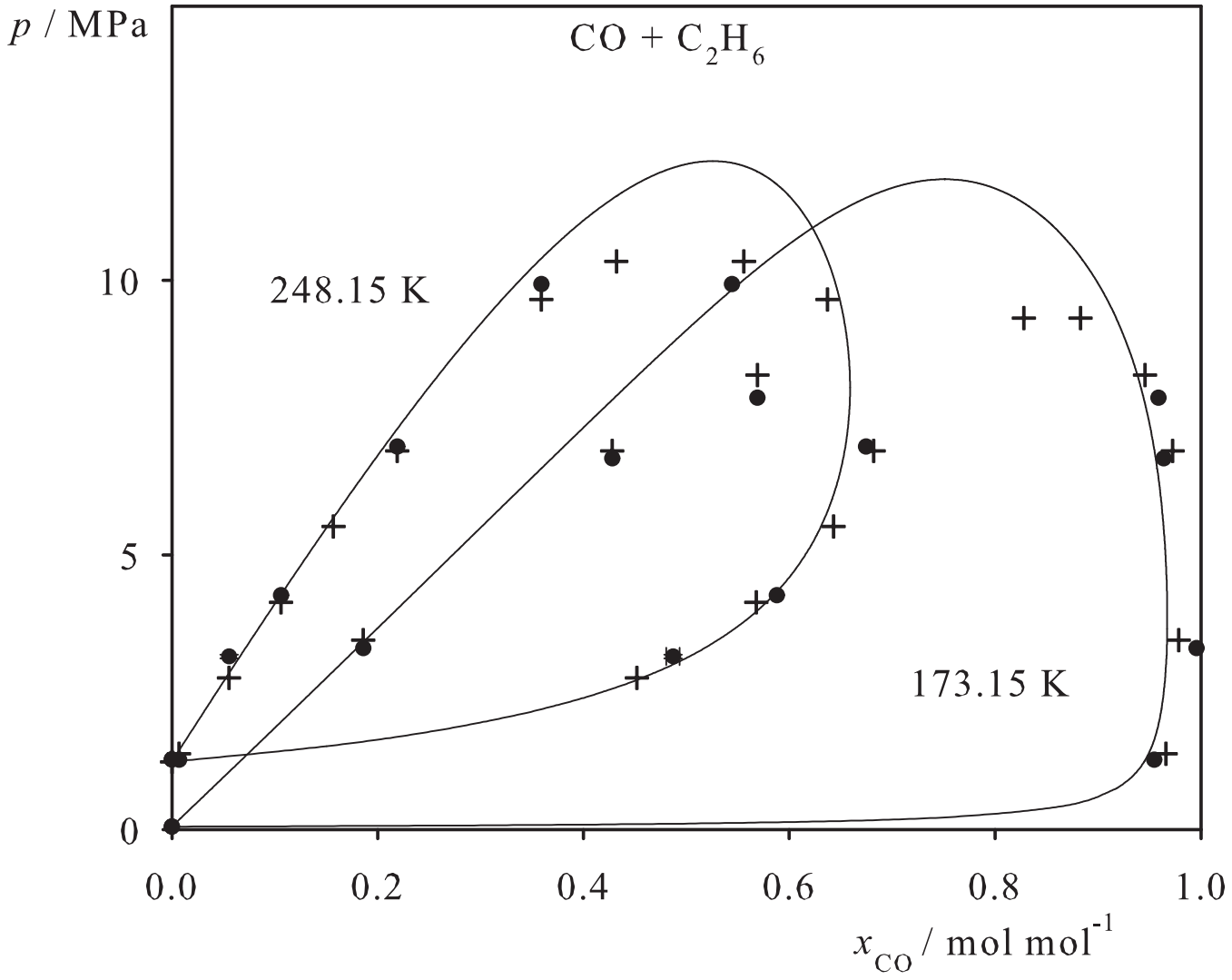

Fig. 58. Binary vapor-liquid equilibrium phase diagram: simulation data ●, experimental data + (cf. Table 2 of the manuscript for the reference) and Peng-Robinson equation of state —.

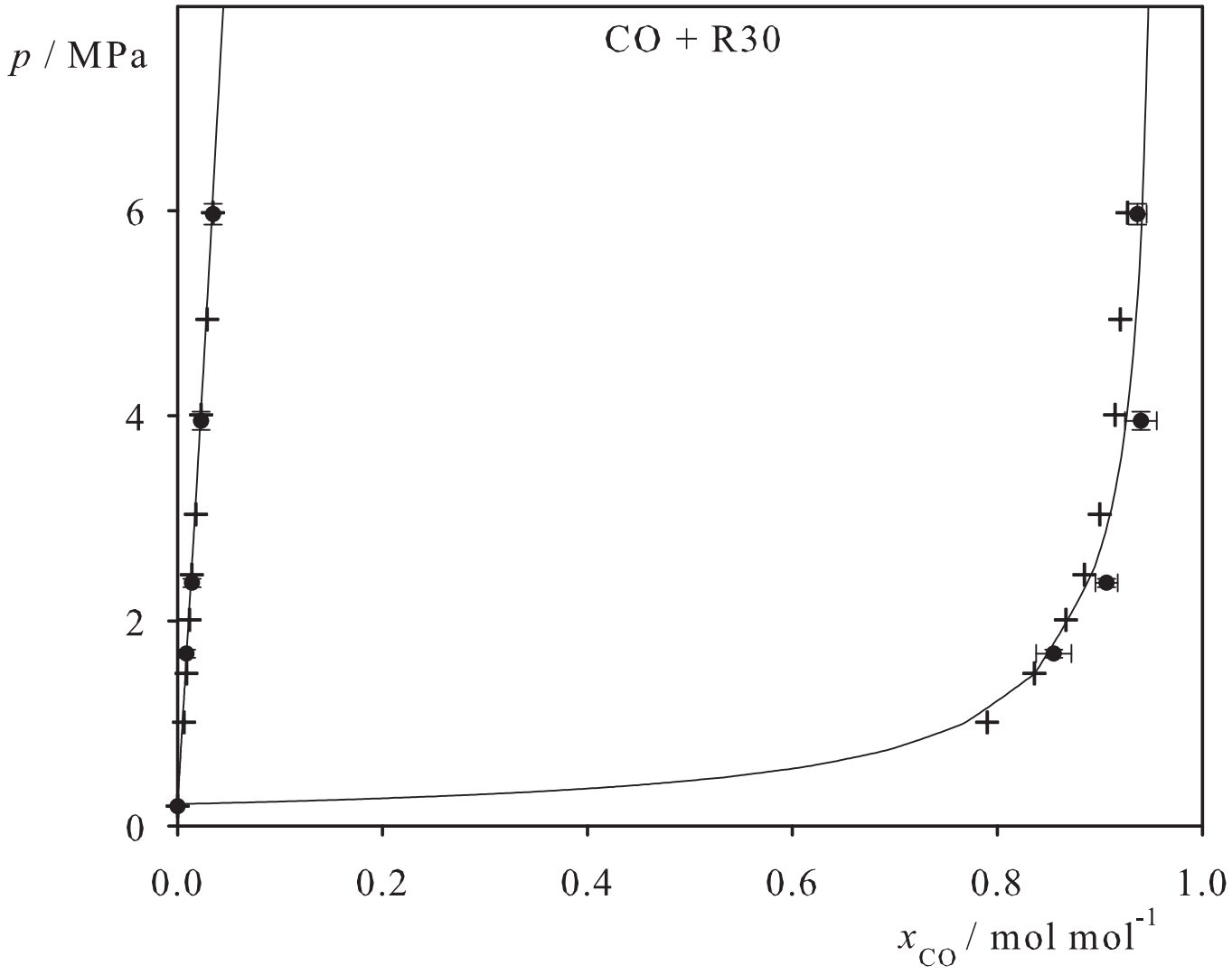

Fig. 59. Binary vapor-liquid equilibrium phase diagram: simulation data ●, experimental data + (cf. Table 2 of the manuscript for the reference) and Peng-Robinson equation of state —.

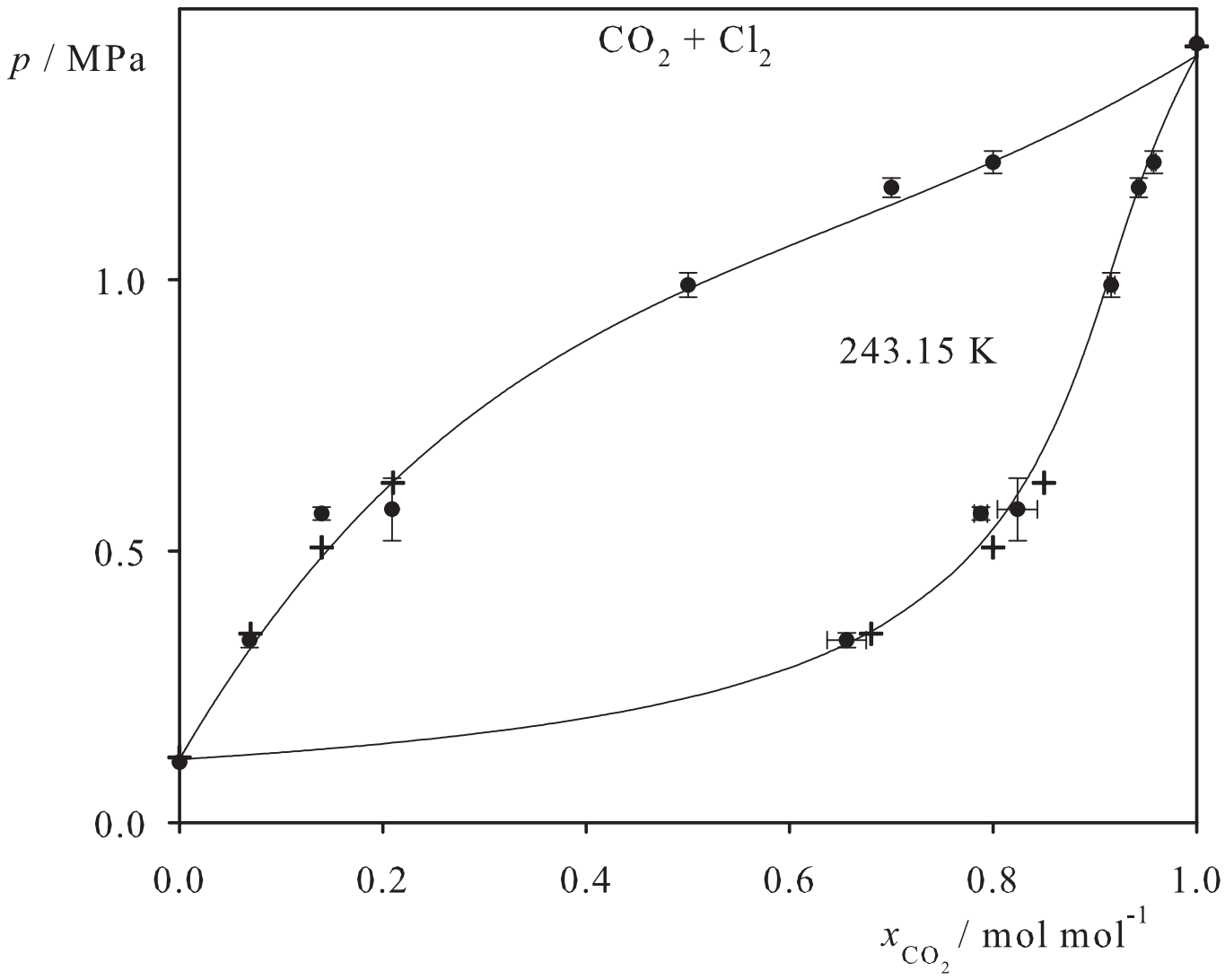

Fig. 60. Binary vapor-liquid equilibrium phase diagram: simulation data ●, experimental data + (cf. Table 2 of the manuscript for the reference) and Peng-Robinson equation of state —.

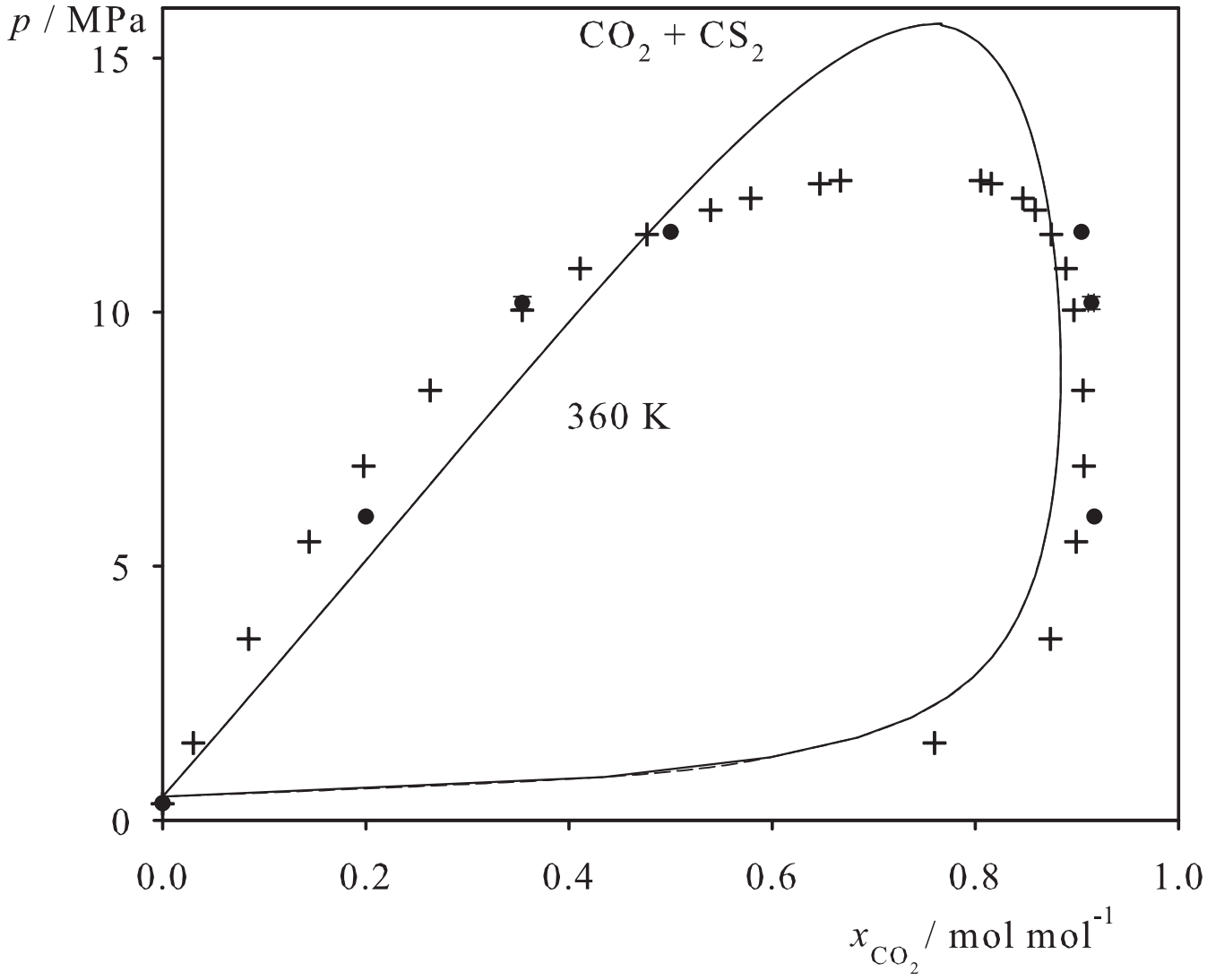

Fig. 61. Binary vapor-liquid equilibrium phase diagram: simulation data ●, experimental data + (cf. Table 2 of the manuscript for the reference) and Peng-Robinson equation of state —.

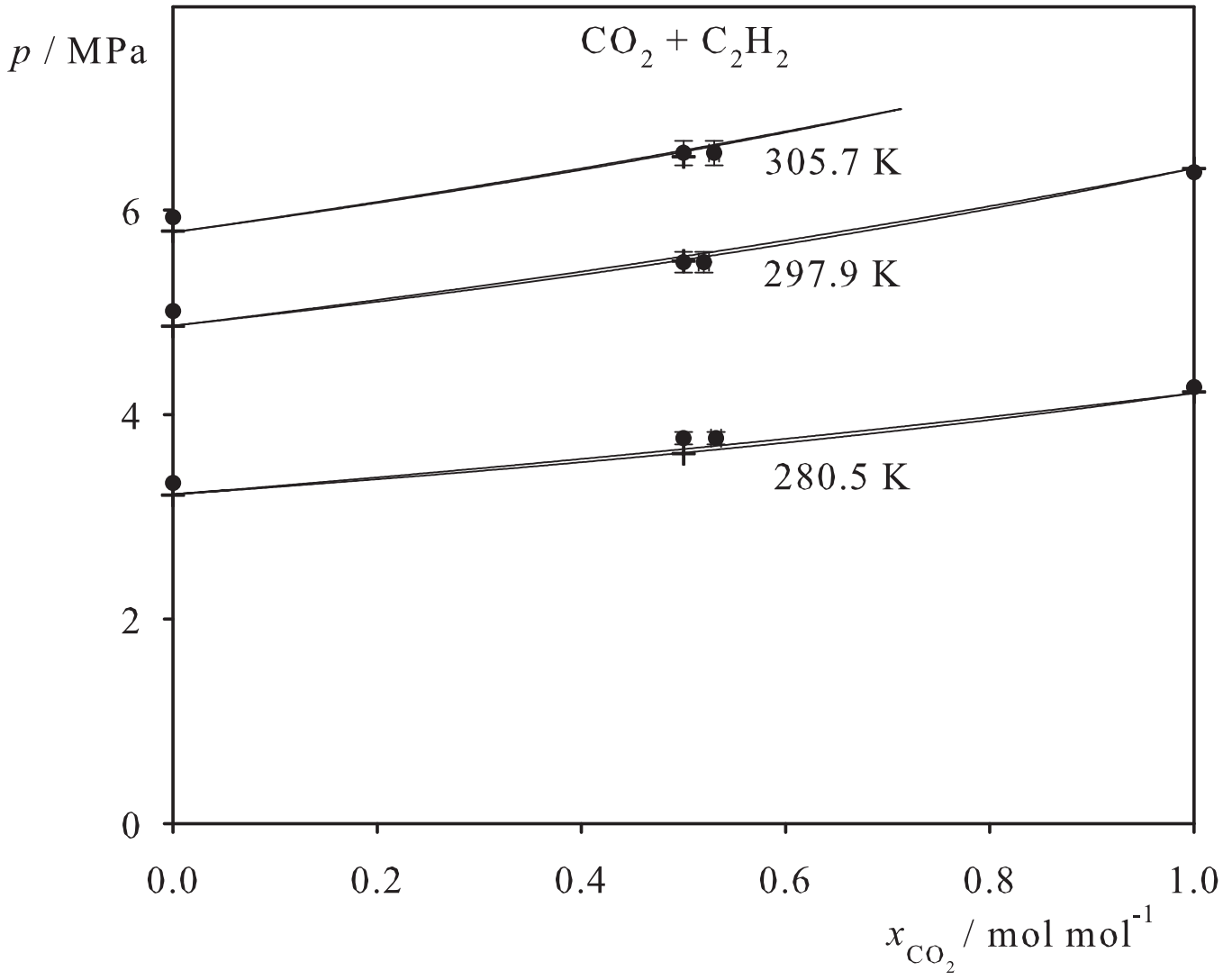

Fig. 62. Binary vapor-liquid equilibrium phase diagram: simulation data ●, experimental data + (cf. Table 2 of the manuscript for the reference) and Peng-Robinson equation of state —.

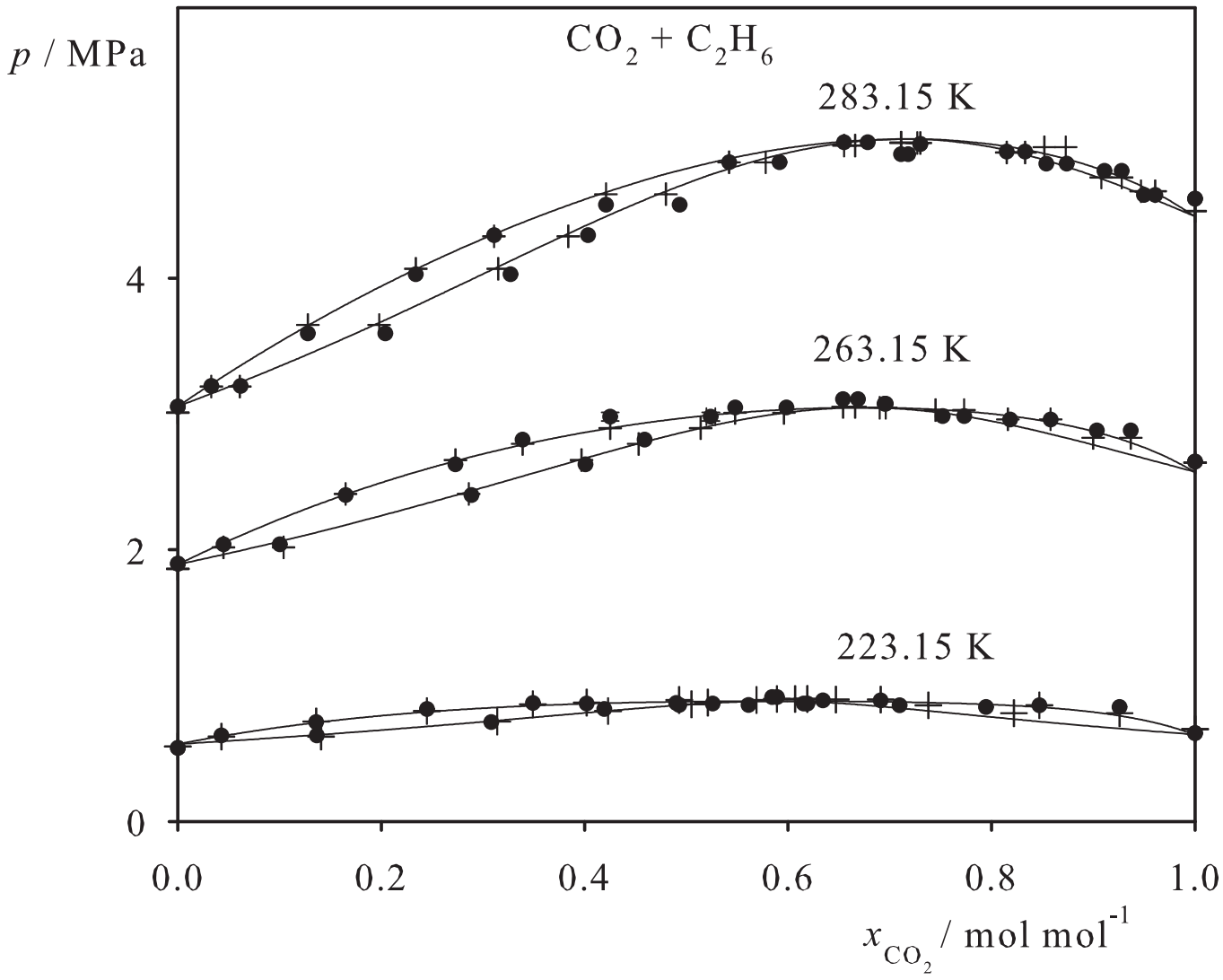

Fig. 63. Binary vapor-liquid equilibrium phase diagram: simulation data ●, experimental data + (cf. Table 2 of the manuscript for the reference) and Peng-Robinson equation of state —.

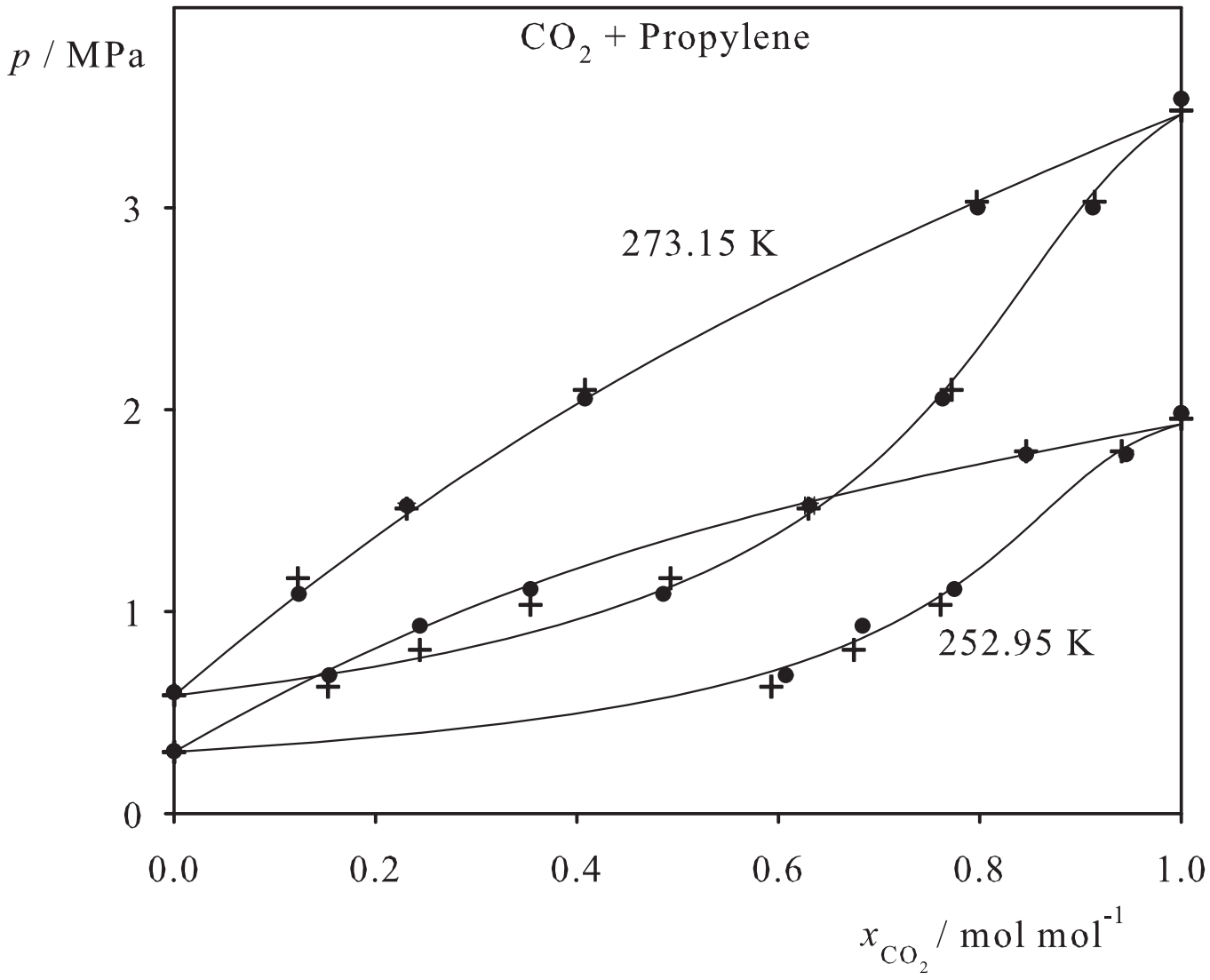

Fig. 64. Binary vapor-liquid equilibrium phase diagram: simulation data ●, experimental data + (cf. Table 2 of the manuscript for the reference) and Peng-Robinson equation of state —.

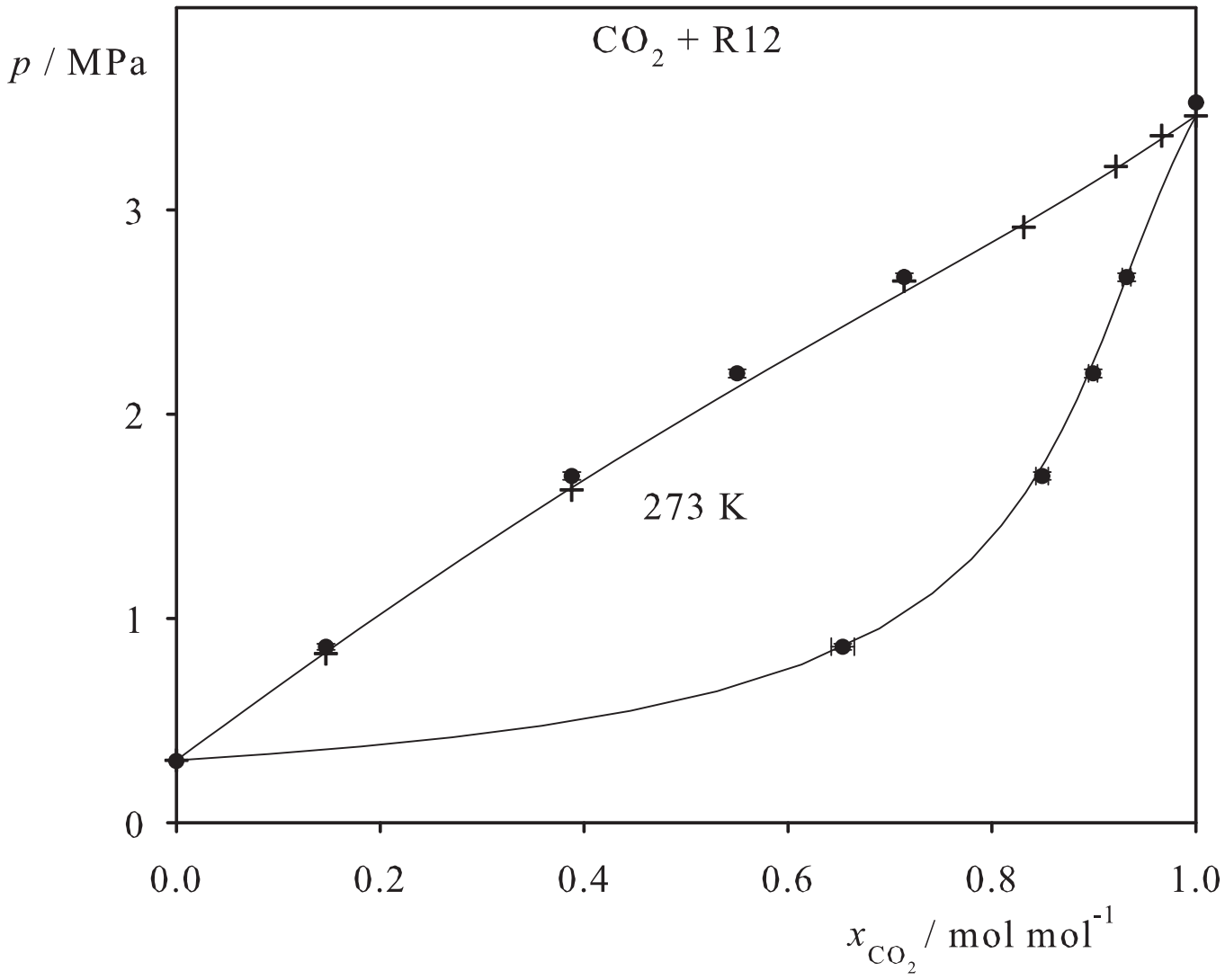

Fig. 65. Binary vapor-liquid equilibrium phase diagram: simulation data ●, experimental data + (cf. Table 2 of the manuscript for the reference) and Peng-Robinson equation of state —.

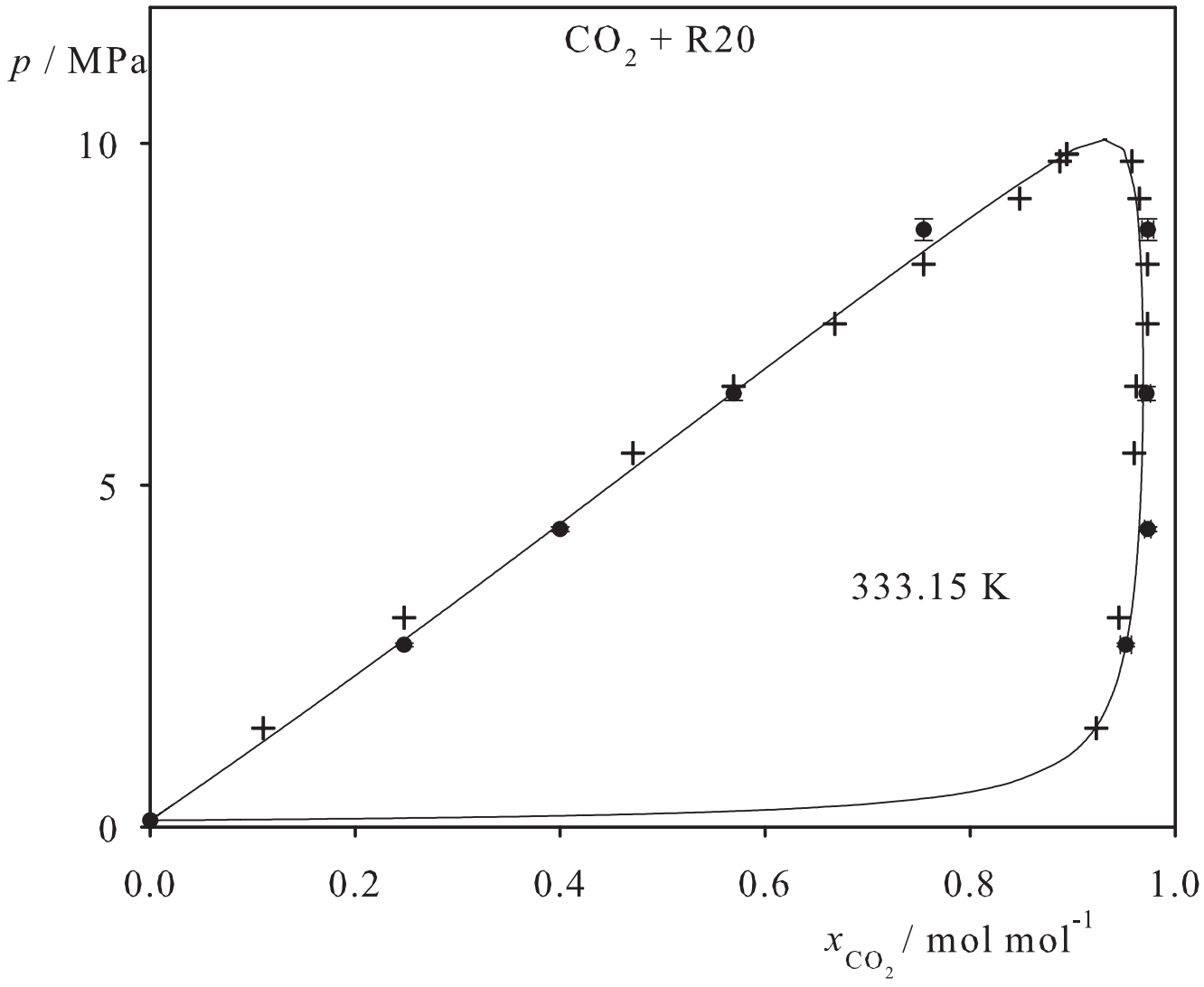

Fig. 66. Binary vapor-liquid equilibrium phase diagram: simulation data ●, experimental data + (cf. Table 2 of the manuscript for the reference) and Peng-Robinson equation of state —.

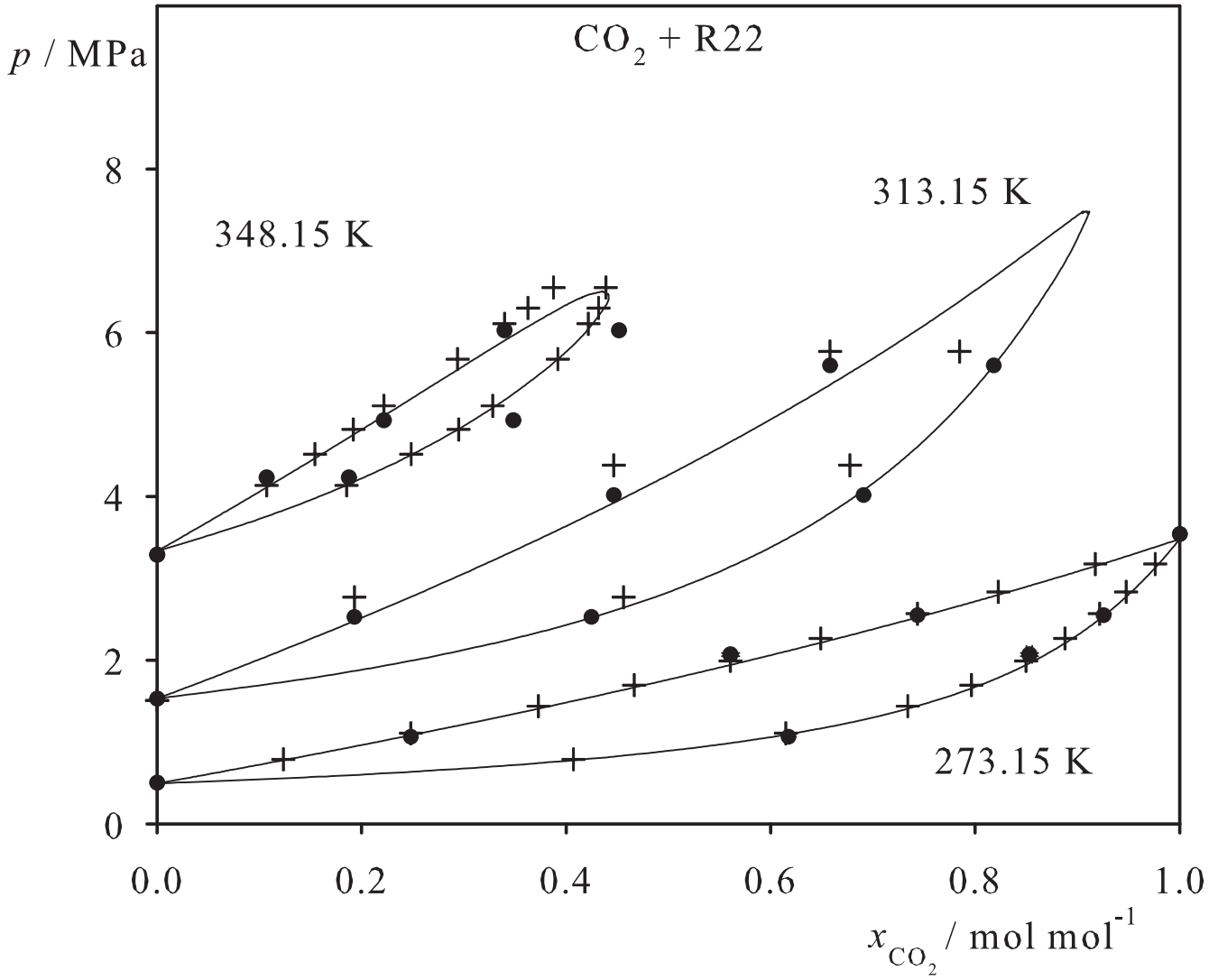

Fig. 67. Binary vapor-liquid equilibrium phase diagram: simulation data ●, experimental data + (cf. Table 2 of the manuscript for the reference) and Peng-Robinson equation of state —.

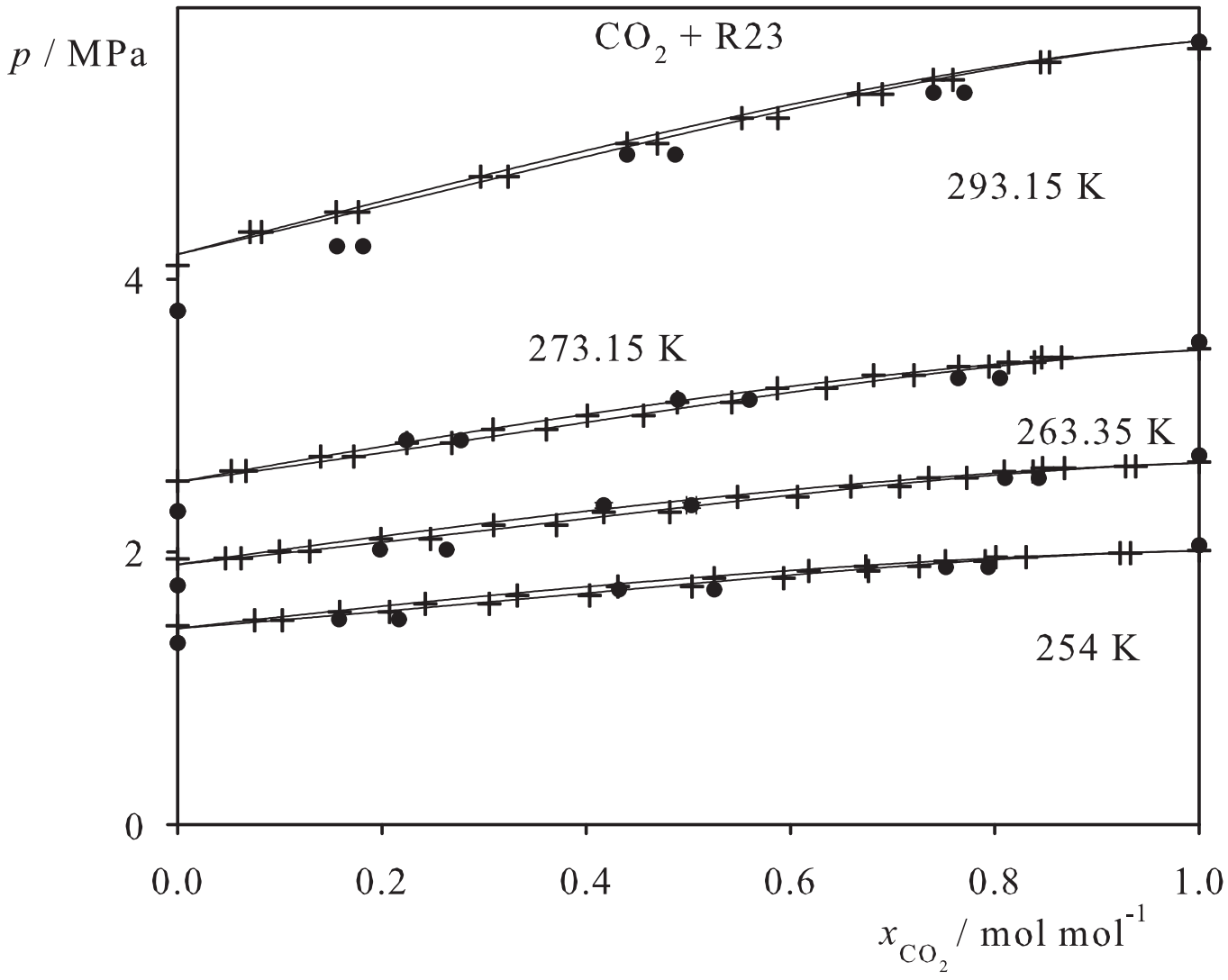

Fig. 68. Binary vapor-liquid equilibrium phase diagram: simulation data ●, experimental data + (cf. Table 2 of the manuscript for the reference) and Peng-Robinson equation of state —.

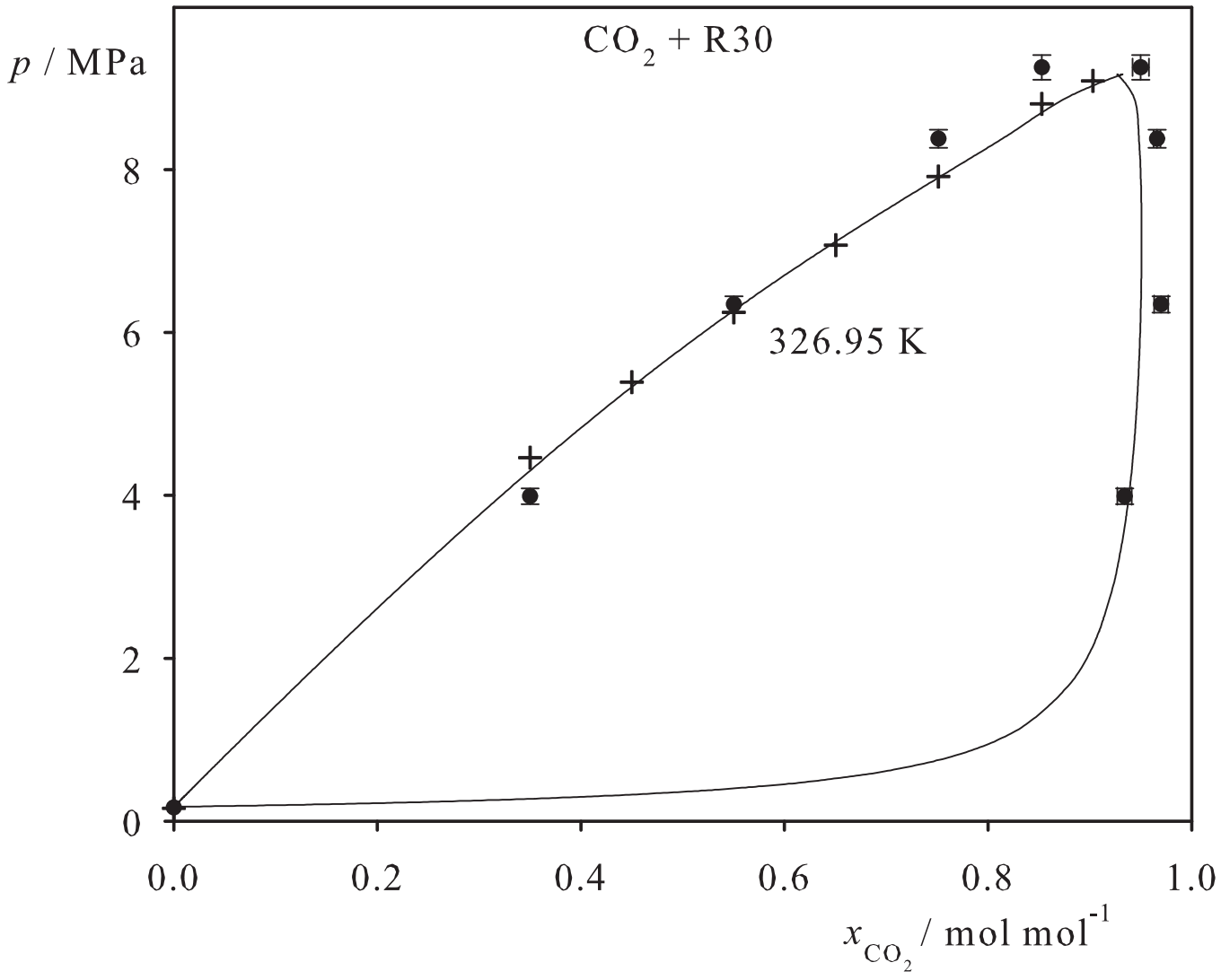

Fig. 69. Binary vapor-liquid equilibrium phase diagram: simulation data ●, experimental data + (cf. Table 2 of the manuscript for the reference) and Peng-Robinson equation of state —.

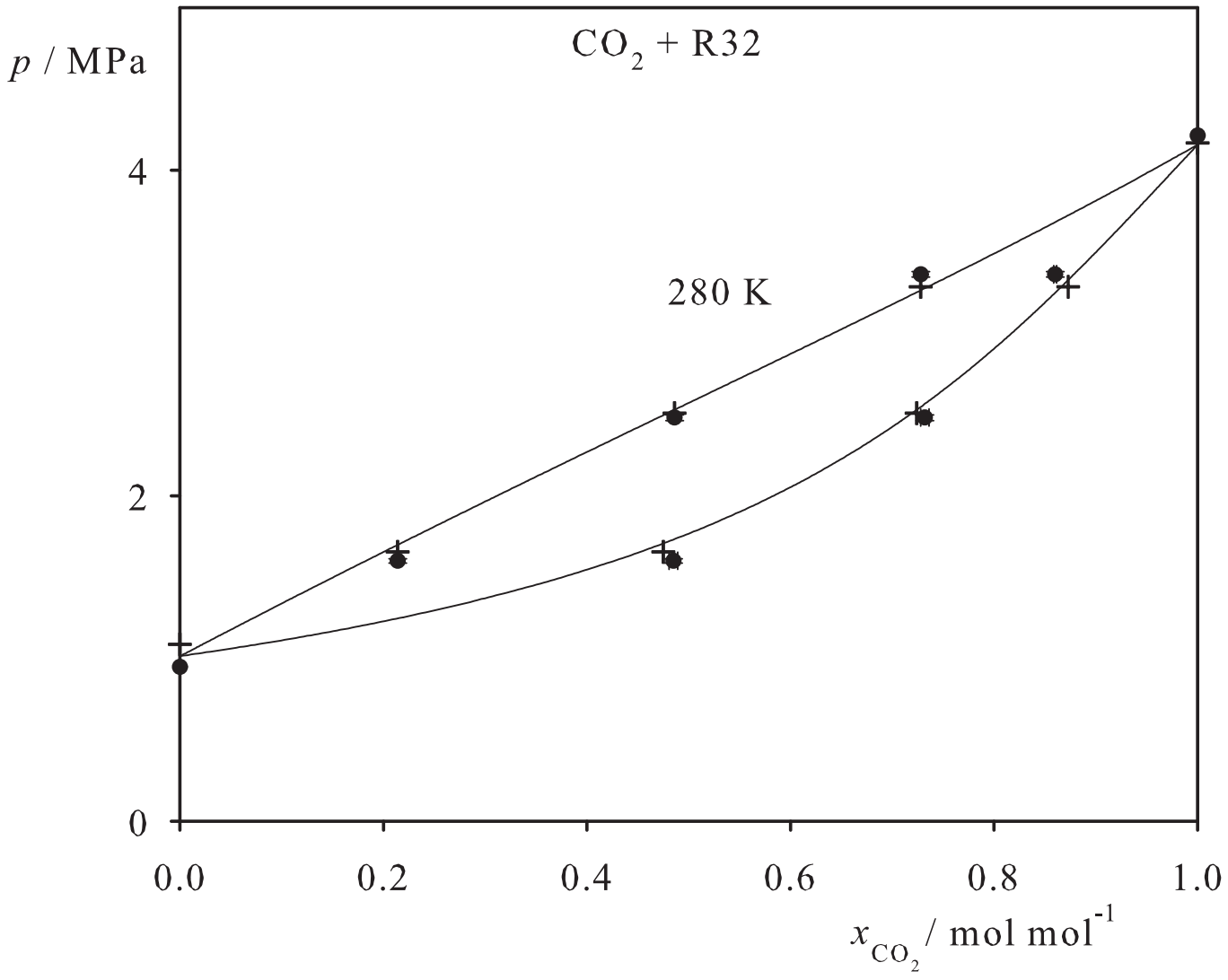

Fig. 70. Binary vapor-liquid equilibrium phase diagram: simulation data ●, experimental data + (cf. Table 2 of the manuscript for the reference) and Peng-Robinson equation of state —.

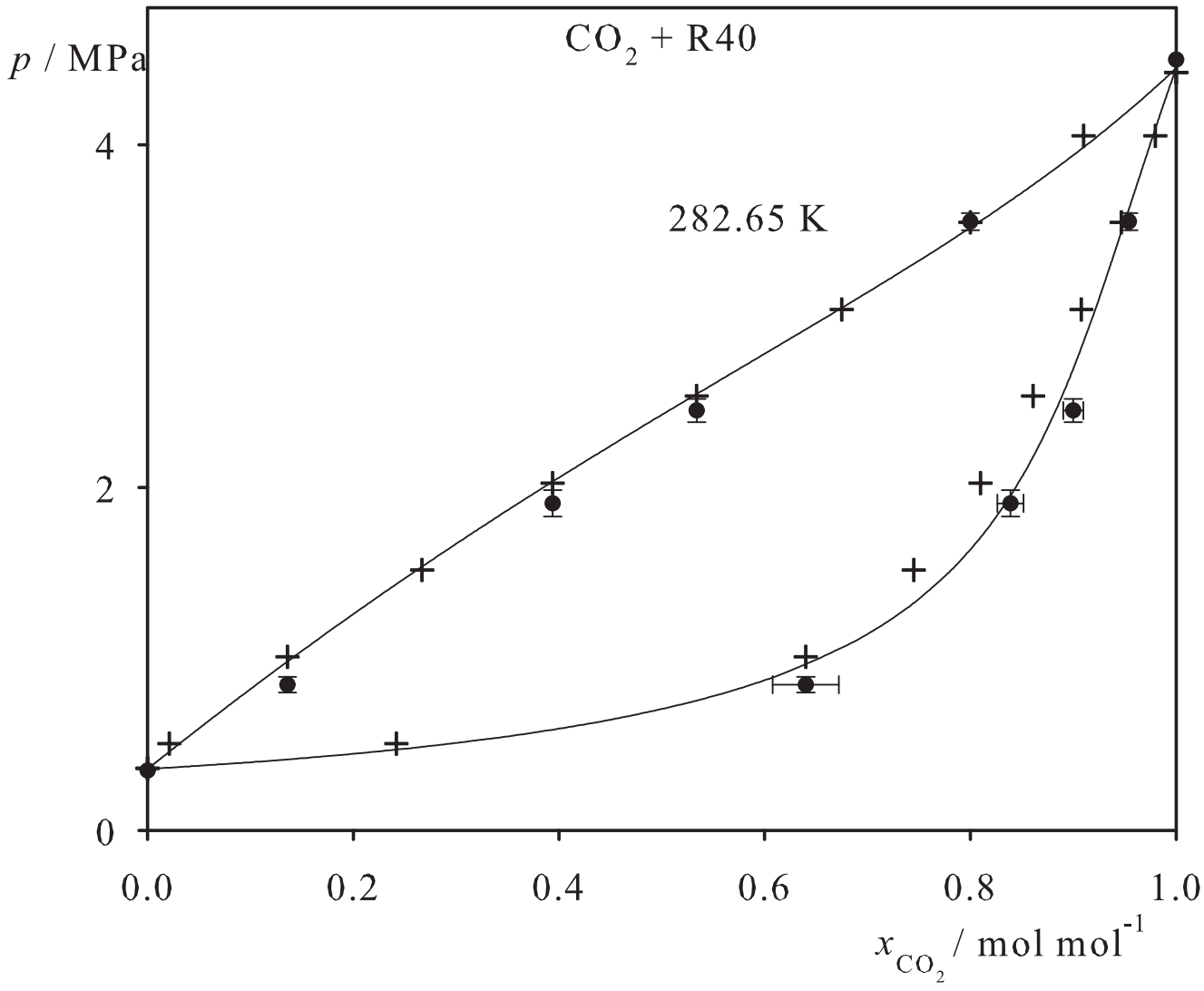

Fig. 71. Binary vapor-liquid equilibrium phase diagram: simulation data ●, experimental data + (cf. Table 2 of the manuscript for the reference) and Peng-Robinson equation of state —.

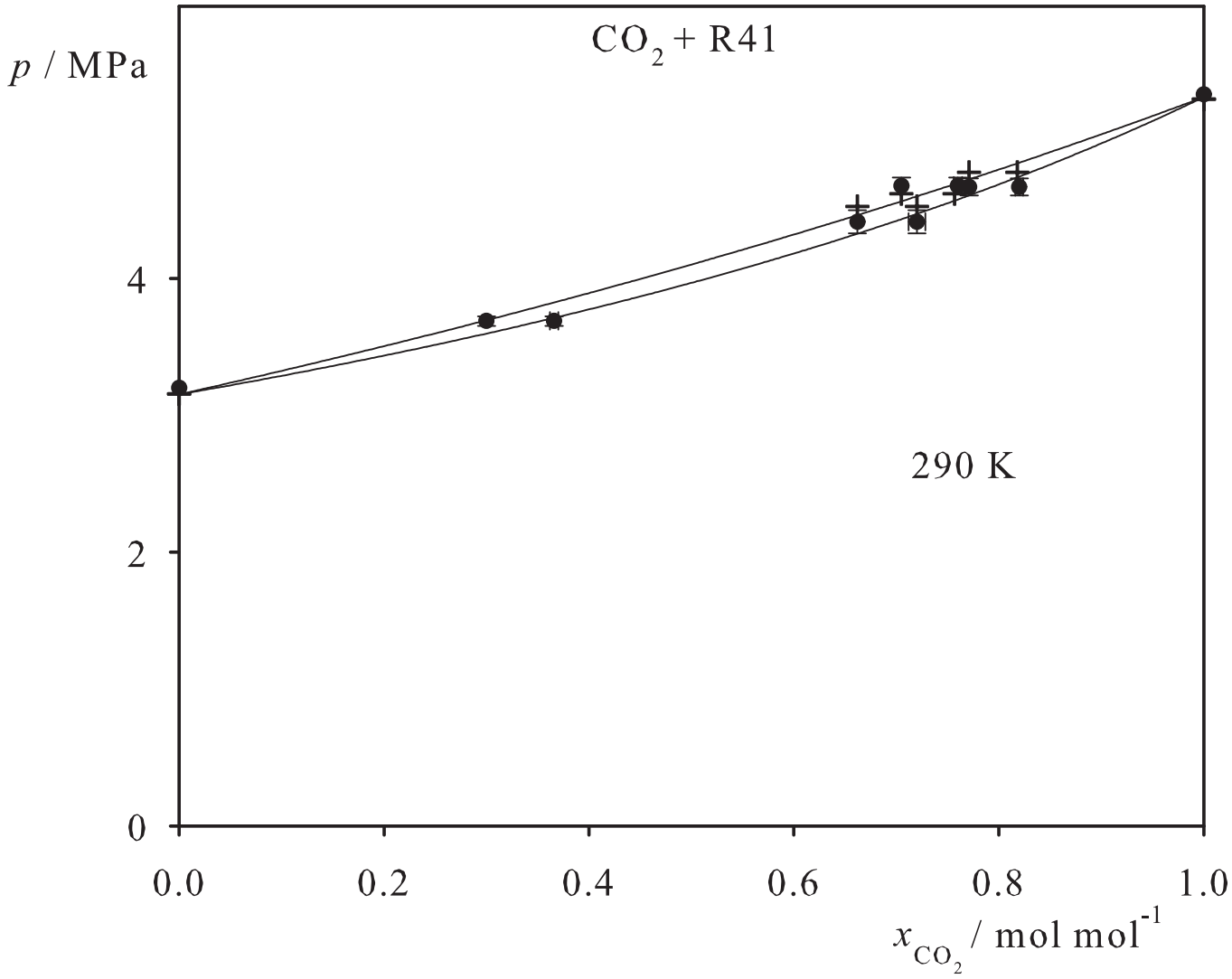

Fig. 72. Binary vapor-liquid equilibrium phase diagram: simulation data ●, experimental data + (cf. Table 2 of the manuscript for the reference) and Peng-Robinson equation of state —.

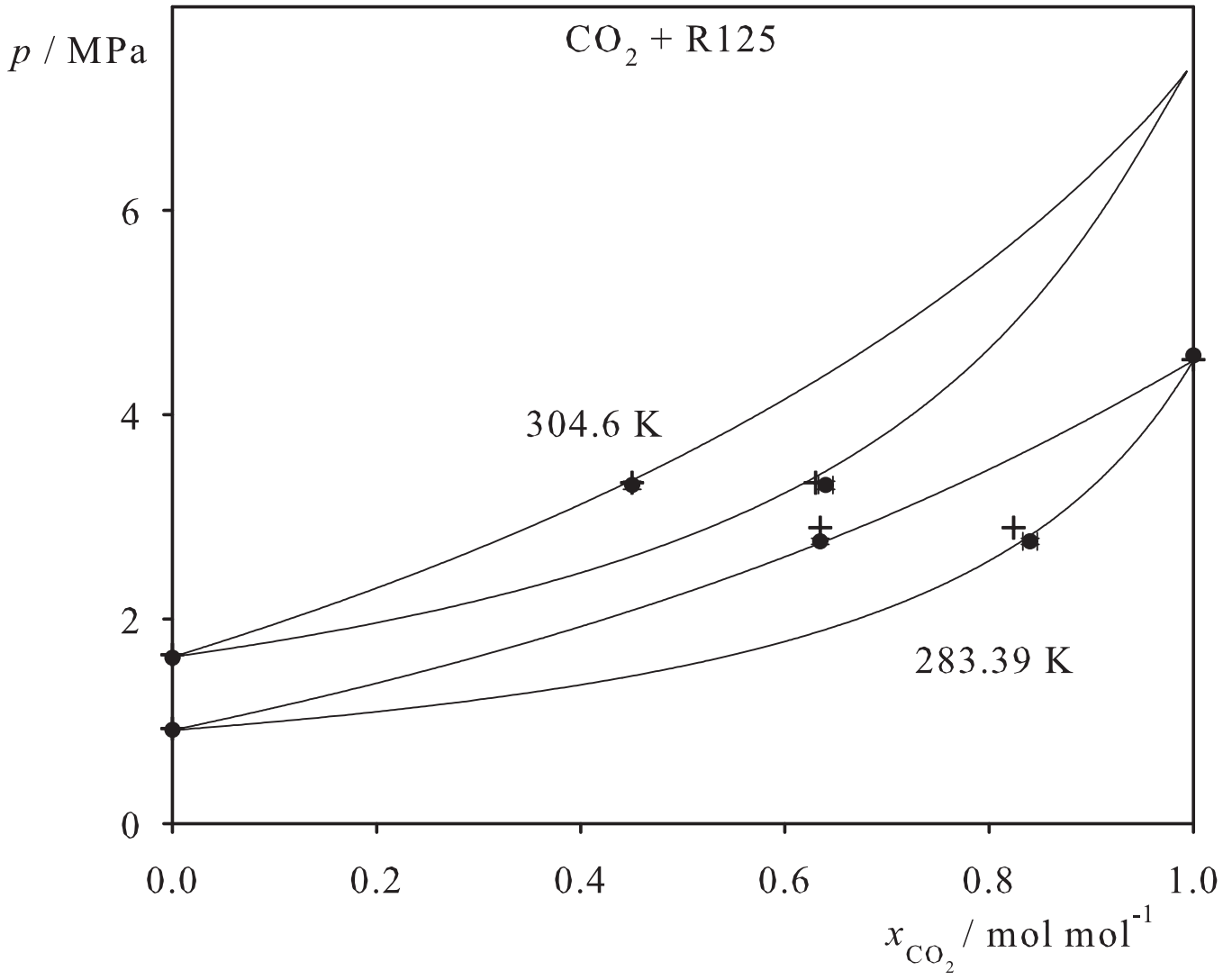

Fig. 73. Binary vapor-liquid equilibrium phase diagram: simulation data ●, experimental data + (cf. Table 2 of the manuscript for the reference) and Peng-Robinson equation of state —.

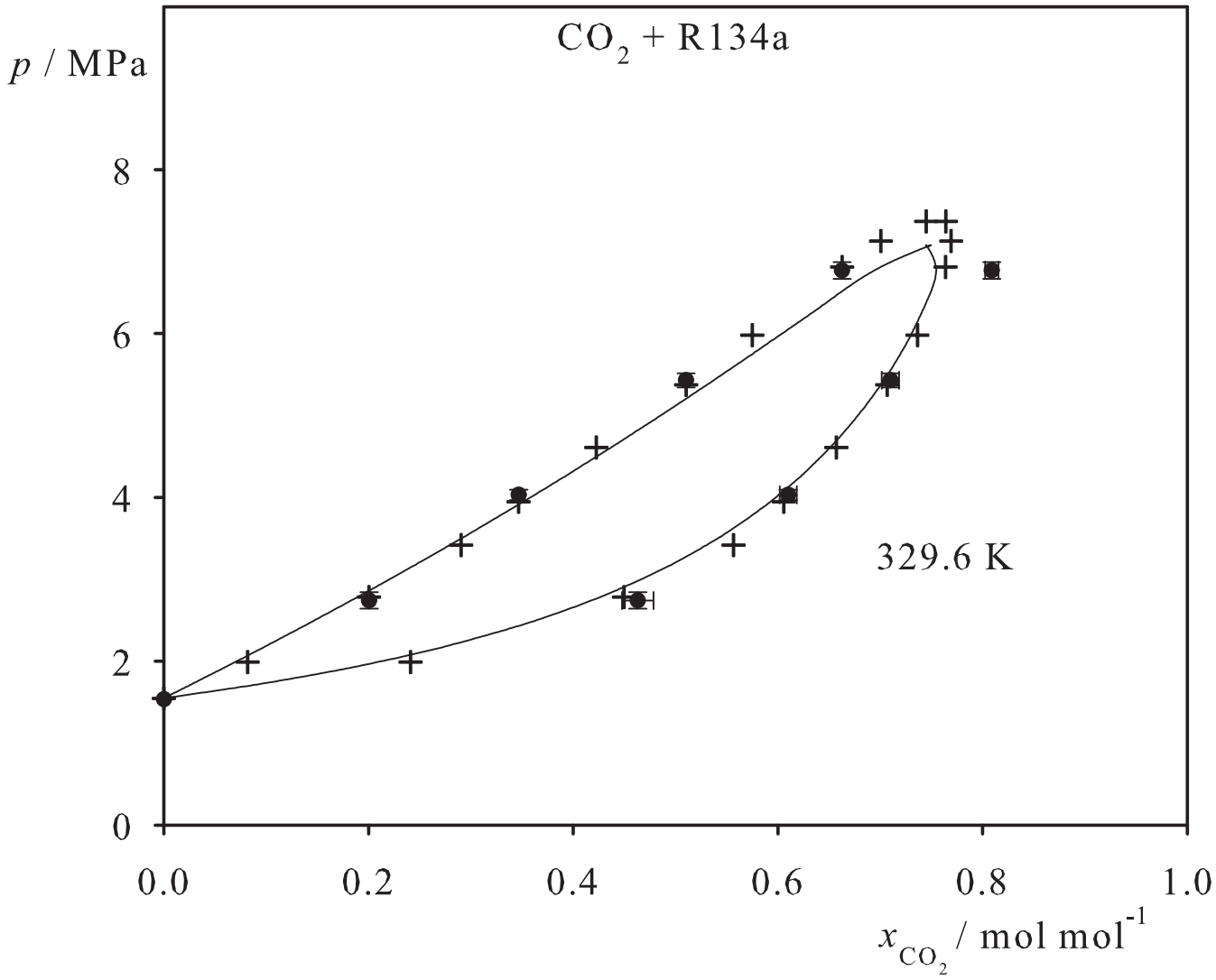

Fig. 74. Binary vapor-liquid equilibrium phase diagram: simulation data ●, experimental data + (cf. Table 2 of the manuscript for the reference) and Peng-Robinson equation of state —.

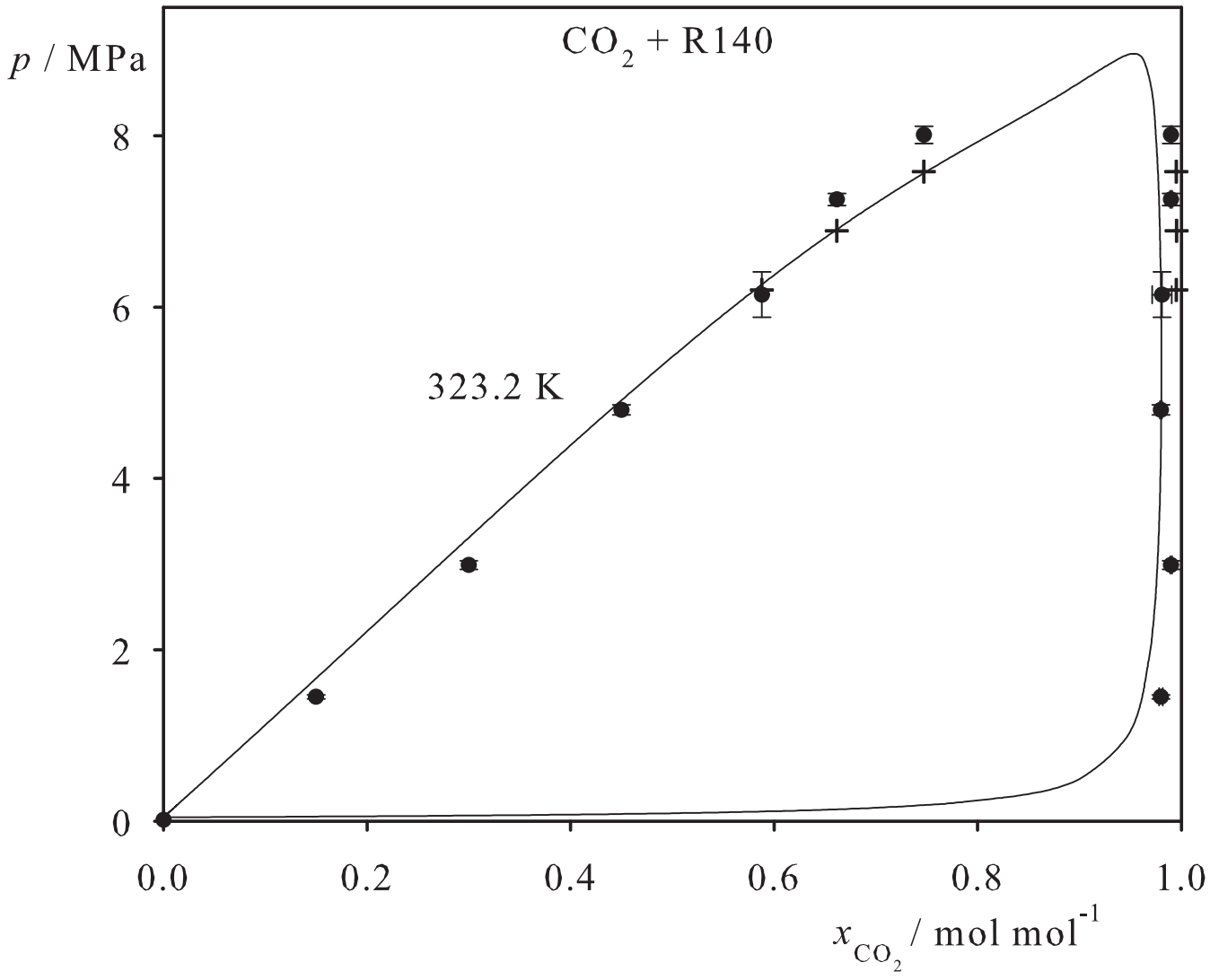

Fig. 75. Binary vapor-liquid equilibrium phase diagram: simulation data ●, experimental data + (cf. Table 2 of the manuscript for the reference) and Peng-Robinson equation of state —.

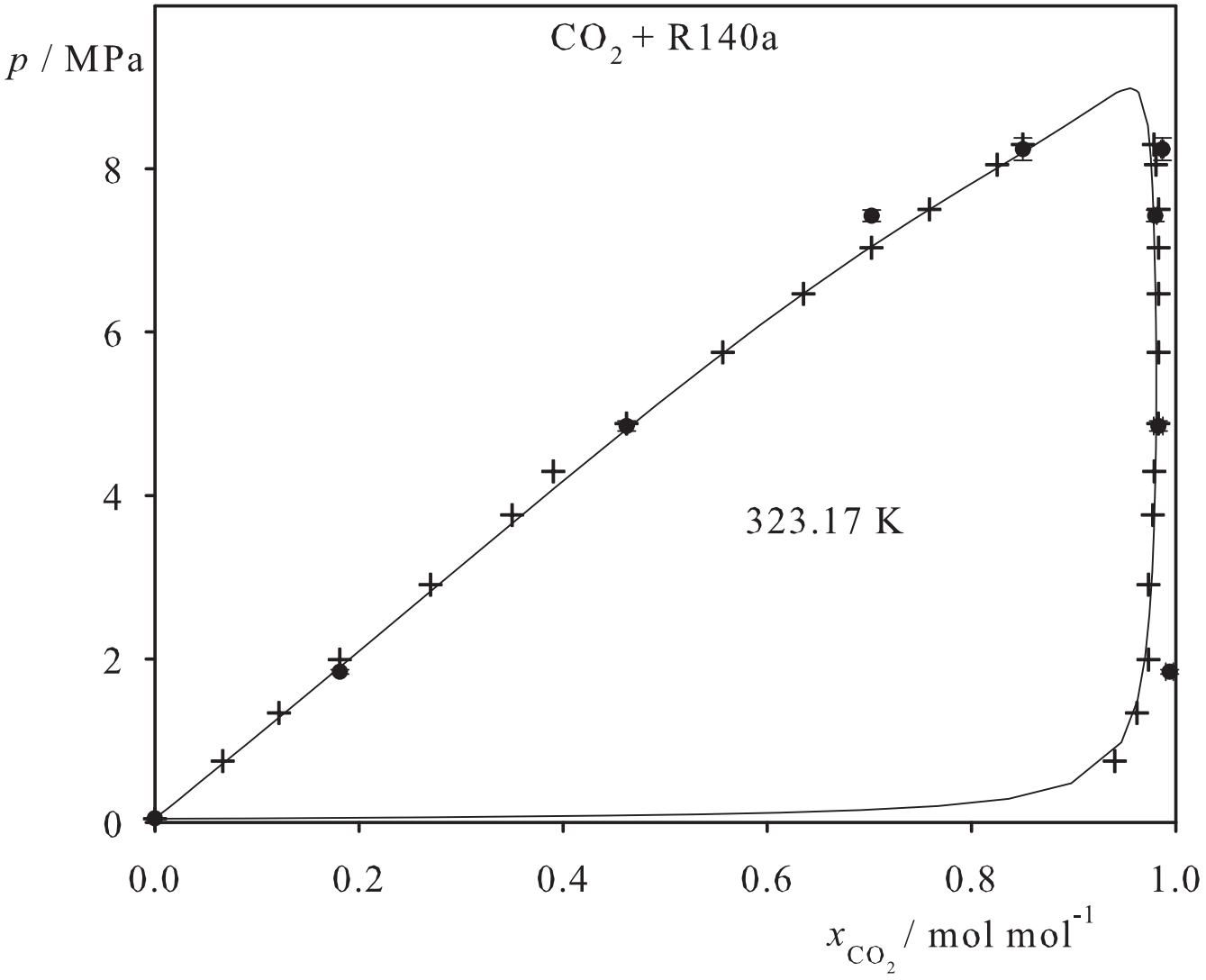

Fig. 76. Binary vapor-liquid equilibrium phase diagram: simulation data ●, experimental data + (cf. Table 2 of the manuscript for the reference) and Peng-Robinson equation of state —.

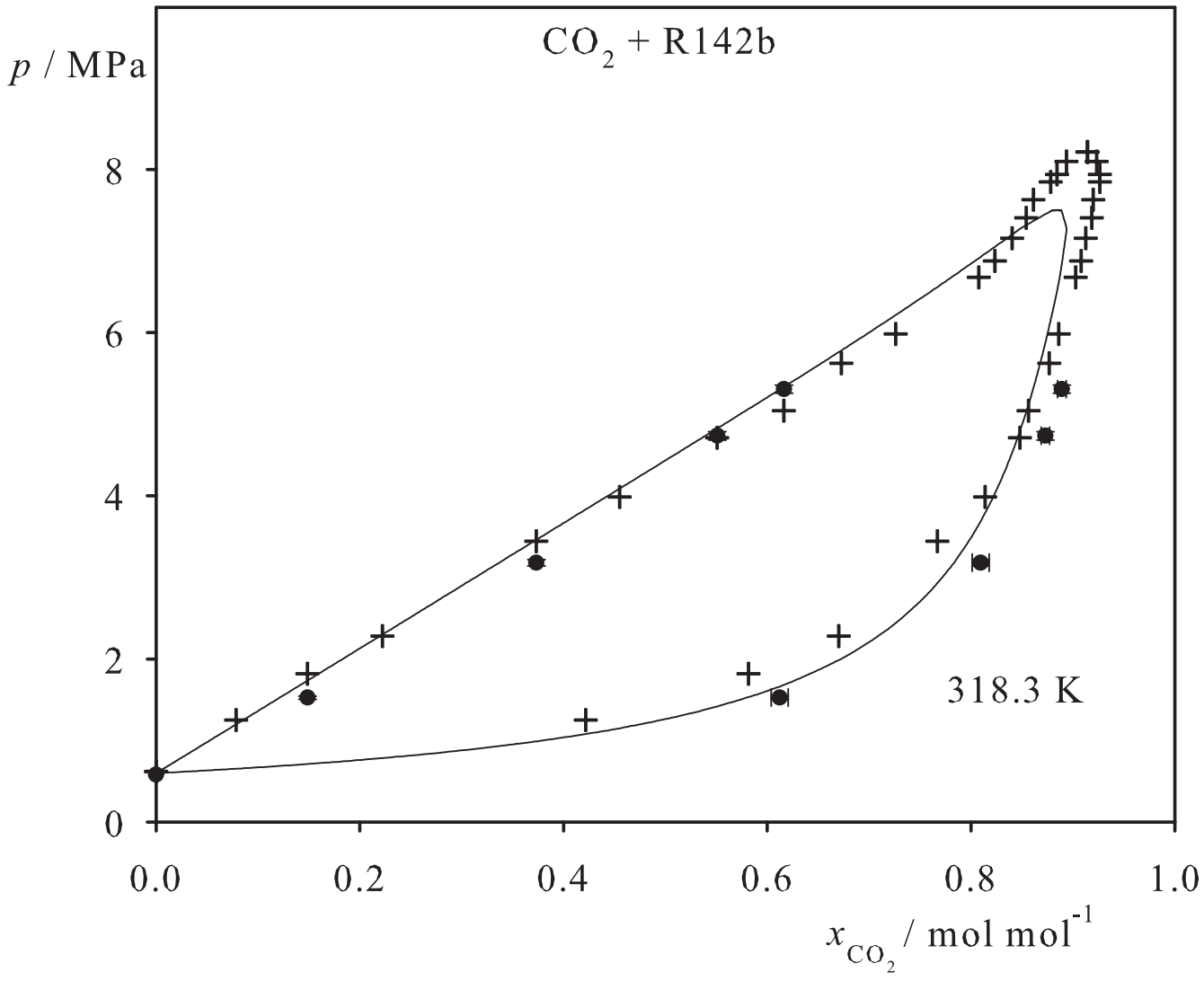

Fig. 77. Binary vapor-liquid equilibrium phase diagram: simulation data ●, experimental data + (cf. Table 2 of the manuscript for the reference) and Peng-Robinson equation of state —.

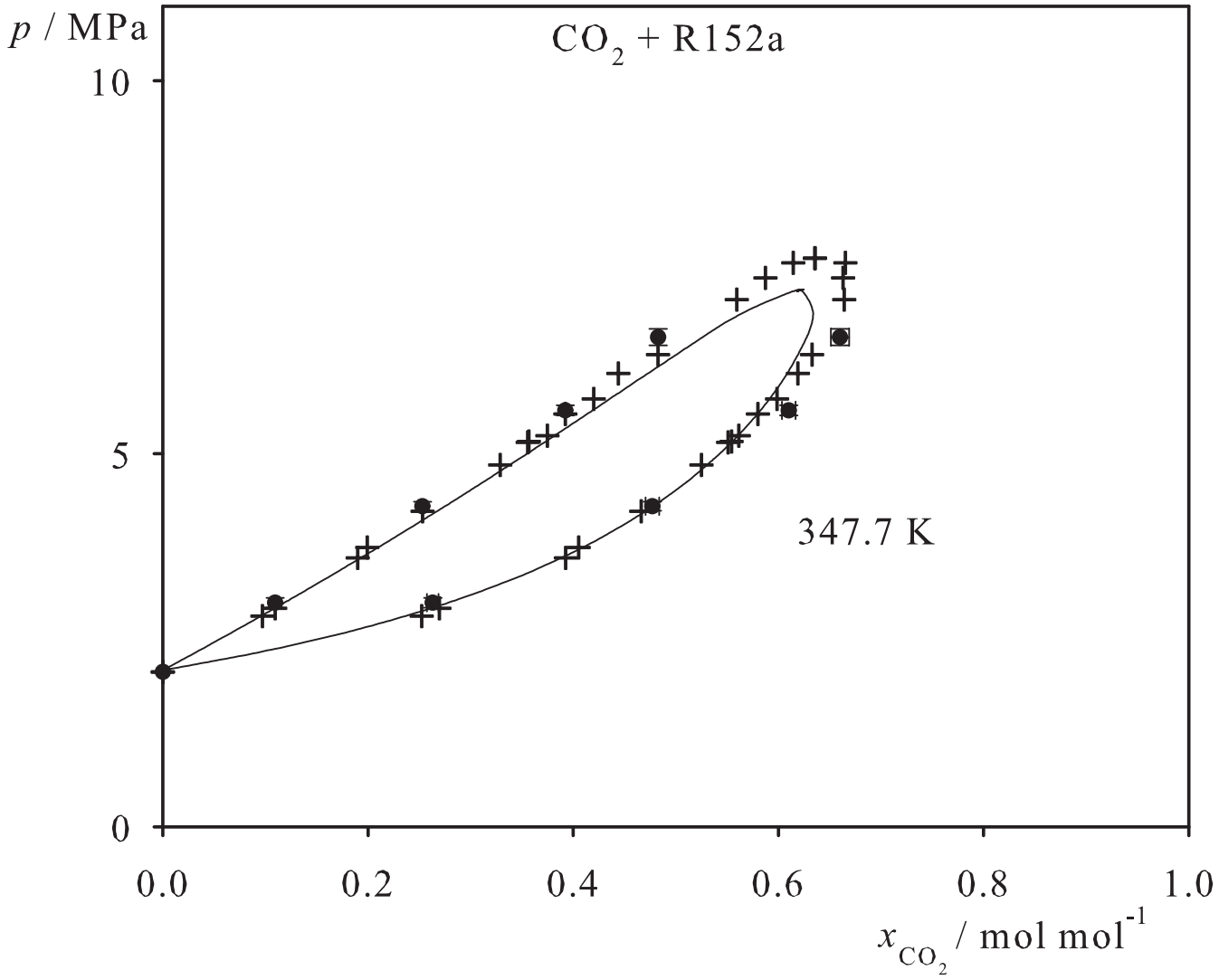

Fig. 78. Binary vapor-liquid equilibrium phase diagram: simulation data ●, experimental data + (cf. Table 2 of the manuscript for the reference) and Peng-Robinson equation of state —.

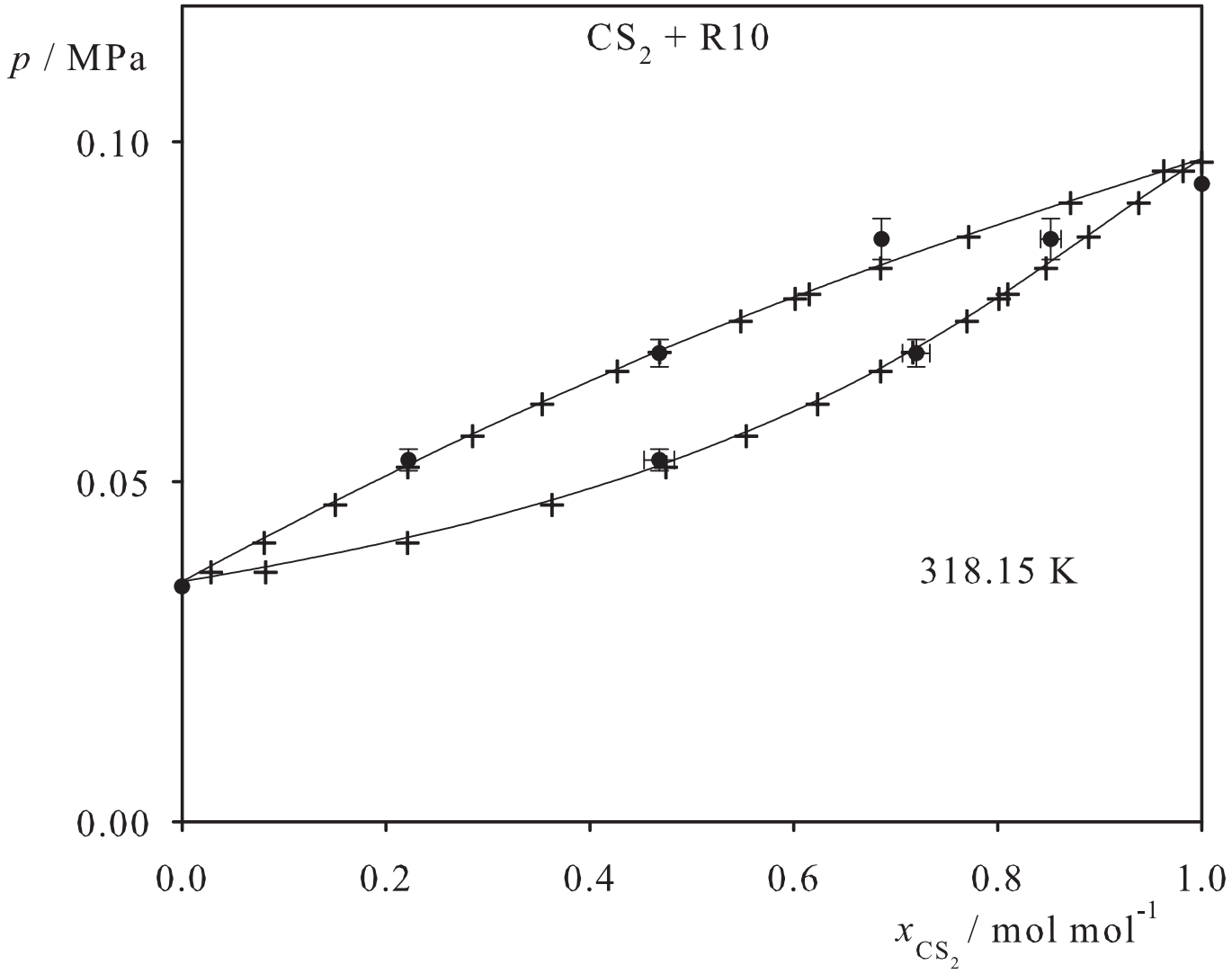

Fig. 79. Binary vapor-liquid equilibrium phase diagram: simulation data ●, experimental data + (cf. Table 2 of the manuscript for the reference) and Peng-Robinson equation of state —.

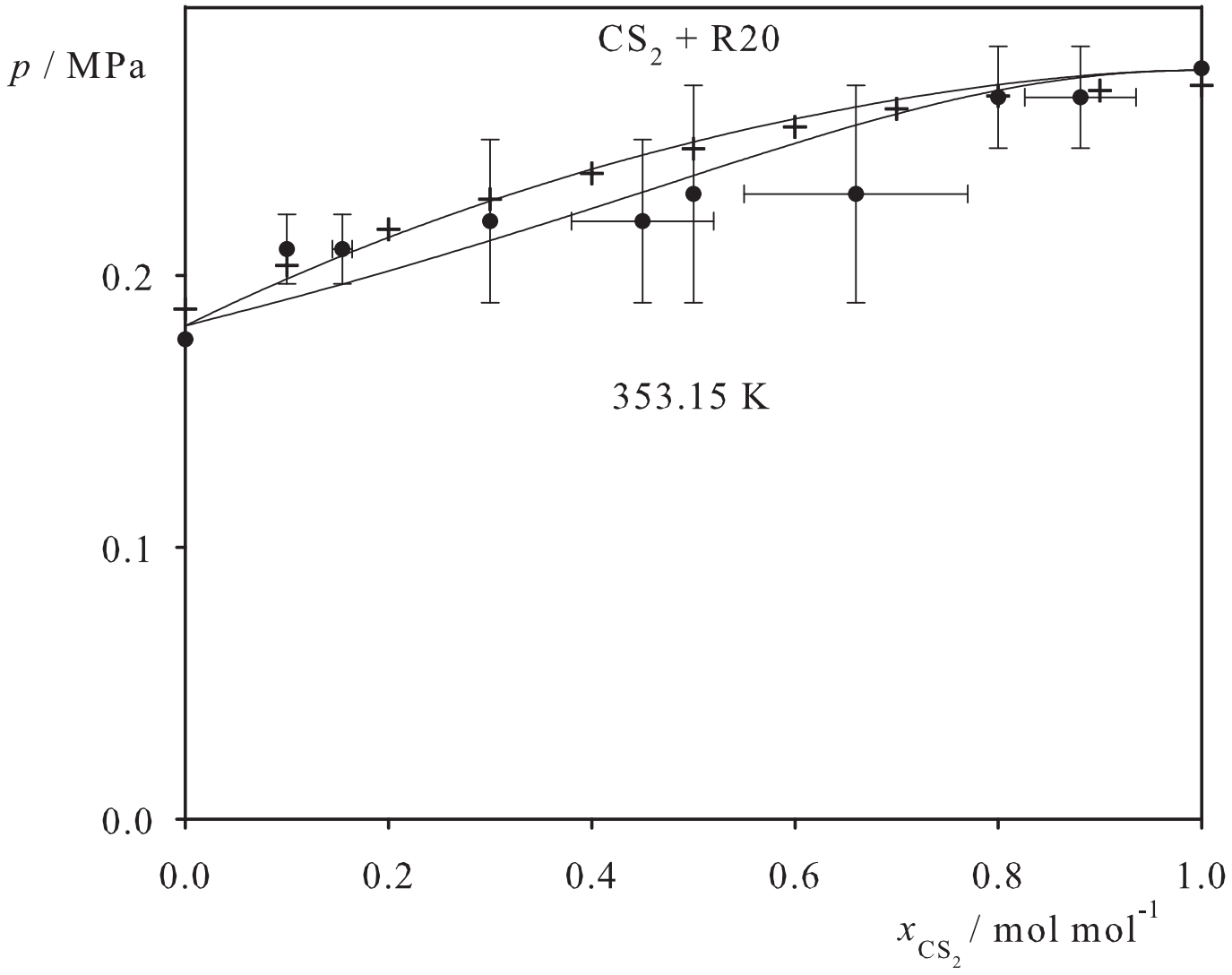

Fig. 80. Binary vapor-liquid equilibrium phase diagram: simulation data ●, experimental data + (cf. Table 2 of the manuscript for the reference) and Peng-Robinson equation of state —.

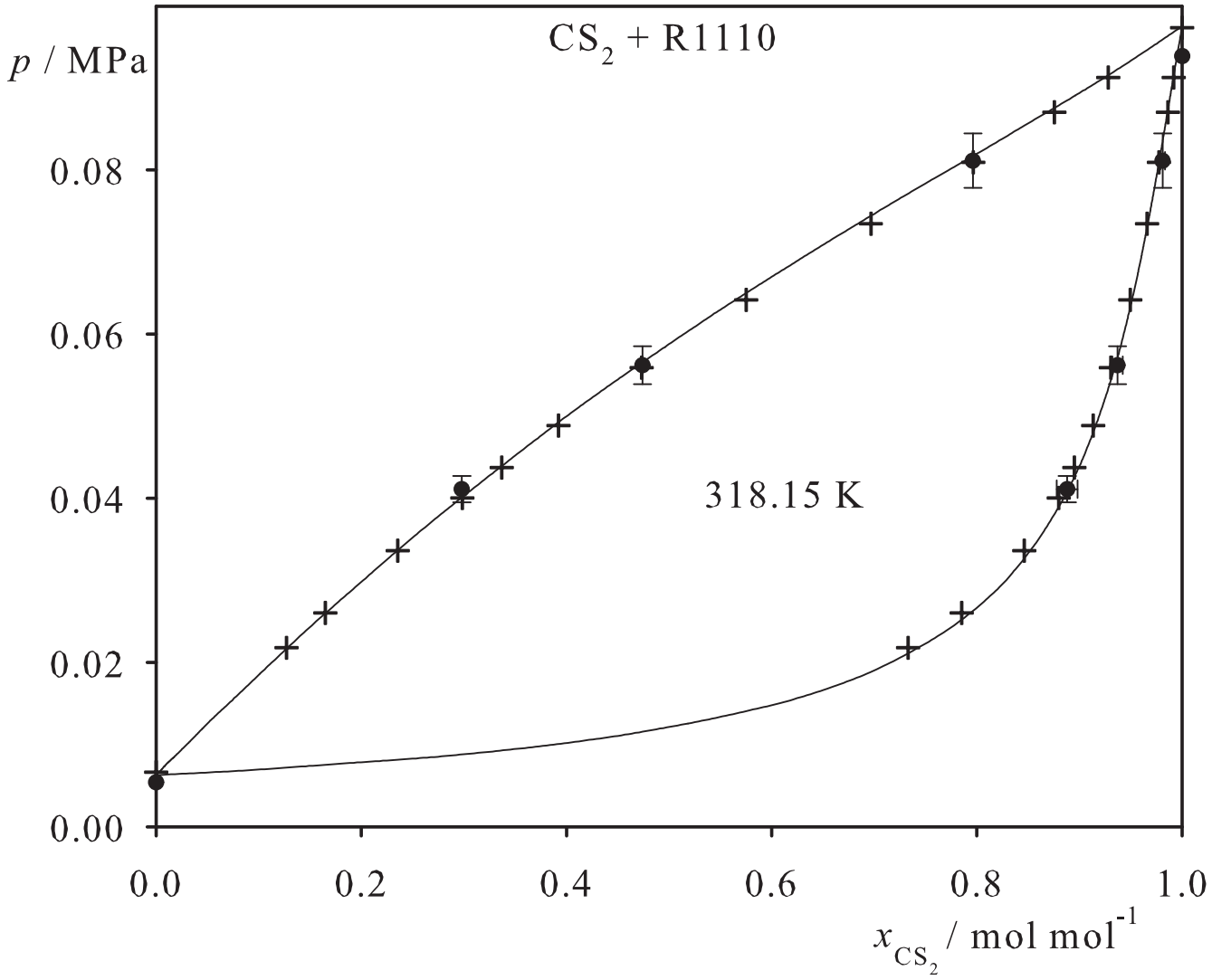

Fig. 81. Binary vapor-liquid equilibrium phase diagram: simulation data ●, experimental data + (cf. Table 2 of the manuscript for the reference) and Peng-Robinson equation of state —.

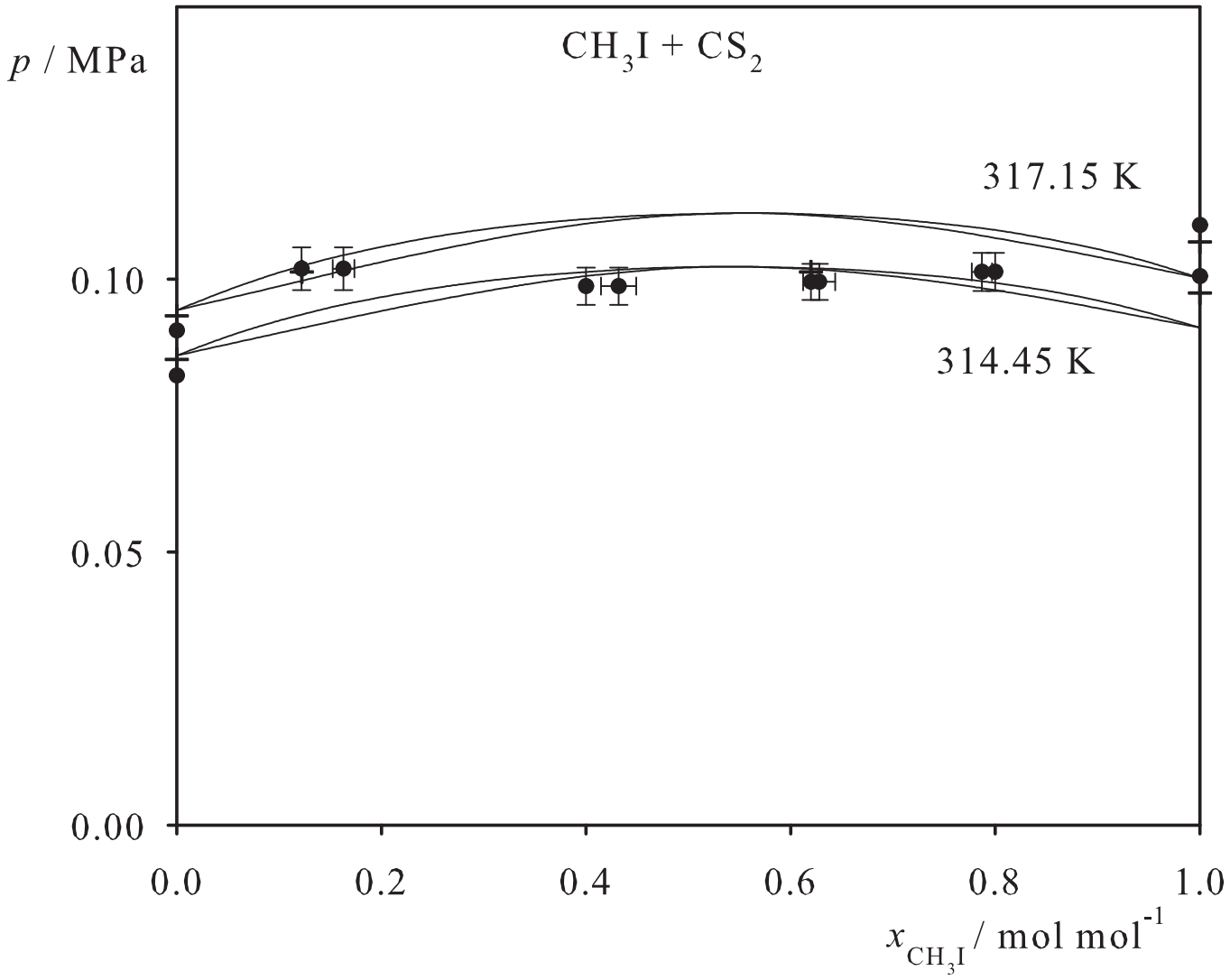

Fig. 82. Binary vapor-liquid equilibrium phase diagram: simulation data ●, experimental data + (cf. Table 2 of the manuscript for the reference) and Peng-Robinson equation of state —.

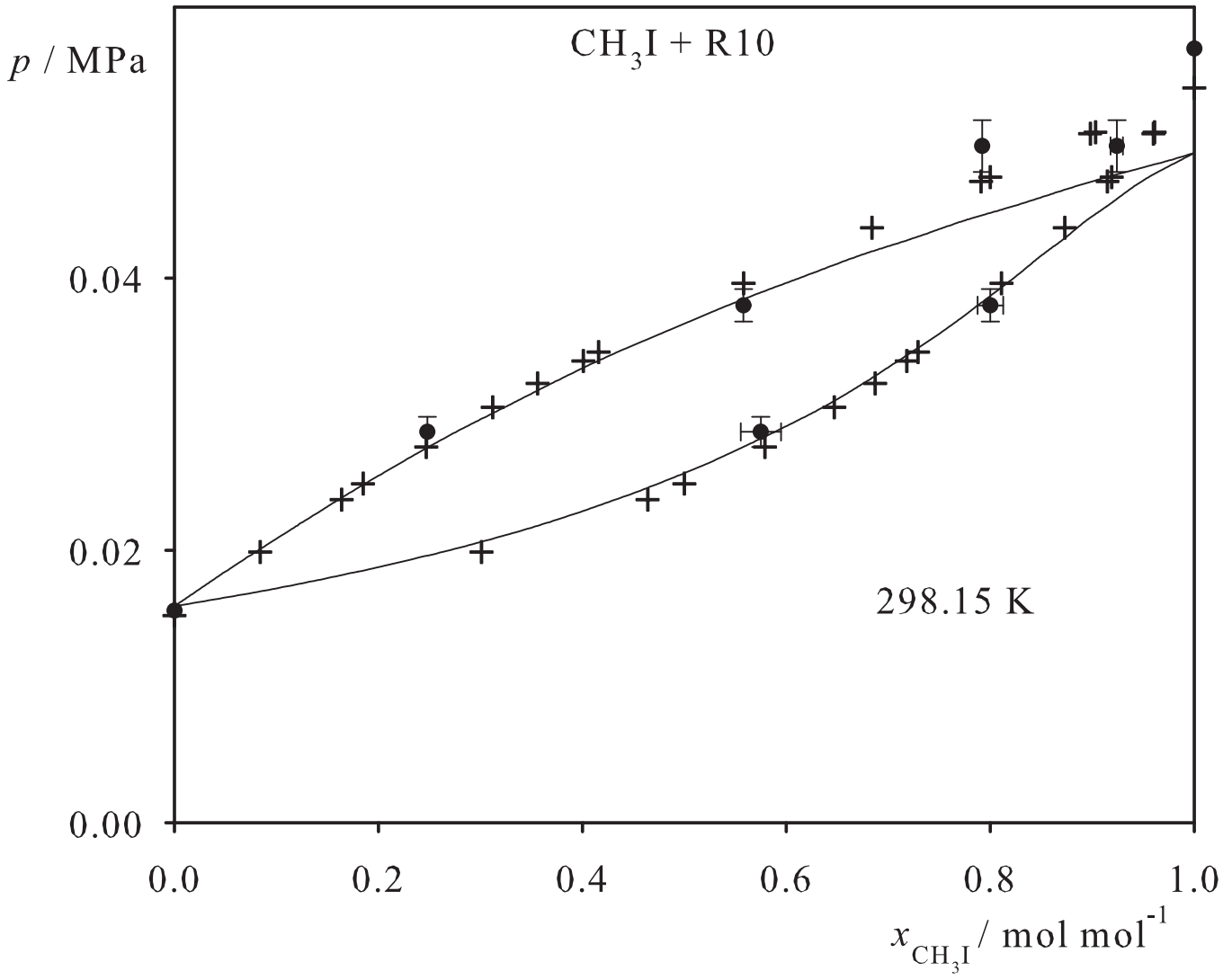

Fig. 83. Binary vapor-liquid equilibrium phase diagram: simulation data ●, experimental data + (cf. Table 2 of the manuscript for the reference) and Peng-Robinson equation of state —.

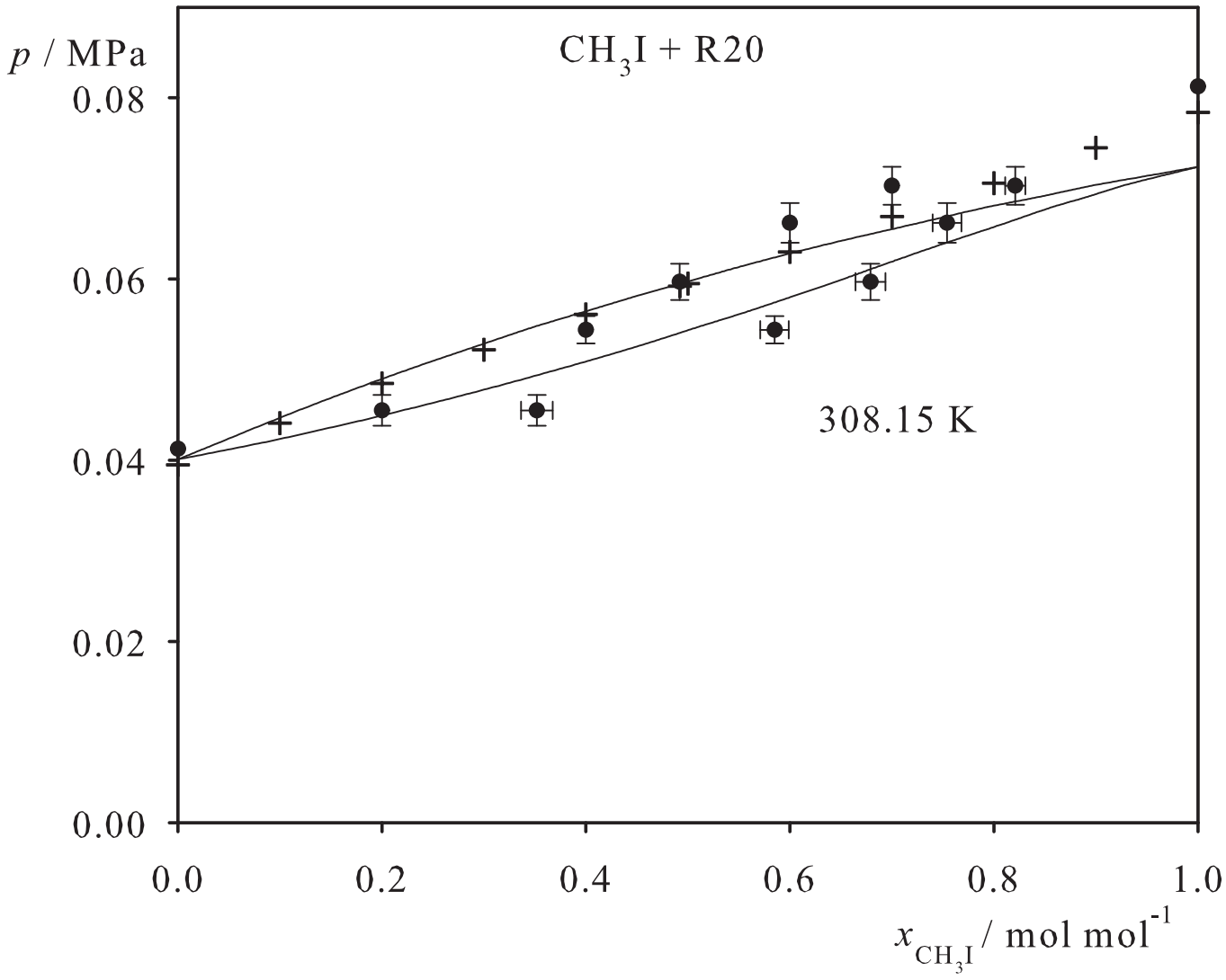

Fig. 84. Binary vapor-liquid equilibrium phase diagram: simulation data ●, experimental data + (cf. Table 2 of the manuscript for the reference) and Peng-Robinson equation of state —.

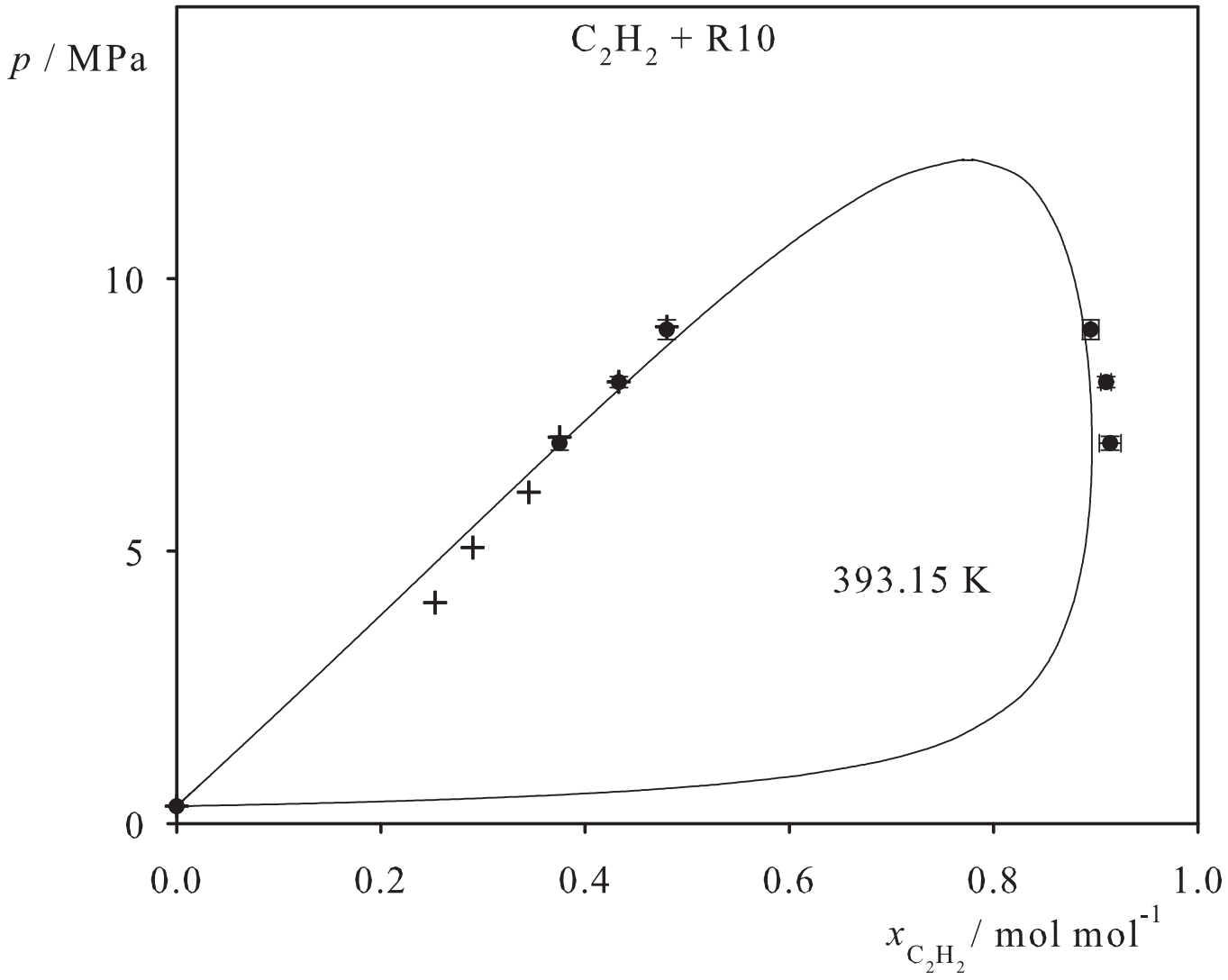

Fig. 85. Binary vapor-liquid equilibrium phase diagram: simulation data ●, experimental data + (cf. Table 2 of the manuscript for the reference) and Peng-Robinson equation of state —.

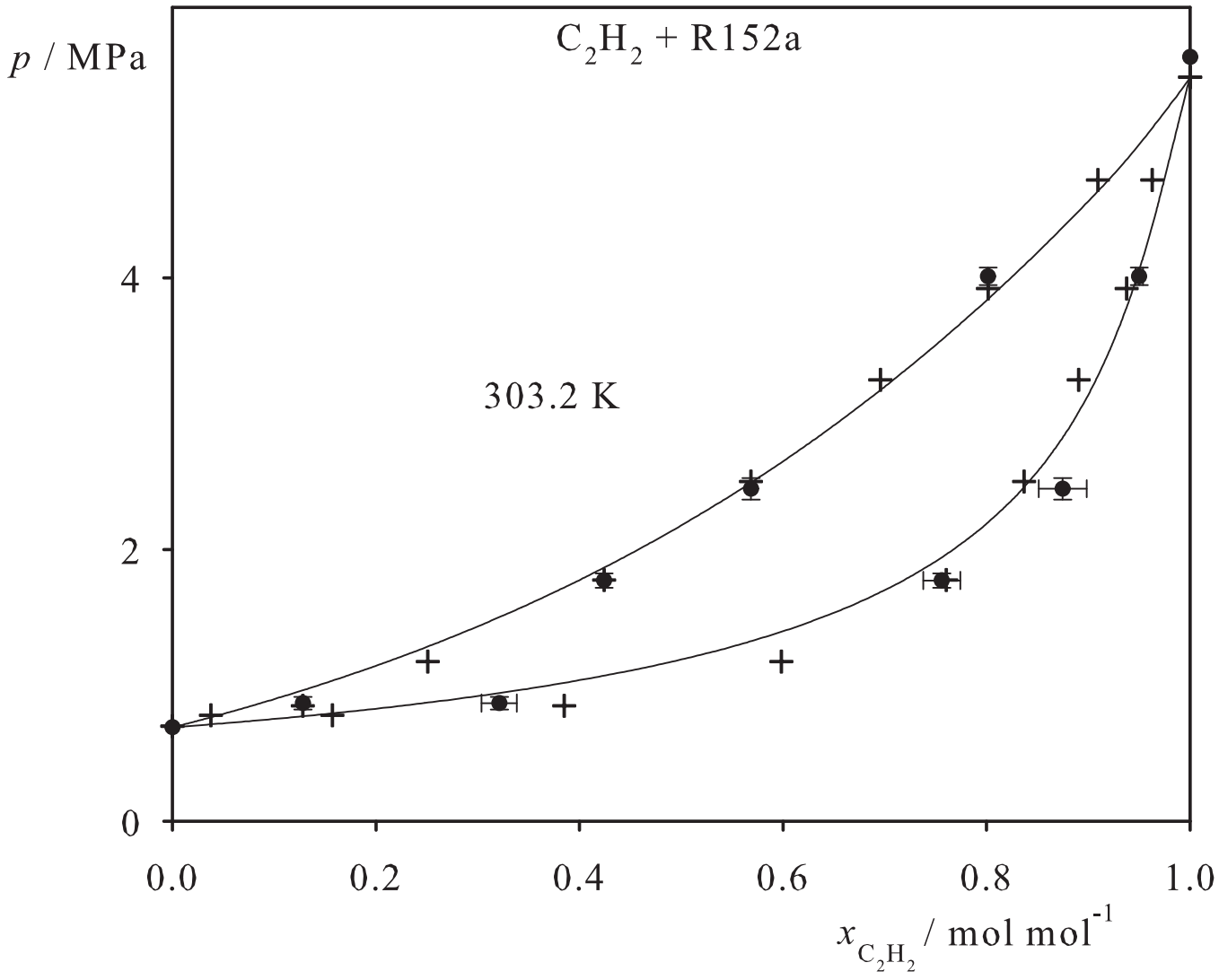

Fig. 86. Binary vapor-liquid equilibrium phase diagram: simulation data ●, experimental data + (cf. Table 2 of the manuscript for the reference) and Peng-Robinson equation of state —.

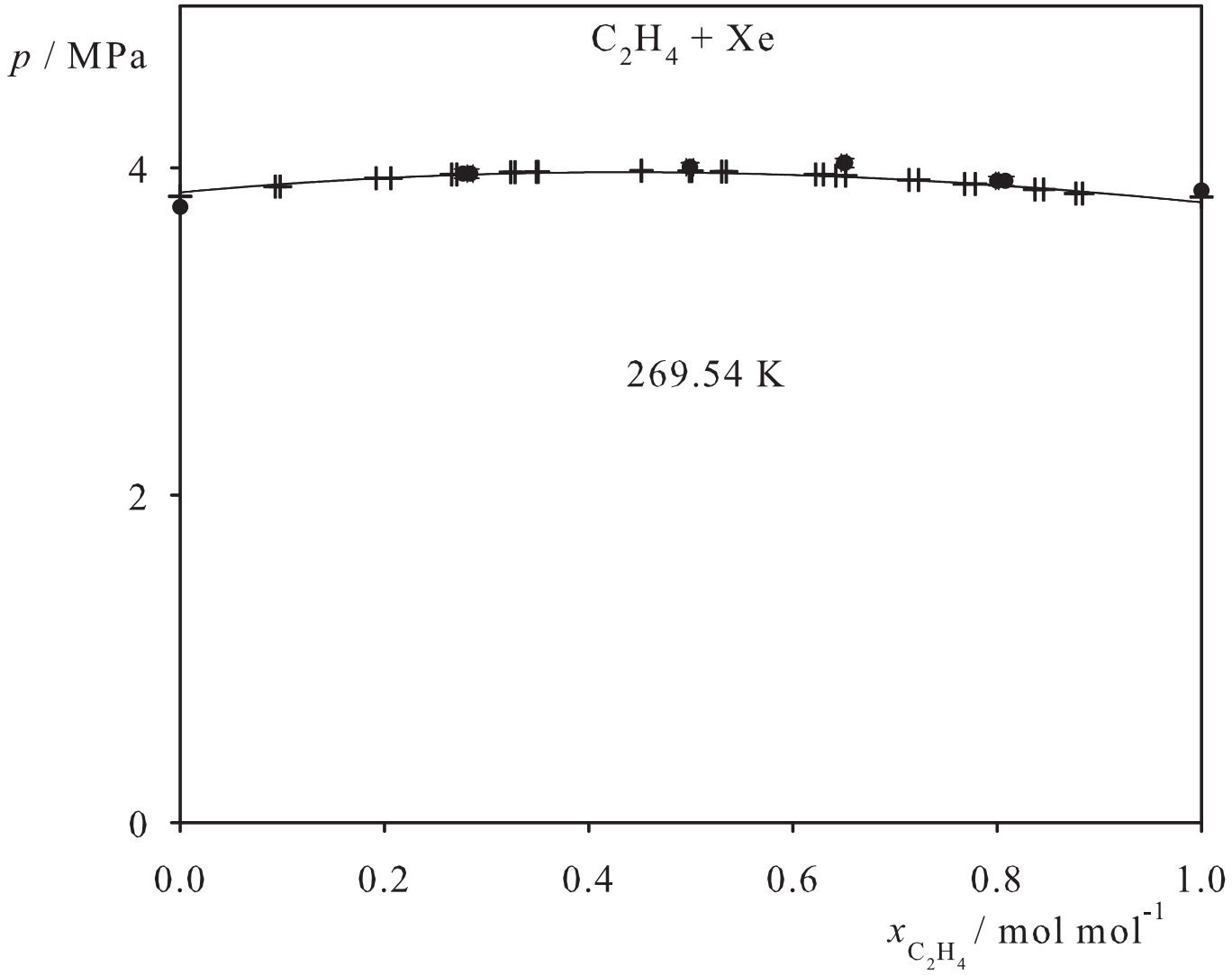

Fig. 87. Binary vapor-liquid equilibrium phase diagram: simulation data ●, experimental data + (cf. Table 2 of the manuscript for the reference) and Peng-Robinson equation of state —.

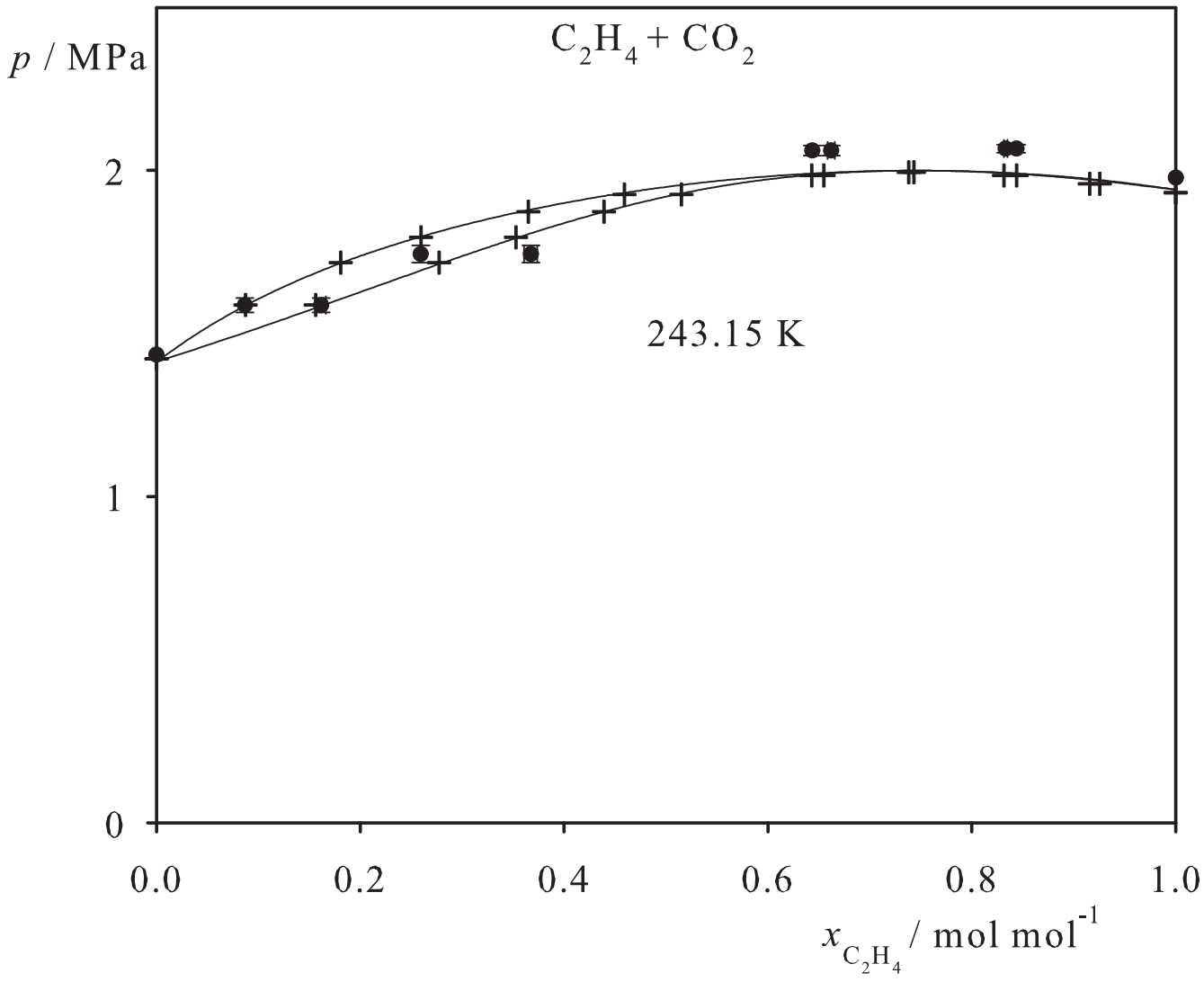

Fig. 88. Binary vapor-liquid equilibrium phase diagram: simulation data ●, experimental data + (cf. Table 2 of the manuscript for the reference) and Peng-Robinson equation of state —.

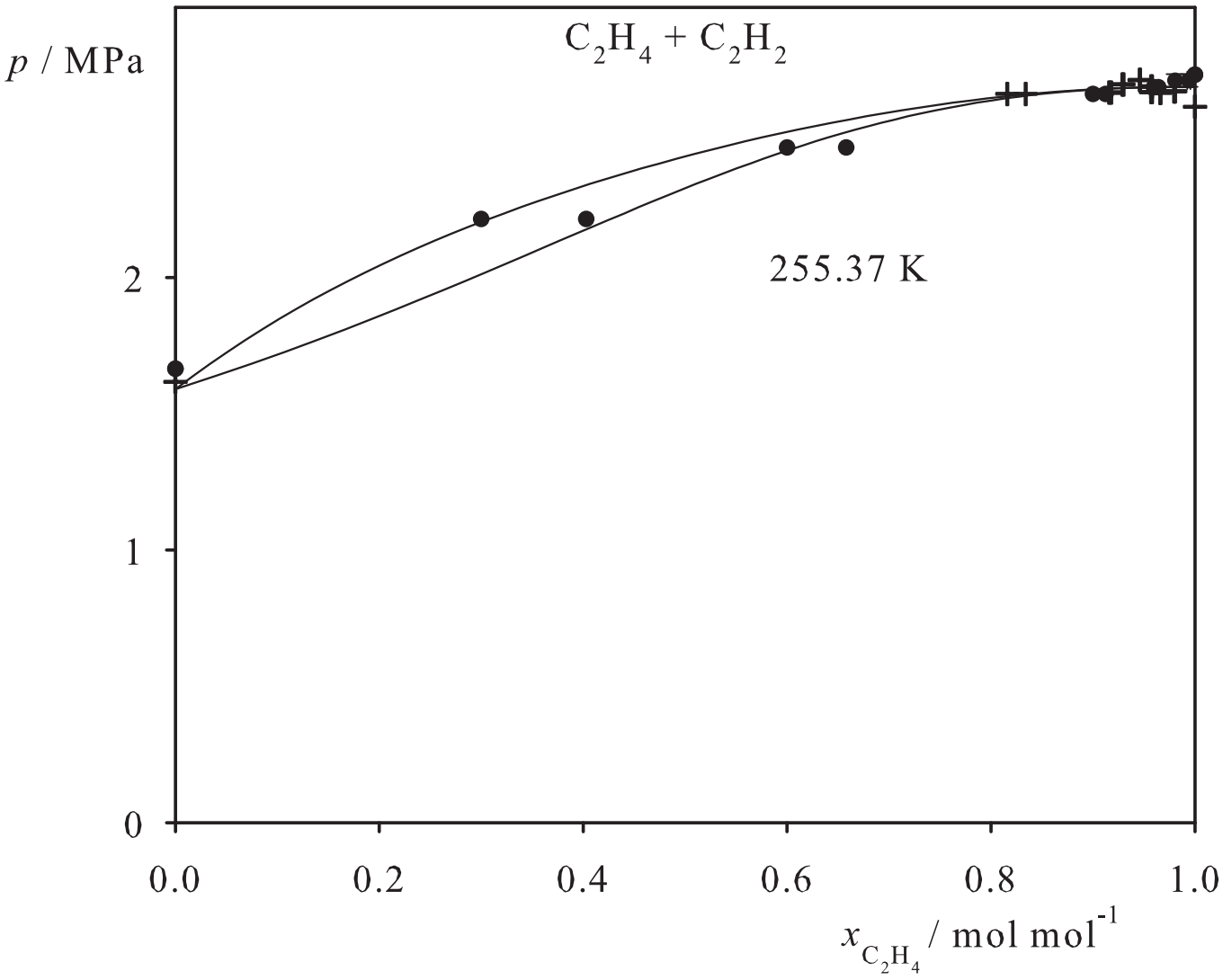

Fig. 89. Binary vapor-liquid equilibrium phase diagram: simulation data ●, experimental data + (cf. Table 2 of the manuscript for the reference) and Peng-Robinson equation of state —.

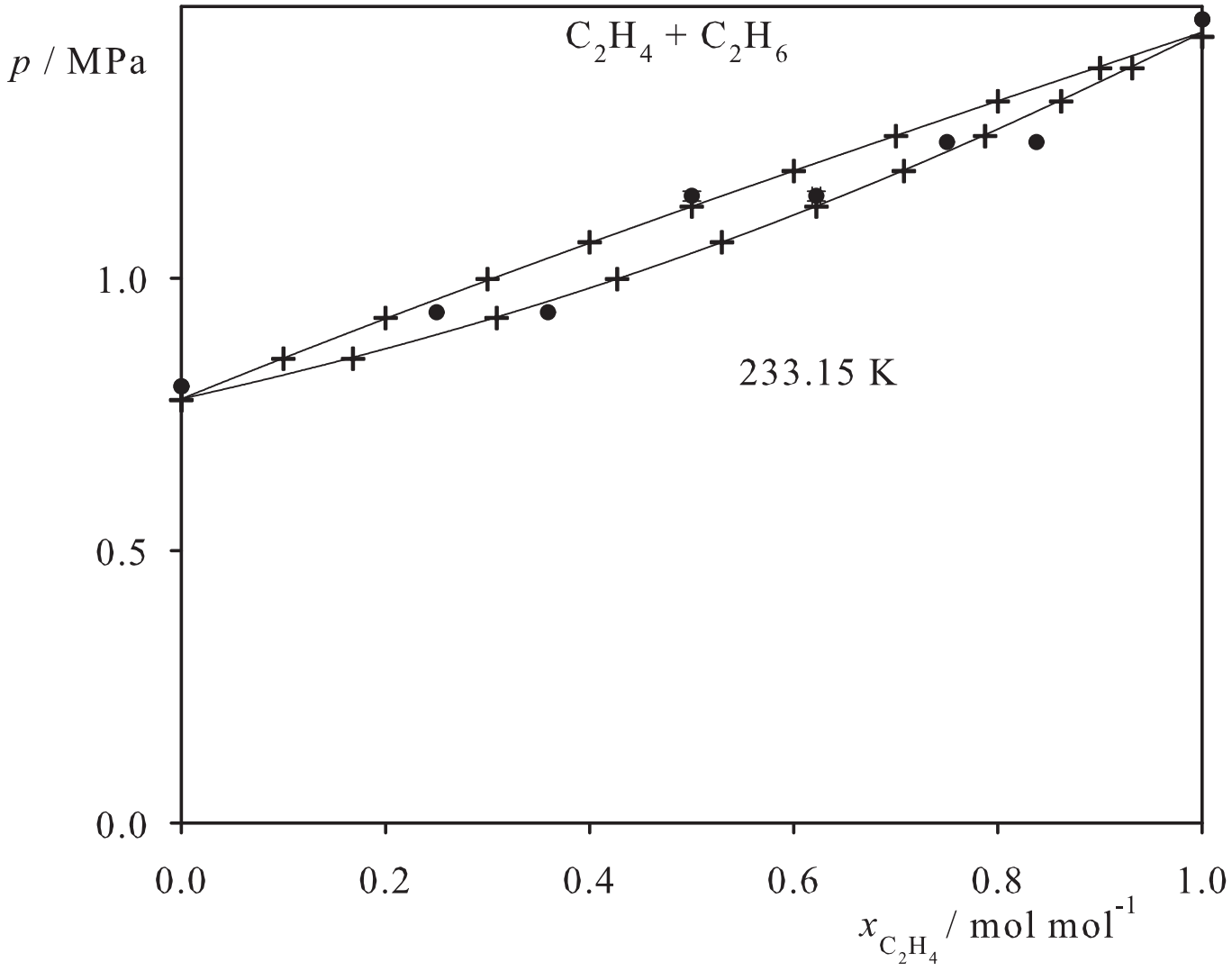

Fig. 90. Binary vapor-liquid equilibrium phase diagram: simulation data ●, experimental data + (cf. Table 2 of the manuscript for the reference) and Peng-Robinson equation of state —.

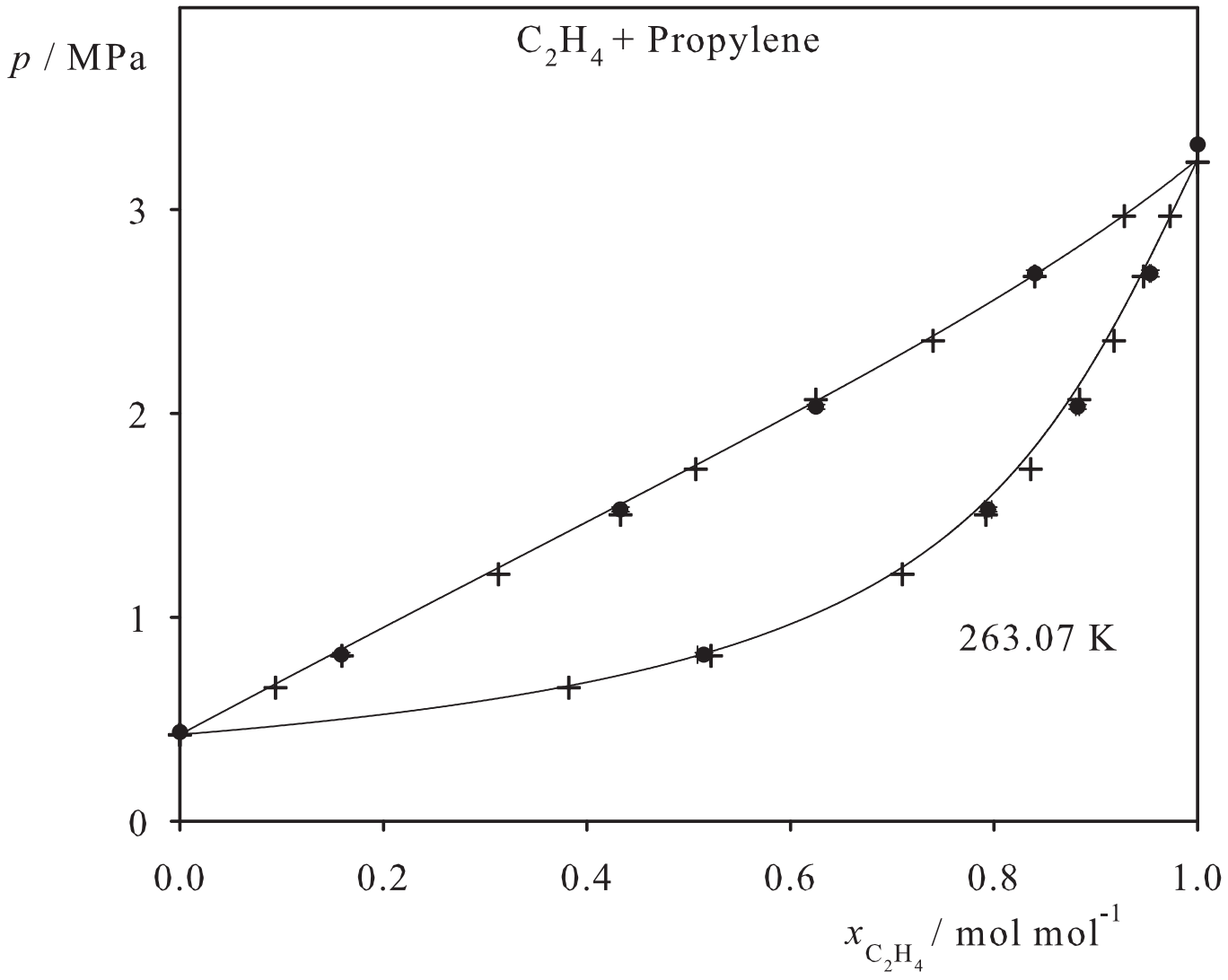

Fig. 91. Binary vapor-liquid equilibrium phase diagram: simulation data ●, experimental data + (cf. Table 2 of the manuscript for the reference) and Peng-Robinson equation of state —.

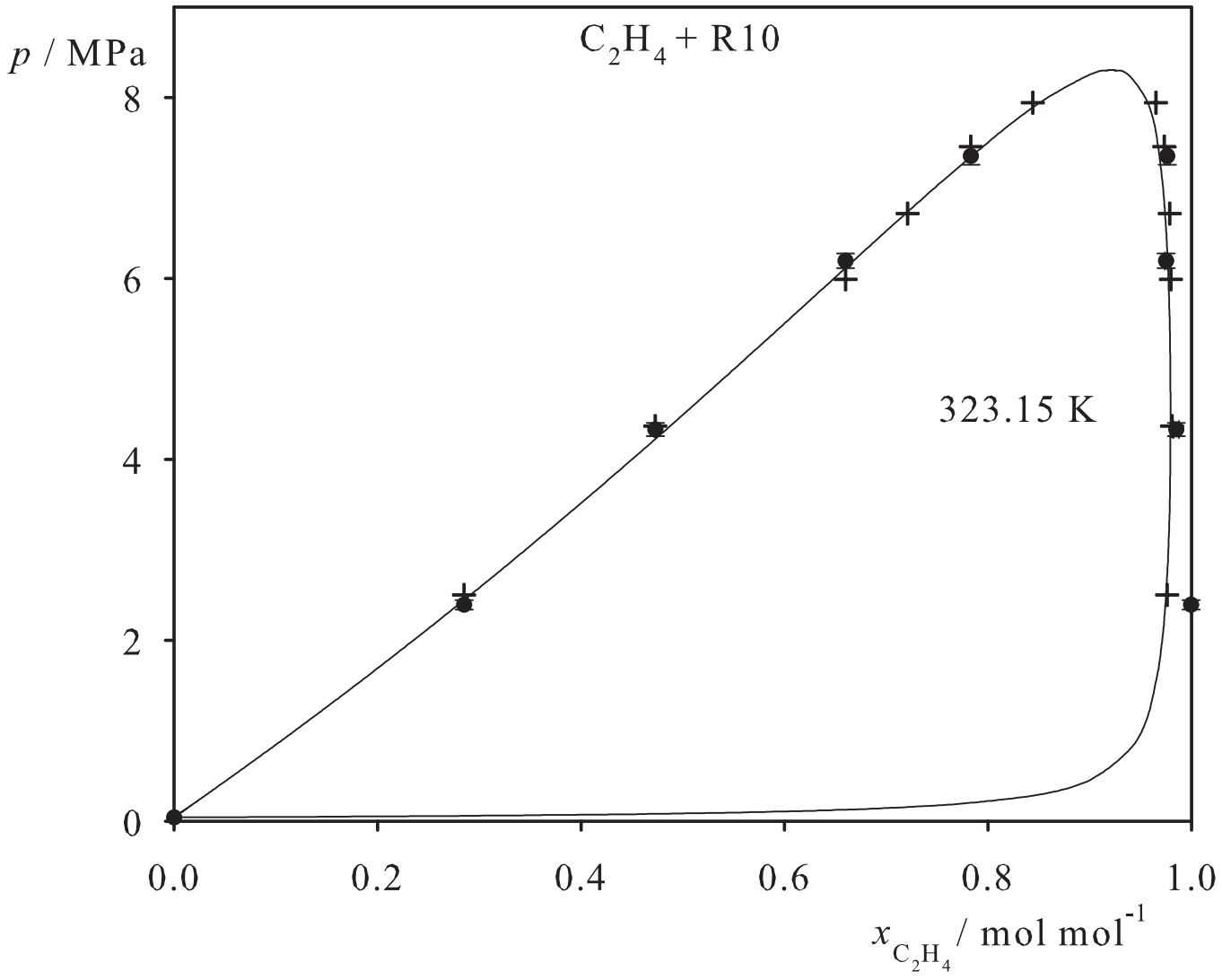

Fig. 92. Binary vapor-liquid equilibrium phase diagram: simulation data ●, experimental data + (cf. Table 2 of the manuscript for the reference) and Peng-Robinson equation of state —.

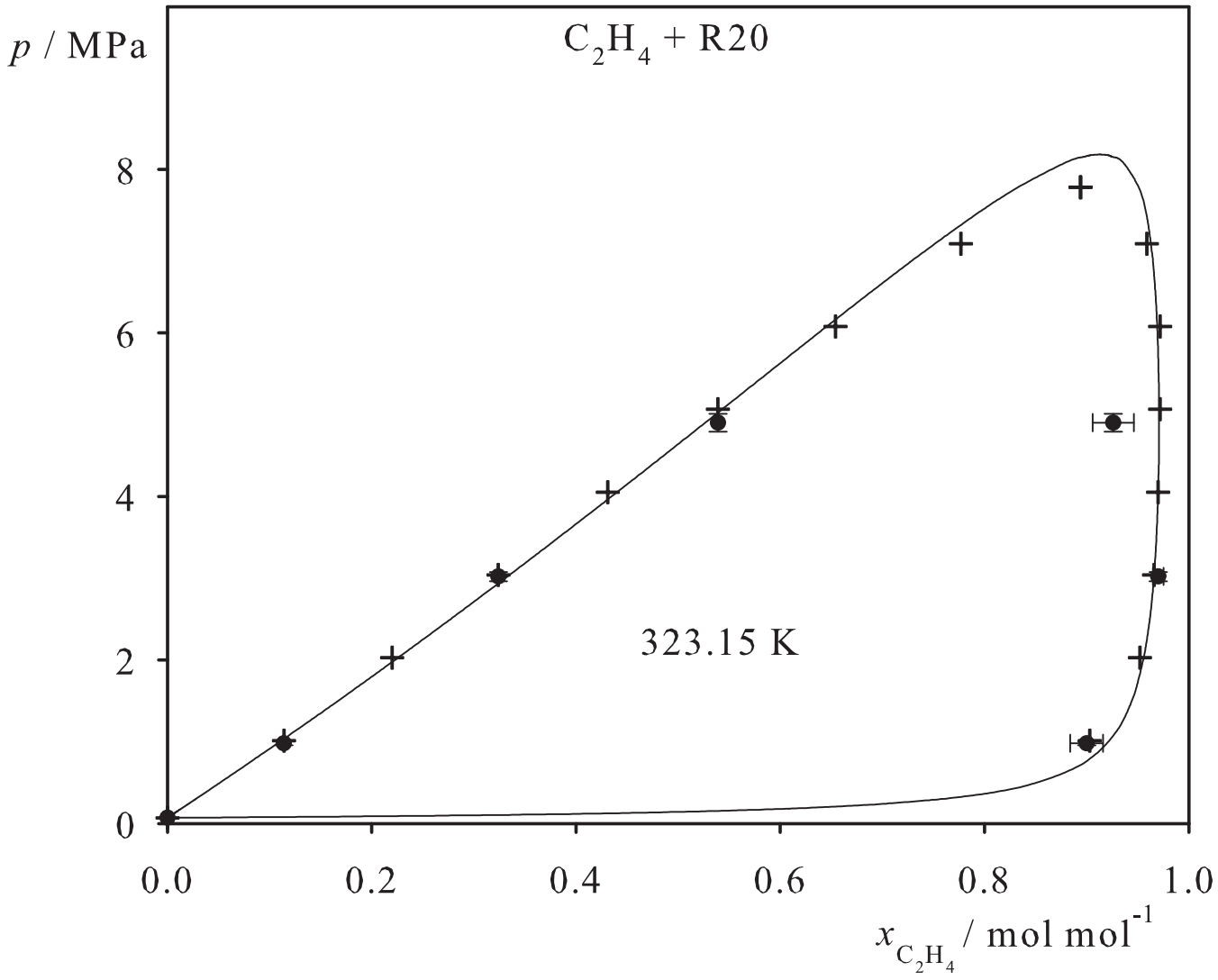

Fig. 93. Binary vapor-liquid equilibrium phase diagram: simulation data ●, experimental data + (cf. Table 2 of the manuscript for the reference) and Peng-Robinson equation of state —.

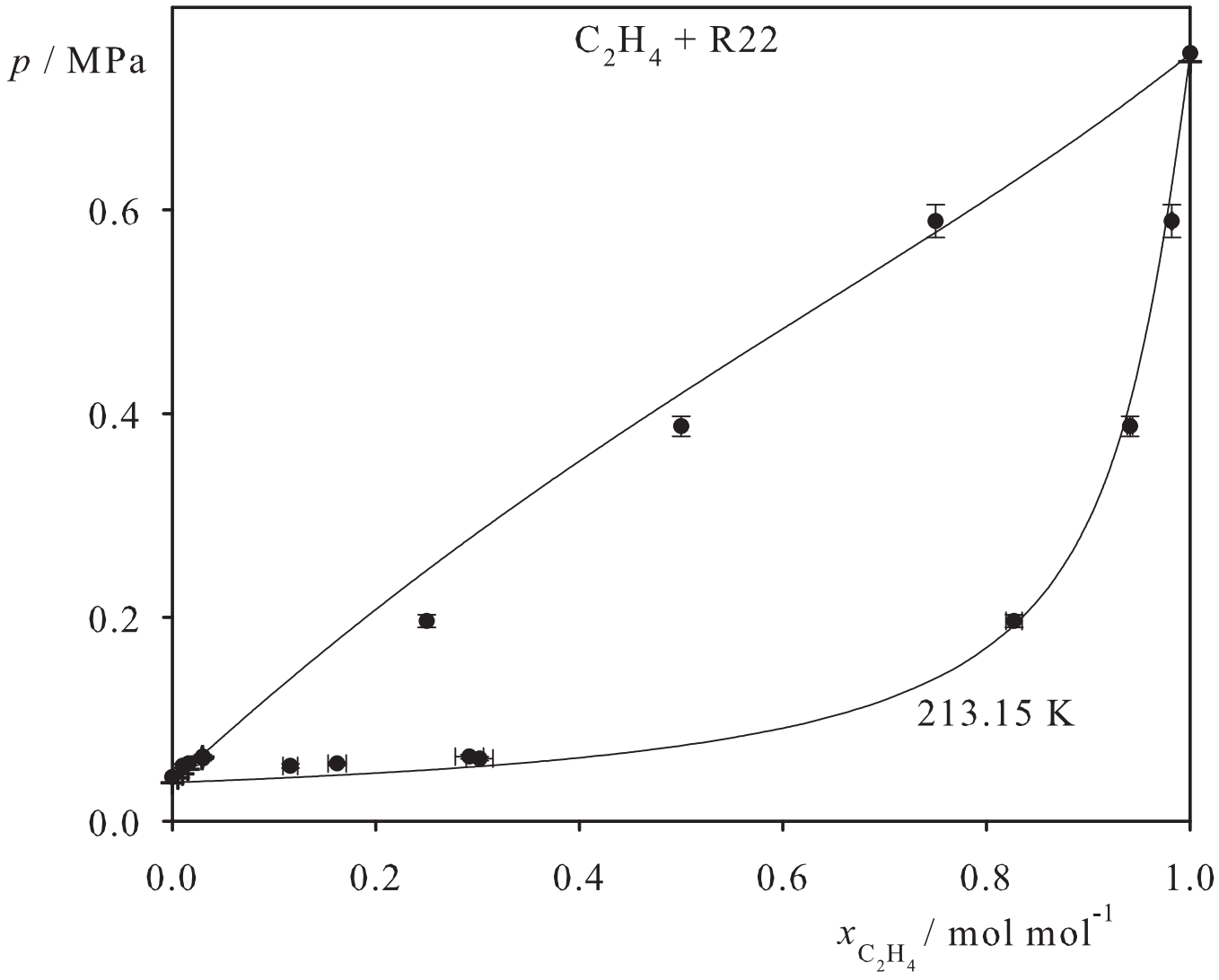

Fig. 94. Binary vapor-liquid equilibrium phase diagram: simulation data ●, experimental data + (cf. Table 2 of the manuscript for the reference) and Peng-Robinson equation of state —.

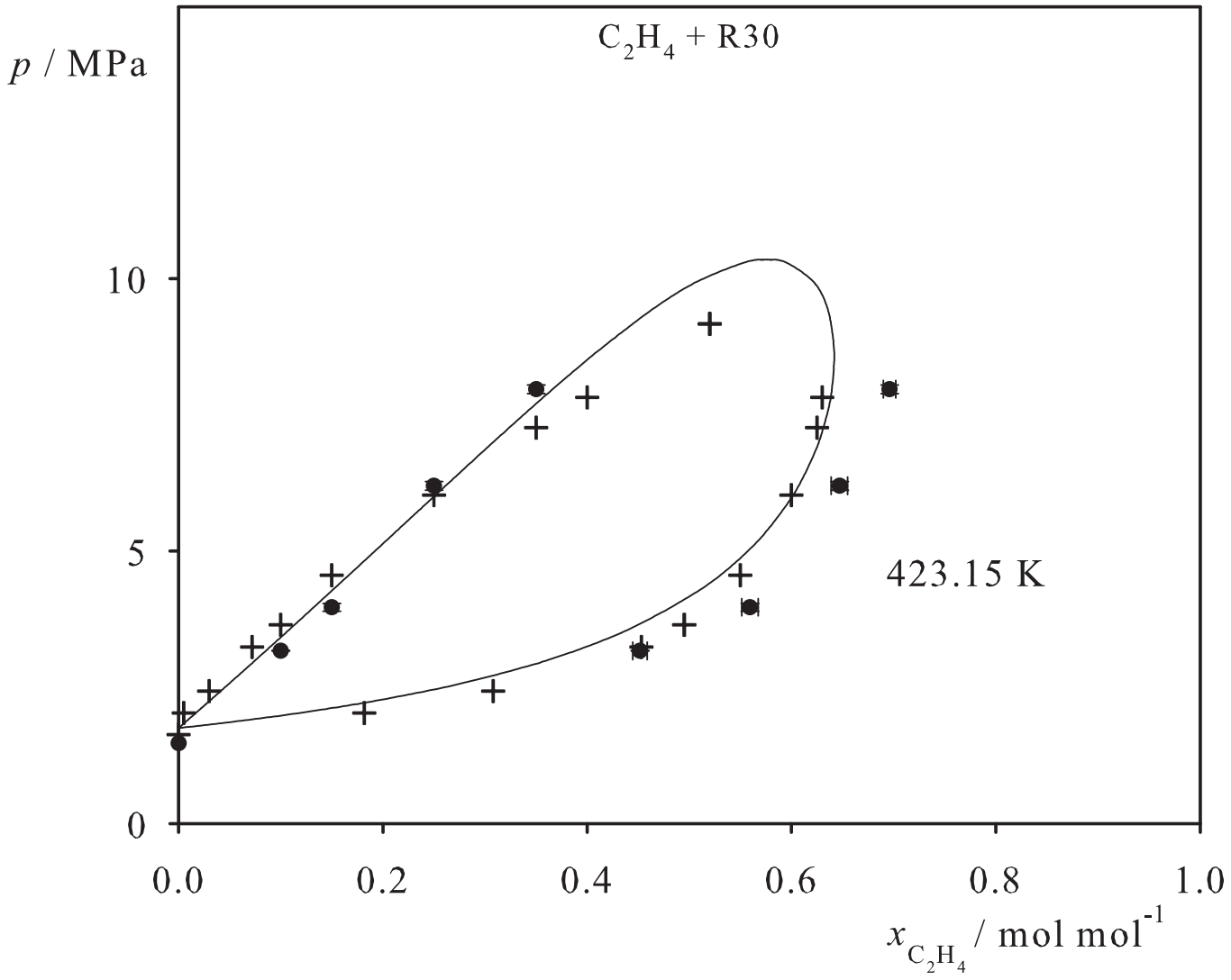

Fig. 95. Binary vapor-liquid equilibrium phase diagram: simulation data ●, experimental data + (cf. Table 2 of the manuscript for the reference) and Peng-Robinson equation of state —.

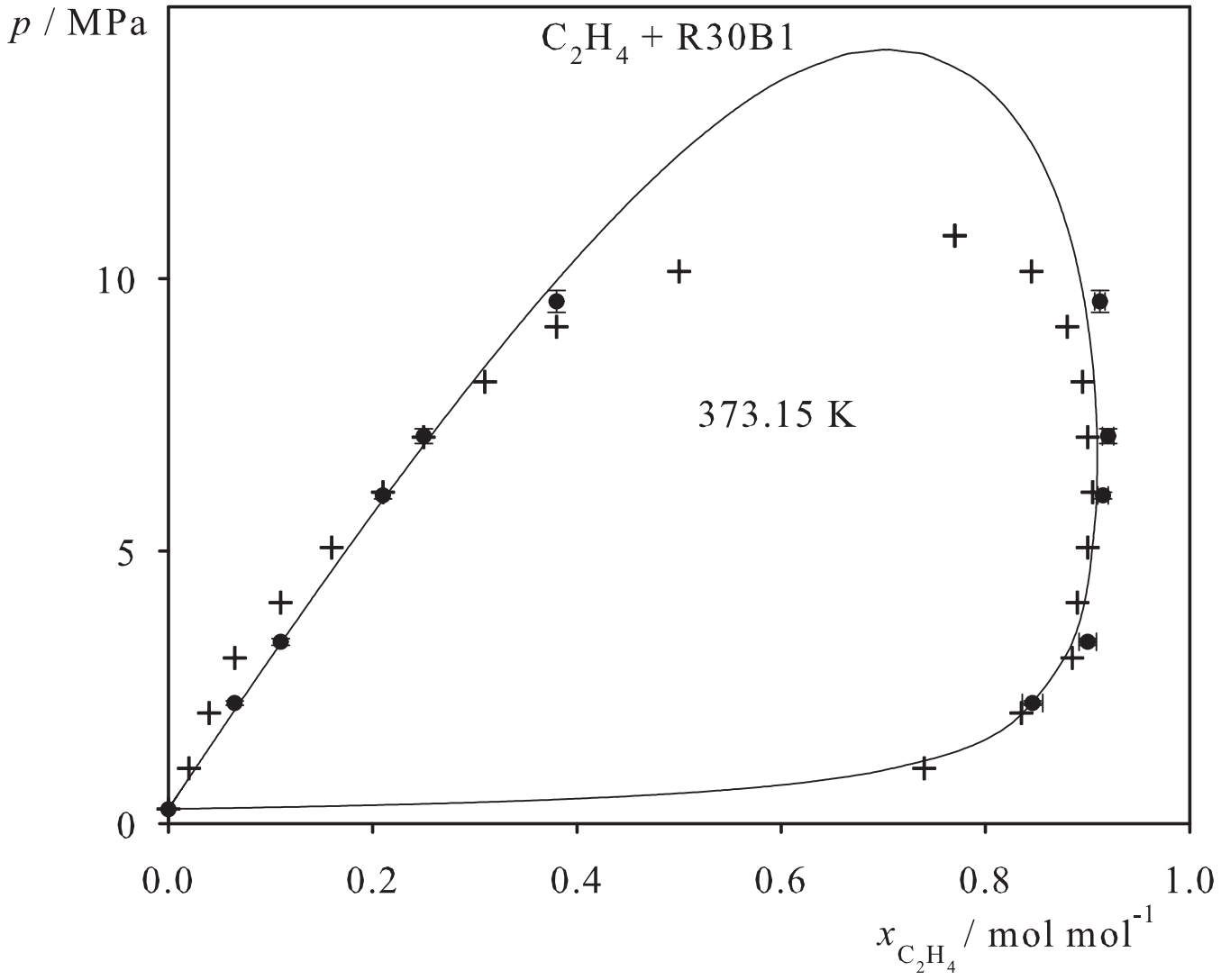

Fig. 96. Binary vapor-liquid equilibrium phase diagram: simulation data ●, experimental data + (cf. Table 2 of the manuscript for the reference) and Peng-Robinson equation of state —.

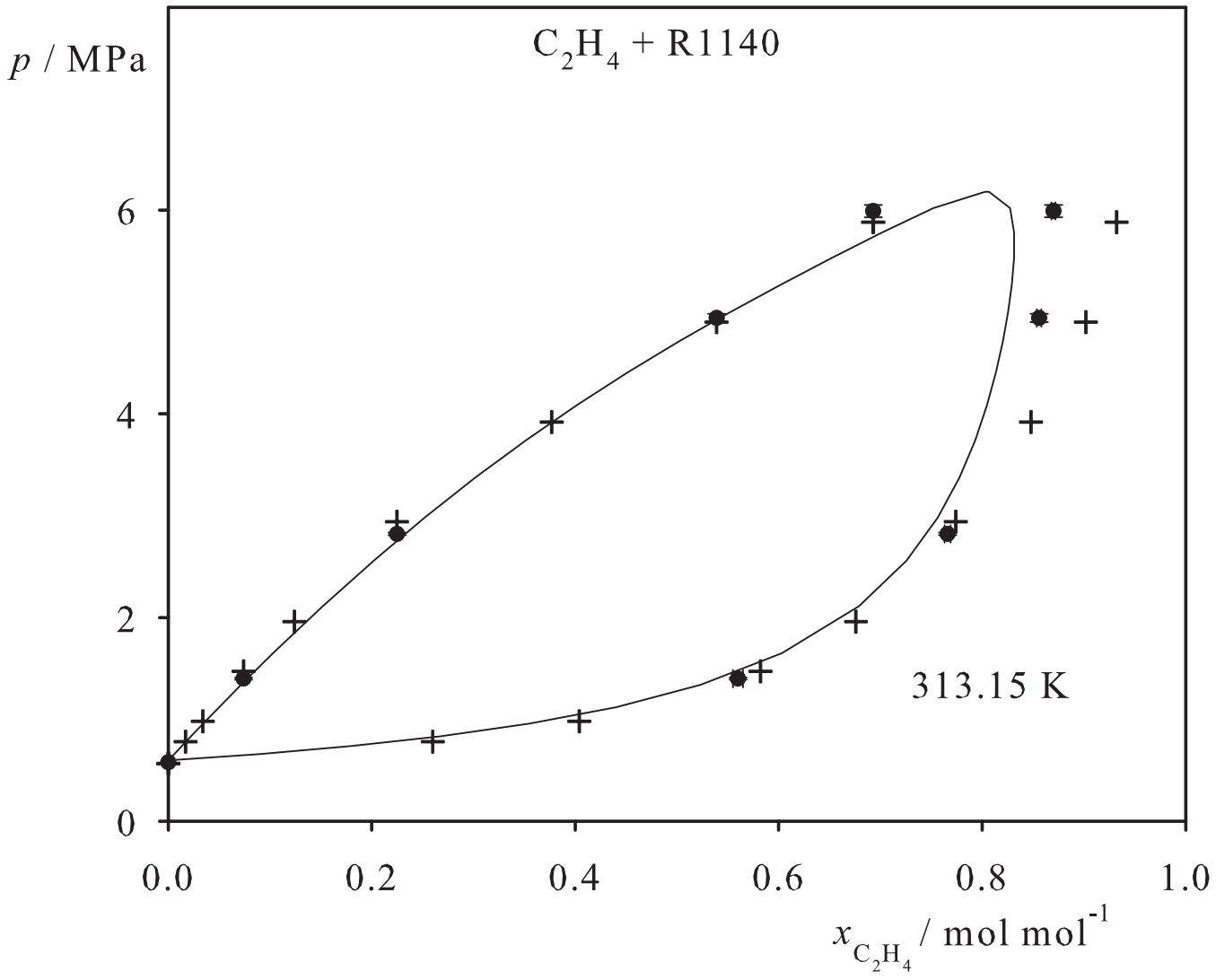

Fig. 97. Binary vapor-liquid equilibrium phase diagram: simulation data ●, experimental data + (cf. Table 2 of the manuscript for the reference) and Peng-Robinson equation of state —.

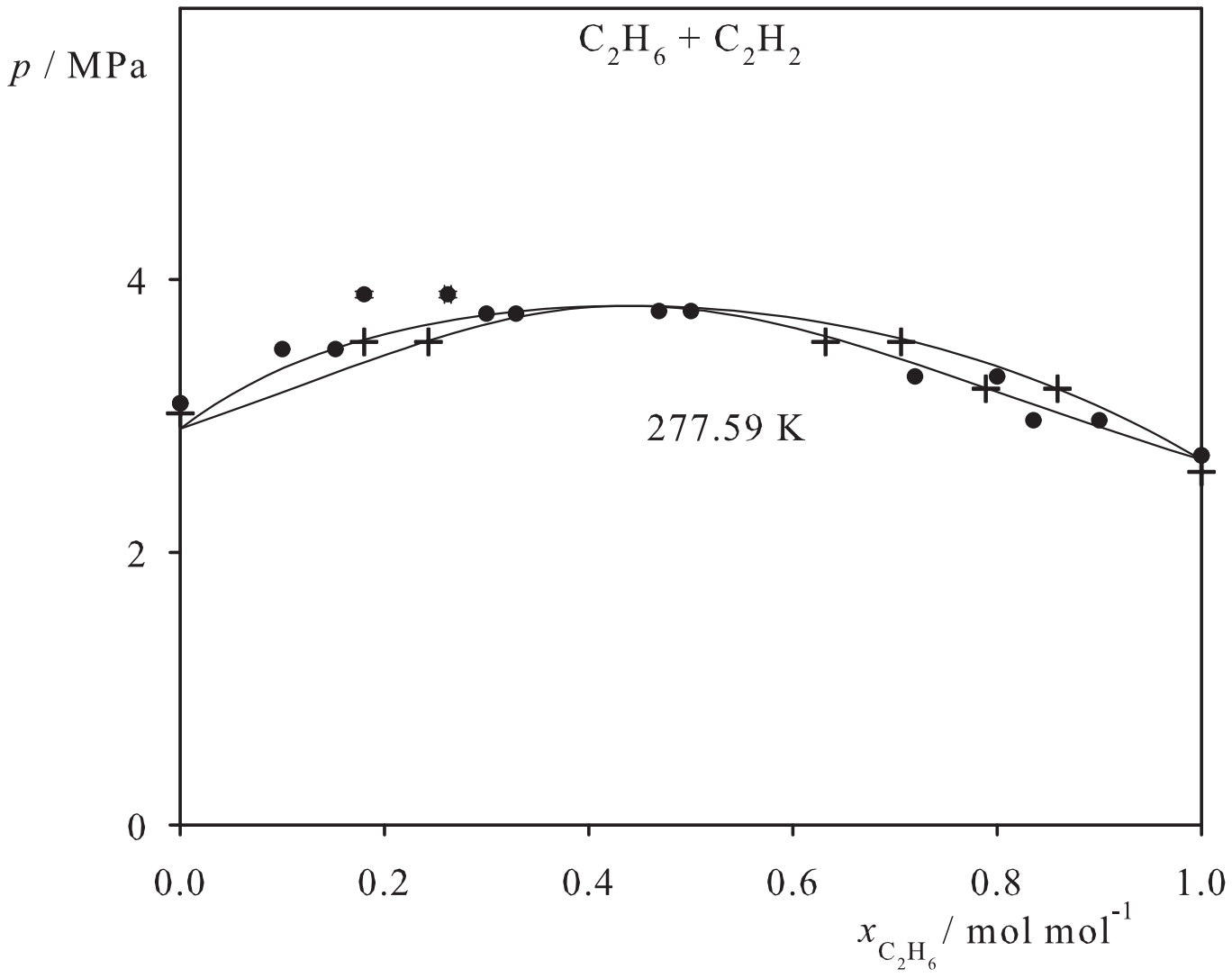

Fig. 98. Binary vapor-liquid equilibrium phase diagram: simulation data ●, experimental data + (cf. Table 2 of the manuscript for the reference) and Peng-Robinson equation of state —.

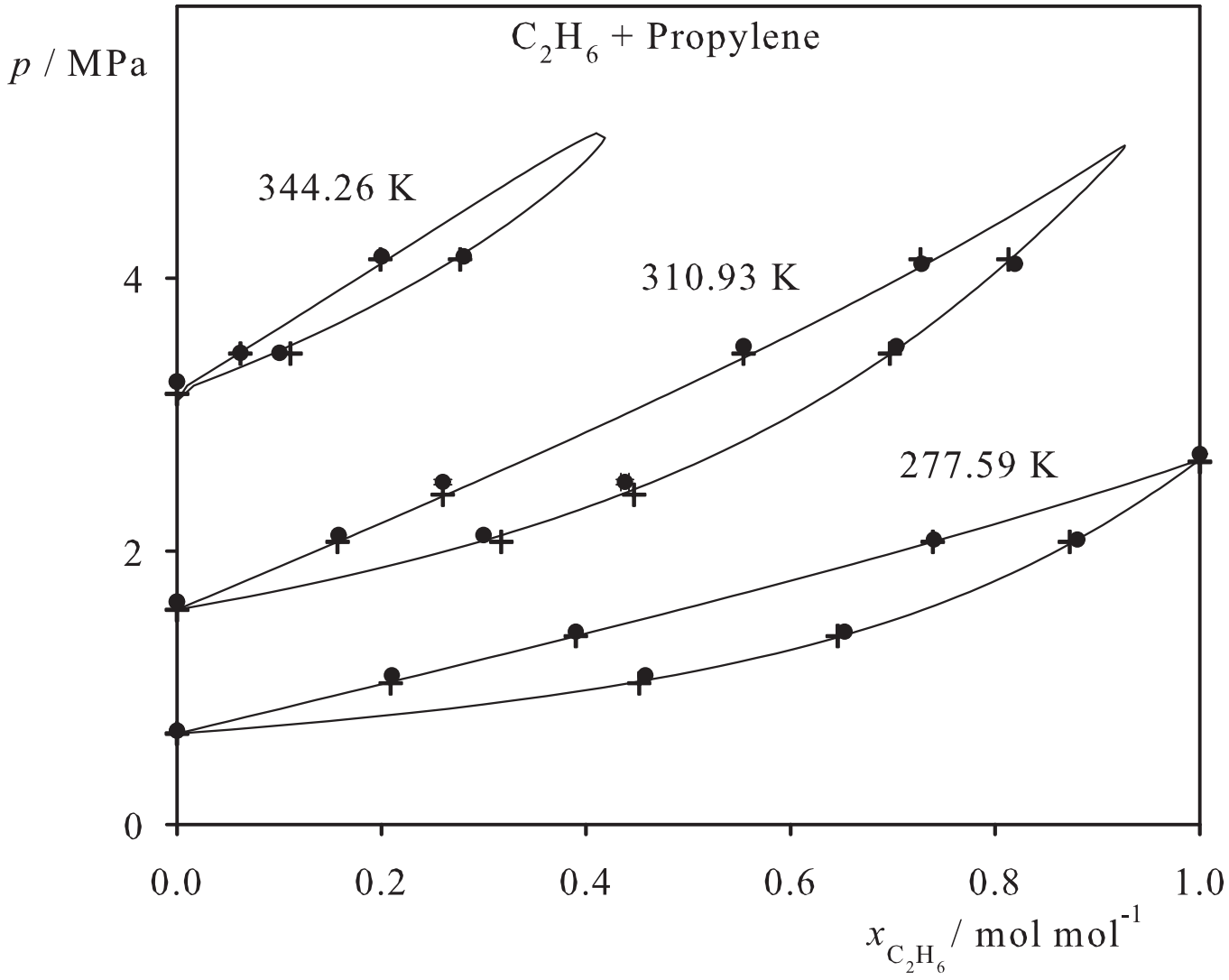

Fig. 99. Binary vapor-liquid equilibrium phase diagram: simulation data ●, experimental data + (cf. Table 2 of the manuscript for the reference) and Peng-Robinson equation of state —.

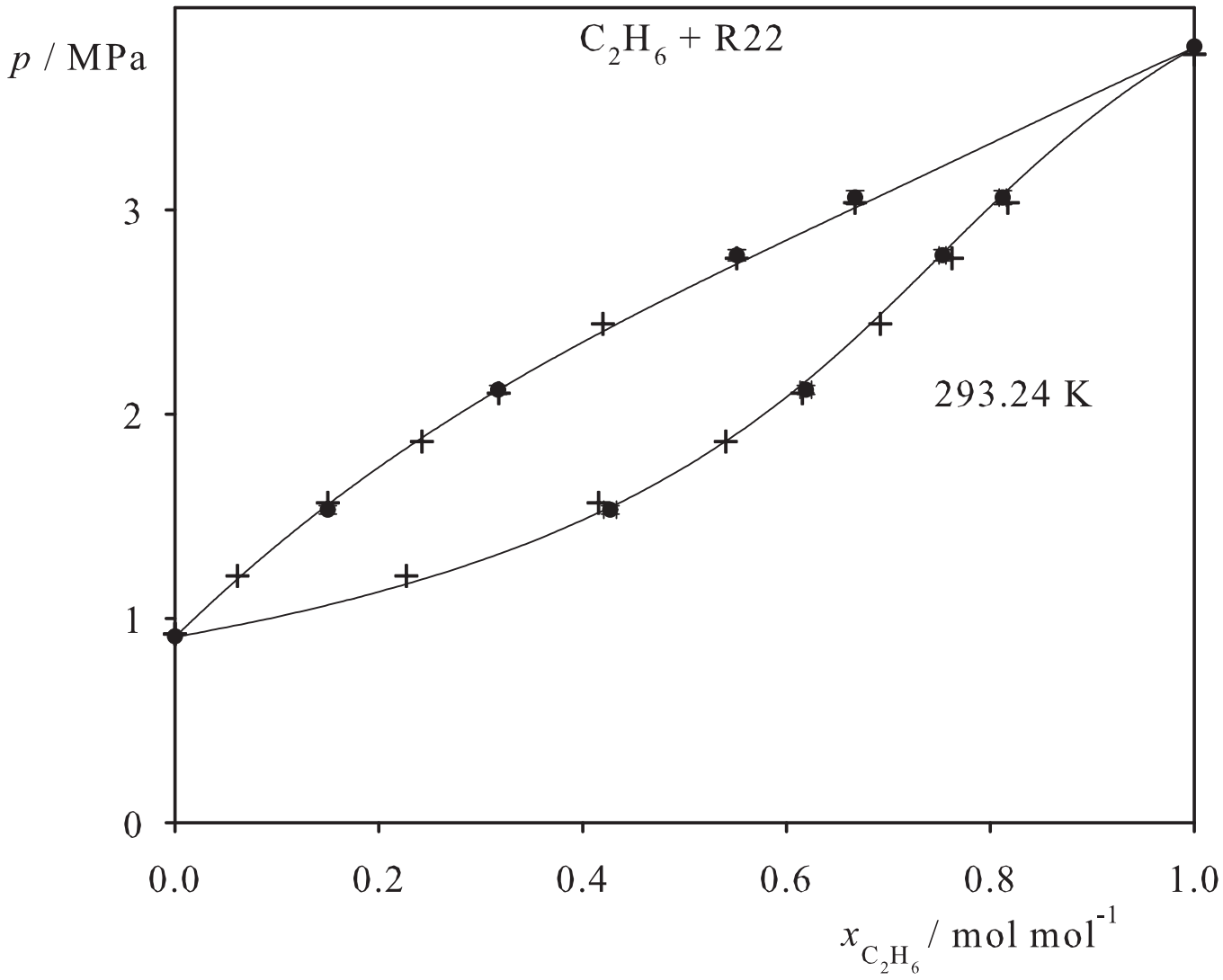

Fig. 100. Binary vapor-liquid equilibrium phase diagram: simulation data ●, experimental data + (cf. Table 2 of the manuscript for the reference) and Peng-Robinson equation of state —.

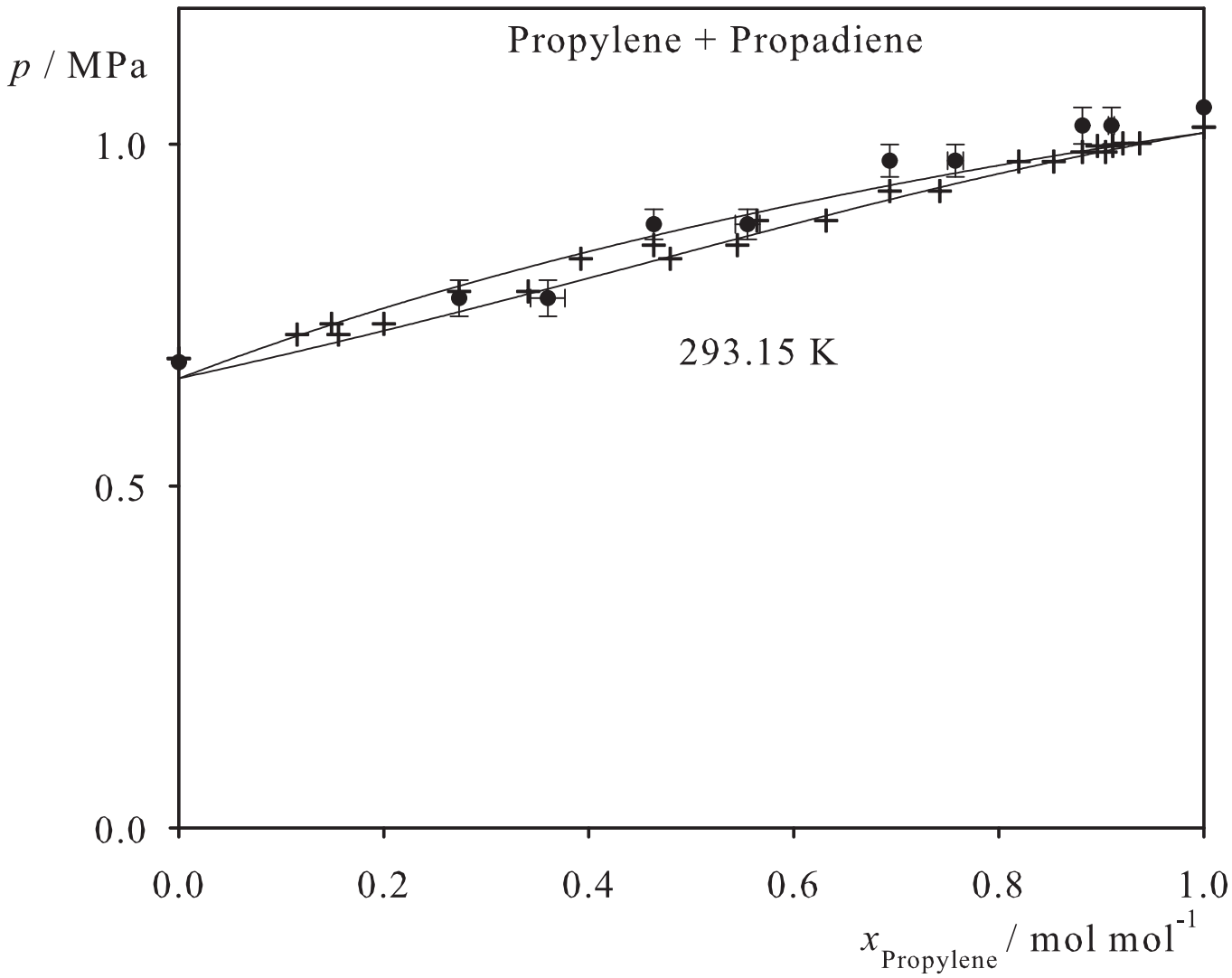

Fig. 101. Binary vapor-liquid equilibrium phase diagram: simulation data ●, experimental data + (cf. Table 2 of the manuscript for the reference) and Peng-Robinson equation of state —.

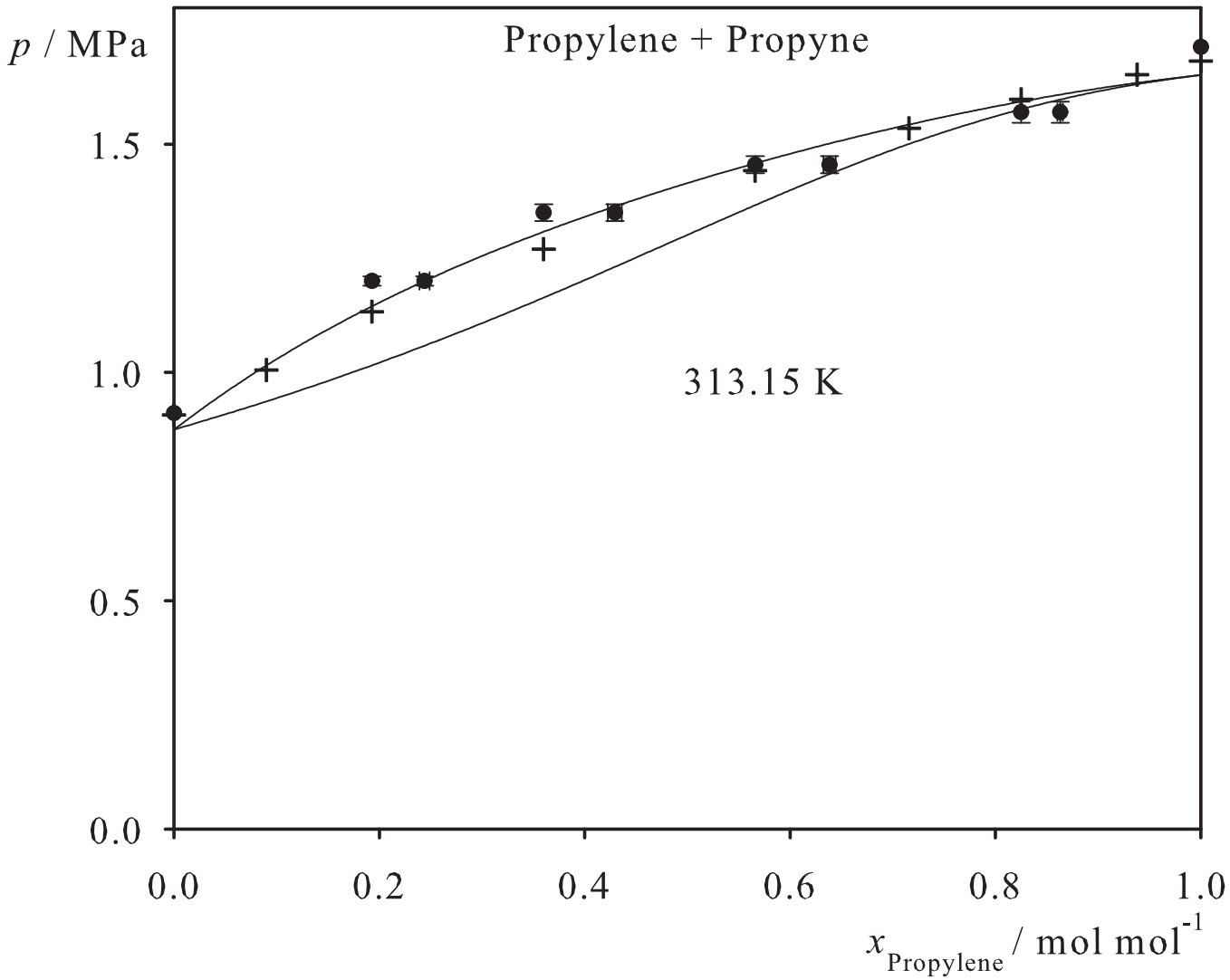

Fig. 102. Binary vapor-liquid equilibrium phase diagram: simulation data ●, experimental data + (cf. Table 2 of the manuscript for the reference) and Peng-Robinson equation of state —.

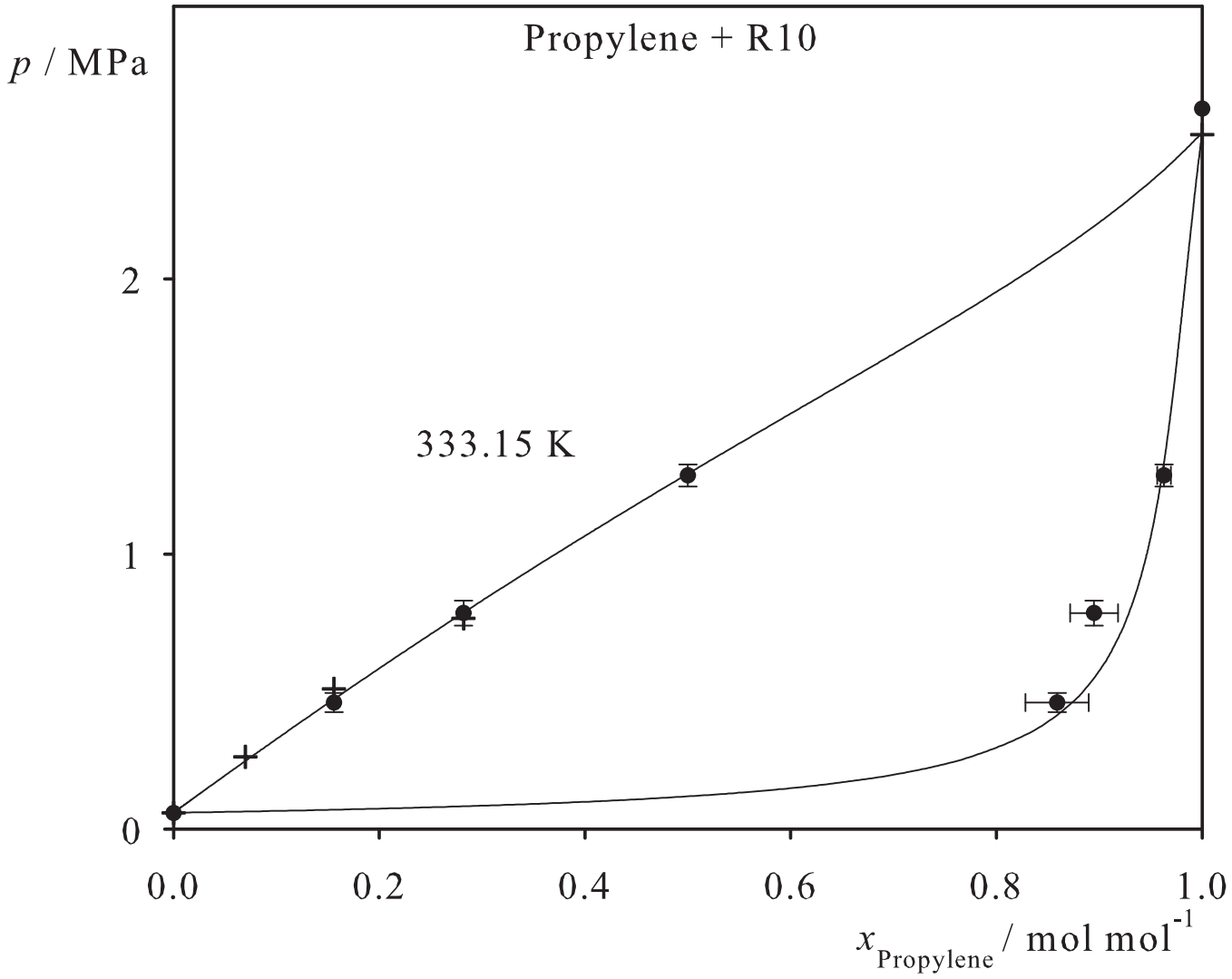

Fig. 103. Binary vapor-liquid equilibrium phase diagram: simulation data ●, experimental data + (cf. Table 2 of the manuscript for the reference) and Peng-Robinson equation of state —.

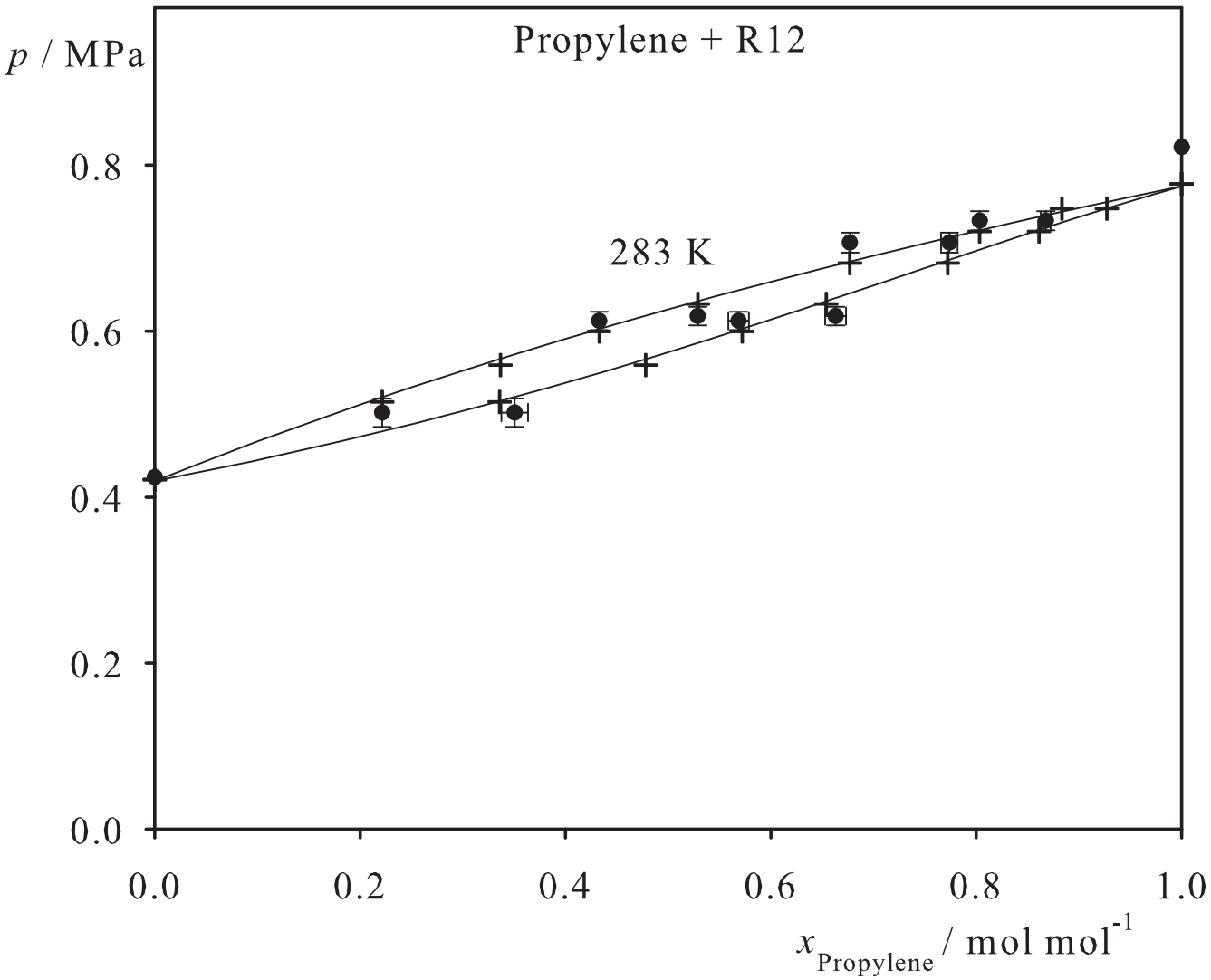

Fig. 104. Binary vapor-liquid equilibrium phase diagram: simulation data ●, experimental data + (cf. Table 2 of the manuscript for the reference) and Peng-Robinson equation of state —.

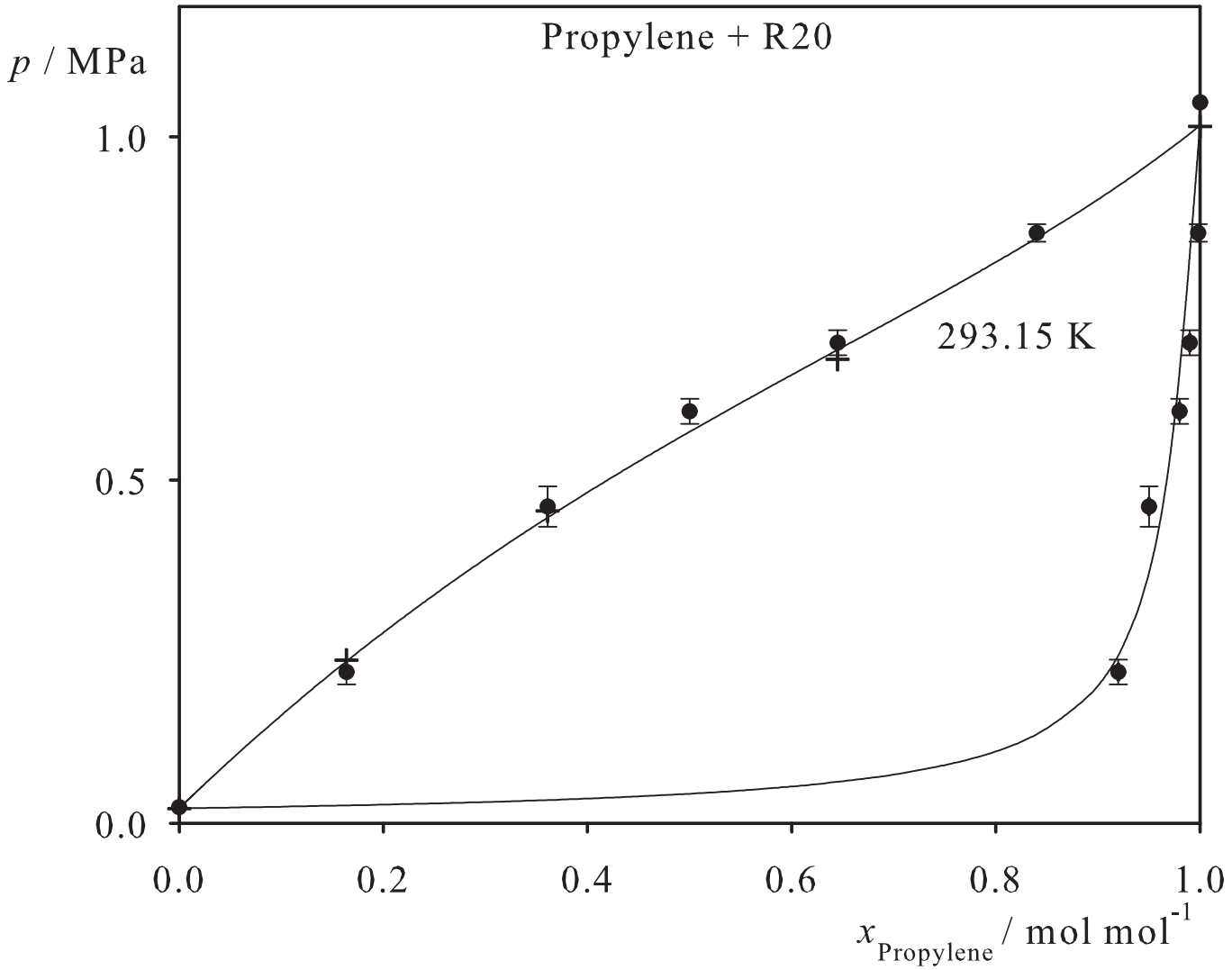

Fig. 105. Binary vapor-liquid equilibrium phase diagram: simulation data ●, experimental data + (cf. Table 2 of the manuscript for the reference) and Peng-Robinson equation of state —.

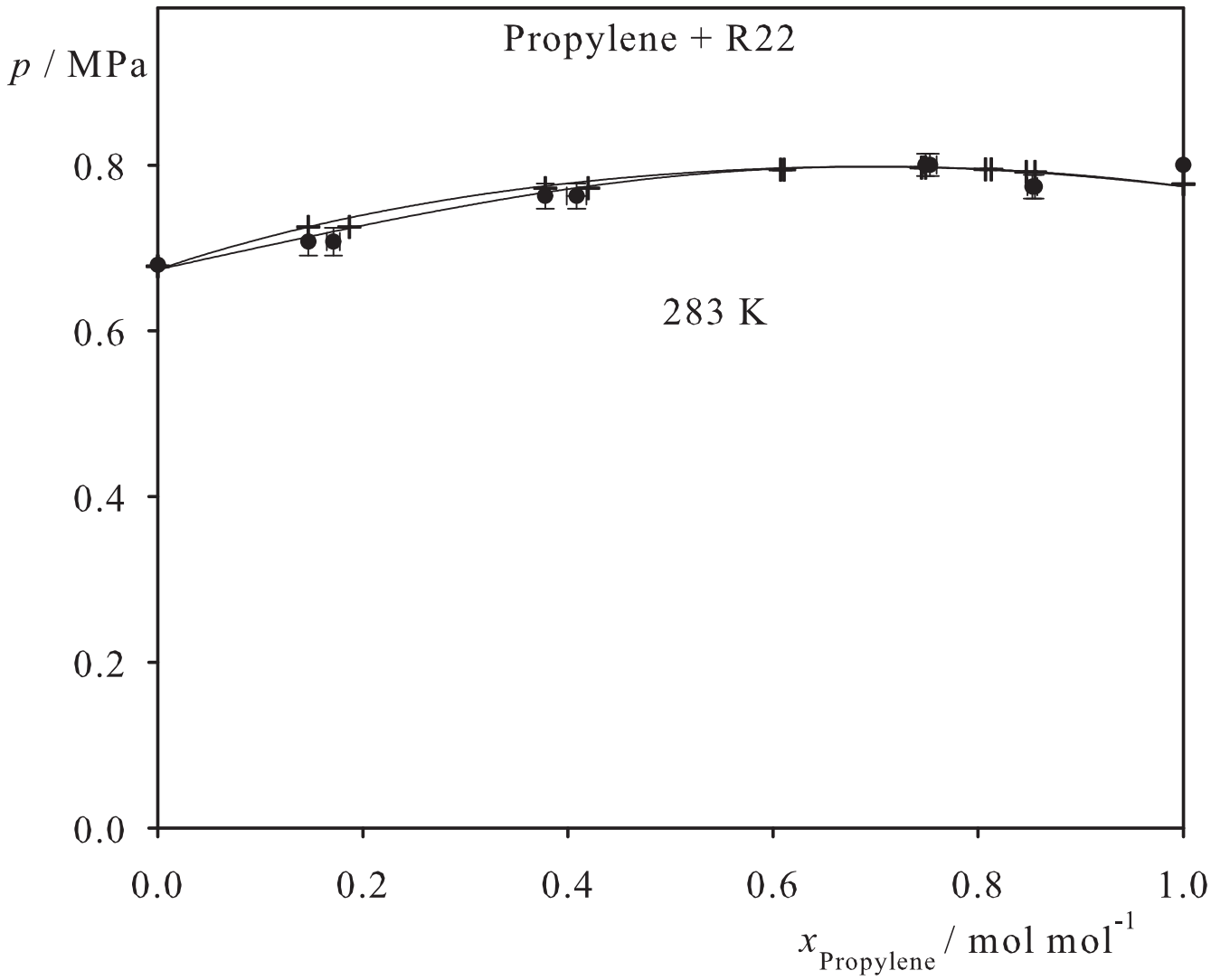

Fig. 106. Binary vapor-liquid equilibrium phase diagram: simulation data ●, experimental data + (cf. Table 2 of the manuscript for the reference) and Peng-Robinson equation of state —.

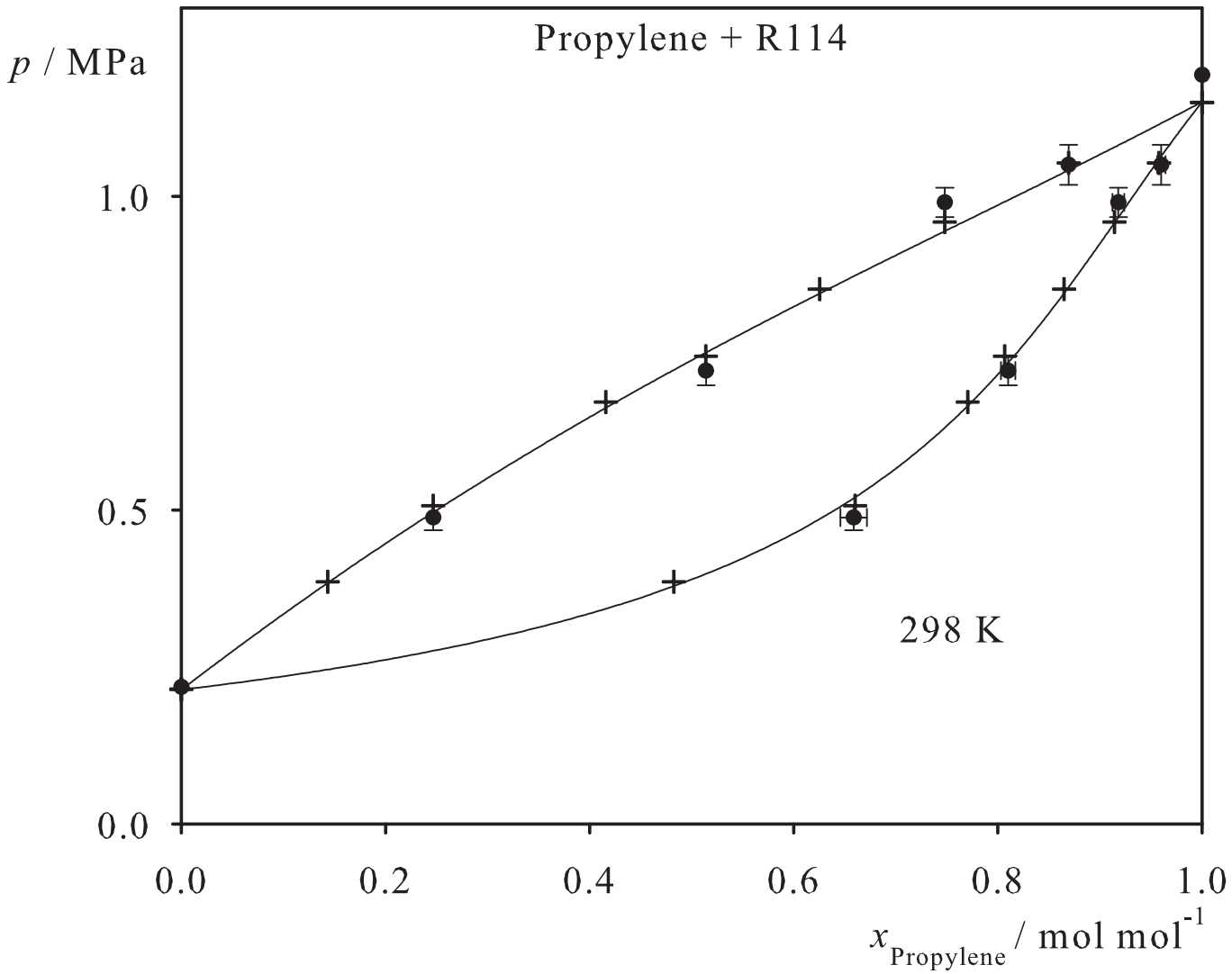

Fig. 107. Binary vapor-liquid equilibrium phase diagram: simulation data ●, experimental data + (cf. Table 2 of the manuscript for the reference) and Peng-Robinson equation of state —.

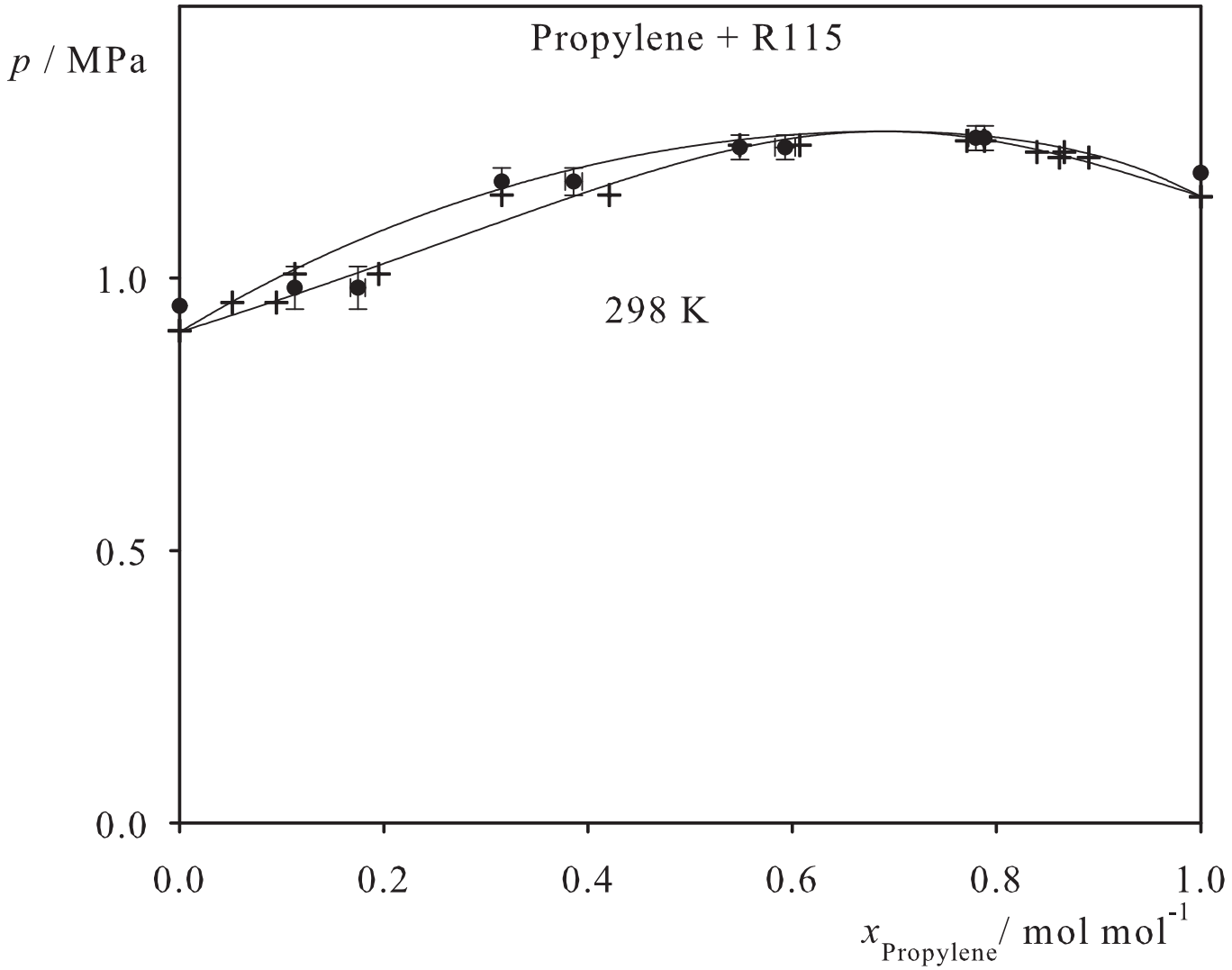

Fig. 108. Binary vapor-liquid equilibrium phase diagram: simulation data ●, experimental data + (cf. Table 2 of the manuscript for the reference) and Peng-Robinson equation of state —.

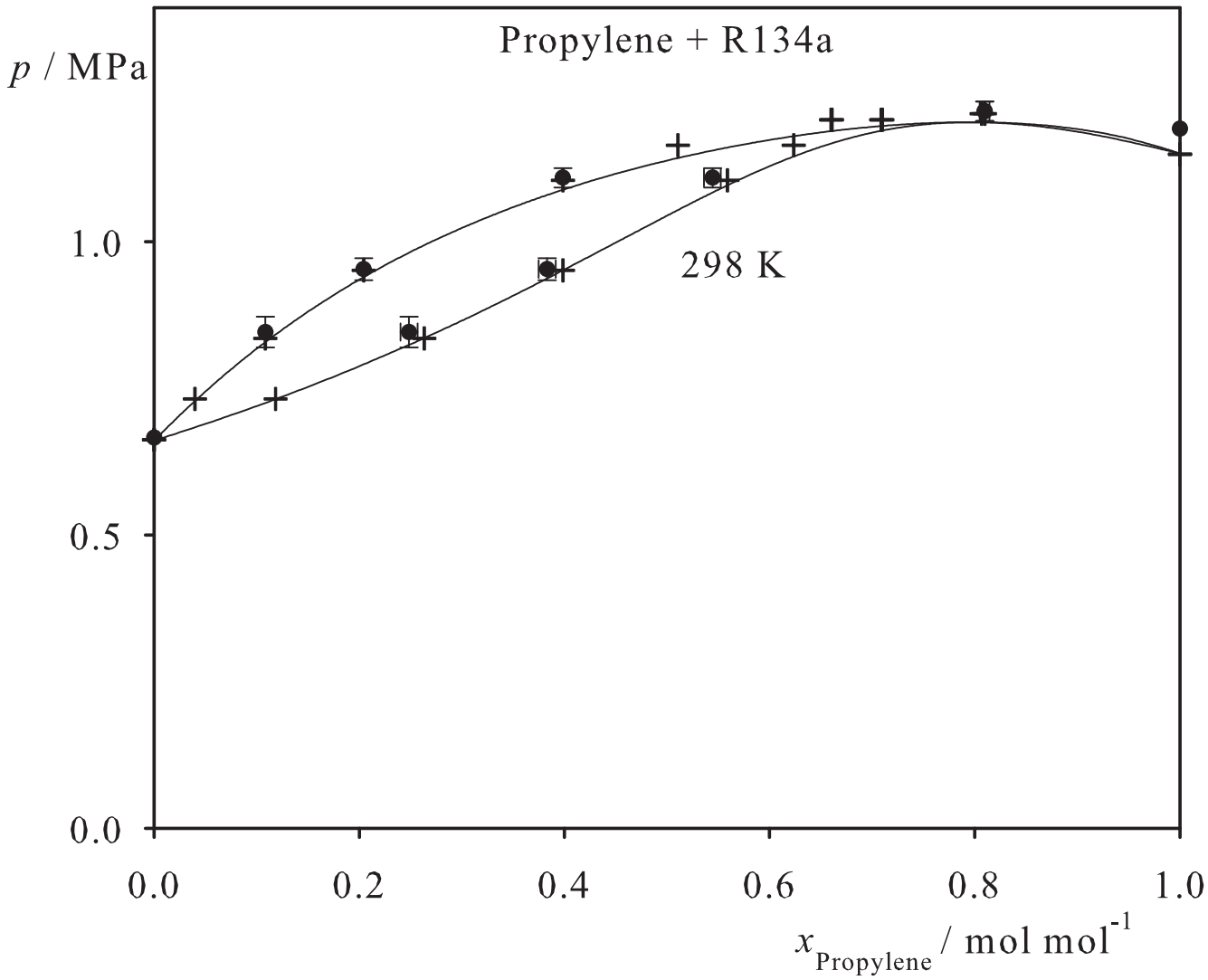

Fig. 109. Binary vapor-liquid equilibrium phase diagram: simulation data ●, experimental data + (cf. Table 2 of the manuscript for the reference) and Peng-Robinson equation of state —.

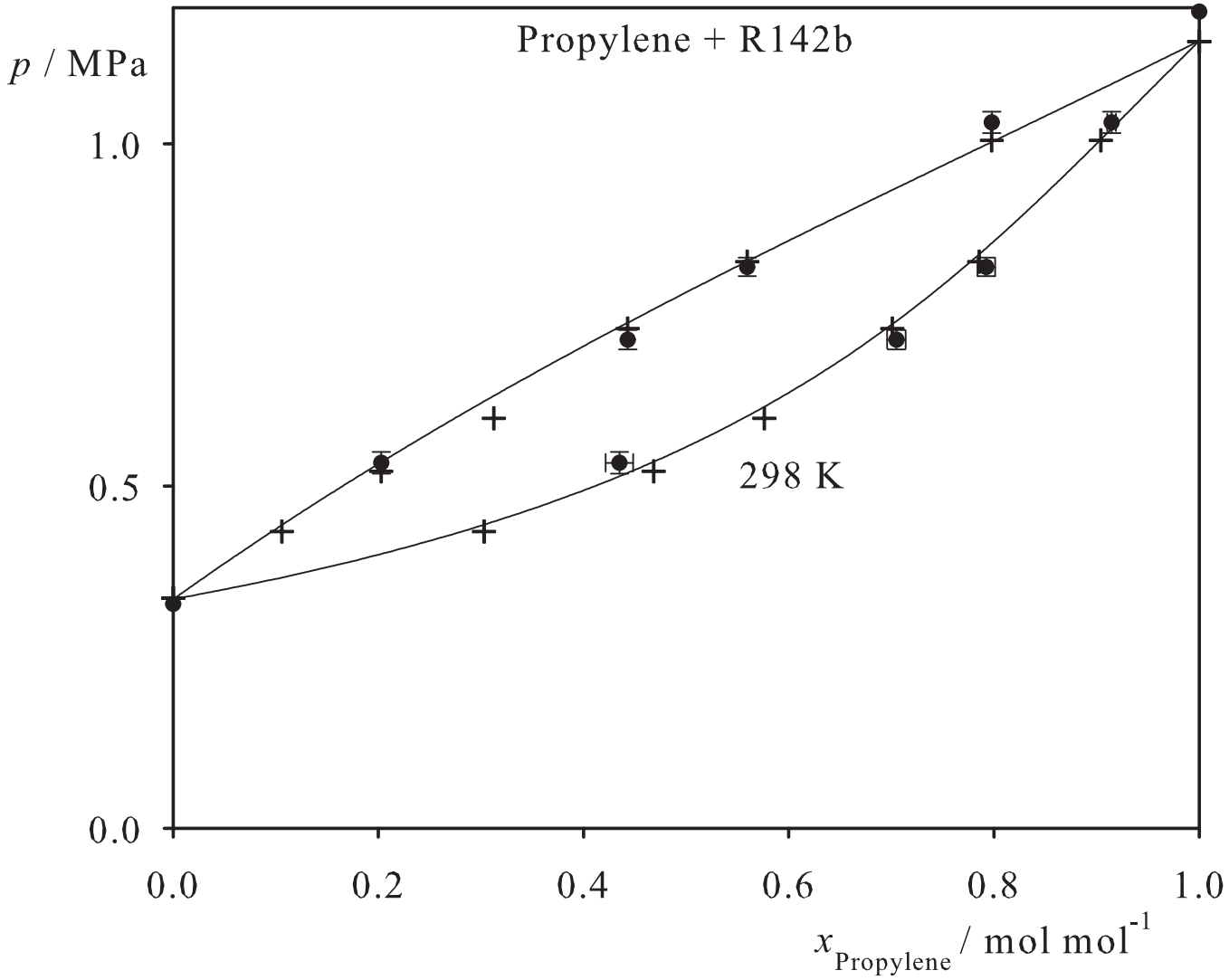

Fig. 110. Binary vapor-liquid equilibrium phase diagram: simulation data ●, experimental data + (cf. Table 2 of the manuscript for the reference) and Peng-Robinson equation of state —.

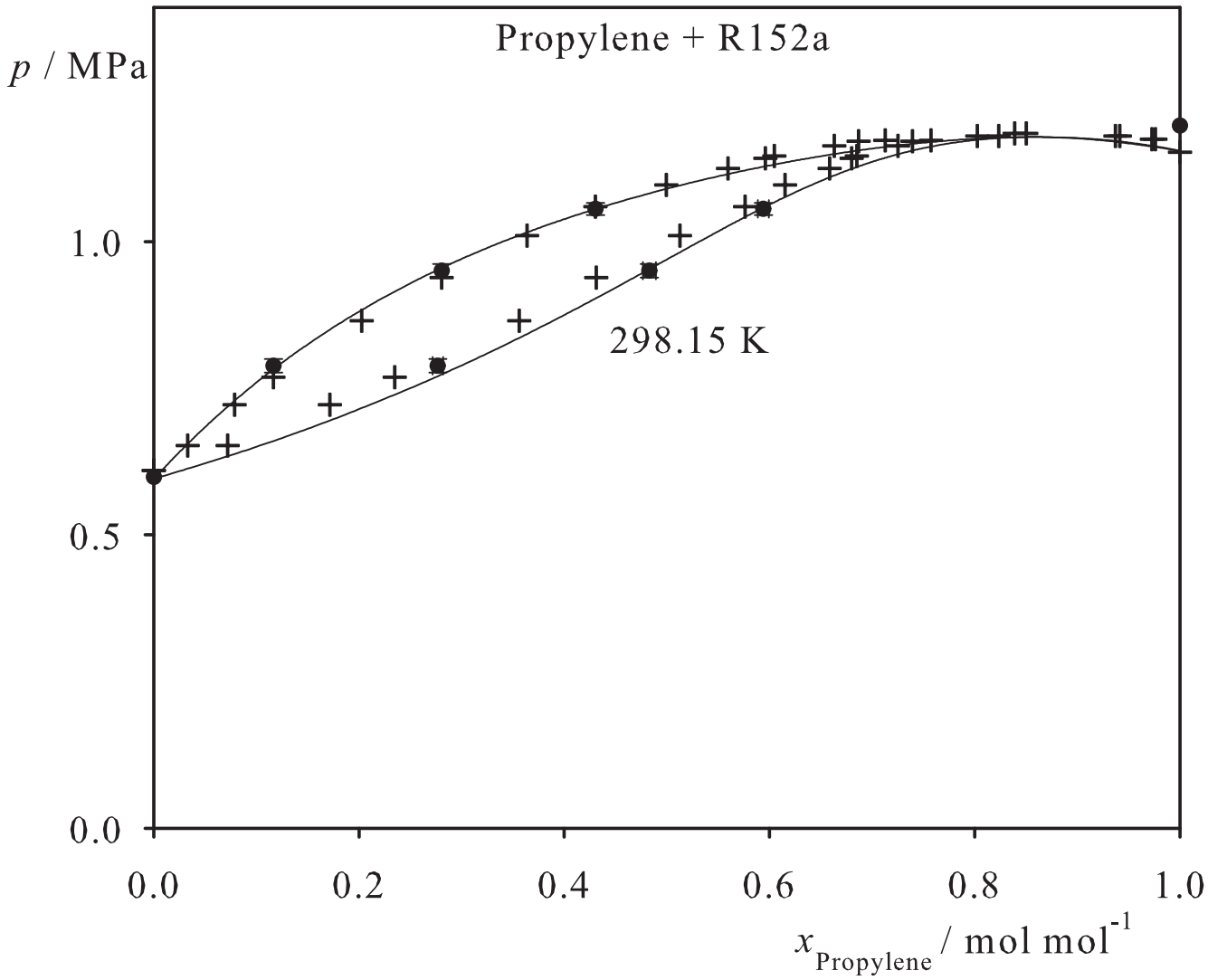

Fig. 111. Binary vapor-liquid equilibrium phase diagram: simulation data ●, experimental data + (cf. Table 2 of the manuscript for the reference) and Peng-Robinson equation of state —.

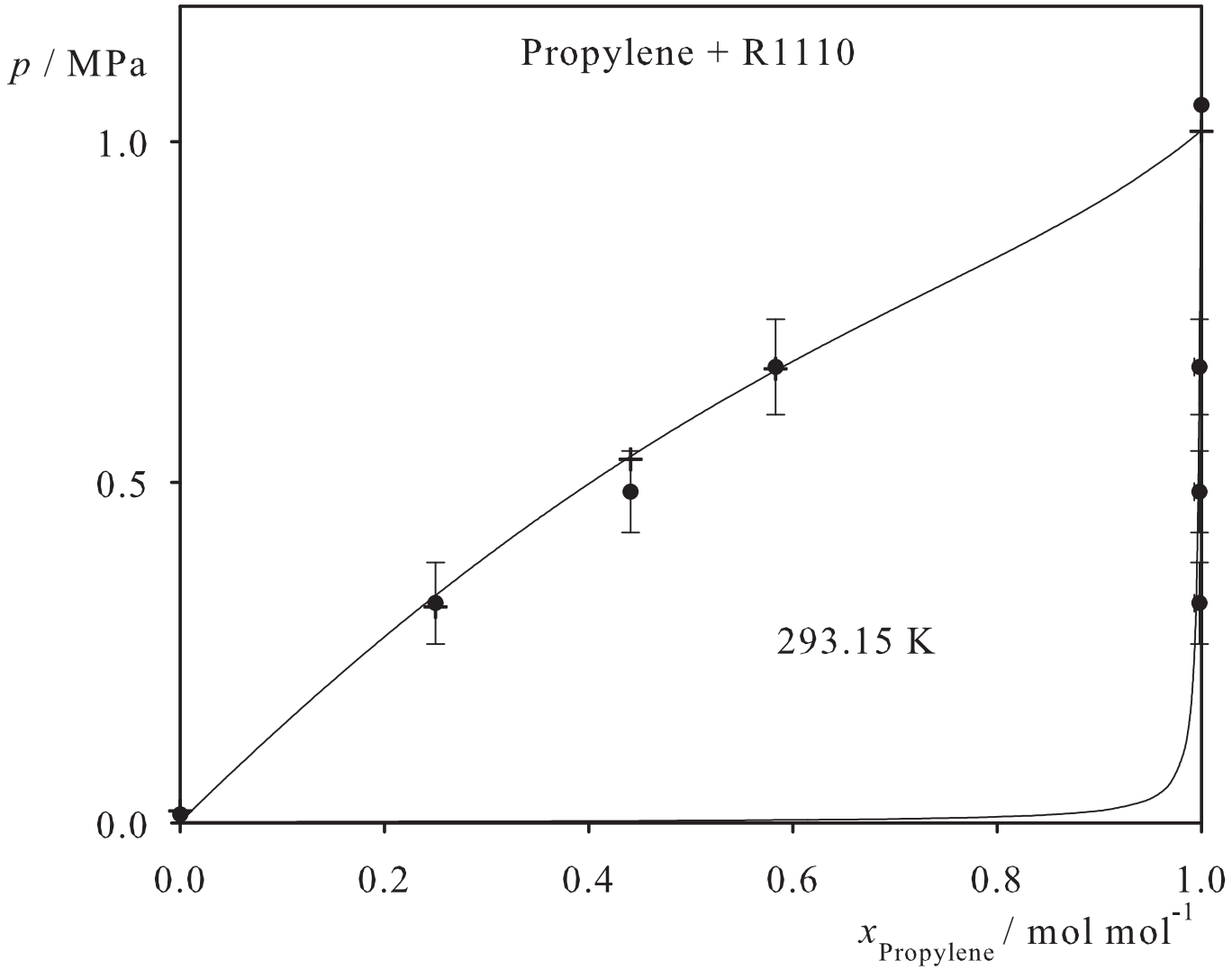

Fig. 112. Binary vapor-liquid equilibrium phase diagram: simulation data ●, experimental data + (cf. Table 2 of the manuscript for the reference) and Peng-Robinson equation of state —.

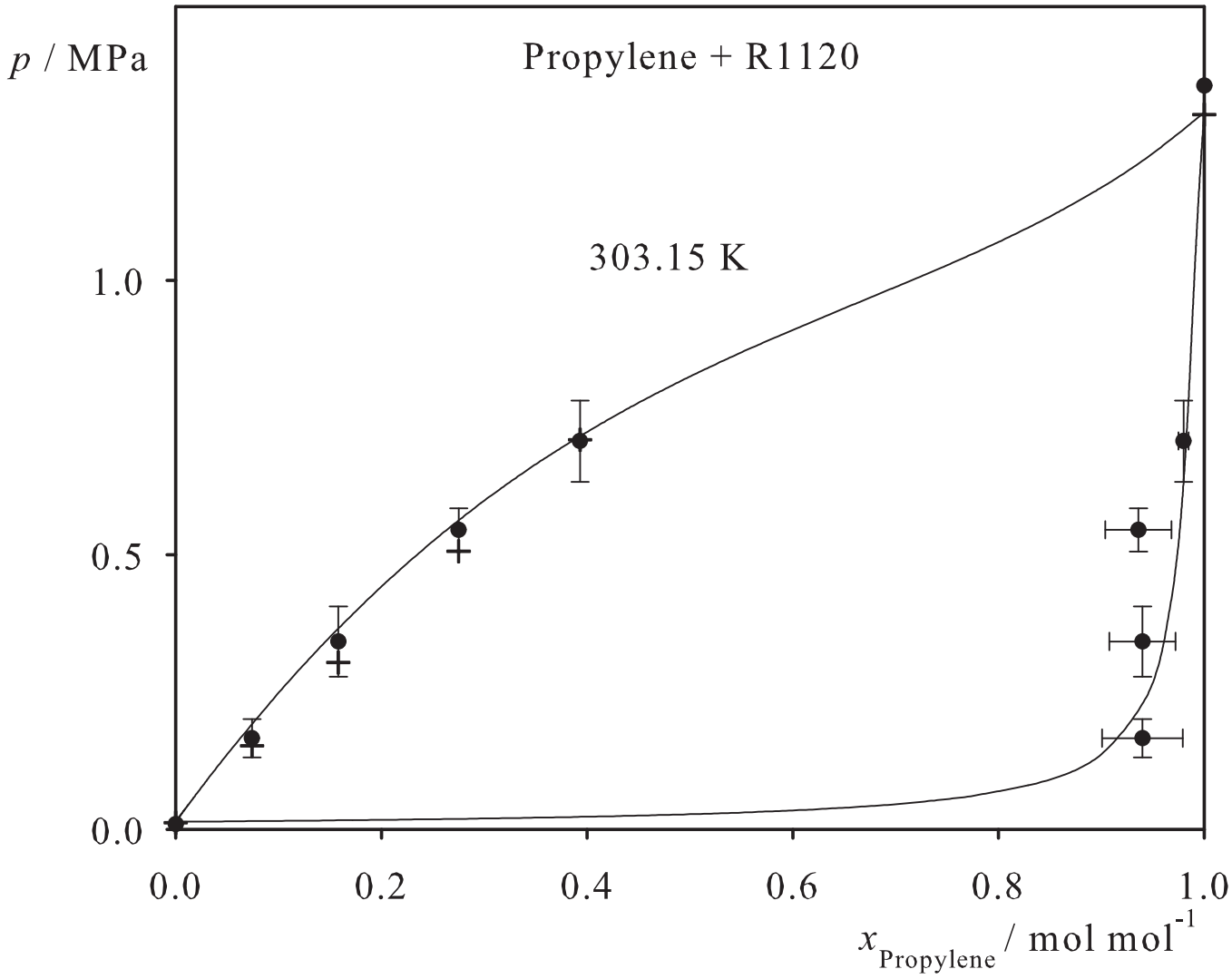

Fig. 113. Binary vapor-liquid equilibrium phase diagram: simulation data ●, experimental data + (cf. Table 2 of the manuscript for the reference) and Peng-Robinson equation of state —.

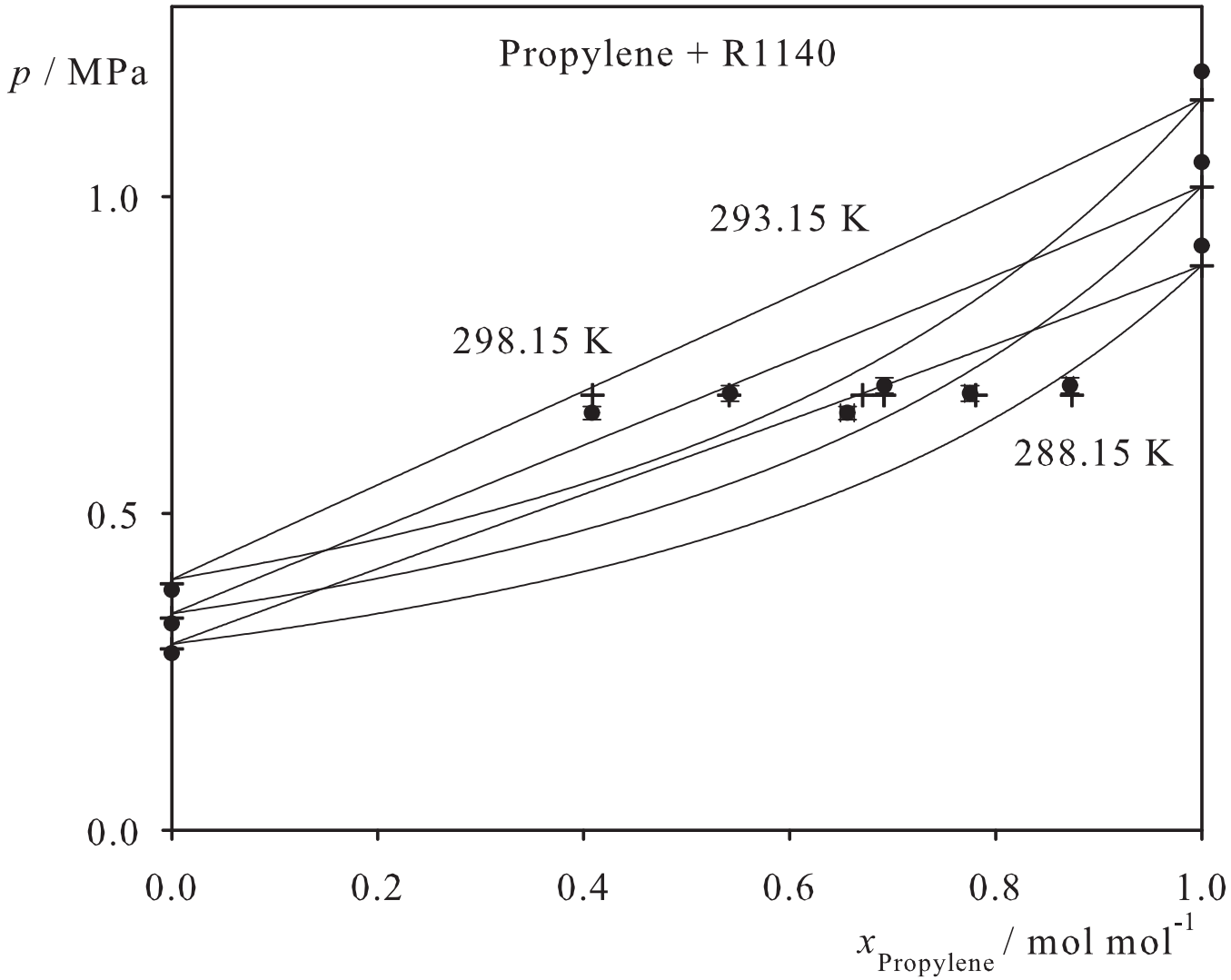

Fig. 114. Binary vapor-liquid equilibrium phase diagram: simulation data ●, experimental data + (cf. Table 2 of the manuscript for the reference) and Peng-Robinson equation of state —.

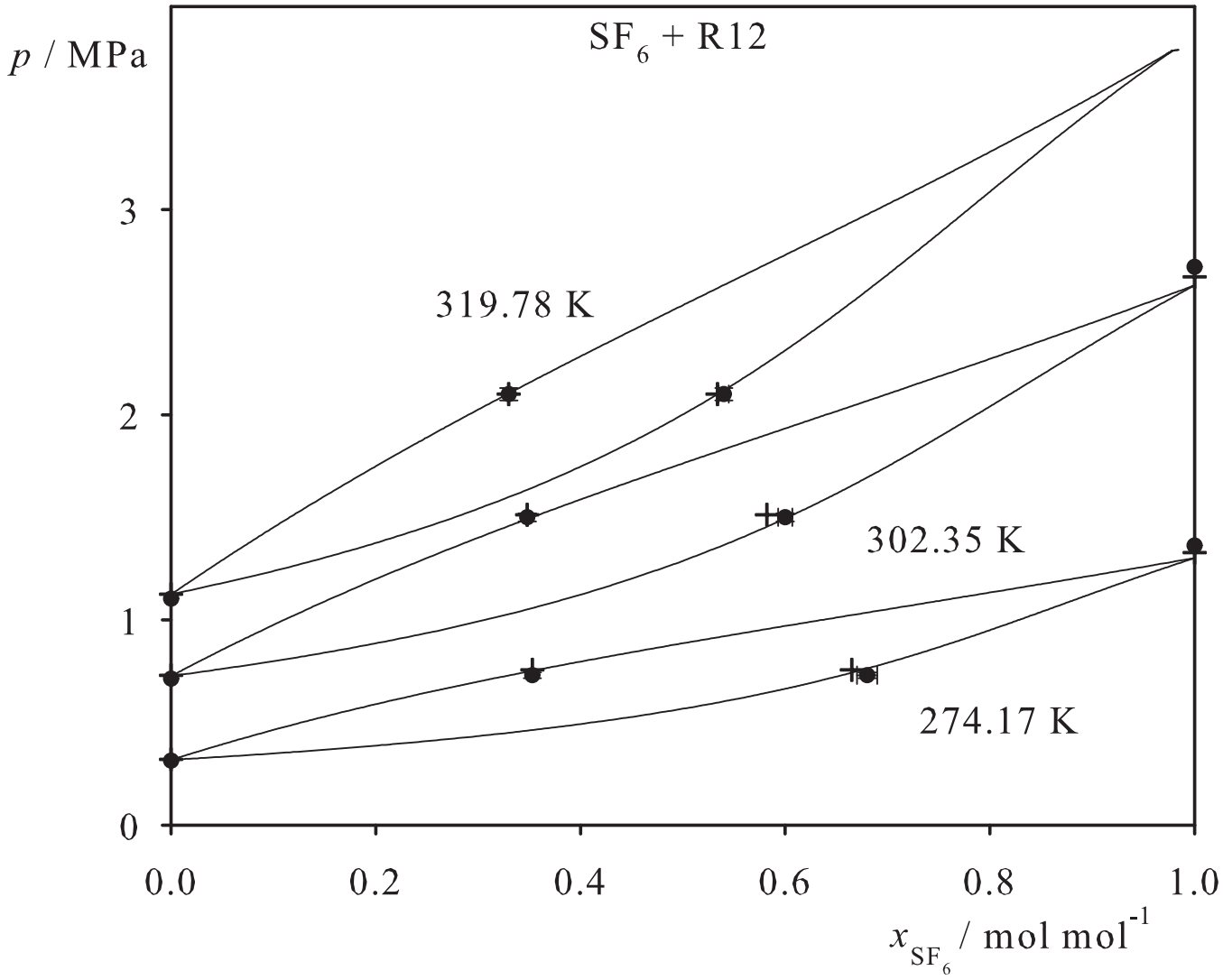

Fig. 115. Binary vapor-liquid equilibrium phase diagram: simulation data ●, experimental data + (cf. Table 2 of the manuscript for the reference) and Peng-Robinson equation of state —.

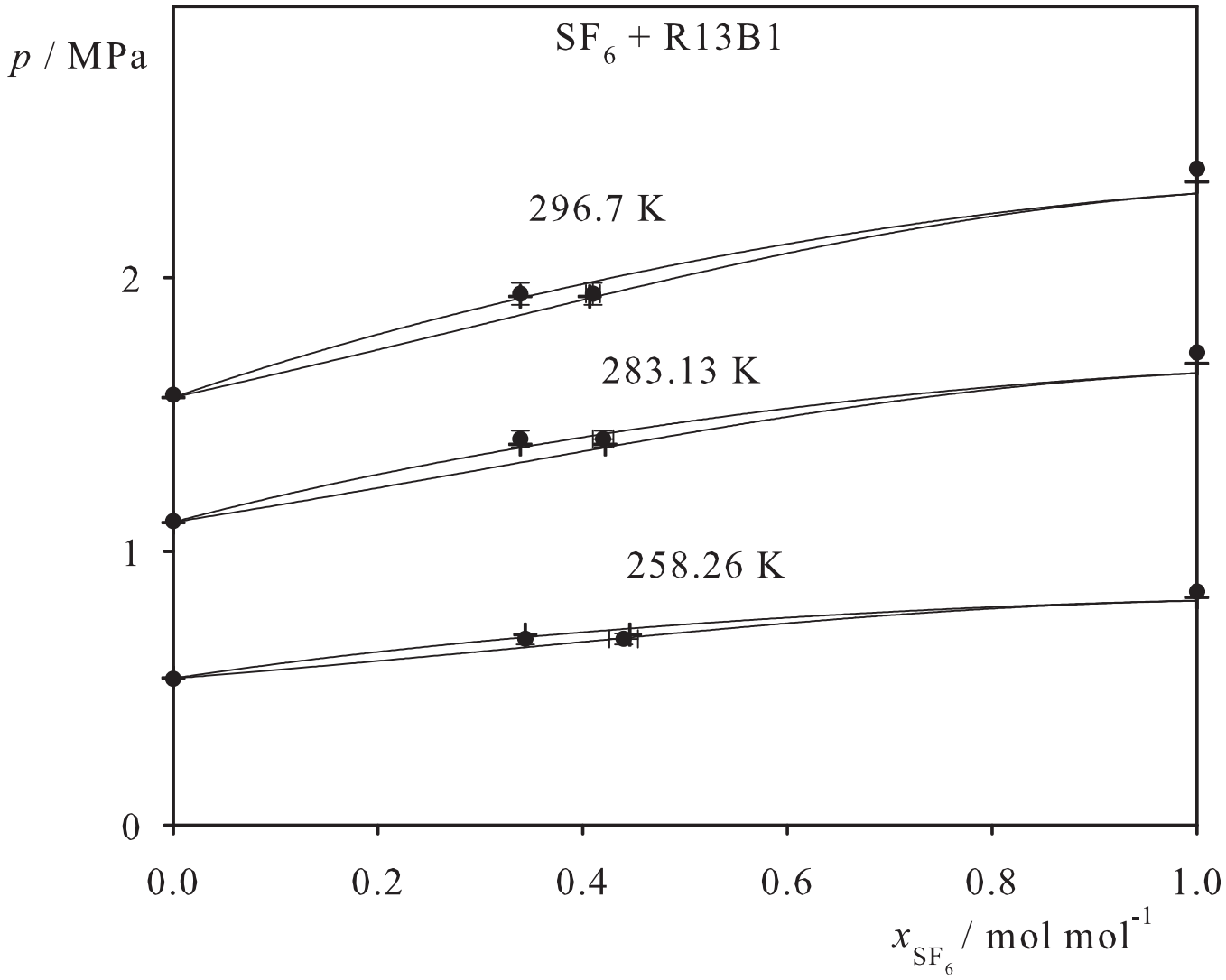

Fig. 116. Binary vapor-liquid equilibrium phase diagram: simulation data ●, experimental data + (cf. Table 2 of the manuscript for the reference) and Peng-Robinson equation of state —.

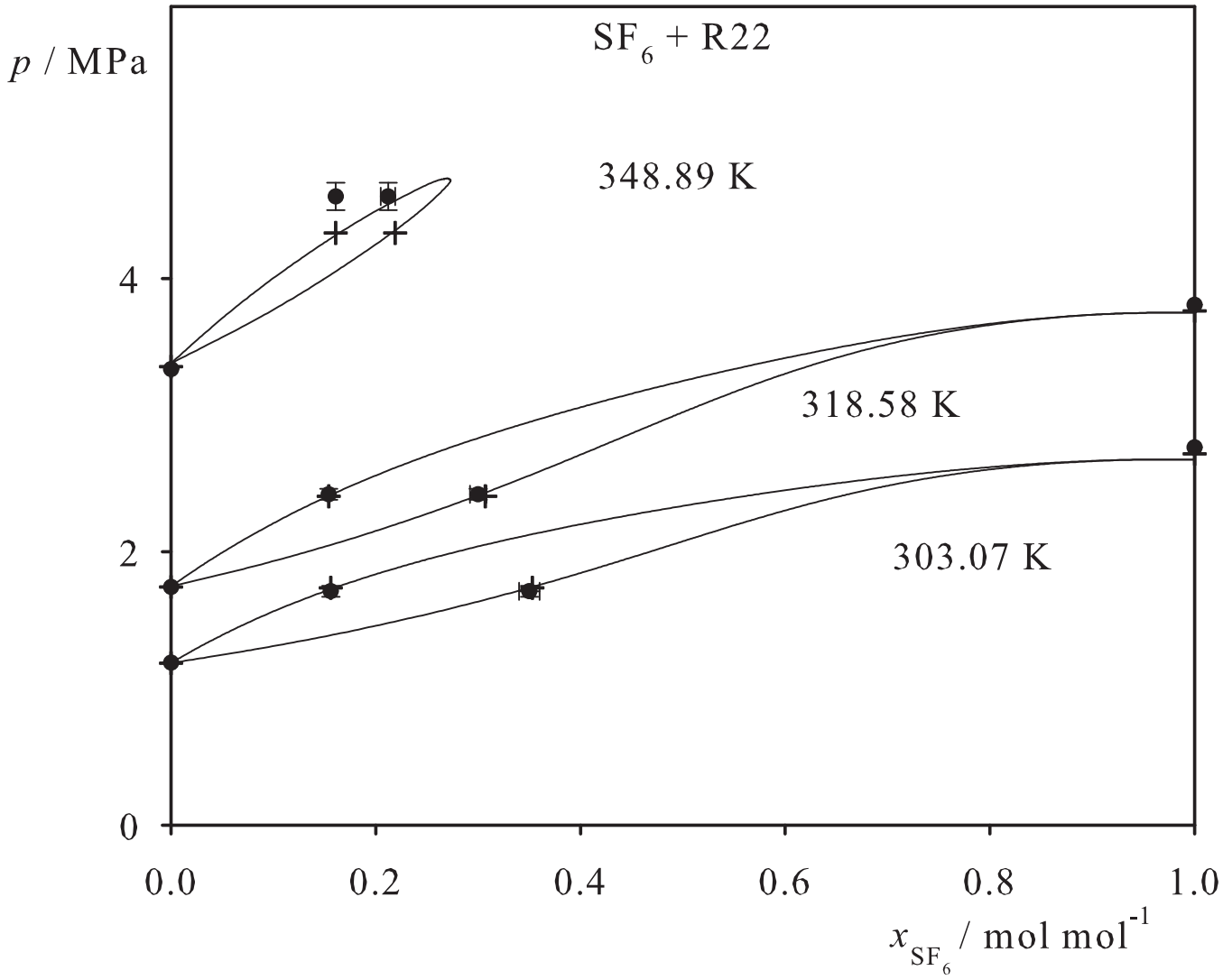

Fig. 117. Binary vapor-liquid equilibrium phase diagram: simulation data ●, experimental data + (cf. Table 2 of the manuscript for the reference) and Peng-Robinson equation of state —.

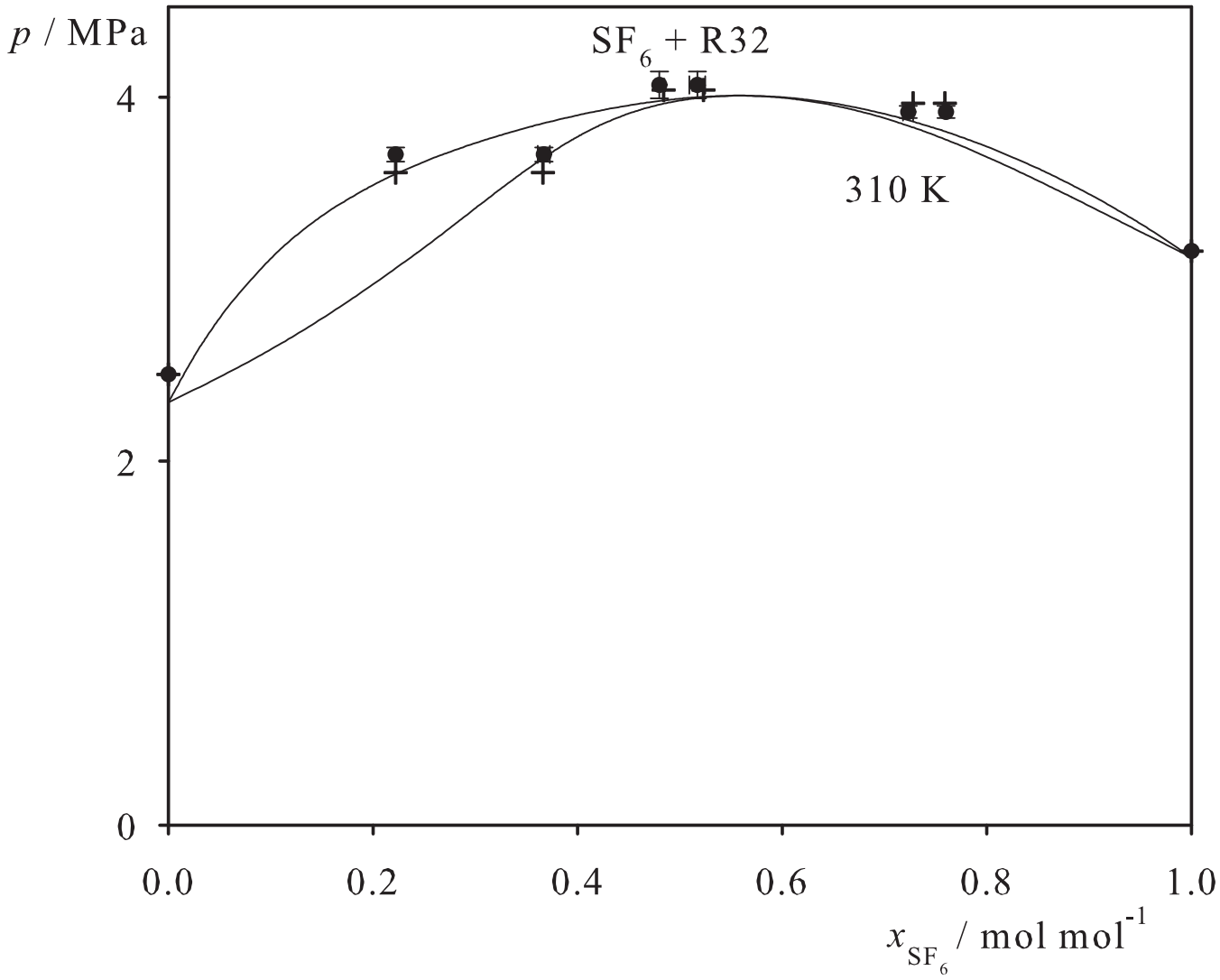

Fig. 118. Binary vapor-liquid equilibrium phase diagram: simulation data ●, experimental data + (cf. Table 2 of the manuscript for the reference) and Peng-Robinson equation of state —.

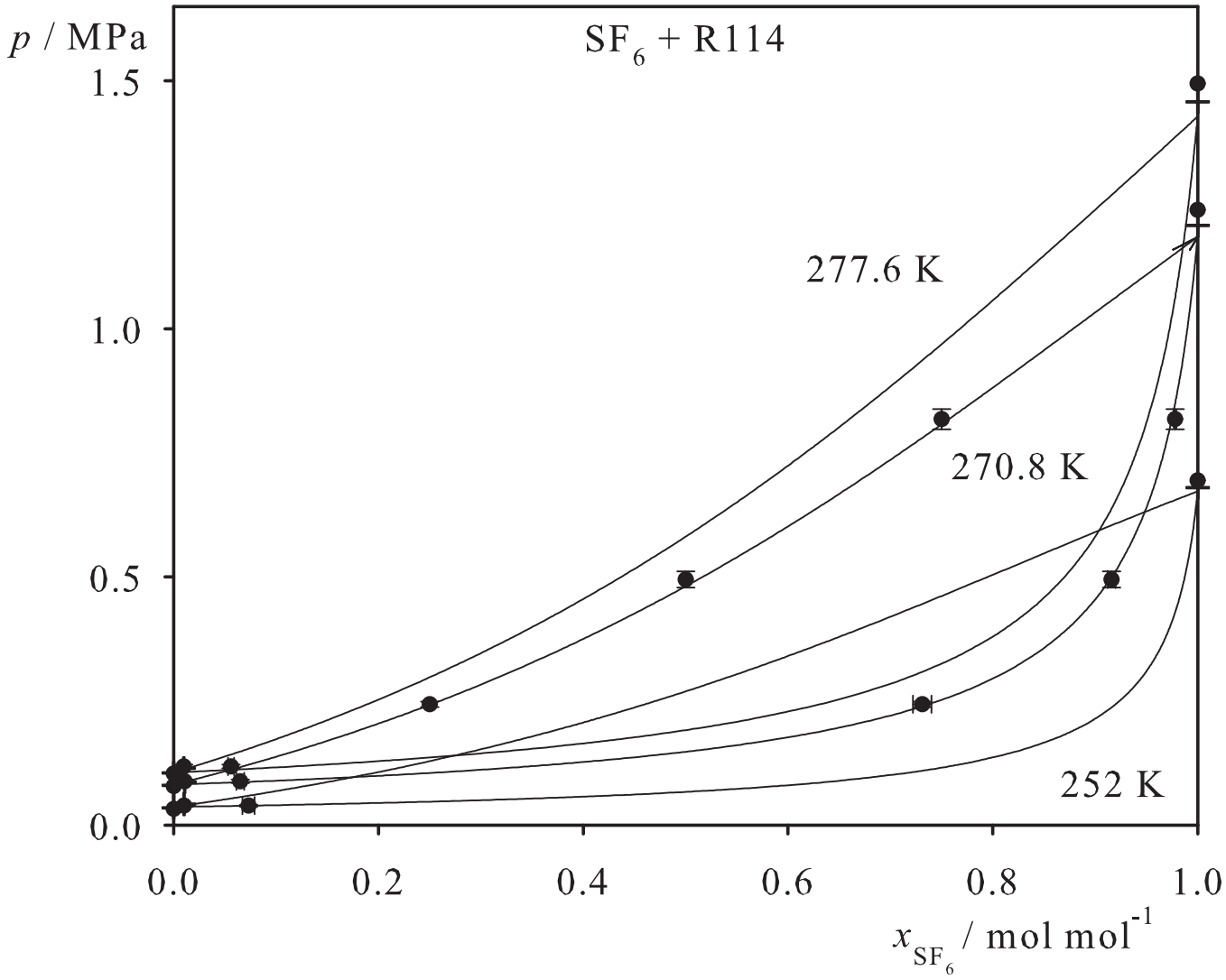

Fig. 119. Binary vapor-liquid equilibrium phase diagram: simulation data ●, experimental data + (cf. Table 2 of the manuscript for the reference) and Peng-Robinson equation of state —.

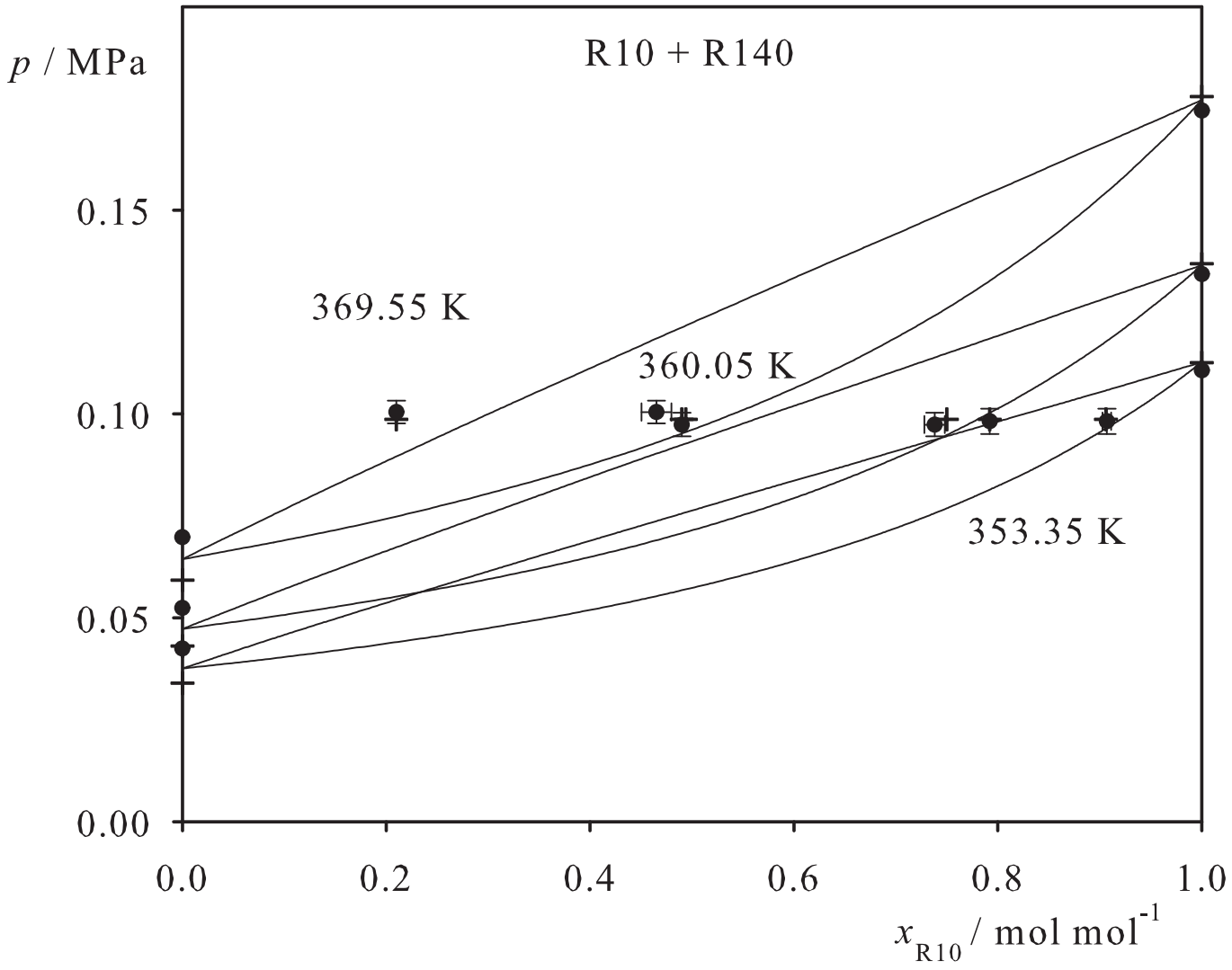

Fig. 120. Binary vapor-liquid equilibrium phase diagram: simulation data ●, experimental data + (cf. Table 2 of the manuscript for the reference) and Peng-Robinson equation of state —.

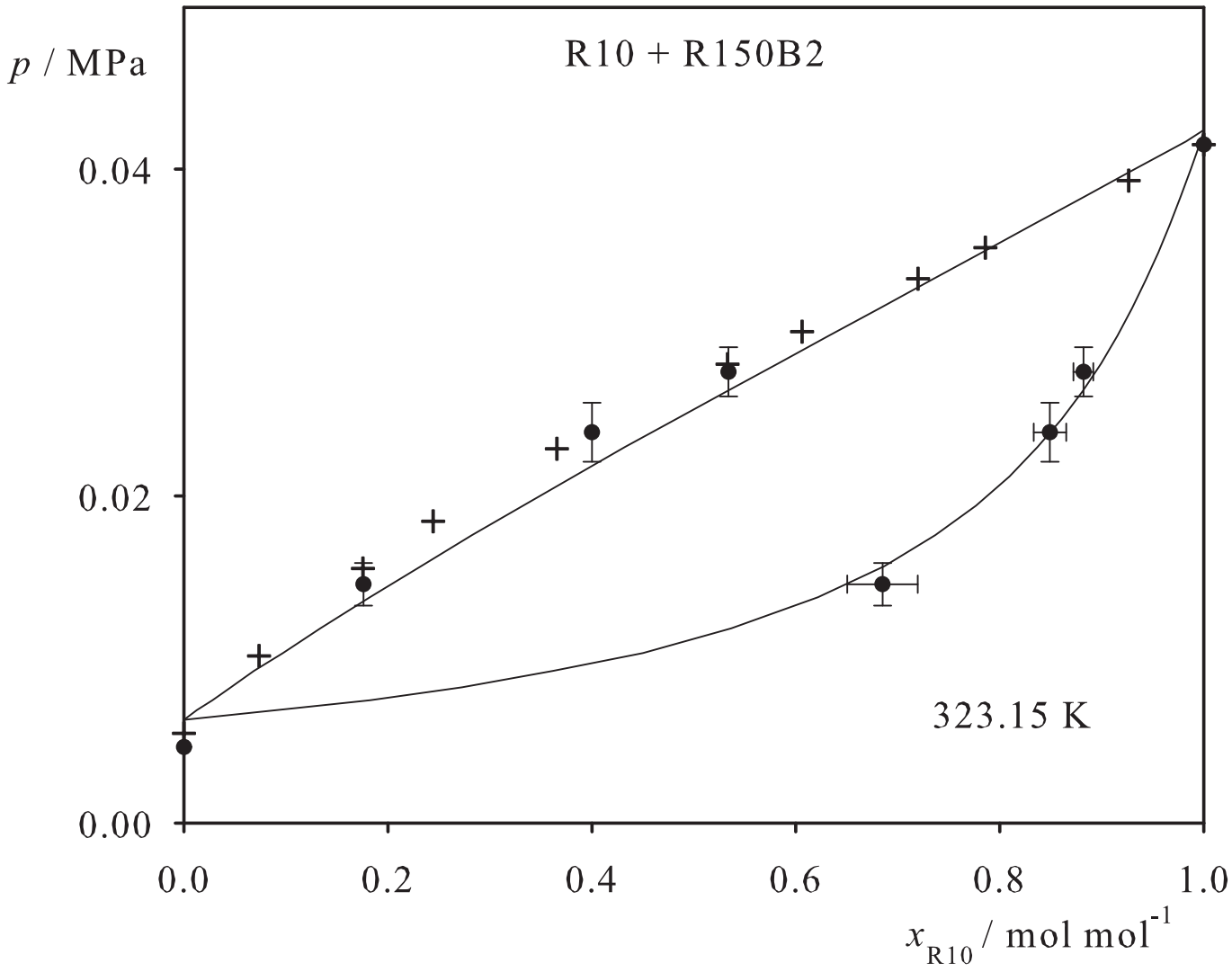

Fig. 121. Binary vapor-liquid equilibrium phase diagram: simulation data ●, experimental data + (cf. Table 2 of the manuscript for the reference) and Peng-Robinson equation of state —.

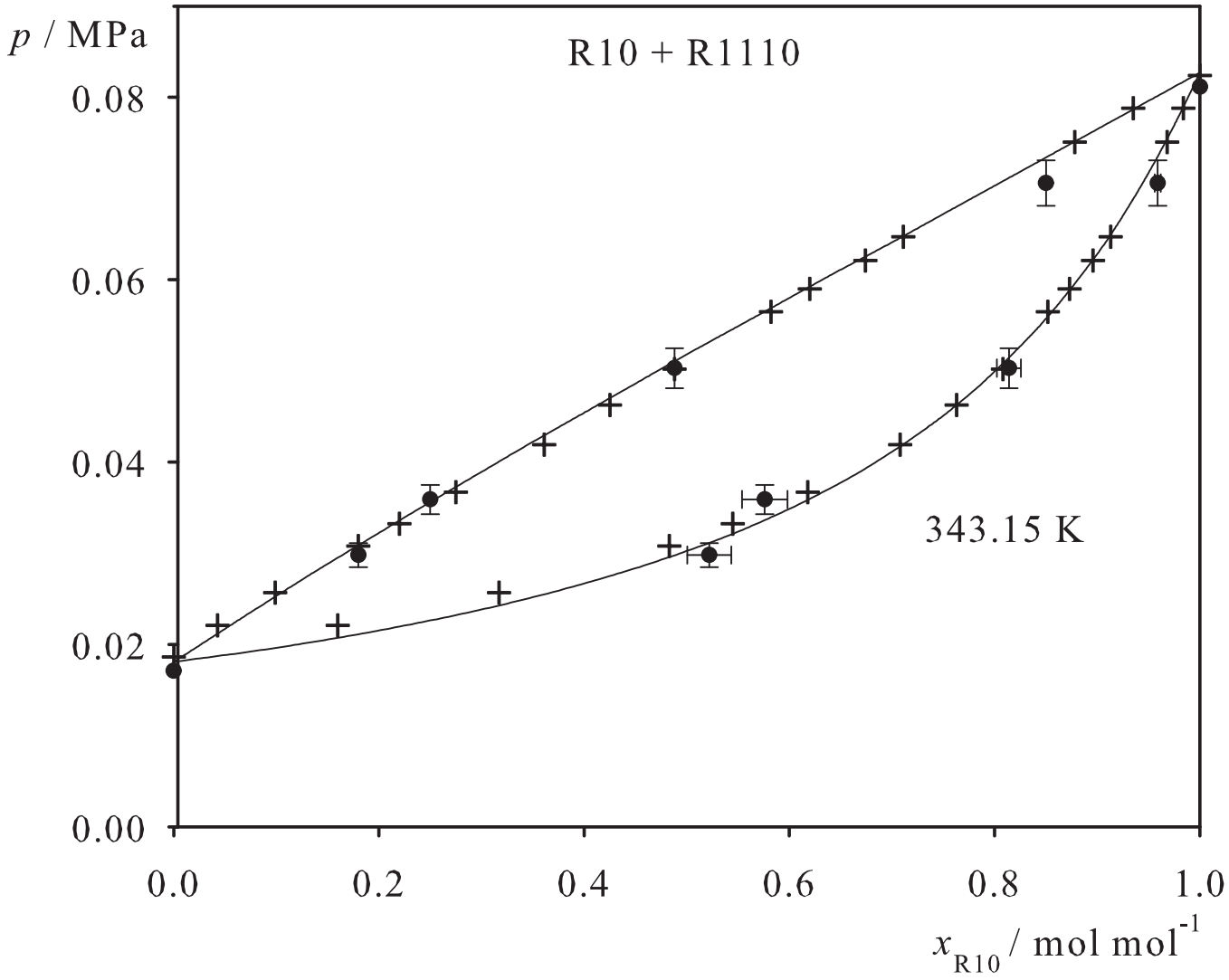

Fig. 122. Binary vapor-liquid equilibrium phase diagram: simulation data ●, experimental data + (cf. Table 2 of the manuscript for the reference) and Peng-Robinson equation of state —.

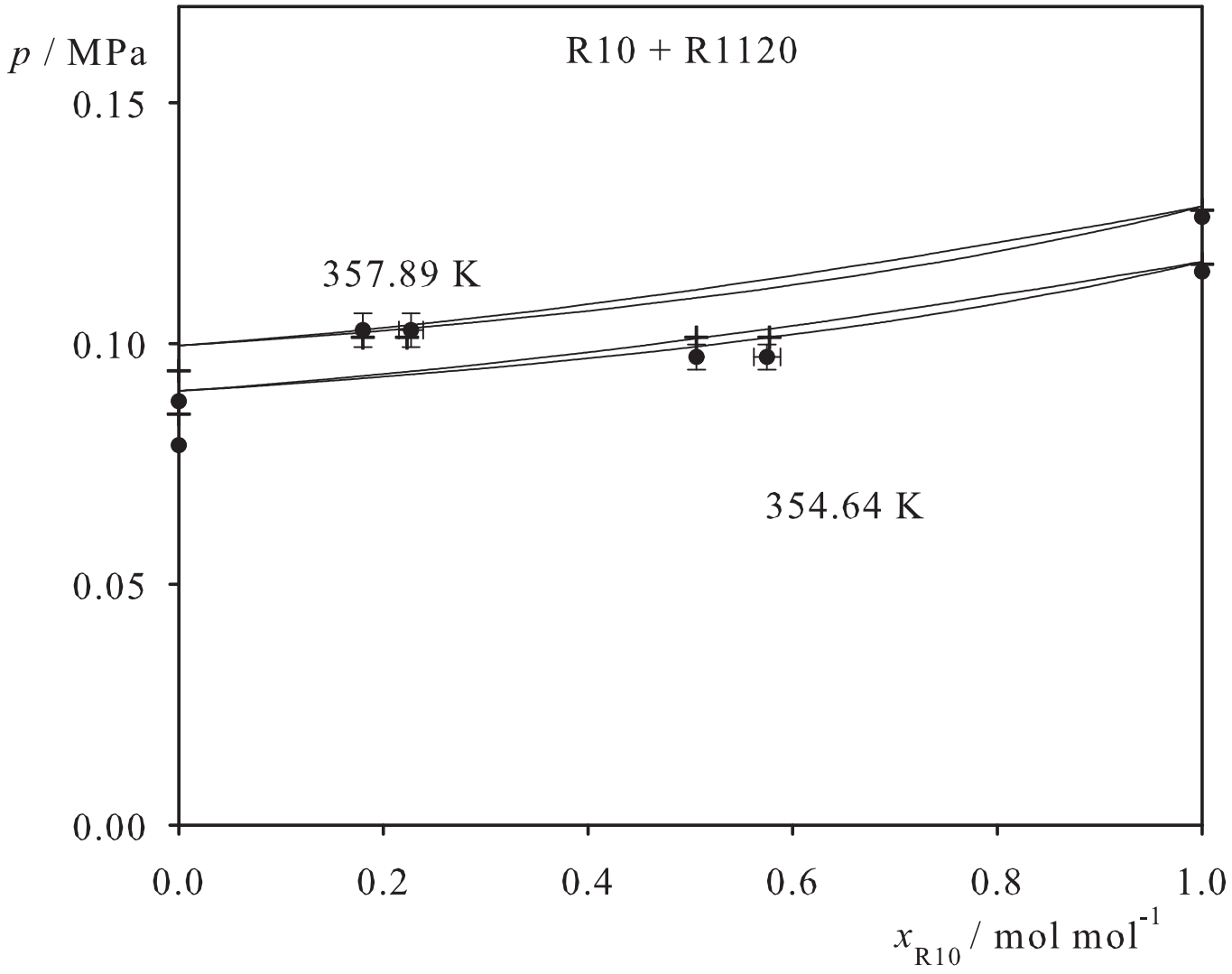

Fig. 123. Binary vapor-liquid equilibrium phase diagram: simulation data ●, experimental data + (cf. Table 2 of the manuscript for the reference) and Peng-Robinson equation of state —.

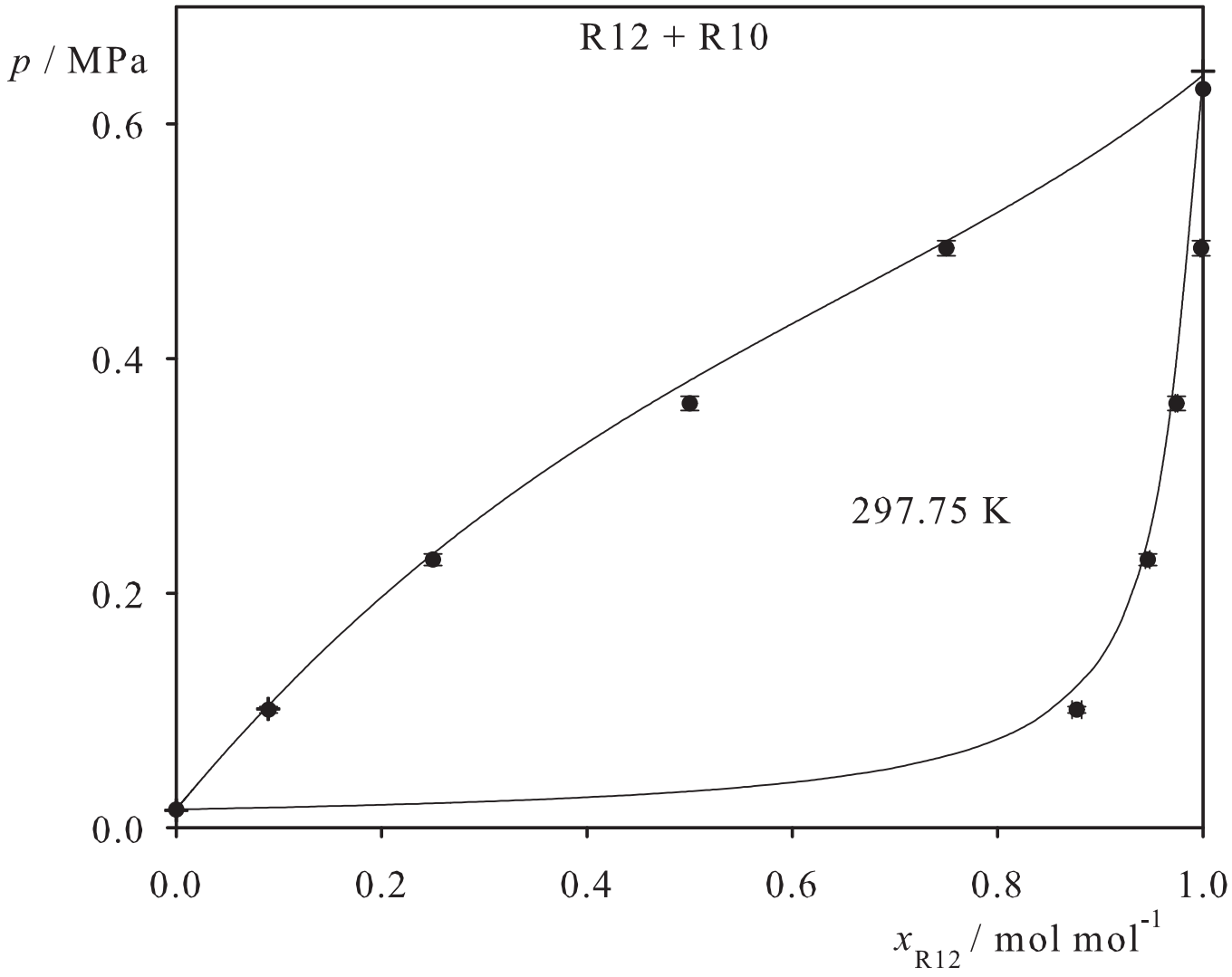

Fig. 124. Binary vapor-liquid equilibrium phase diagram: simulation data ●, experimental data + (cf. Table 2 of the manuscript for the reference) and Peng-Robinson equation of state —.

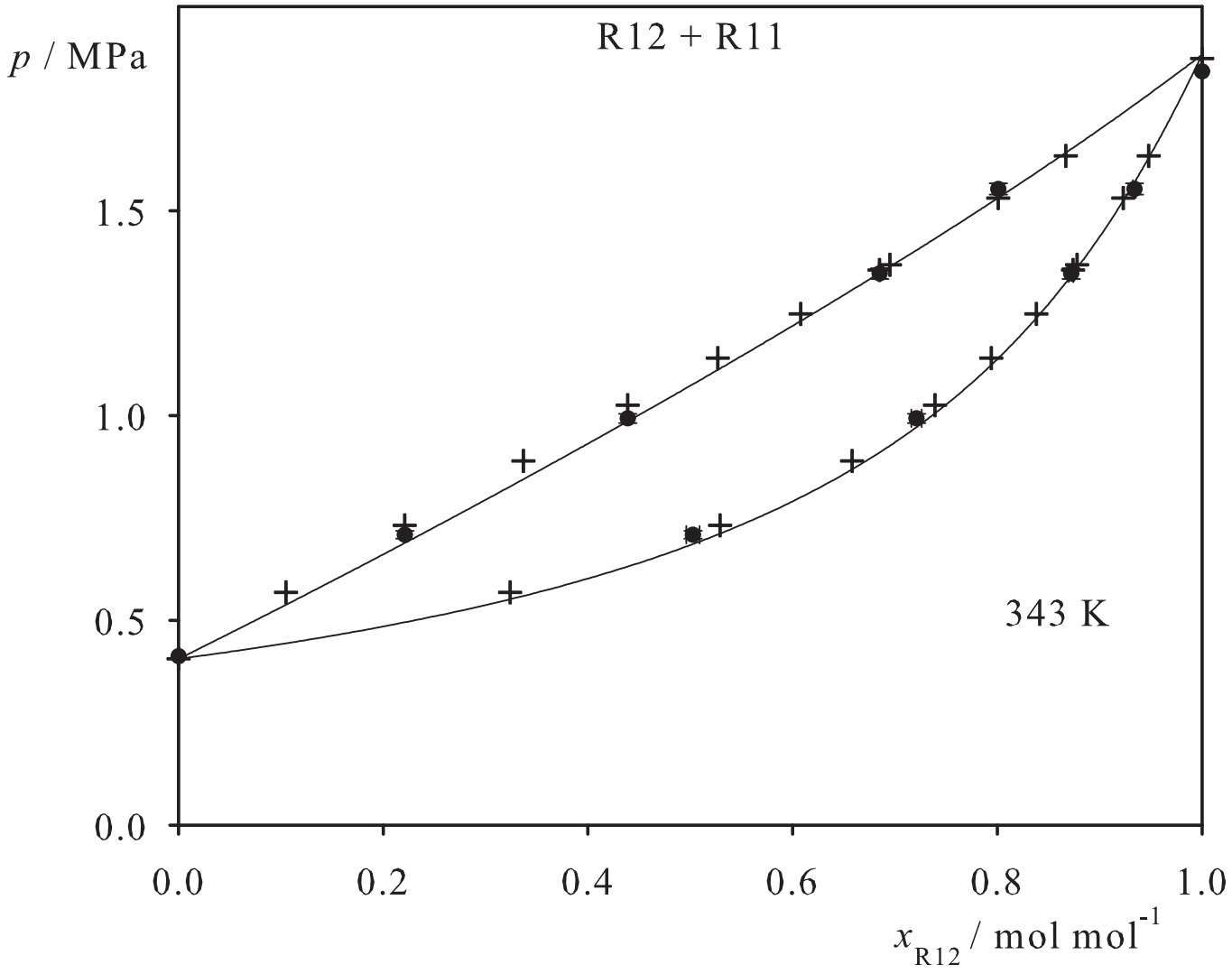

Fig. 125. Binary vapor-liquid equilibrium phase diagram: simulation data ●, experimental data + (cf. Table 2 of the manuscript for the reference) and Peng-Robinson equation of state —.

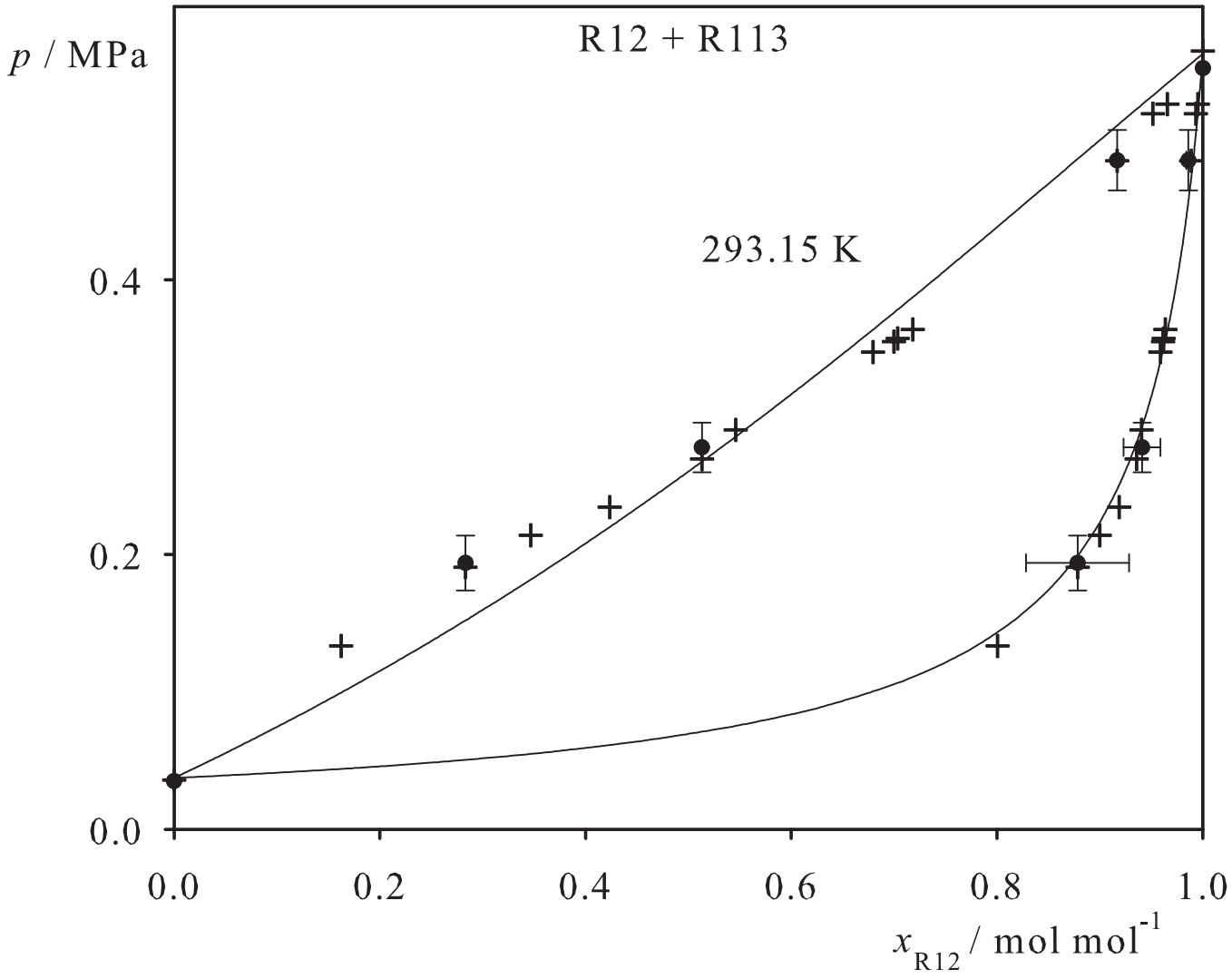

Fig. 126. Binary vapor-liquid equilibrium phase diagram: simulation data ●, experimental data + (cf. Table 2 of the manuscript for the reference) and Peng-Robinson equation of state —.

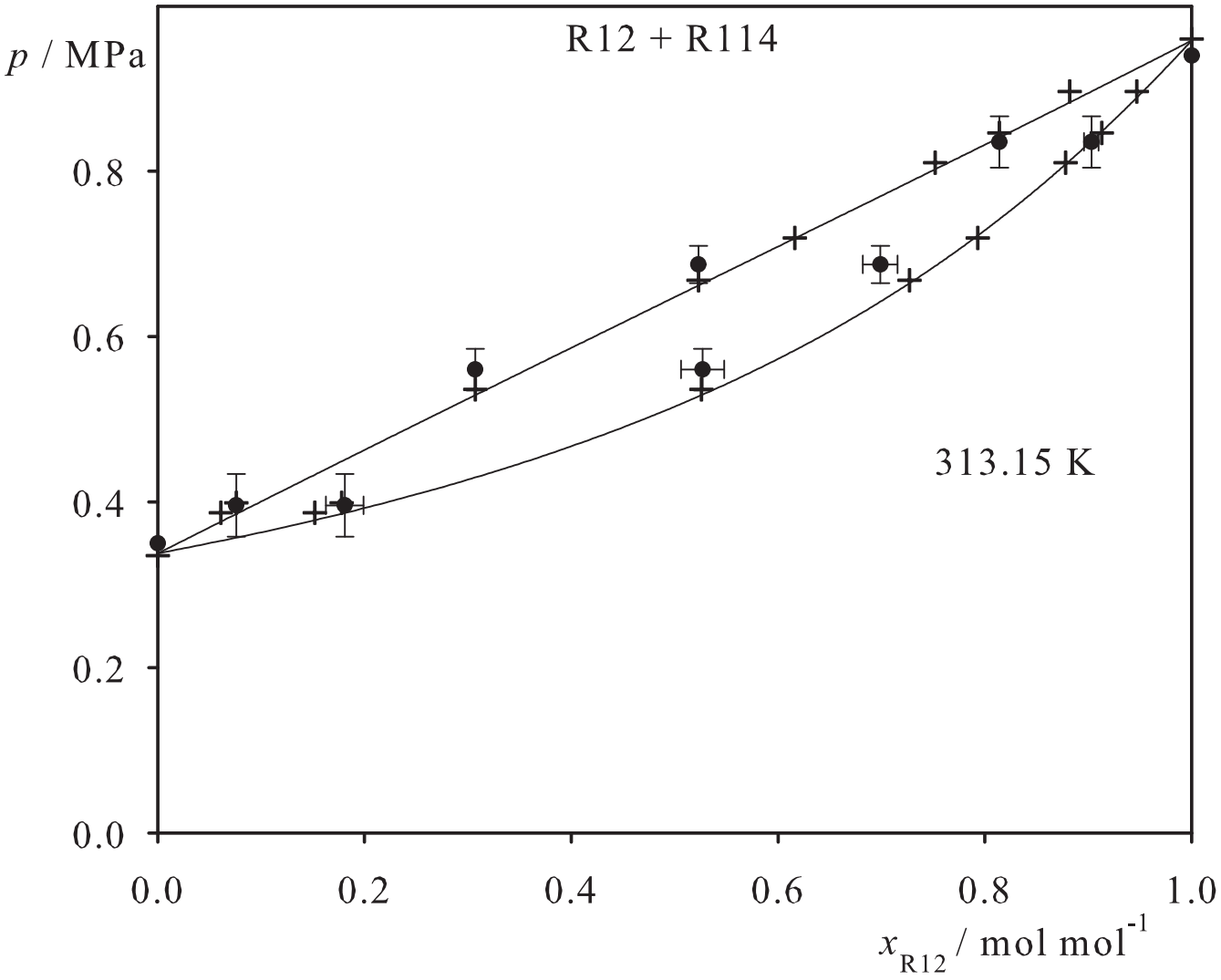

Fig. 127. Binary vapor-liquid equilibrium phase diagram: simulation data ●, experimental data + (cf. Table 2 of the manuscript for the reference) and Peng-Robinson equation of state —.

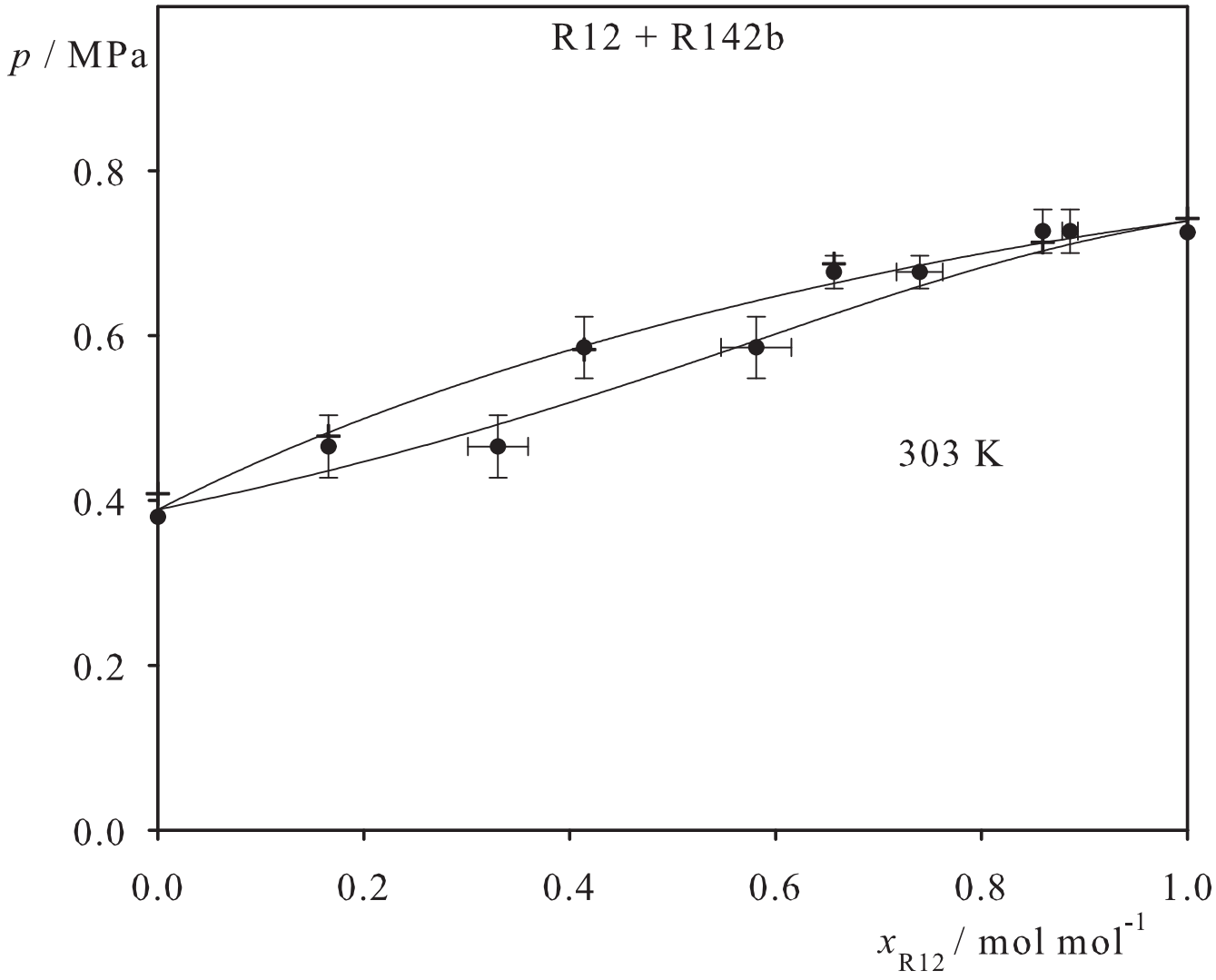

Fig. 128. Binary vapor-liquid equilibrium phase diagram: simulation data ●, experimental data + (cf. Table 2 of the manuscript for the reference) and Peng-Robinson equation of state —.

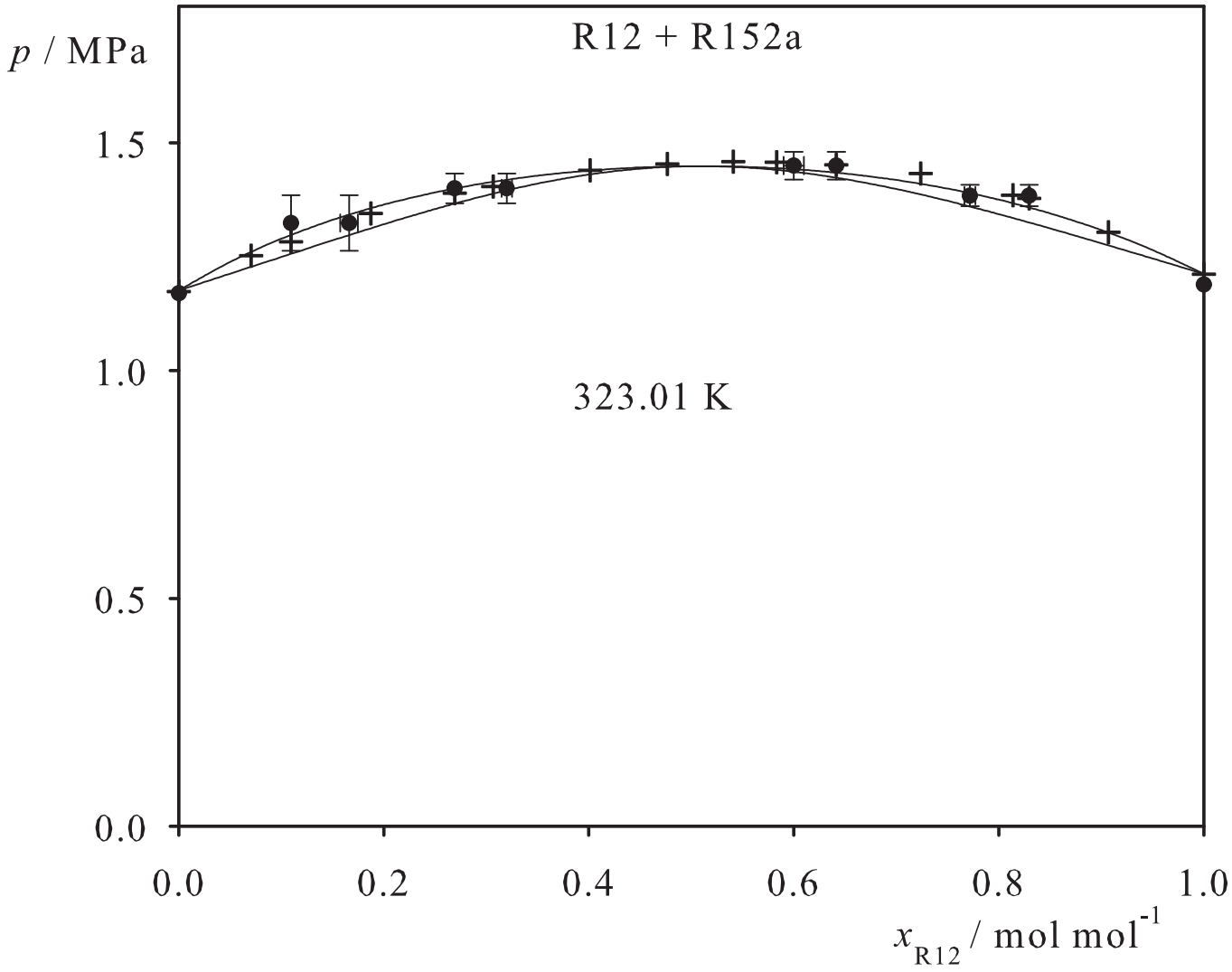

Fig. 129. Binary vapor-liquid equilibrium phase diagram: simulation data ●, experimental data + (cf. Table 2 of the manuscript for the reference) and Peng-Robinson equation of state —.

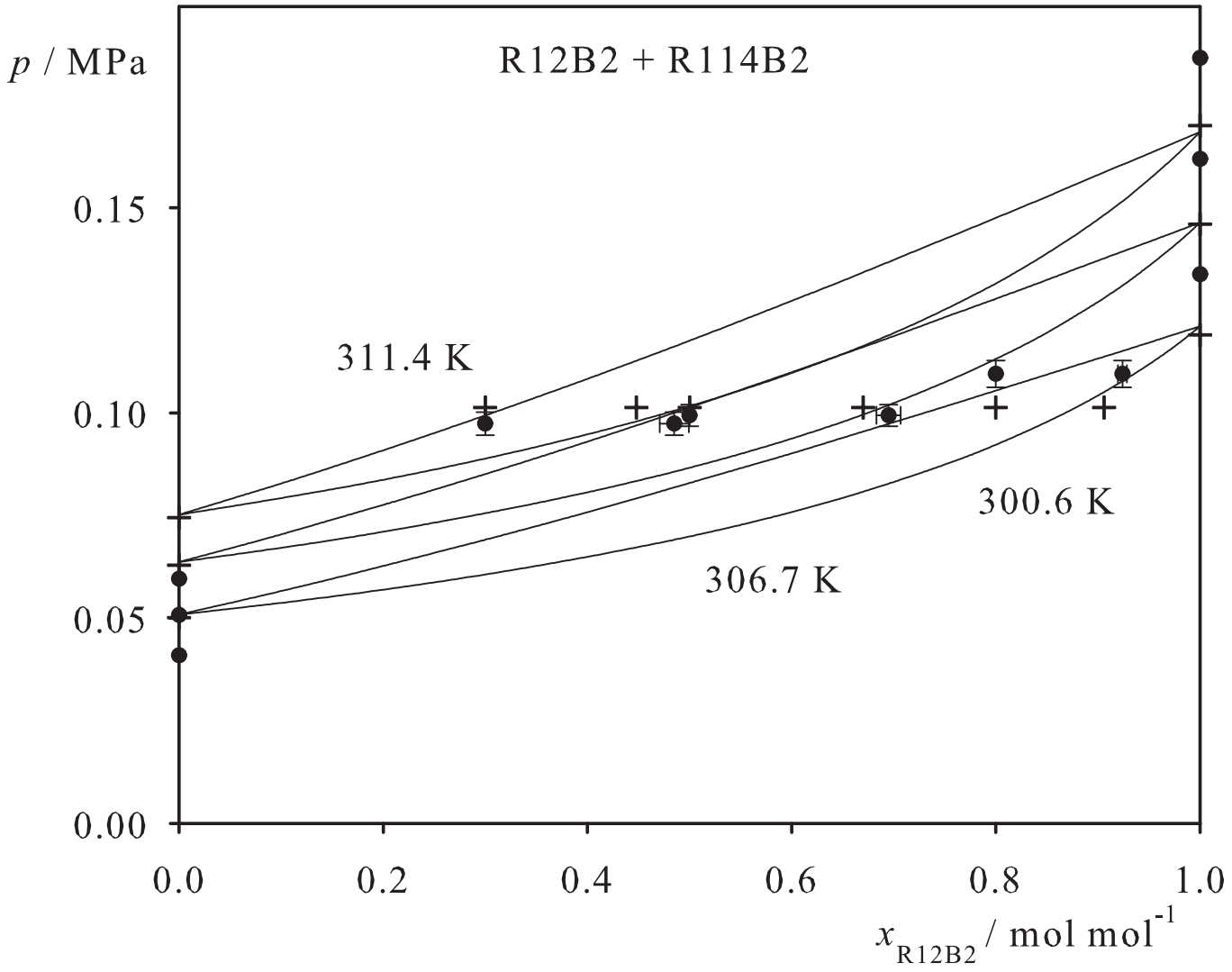

Fig. 130. Binary vapor-liquid equilibrium phase diagram: simulation data ●, experimental data + (cf. Table 2 of the manuscript for the reference) and Peng-Robinson equation of state —.

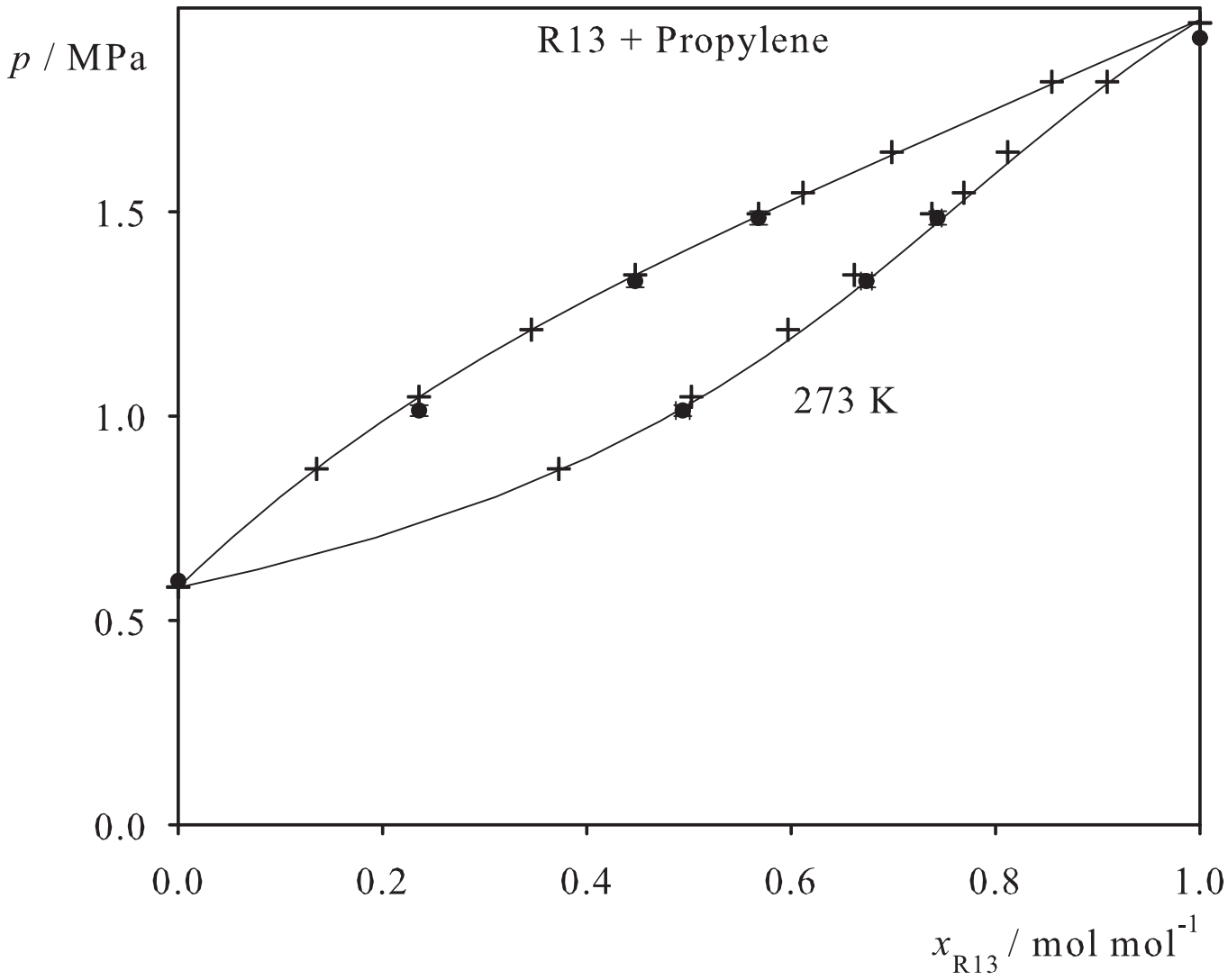

Fig. 131. Binary vapor-liquid equilibrium phase diagram: simulation data ●, experimental data + (cf. Table 2 of the manuscript for the reference) and Peng-Robinson equation of state —.

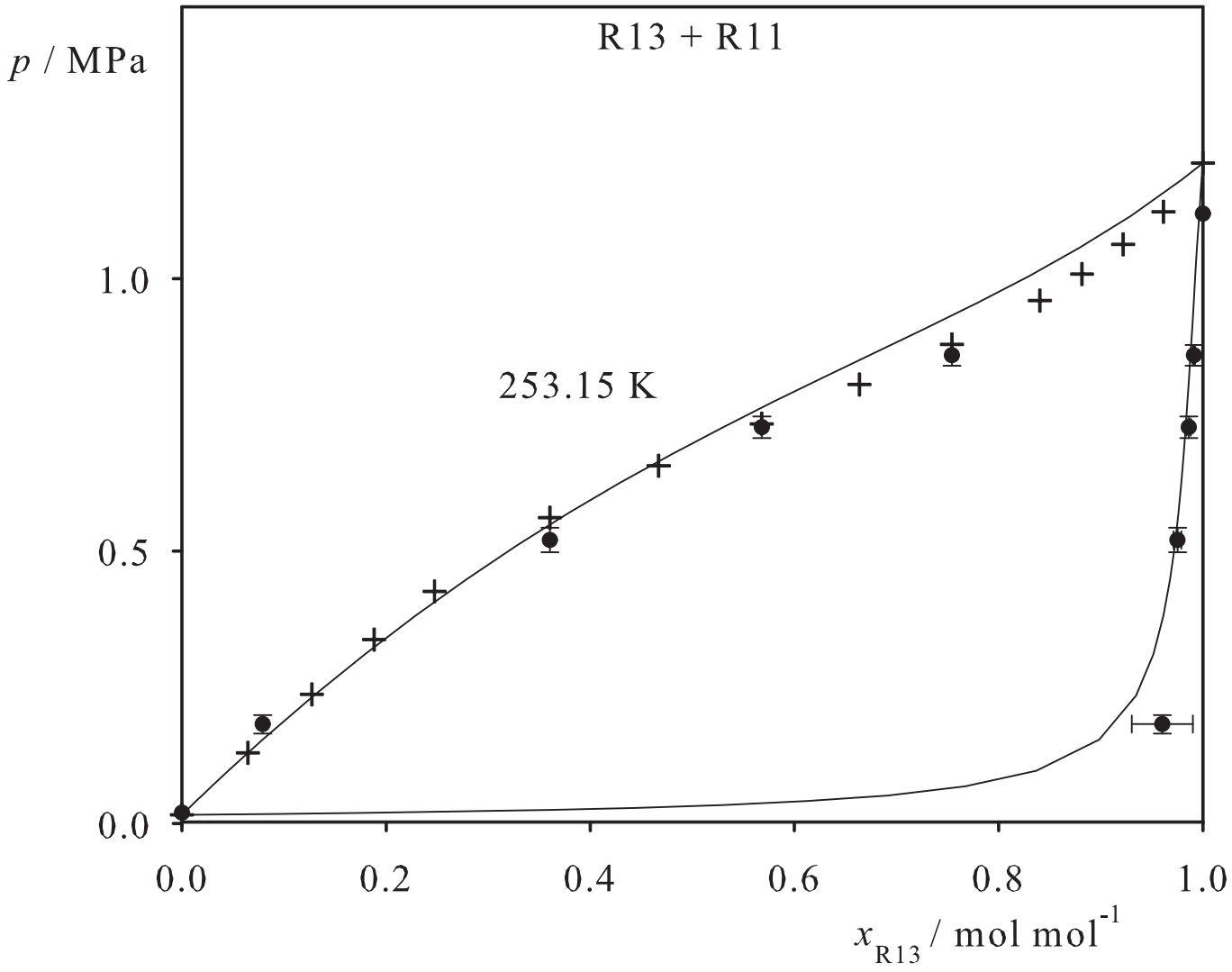

Fig. 132. Binary vapor-liquid equilibrium phase diagram: simulation data ●, experimental data + (cf. Table 2 of the manuscript for the reference) and Peng-Robinson equation of state —.

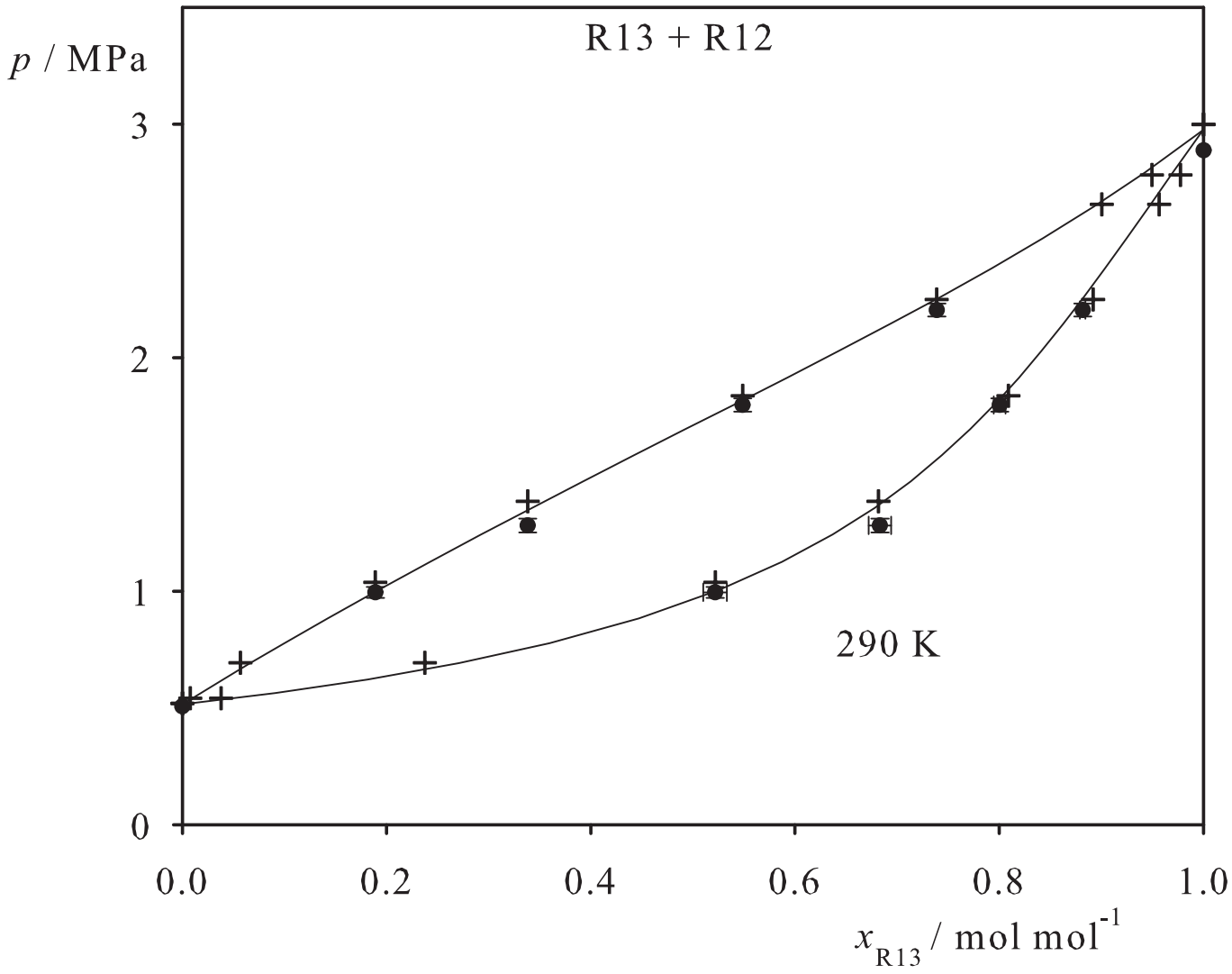

Fig. 133. Binary vapor-liquid equilibrium phase diagram: simulation data ●, experimental data + (cf. Table 2 of the manuscript for the reference) and Peng-Robinson equation of state —.

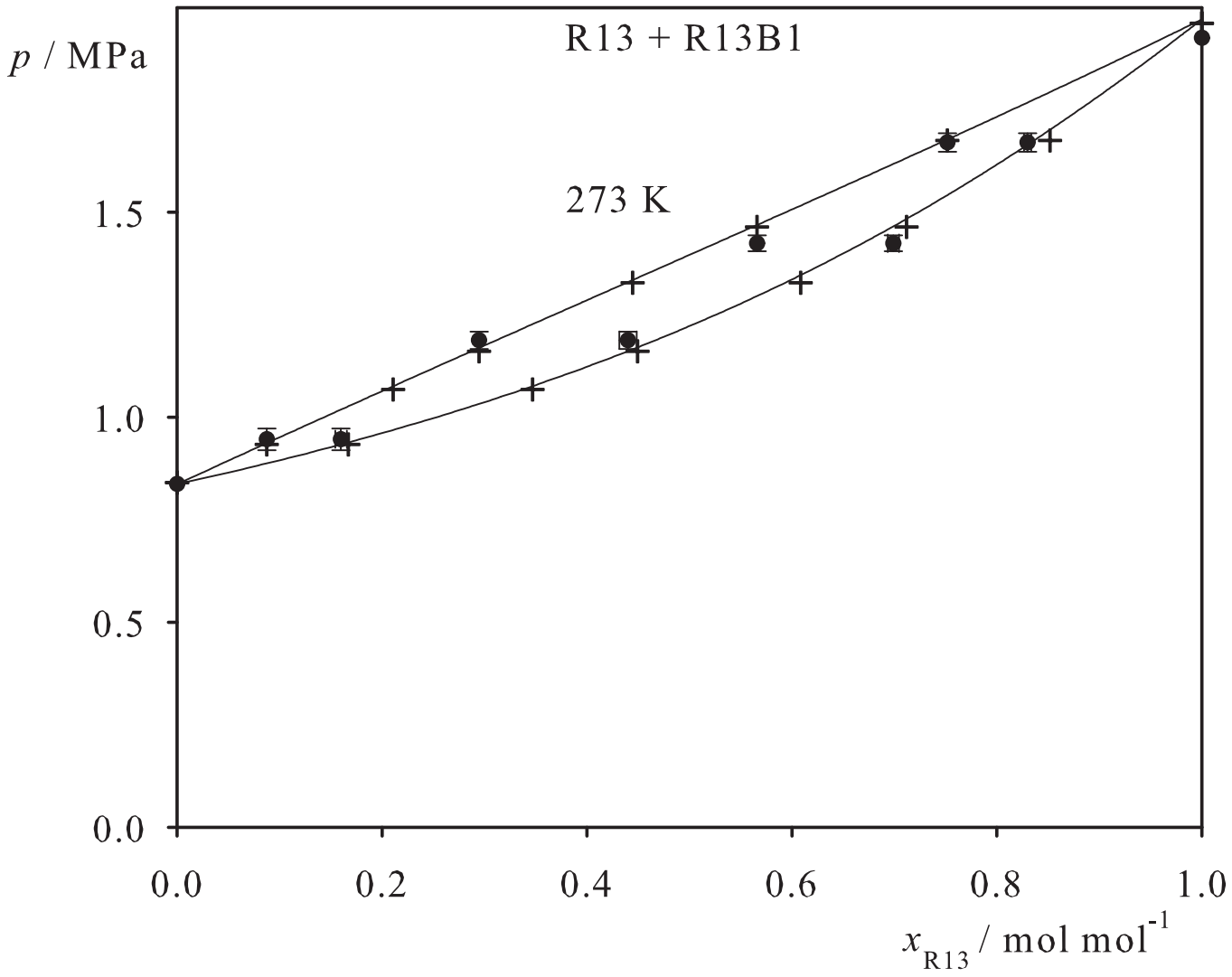

Fig. 134. Binary vapor-liquid equilibrium phase diagram: simulation data ●, experimental data + (cf. Table 2 of the manuscript for the reference) and Peng-Robinson equation of state —.

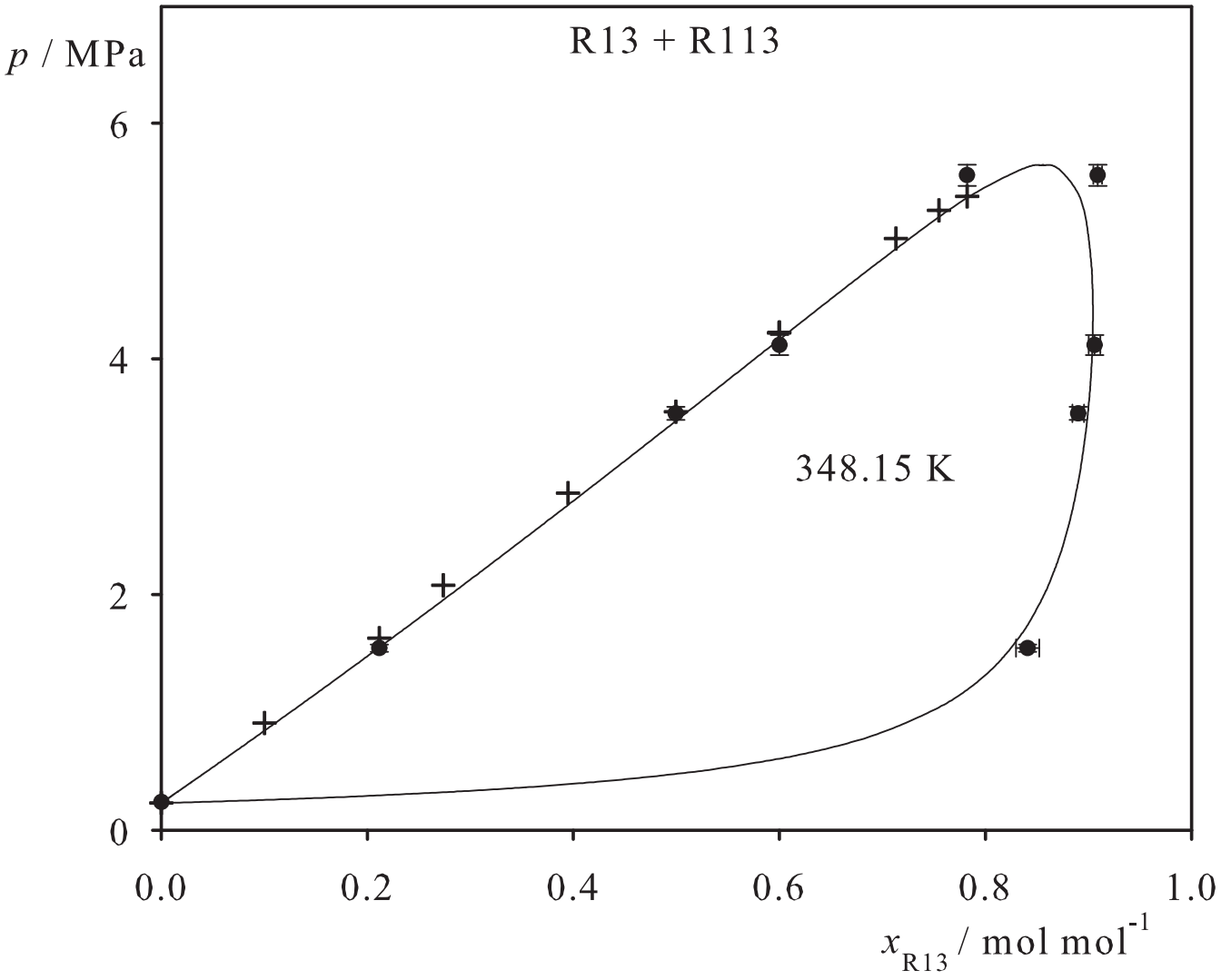

Fig. 135. Binary vapor-liquid equilibrium phase diagram: simulation data ●, experimental data + (cf. Table 2 of the manuscript for the reference) and Peng-Robinson equation of state —.

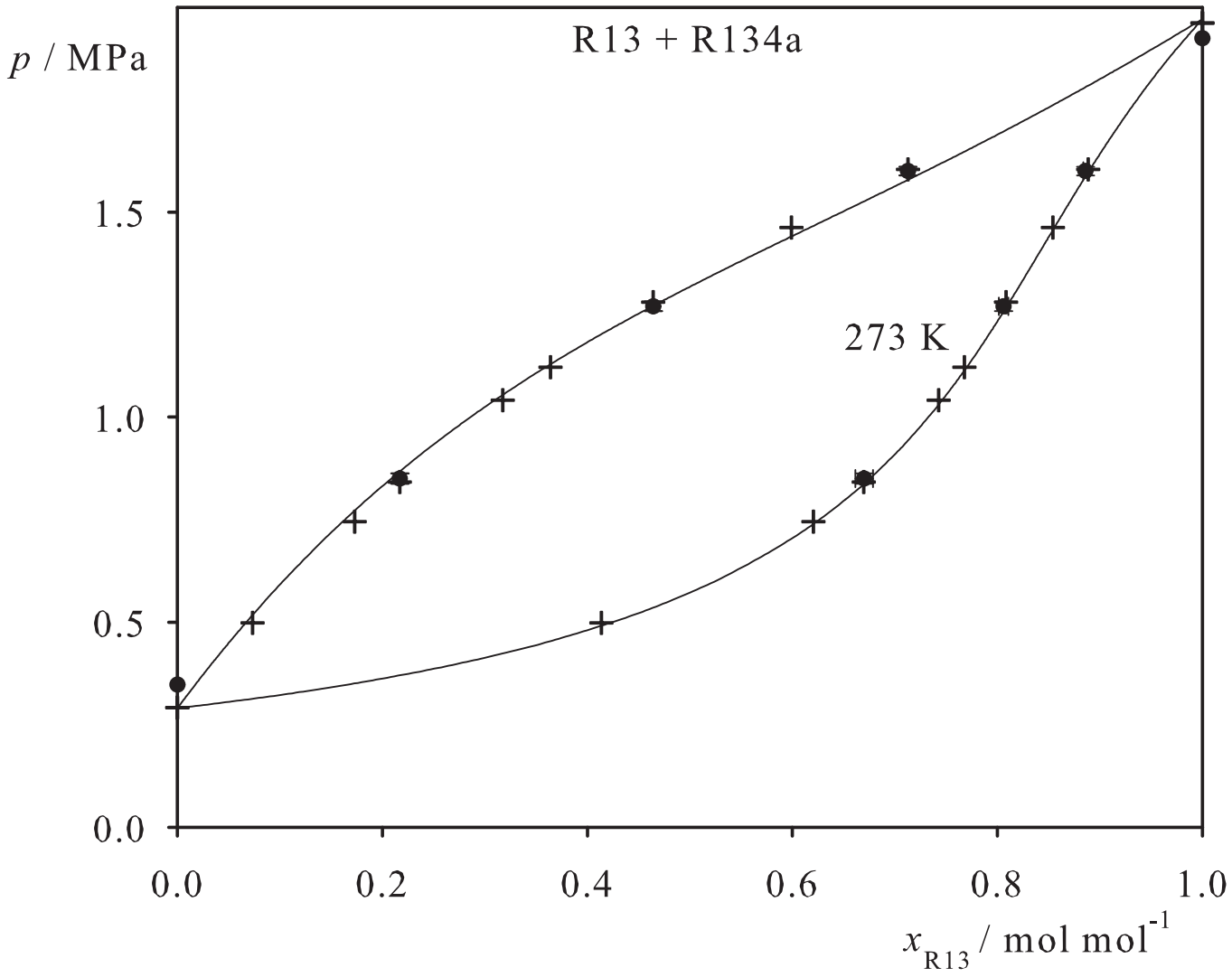

Fig. 136. Binary vapor-liquid equilibrium phase diagram: simulation data ●, experimental data + (cf. Table 2 of the manuscript for the reference) and Peng-Robinson equation of state —.

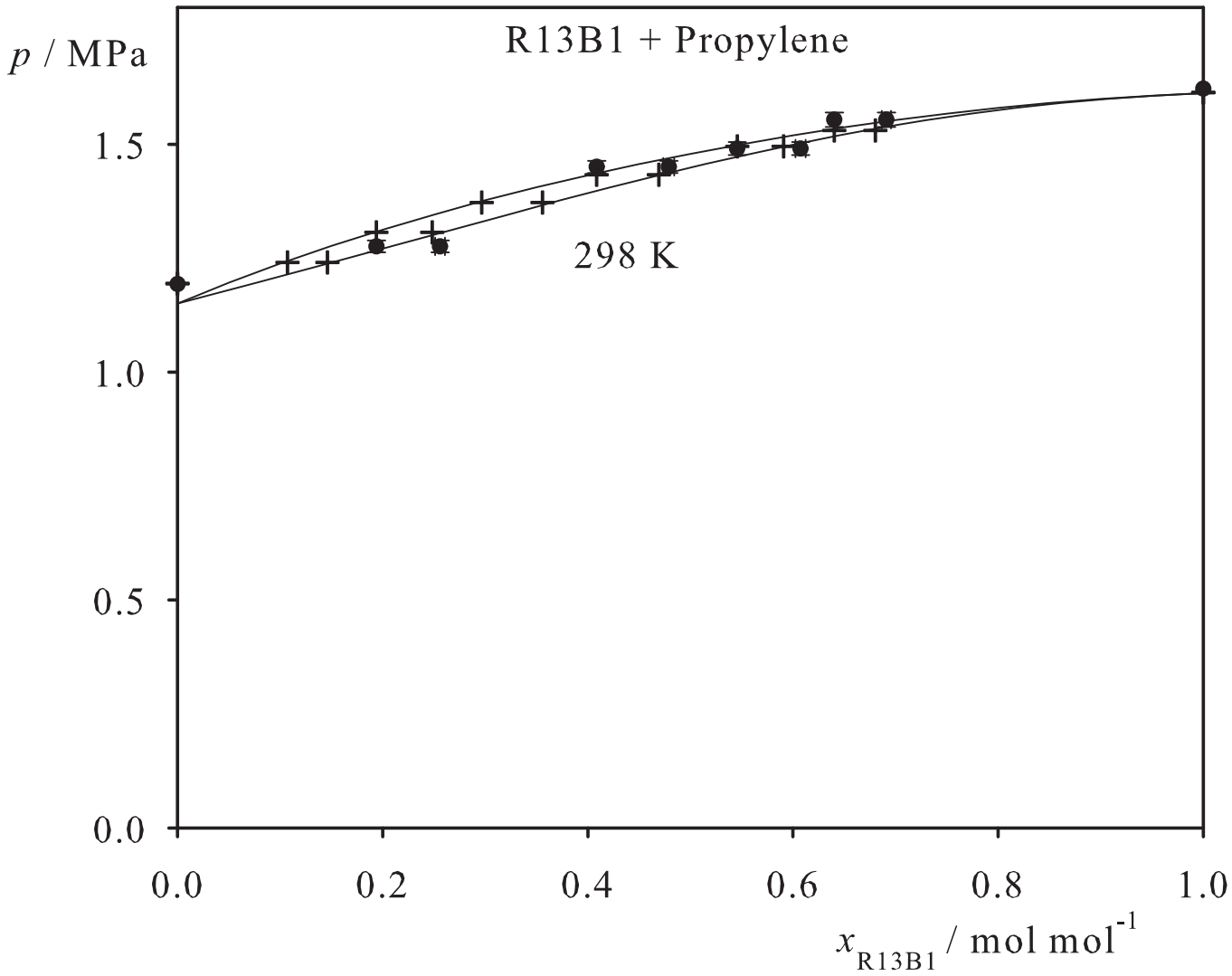

Fig. 137. Binary vapor-liquid equilibrium phase diagram: simulation data ●, experimental data + (cf. Table 2 of the manuscript for the reference) and Peng-Robinson equation of state —.

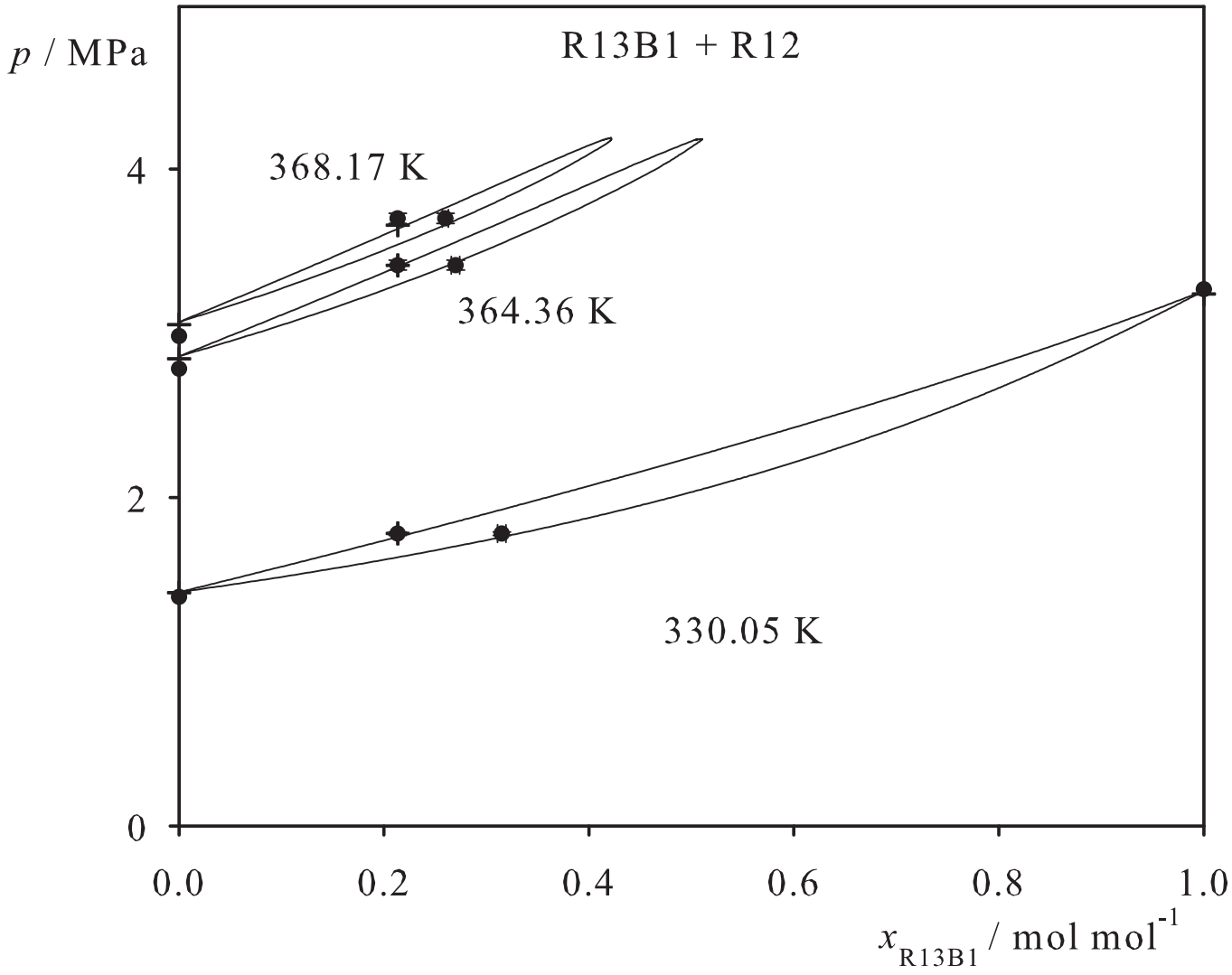

Fig. 138. Binary vapor-liquid equilibrium phase diagram: simulation data ●, experimental data + (cf. Table 2 of the manuscript for the reference) and Peng-Robinson equation of state —.

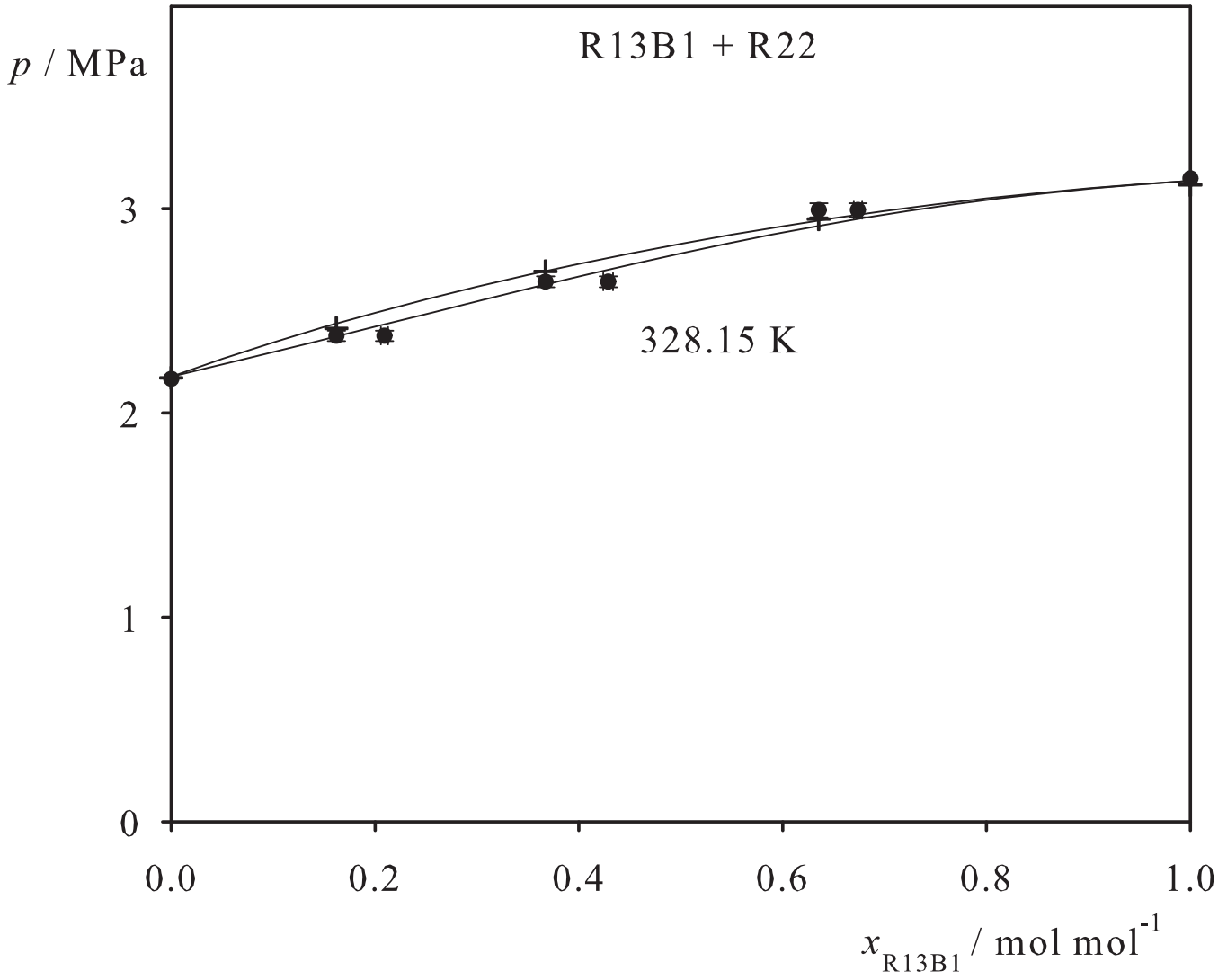

Fig. 139. Binary vapor-liquid equilibrium phase diagram: simulation data ●, experimental data + (cf. Table 2 of the manuscript for the reference) and Peng-Robinson equation of state —.

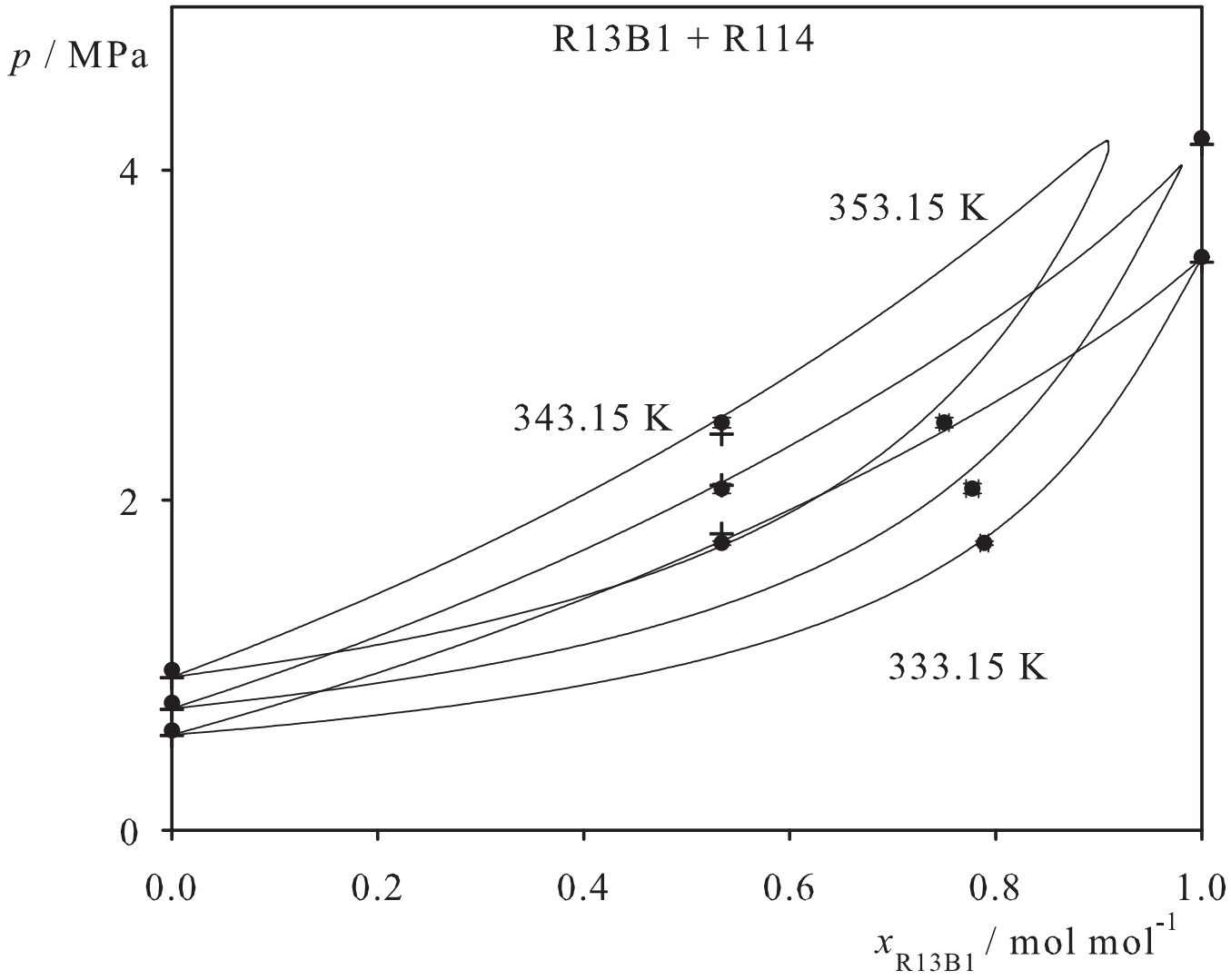

Fig. 140. Binary vapor-liquid equilibrium phase diagram: simulation data ●, experimental data + (cf. Table 2 of the manuscript for the reference) and Peng-Robinson equation of state —.

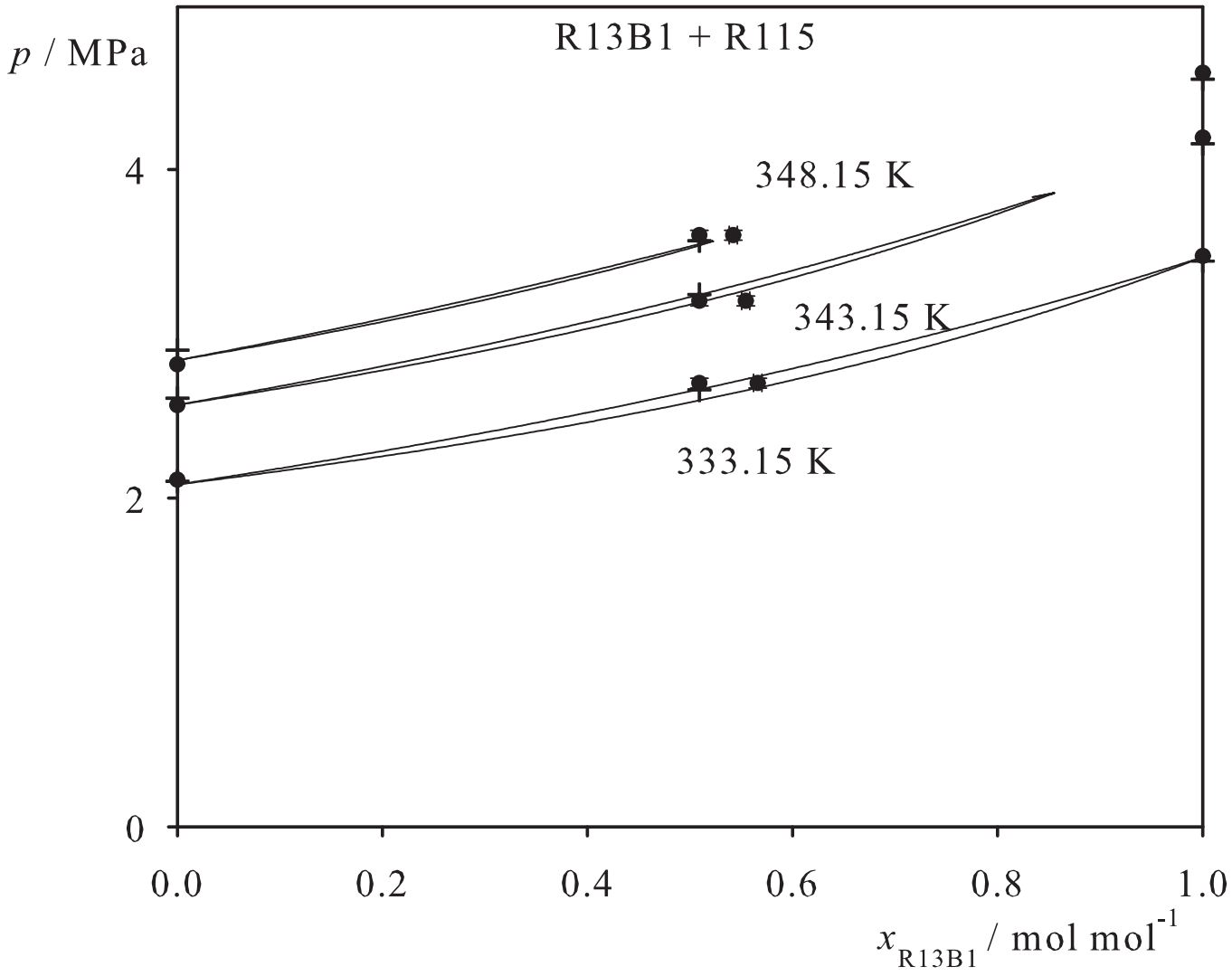

Fig. 141. Binary vapor-liquid equilibrium phase diagram: simulation data ●, experimental data + (cf. Table 2 of the manuscript for the reference) and Peng-Robinson equation of state —.

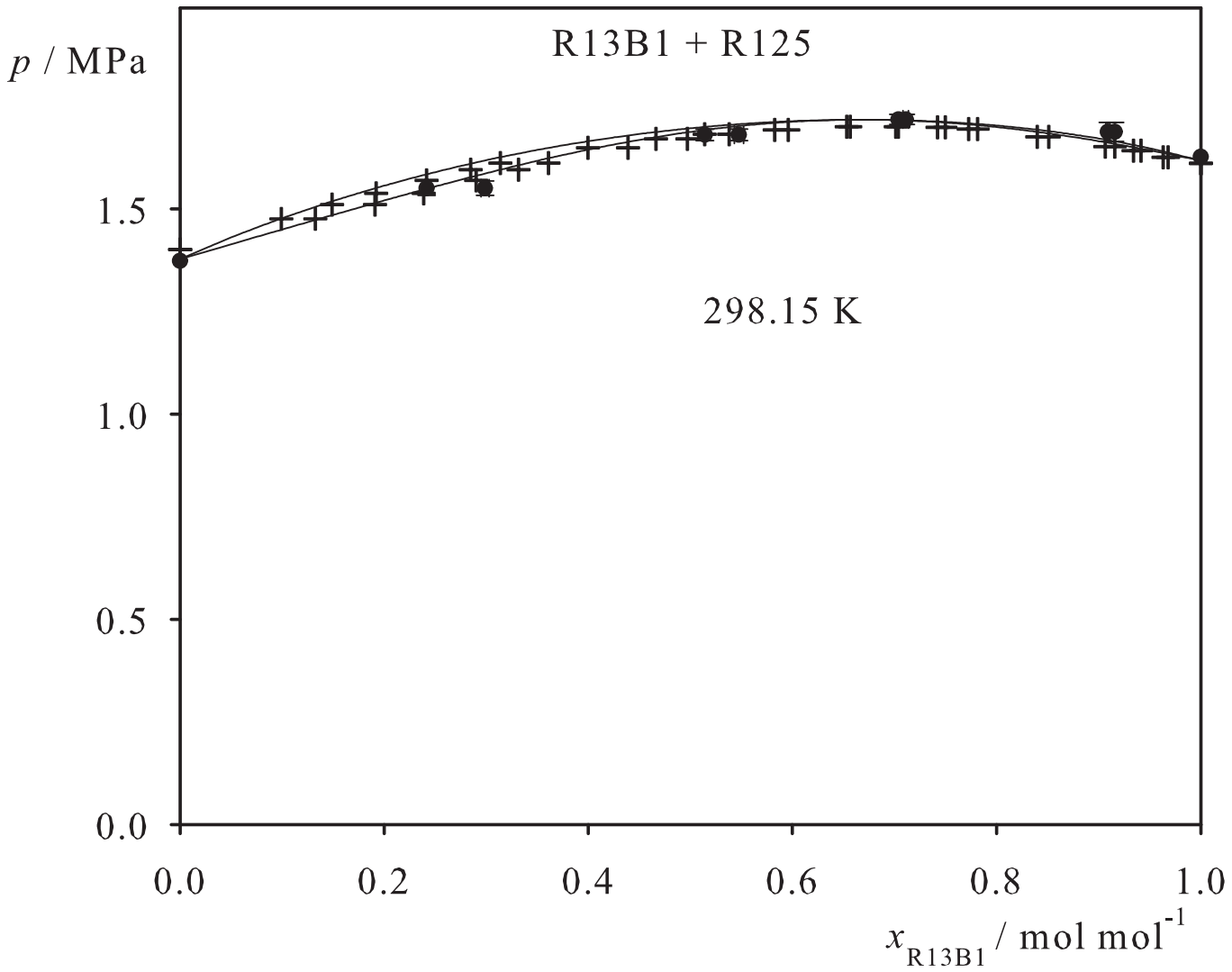

Fig. 142. Binary vapor-liquid equilibrium phase diagram: simulation data ●, experimental data + (cf. Table 2 of the manuscript for the reference) and Peng-Robinson equation of state —.

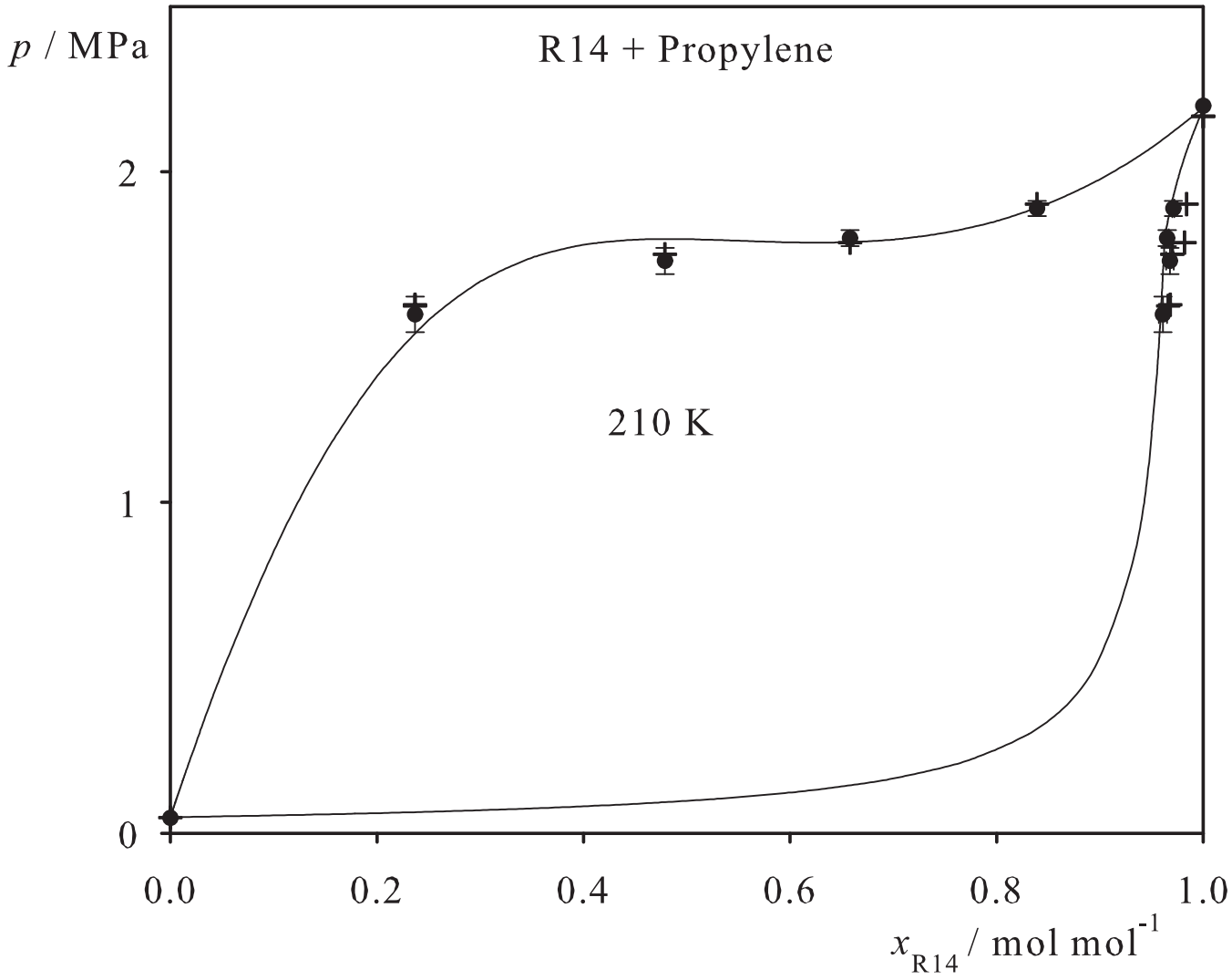

Fig. 143. Binary vapor-liquid equilibrium phase diagram: simulation data ●, experimental data + (cf. Table 2 of the manuscript for the reference) and Peng-Robinson equation of state —.

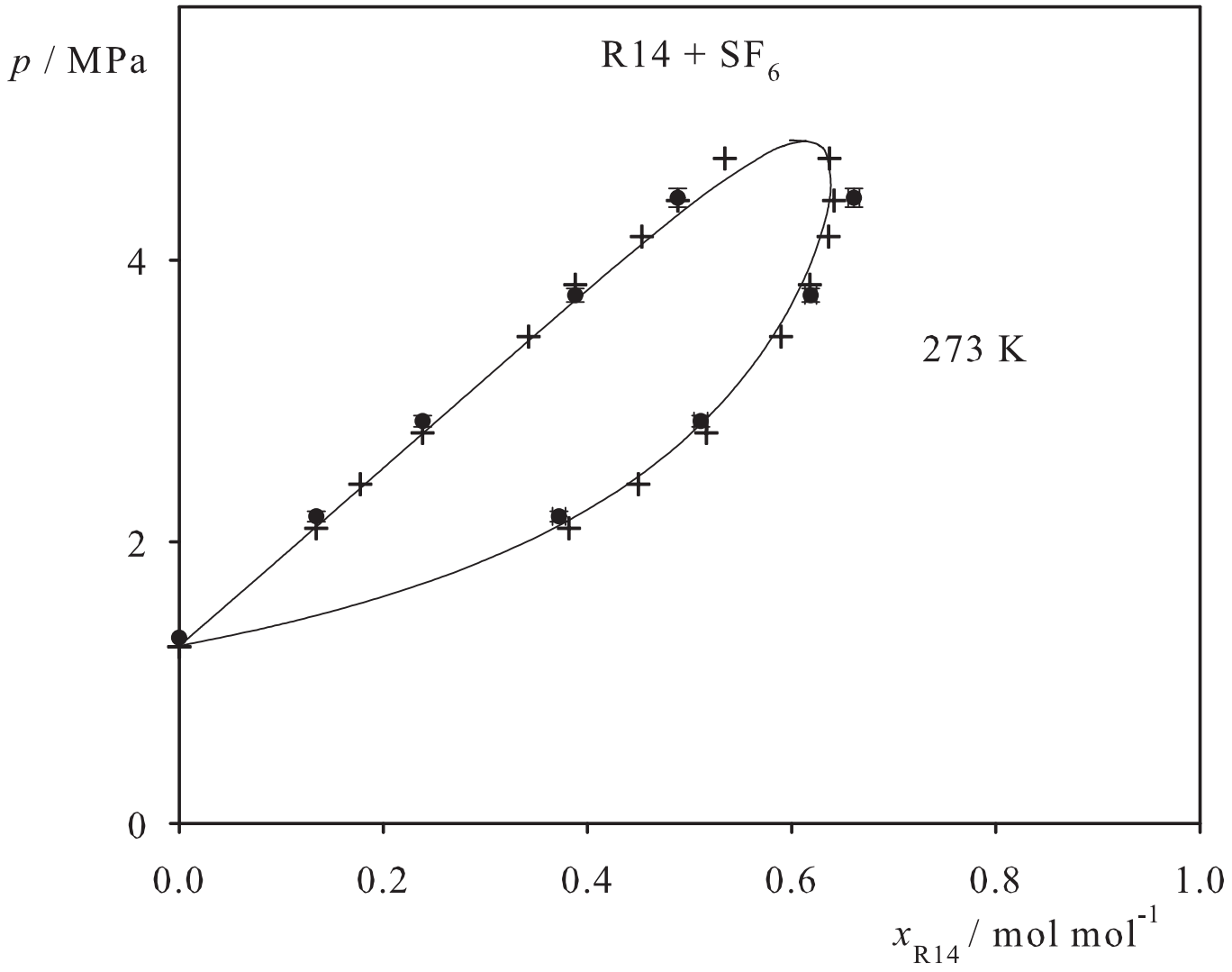

Fig. 144. Binary vapor-liquid equilibrium phase diagram: simulation data ●, experimental data + (cf. Table 2 of the manuscript for the reference) and Peng-Robinson equation of state —.

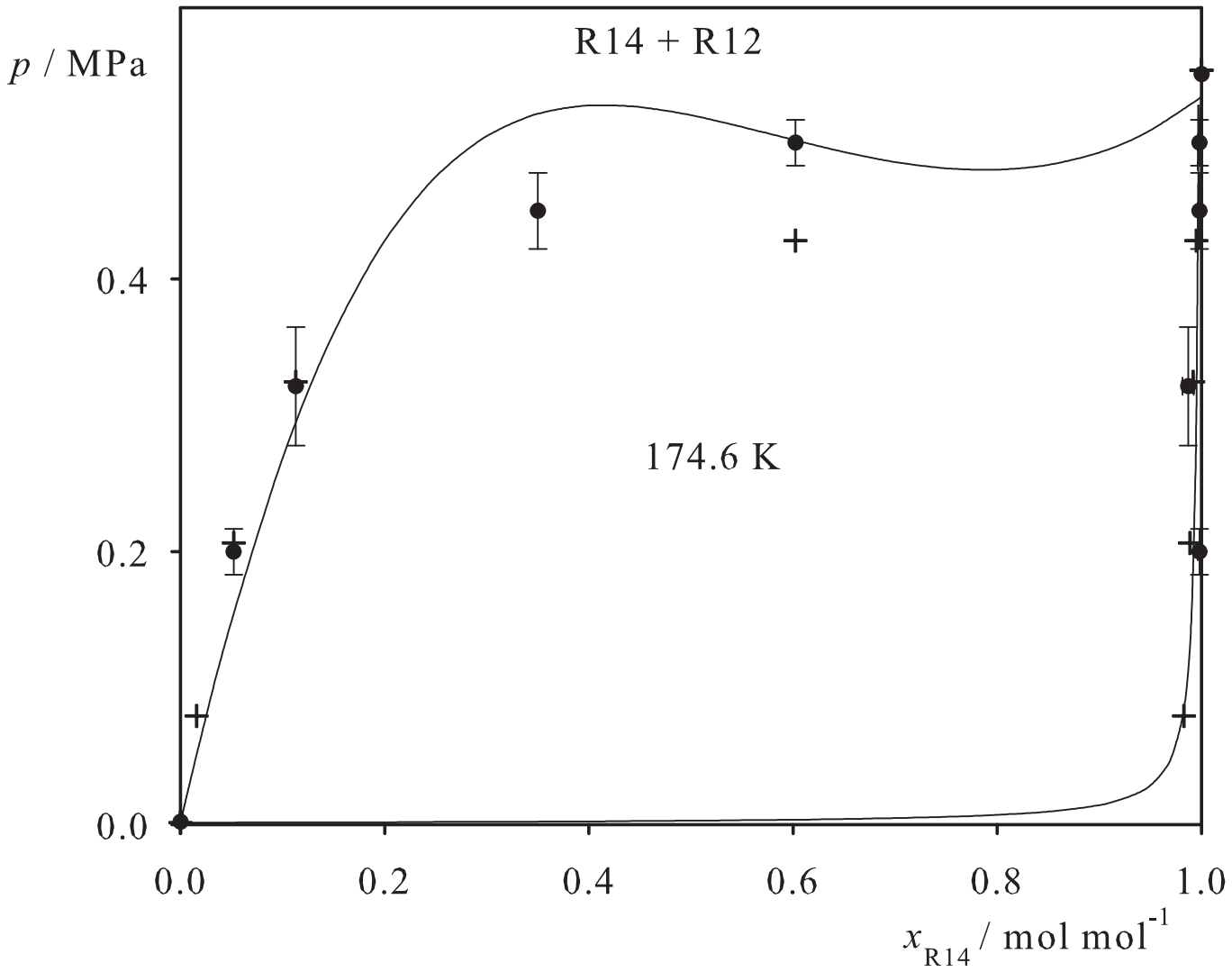

Fig. 145. Binary vapor-liquid equilibrium phase diagram: simulation data ●, experimental data + (cf. Table 2 of the manuscript for the reference) and Peng-Robinson equation of state —.

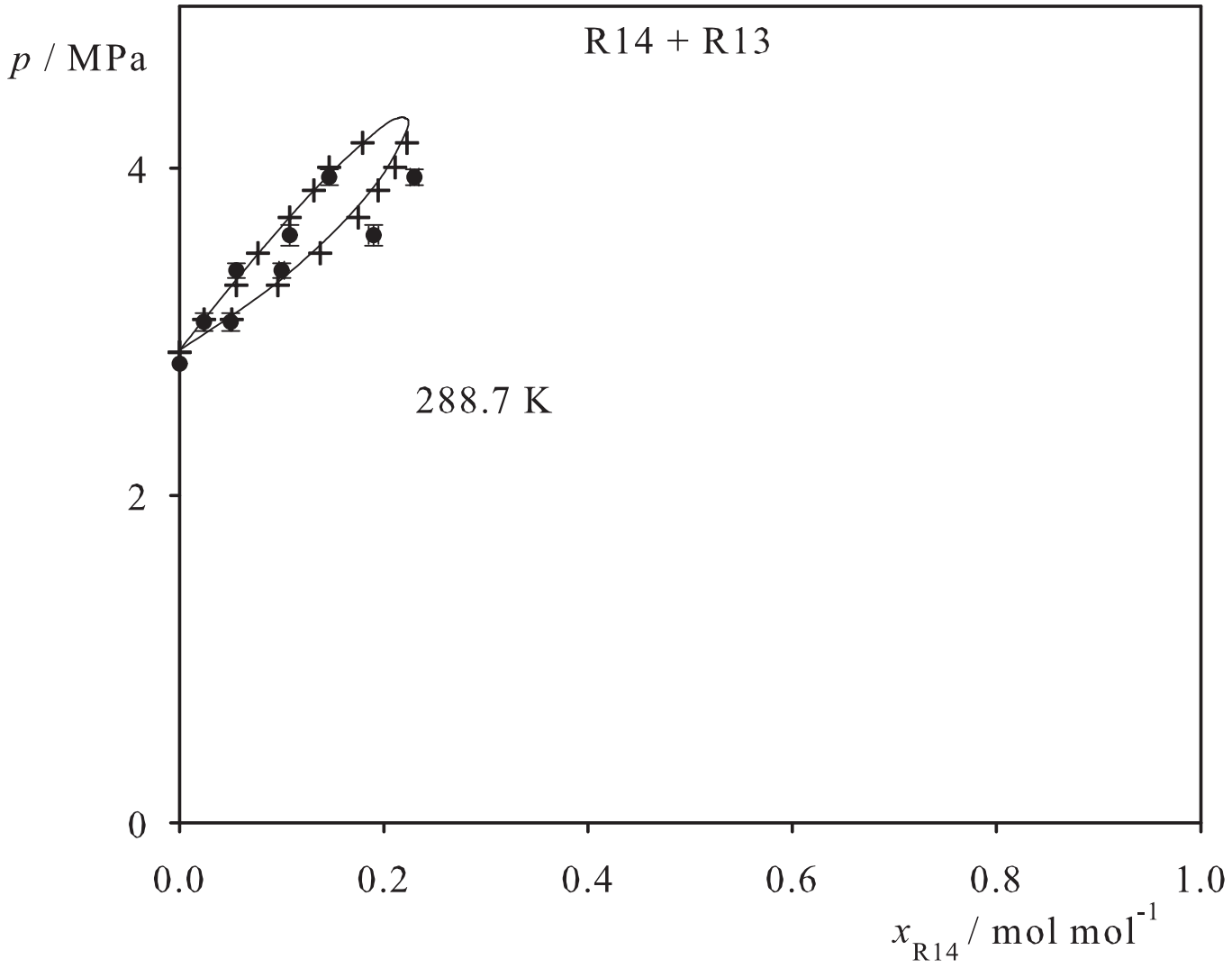

Fig. 146. Binary vapor-liquid equilibrium phase diagram: simulation data ●, experimental data + (cf. Table 2 of the manuscript for the reference) and Peng-Robinson equation of state —.

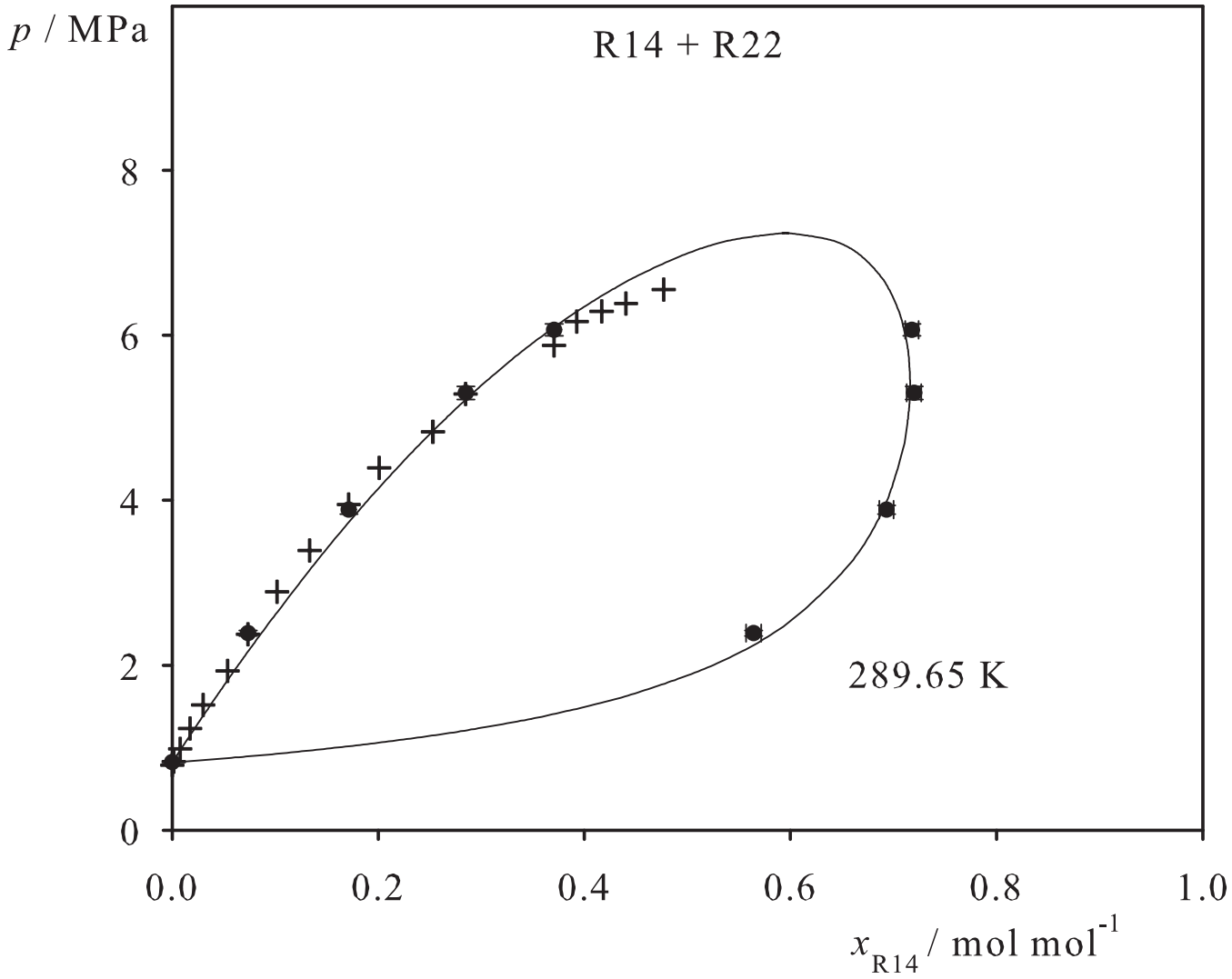

Fig. 147. Binary vapor-liquid equilibrium phase diagram: simulation data ●, experimental data + (cf. Table 2 of the manuscript for the reference) and Peng-Robinson equation of state —.

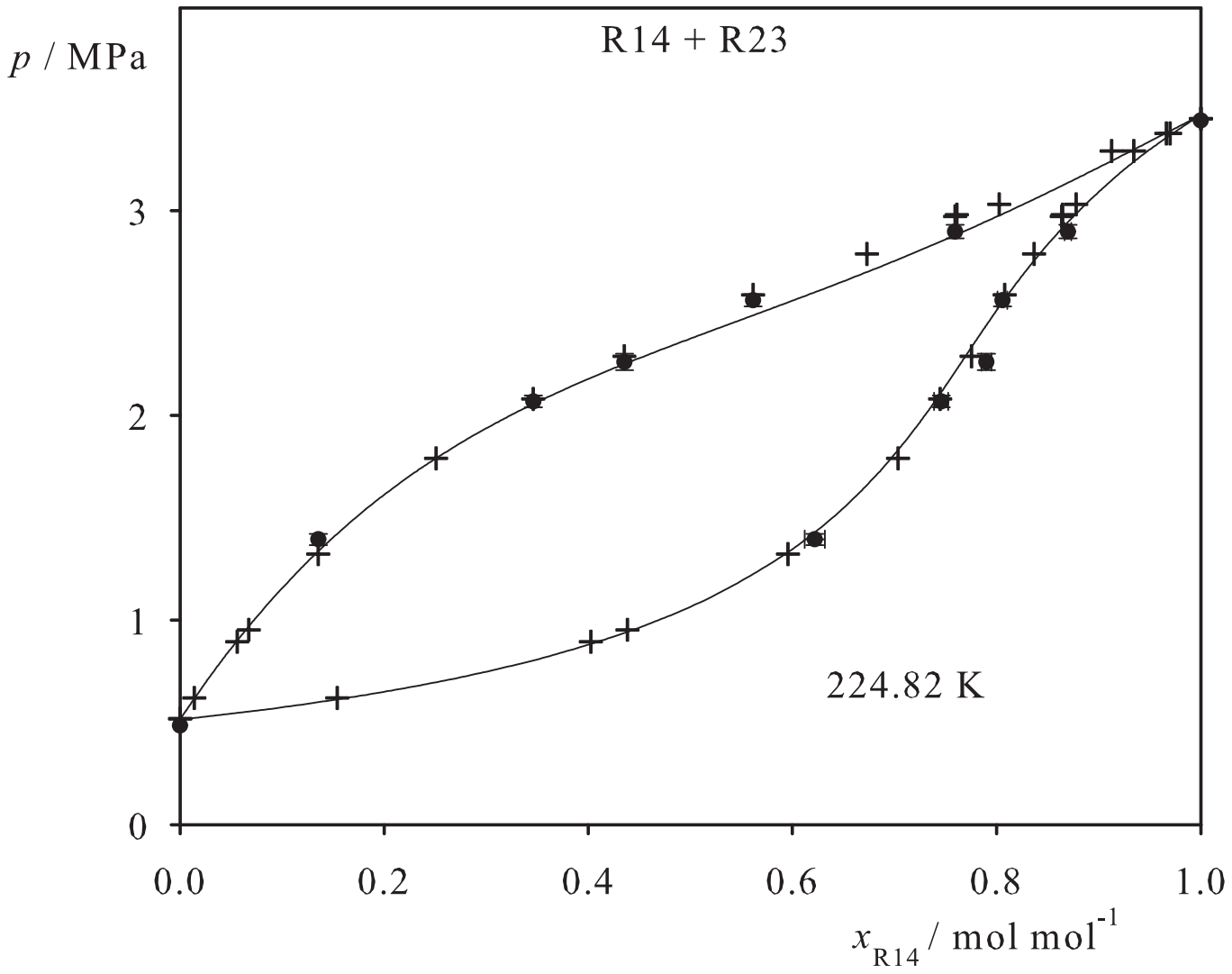

Fig. 148. Binary vapor-liquid equilibrium phase diagram: simulation data ● and experimental data + (cf. Table 2 of the manuscript for the reference).

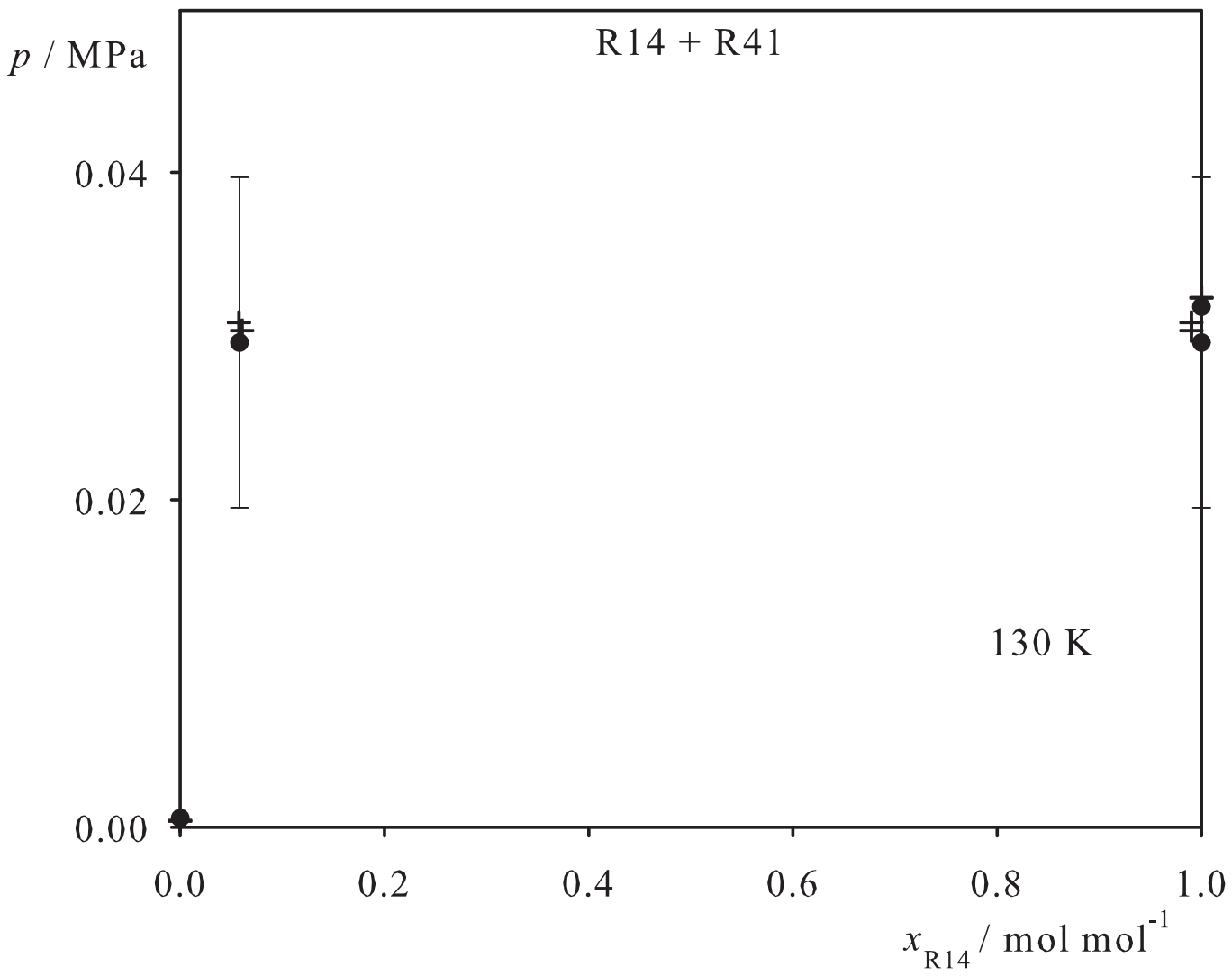

Fig. 149. Binary vapor-liquid equilibrium phase diagram: simulation data ●, experimental data + (cf. Table 2 of the manuscript for the reference) and Peng-Robinson equation of state —.

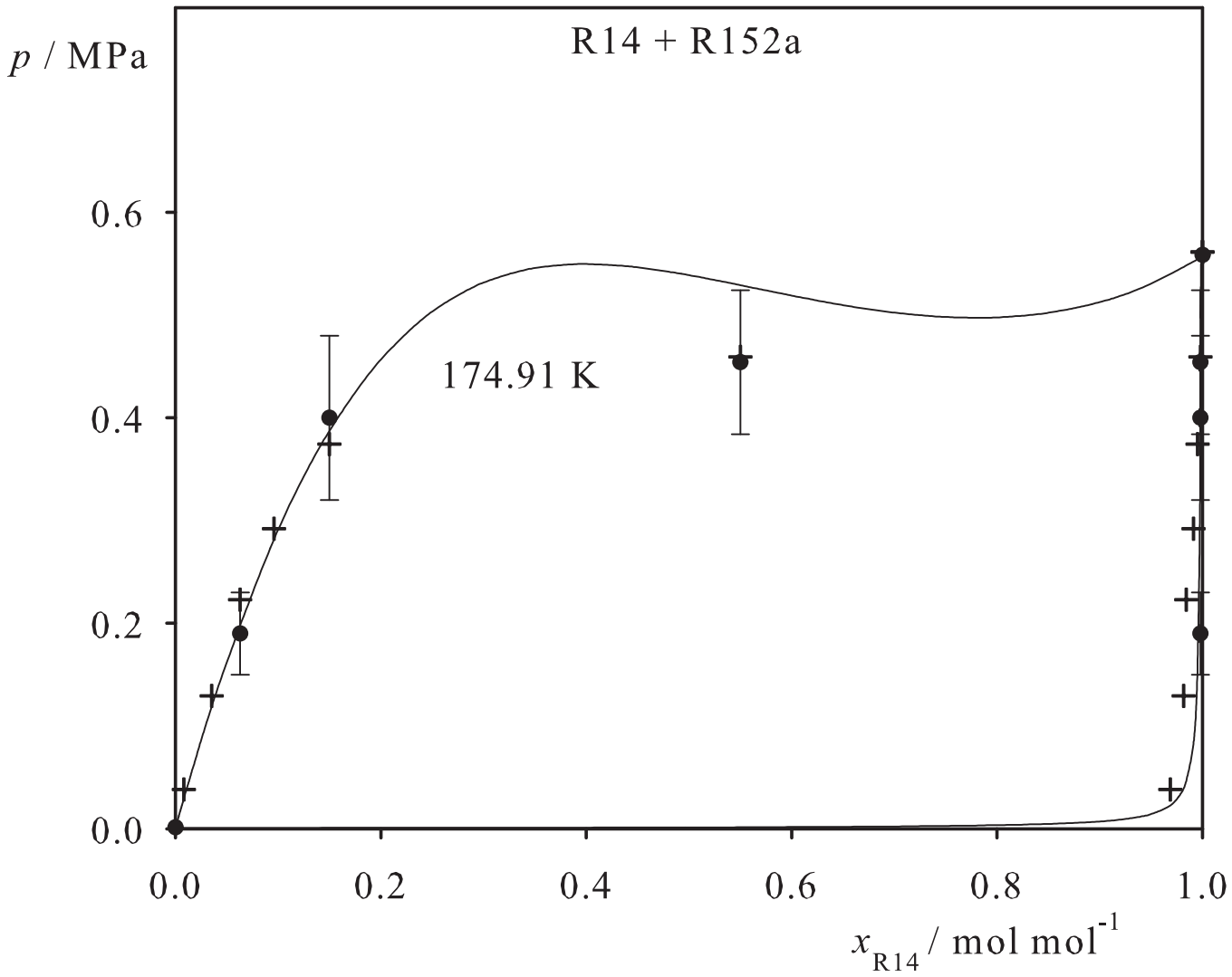

Fig. 150. Binary vapor-liquid equilibrium phase diagram: simulation data ●, experimental data + (cf. Table 2 of the manuscript for the reference) and Peng-Robinson equation of state —.

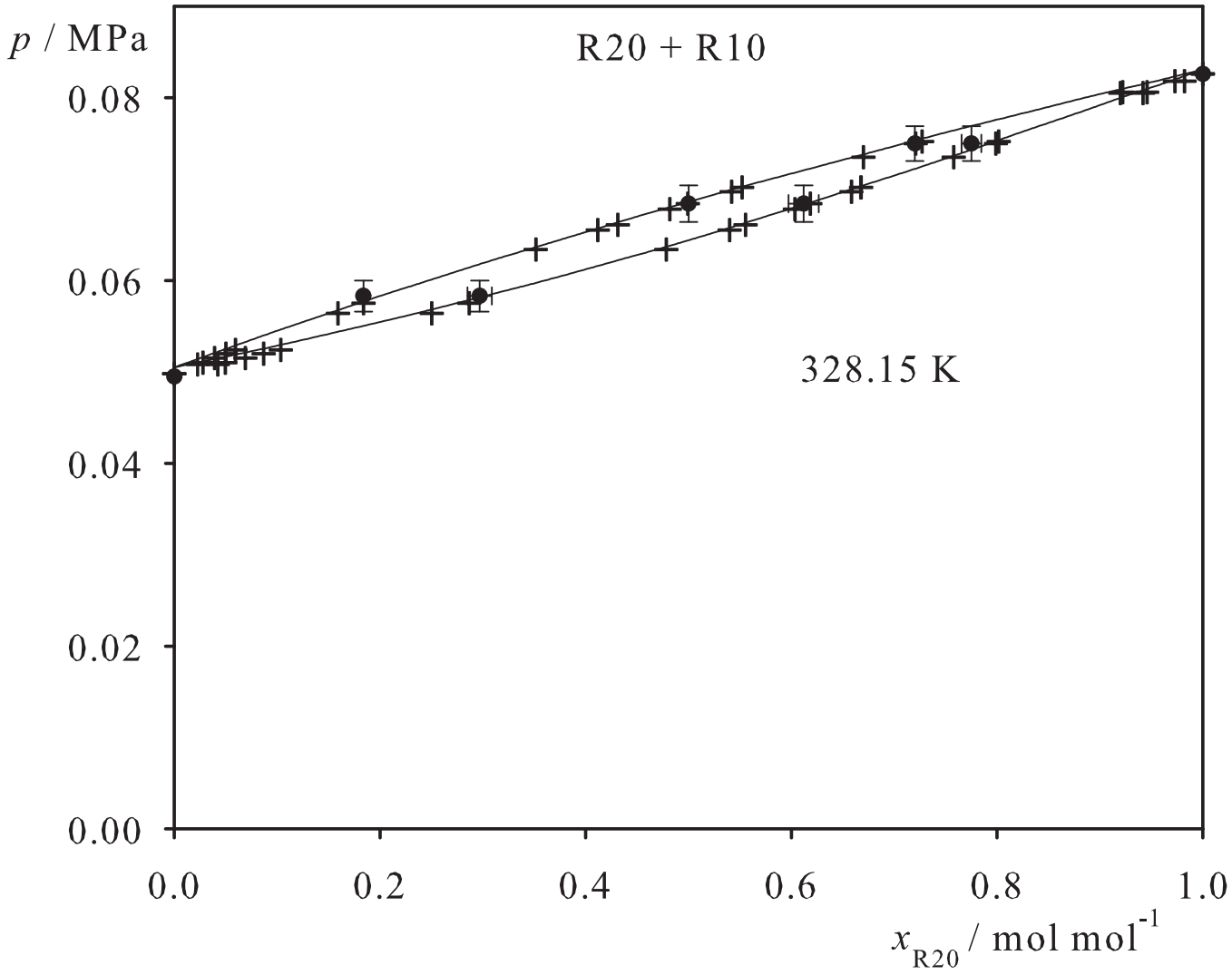

Fig. 151. Binary vapor-liquid equilibrium phase diagram: simulation data ●, experimental data + (cf. Table 2 of the manuscript for the reference) and Peng-Robinson equation of state —.

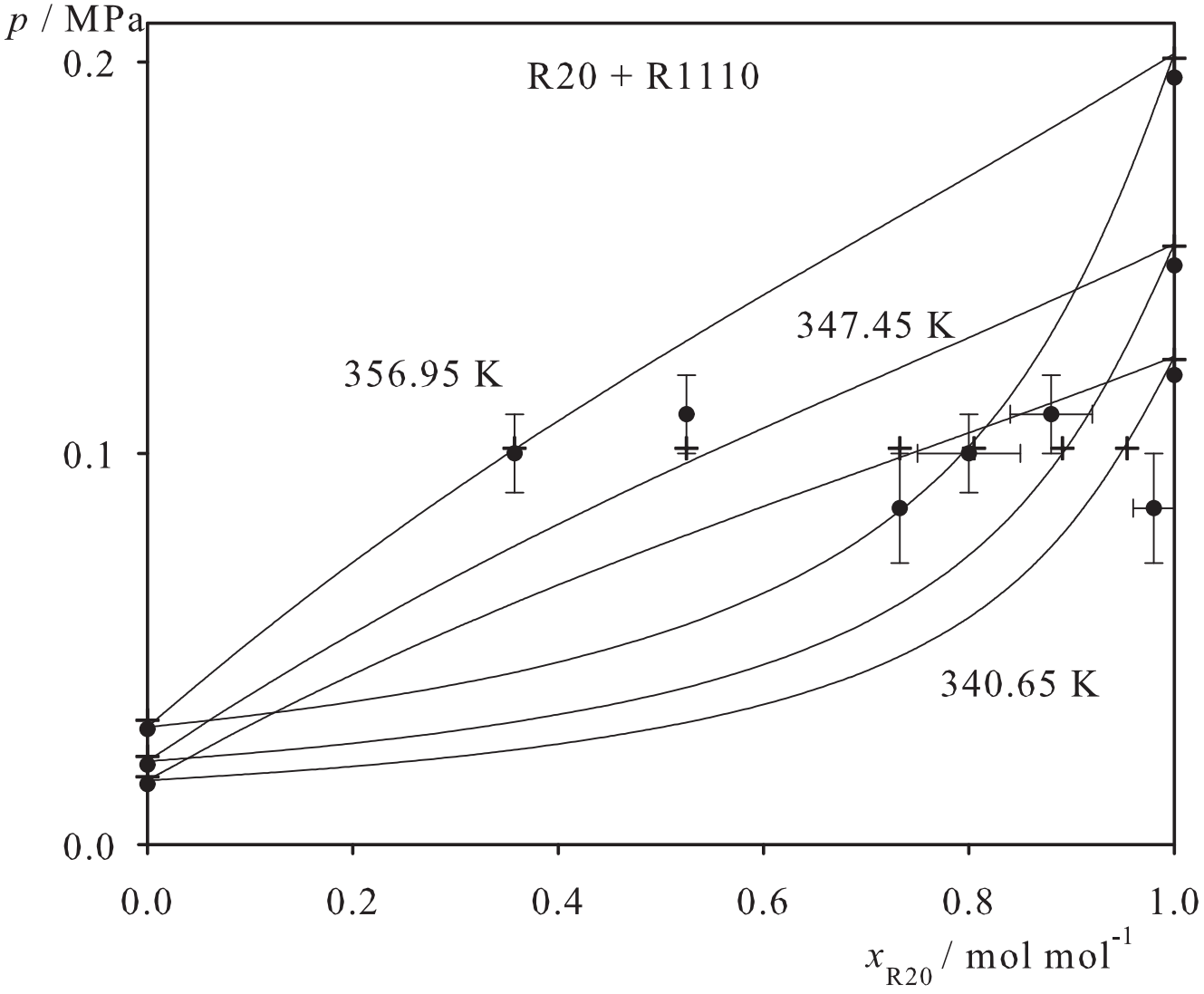

Fig. 152. Binary vapor-liquid equilibrium phase diagram: simulation data ●, experimental data + (cf. Table 2 of the manuscript for the reference) and Peng-Robinson equation of state —.

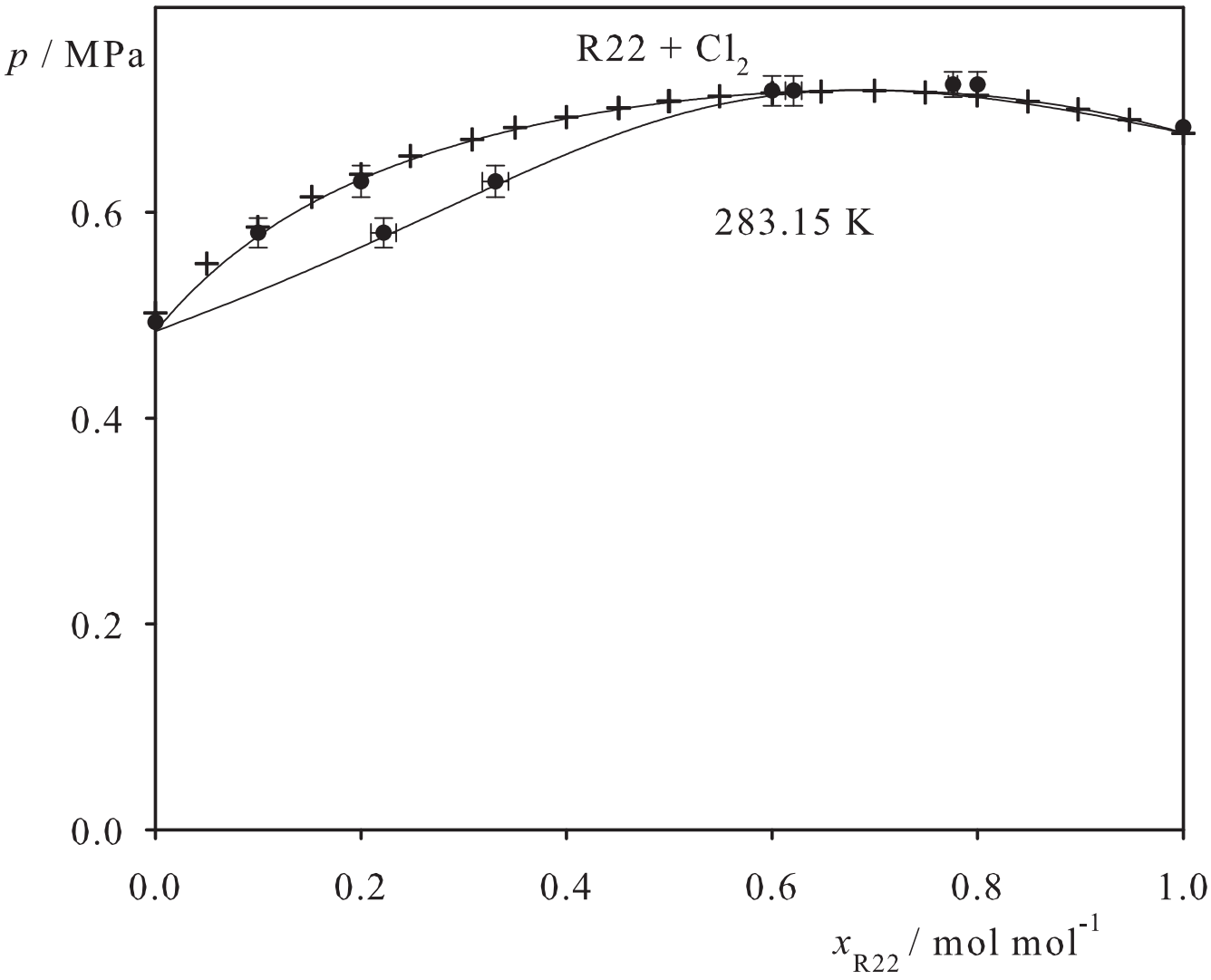

Fig. 153. Binary vapor-liquid equilibrium phase diagram: simulation data ●, experimental data + (cf. Table 2 of the manuscript for the reference) and Peng-Robinson equation of state —.

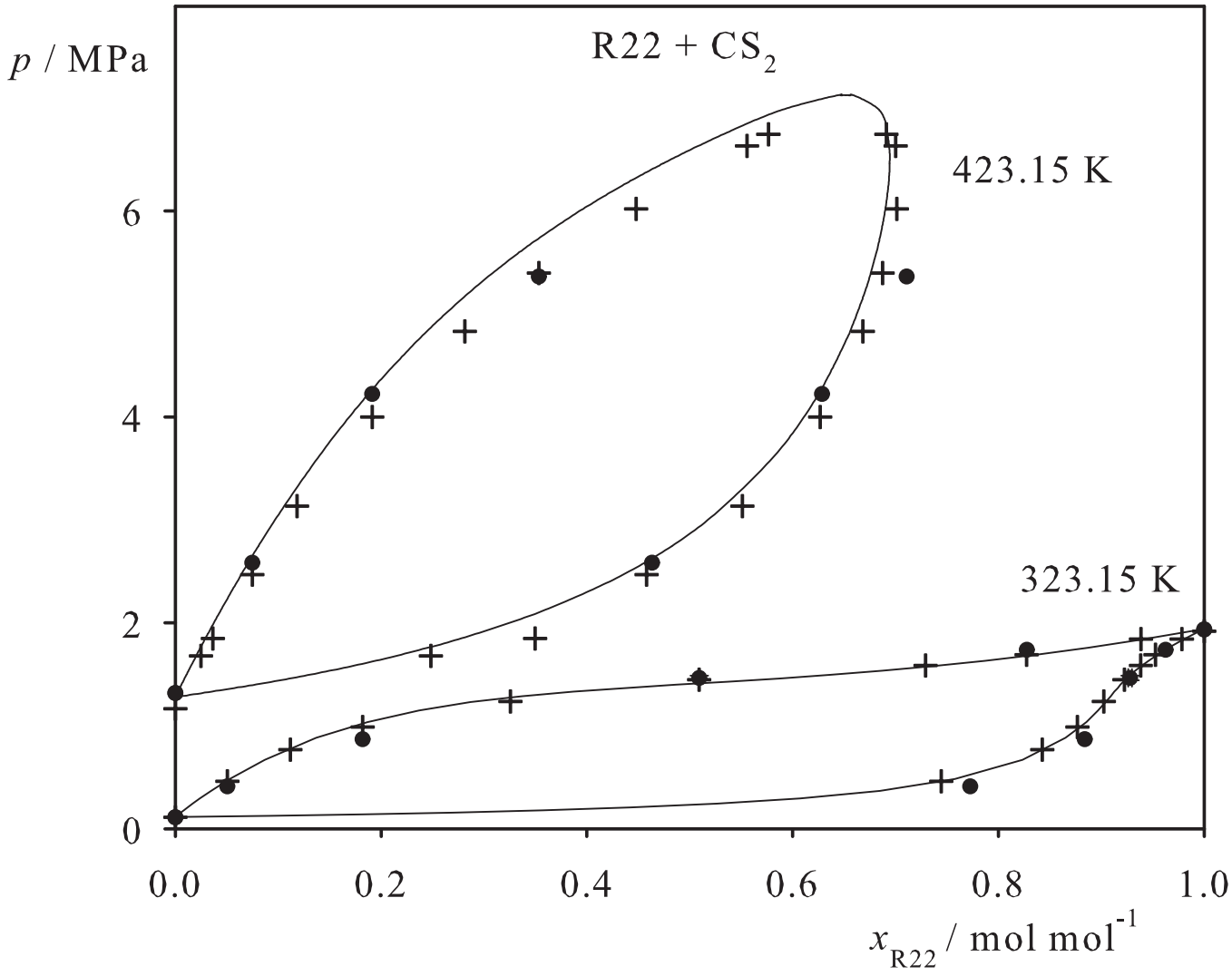

Fig. 154. Binary vapor-liquid equilibrium phase diagram: simulation data ●, experimental data + (cf. Table 2 of the manuscript for the reference) and Peng-Robinson equation of state —.

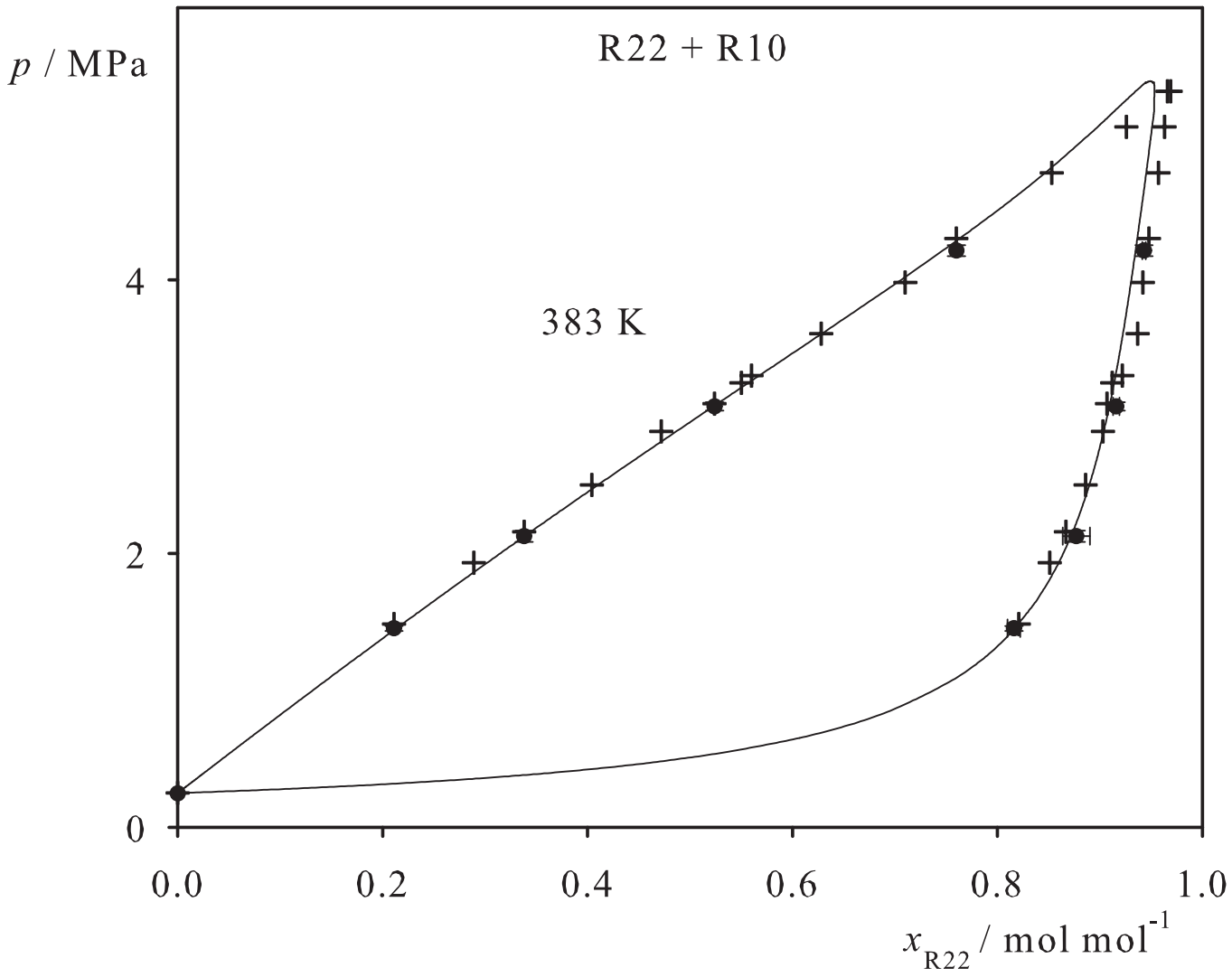

Fig. 155. Binary vapor-liquid equilibrium phase diagram: simulation data ●, experimental data + (cf. Table 2 of the manuscript for the reference) and Peng-Robinson equation of state —.

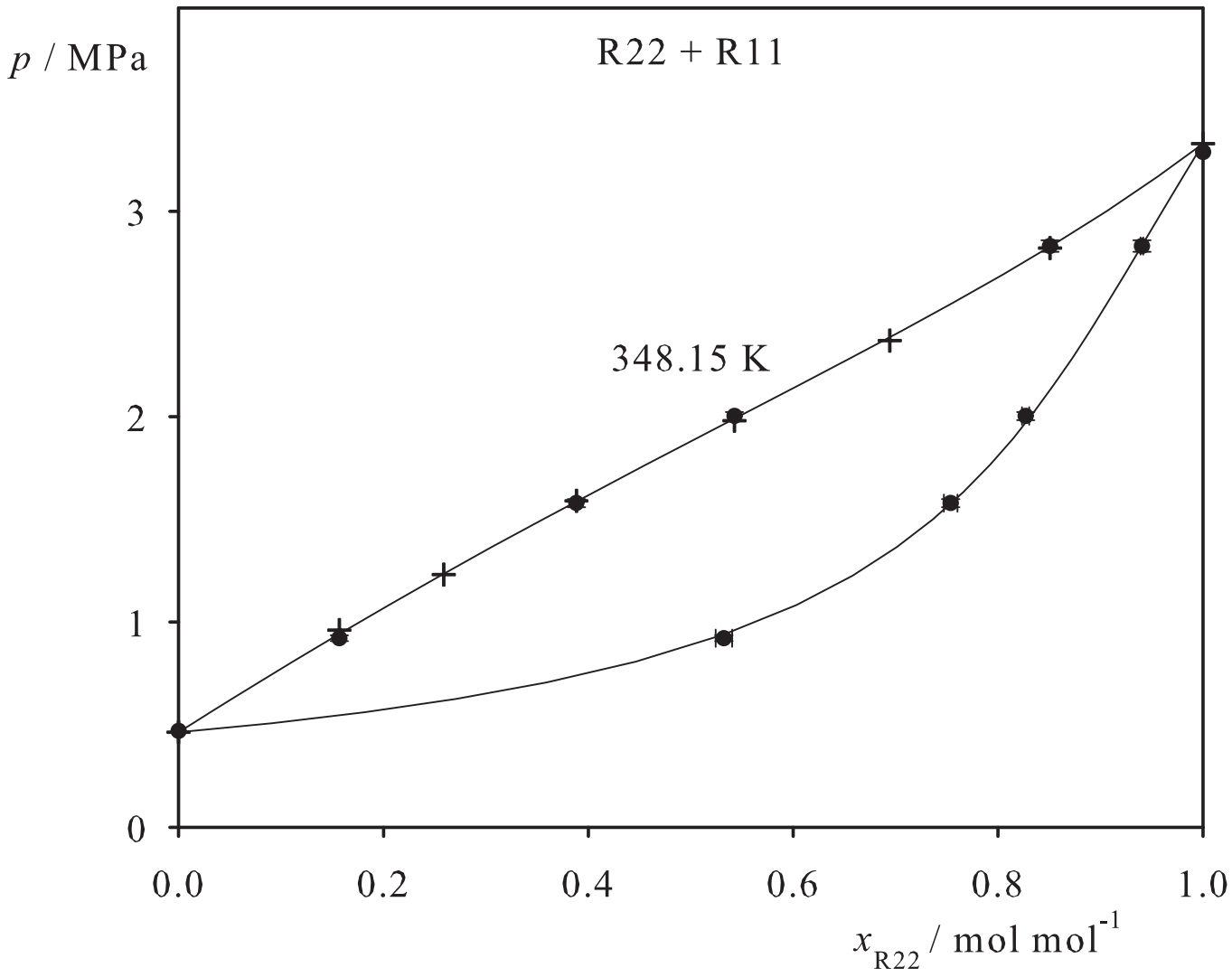

Fig. 156. Binary vapor-liquid equilibrium phase diagram: simulation data ●, experimental data + (cf. Table 2 of the manuscript for the reference) and Peng-Robinson equation of state —.

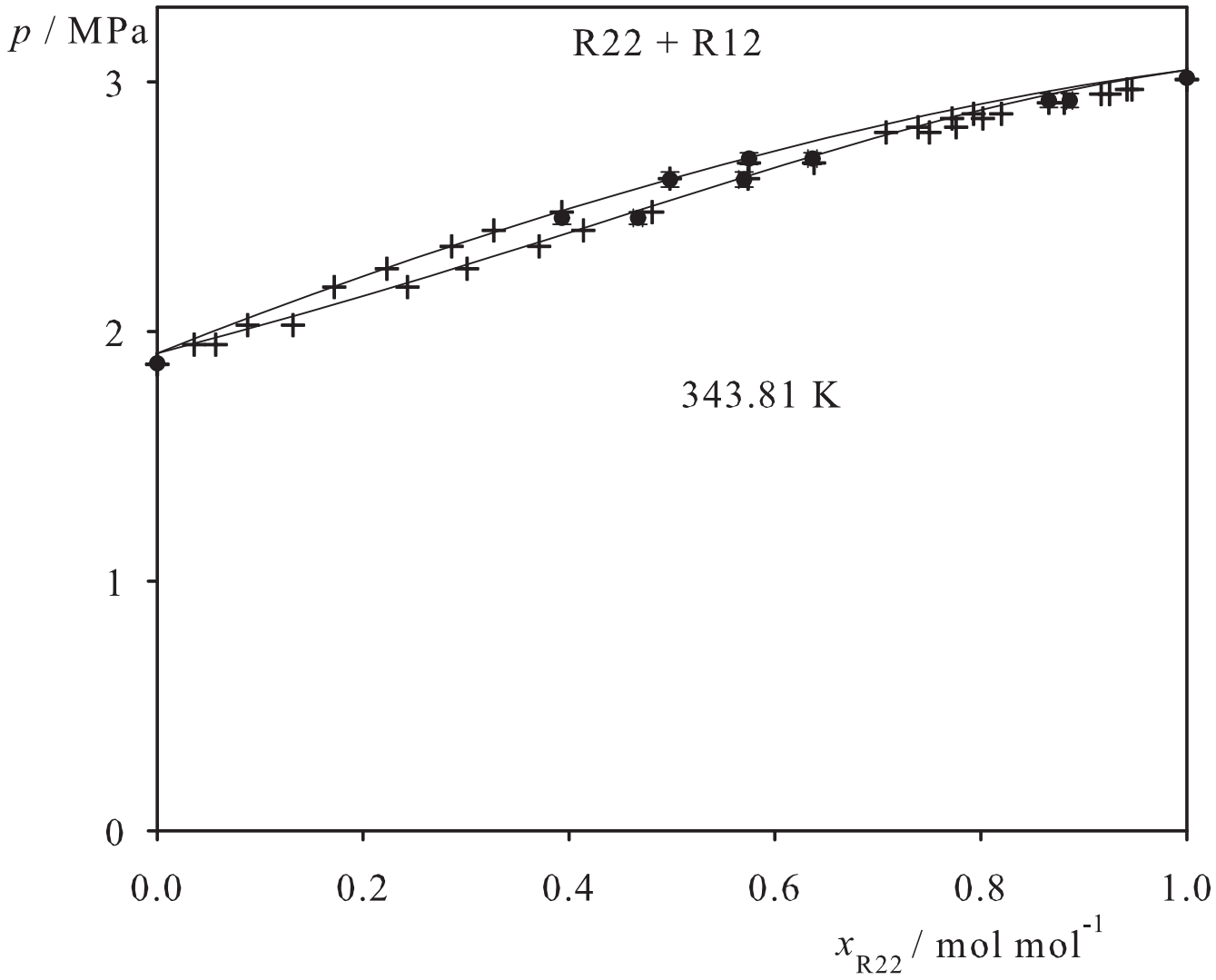

Fig. 157. Binary vapor-liquid equilibrium phase diagram: simulation data ●, experimental data + (cf. Table 2 of the manuscript for the reference) and Peng-Robinson equation of state —.

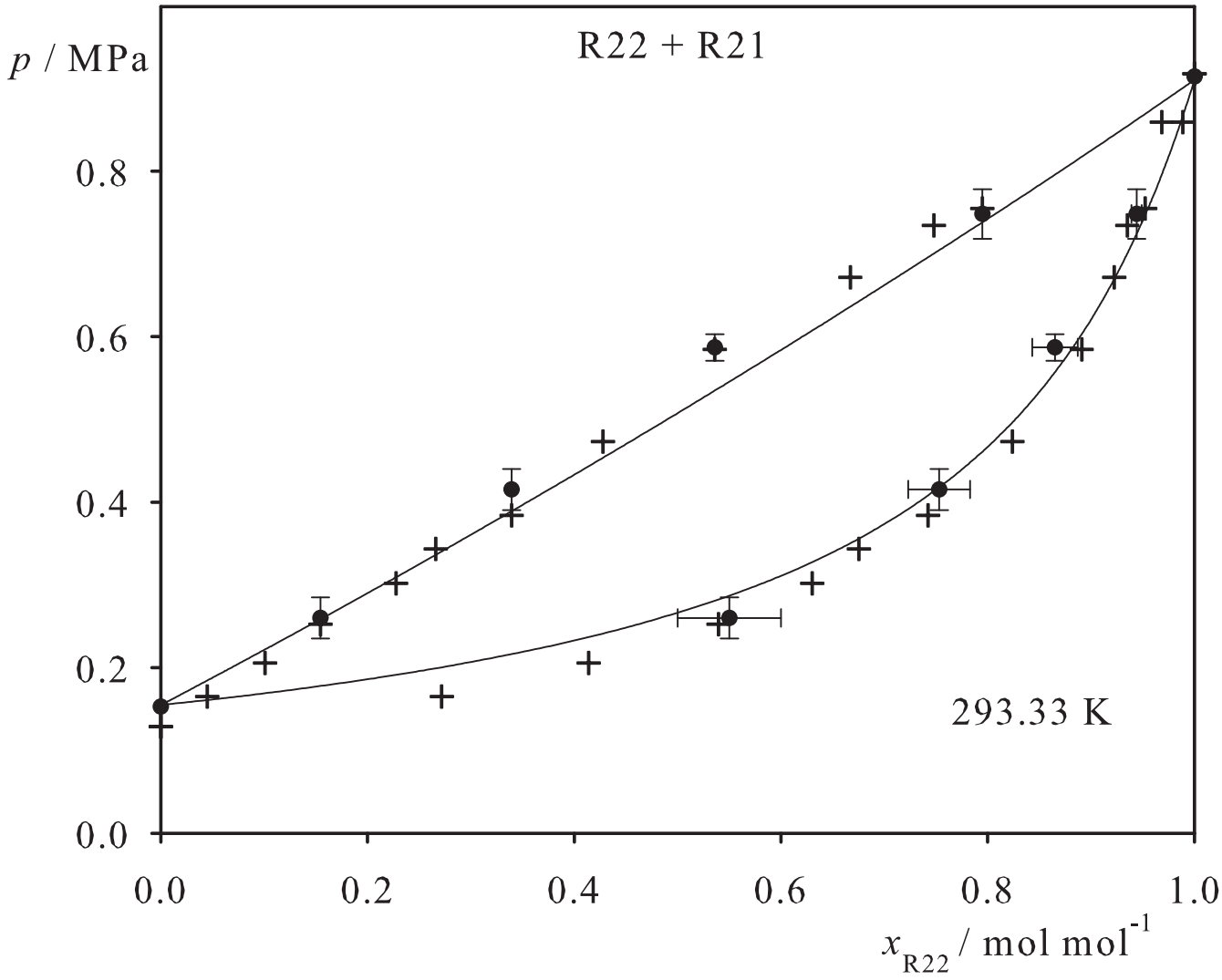

Fig. 158. Binary vapor-liquid equilibrium phase diagram: simulation data ●, experimental data + (cf. Table 2 of the manuscript for the reference) and Peng-Robinson equation of state —.

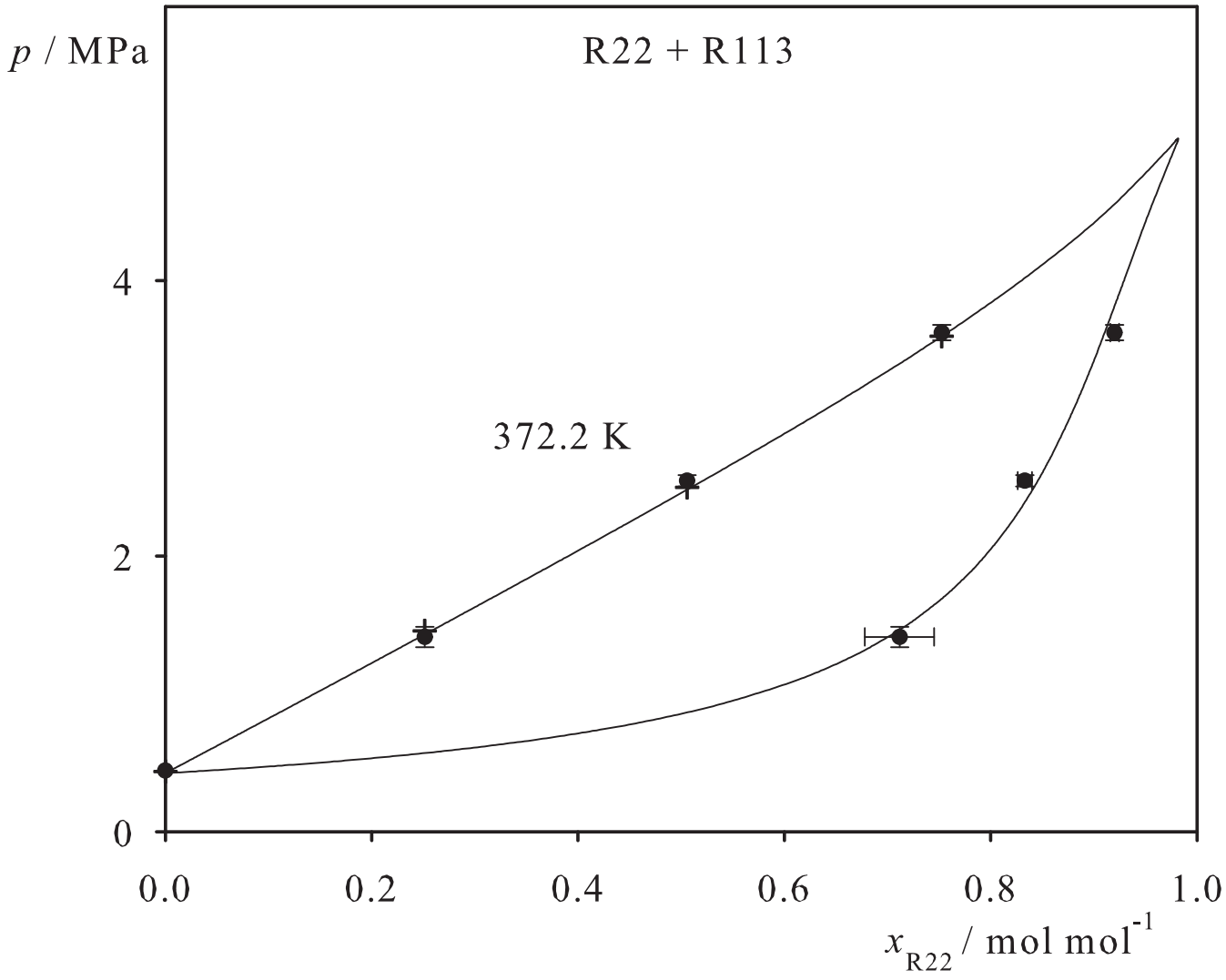

Fig. 159. Binary vapor-liquid equilibrium phase diagram: simulation data ●, experimental data + (cf. Table 2 of the manuscript for the reference) and Peng-Robinson equation of state —.

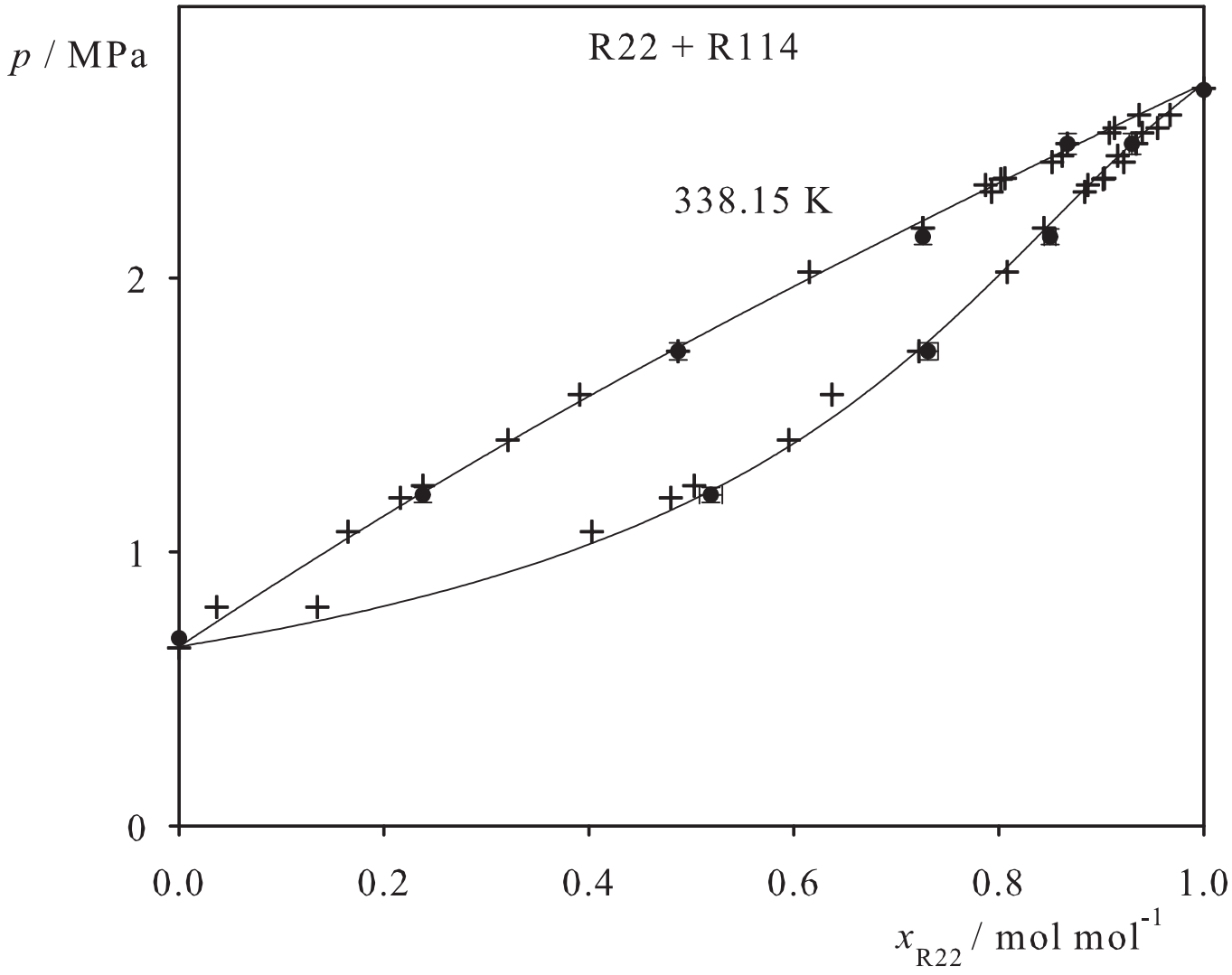

Fig. 160. Binary vapor-liquid equilibrium phase diagram: simulation data ●, experimental data + (cf. Table 2 of the manuscript for the reference) and Peng-Robinson equation of state —.

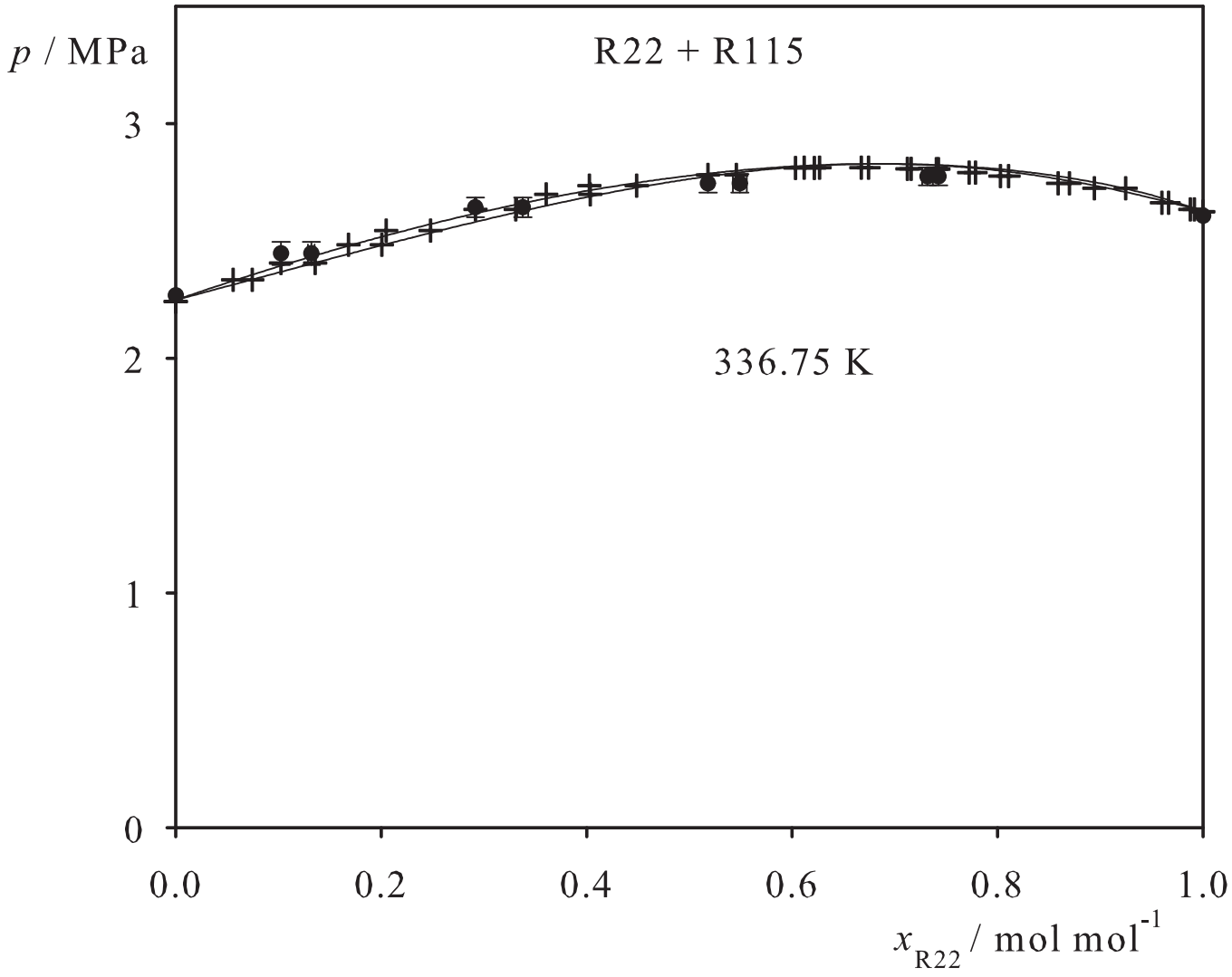

Fig. 161. Binary vapor-liquid equilibrium phase diagram: simulation data ●, experimental data + (cf. Table 2 of the manuscript for the reference) and Peng-Robinson equation of state —.

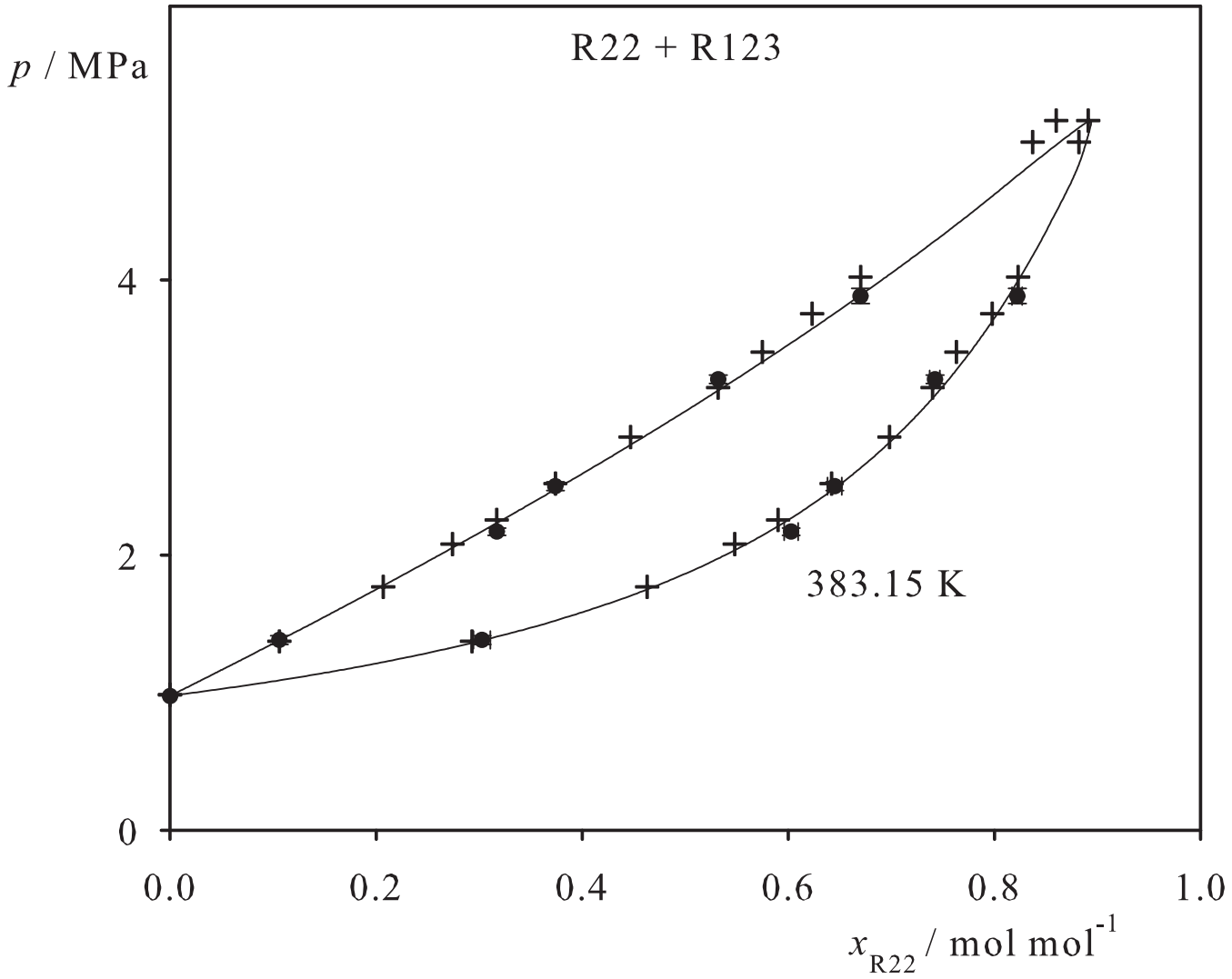

Fig. 162. Binary vapor-liquid equilibrium phase diagram: simulation data ●, experimental data + (cf. Table 2 of the manuscript for the reference) and Peng-Robinson equation of state —.

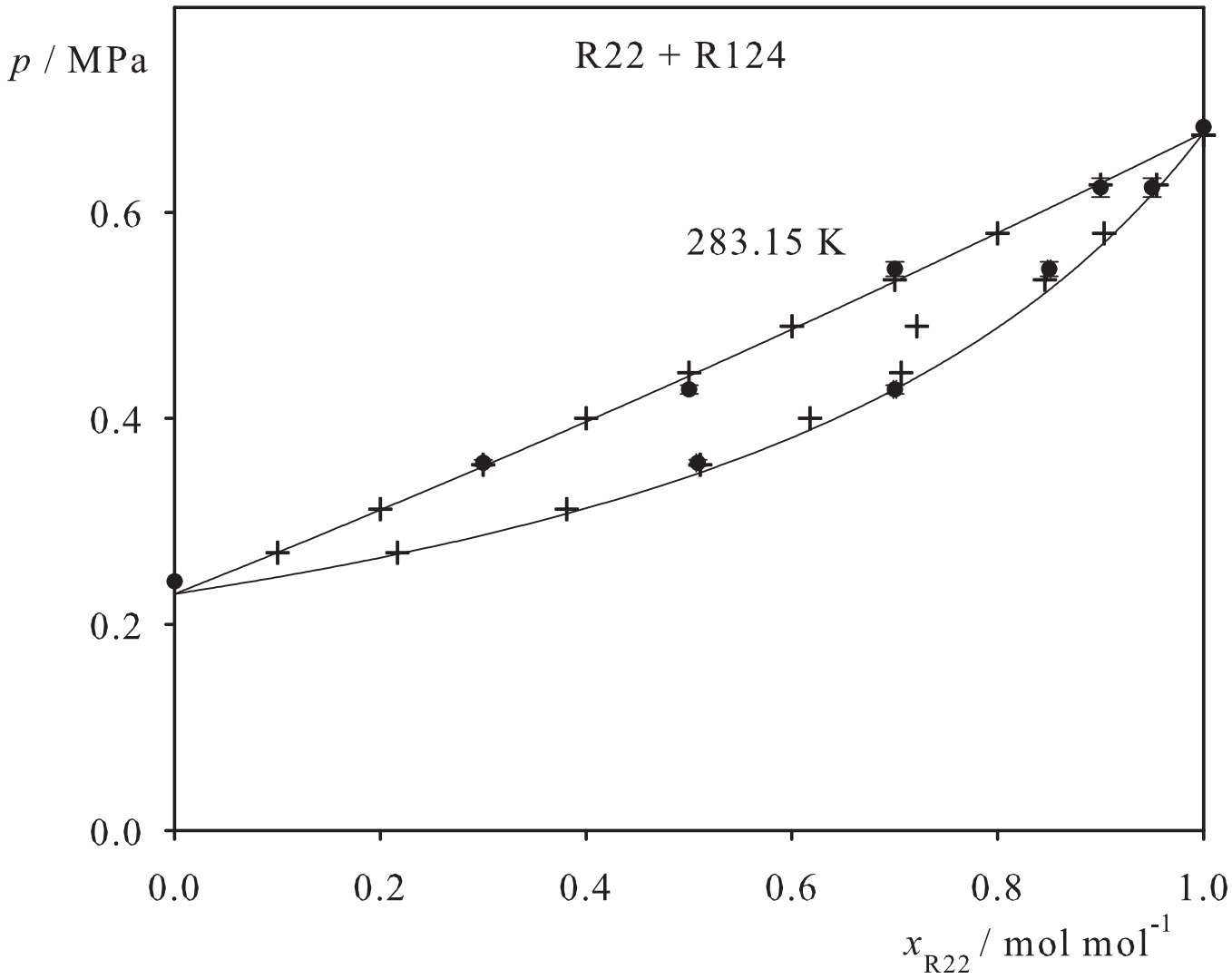

Fig. 163. Binary vapor-liquid equilibrium phase diagram: simulation data ●, experimental data + (cf. Table 2 of the manuscript for the reference) and Peng-Robinson equation of state —.

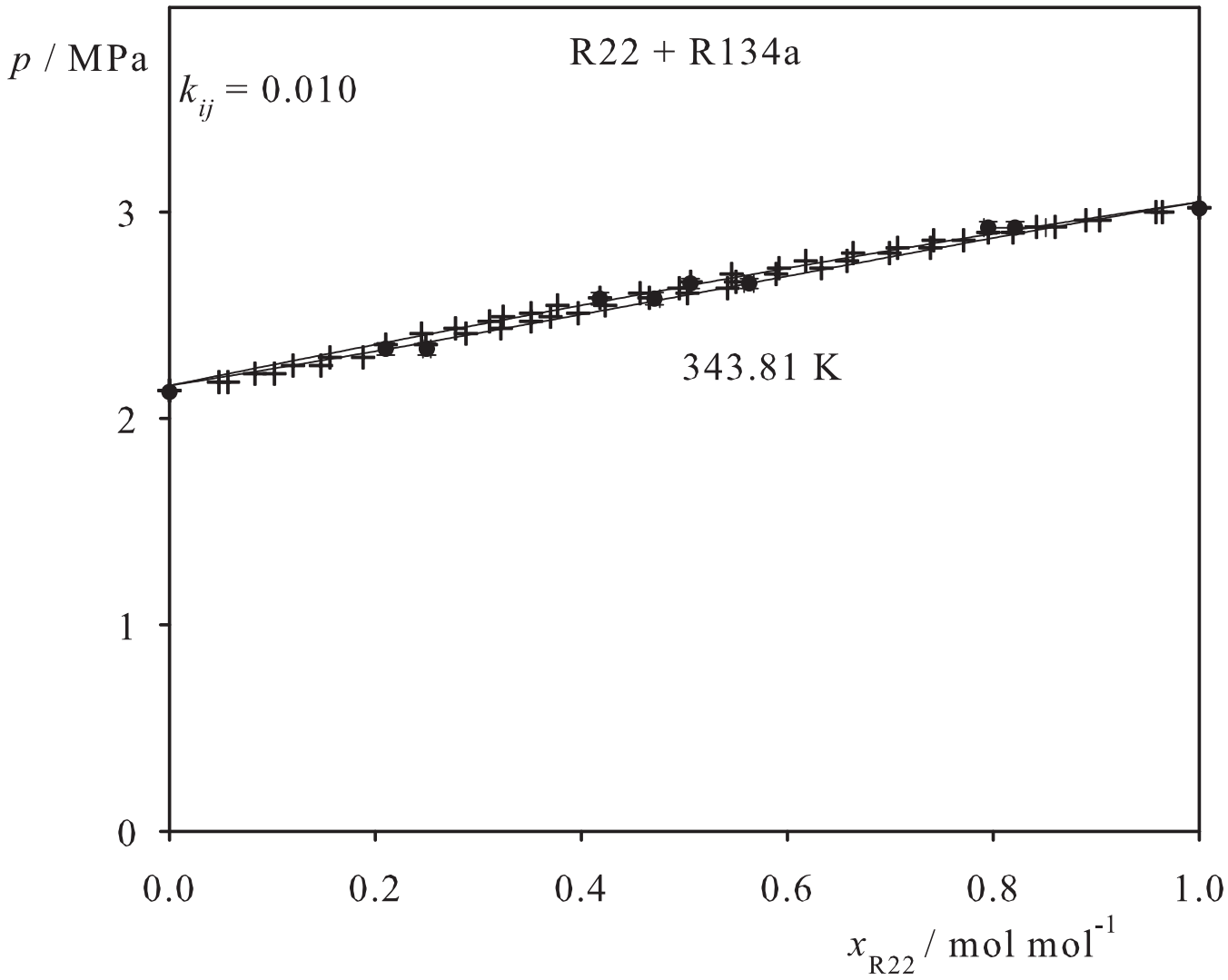

Fig. 164. Binary vapor-liquid equilibrium phase diagram: simulation data ●, experimental data + (cf. Table 2 of the manuscript for the reference) and Peng-Robinson equation of state —.

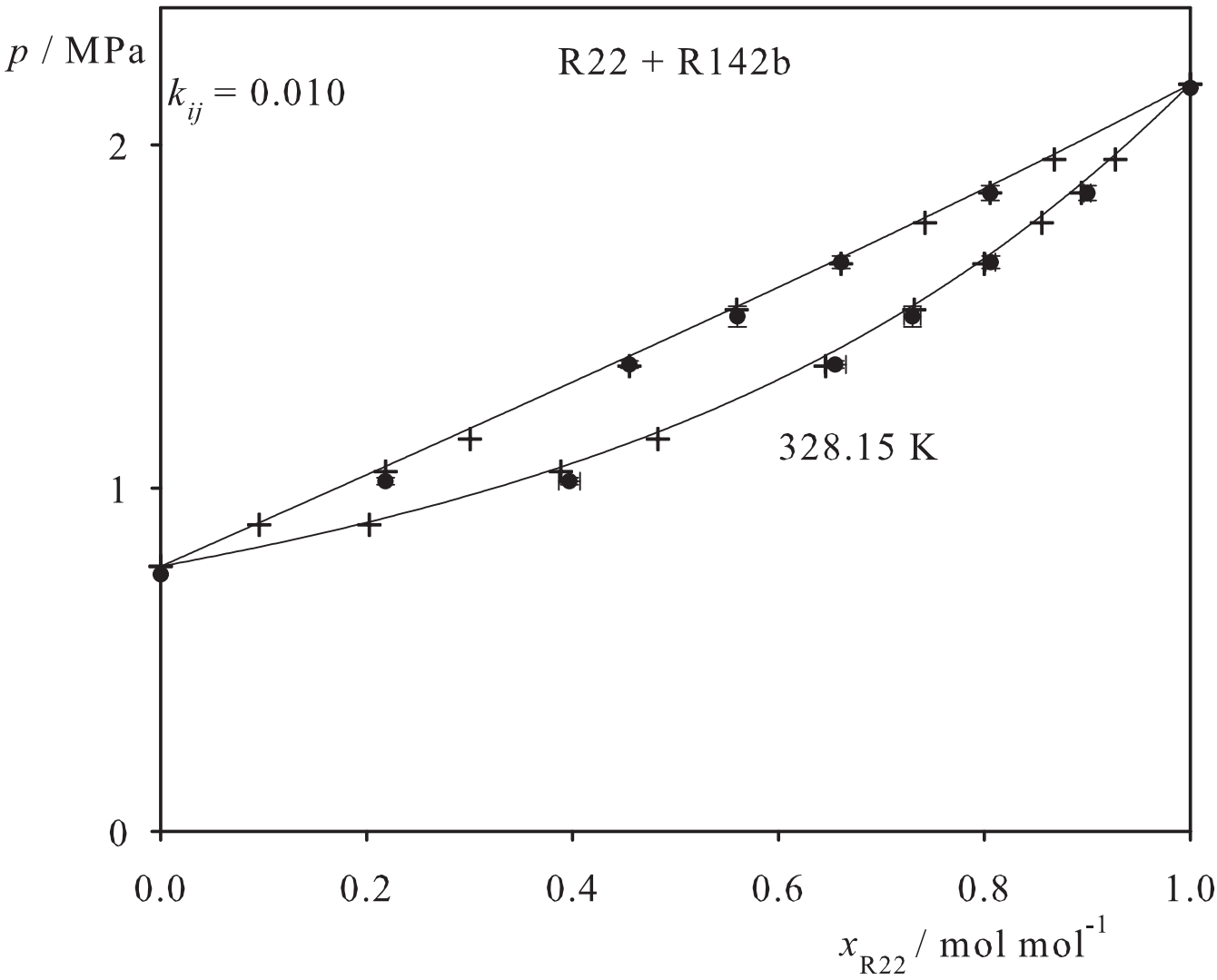

Fig. 165. Binary vapor-liquid equilibrium phase diagram: simulation data ●, experimental data + (cf. Table 2 of the manuscript for the reference) and Peng-Robinson equation of state —.

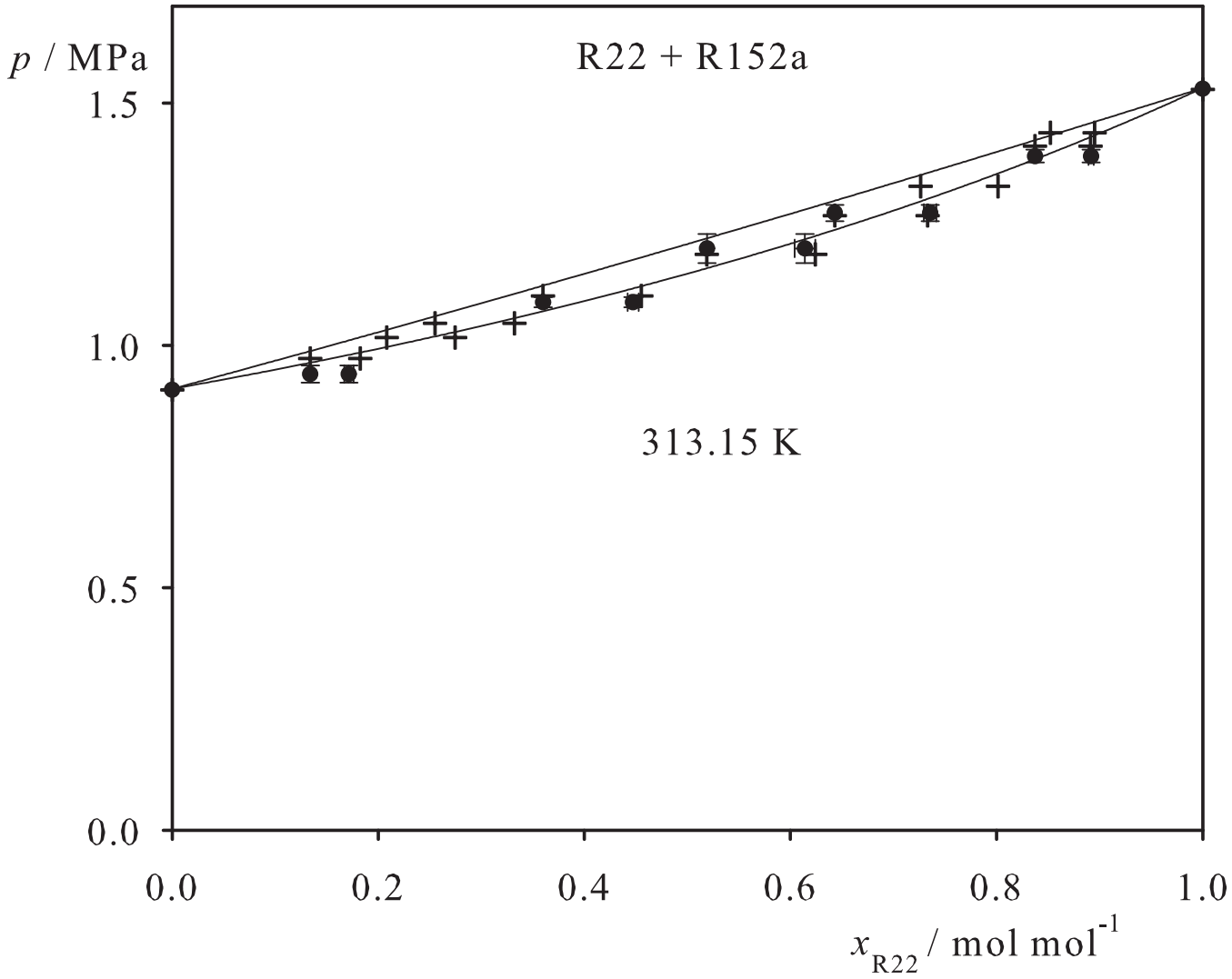

Fig. 166. Binary vapor-liquid equilibrium phase diagram: simulation data ●, experimental data + (cf. Table 2 of the manuscript for the reference) and Peng-Robinson equation of state —.

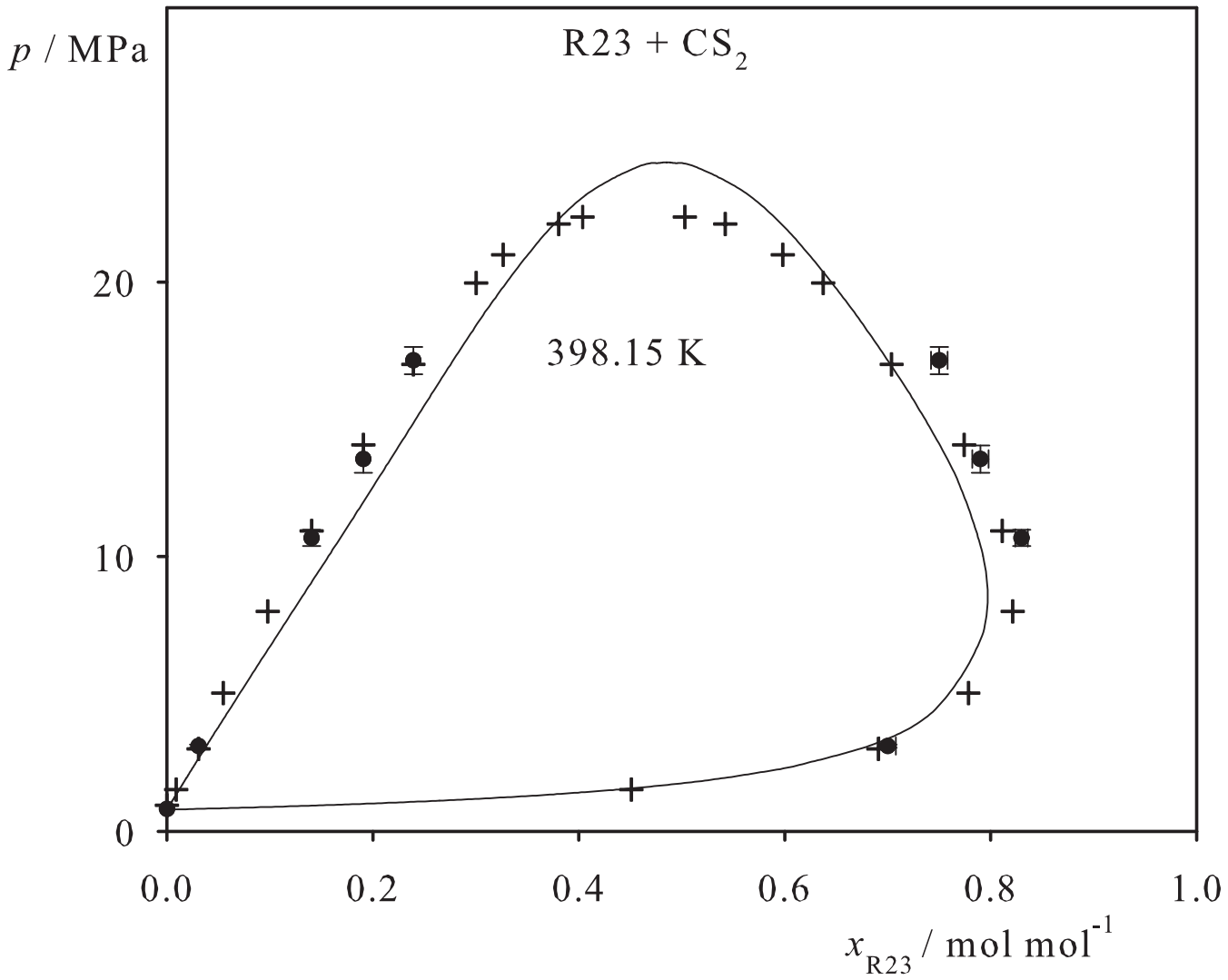

Fig. 167. Binary vapor-liquid equilibrium phase diagram: simulation data ●, experimental data + (cf. Table 2 of the manuscript for the reference) and Peng-Robinson equation of state —.

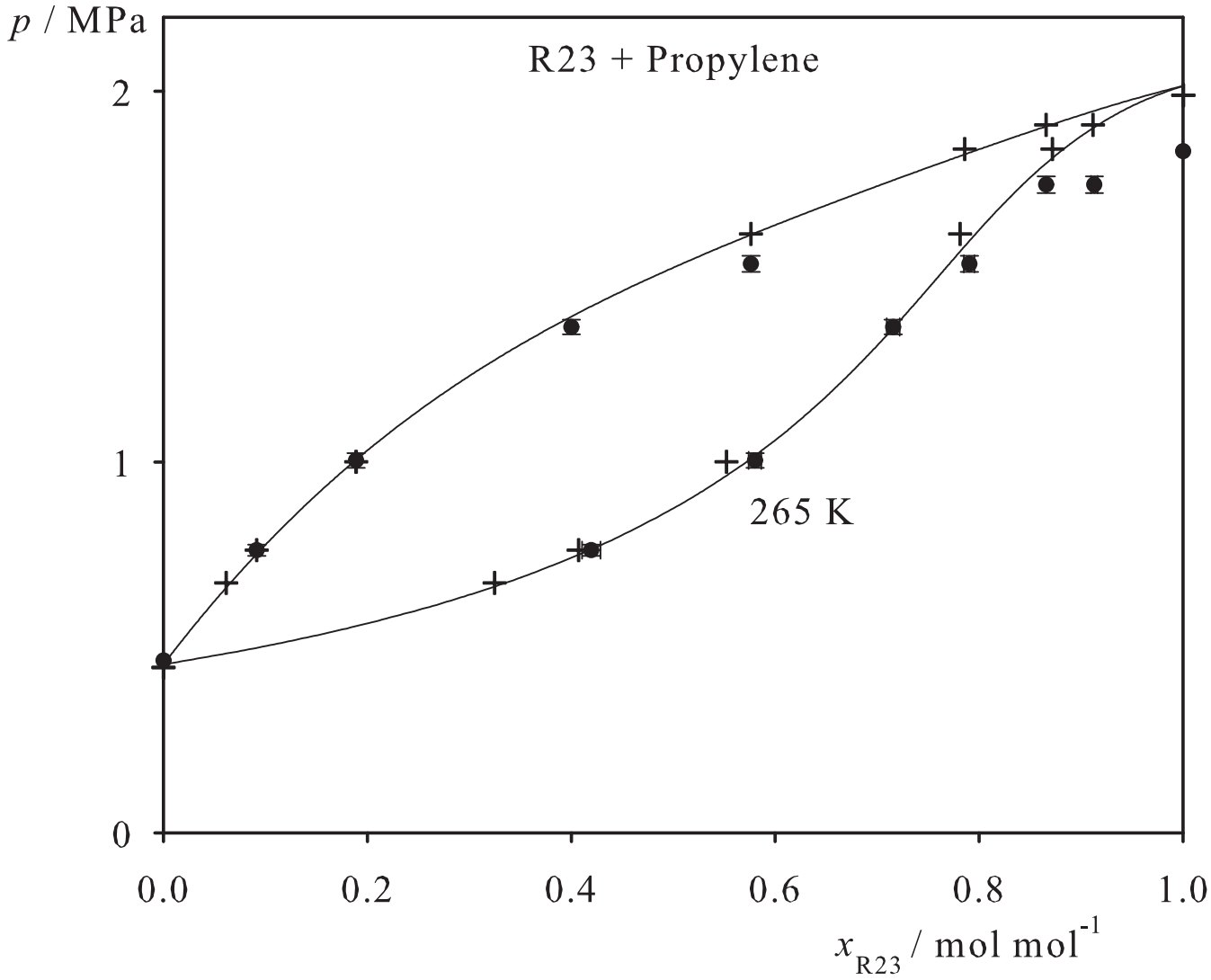

Fig. 168. Binary vapor-liquid equilibrium phase diagram: simulation data ●, experimental data + (cf. Table 2 of the manuscript for the reference) and Peng-Robinson equation of state —.

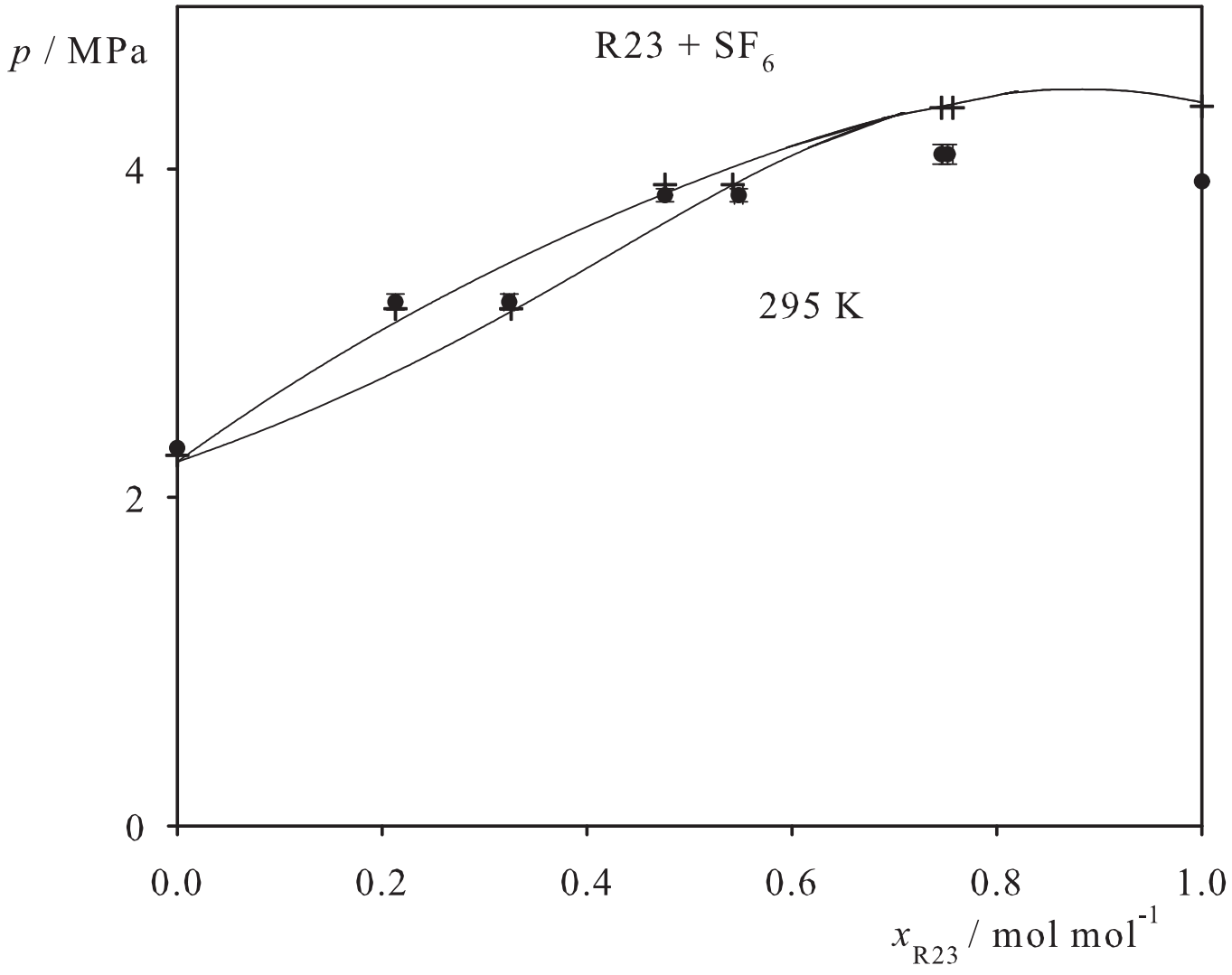

Fig. 169. Binary vapor-liquid equilibrium phase diagram: simulation data ●, experimental data + (cf. Table 2 of the manuscript for the reference) and Peng-Robinson equation of state —.

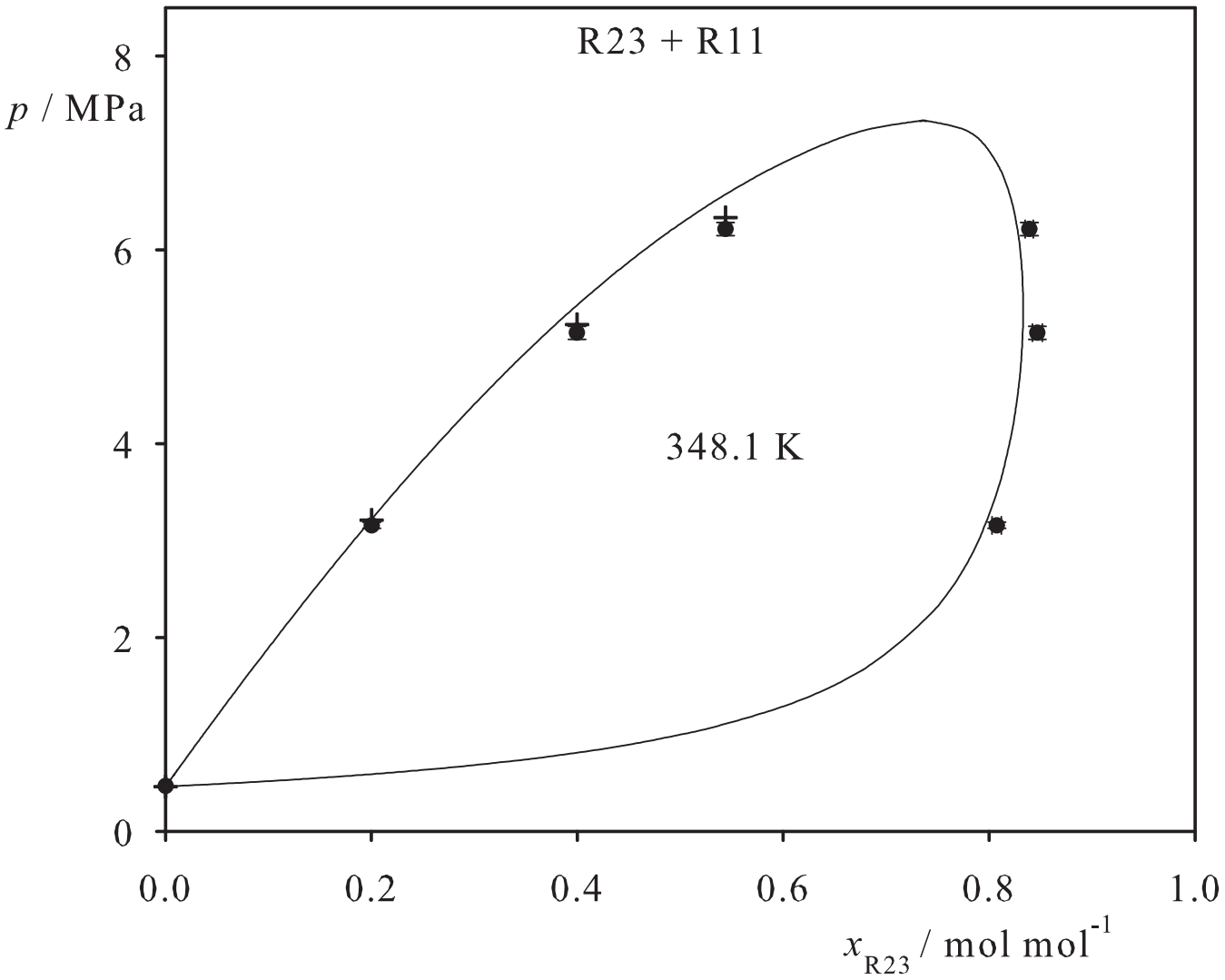

Fig. 170. Binary vapor-liquid equilibrium phase diagram: simulation data ●, experimental data + (cf. Table 2 of the manuscript for the reference) and Peng-Robinson equation of state —.

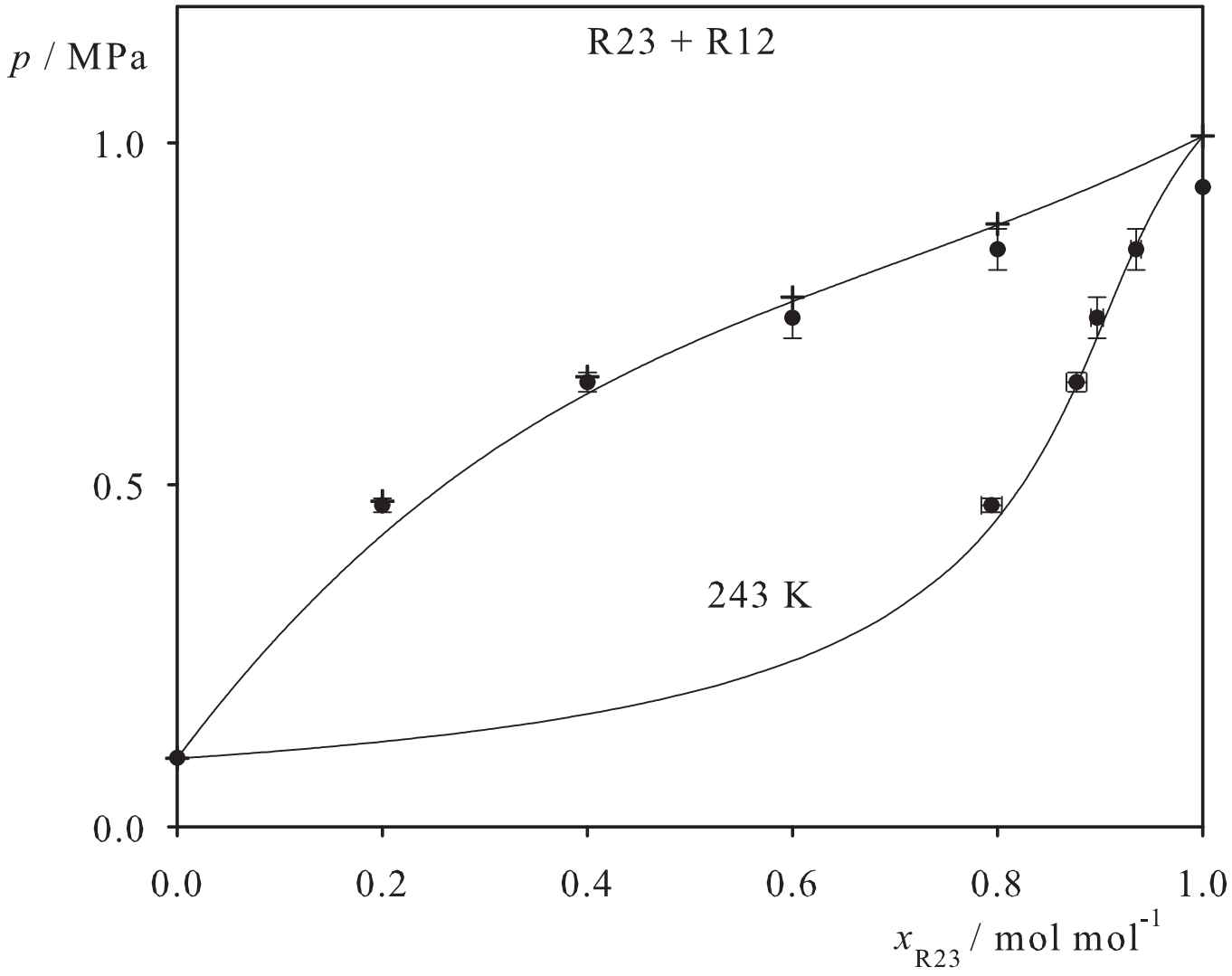

Fig. 171. Binary vapor-liquid equilibrium phase diagram: simulation data ●, experimental data + (cf. Table 2 of the manuscript for the reference) and Peng-Robinson equation of state —.

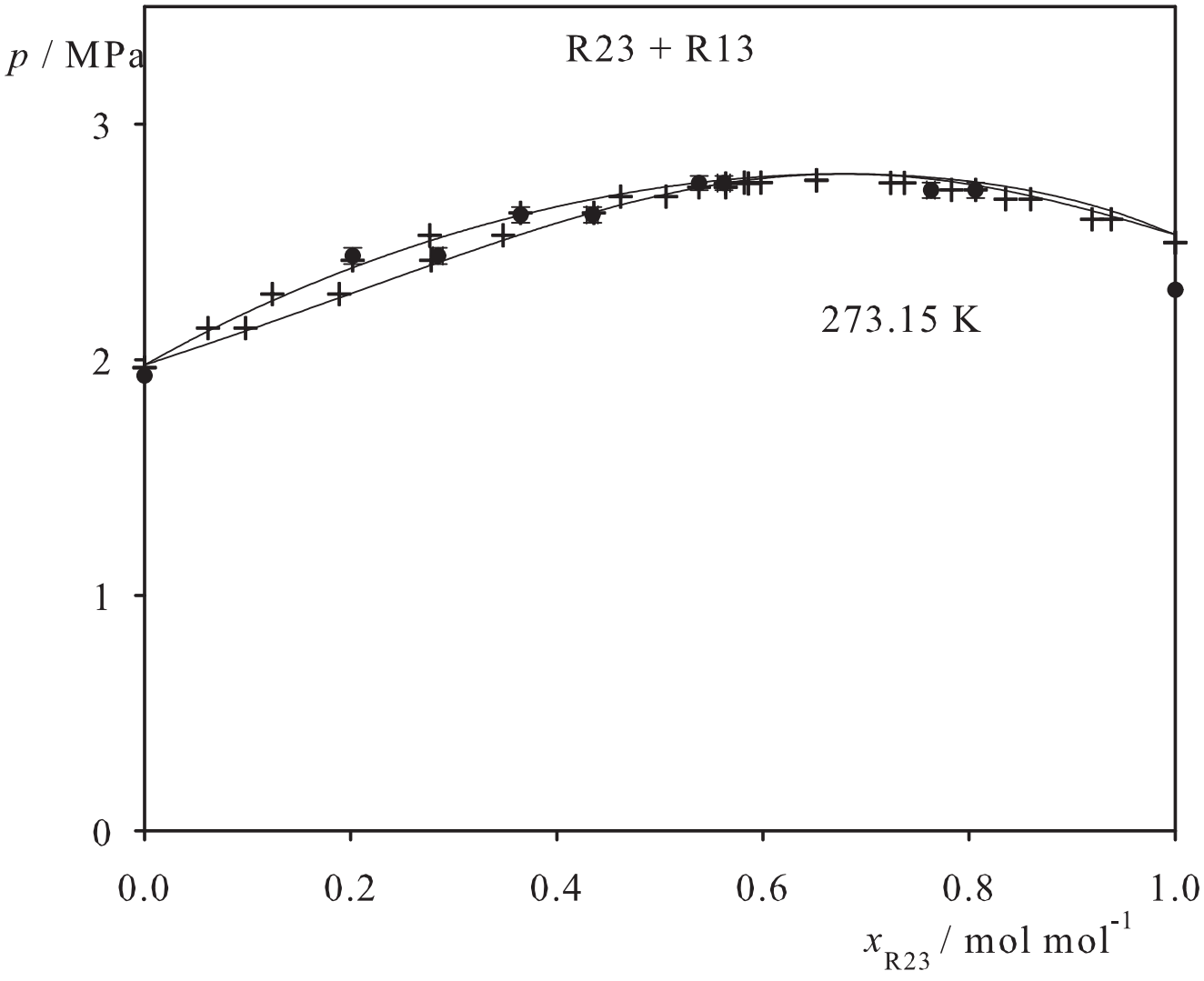

Fig. 172. Binary vapor-liquid equilibrium phase diagram: simulation data ●, experimental data + (cf. Table 2 of the manuscript for the reference) and Peng-Robinson equation of state —.

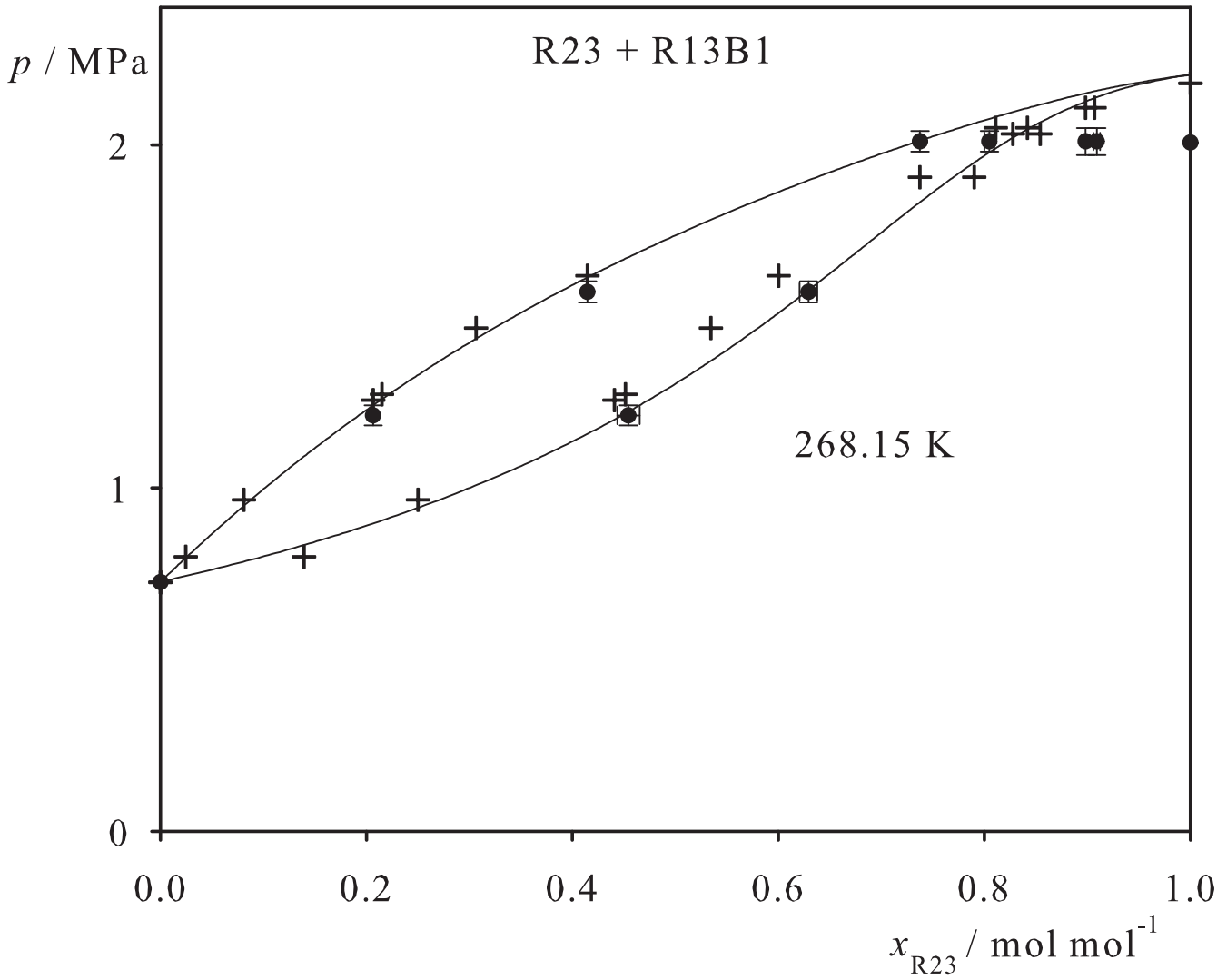

Fig. 173. Binary vapor-liquid equilibrium phase diagram: simulation data ●, experimental data + (cf. Table 2 of the manuscript for the reference) and Peng-Robinson equation of state —.

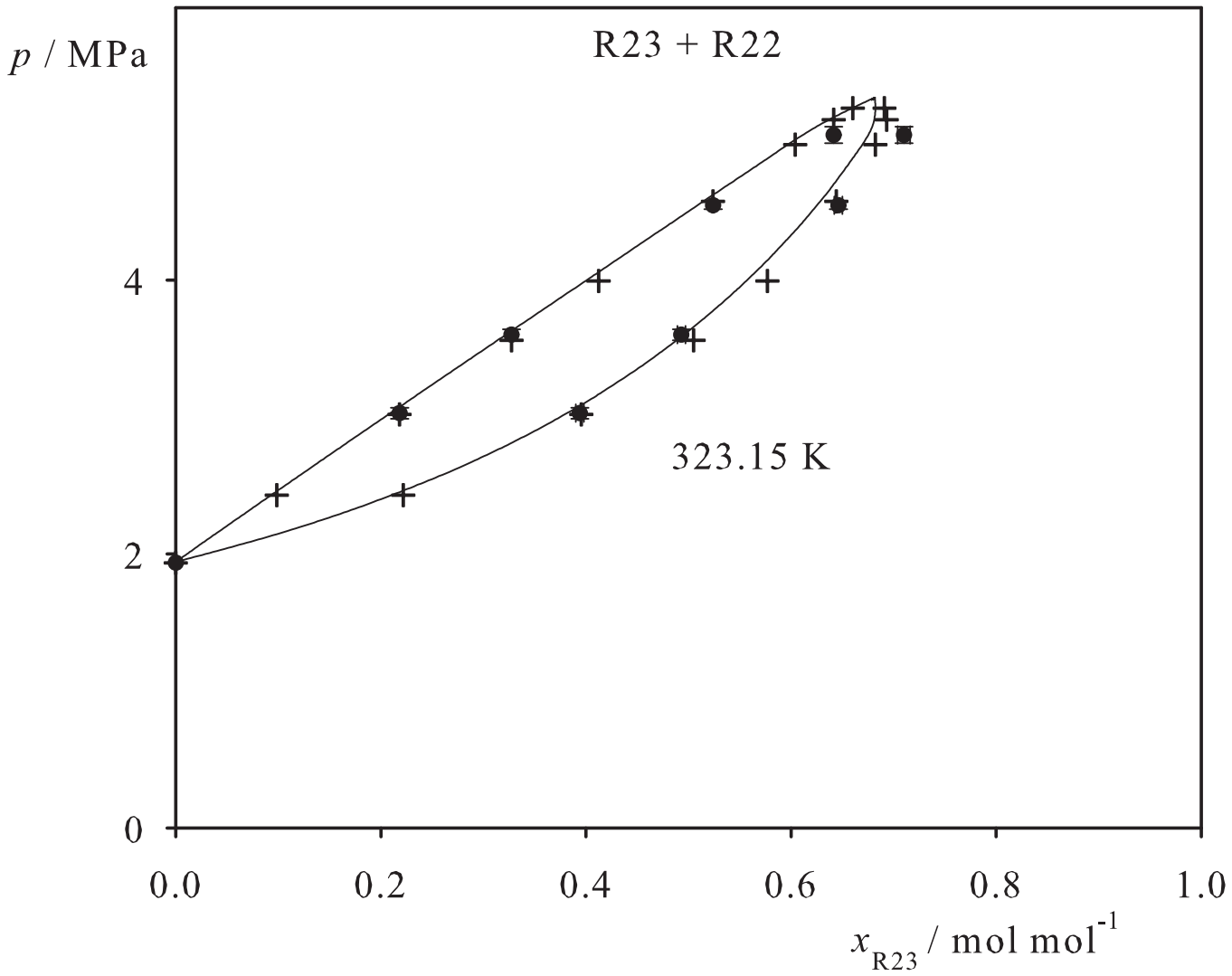

Fig. 174. Binary vapor-liquid equilibrium phase diagram: simulation data ●, experimental data + (cf. Table 2 of the manuscript for the reference) and Peng-Robinson equation of state —.

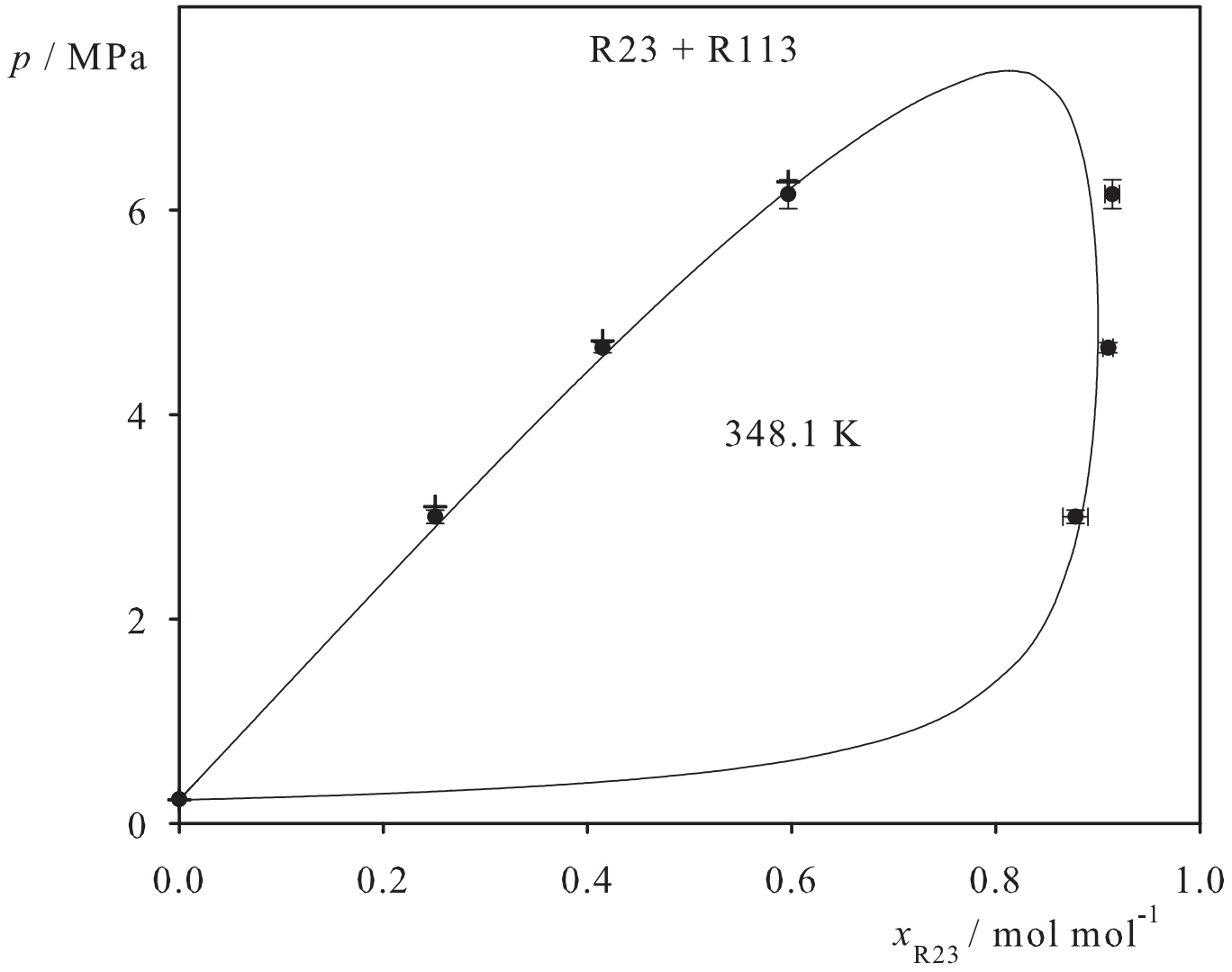

Fig. 175. Binary vapor-liquid equilibrium phase diagram: simulation data ●, experimental data + (cf. Table 2 of the manuscript for the reference) and Peng-Robinson equation of state —.

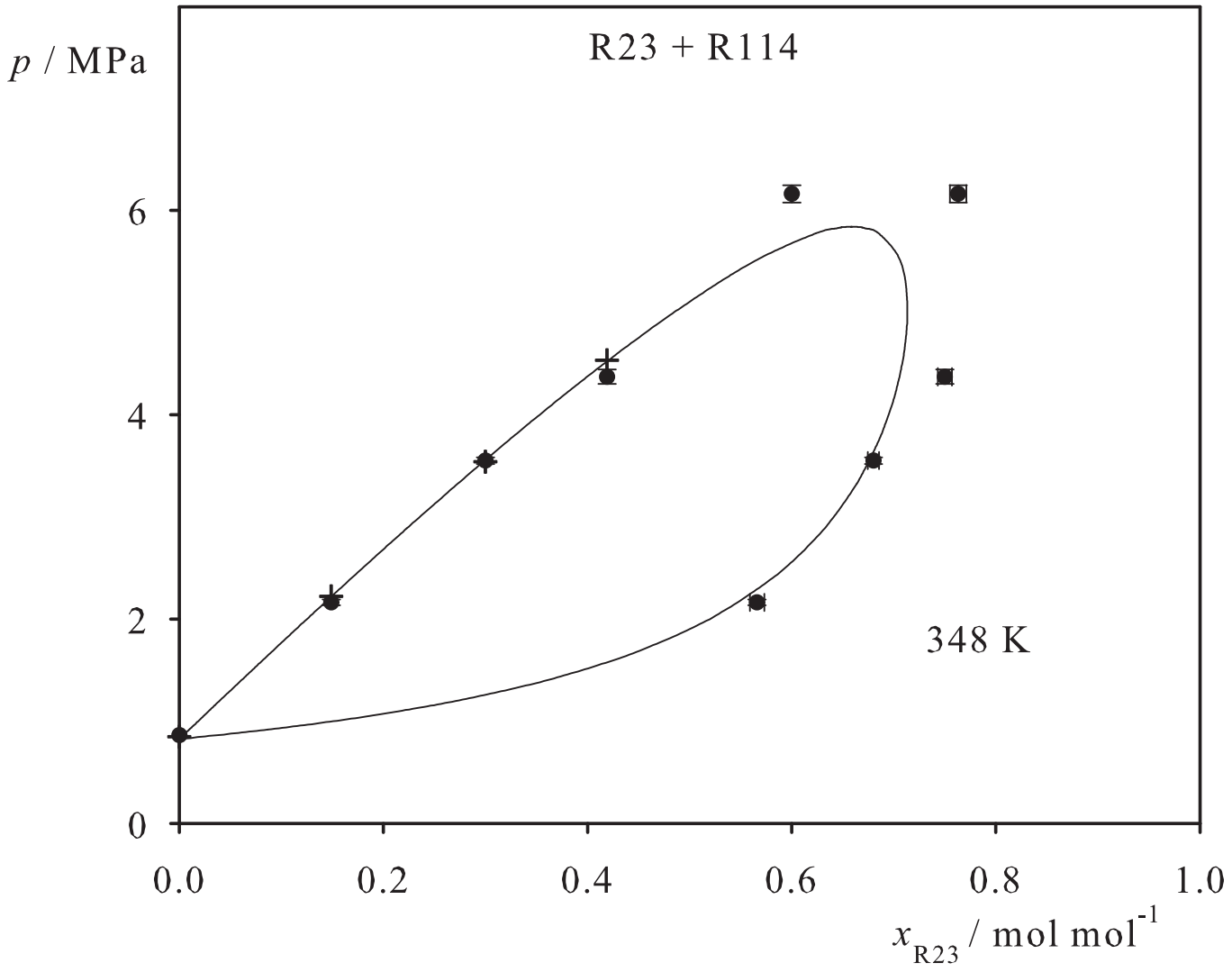

Fig. 176. Binary vapor-liquid equilibrium phase diagram: simulation data ●, experimental data + (cf. Table 2 of the manuscript for the reference) and Peng-Robinson equation of state —.

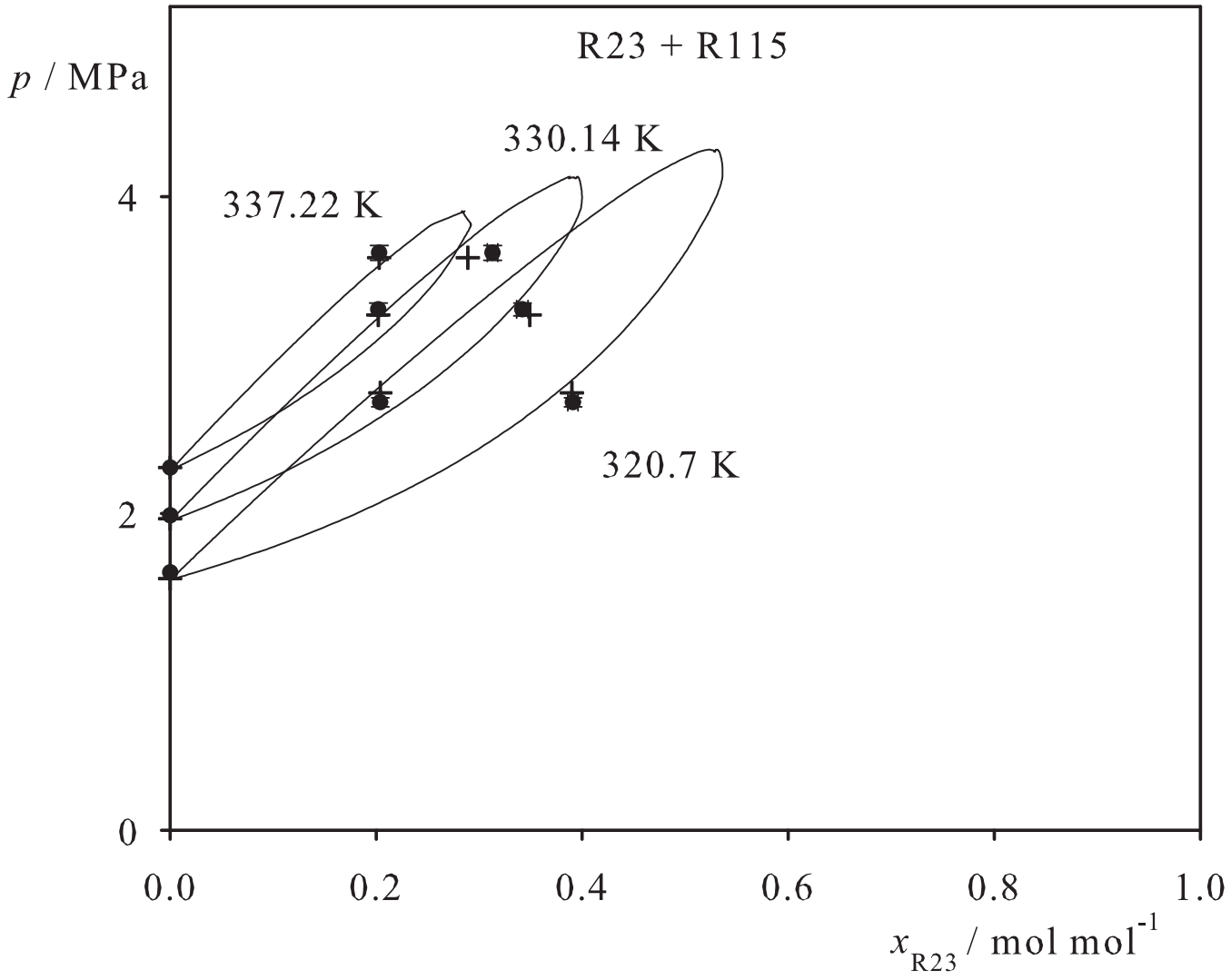

Fig. 177. Binary vapor-liquid equilibrium phase diagram: simulation data ●, experimental data + (cf. Table 2 of the manuscript for the reference) and Peng-Robinson equation of state —.

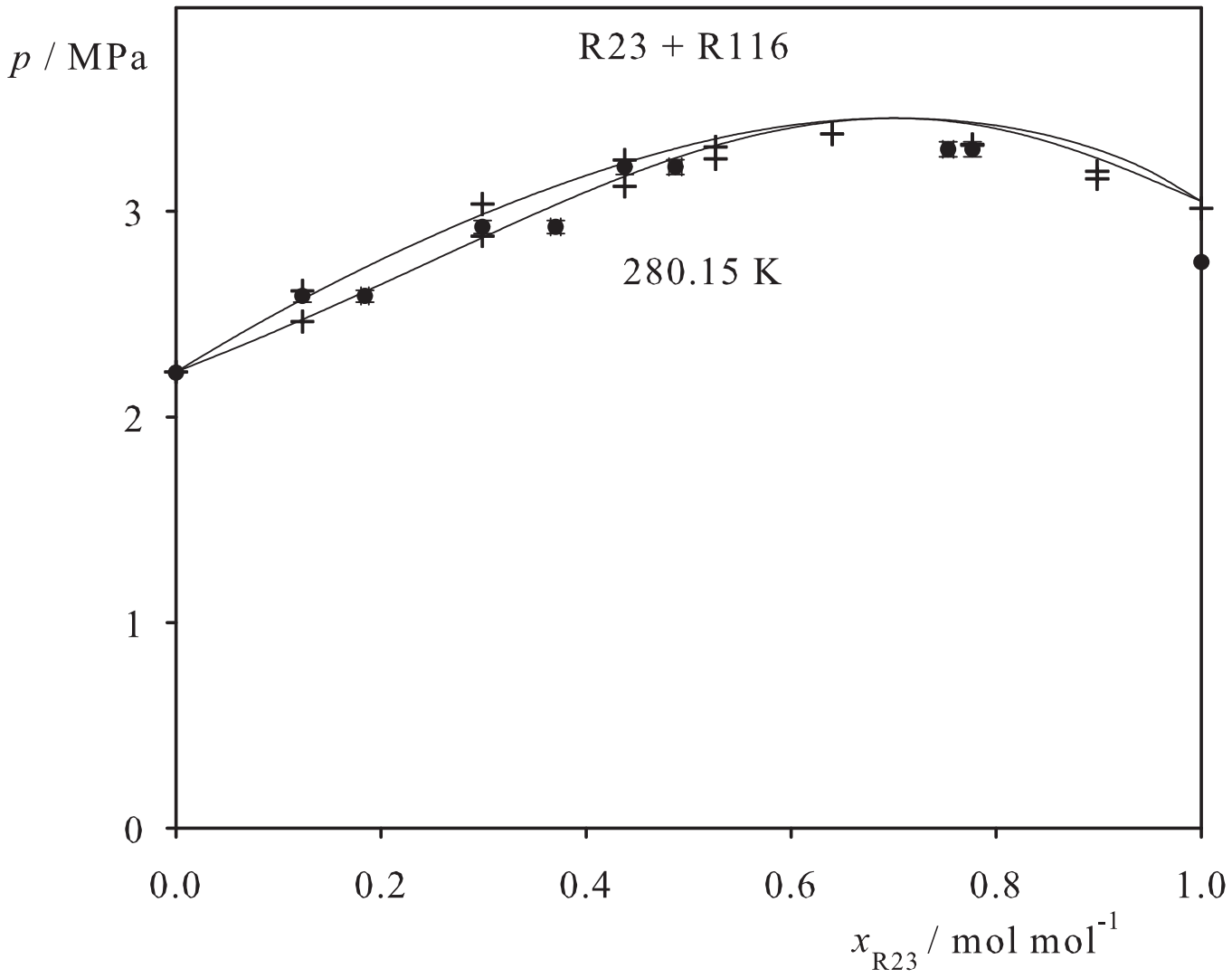

Fig. 178. Binary vapor-liquid equilibrium phase diagram: simulation data ●, experimental data + (cf. Table 2 of the manuscript for the reference) and Peng-Robinson equation of state —.

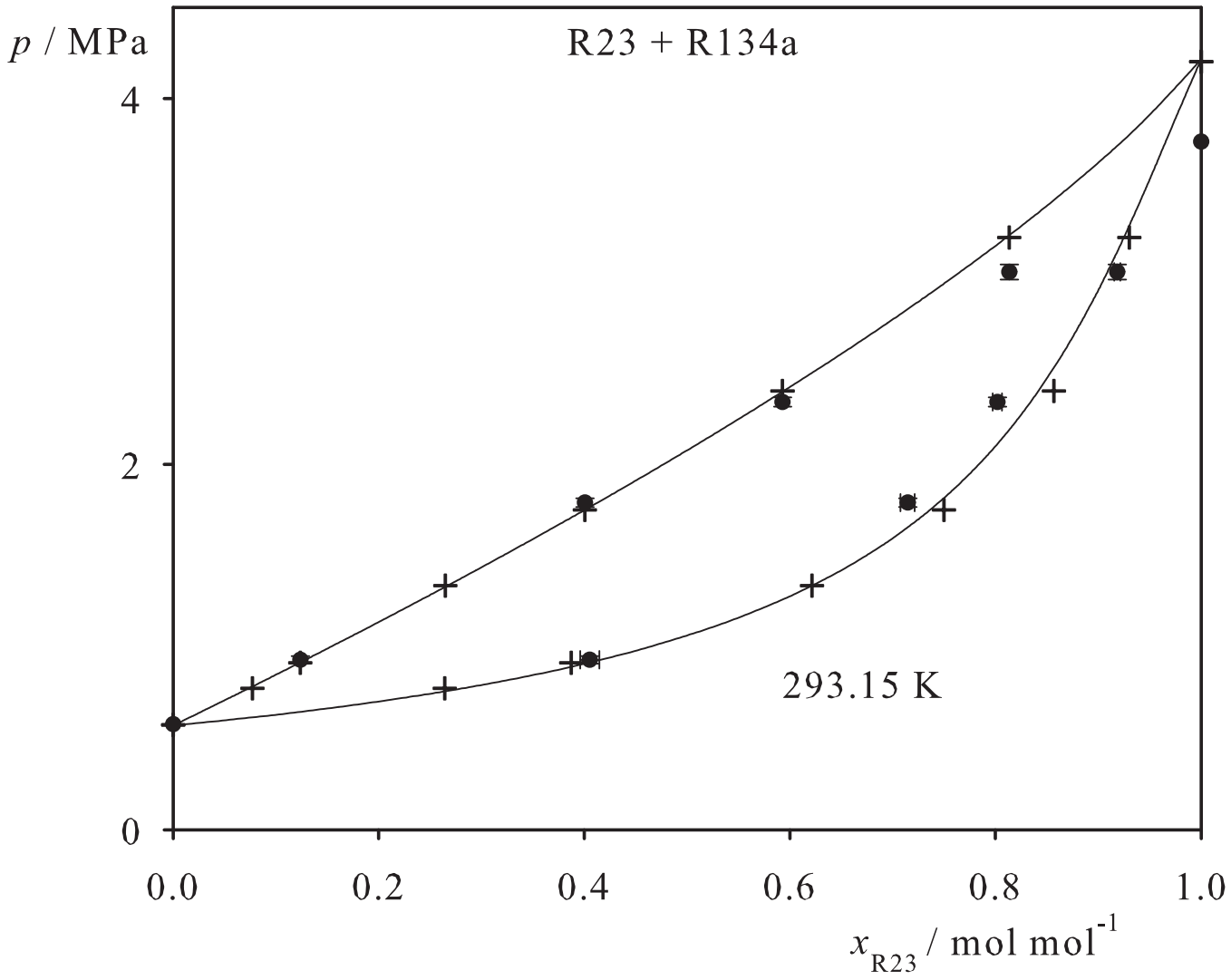

Fig. 179. Binary vapor-liquid equilibrium phase diagram: simulation data ●, experimental data + (cf. Table 2 of the manuscript for the reference) and Peng-Robinson equation of state —.

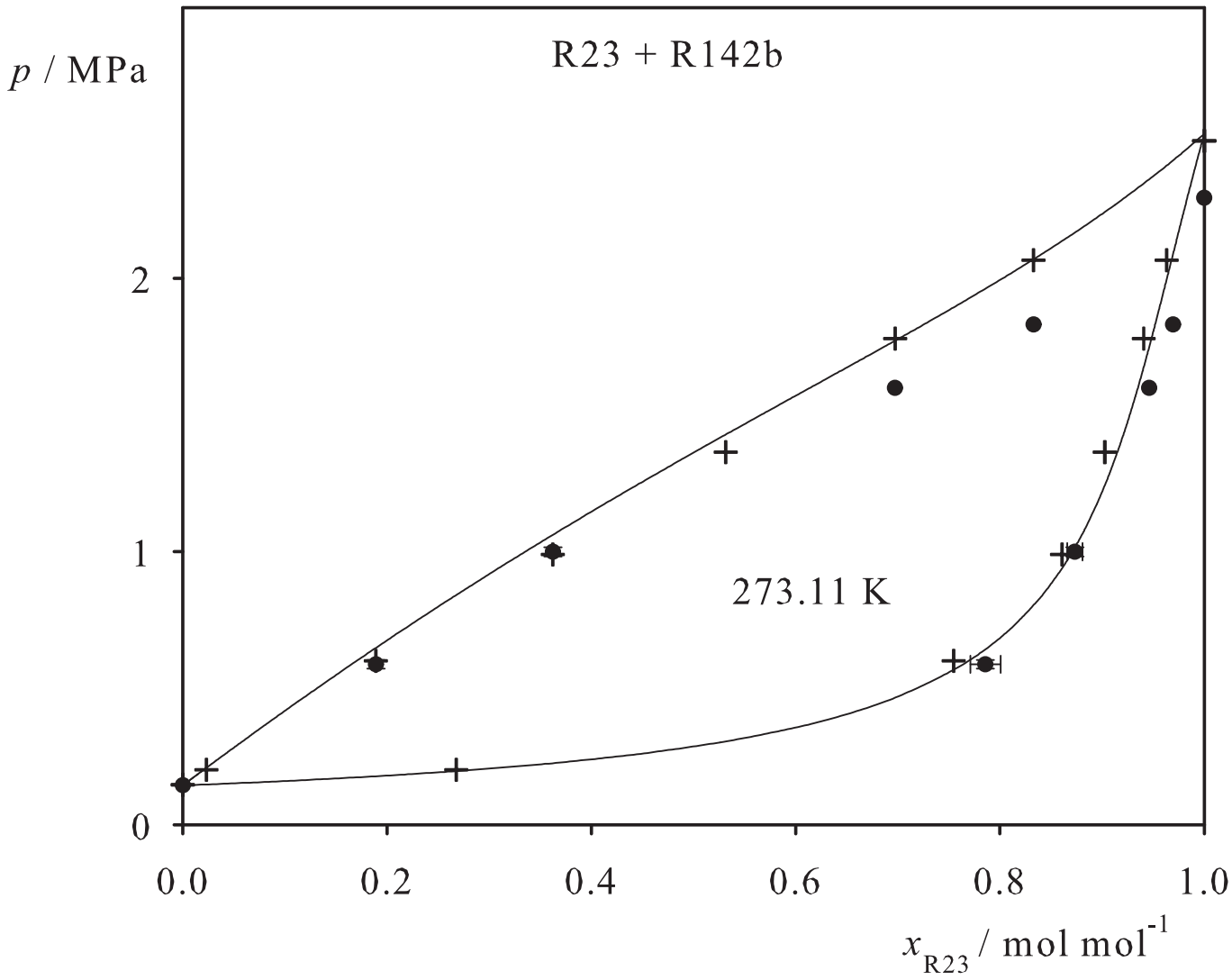

Fig. 180. Binary vapor-liquid equilibrium phase diagram: simulation data ●, experimental data + (cf. Table 2 of the manuscript for the reference) and Peng-Robinson equation of state —.

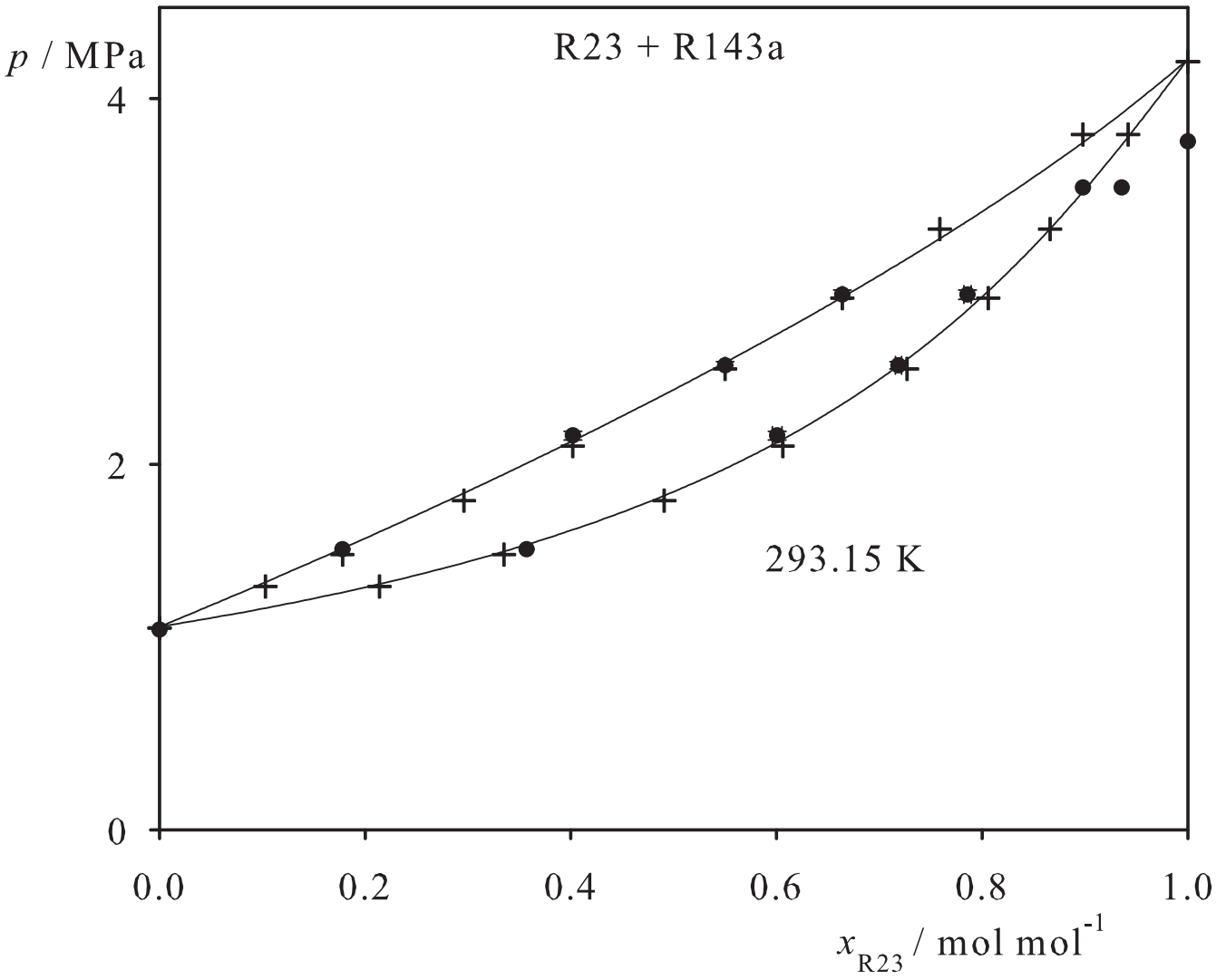

Fig. 181. Binary vapor-liquid equilibrium phase diagram: simulation data ●, experimental data + (cf. Table 2 of the manuscript for the reference) and Peng-Robinson equation of state —.

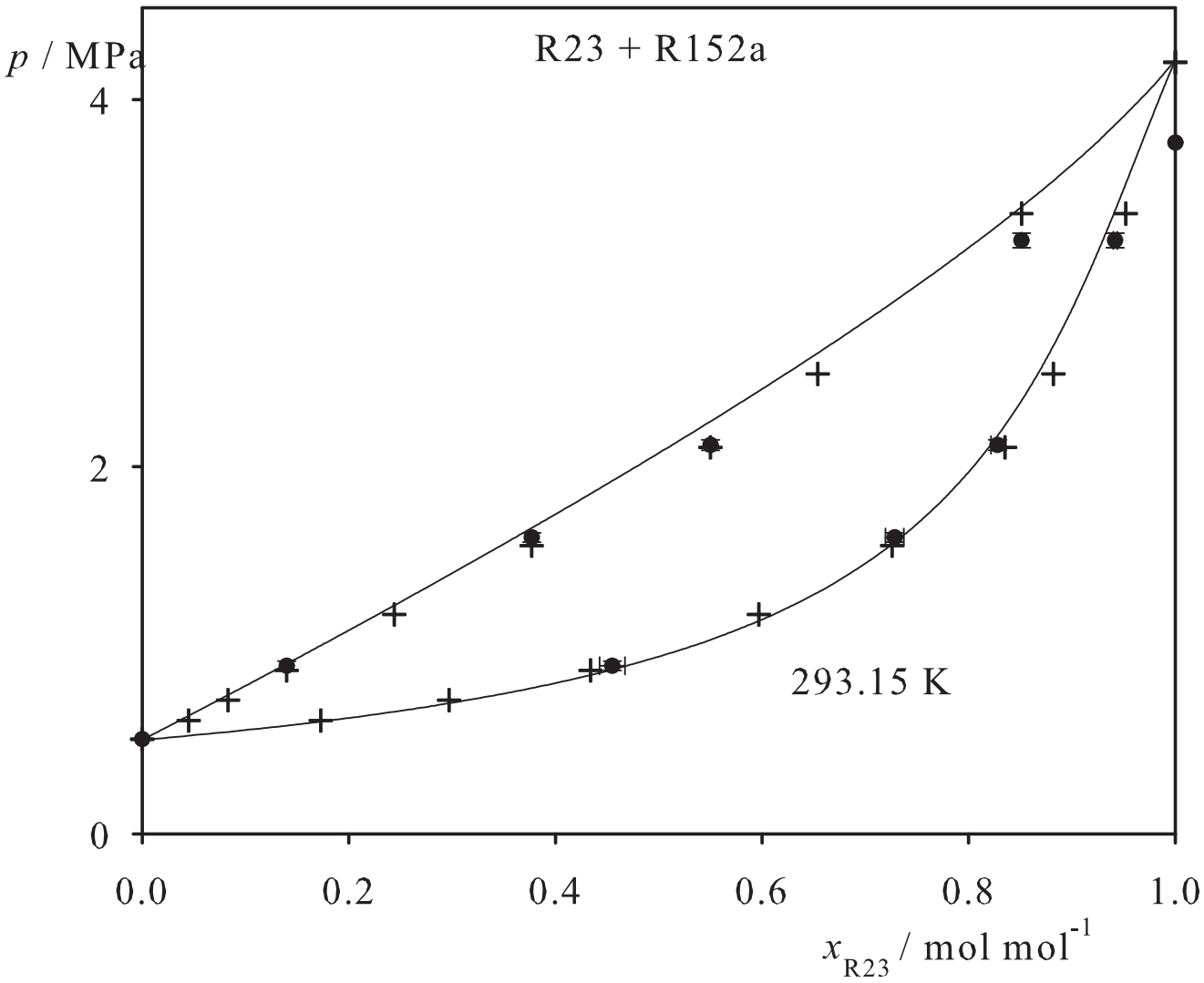

Fig. 182. Binary vapor-liquid equilibrium phase diagram: simulation data ●, experimental data + (cf. Table 2 of the manuscript for the reference) and Peng-Robinson equation of state —.

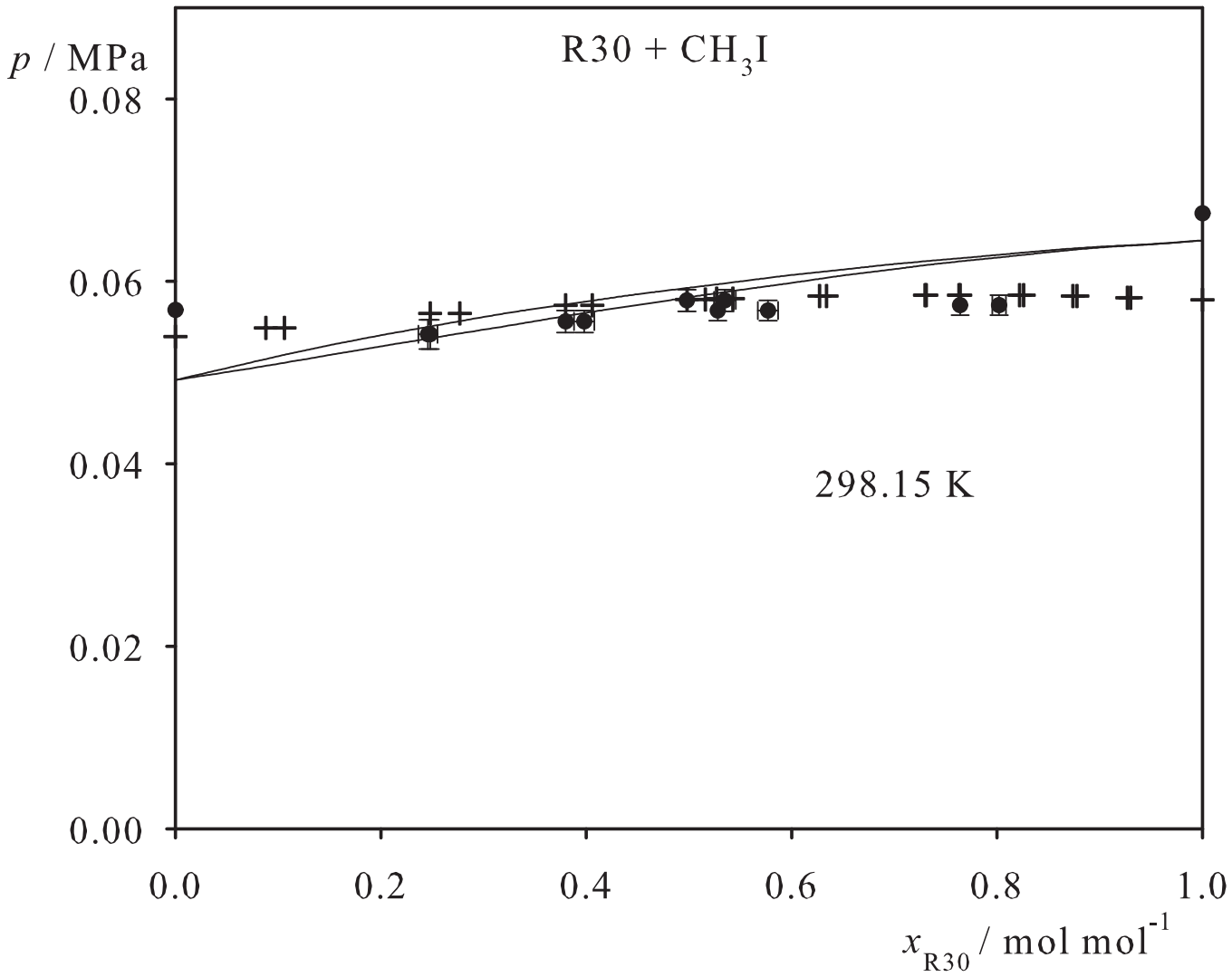

Fig. 183. Binary vapor-liquid equilibrium phase diagram: simulation data ●, experimental data + (cf. Table 2 of the manuscript for the reference) and Peng-Robinson equation of state —.

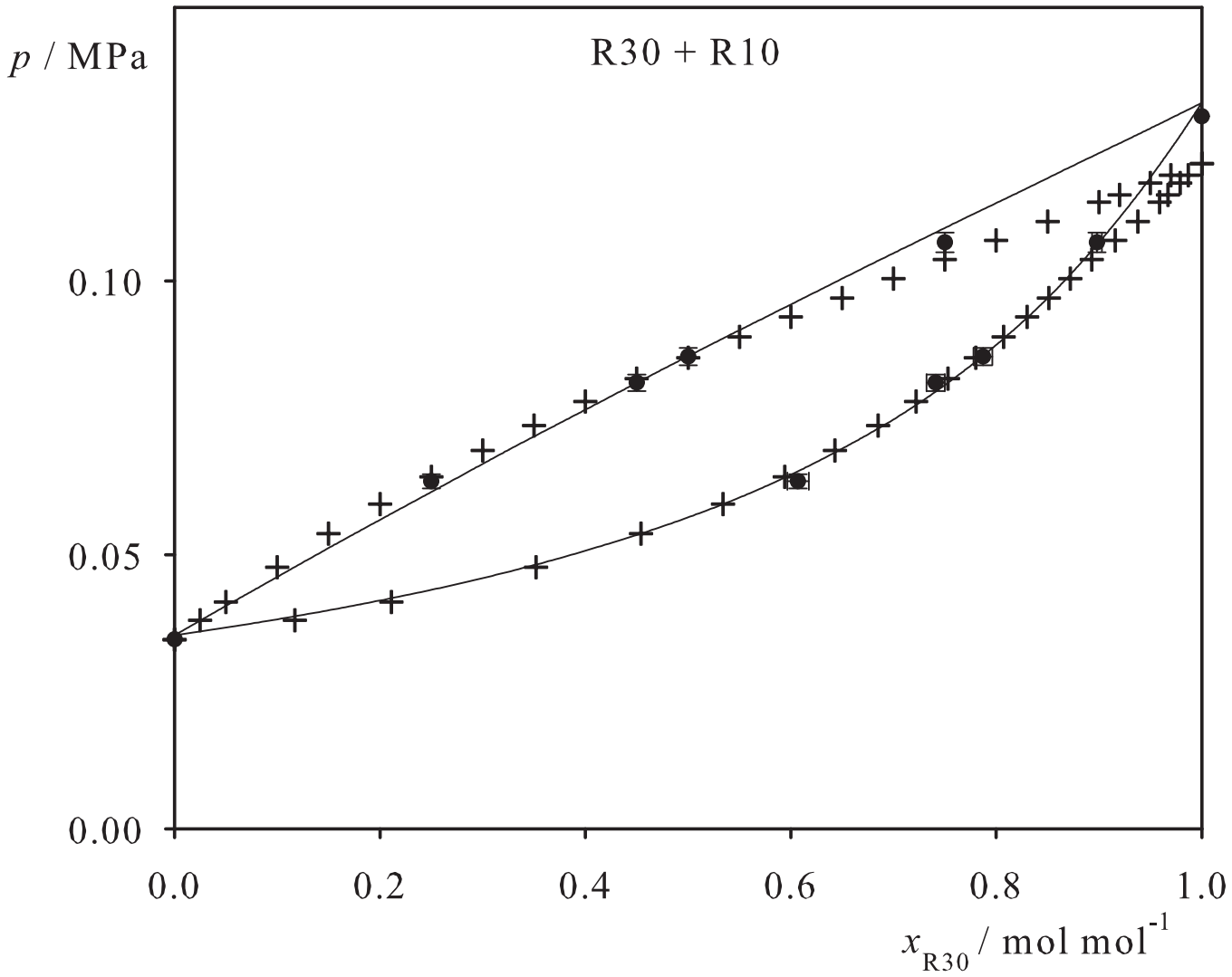

Fig. 184. Binary vapor-liquid equilibrium phase diagram: simulation data ●, experimental data + (cf. Table 2 of the manuscript for the reference) and Peng-Robinson equation of state —.

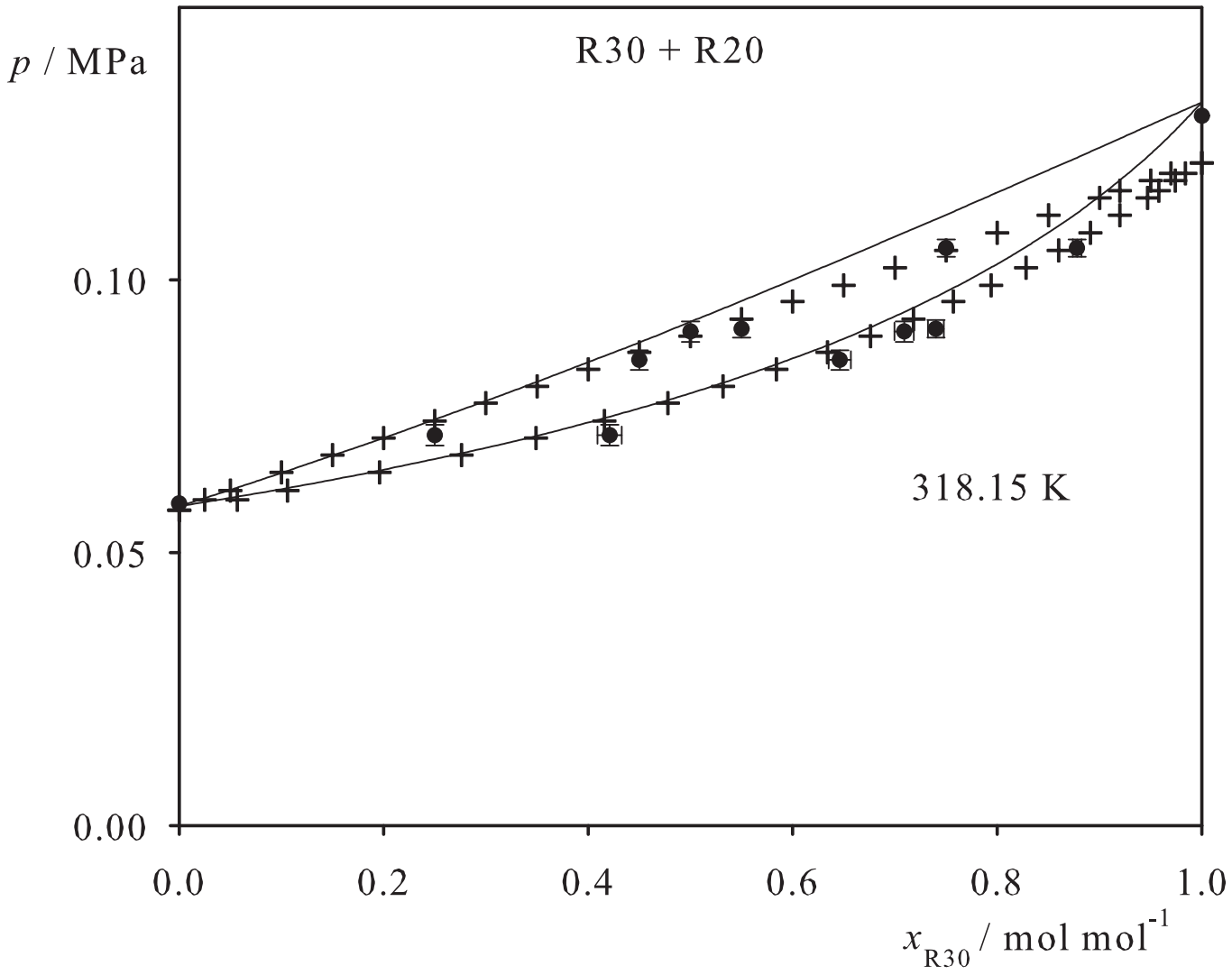

Fig. 185. Binary vapor-liquid equilibrium phase diagram: simulation data ●, experimental data + (cf. Table 2 of the manuscript for the reference) and Peng-Robinson equation of state —.

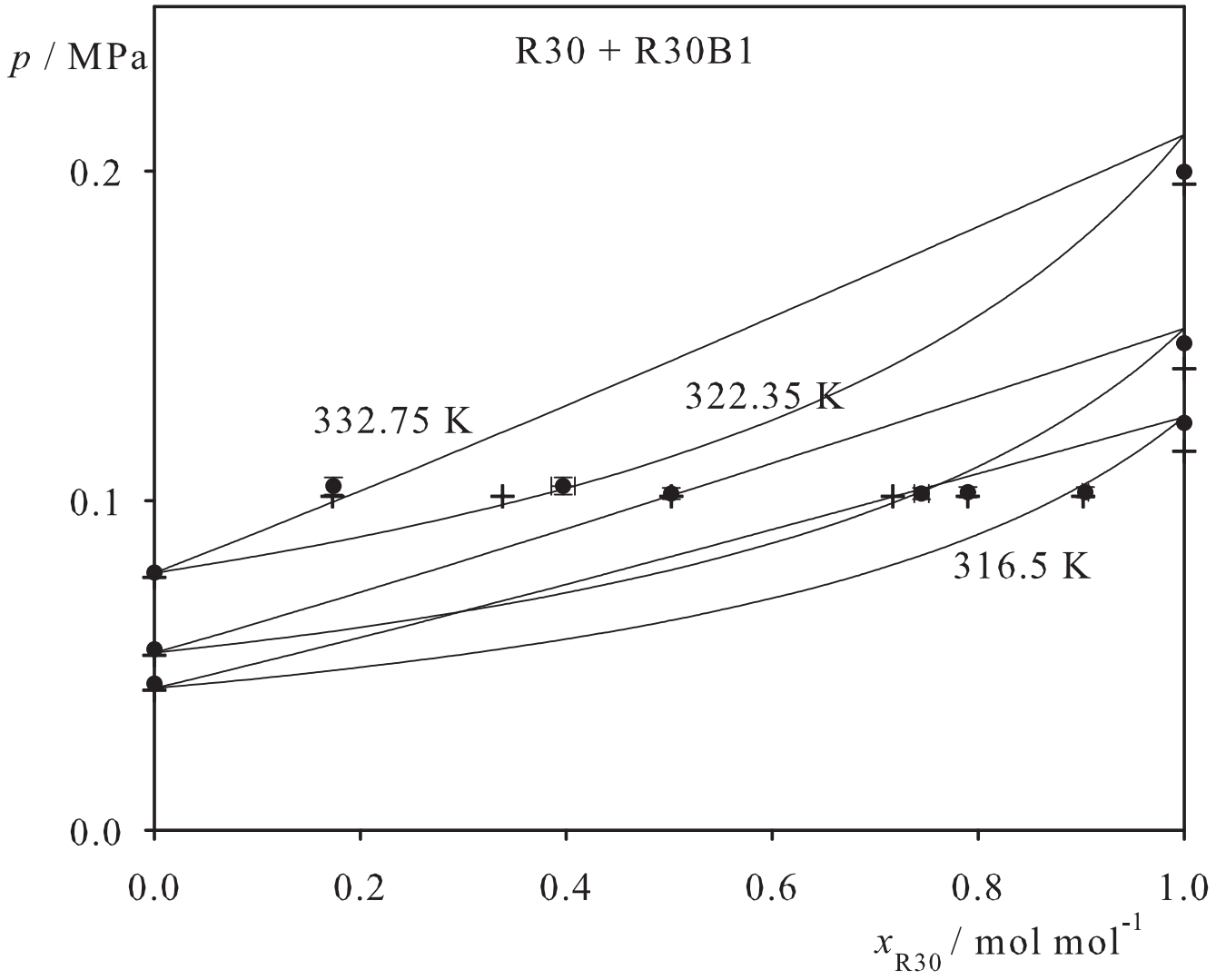

Fig. 186. Binary vapor-liquid equilibrium phase diagram: simulation data ●, experimental data + (cf. Table 2 of the manuscript for the reference) and Peng-Robinson equation of state —.

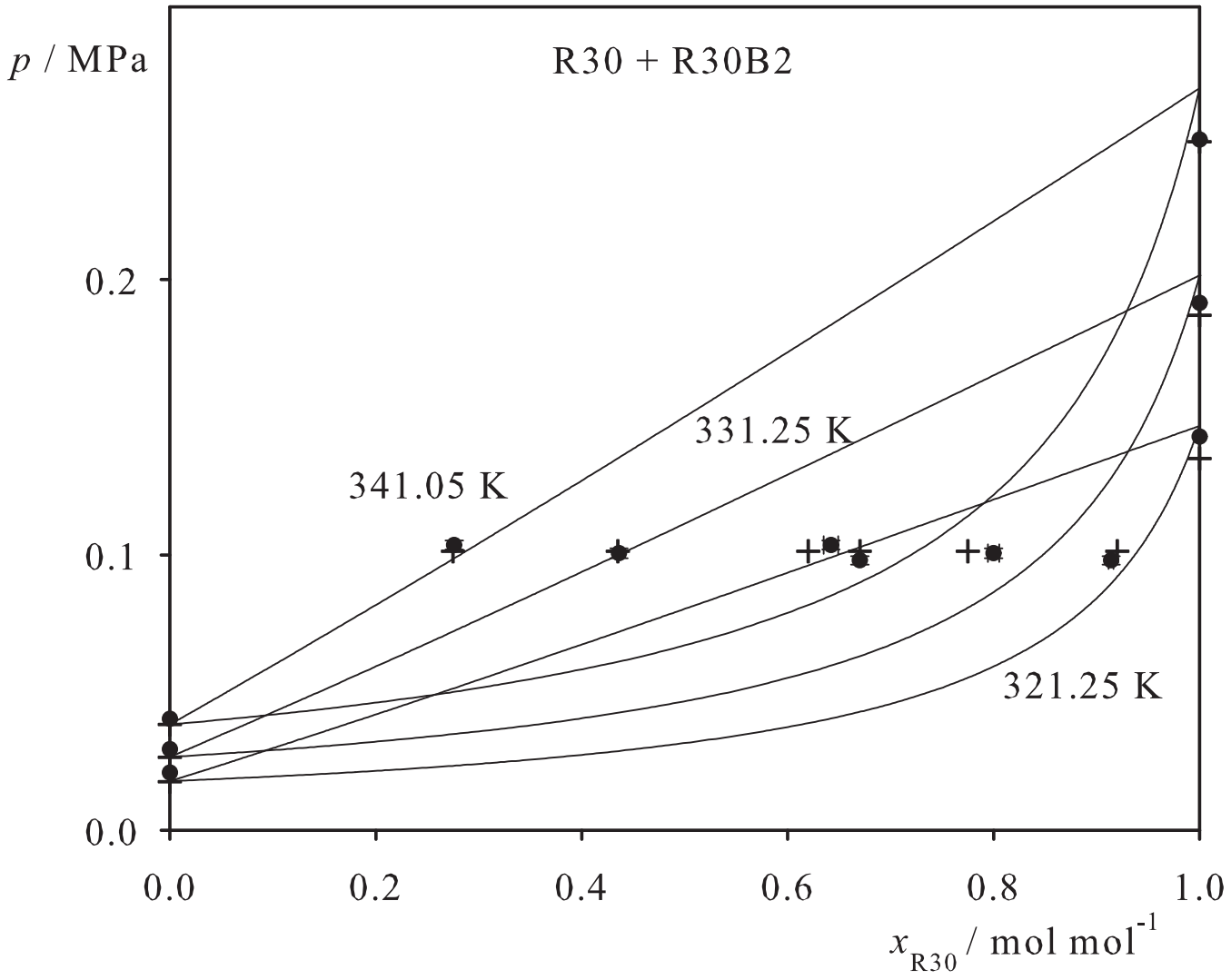

Fig. 187. Binary vapor-liquid equilibrium phase diagram: simulation data ●, experimental data + (cf. Table 2 of the manuscript for the reference) and Peng-Robinson equation of state —.

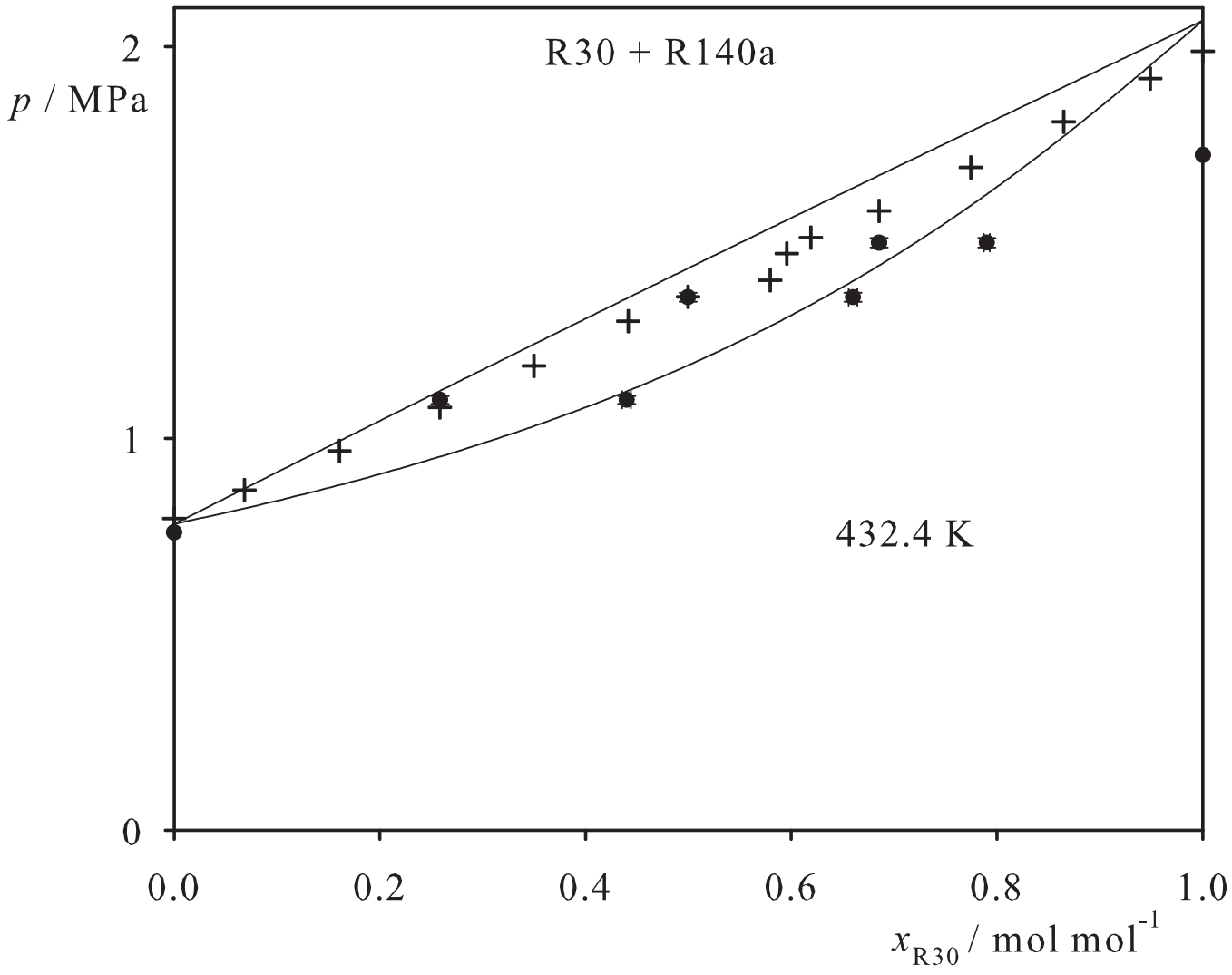

Fig. 188. Binary vapor-liquid equilibrium phase diagram: simulation data ●, experimental data + (cf. Table 2 of the manuscript for the reference) and Peng-Robinson equation of state —.

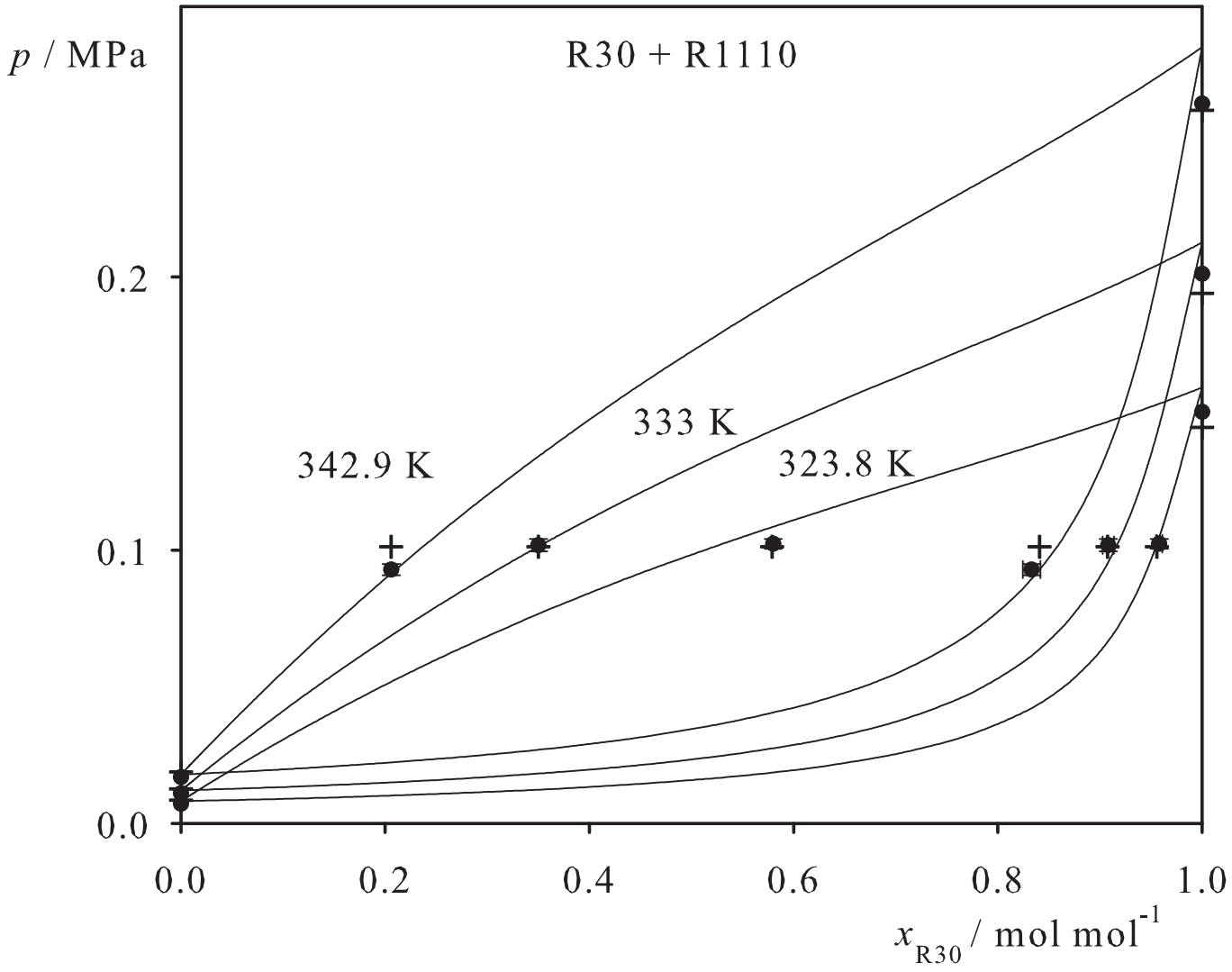

Fig. 189. Binary vapor-liquid equilibrium phase diagram: simulation data ●, experimental data + (cf. Table 2 of the manuscript for the reference) and Peng-Robinson equation of state —.

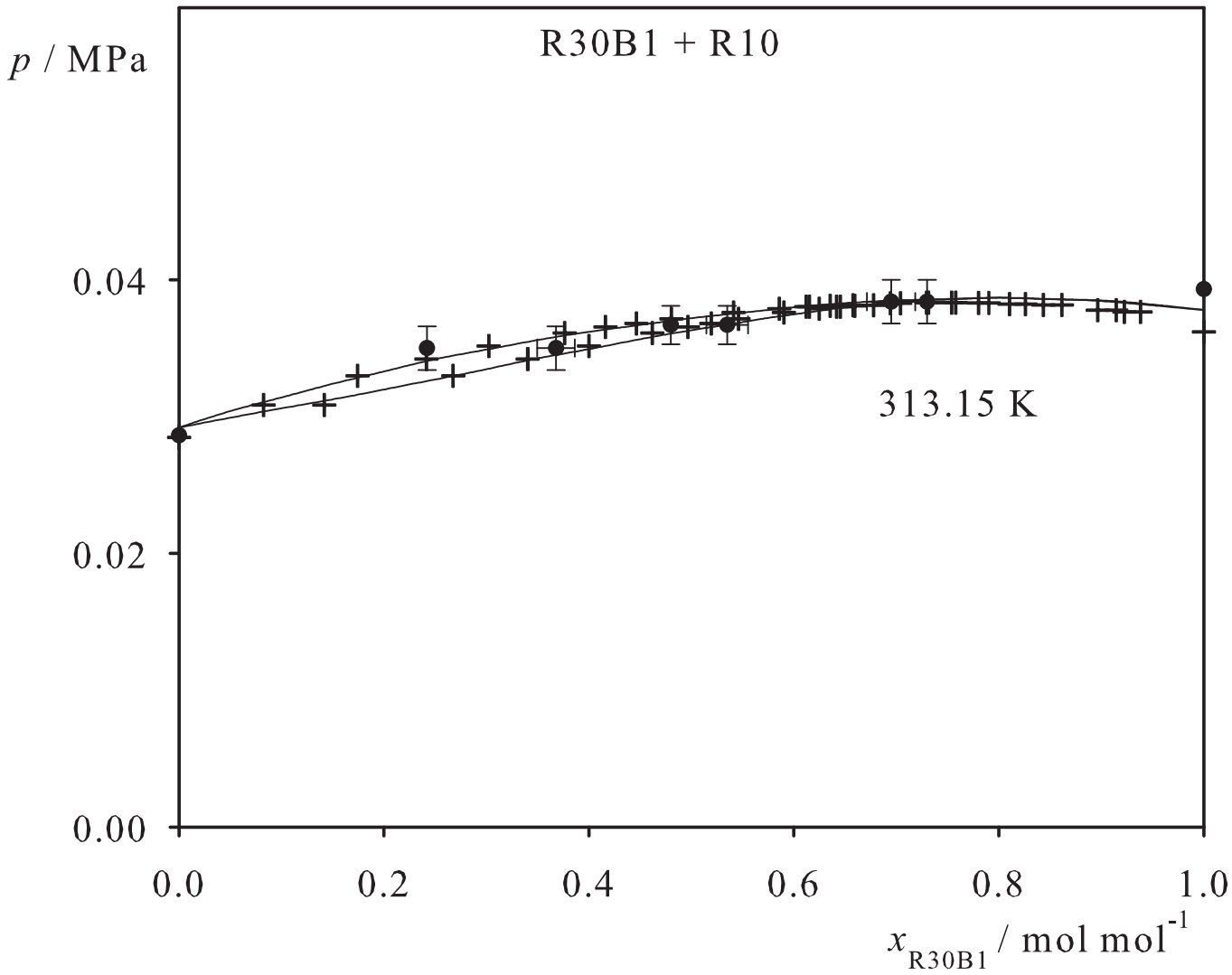

Fig. 190. Binary vapor-liquid equilibrium phase diagram: simulation data ●, experimental data + (cf. Table 2 of the manuscript for the reference) and Peng-Robinson equation of state —.

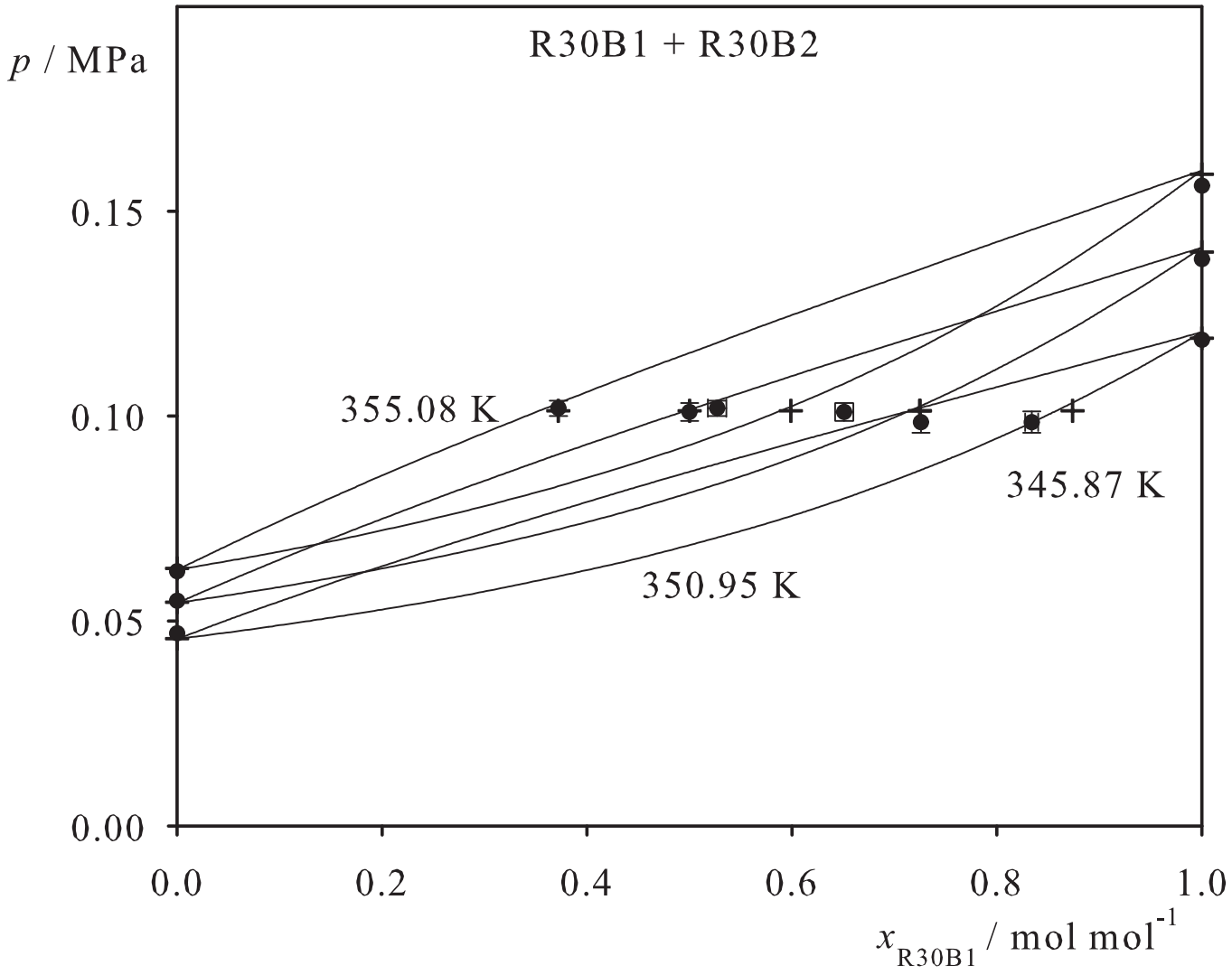

Fig. 191. Binary vapor-liquid equilibrium phase diagram: simulation data ●, experimental data + (cf. Table 2 of the manuscript for the reference) and Peng-Robinson equation of state —.

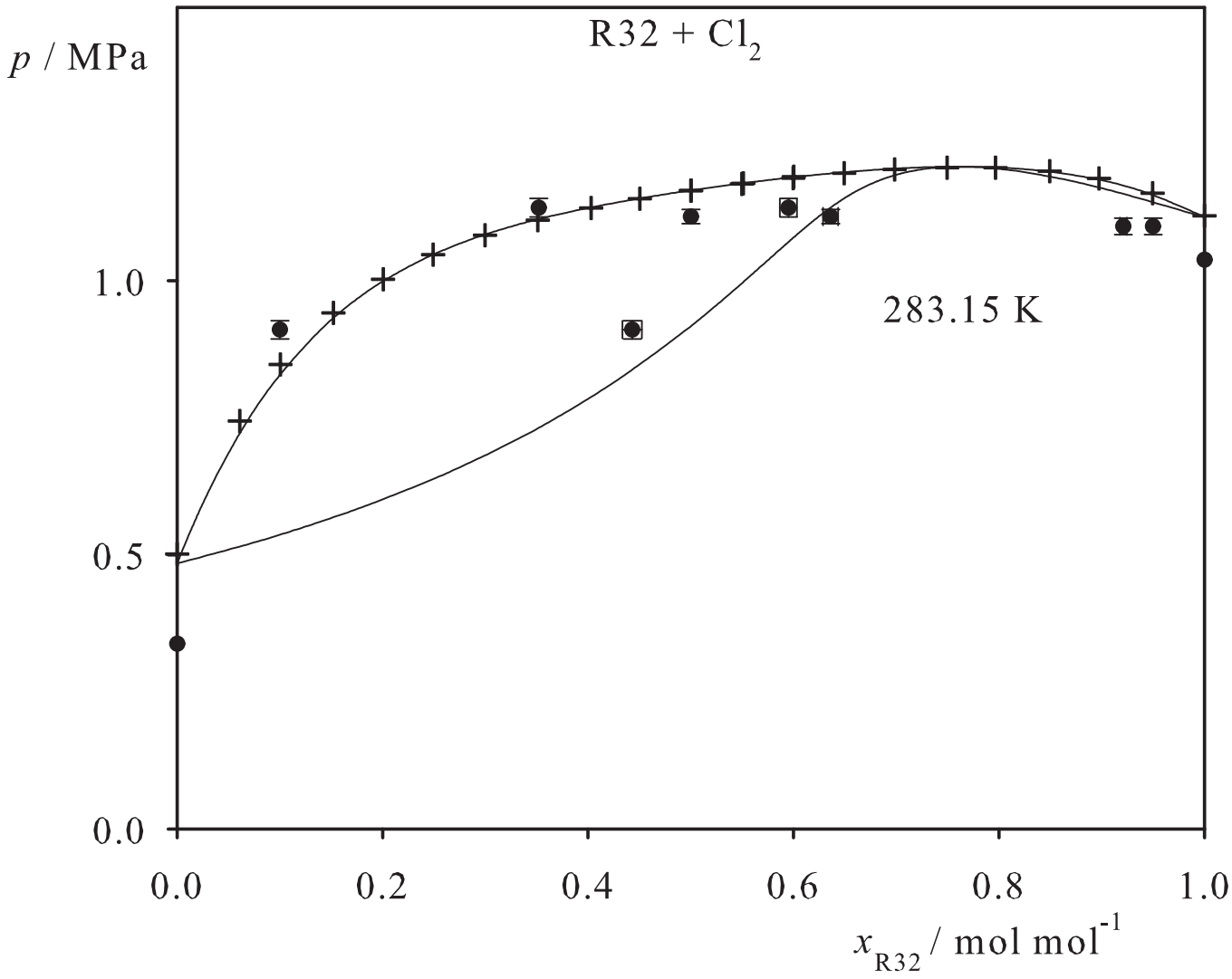

Fig. 192. Binary vapor-liquid equilibrium phase diagram: simulation data ●, experimental data + (cf. Table 2 of the manuscript for the reference) and Peng-Robinson equation of state —.

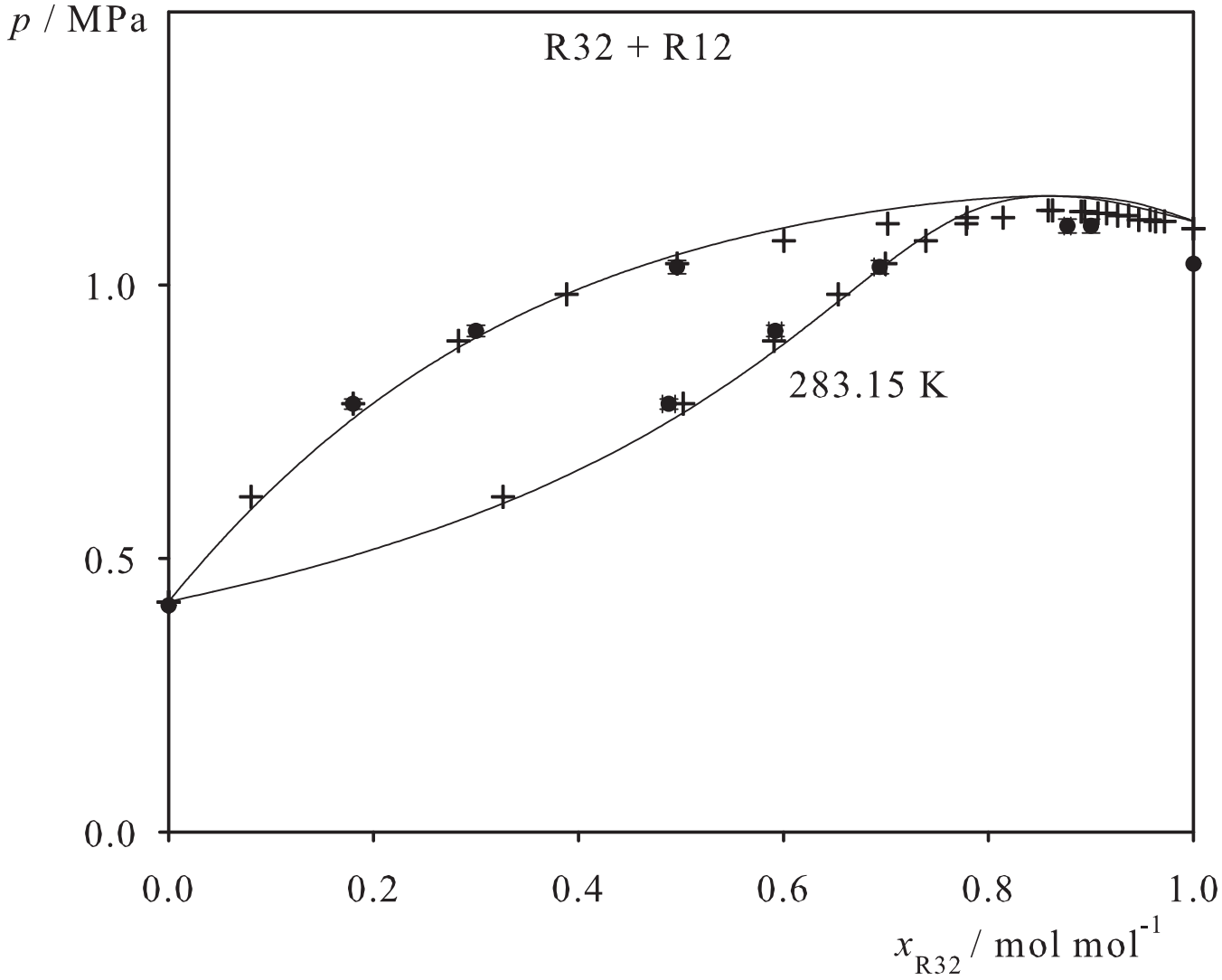

Fig. 193. Binary vapor-liquid equilibrium phase diagram: simulation data ●, experimental data + (cf. Table 2 of the manuscript for the reference) and Peng-Robinson equation of state —.

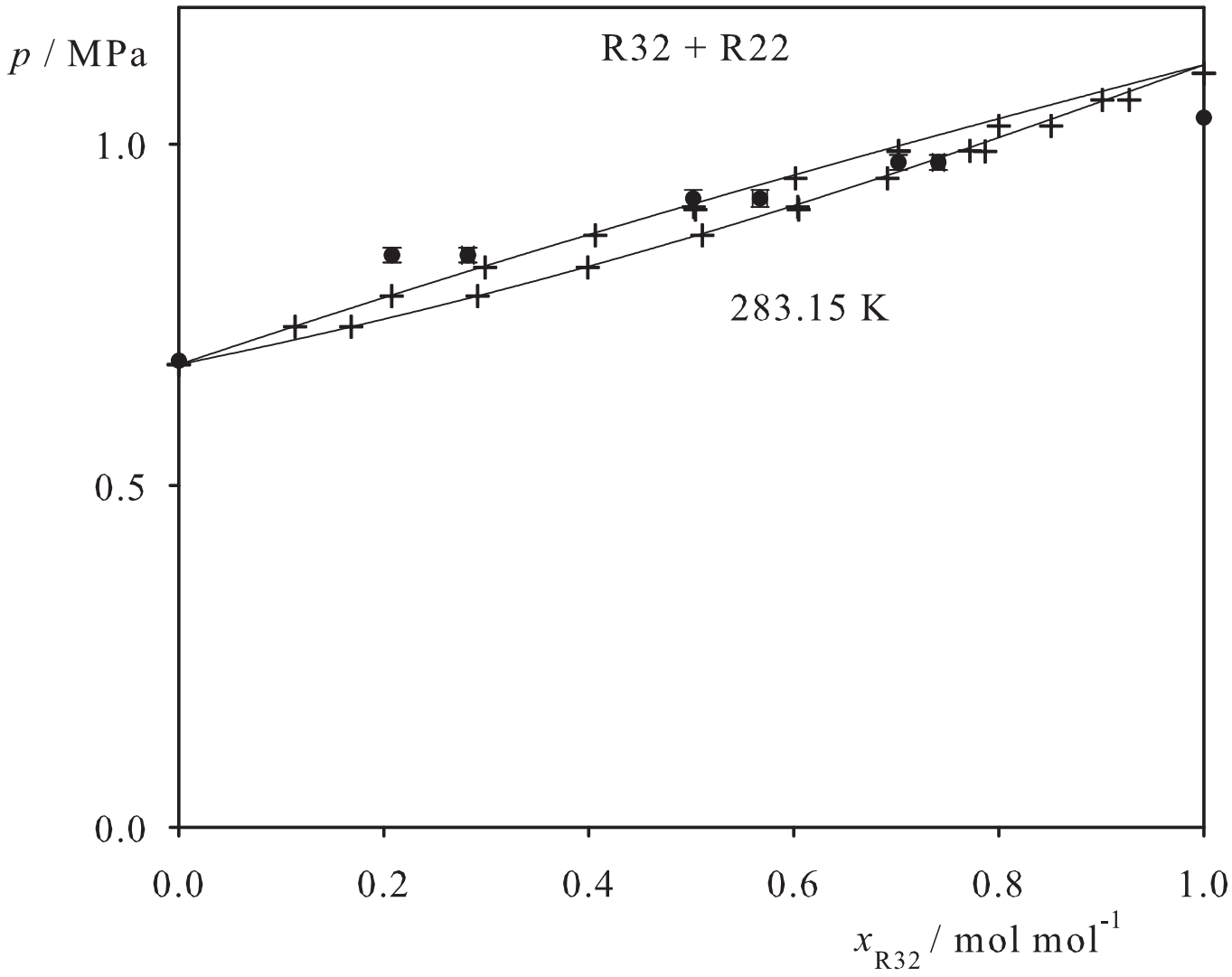

Fig. 194. Binary vapor-liquid equilibrium phase diagram: simulation data ●, experimental data + (cf. Table 2 of the manuscript for the reference) and Peng-Robinson equation of state —.

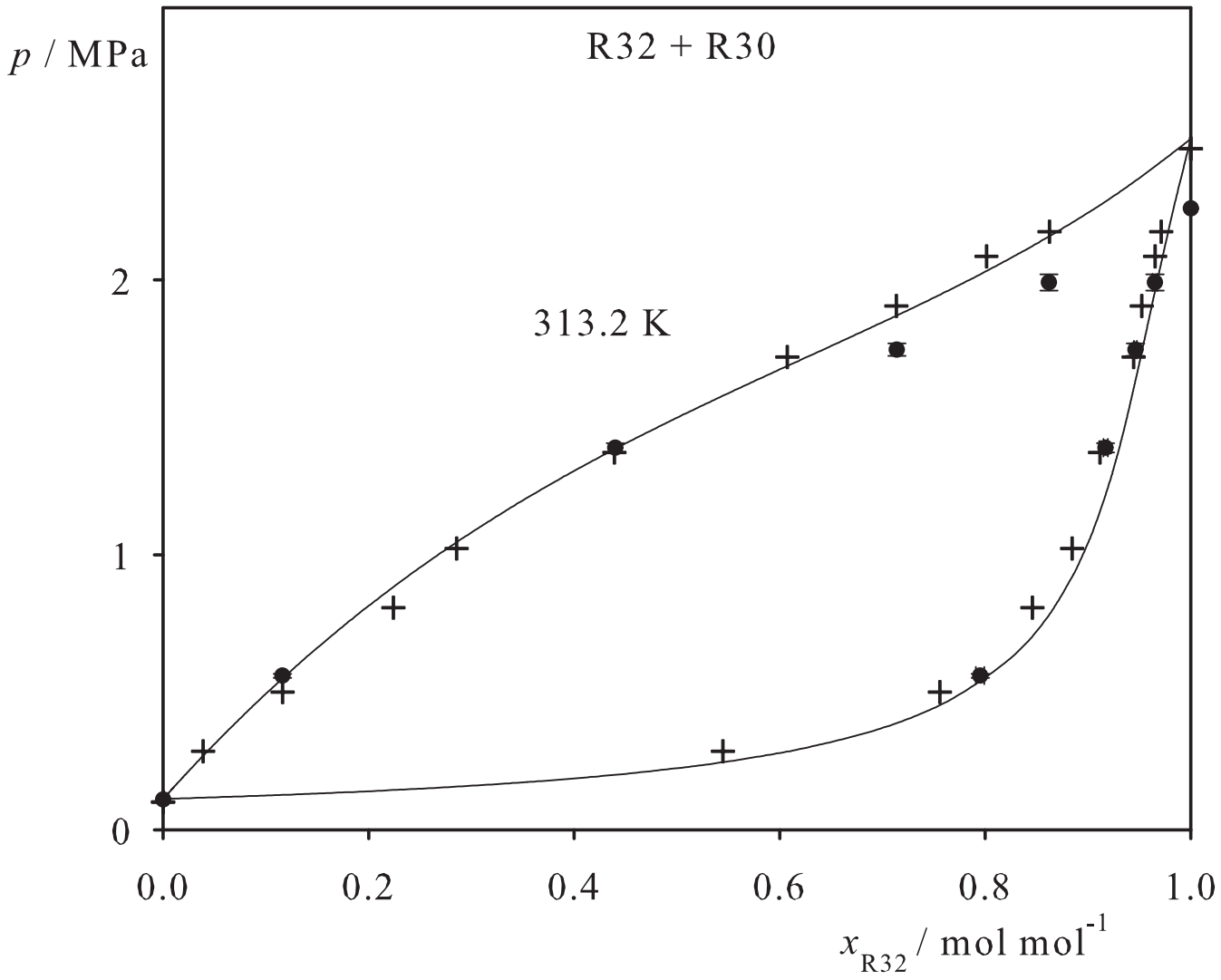

Fig. 195. Binary vapor-liquid equilibrium phase diagram: simulation data ●, experimental data + (cf. Table 2 of the manuscript for the reference) and Peng-Robinson equation of state —.

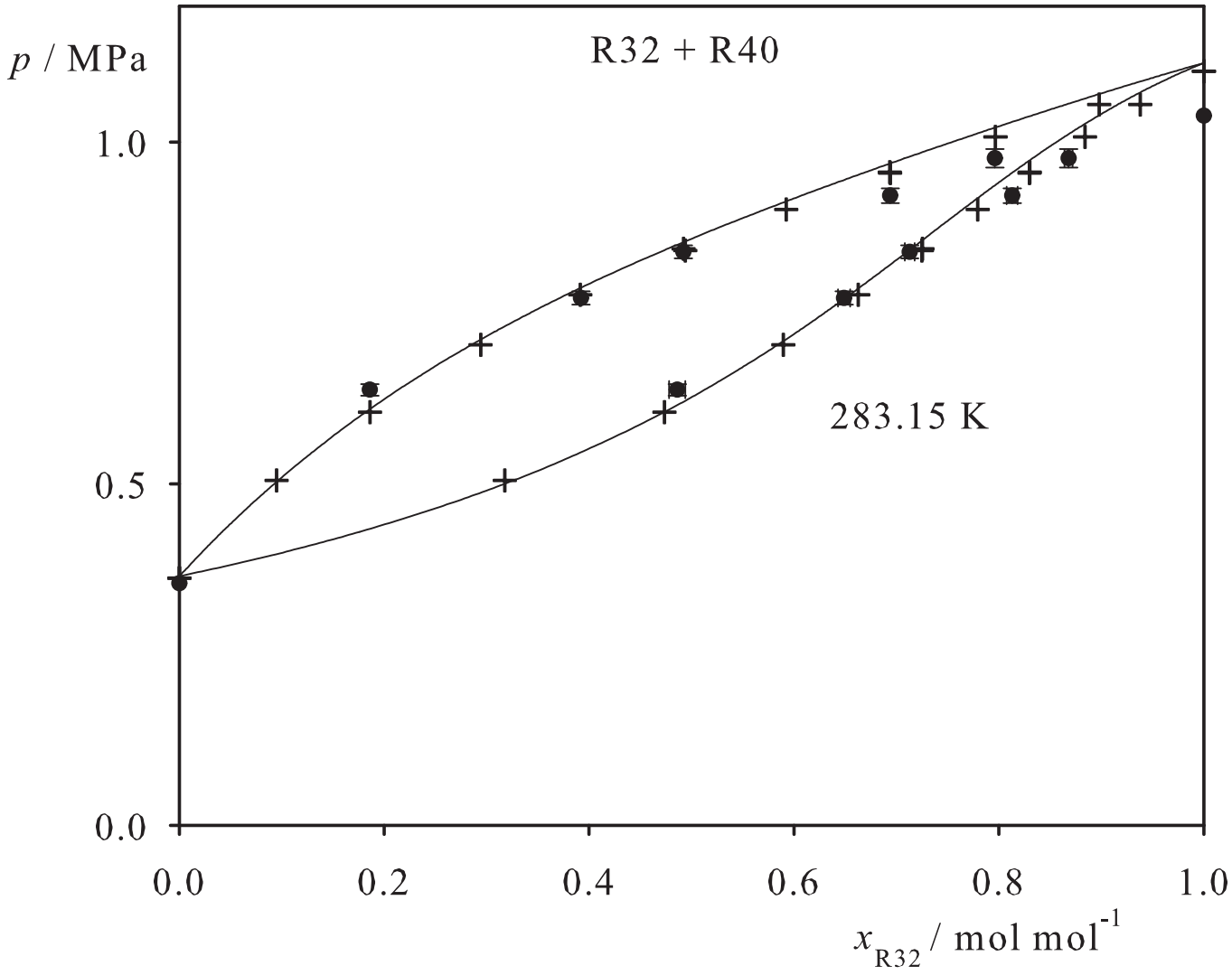

Fig. 196. Binary vapor-liquid equilibrium phase diagram: simulation data ●, experimental data + (cf. Table 2 of the manuscript for the reference) and Peng-Robinson equation of state —.

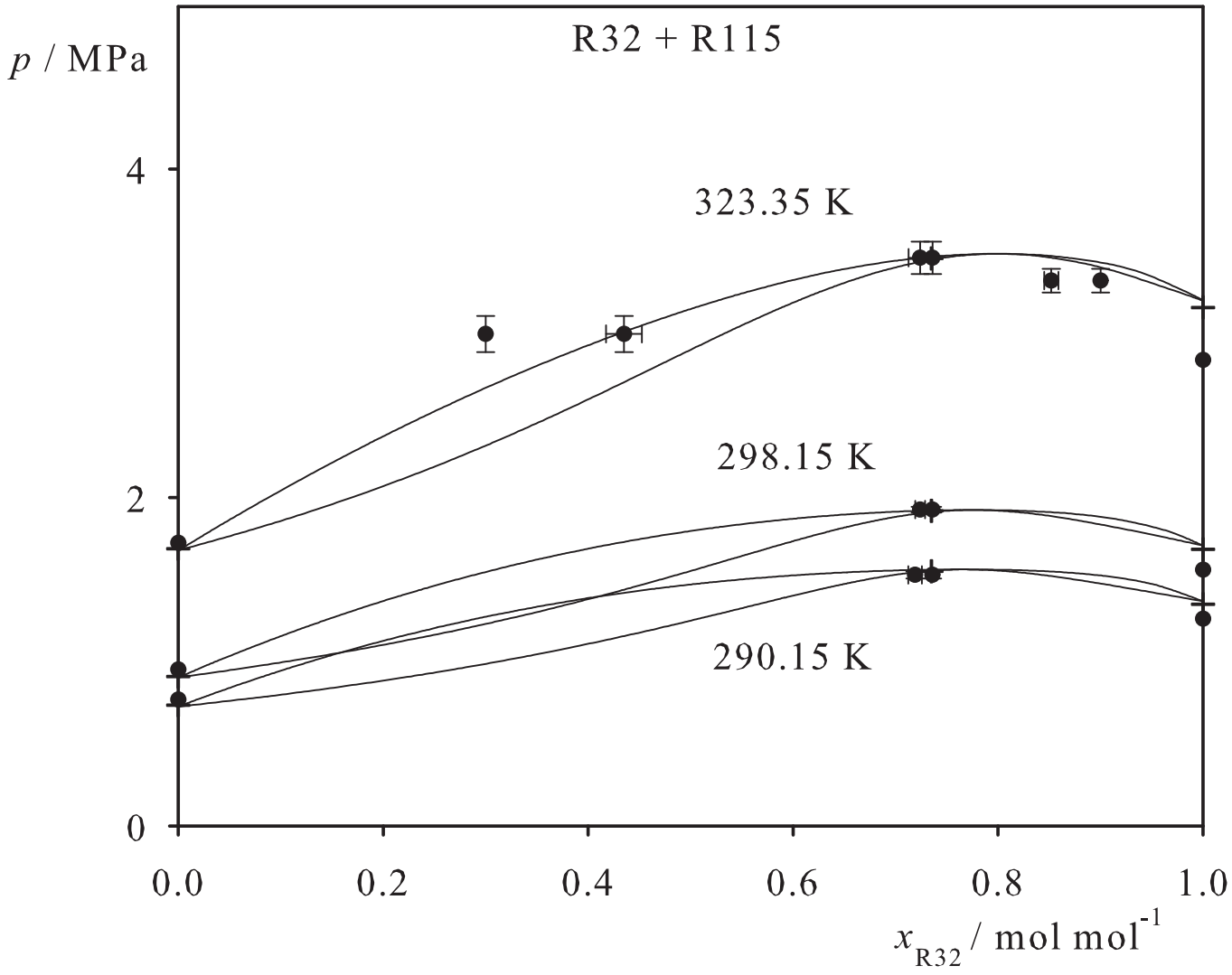

Fig. 197. Binary vapor-liquid equilibrium phase diagram: simulation data ●, experimental data + (cf. Table 2 of the manuscript for the reference) and Peng-Robinson equation of state —.

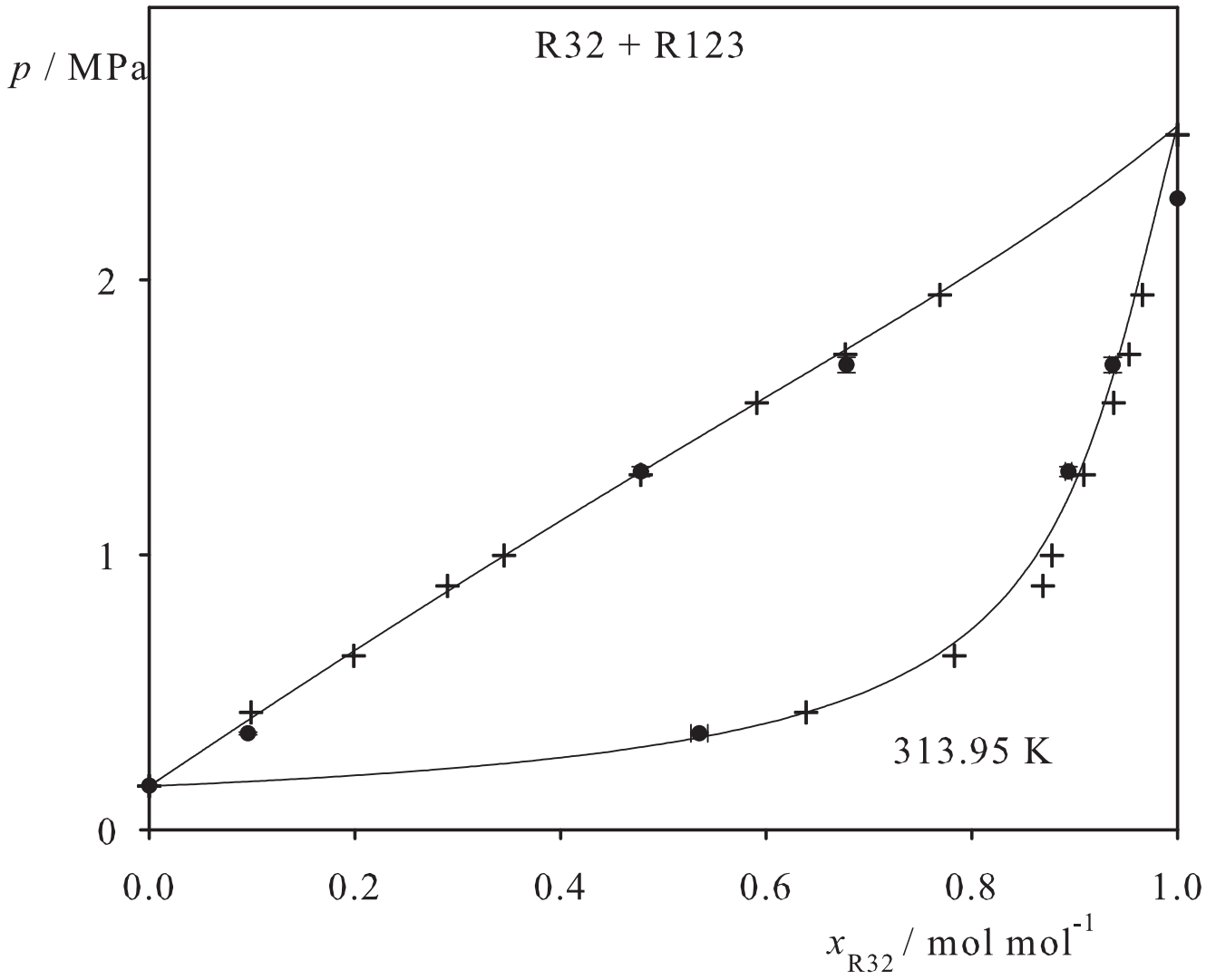

Fig. 198. Binary vapor-liquid equilibrium phase diagram: simulation data ●, experimental data + (cf. Table 2 of the manuscript for the reference) and Peng-Robinson equation of state —.

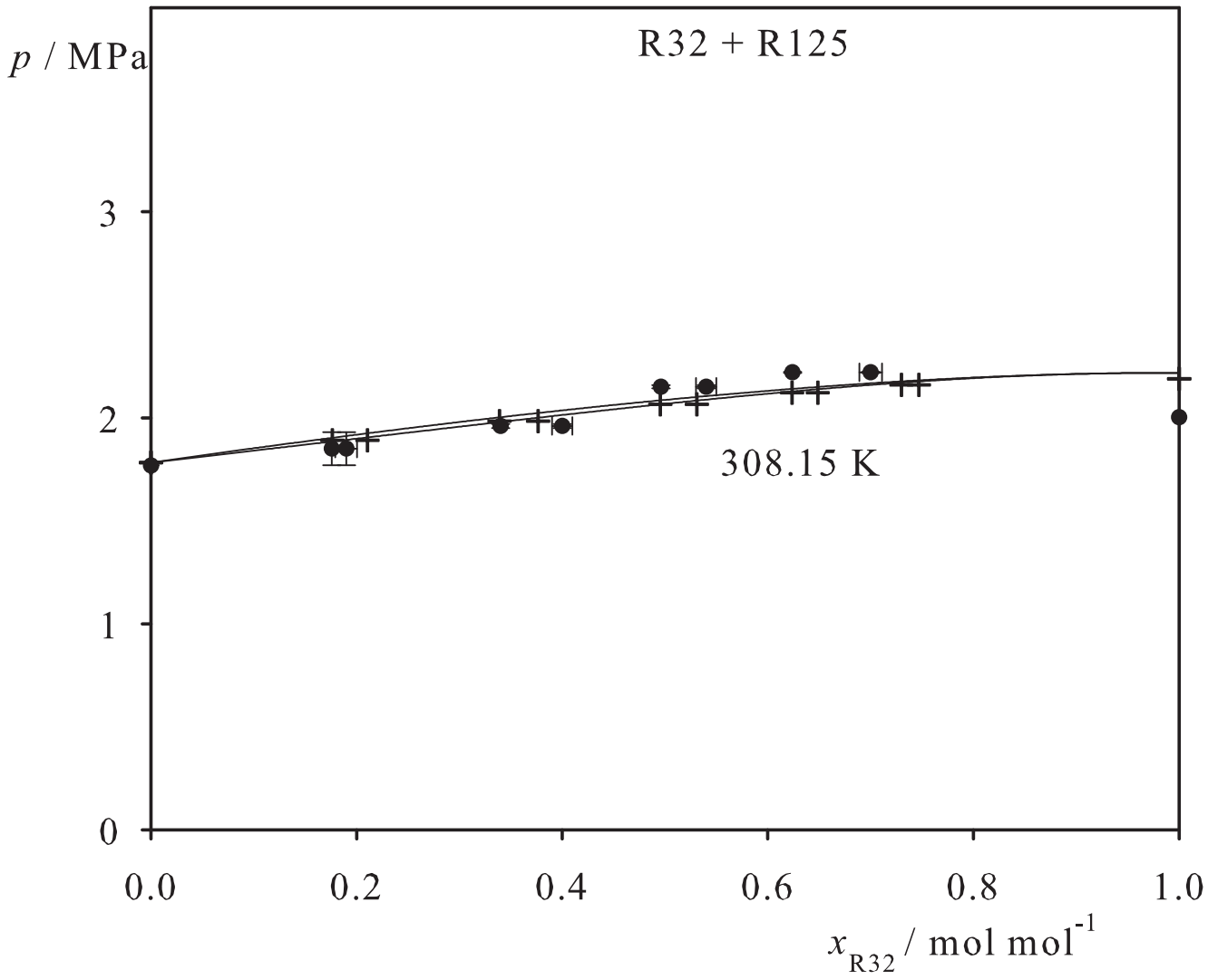

Fig. 199. Binary vapor-liquid equilibrium phase diagram: simulation data ●, experimental data + (cf. Table 2 of the manuscript for the reference) and Peng-Robinson equation of state —.

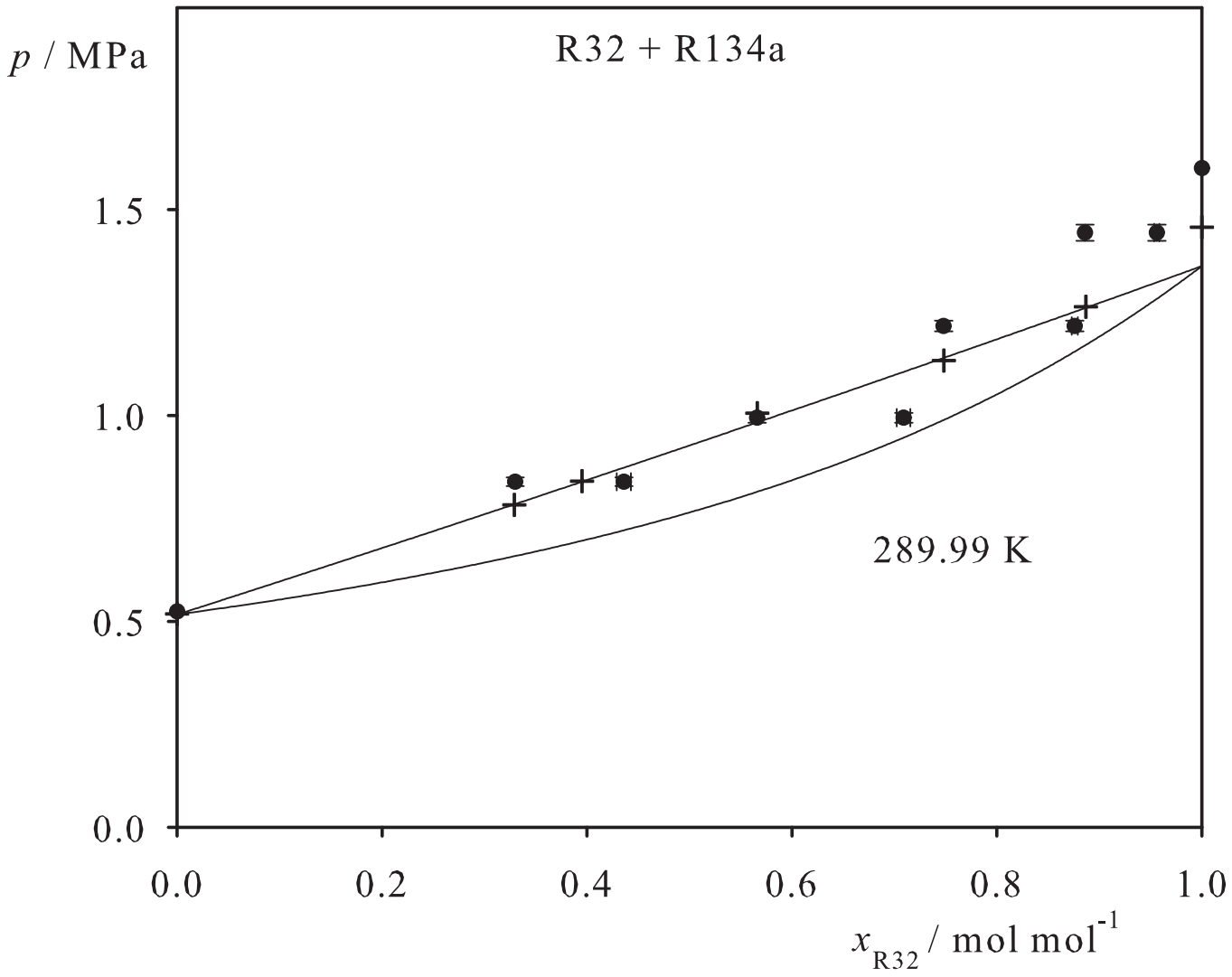

Fig. 200. Binary vapor-liquid equilibrium phase diagram: simulation data ●, experimental data + (cf. Table 2 of the manuscript for the reference) and Peng-Robinson equation of state —.

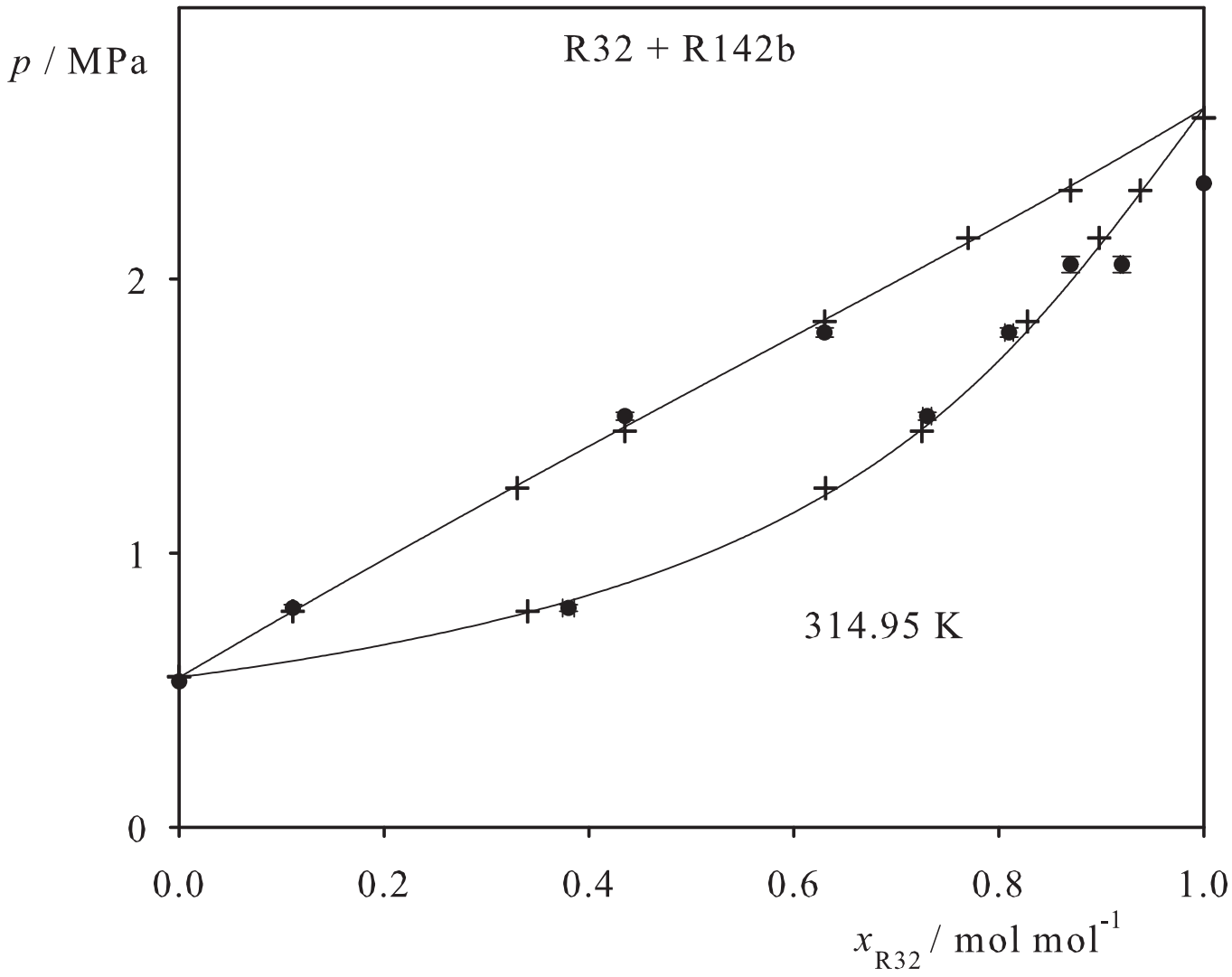

Fig. 201. Binary vapor-liquid equilibrium phase diagram: simulation data ●, experimental data + (cf. Table 2 of the manuscript for the reference) and Peng-Robinson equation of state —.

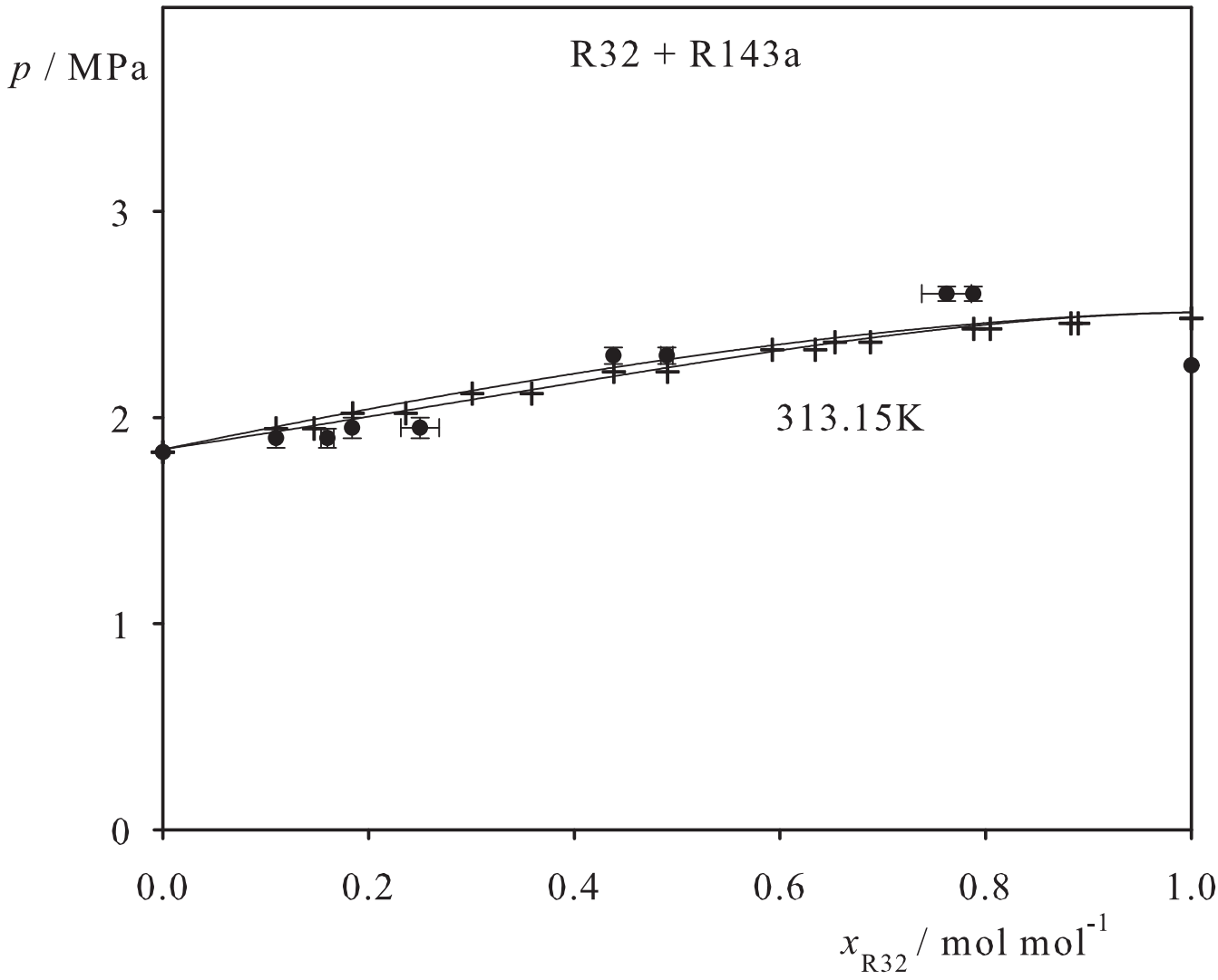

Fig. 202. Binary vapor-liquid equilibrium phase diagram: simulation data ●, experimental data + (cf. Table 2 of the manuscript for the reference) and Peng-Robinson equation of state —.

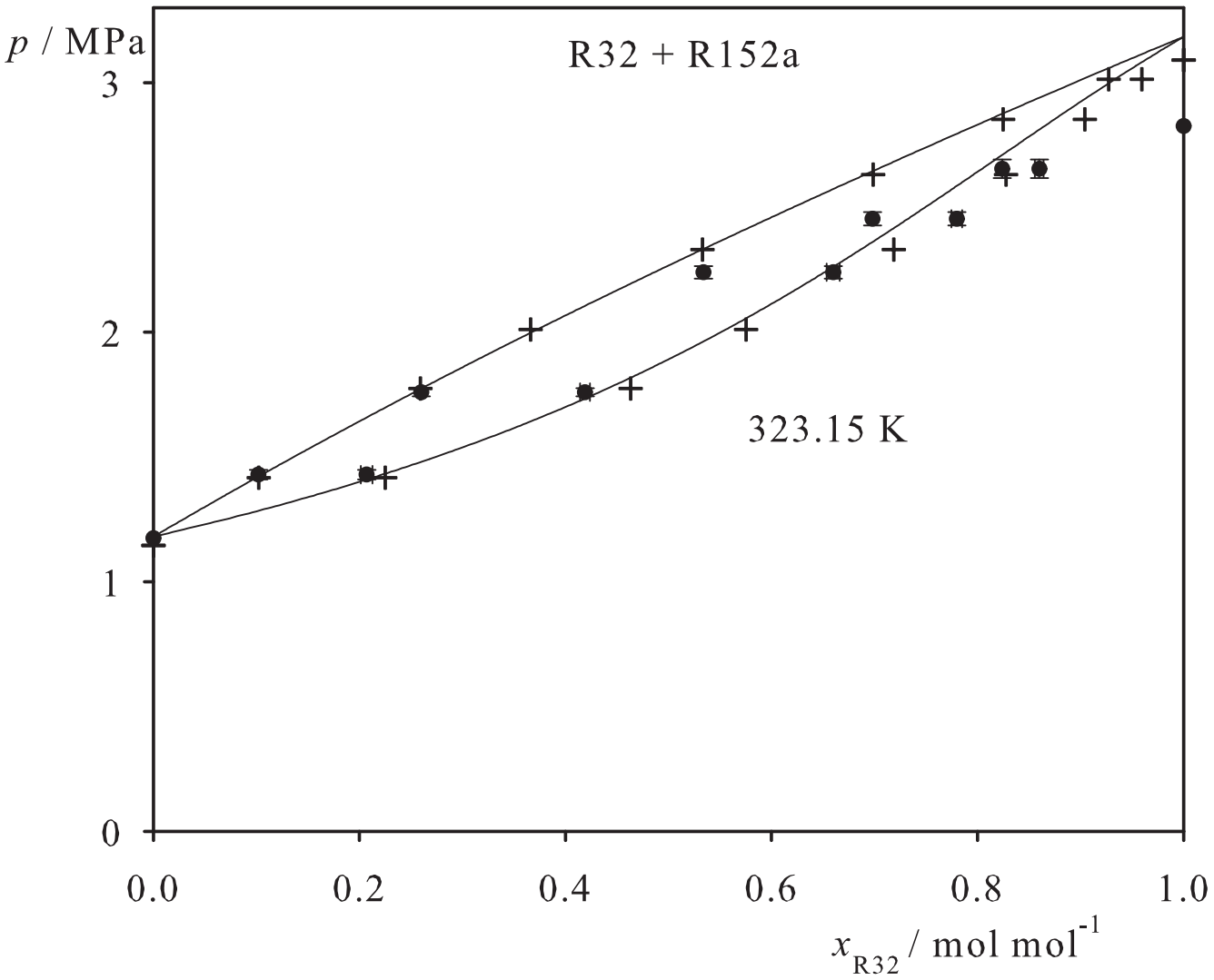

Fig. 203. Binary vapor-liquid equilibrium phase diagram: simulation data ●, experimental data + (cf. Table 2 of the manuscript for the reference) and Peng-Robinson equation of state —.

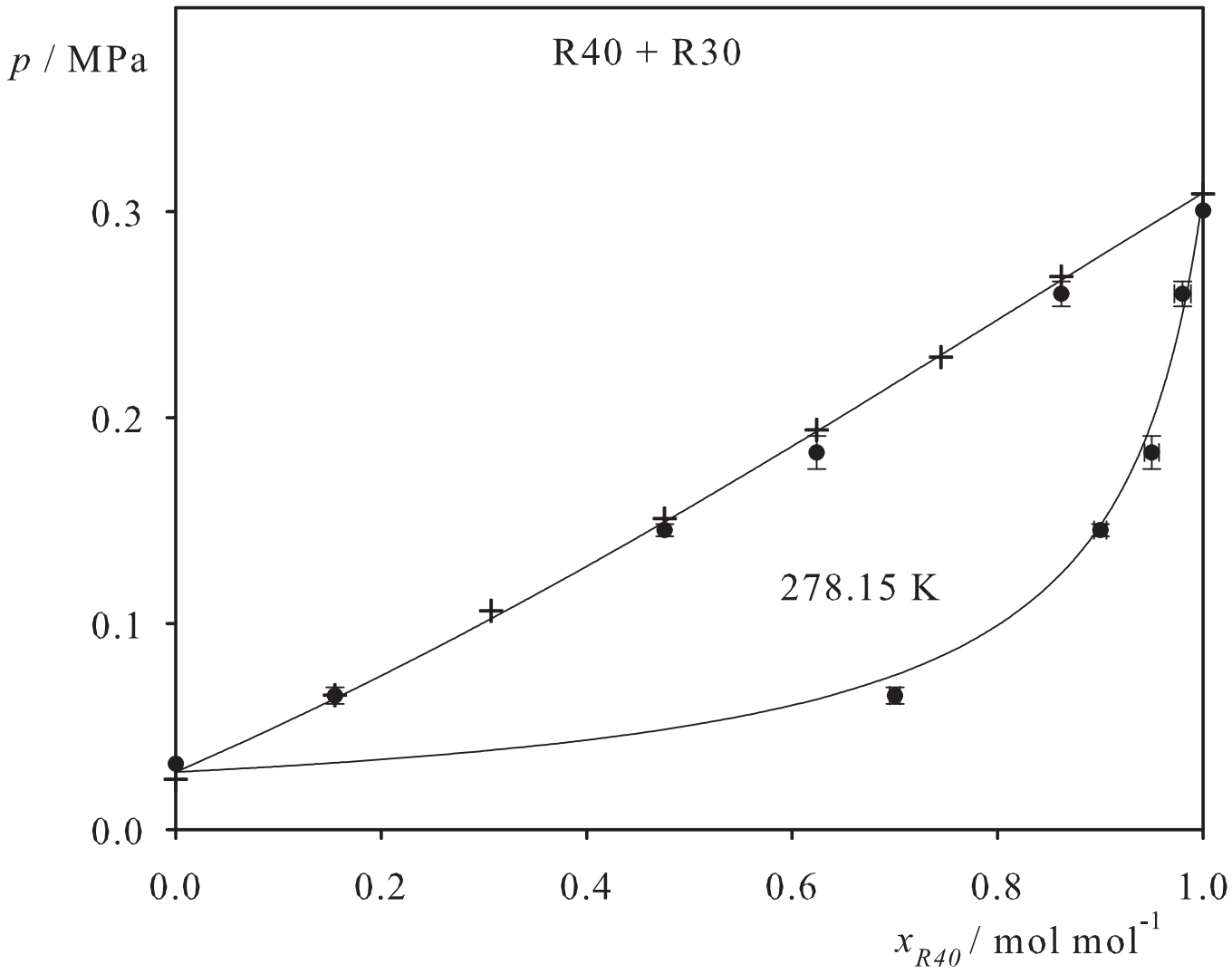

Fig. 204. Binary vapor-liquid equilibrium phase diagram: simulation data ●, experimental data + (cf. Table 2 of the manuscript for the reference) and Peng-Robinson equation of state —.

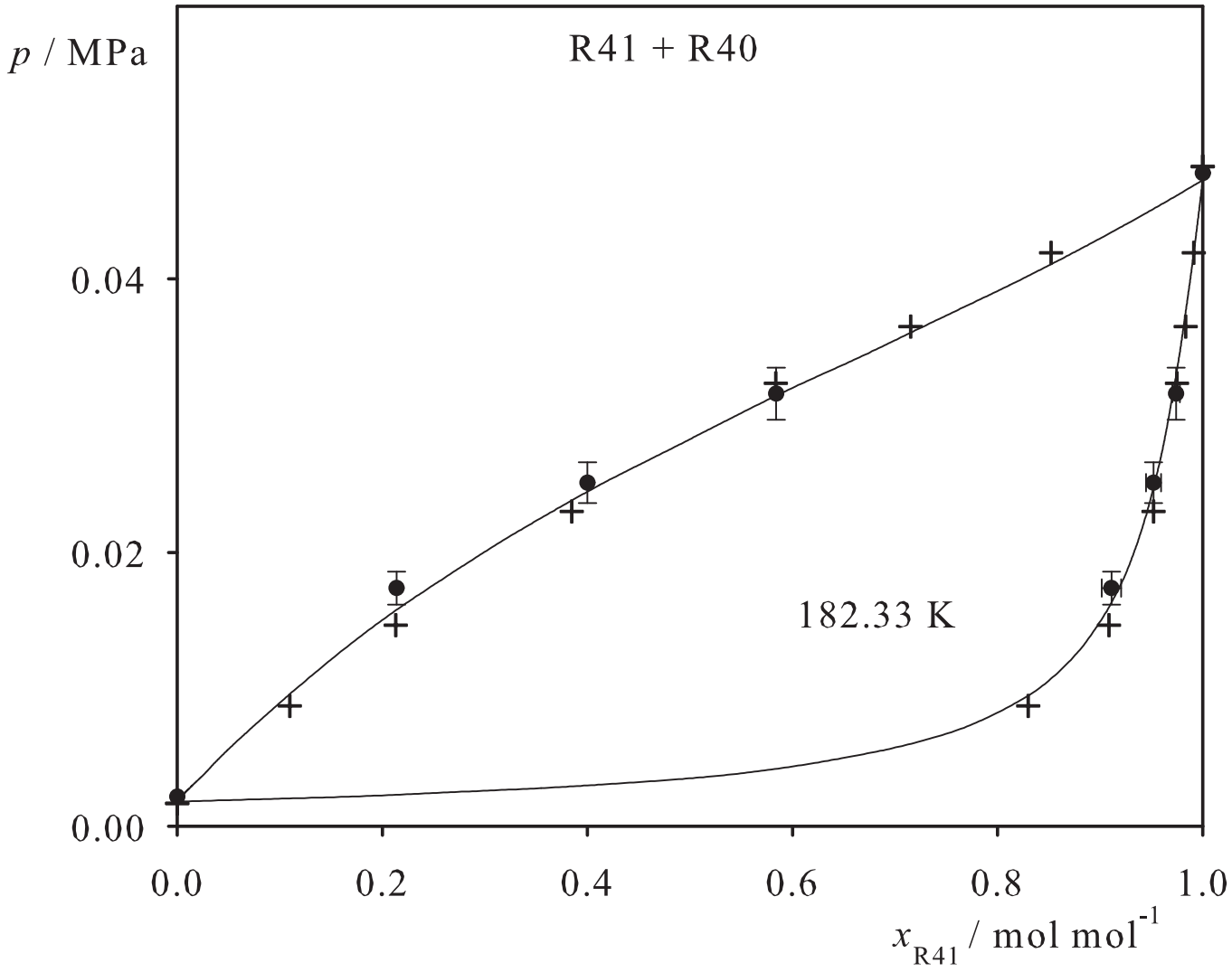

Fig. 205. Binary vapor-liquid equilibrium phase diagram: simulation data ●, experimental data + (cf. Table 2 of the manuscript for the reference) and Peng-Robinson equation of state —.

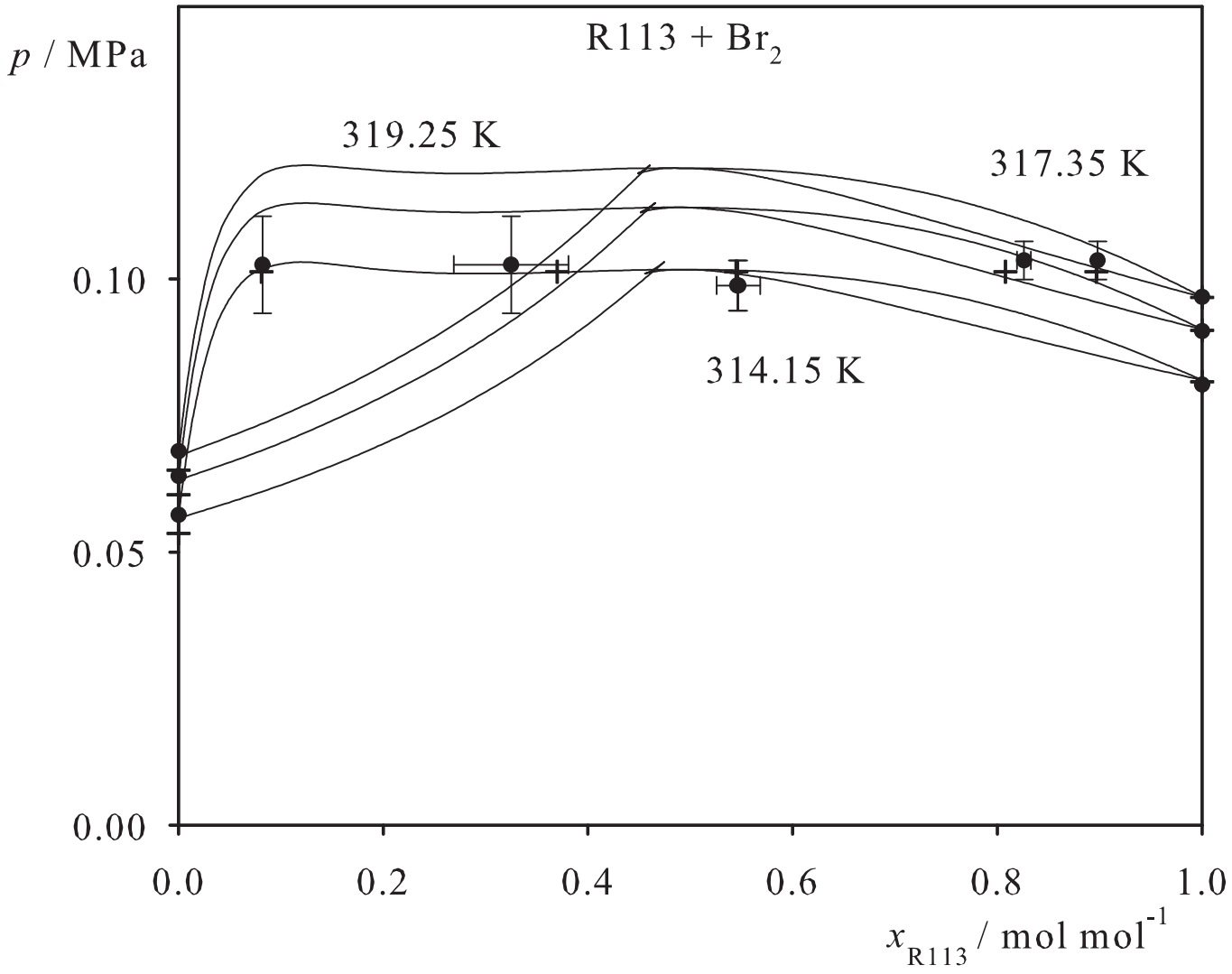

Fig. 206. Binary vapor-liquid equilibrium phase diagram: simulation data ●, experimental data + (cf. Table 2 of the manuscript for the reference) and Peng-Robinson equation of state —.

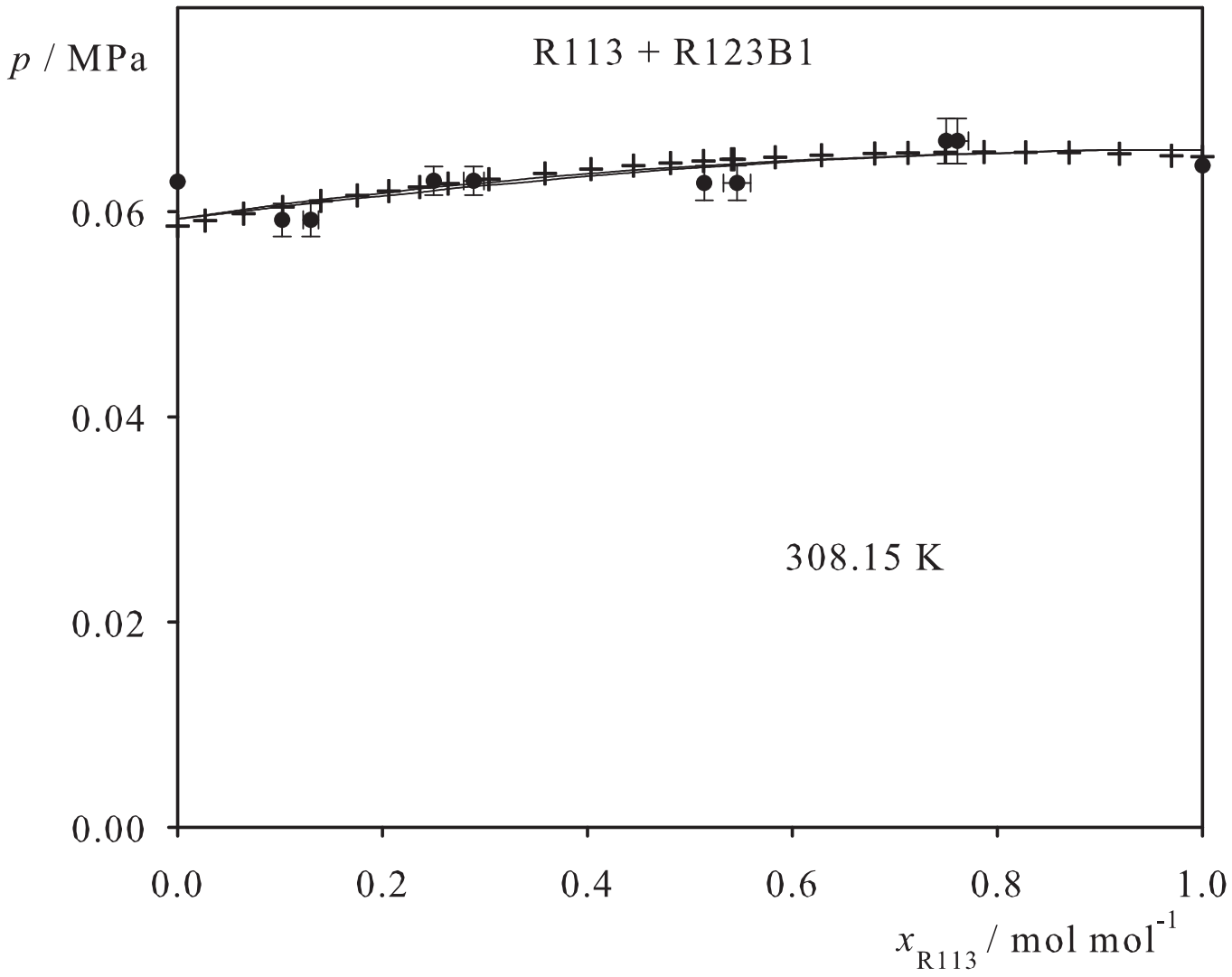

Fig. 207. Binary vapor-liquid equilibrium phase diagram: simulation data ●, experimental data + (cf. Table 2 of the manuscript for the reference) and Peng-Robinson equation of state —.

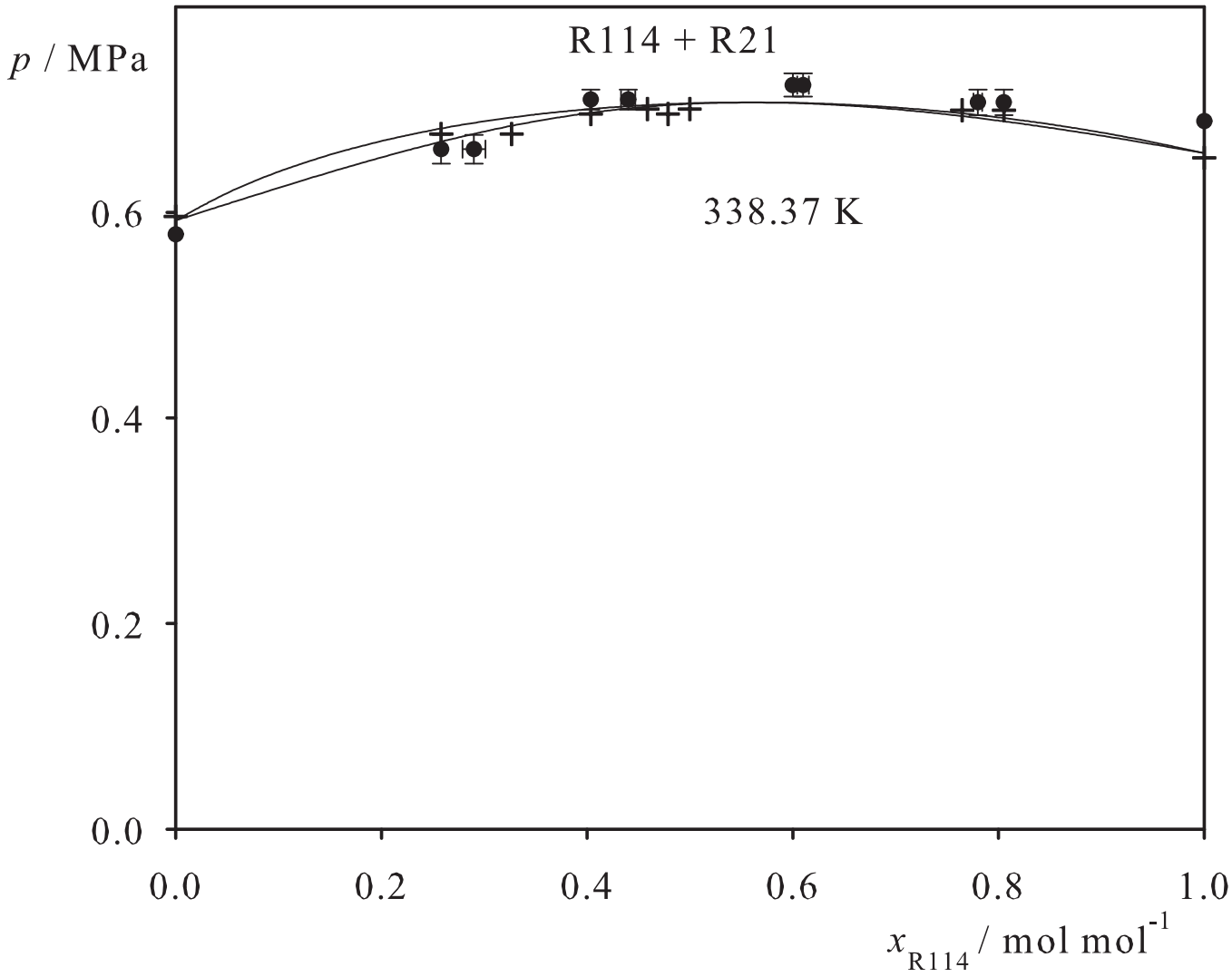

Fig. 208. Binary vapor-liquid equilibrium phase diagram: simulation data ●, experimental data + (cf. Table 2 of the manuscript for the reference) and Peng-Robinson equation of state —.

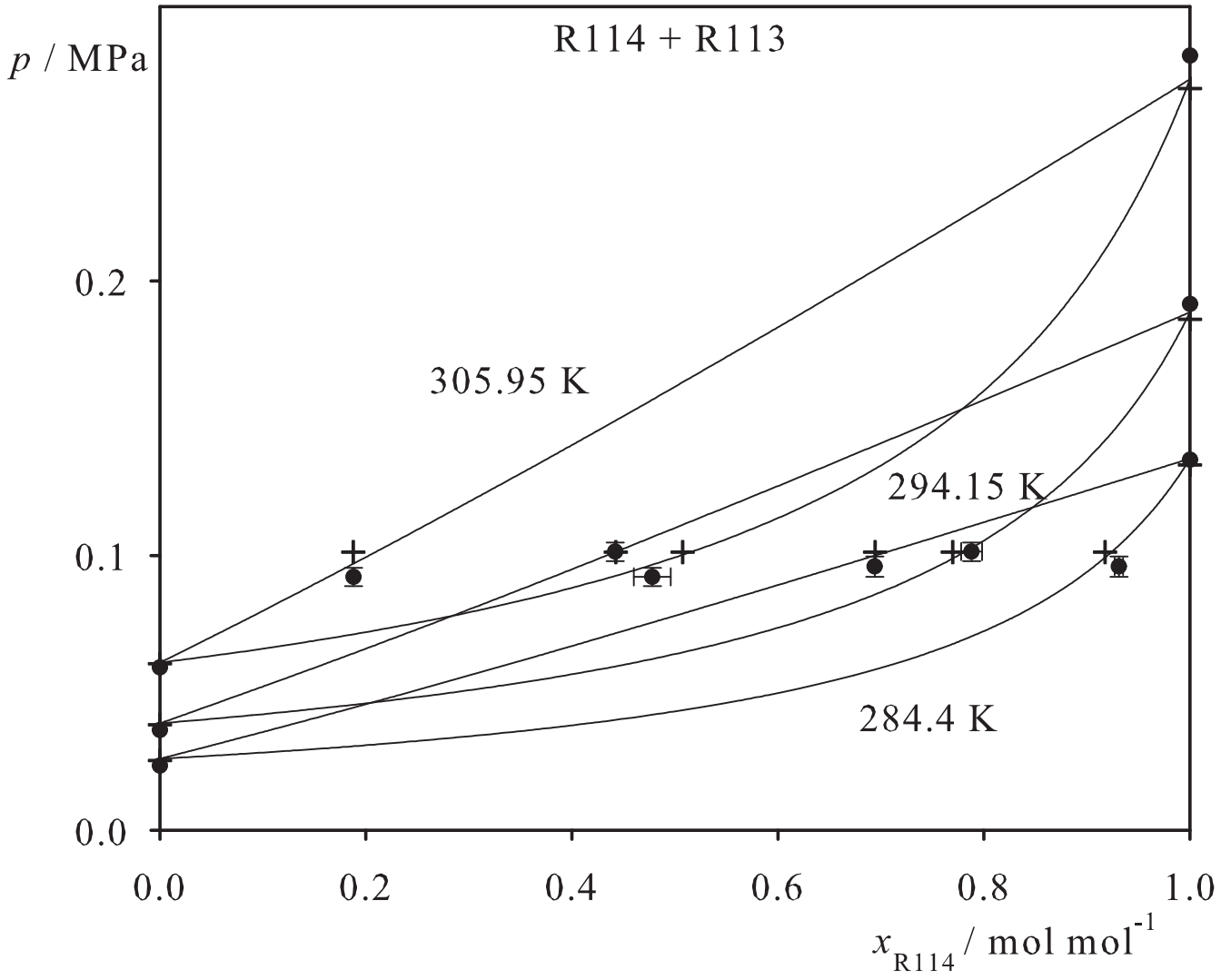

Fig. 209. Binary vapor-liquid equilibrium phase diagram: simulation data ●, experimental data + (cf. Table 2 of the manuscript for the reference) and Peng-Robinson equation of state —.

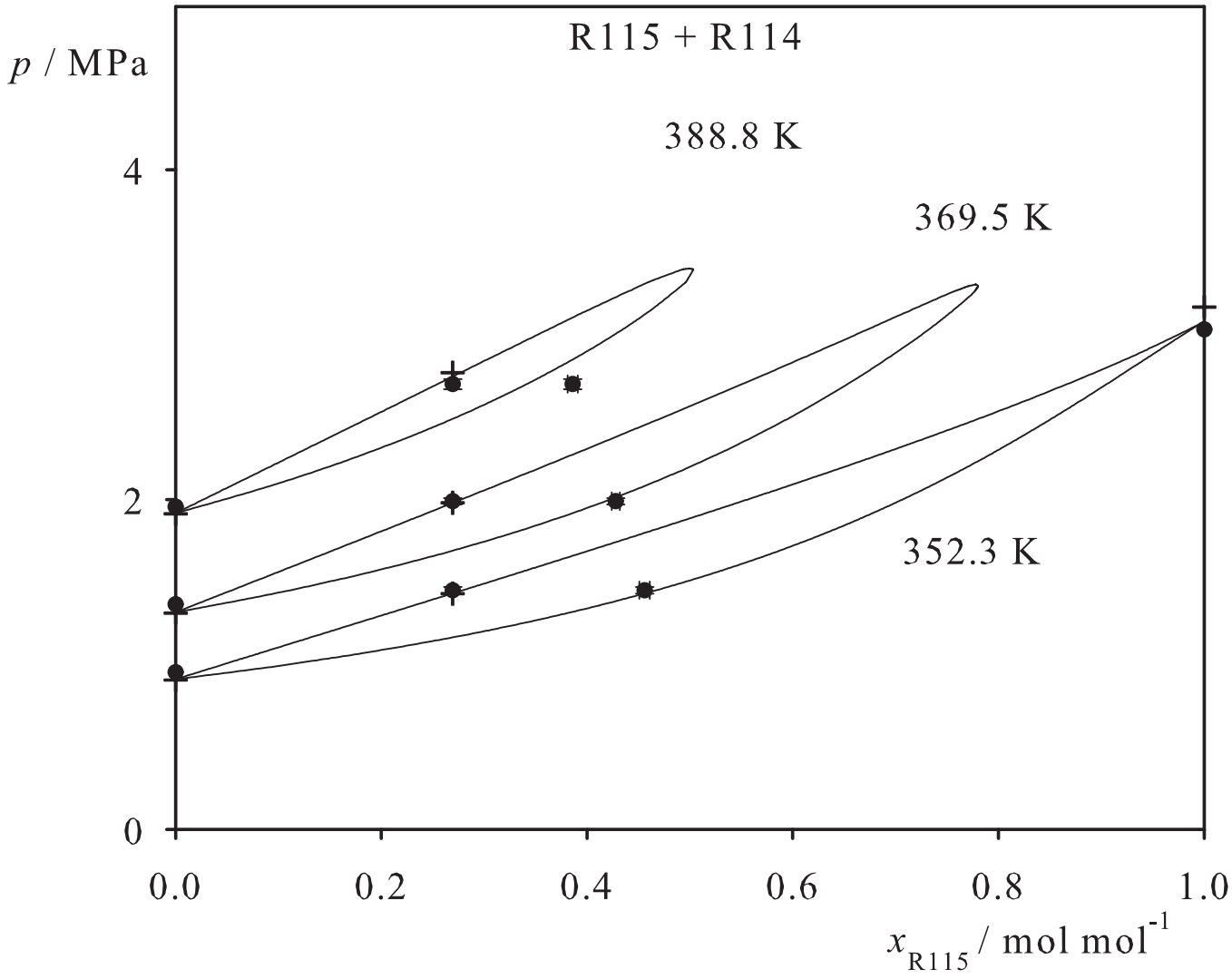

Fig. 210. Binary vapor-liquid equilibrium phase diagram: simulation data ●, experimental data + (cf. Table 2 of the manuscript for the reference) and Peng-Robinson equation of state —.

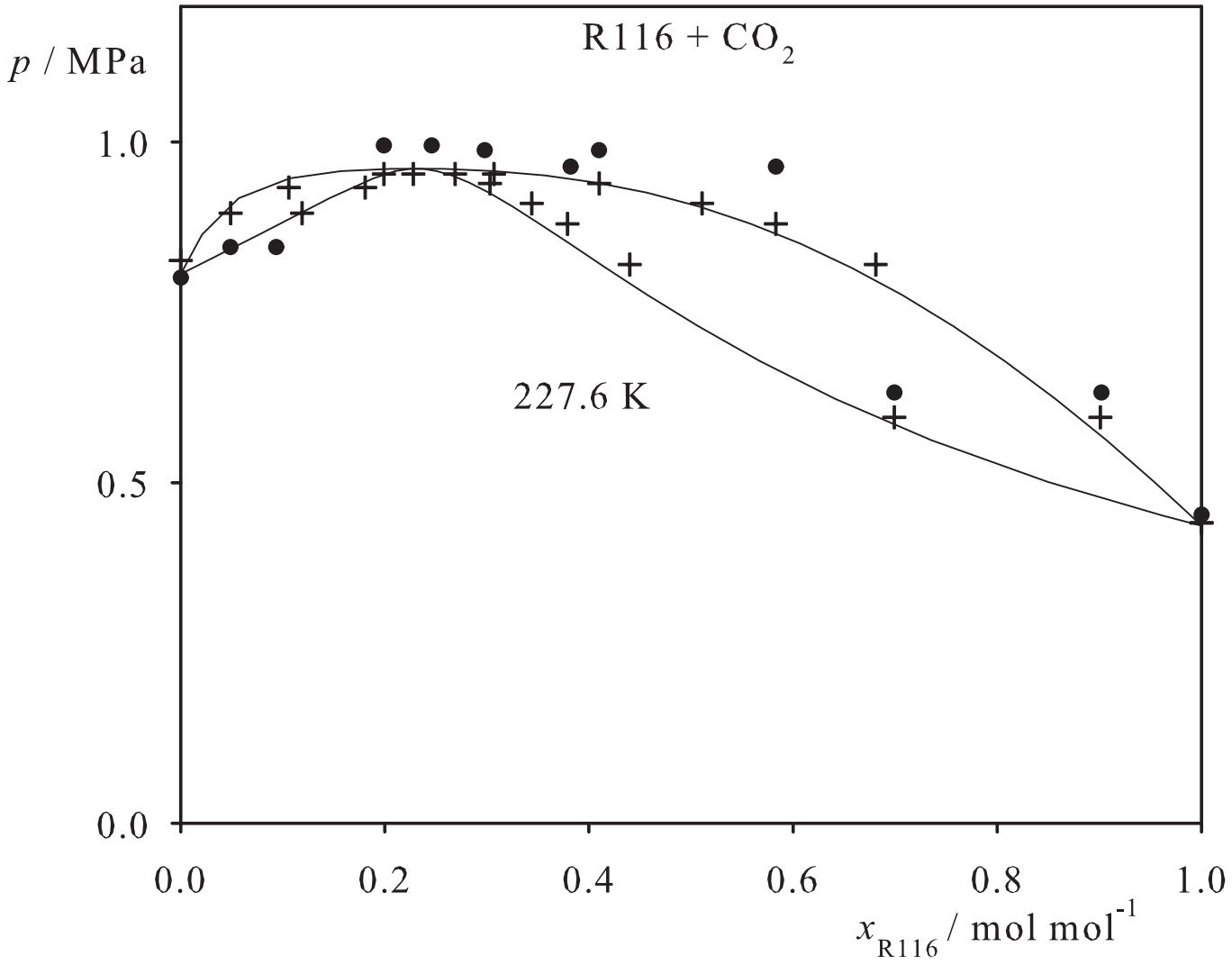

Fig. 211. Binary vapor-liquid equilibrium phase diagram: simulation data ●, experimental data + (cf. Table 2 of the manuscript for the reference) and Peng-Robinson equation of state —.

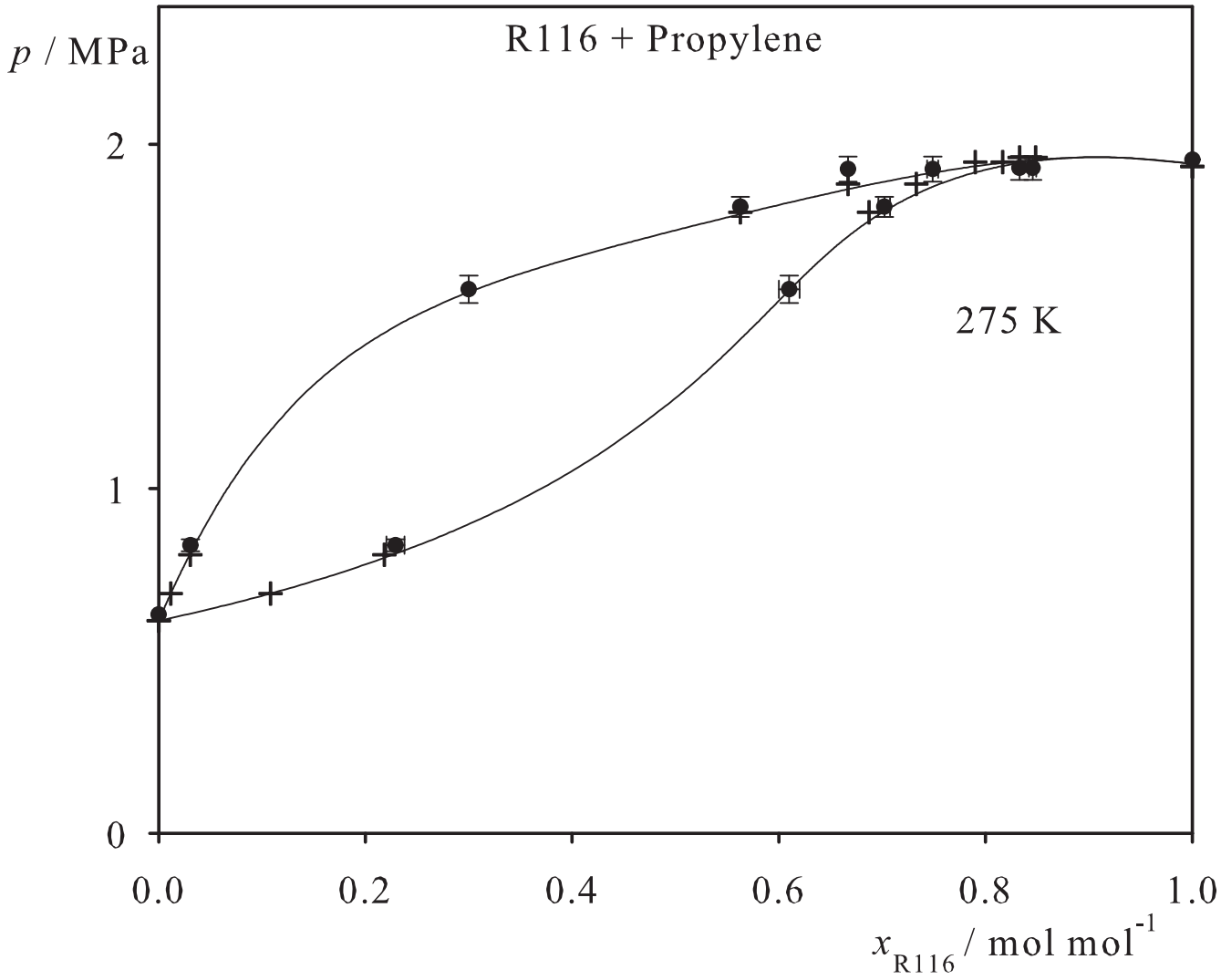

Fig. 212. Binary vapor-liquid equilibrium phase diagram: simulation data ●, experimental data + (cf. Table 2 of the manuscript for the reference) and Peng-Robinson equation of state —.

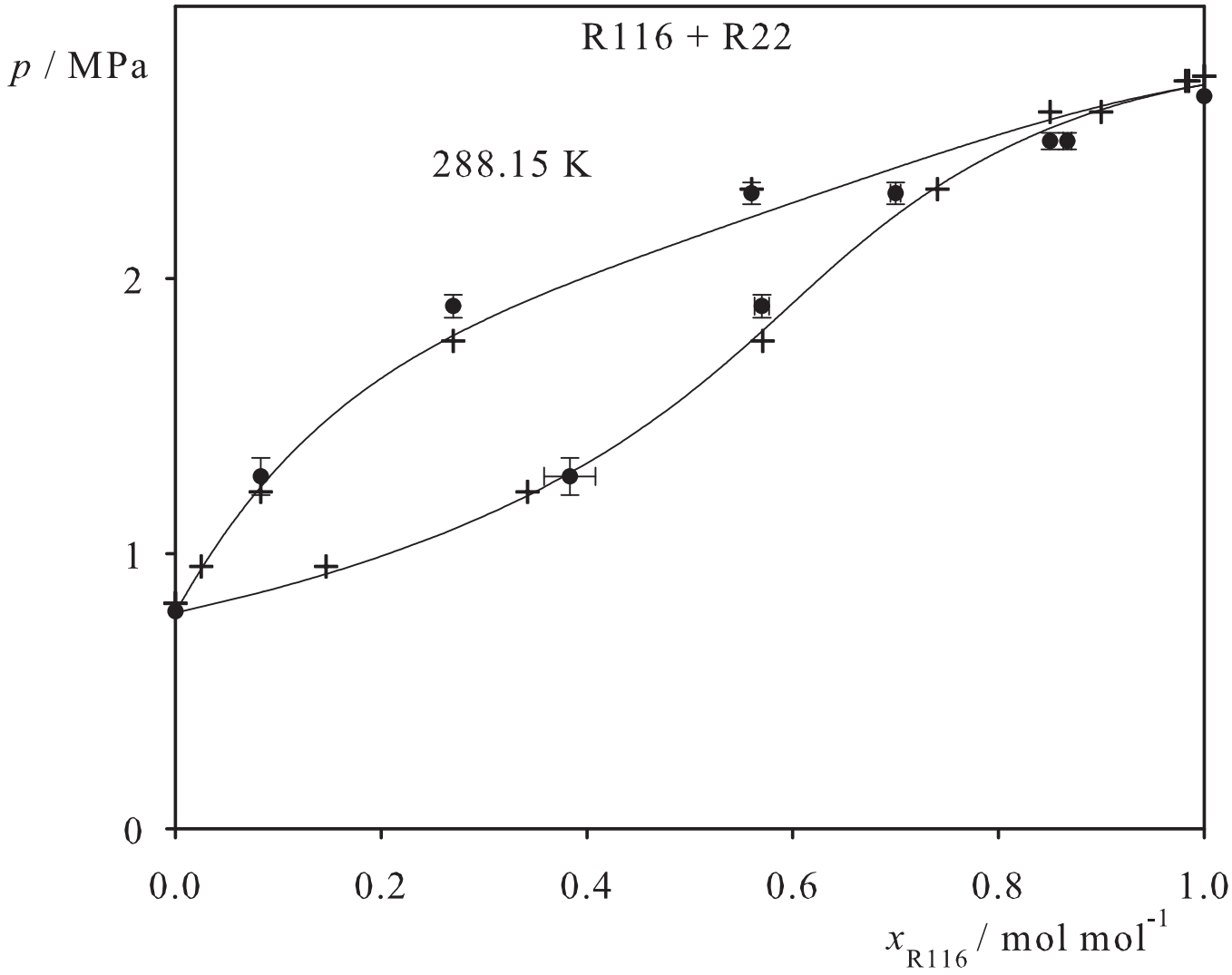

Fig. 213. Binary vapor-liquid equilibrium phase diagram: simulation data ●, experimental data + (cf. Table 2 of the manuscript for the reference) and Peng-Robinson equation of state —.

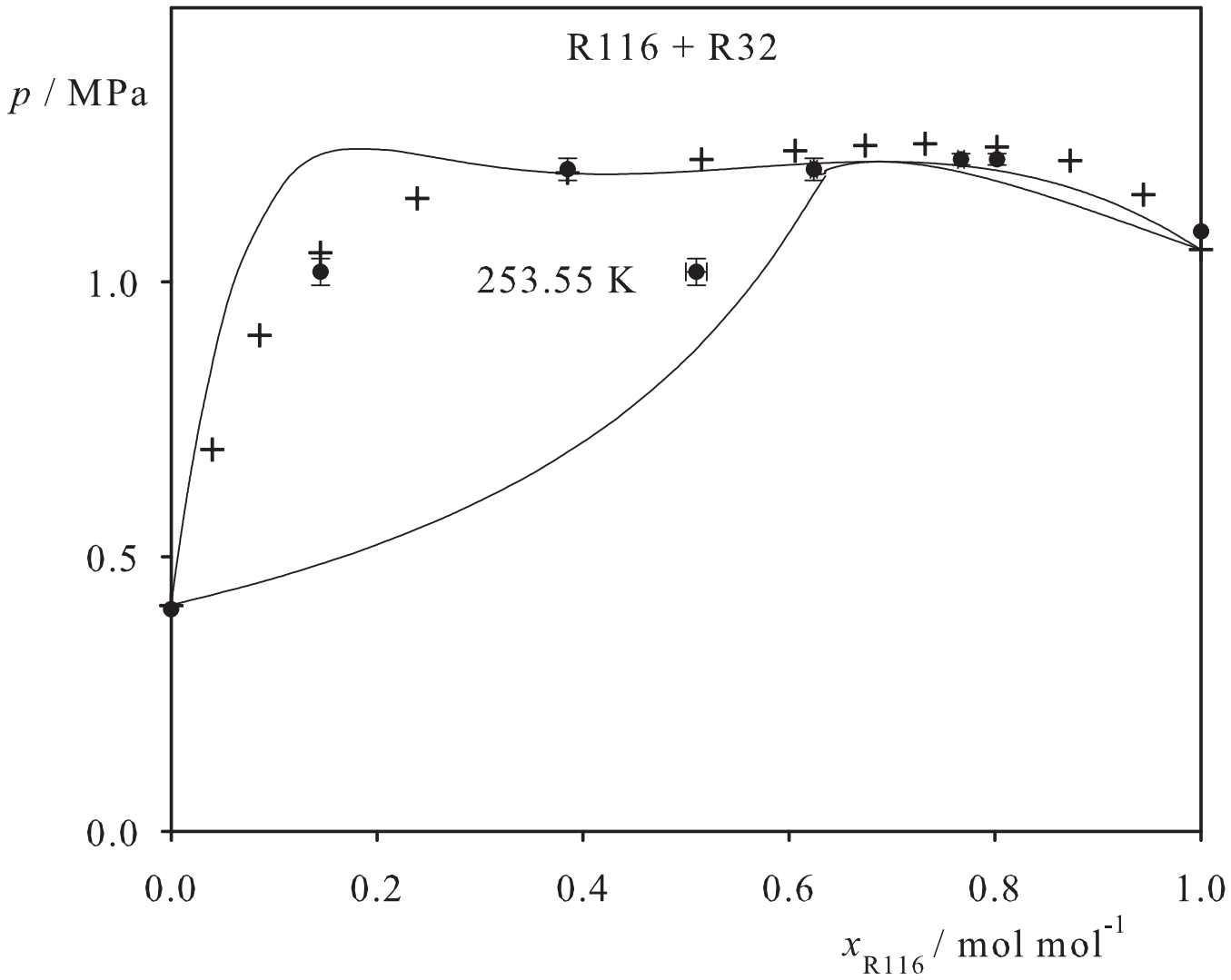

Fig. 214. Binary vapor-liquid equilibrium phase diagram: simulation data ●, experimental data + (cf. Table 2 of the manuscript for the reference) and Peng-Robinson equation of state —.

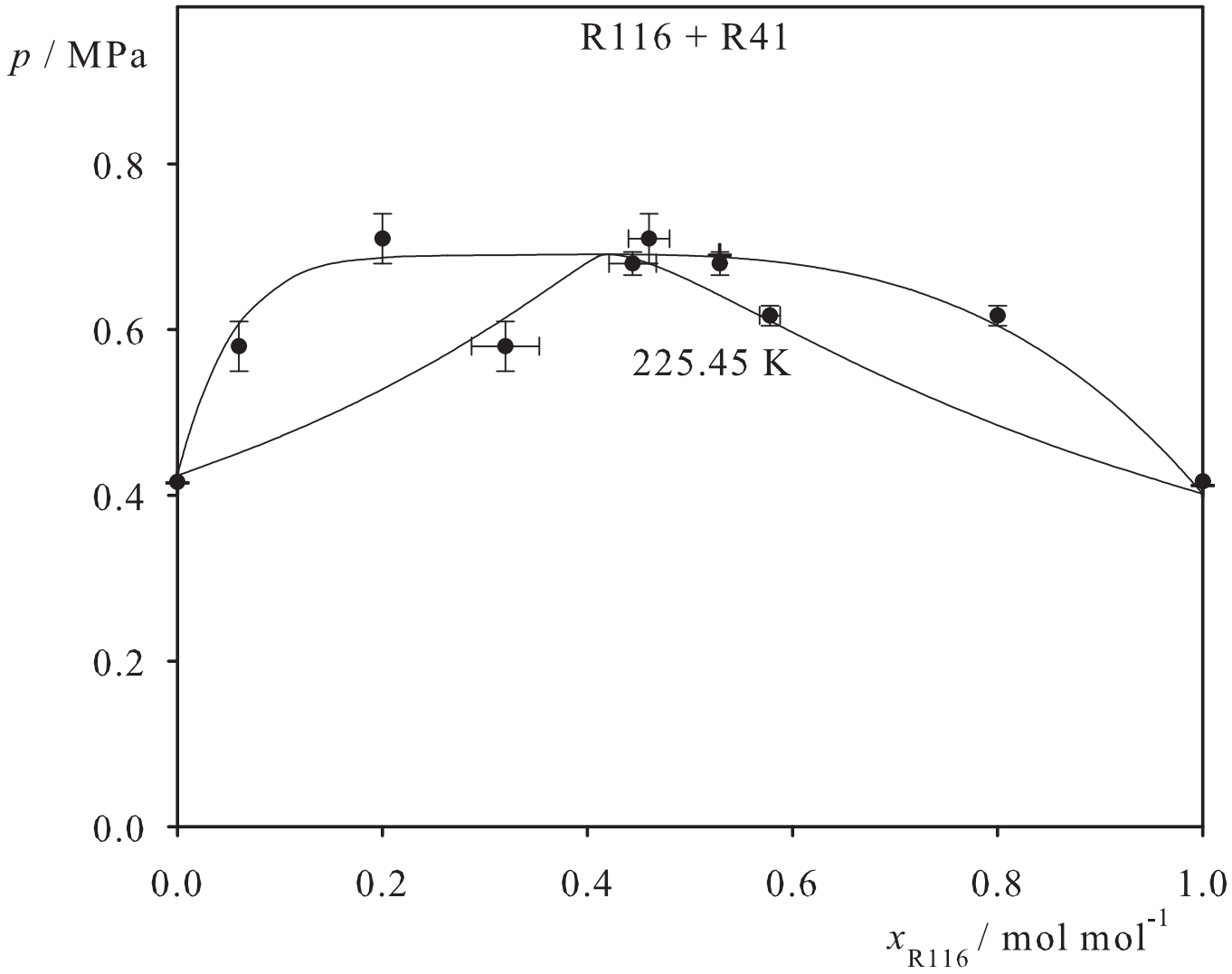

Fig. 215. Binary vapor-liquid equilibrium phase diagram: simulation data ●, experimental data + (cf. Table 2 of the manuscript for the reference) and Peng-Robinson equation of state —.

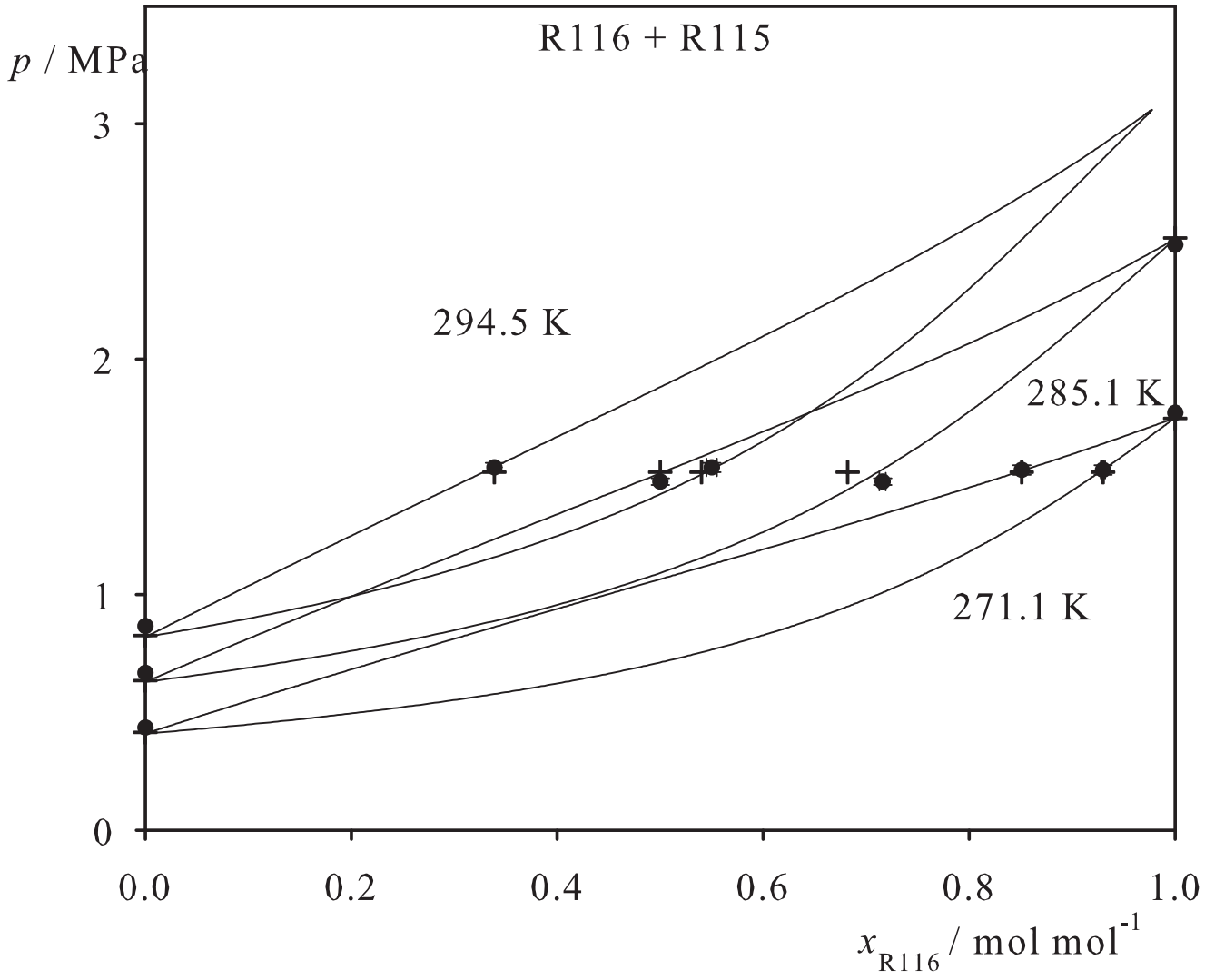

Fig. 216. Binary vapor-liquid equilibrium phase diagram: simulation data ●, experimental data + (cf. Table 2 of the manuscript for the reference) and Peng-Robinson equation of state —.

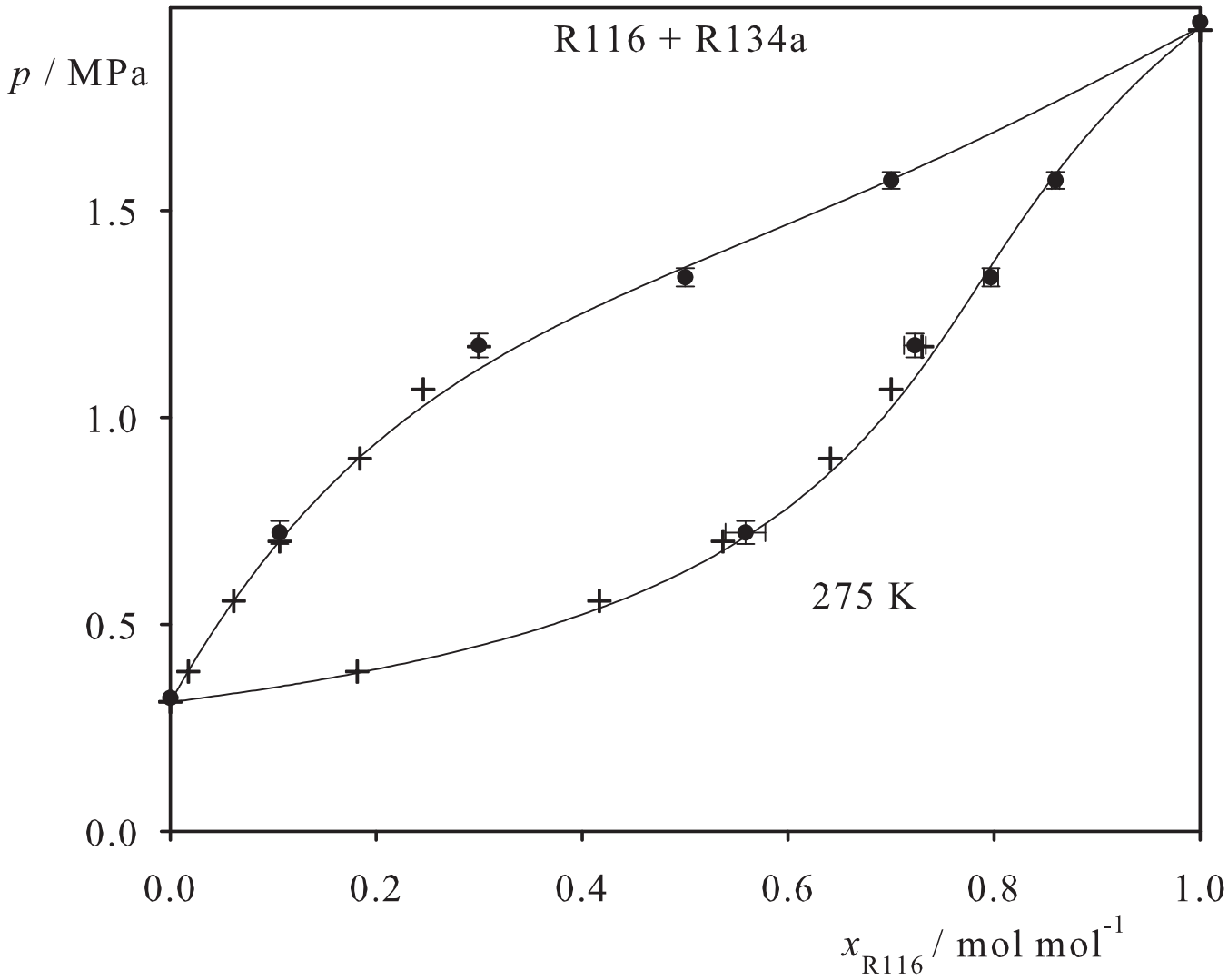

Fig. 217. Binary vapor-liquid equilibrium phase diagram: simulation data ●, experimental data + (cf. Table 2 of the manuscript for the reference) and Peng-Robinson equation of state —.

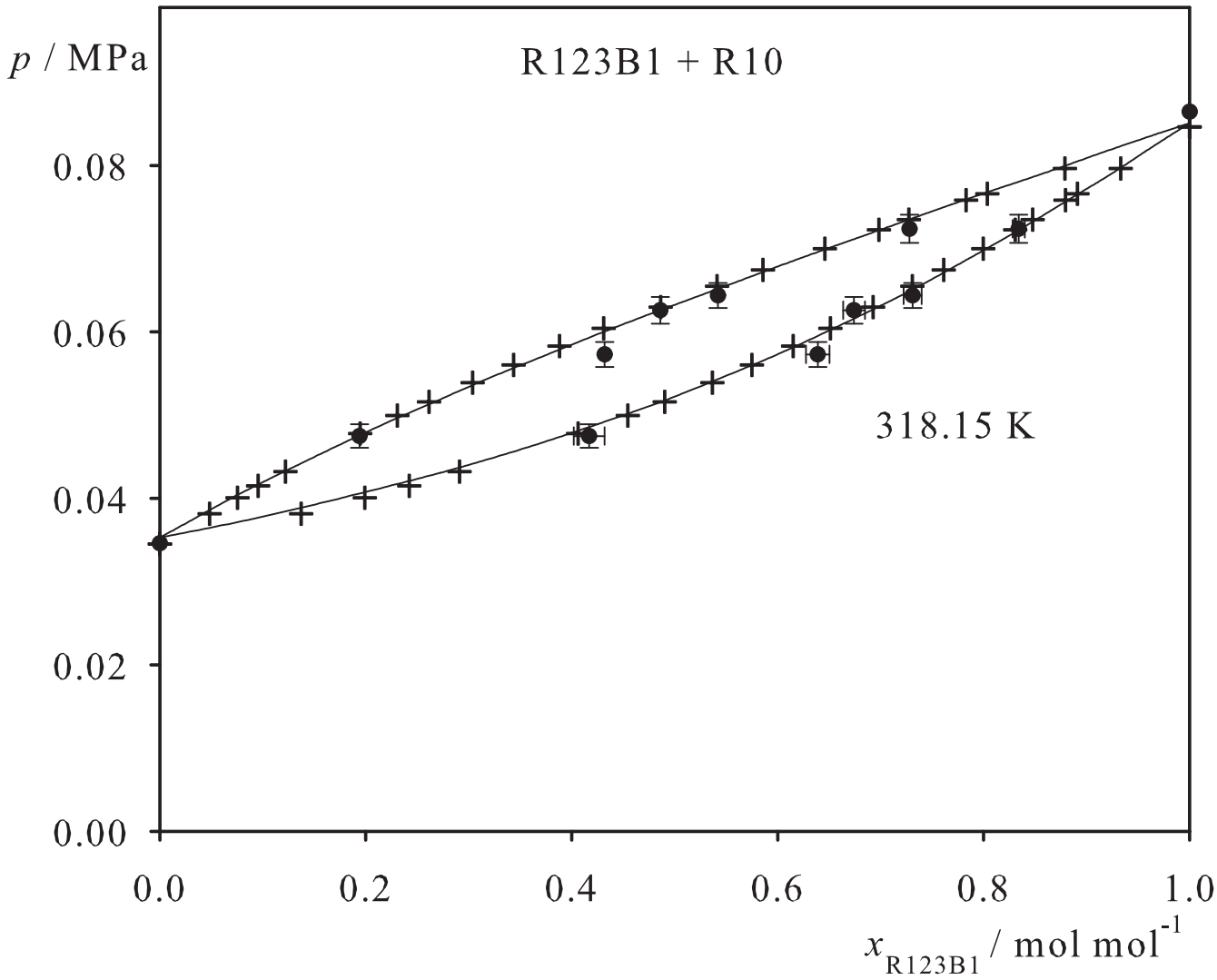

Fig. 218. Binary vapor-liquid equilibrium phase diagram: simulation data ●, experimental data + (cf. Table 2 of the manuscript for the reference) and Peng-Robinson equation of state —.

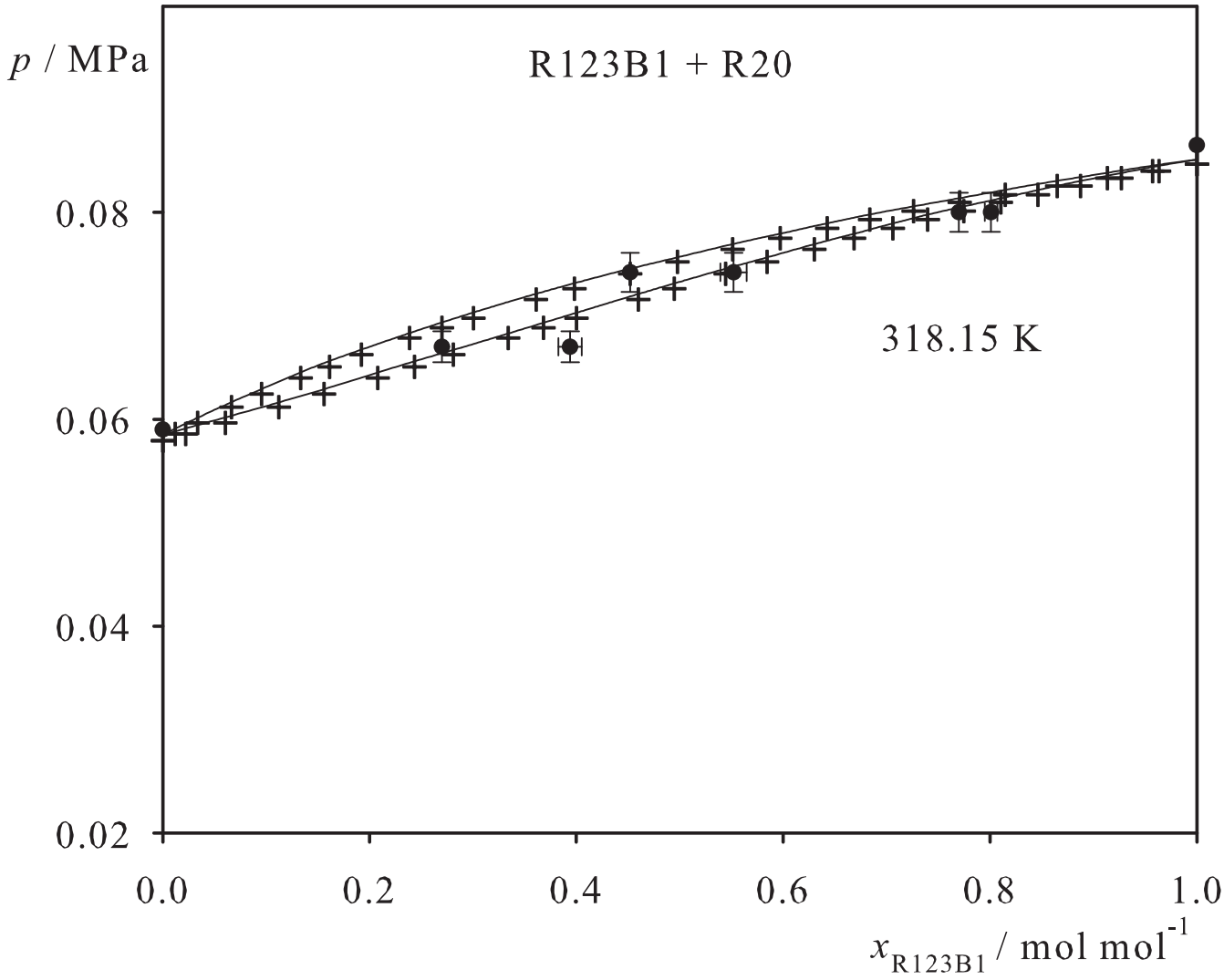

Fig. 219. Binary vapor-liquid equilibrium phase diagram: simulation data ●, experimental data + (cf. Table 2 of the manuscript for the reference) and Peng-Robinson equation of state —.

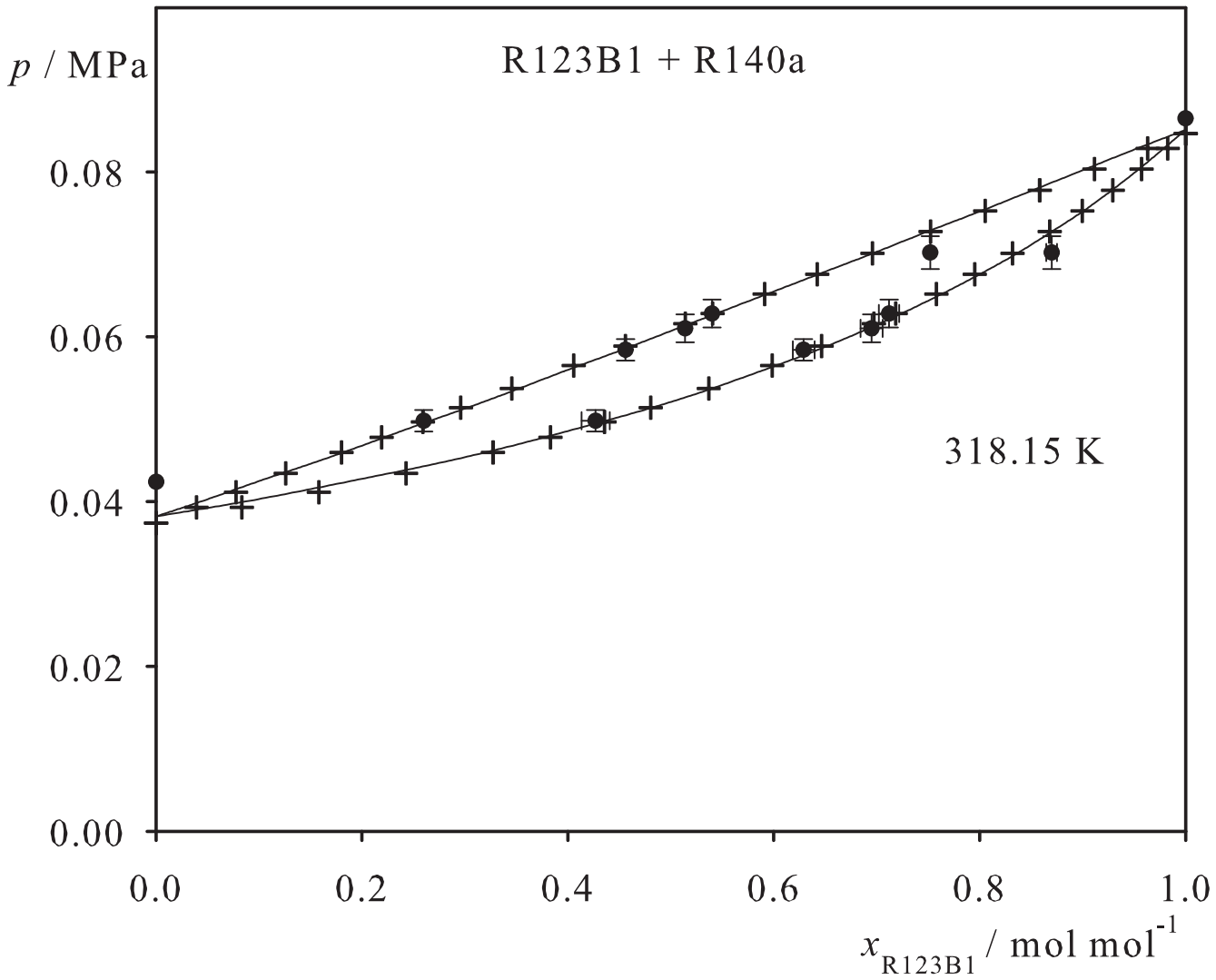

Fig. 220. Binary vapor-liquid equilibrium phase diagram: simulation data ●, experimental data + (cf. Table 2 of the manuscript for the reference) and Peng-Robinson equation of state —.

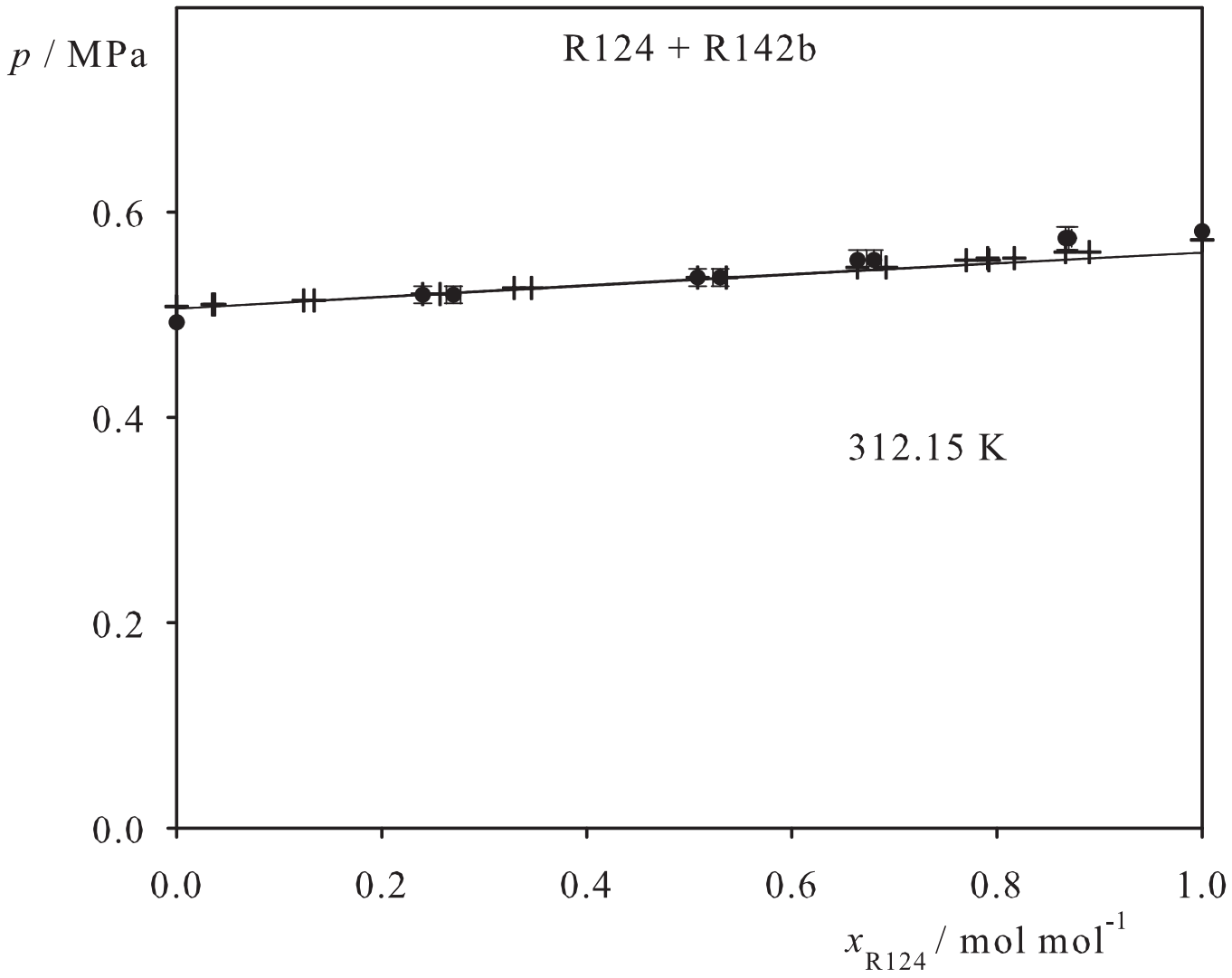

Fig. 221. Binary vapor-liquid equilibrium phase diagram: simulation data ●, experimental data + (cf. Table 2 of the manuscript for the reference) and Peng-Robinson equation of state —.

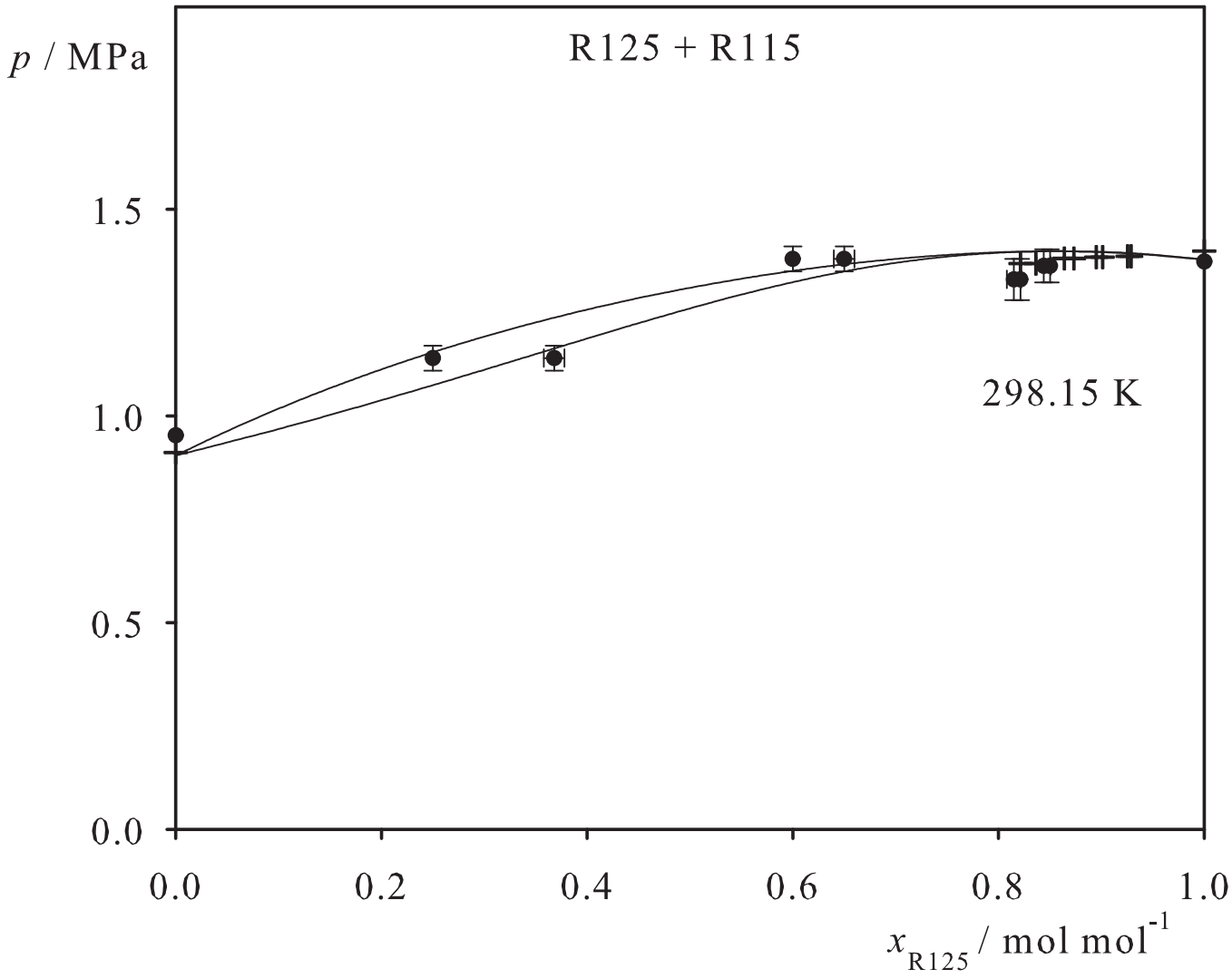

Fig. 222. Binary vapor-liquid equilibrium phase diagram: simulation data ●, experimental data + (cf. Table 2 of the manuscript for the reference) and Peng-Robinson equation of state —.

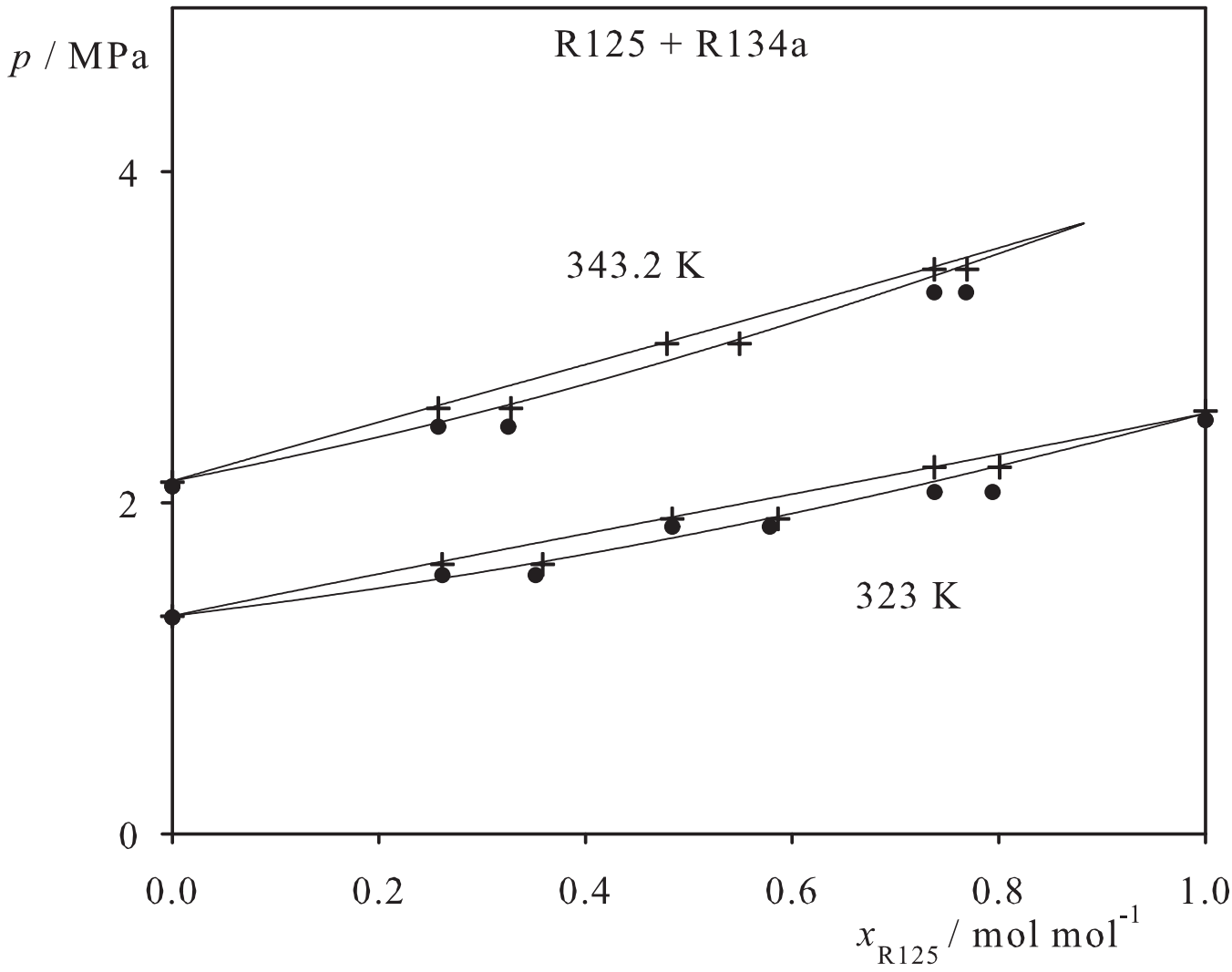

Fig. 223. Binary vapor-liquid equilibrium phase diagram: simulation data ● and experimental data + (cf. Table 2 of the manuscript for the reference).

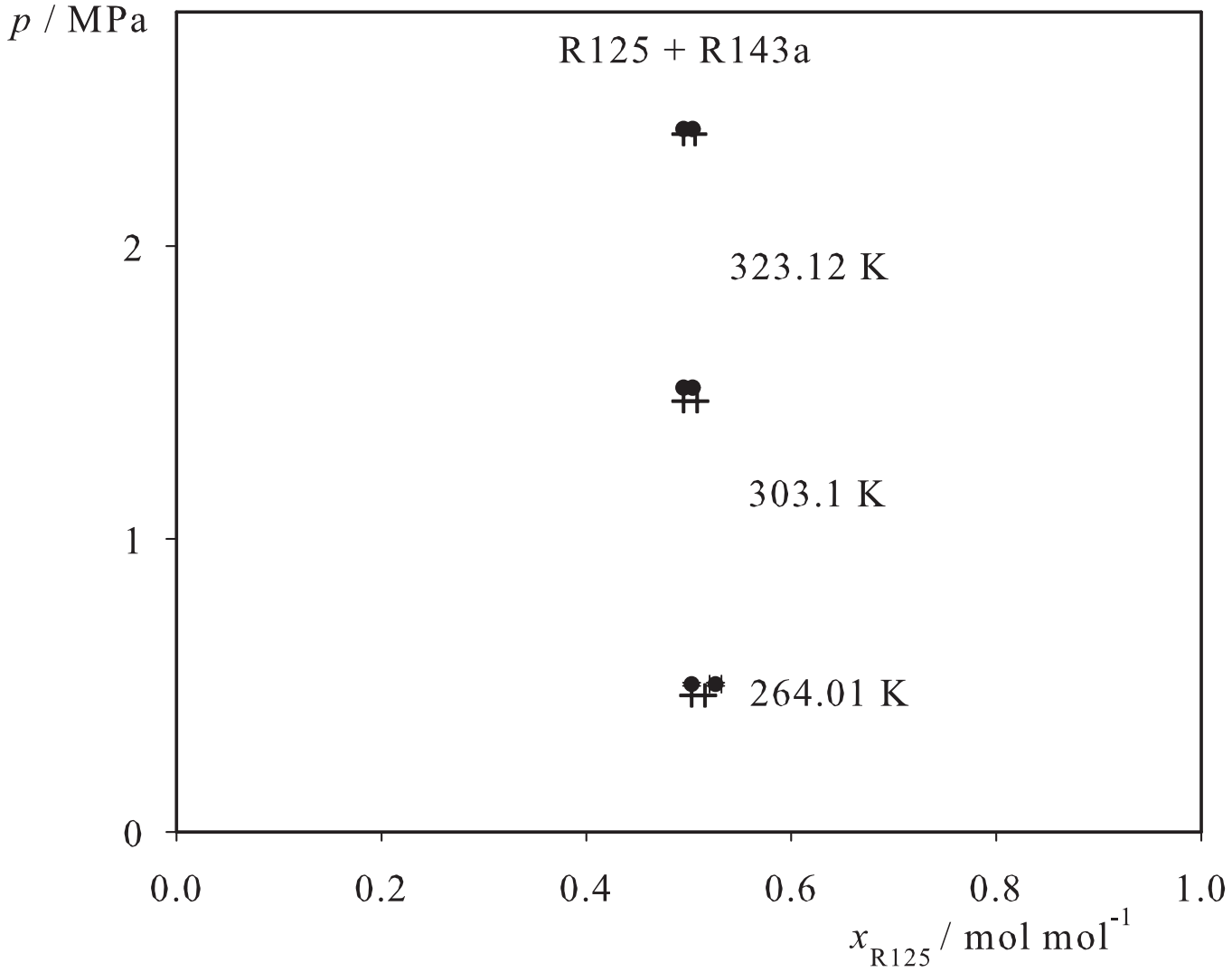

Fig. 224. Binary vapor-liquid equilibrium phase diagram: simulation data ●, experimental data + (cf. Table 2 of the manuscript for the reference) and Peng-Robinson equation of state —.

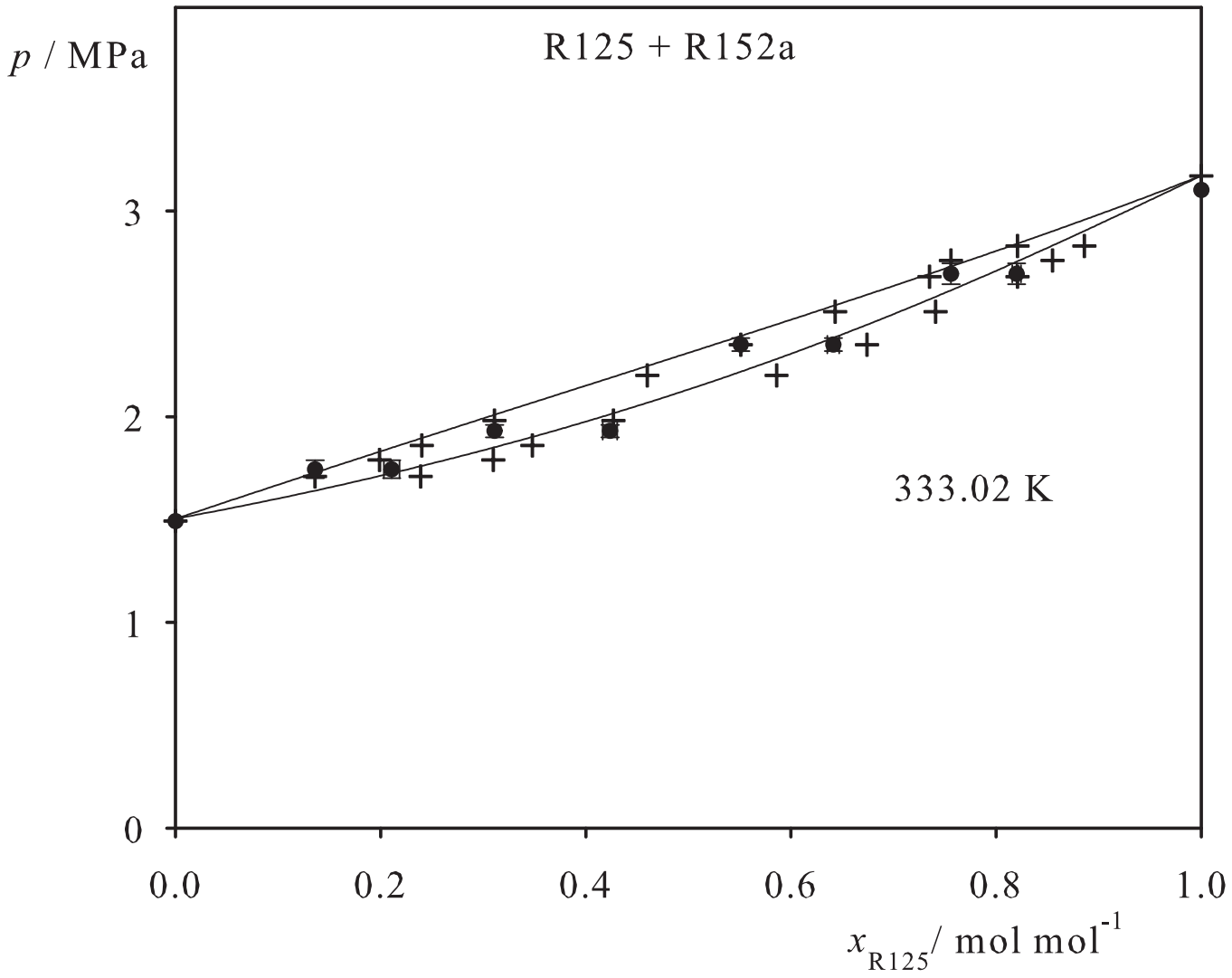

Fig. 225. Binary vapor-liquid equilibrium phase diagram: simulation data ●, experimental data + (cf. Table 2 of the manuscript for the reference) and Peng-Robinson equation of state —.

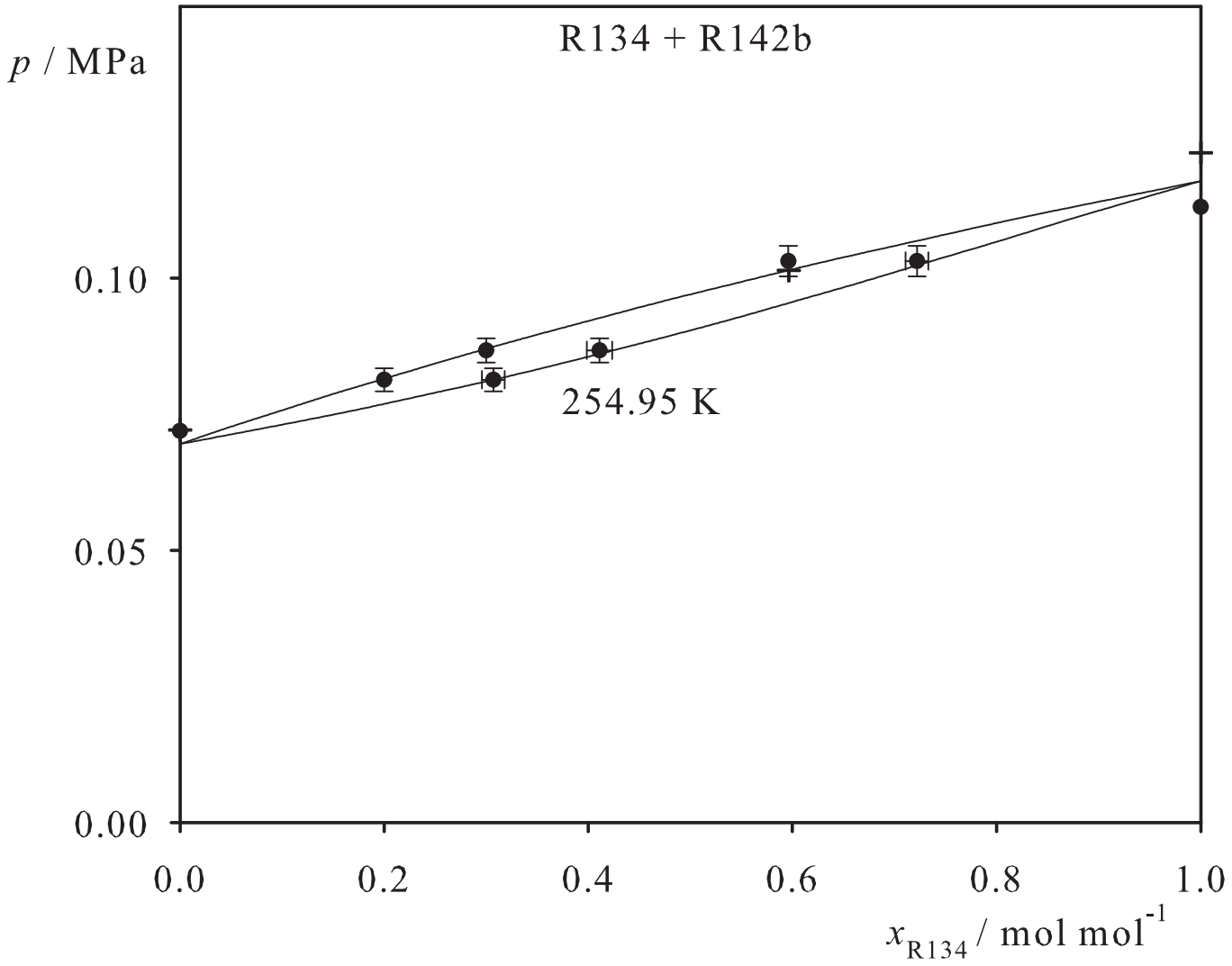

Fig. 226. Binary vapor-liquid equilibrium phase diagram: simulation data ●, experimental data + (cf. Table 2 of the manuscript for the reference) and Peng-Robinson equation of state —.

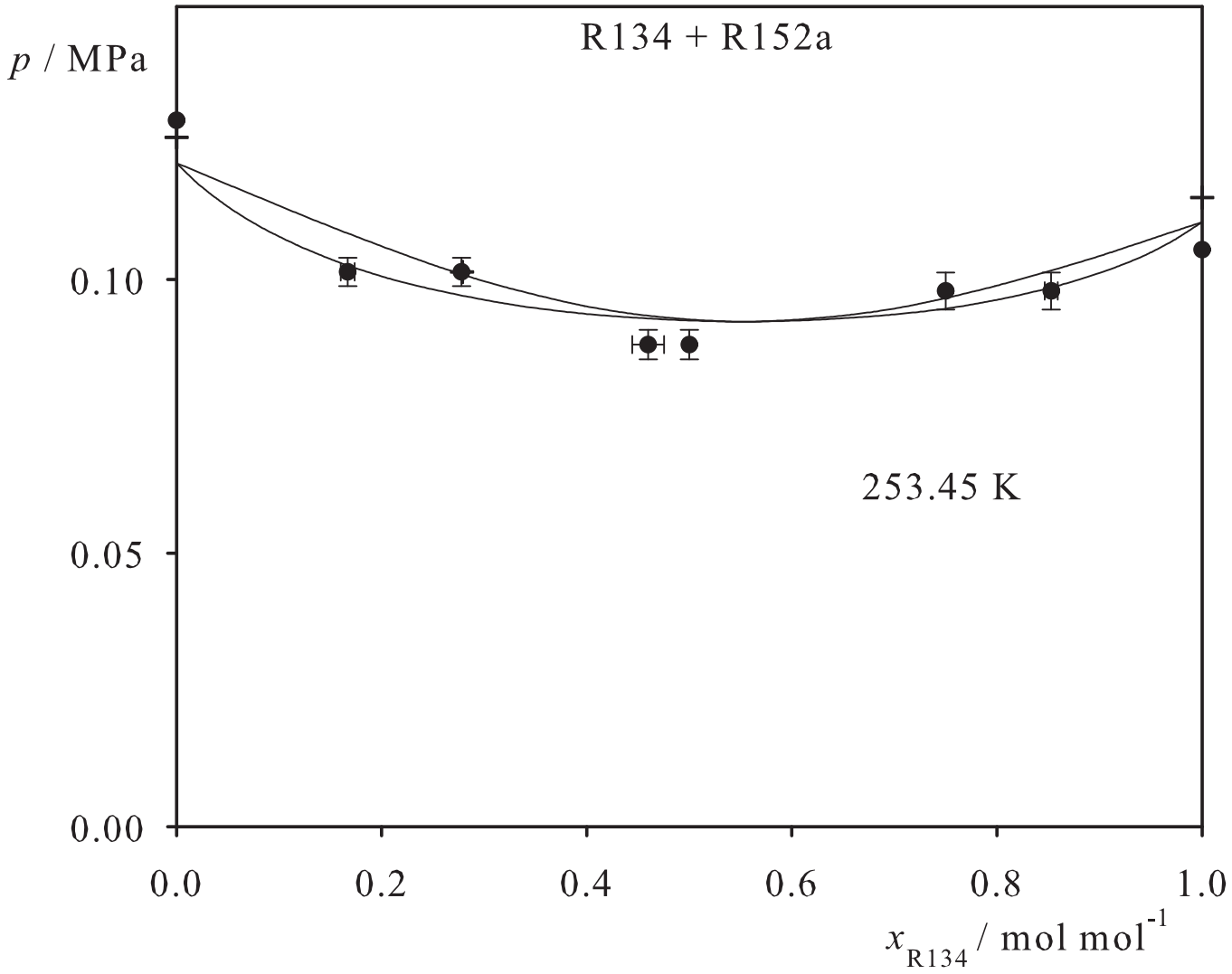

Fig. 227. Binary vapor-liquid equilibrium phase diagram: simulation data ●, experimental data + (cf. Table 2 of the manuscript for the reference) and Peng-Robinson equation of state —.

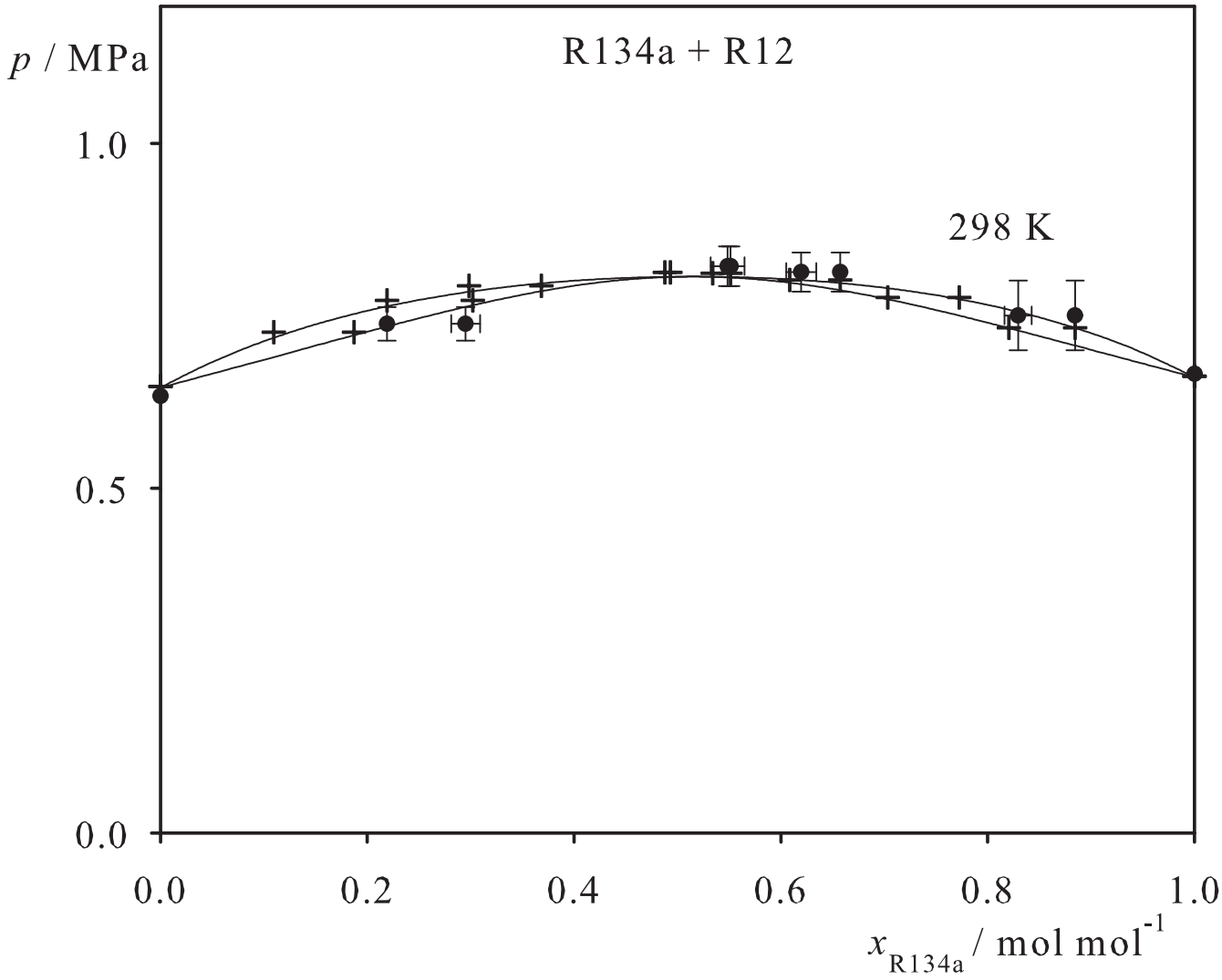

Fig. 228. Binary vapor-liquid equilibrium phase diagram: simulation data ●, experimental data + (cf. Table 2 of the manuscript for the reference) and Peng-Robinson equation of state —.

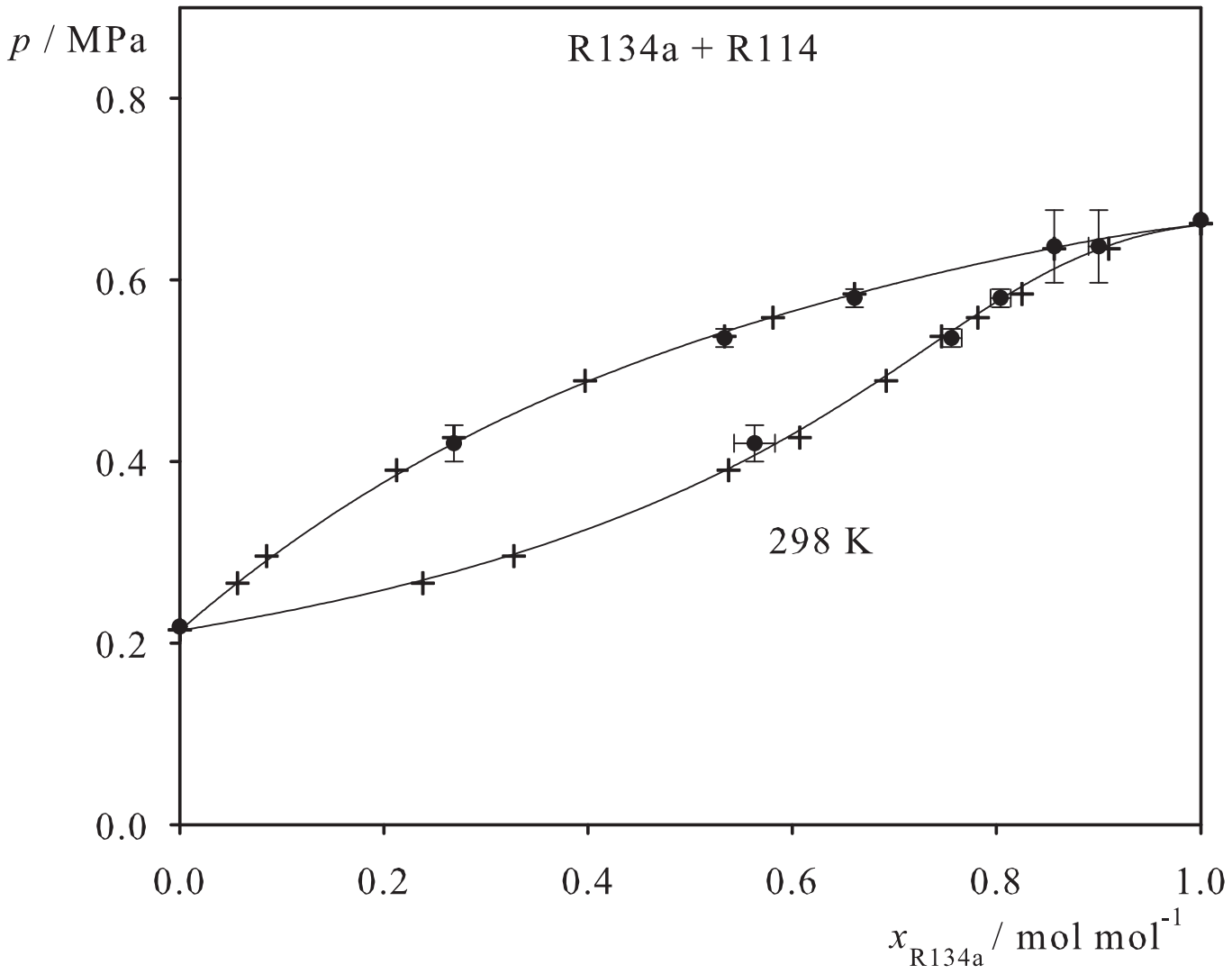

Fig. 229. Binary vapor-liquid equilibrium phase diagram: simulation data ●, experimental data + (cf. Table 2 of the manuscript for the reference) and Peng-Robinson equation of state —.

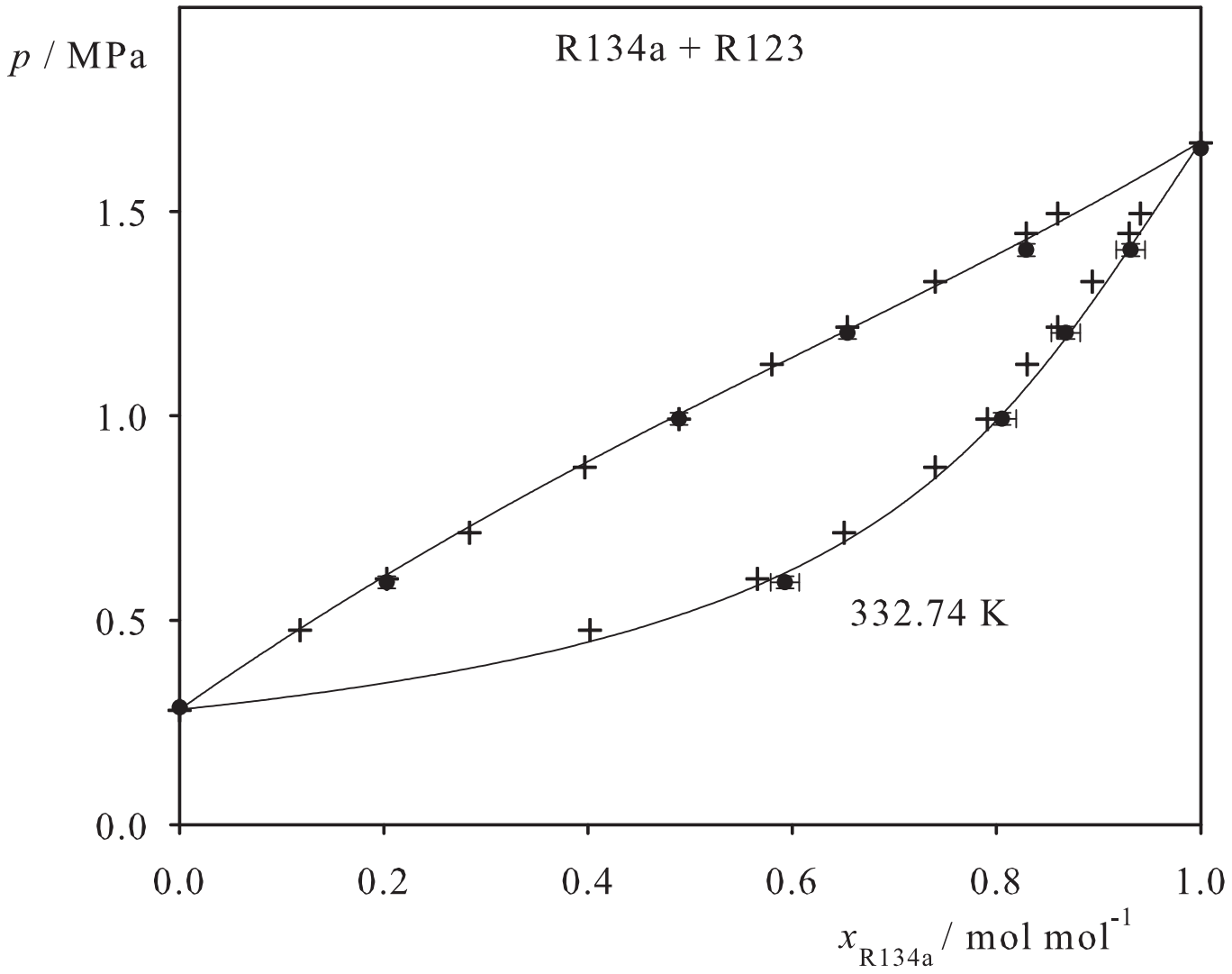

Fig. 230. Binary vapor-liquid equilibrium phase diagram: simulation data ●, experimental data + (cf. Table 2 of the manuscript for the reference) and Peng-Robinson equation of state —.

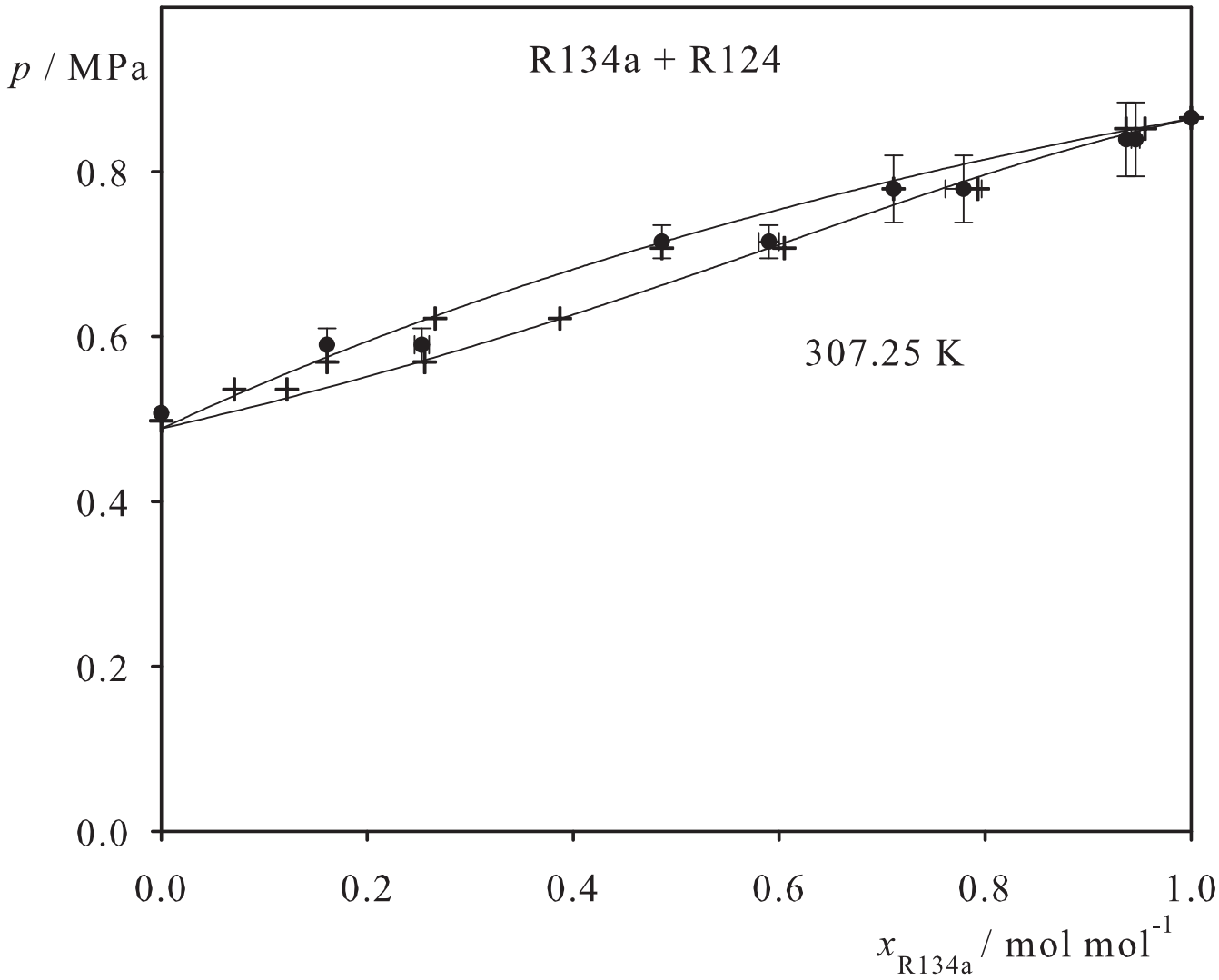

Fig. 231. Binary vapor-liquid equilibrium phase diagram: simulation data ●, experimental data + (cf. Table 2 of the manuscript for the reference) and Peng-Robinson equation of state —.

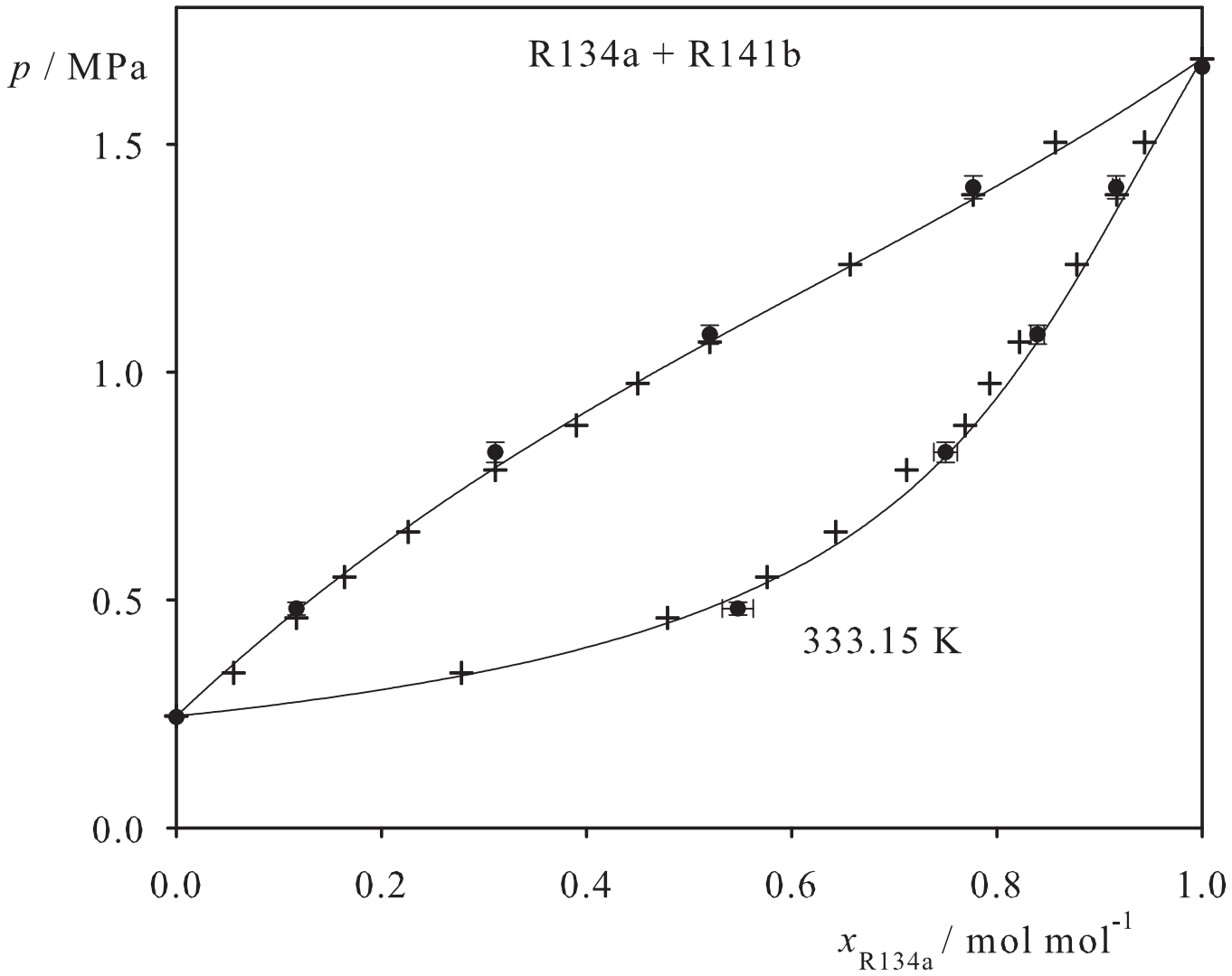

Fig. 232. Binary vapor-liquid equilibrium phase diagram: simulation data ●, experimental data + (cf. Table 2 of the manuscript for the reference) and Peng-Robinson equation of state —.

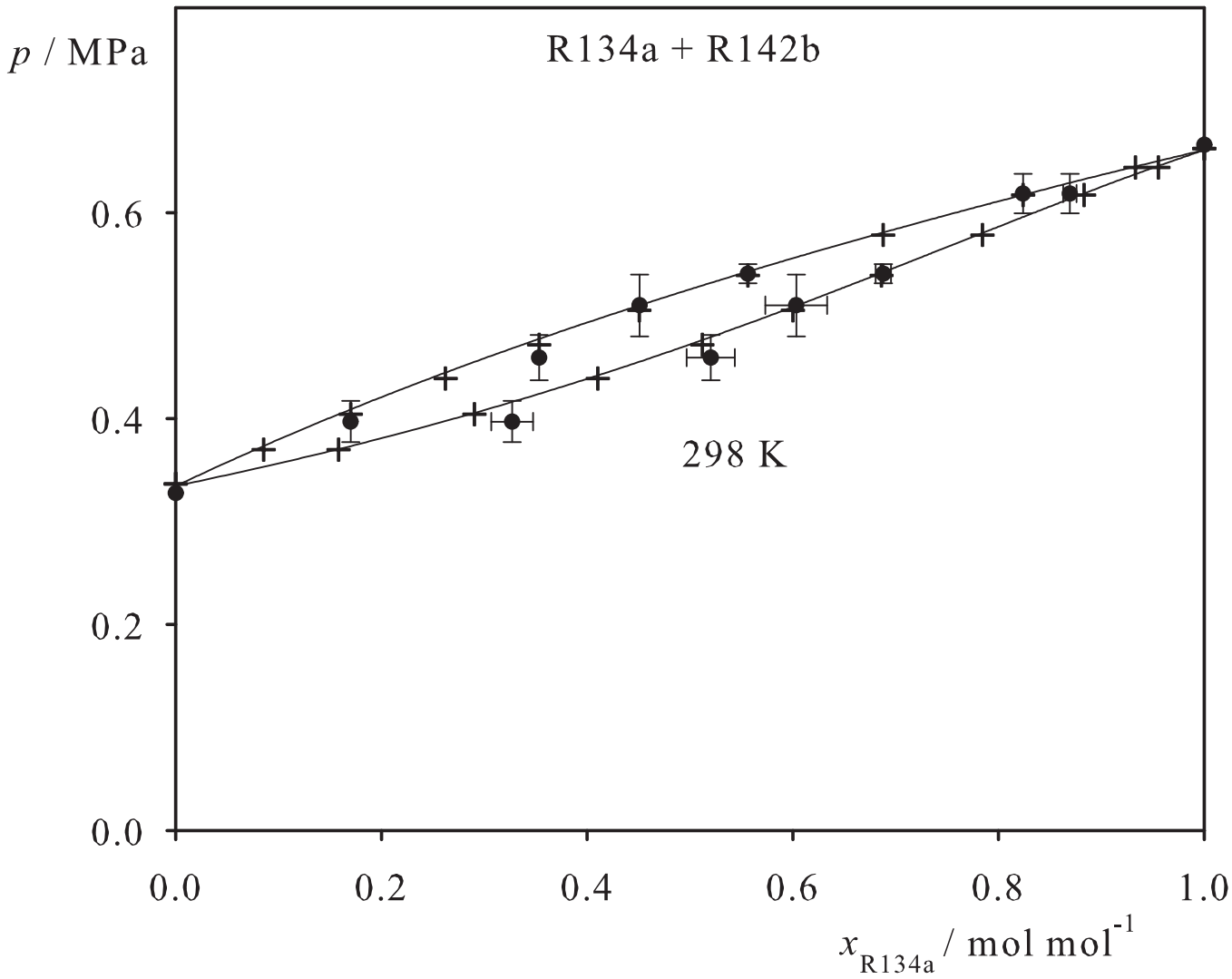

Fig. 233. Binary vapor-liquid equilibrium phase diagram: simulation data ●, experimental data + (cf. Table 2 of the manuscript for the reference) and Peng-Robinson equation of state —.

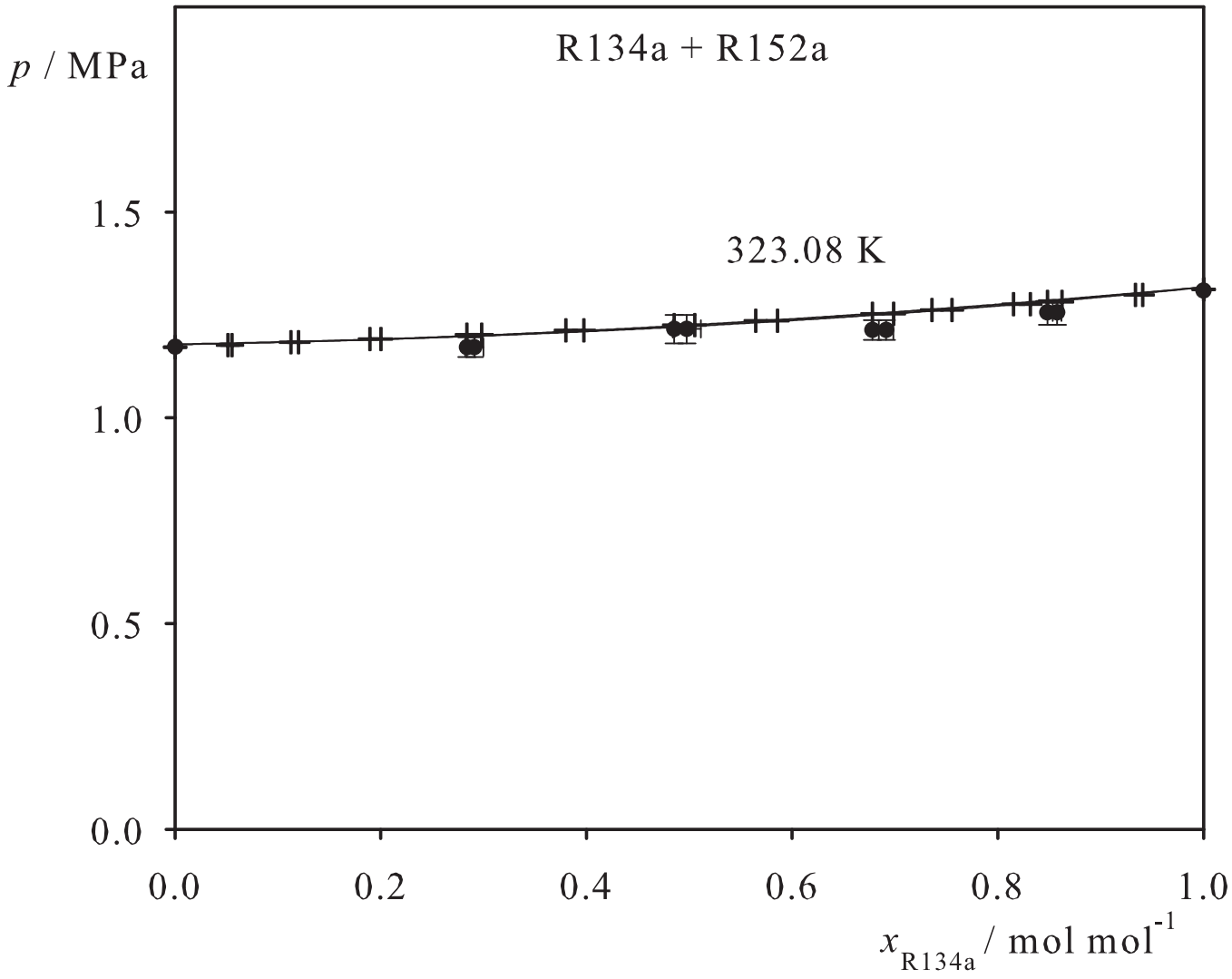

Fig. 234. Binary vapor-liquid equilibrium phase diagram: simulation data ●, experimental data + (cf. Table 2 of the manuscript for the reference) and Peng-Robinson equation of state —.

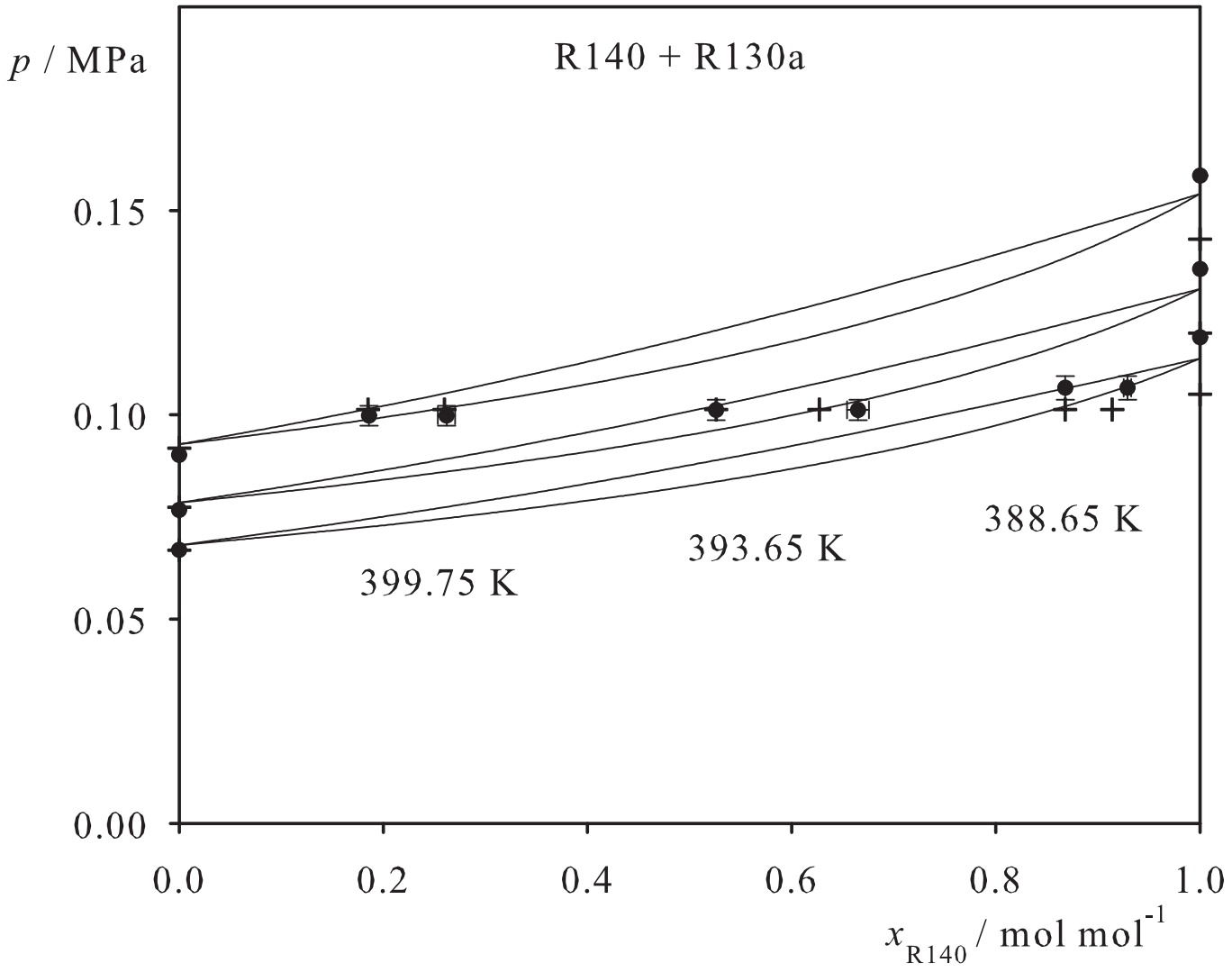

Fig. 235. Binary vapor-liquid equilibrium phase diagram: simulation data ●, experimental data + (cf. Table 2 of the manuscript for the reference) and Peng-Robinson equation of state —.

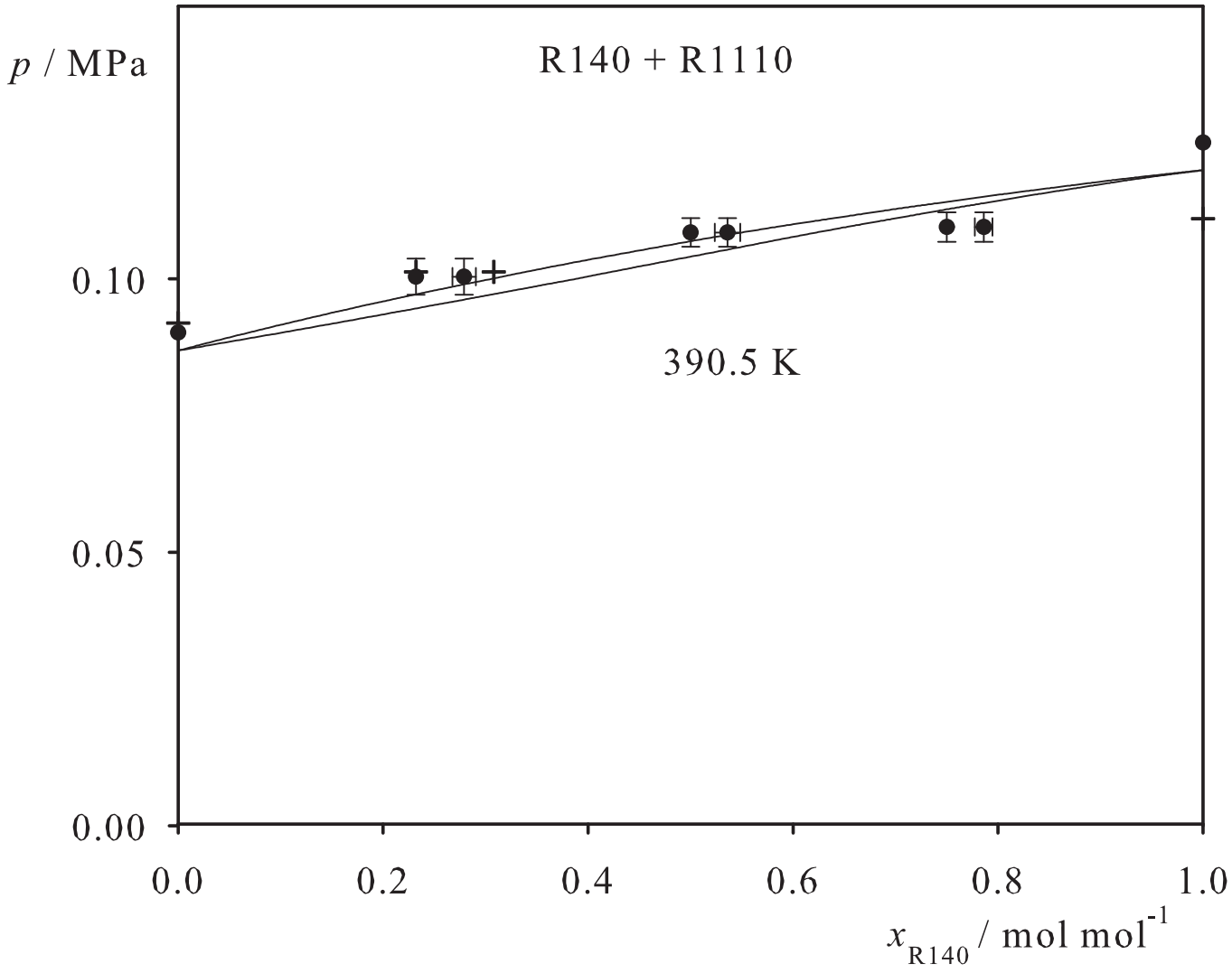

Fig. 236. Binary vapor-liquid equilibrium phase diagram: simulation data ●, experimental data + (cf. Table 2 of the manuscript for the reference) and Peng-Robinson equation of state —.

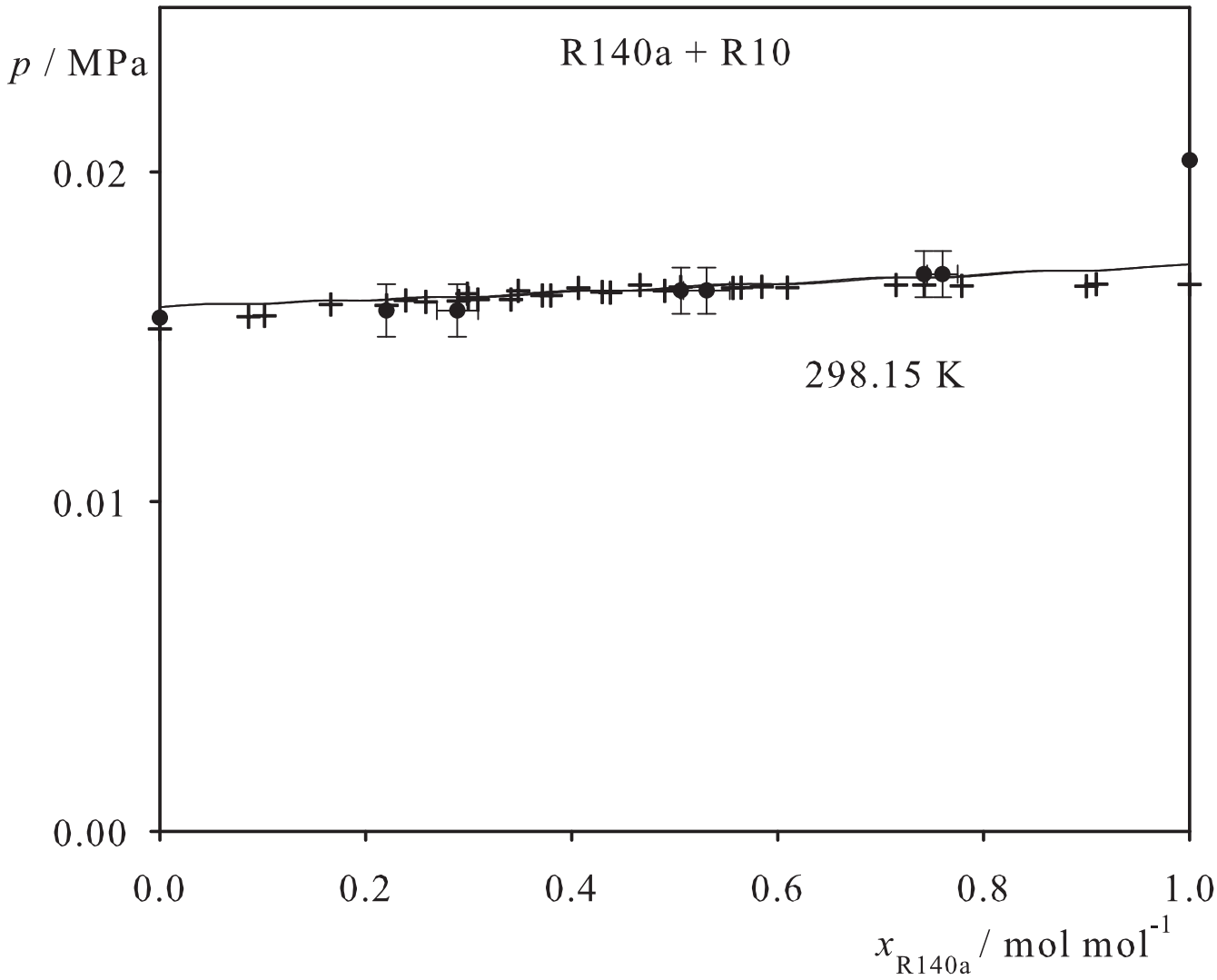

Fig. 237. Binary vapor-liquid equilibrium phase diagram: simulation data ●, experimental data + (cf. Table 2 of the manuscript for the reference) and Peng-Robinson equation of state —.

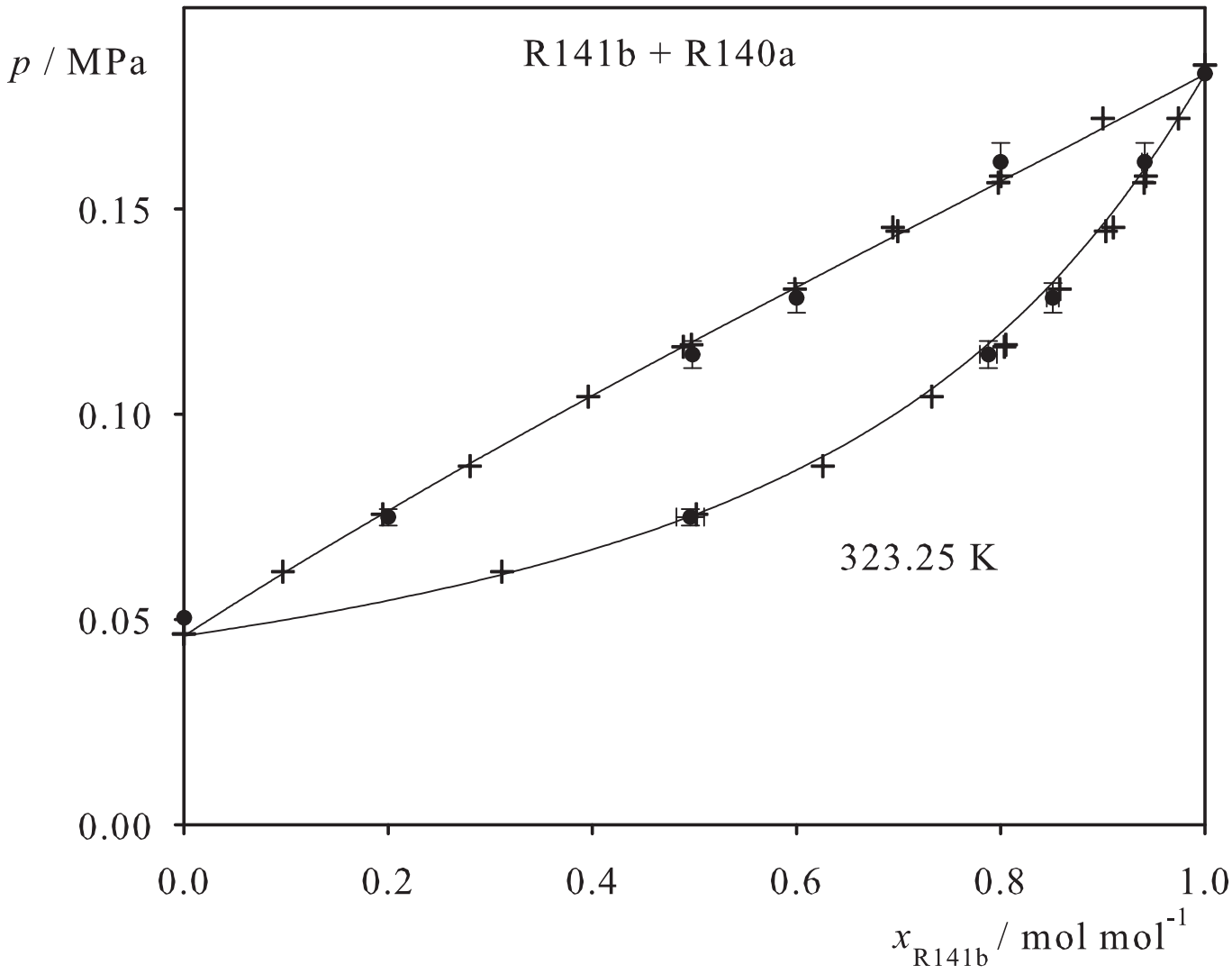

Fig. 238. Binary vapor-liquid equilibrium phase diagram: simulation data ●, experimental data + (cf. Table 2 of the manuscript for the reference) and Peng-Robinson equation of state —.

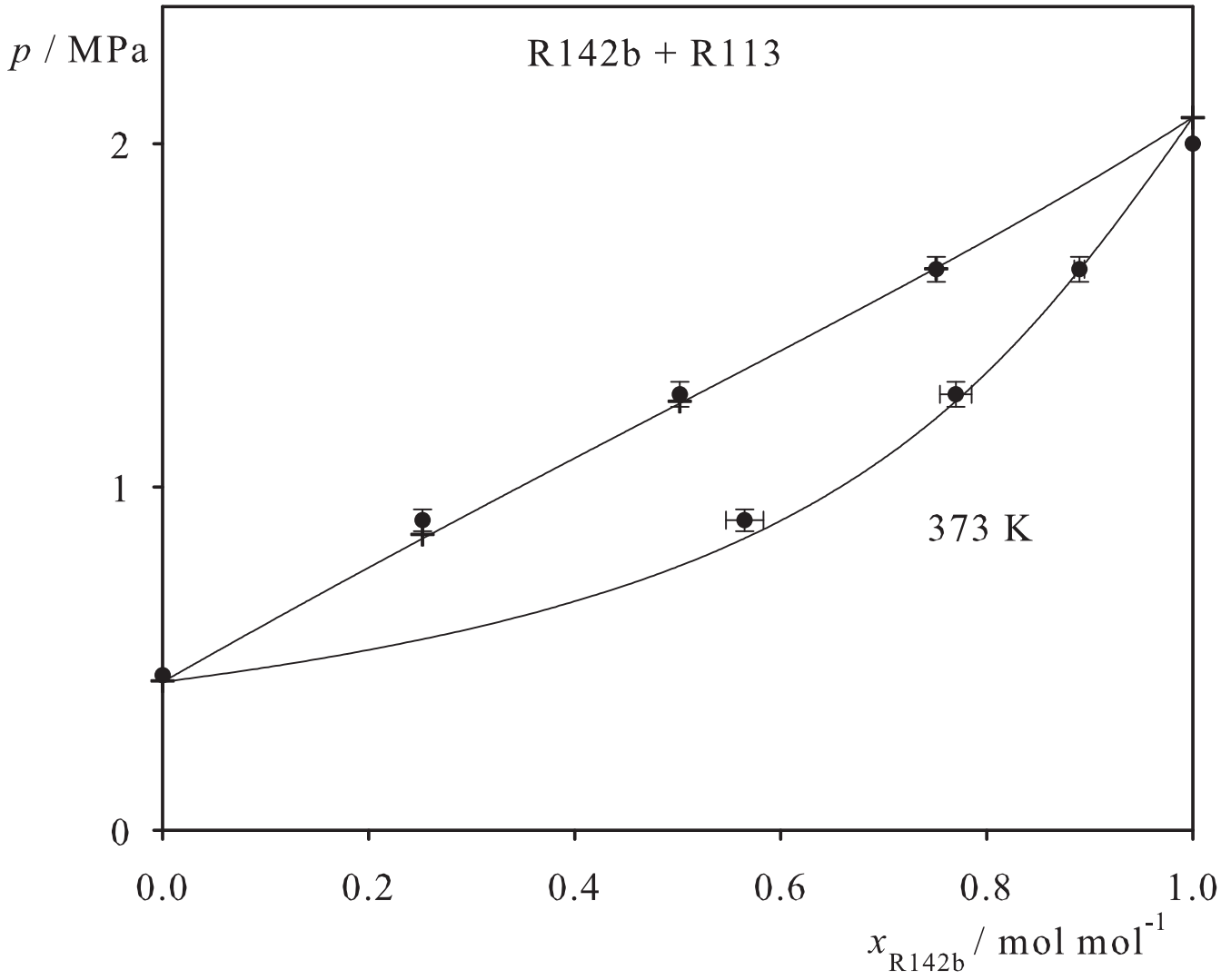

Fig. 239. Binary vapor-liquid equilibrium phase diagram: simulation data ●, experimental data + (cf. Table 2 of the manuscript for the reference) and Peng-Robinson equation of state —.

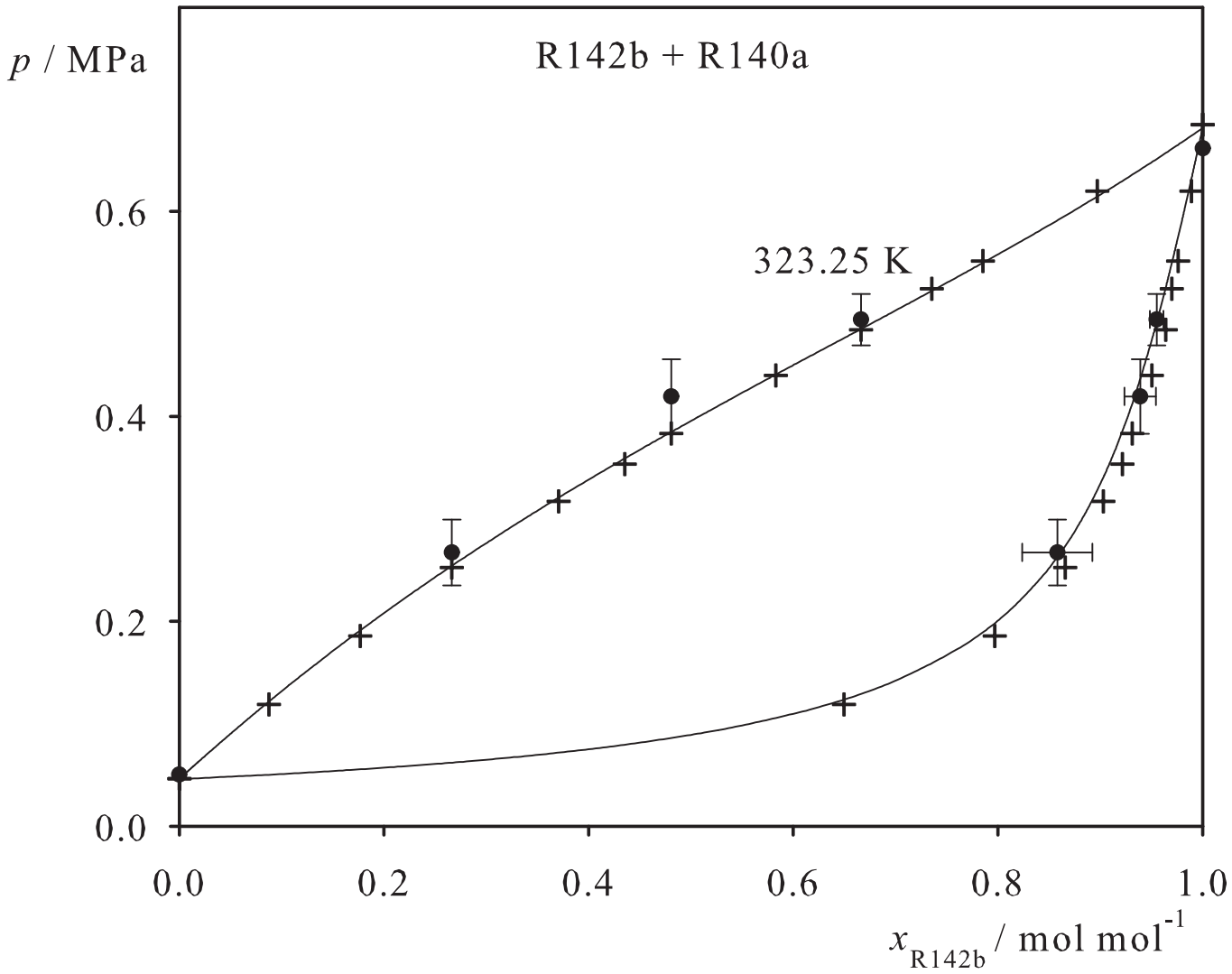

Fig. 240. Binary vapor-liquid equilibrium phase diagram: simulation data ●, experimental data + (cf. Table 2 of the manuscript for the reference) and Peng-Robinson equation of state —.

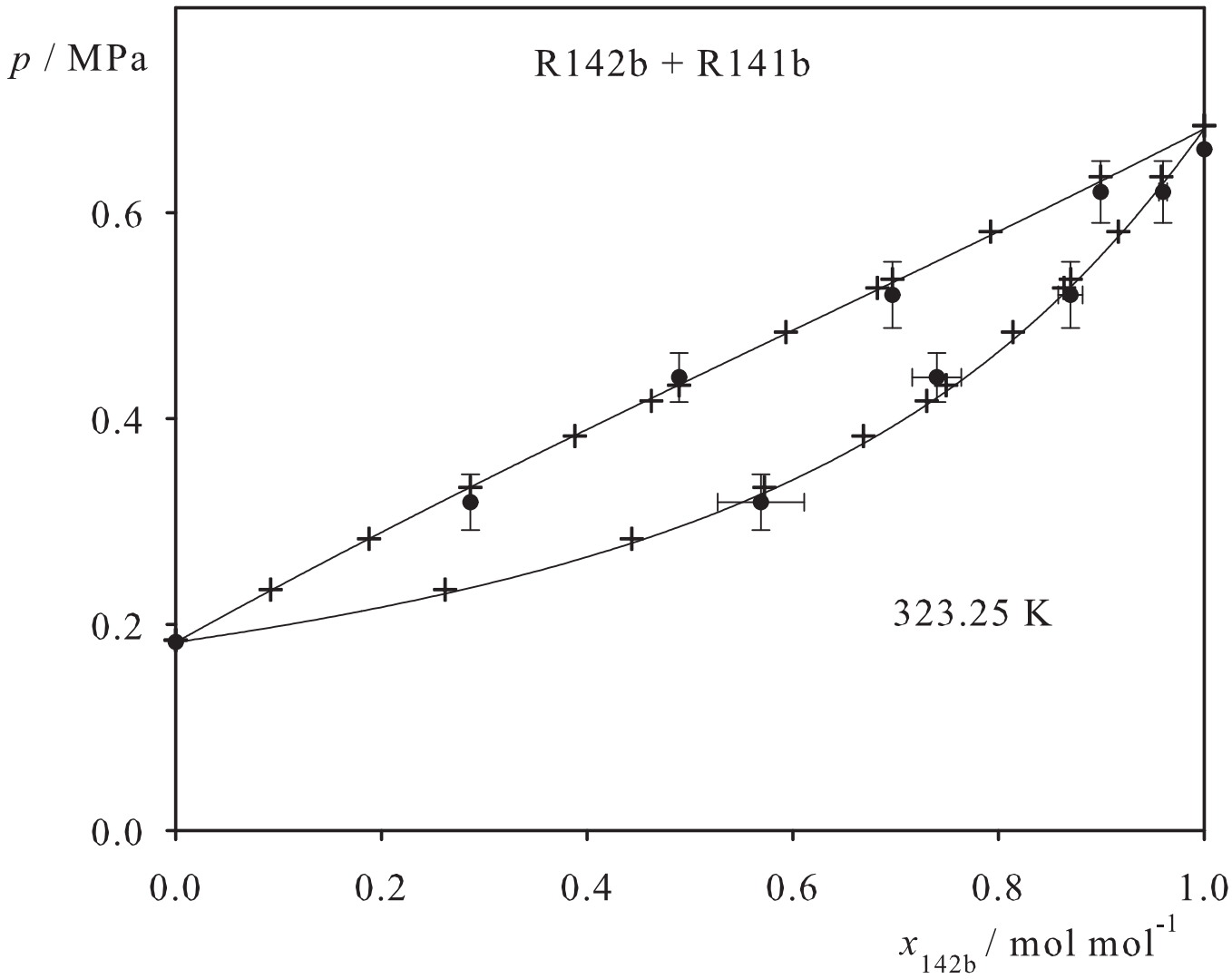

Fig. 241. Binary vapor-liquid equilibrium phase diagram: simulation data ●, experimental data + (cf. Table 2 of the manuscript for the reference) and Peng-Robinson equation of state —.

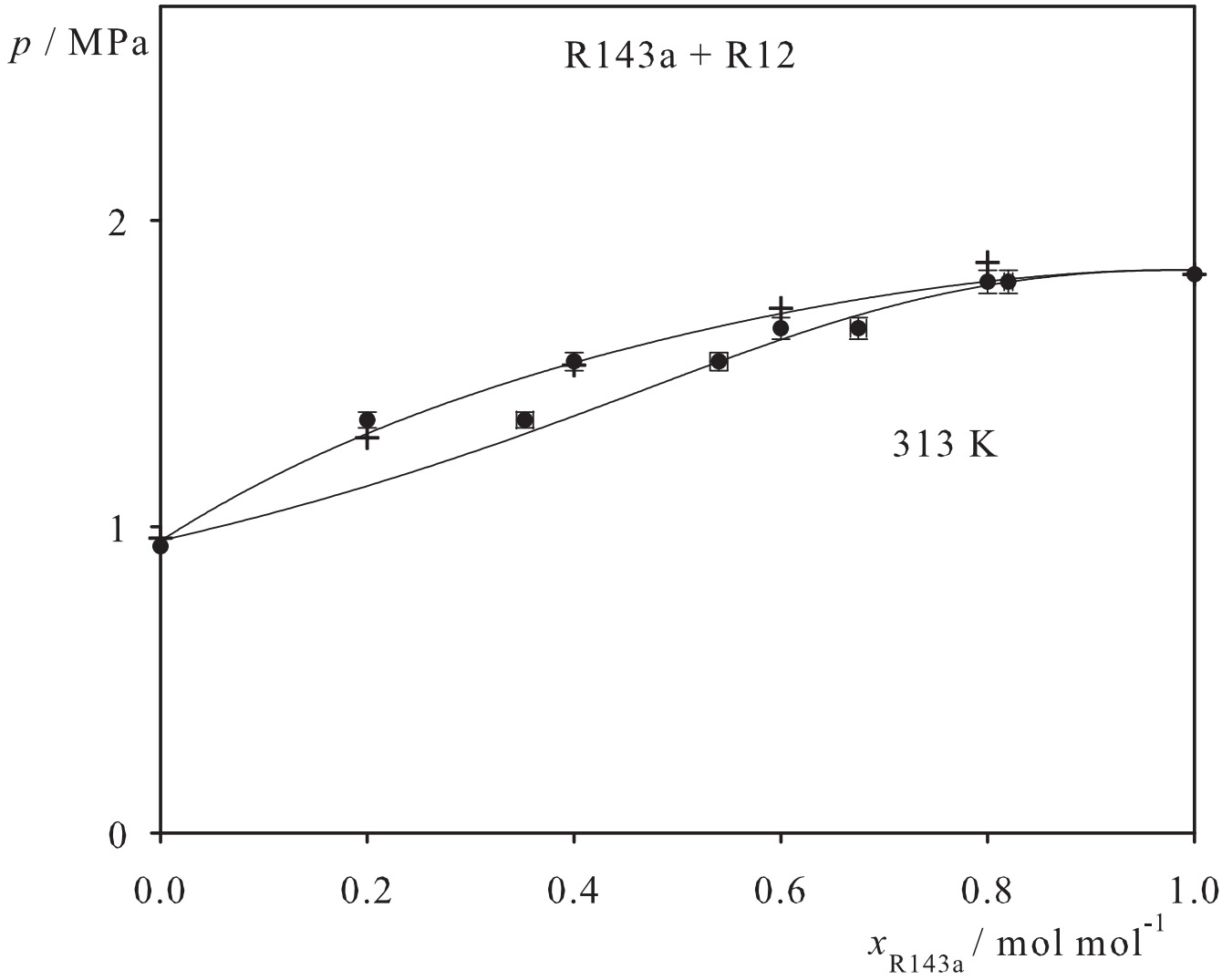

Fig. 242. Binary vapor-liquid equilibrium phase diagram: simulation data ●, experimental data + (cf. Table 2 of the manuscript for the reference) and Peng-Robinson equation of state —.

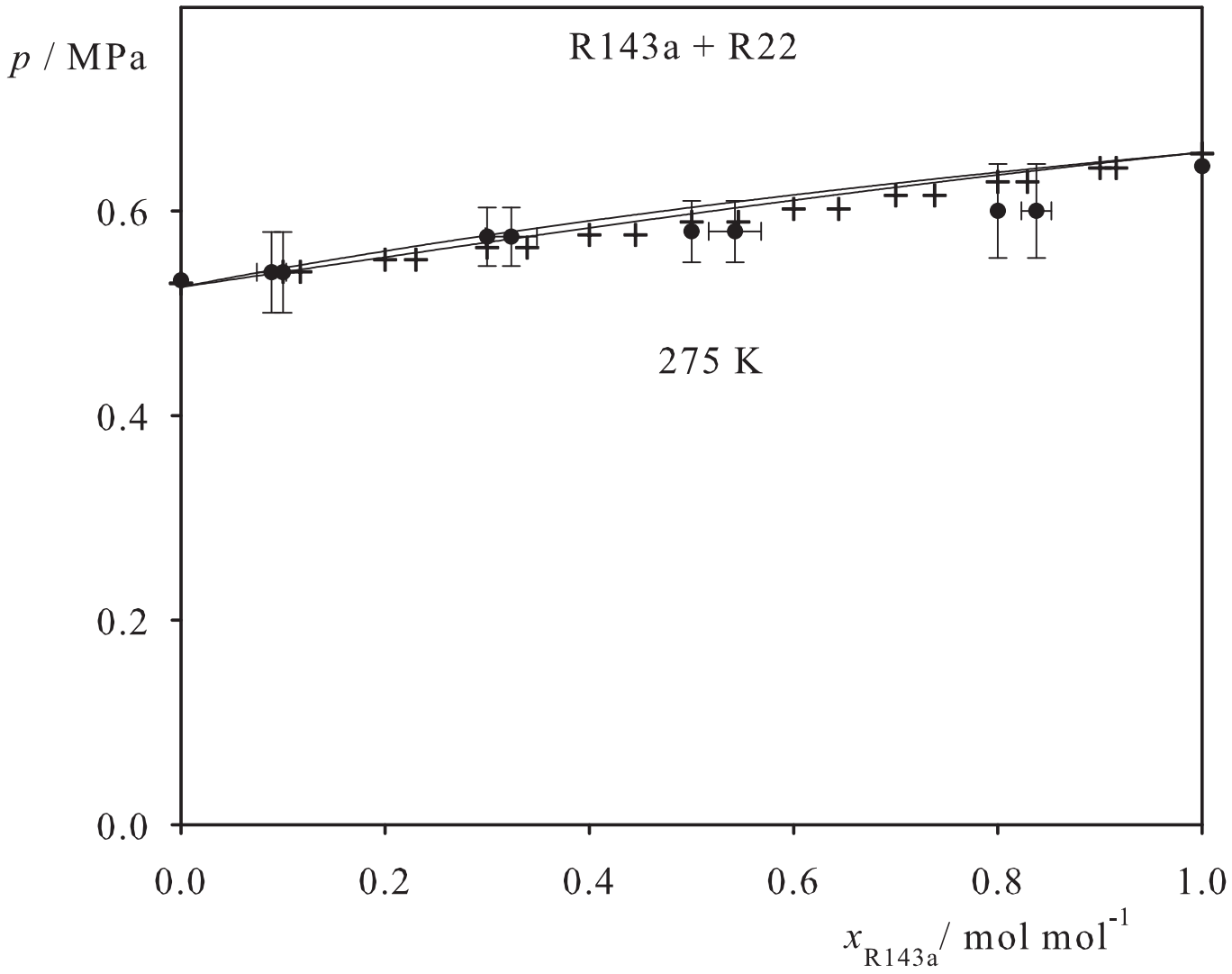

Fig. 243. Binary vapor-liquid equilibrium phase diagram: simulation data ●, experimental data + (cf. Table 2 of the manuscript for the reference) and Peng-Robinson equation of state —.

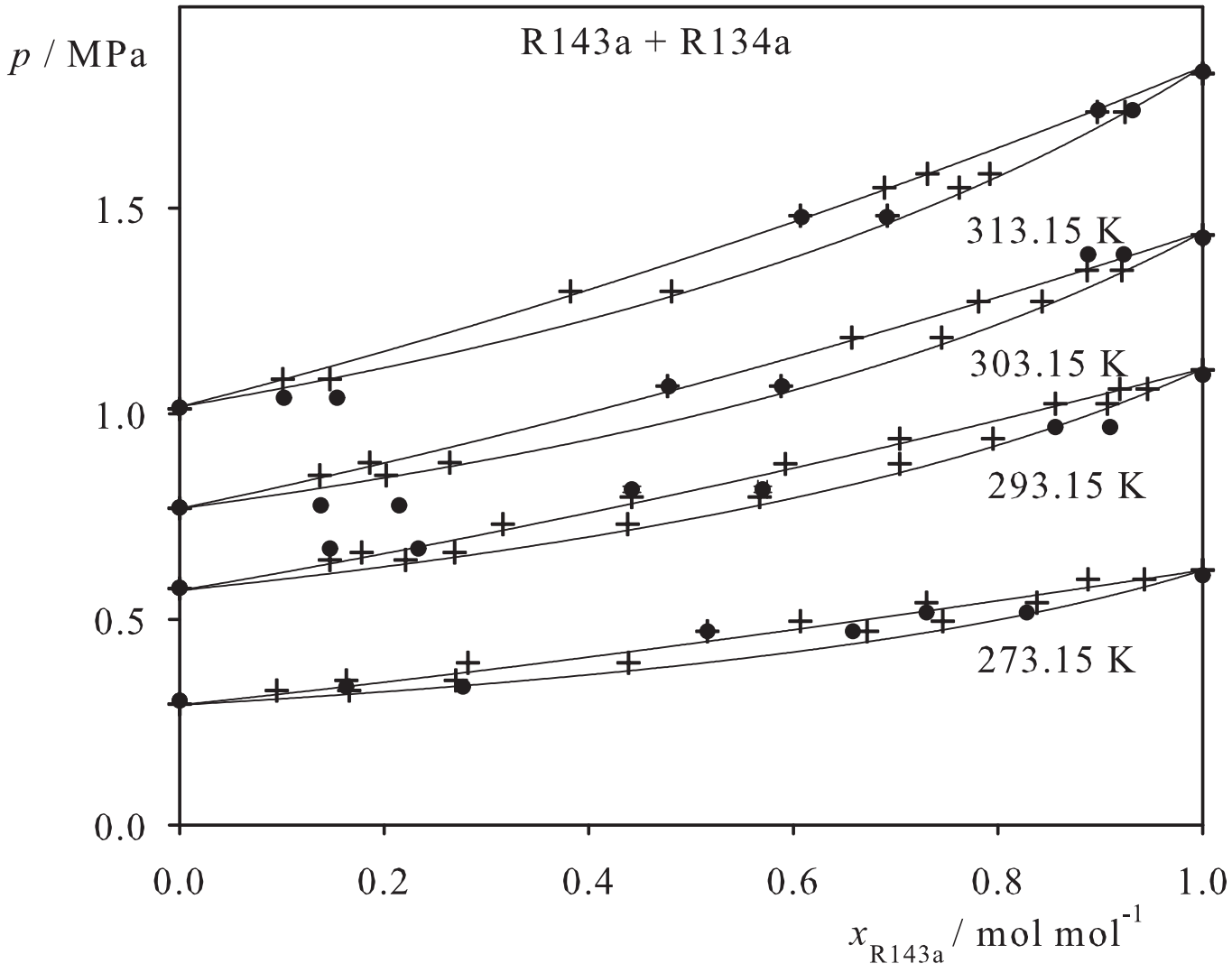

Fig. 244. Binary vapor-liquid equilibrium phase diagram: simulation data ●, experimental data + (cf. Table 2 of the manuscript for the reference) and Peng-Robinson equation of state —.

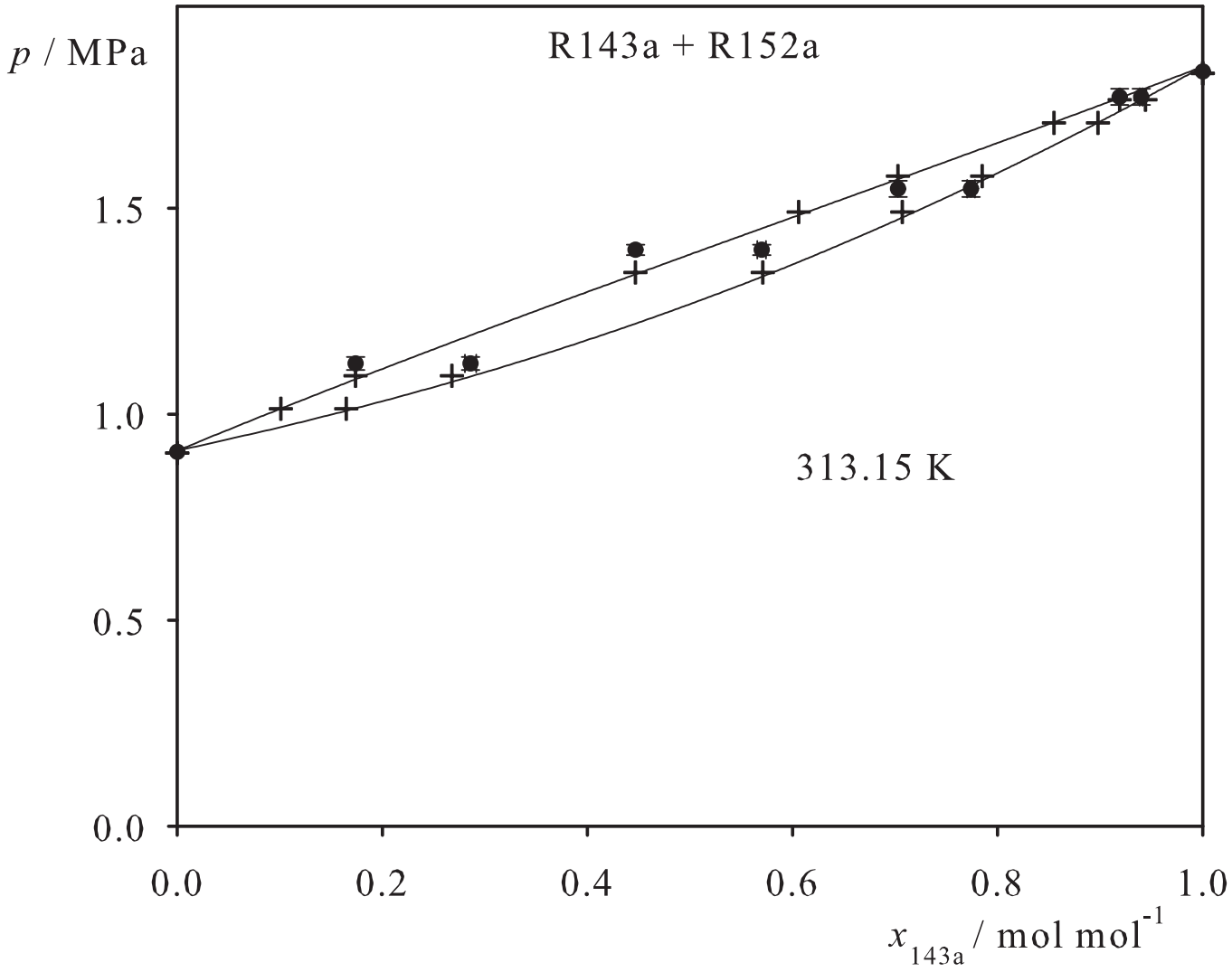

Fig. 245. Binary vapor-liquid equilibrium phase diagram: simulation data ●, experimental data + (cf. Table 2 of the manuscript for the reference) and Peng-Robinson equation of state —.

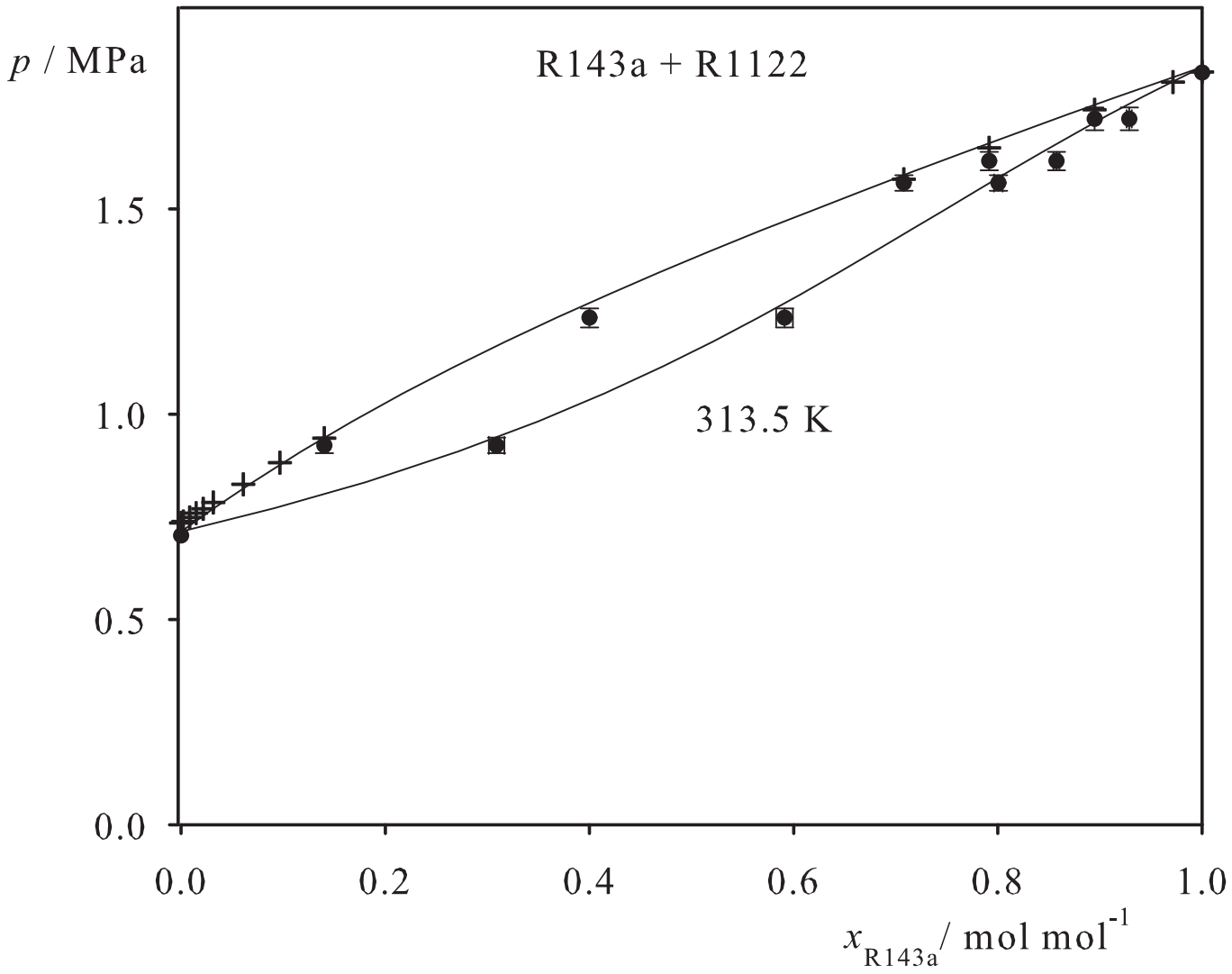

Fig. 246. Binary vapor-liquid equilibrium phase diagram: simulation data ●, experimental data + (cf. Table 2 of the manuscript for the reference) and Peng-Robinson equation of state —.

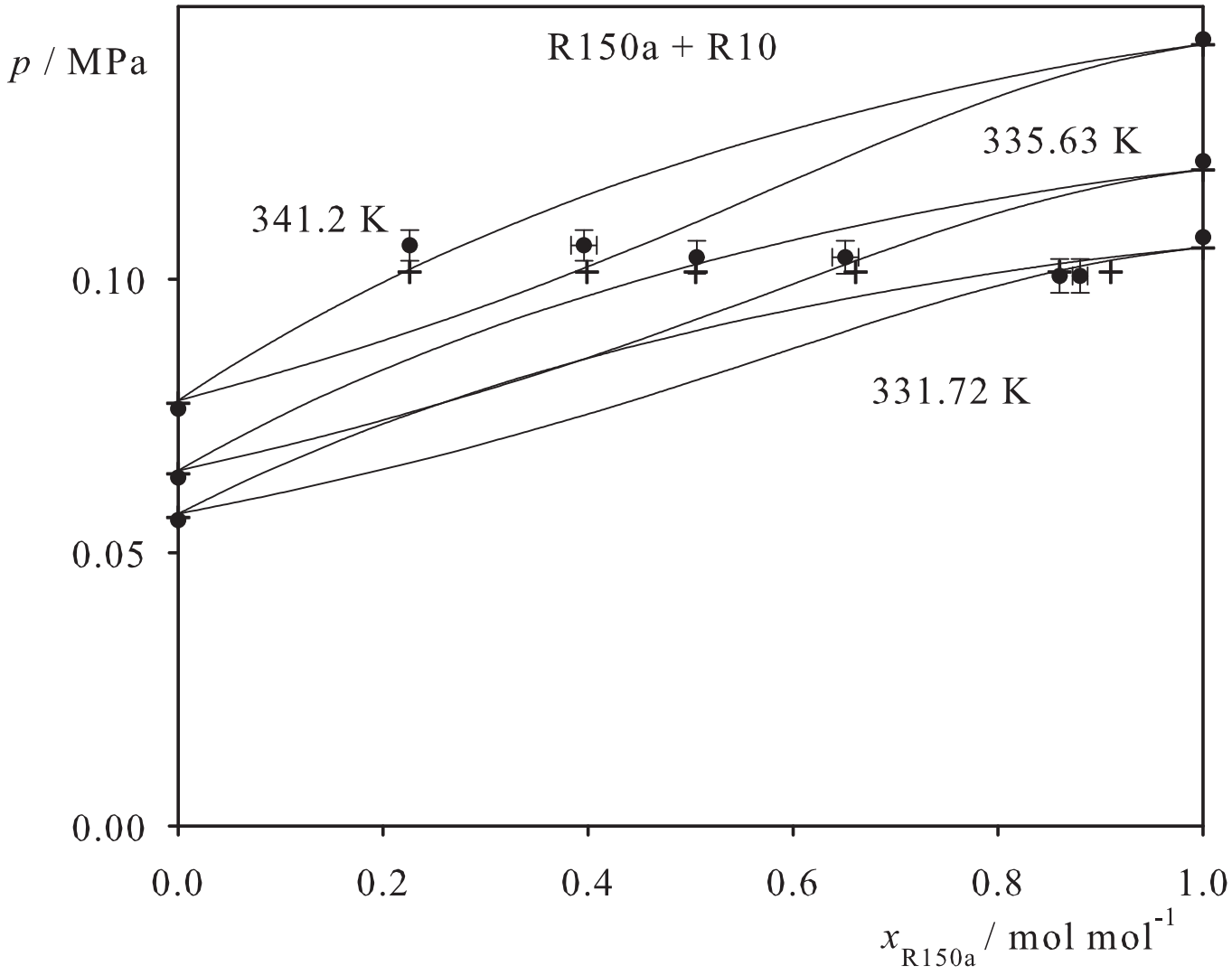

Fig. 247. Binary vapor-liquid equilibrium phase diagram: simulation data ● and experimental data + (cf. Table 2 of the manuscript for the reference).

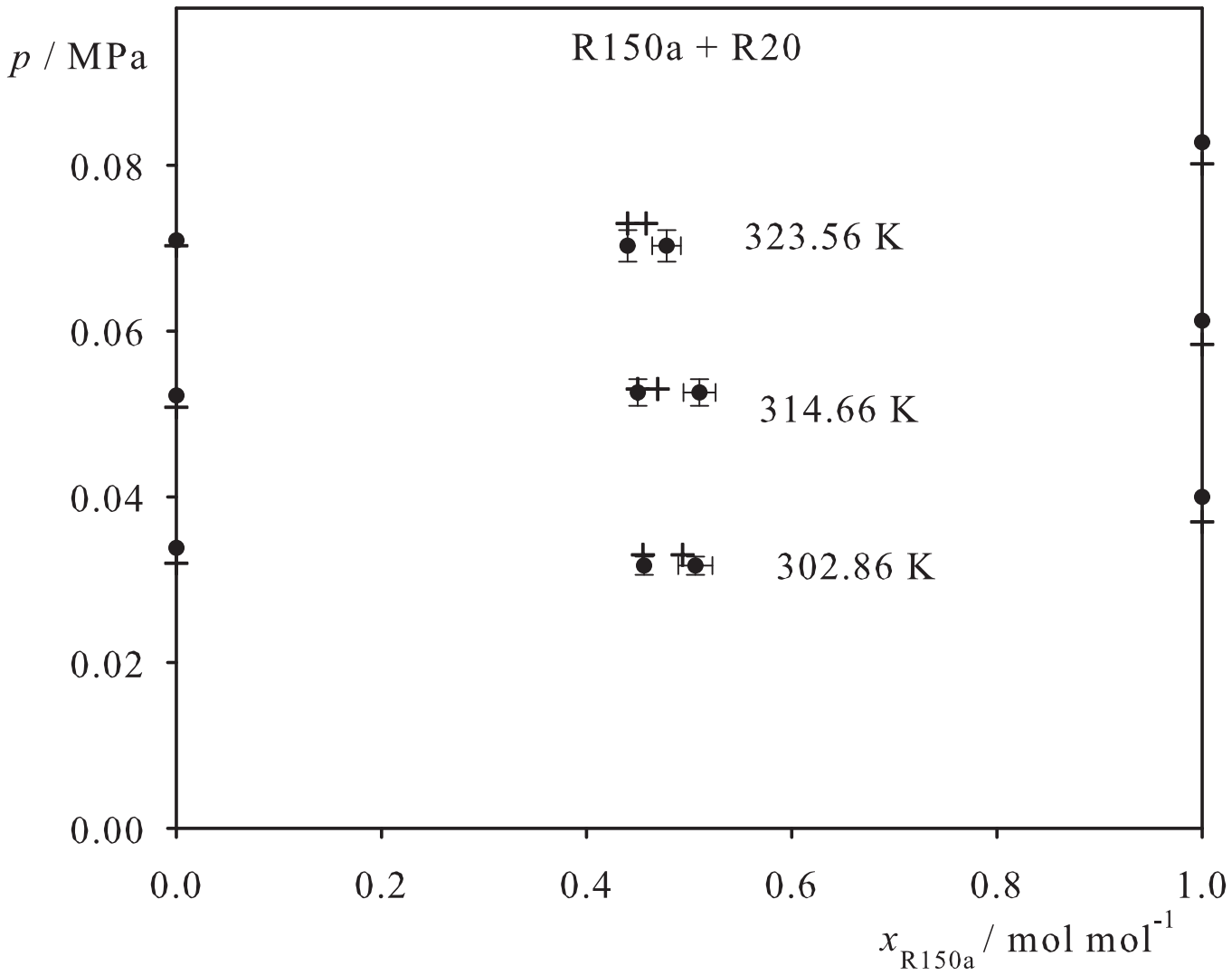

Fig. 248. Binary vapor-liquid equilibrium phase diagram: simulation data ●, experimental data + (cf. Table 2 of the manuscript for the reference) and Peng-Robinson equation of state —.

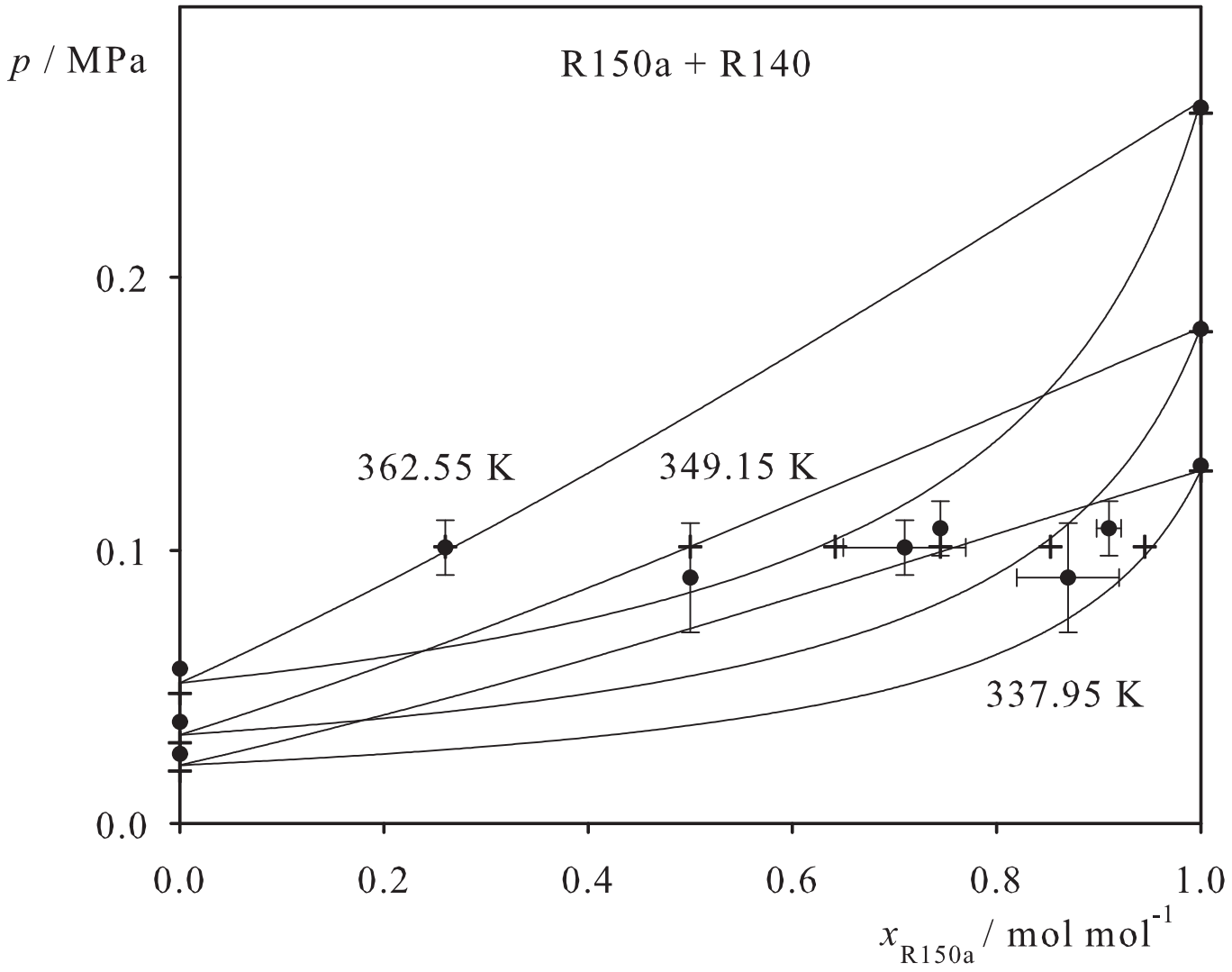

Fig. 249. Binary vapor-liquid equilibrium phase diagram: simulation data ●, experimental data + (cf. Table 2 of the manuscript for the reference) and Peng-Robinson equation of state —.

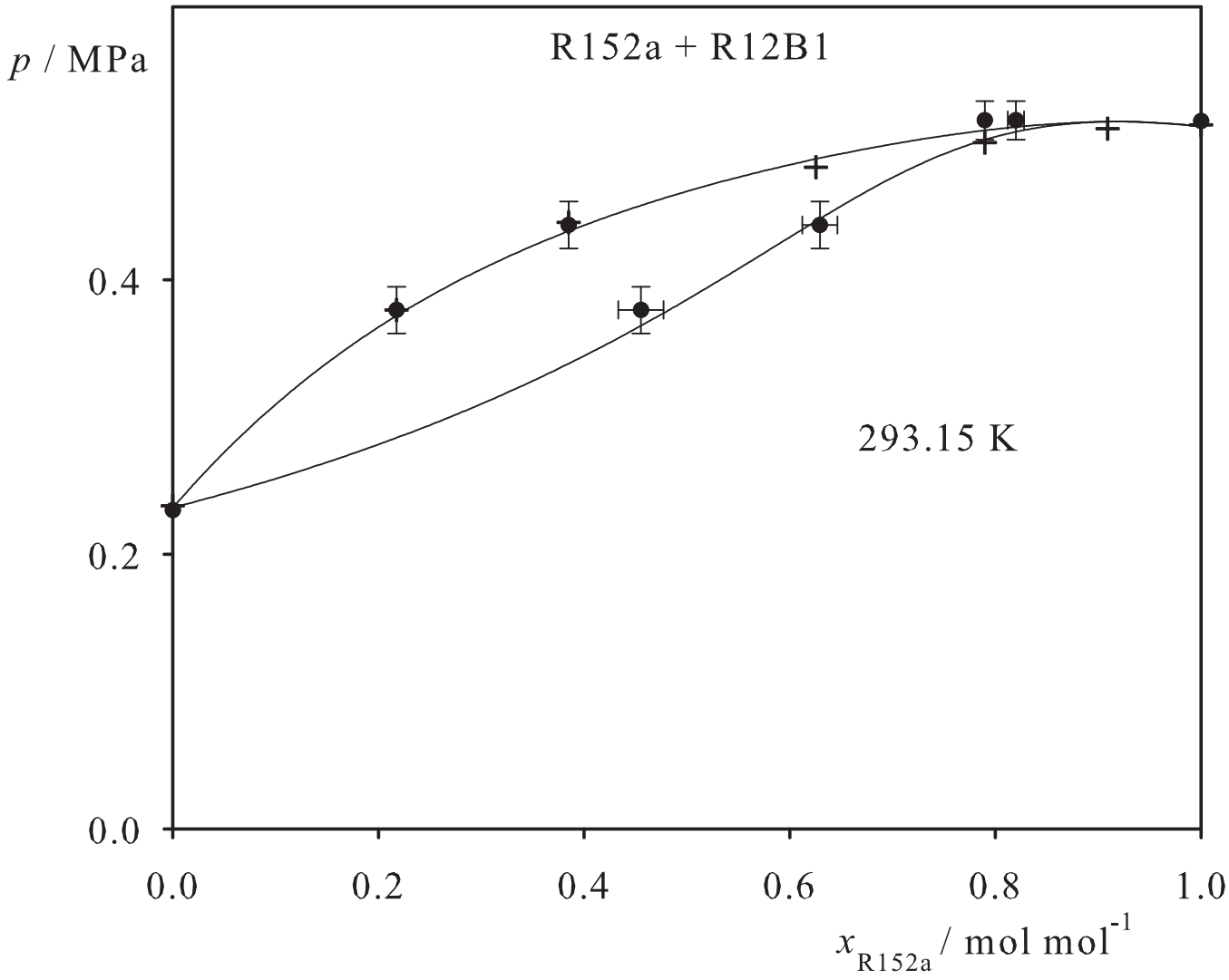

Fig. 250. Binary vapor-liquid equilibrium phase diagram: simulation data ●, experimental data + (cf. Table 2 of the manuscript for the reference) and Peng-Robinson equation of state —.

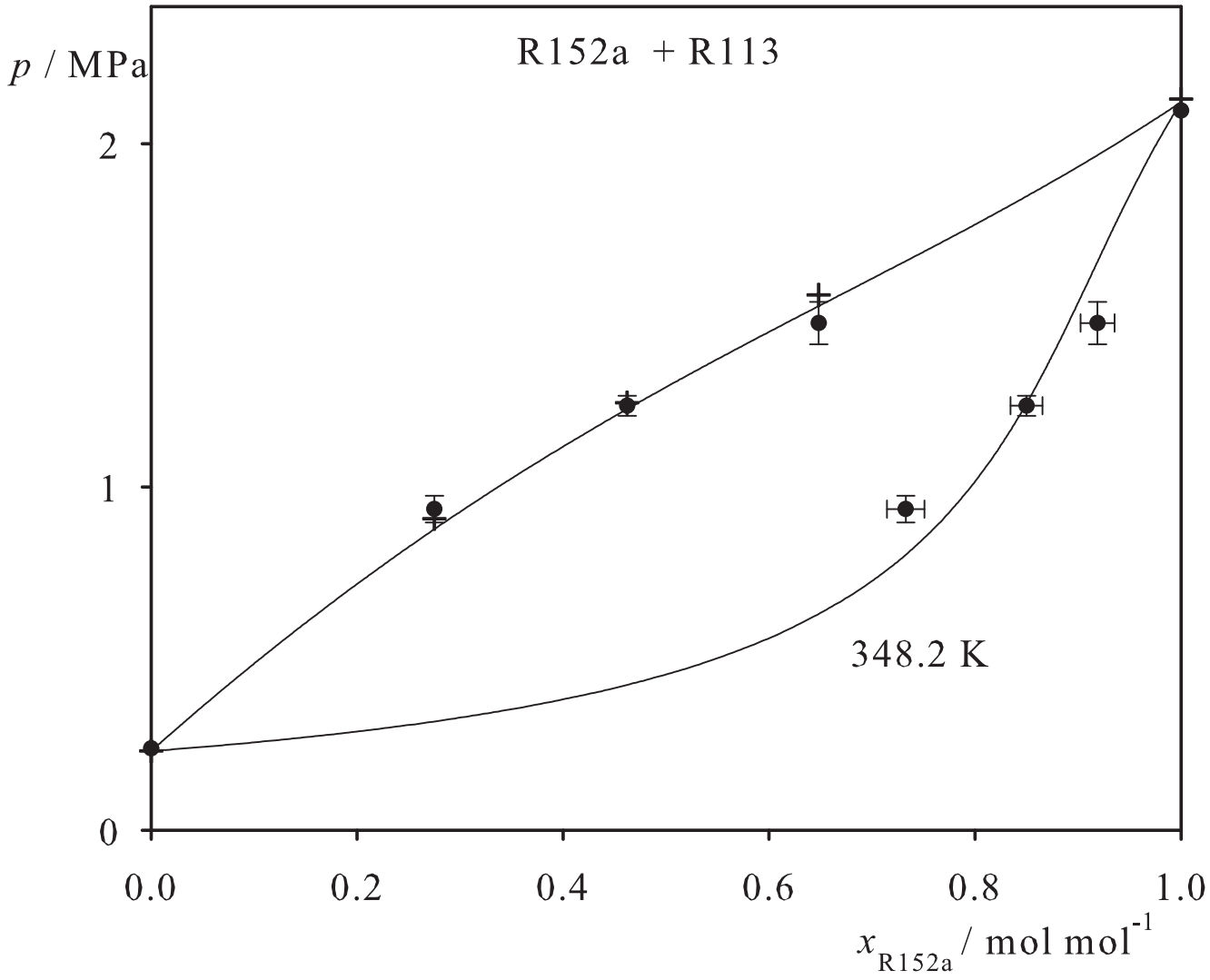

Fig. 251. Binary vapor-liquid equilibrium phase diagram: simulation data ●, experimental data + (cf. Table 2 of the manuscript for the reference) and Peng-Robinson equation of state —.

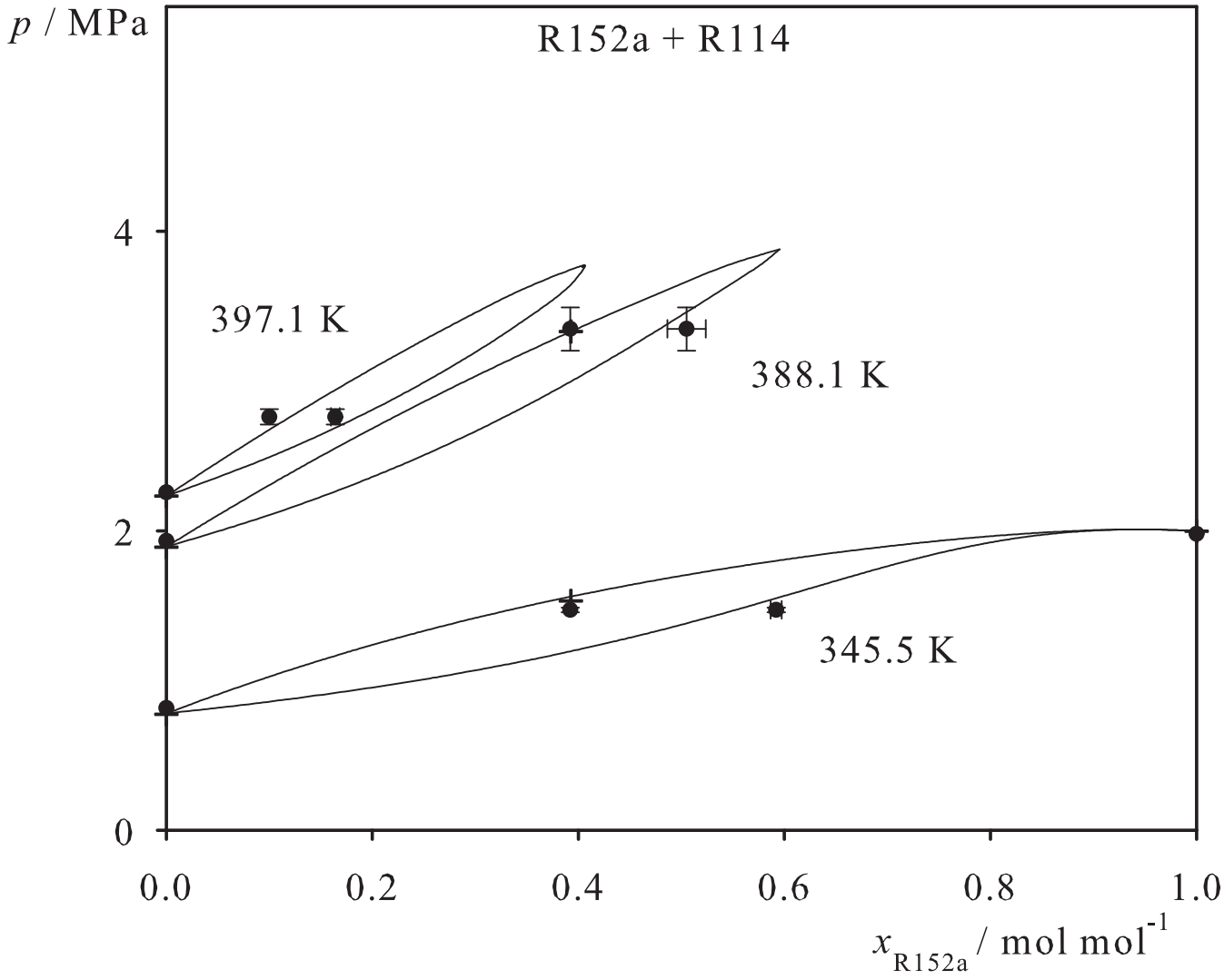

Fig. 252. Binary vapor-liquid equilibrium phase diagram: simulation data ●, experimental data + (cf. Table 2 of the manuscript for the reference) and Peng-Robinson equation of state —.

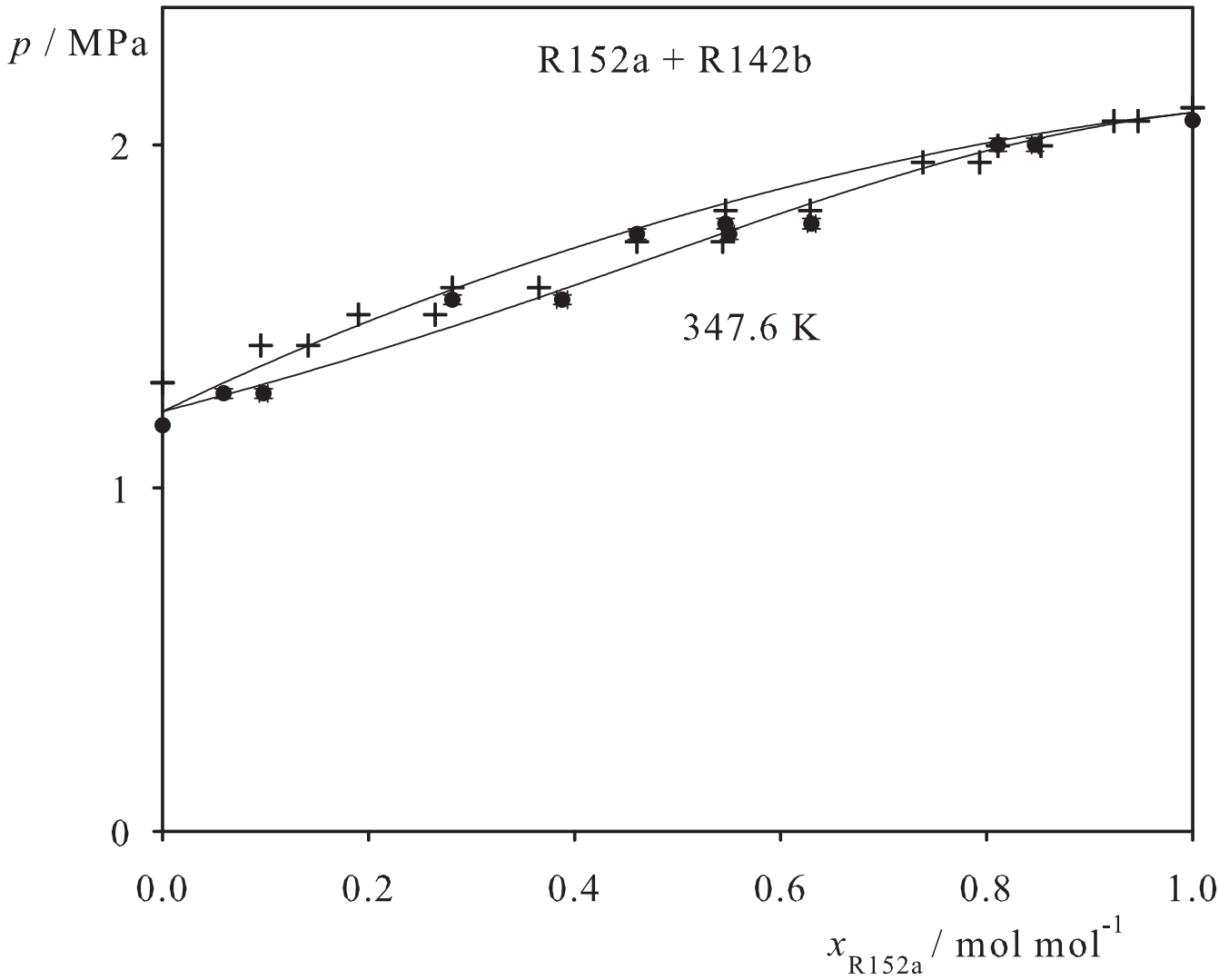

Fig. 253. Binary vapor-liquid equilibrium phase diagram: simulation data ●, experimental data + (cf. Table 2 of the manuscript for the reference) and Peng-Robinson equation of state —.

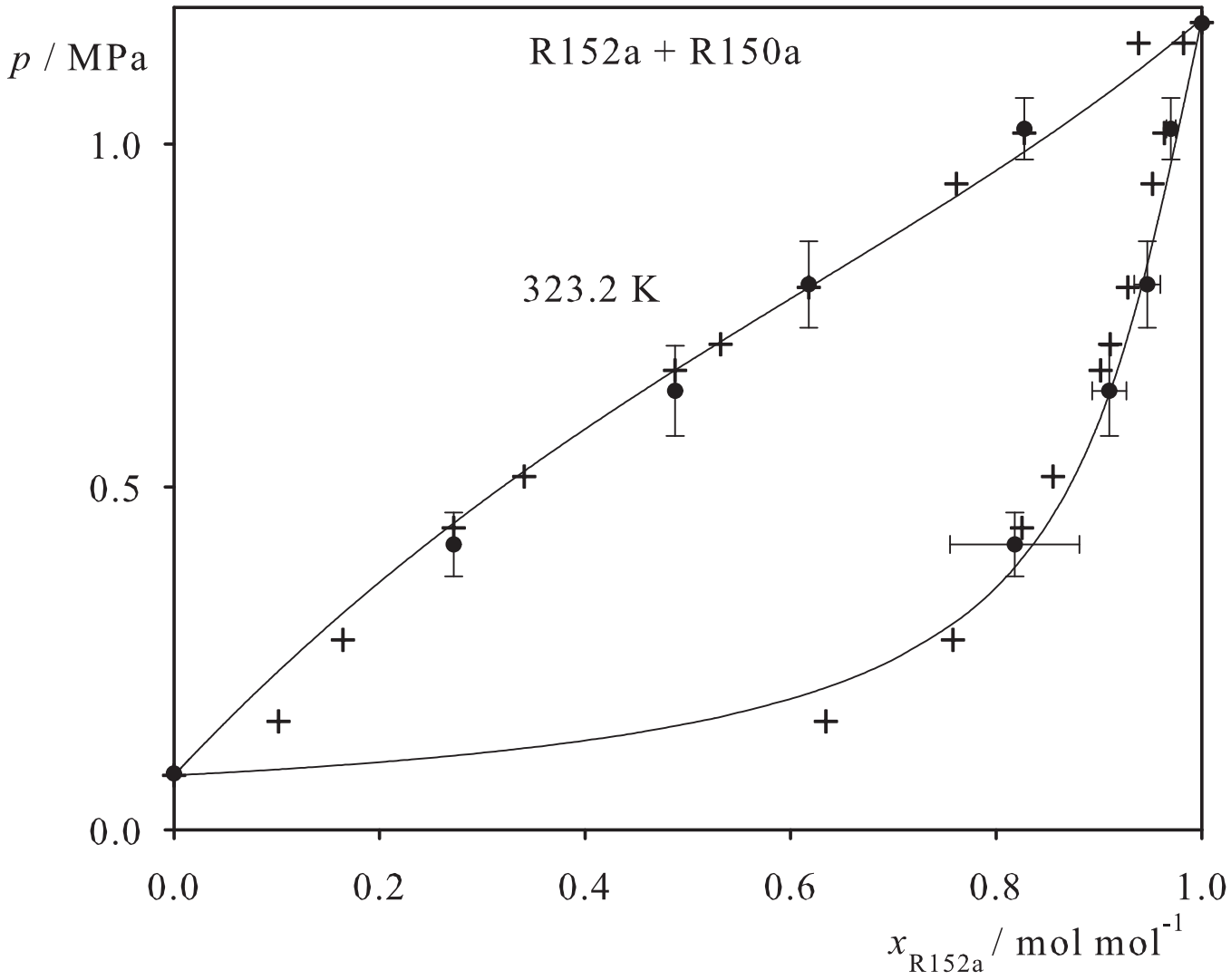

Fig. 254. Binary vapor-liquid equilibrium phase diagram: simulation data ●, experimental data + (cf. Table 2 of the manuscript for the reference) and Peng-Robinson equation of state —.

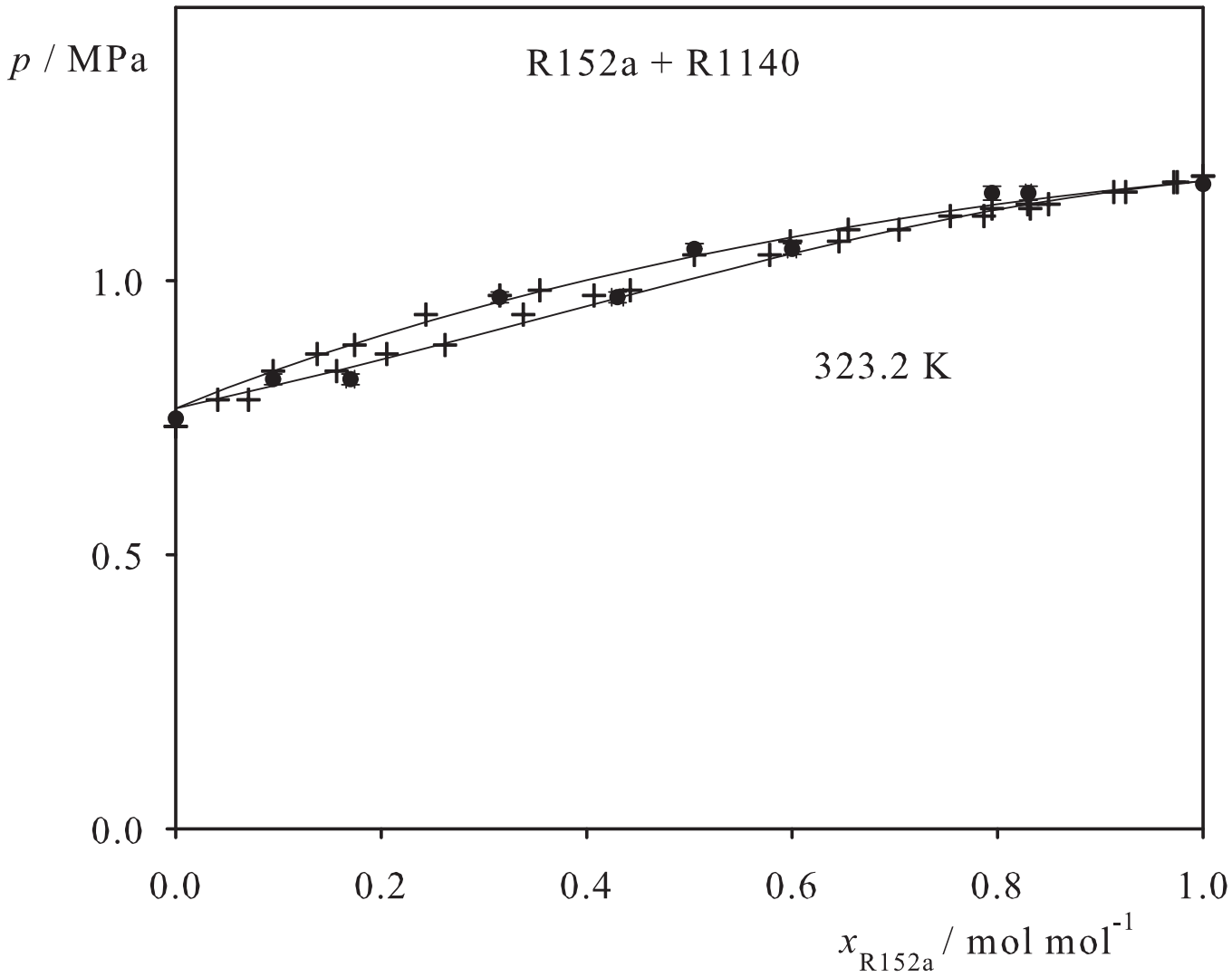

Fig. 255. Binary vapor-liquid equilibrium phase diagram: simulation data ●, experimental data + (cf. Table 2 of the manuscript for the reference) and Peng-Robinson equation of state —.

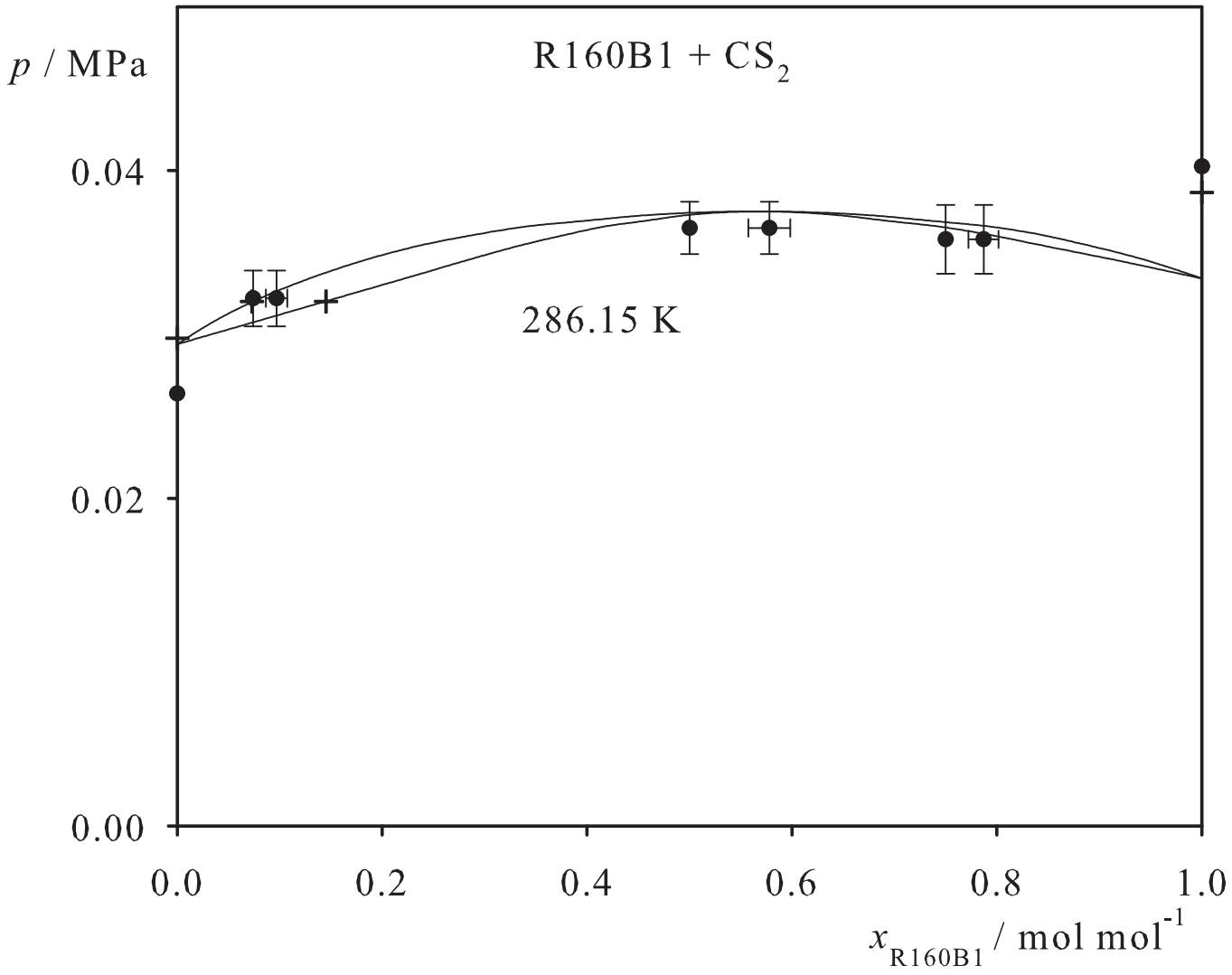

Fig. 256. Binary vapor-liquid equilibrium phase diagram: simulation data ●, experimental data + (cf. Table 2 of the manuscript for the reference) and Peng-Robinson equation of state —.

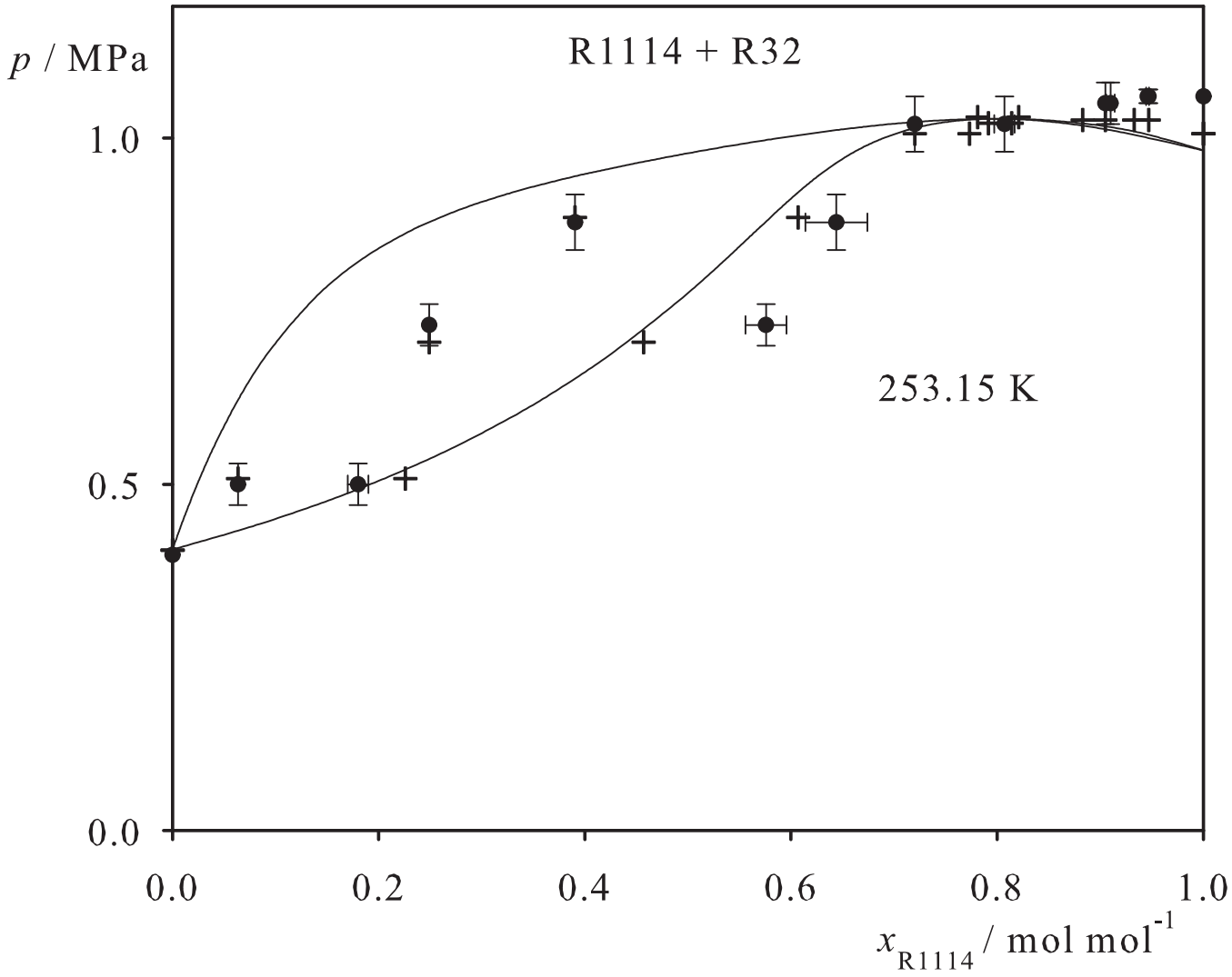

Fig. 257. Binary vapor-liquid equilibrium phase diagram: simulation data ●, experimental data + (cf. Table 2 of the manuscript for the reference) and Peng-Robinson equation of state —.

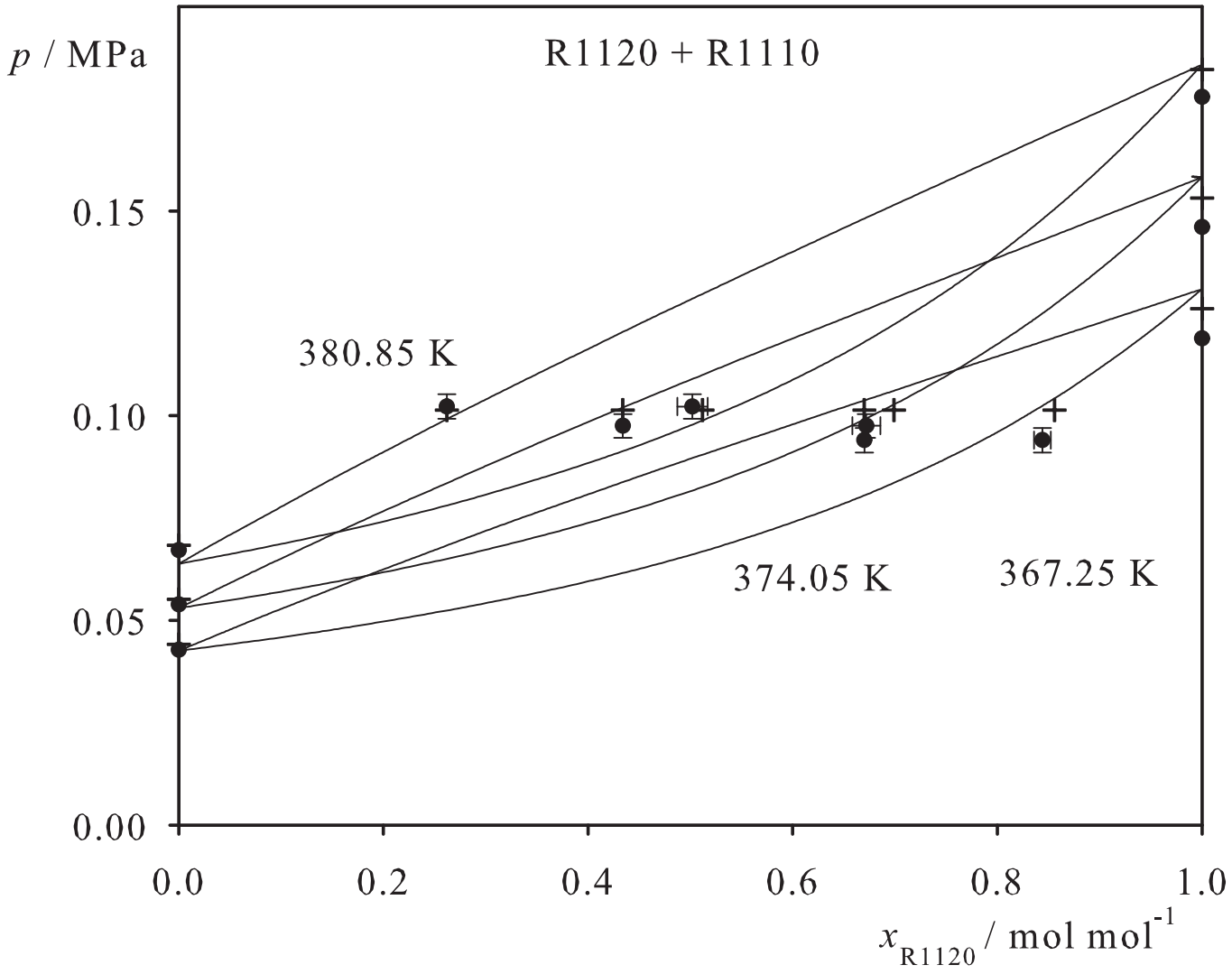

Fig. 258. Binary vapor-liquid equilibrium phase diagram: simulation data ●, experimental data + (cf. Table 2 of the manuscript for the reference) and Peng-Robinson equation of state —.

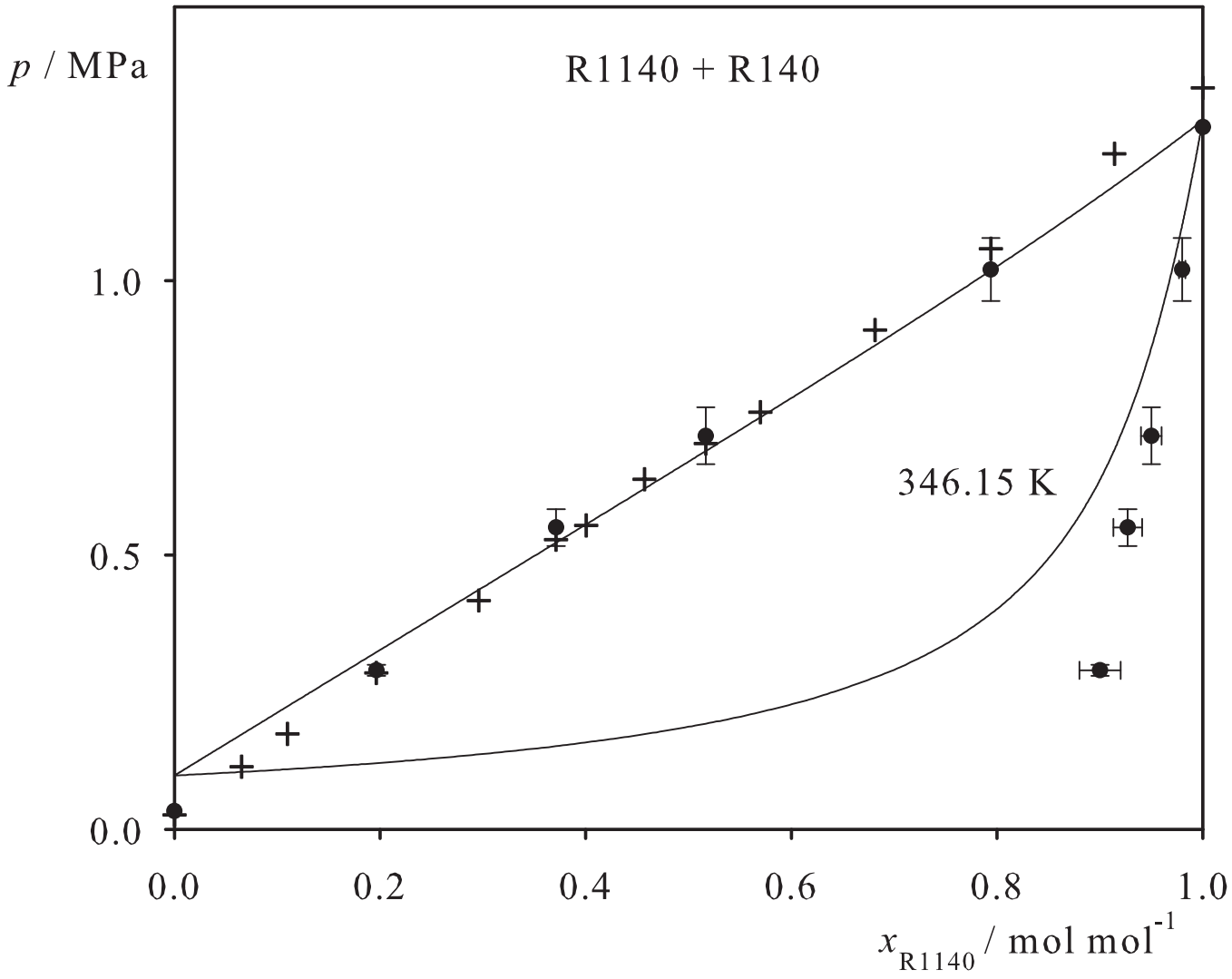

Fig. 259. Binary vapor-liquid equilibrium phase diagram: simulation data ●, experimental data + (cf. Table 2 of the manuscript for the reference) and Peng-Robinson equation of state —.

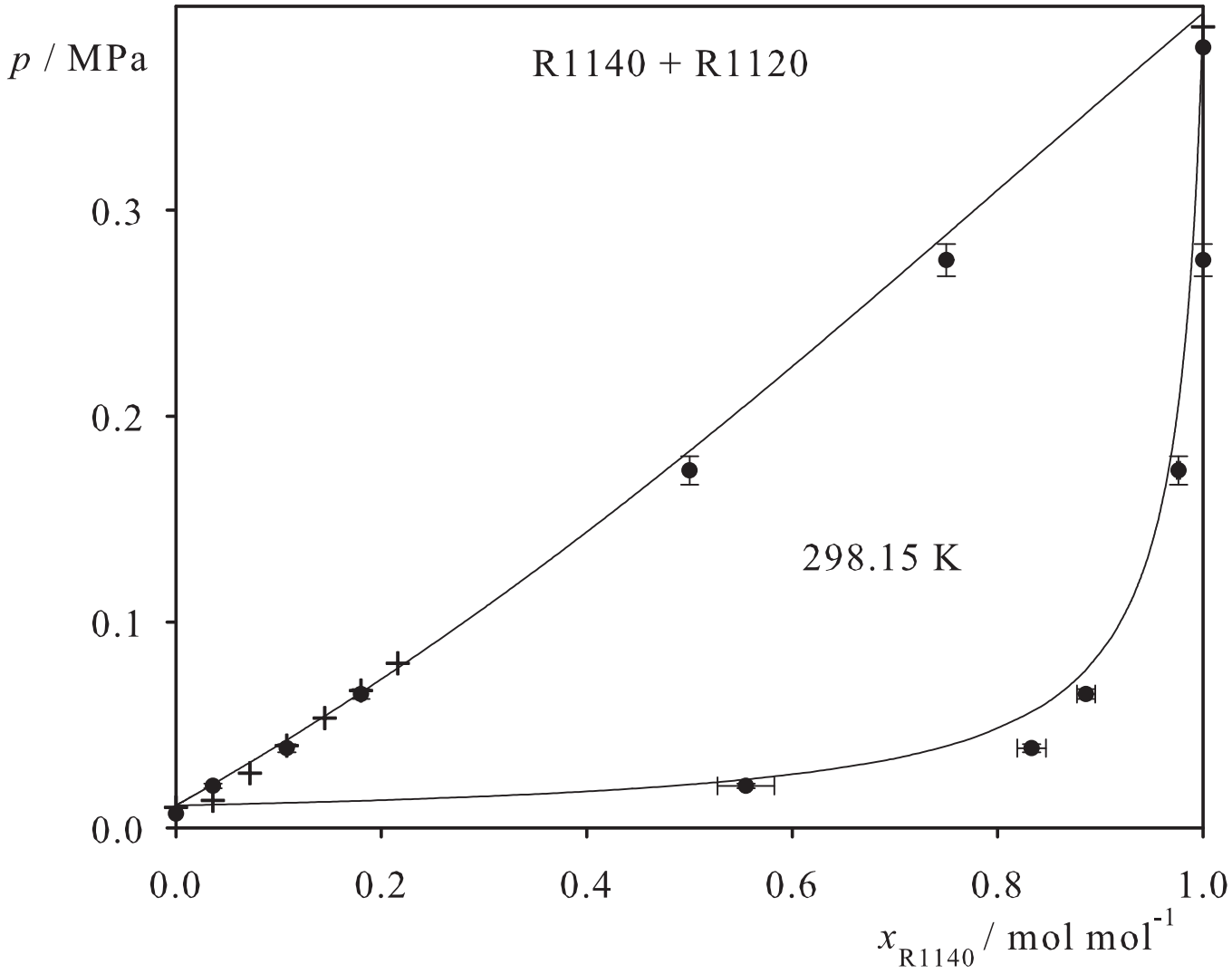

Fig. 260. Binary vapor-liquid equilibrium phase diagram: simulation data ● and experimental data + (cf. Table 3 of the manuscript for the reference).

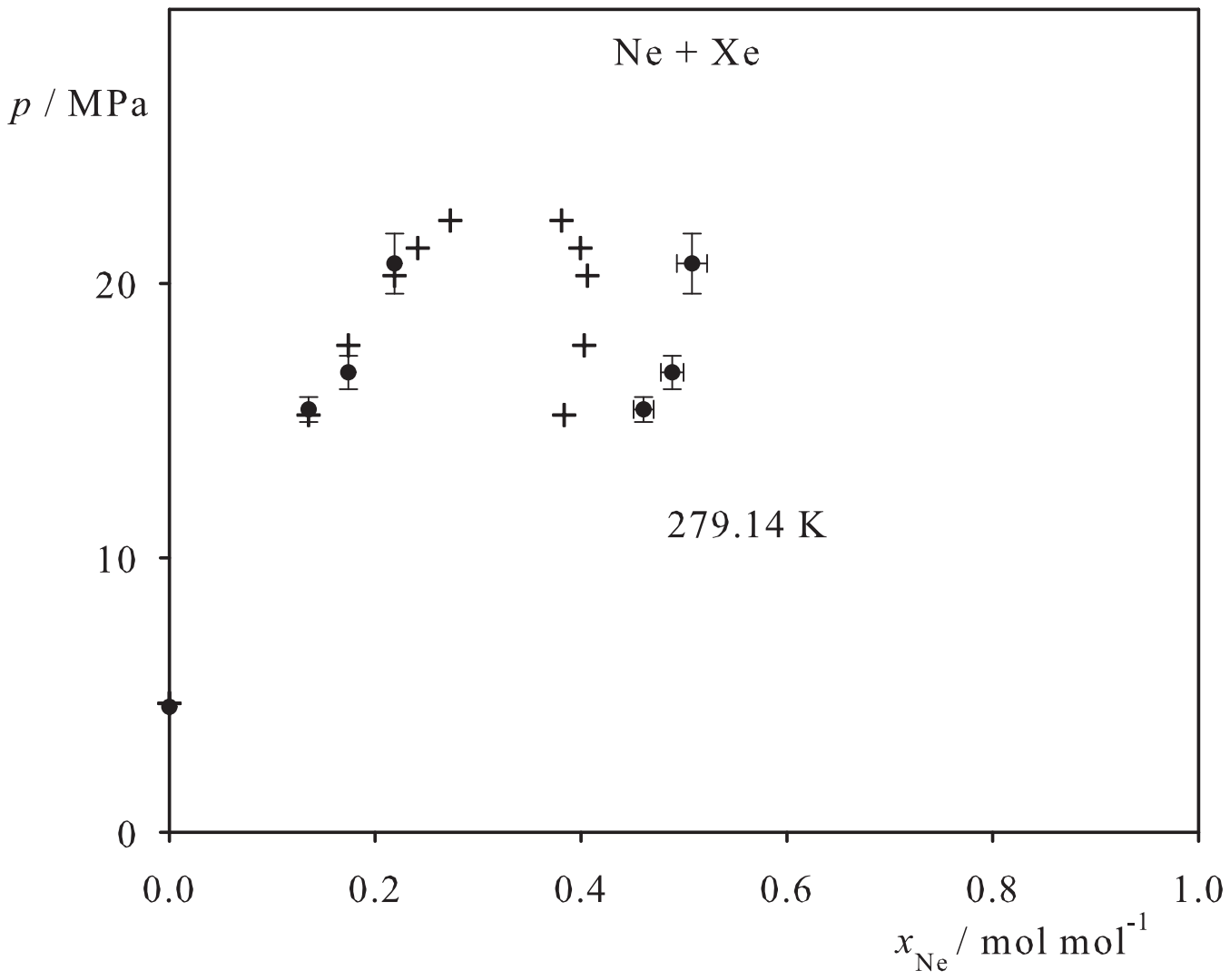

Fig. 261. Binary vapor-liquid equilibrium phase diagram: simulation data ●, experimental data + (cf. Table 3 of the manuscript for the reference) and Peng-Robinson equation of state —.

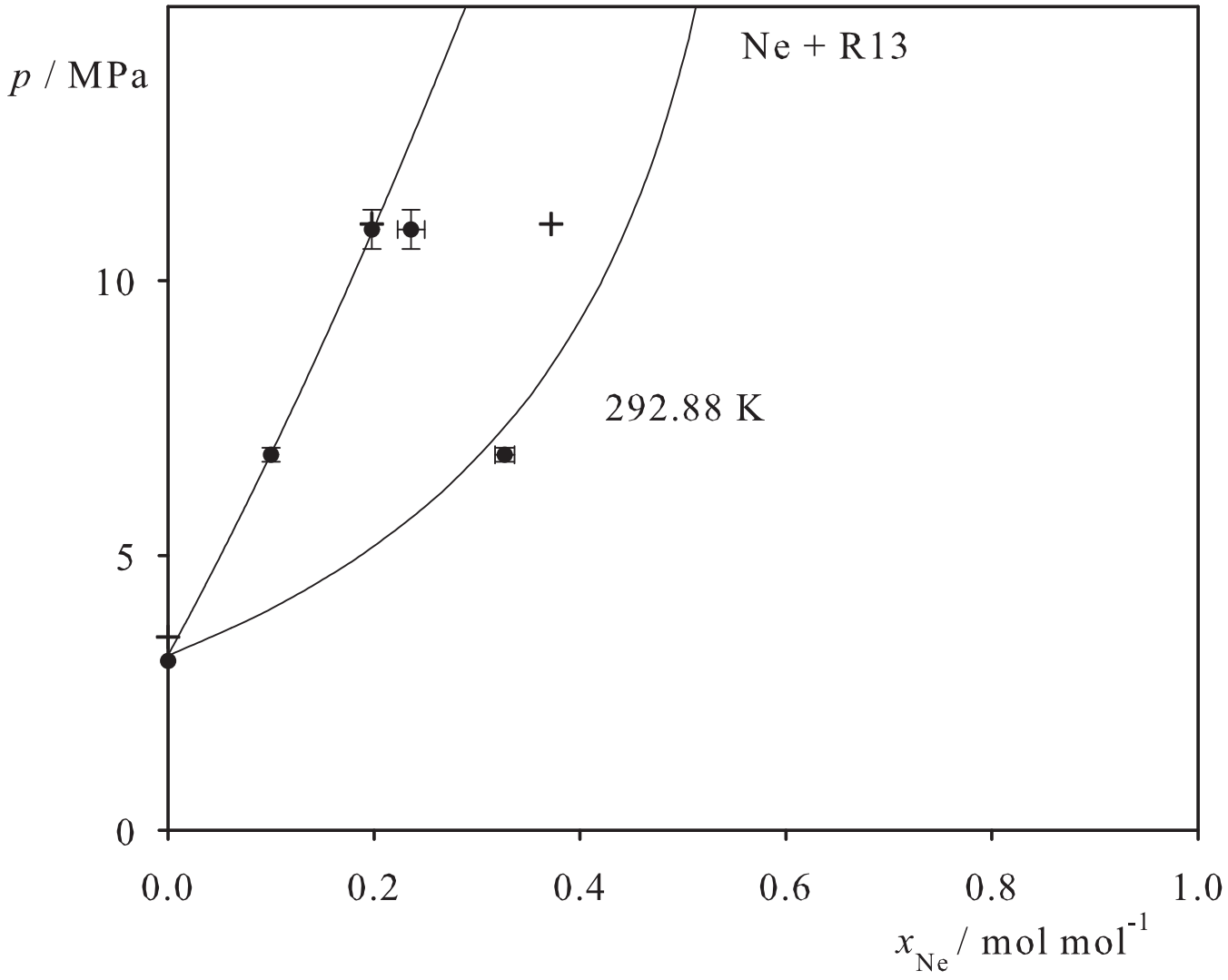

Fig. 262. Binary vapor-liquid equilibrium phase diagram: simulation data ●, experimental data + (cf. Table 3 of the manuscript for the reference) and Peng-Robinson equation of state —.

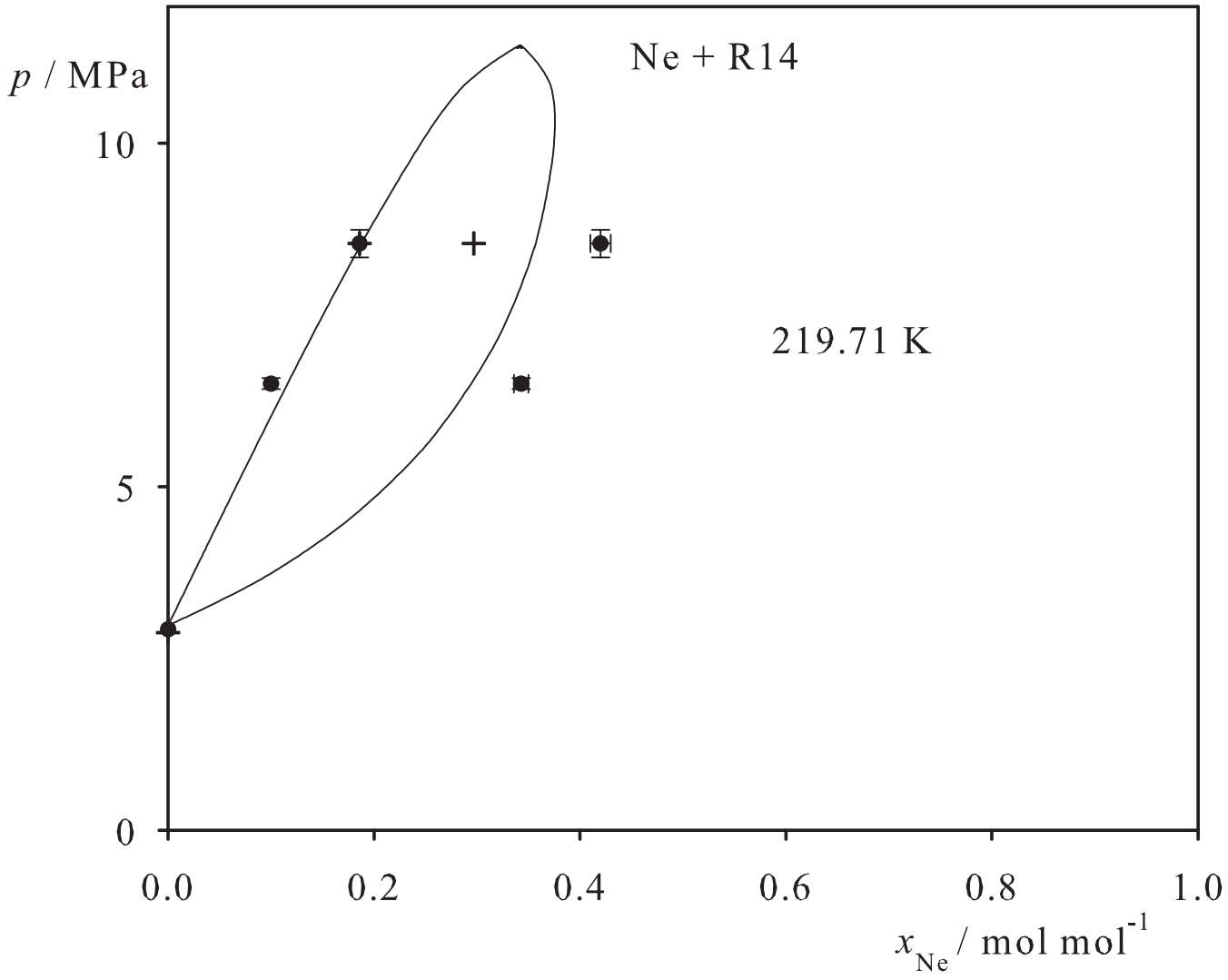

Fig. 263. Binary vapor-liquid equilibrium phase diagram: simulation data ●, experimental data + (cf. Table 3 of the manuscript for the reference) and Peng-Robinson equation of state —.

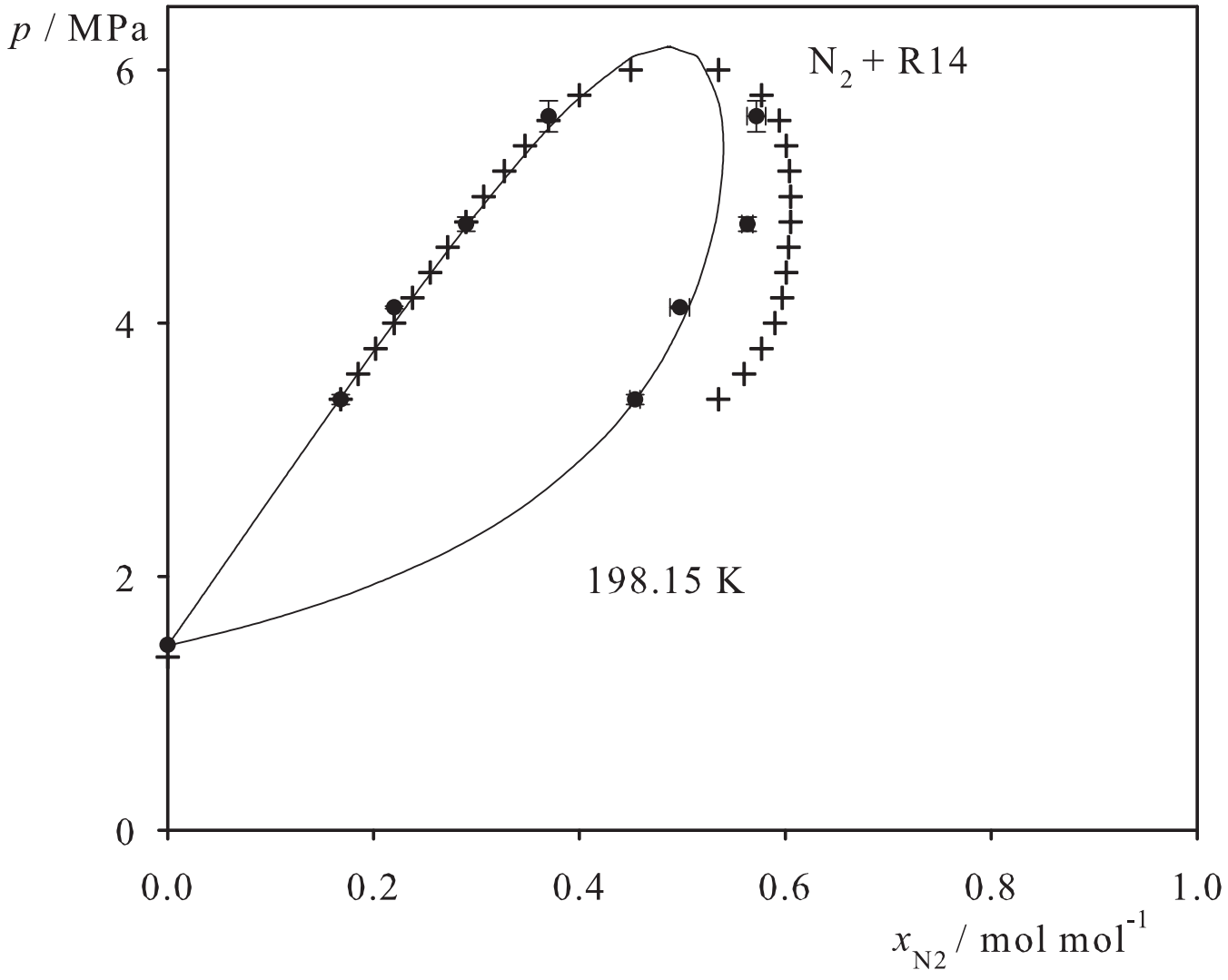

Fig. 264. Binary vapor-liquid equilibrium phase diagram: simulation data ●, experimental data + (cf. Table 3 of the manuscript for the reference) and Peng-Robinson equation of state —.

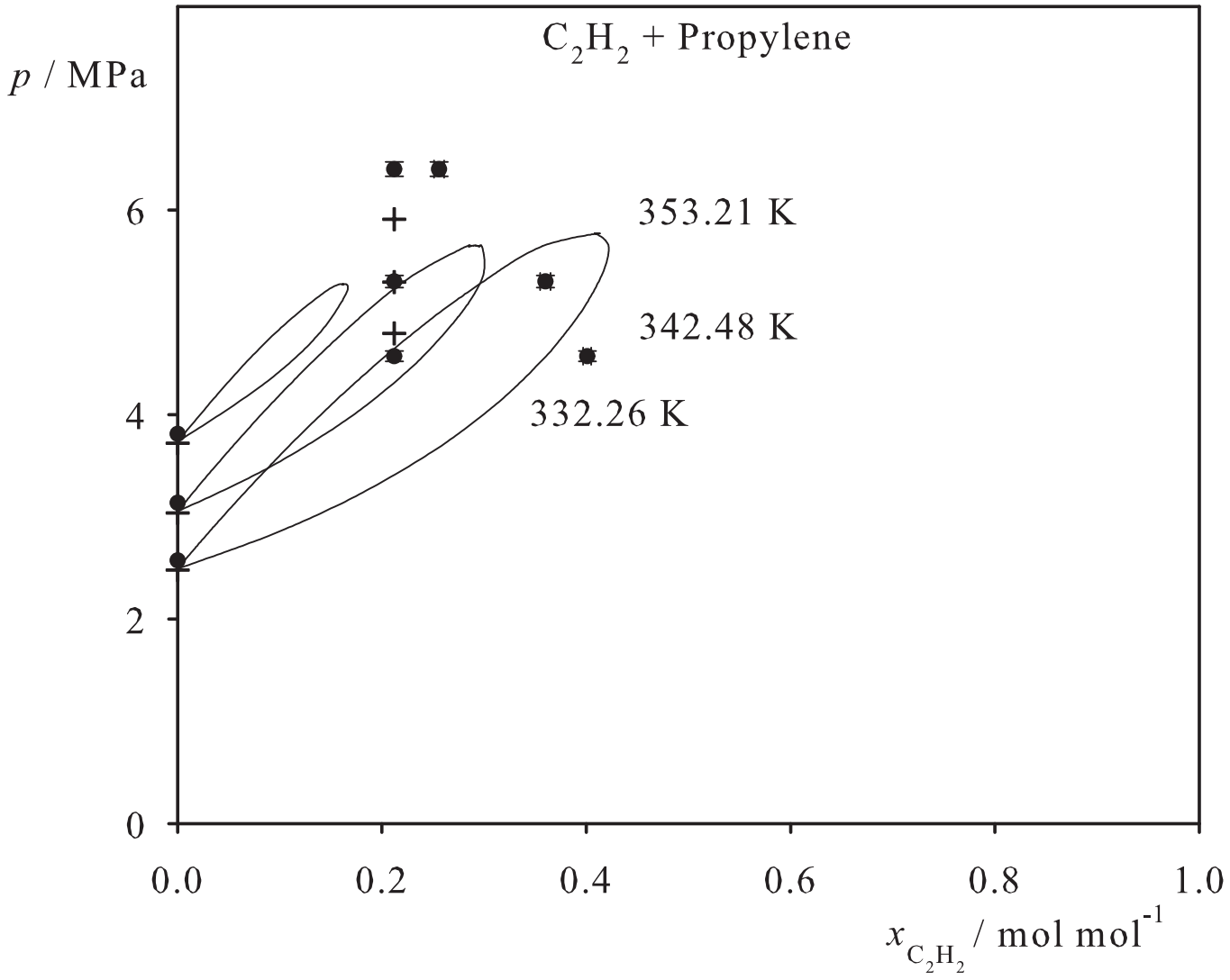

Fig. 265. Binary vapor-liquid equilibrium phase diagram: simulation data ●, experimental data + (cf. Table 3 of the manuscript for the reference) and Peng-Robinson equation of state —.

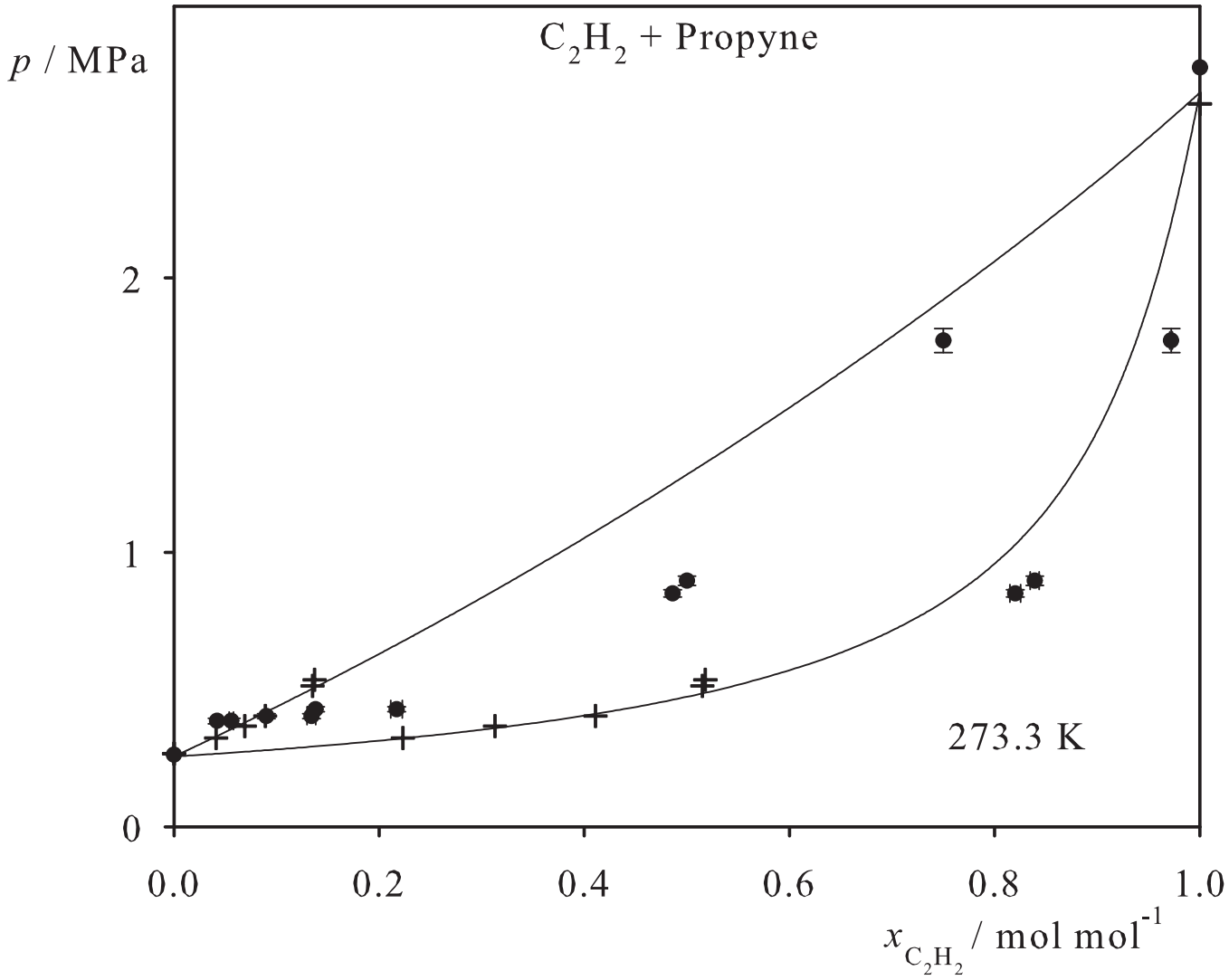

Fig. 266. Binary vapor-liquid equilibrium phase diagram: simulation data ●, experimental data + (cf. Table 3 of the manuscript for the reference) and Peng-Robinson equation of state —.

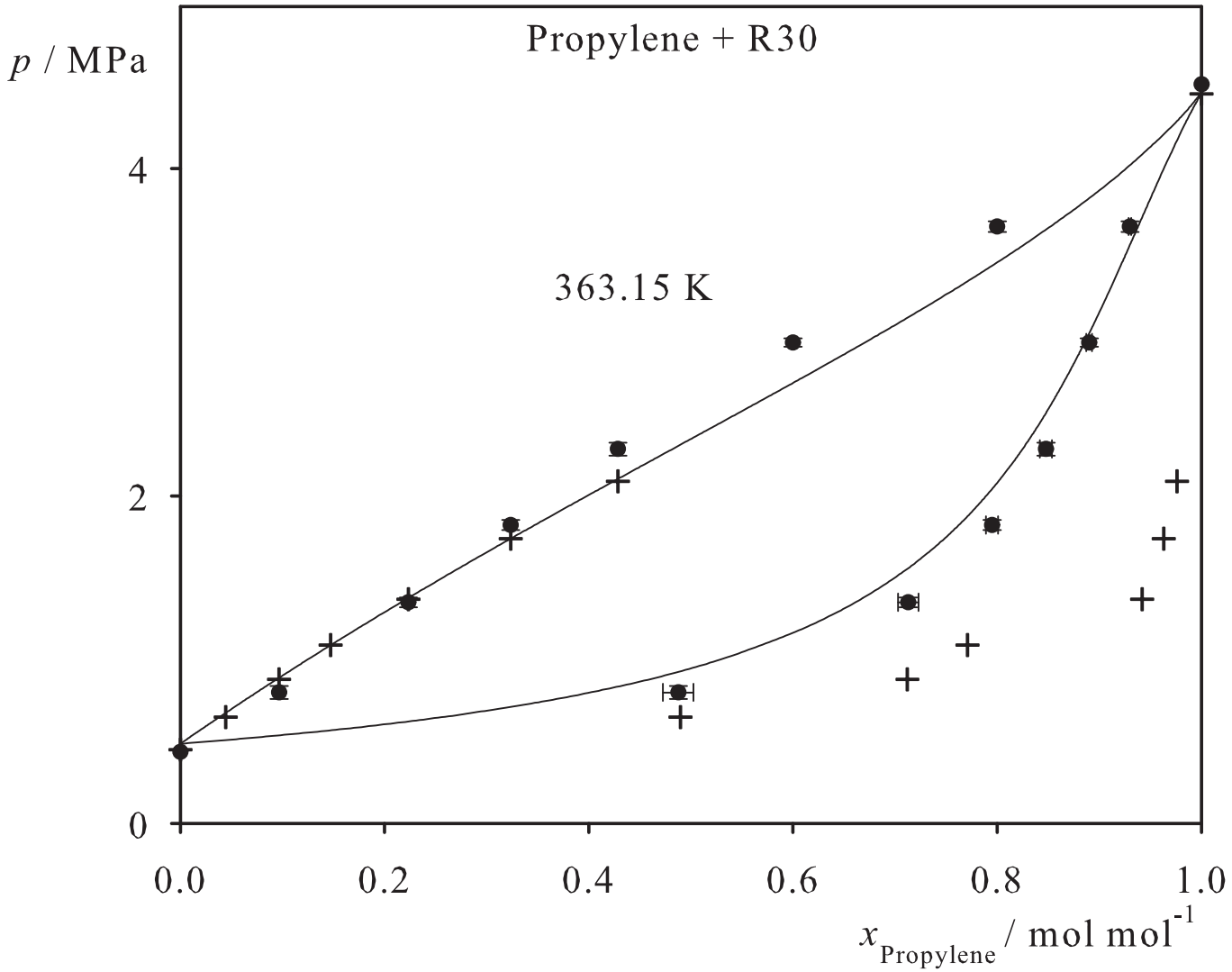

Fig. 267. Binary vapor-liquid equilibrium phase diagram: simulation data ●, experimental data + (cf. Table 3 of the manuscript for the reference) and Peng-Robinson equation of state —.